Investigations of the *In vitro* and *In vivo* Metabolism of a Synthetic C20 Keto Steroid via Chemical Synthesis, Chromatography, and High-Resolution Mass Spectrometry

Doctoral thesis

to attain the

doctoral degree (Dr. rer. nat.)

of the Faculty of Mathematics and Natural Sciences

of the University of Cologne

submitted by

Hui-Chung Wen

from Taiwan

Cologne 5-2025

Reviewers:

Prof. Dr. Mathias Schäfer
Department of Chemistry
University of Cologne

Prof. Dr. Stephanie Kath-Schorr
Department of Chemistry
University of Cologne

Oral examination day 22. August 2025

“Nothing in life is to be feared, it is only to be understood. Now is the time to understand more, so that we may fear less.”

Maria Salomea Skłodowska-Curie

Acknowledgement

This work was conducted from June 2021 to May 2025 in the Department of Chemistry in the University of Cologne and the Institute of Biochemistry in the German Sport University Cologne under the supervision of *Prof. Dr. Mathias Schäfer*, in cooperation with *Prof. Dr. Mario Thevis*.

Firstly, I want to thank my thesis supervisor, *Prof. Dr. Mathias Schäfer*, giving me the opportunity to join this project. I am grateful for his guidance, his encouragement to broaden my knowledge in the mass spectrometry workshops, his support in the investigation of fragmentation mechanisms, and his helpful revision of all my manuscripts. I am always inspired by his enthusiasm for mass spectrometry and his deep passion for chemical mechanism research.

I would further like to express my gratitude to *Prof. Dr. Mario Thevis*, who played a vital role in application for the funding of the *Partnership for Clean Competition*. He always provided insightful advice on my research and offered me chances to present my work at the *Manfred Donike Workshops* in 2023, 2024 and 2025.

Many thanks to *Prof. Dr. Stephanie Kath-Schorr* for kindly allowing me to work on the blue floor, helping me integrate into her group, and inviting me to group seminars and activities. I am delighted that she agreed to be my second thesis reviewer.

I appreciate *Prof. Dr. Mathias Wickleder* for being as the chair of the examination committee, and for dedicating his time to my defense. Big thanks to *Dr. Christof Domnik* for willingly being the recorder in the examination.

I am very grateful to *Dr. Thomas Piper* and *Dr. Felicitas Wagener* for their indispensable support in biochemistry experiments and GC/LC-MS analysis. Special thanks also go to *Dr. Jörg-M. Neudörfl* for performing XRD analysis. Without their help, the publication of the papers would not be possible.

For the synthesis work, I would like to thank *Prof. Dr. Albrecht Berkessel*, *Dr. Tobias Wilczek*, and *Dr. Christina Wartmann* for the valuable suggestions and support.

My deep thanks go to people who gave me advice on thesis contents or formatting, including *Philip Wagner*, *Tristan Möller*, *Dr. Thomas Piper*, *Dr. Felicitas Wagener*, *Dr. Chun-Yu Fu*, *Dr. Jing Li*, *Hans Wagner*, and *Birgit Wagner*.

I am grateful to *Dr. Gregor Fußhöller*, *Astrid Baum*, *Michael Neihs*, *Gamze Gömec*, *Prof. Dr. Andreas Thomas*, *Dr. Sophia Krombholz*, and *Christof Schmitz* for the technical support with mass spectrometry instruments. In addition, thanks to the Horse Department at the *Manfred Donike Institute* for consistently providing derivatization reagents. I am grateful to *Torsten Wick*, the routine sample collection group and all other colleagues, who have expanded my knowledge of doping sample controls.

Many thanks to working groups *Schäfer*, *Thevis*, *Kath-Schorr*, *Berkessel*, *Giernoth* as well as to my dear labmate, *Sarwar Aziz*, for creating a friendly and supporting working environment. I especially enjoy having lunch breaks with all these warm, kind and interesting people.

Special thanks to NMR department, *Dr. Daniel Friedrich*, *Dr. Philipp Hegemann*, *Kathrin König*, and *Daniela Naumann* for maintaining the instruments and manually measuring my samples.

I am grateful to *Sylvia Rakovac*, *Ingo Müller* and *Nihad El Ghachtoun* for managing chemical orders and solvent refills, and to the secretaries *Anja Bitners*, *Janine Keusen*, *Susanne Geuer*, *Doris Sagioglou* and *Sarah Hensel* for administrative support. Many thanks also go to *Andreas Wallraf* for maintaining the building and always bringing me new argon bottles. I would also like to thank the staff in the mechanical and the glass blowing workshops for repairing lab-equipment and glassware.

I am thankful to my family in Taiwan and in Germany as well as to my friends for strong supports and encouragement. I am grateful to meet these warm and amazing people who always share moments of happiness and challenges with me. Your presence made me feel not alone in Germany and gave me the strength to hold on throughout my PhD journey.

Lastly, I want to thank to the funding from *Partnership for Clean Competition.*

Abstract

This study investigates the *in vitro* and *in vivo* metabolism of the synthetic steroid S42, a novel selective androgen receptor modulator (SARM). Its pharmaceutical potential triggered concerns towards illicit use in sports doping. The fragmentation behavior of S42 was examined to support the development of a qualitative and quantitative doping control method based on gas chromatography–electron ionization high-resolution mass spectrometry (GC-EI-HRMS).

Chemically synthesized S42, S42-d4, S42-d7, and their trimethylsilyl (TMS) derivatives were analyzed to characterize key fragment ions found of S42. *In vitro* assays using human liver microsomes and the S9 fraction, a supernatant from homogenized liver tissue, along with *in vivo* rat studies, were conducted to detect metabolites. Many product ions from TMS-metabolites could be identified as they matched those of TMS-S42, with extra TMSO groups, suggesting the actual hydroxylation levels in S42. Comparison of the S42 metabolites and the deuterated metabolites by *in vitro* experiments allowed localization of the oxidation position. To confirm metabolite structures, S42-C20-OH, S42-C6*β*-OH, and S42-C7*α*-OH were synthesized, TMS-derivatized, and GC-MS analyzed as reference compounds for comparison of chromatograms and spectra.

In vitro and *in vivo* phase II metabolites were further analyzed via liquid chromatography–electrospray ionization high-resolution mass spectrometry (LC-ESI-HRMS) in negative mode, with parallel reaction monitoring (PRM) to detect glucuronide and sulfate adducts.

In vitro results indicate that mono-hydroxylation and reduction reactions dominate phase I metabolism, followed by glucuronidation in phase II metabolism. In contrast, triple hydroxylated metabolites were more abundant in rat urine. Sulfate conjugates exhibited stronger LC-MS signals than glucuronides, showing a higher detectability.

Table of contents

1. Introduction

Steroids are essential hormonal compounds involved in a wide range of physiological processes. The use of anabolic androgenic steroids (AASs) can enhance physical strength and increase bone mass.[1] However, their intake is also associated with androgenic side effects such as acne, testicular atrophy, insomnia, and sexual dysfunction.[2] In addition, the risk of serious cardiovascular events, including heart attacks, stroke, and increased mortality, should not be overlooked.[3]

The term “steroid” is often associated with negative connotations due to its illicit use. Anabolic androgenic steroids (AASs) are frequently misused in competitive sports and bodybuilding. One well-known example is testosterone, which gained popularity in the 1990s as a performance-enhancing substance.[4] To ensure fairness in athletic competition, anabolic agents have been banned by the World Anti-Doping Agency (WADA).[5]

Compared to AAS, selective androgen receptor modulators (SARMs) can selectively bind to androgen receptors in specific tissues, which can enhance bone and muscle growth without the side effects of AAS.[6] Therefore, SARMs have become increasingly popular as doping agents, with a growing number of synthetic derivatives being developed and sold on the black market illegally. Therefore, studying SARMs is essential not only for clinical applications but also for improving doping control.

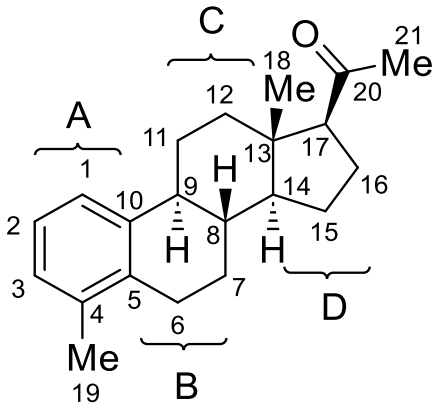

S42 (**1**)

Scheme 1. Structure of novel C20-keto-steroid S42 (**1**) composing of A, B, C, D-ring with specific carbon atom notation.[7]

In 2006, *Uyanik et al.* published a novel synthesized C20 keto steroid S42 (**1**).[7] Subsequent research by *Liu et al.* identified it as a selective androgen receptor

modulator (SARM).[8] S42 (**1**) has been reported to exhibit both anabolic and anti-catabolic properties.[9] It has shown the ability to suppress the proliferation of prostate cancer cells.[10] Despite these promising findings, *Thevis et al.* have raised concerns about the potential misuse of S42 (**1**) in illicit sports doping.[11] To date, no comprehensive studies have been conducted on the metabolic profile of S42 (**1**), and data obtained through gas chromatography-mass spectrometry (GC-MS) analysis remain limited.

To enable future doping control of S42 (**1**), a detailed investigation of its fragmentation behavior in GC-MS and its metabolic profile is essential. In this study, we first focus on elucidating the fragmentation mechanism of S42 (**1**) in GC-MS. Two deuterium-labeled reference compounds, S42-d4 (**1-d4**) and S42-d7 (**1-d7**), were synthesized for comparative fragment interpretation. Trimethylsilyl (TMS) derivatives of these compounds were generated and examined in detail. Subsequent *in vitro* and *in vivo* metabolism studies of S42 (**1**) metabolites bring us a step closer to establishing effective doping control strategies for S42 (**1**).

2. State of knowledge

2.1 Roles of AAS in steroids

2.1.1 General knowledge about steroids and AAS

Steroids nomenclature

The fundamental structure and stereochemistry of steroids are defined by their fused four-ring system and specific spatial configurations. Steroids are classified as triterpenoids and belong to a class of natural compounds characterized by a core structure composed of three six-membered rings (assigned as rings A, B, and C) and one five-membered ring (ring D) (see **Figure 1**).

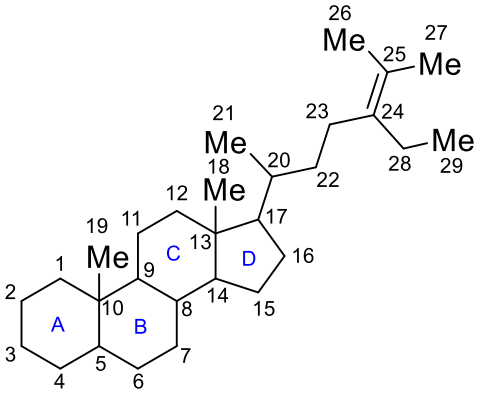

35

Figure 1. IUPAC nomenclature and planar representation of ergost-24-ene steroid skeleton.[12]

The ring numbering system of steroids follows the IUPAC convention, starting with ring A and proceeding sequentially through rings B and C, ending at the side-chain, often referred to as the "bench" structure (see **Figure 1**). Structurally, the three saturated six-membered rings typically adopt a chair conformation, while the five-membered D ring assumes a half-chair conformation.

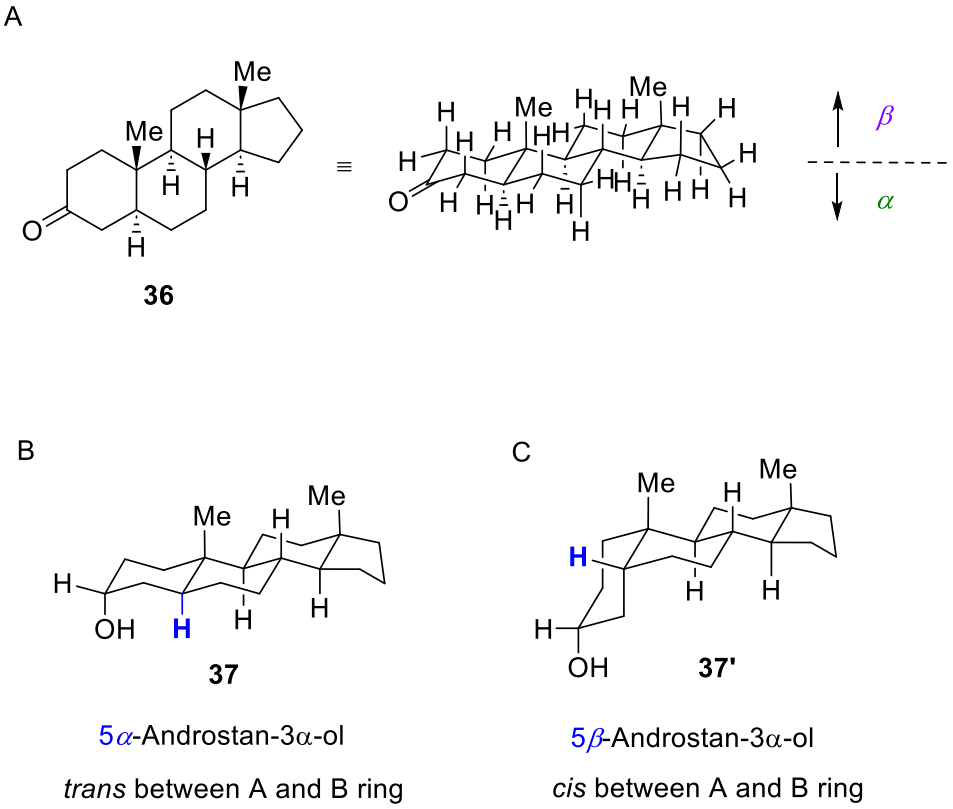

Figure 2. (A) stereochemical configuration of a steroid. The functional group at the axial position is labeled as *β*, and the equatorial position is labeled as *α*. (B) *Trans* form between A and B rings. (C) *Cis* form of A and B rings.[12]

The nomenclature of steroids is defined by the International Union of Pure and Applied Chemistry (IUPAC). A bond is defined as *α*-oriented when it lies below the molecular plane, and *β*-oriented when it lies above (**Figure 2A**). The conformation between rings A and B can be either *trans* or *cis.* A *trans* configuration occurs when the hydrogen atom at carbon 5 is in the *α*-position, whereas a *cis* configuration is present when the hydrogen is in the *β*-position (**Figure 2B**).[13] If the ring system contains a double bond, the symbol Δ (delta) is used to indicate its double position, for example, Δ⁴-testosterone (**46**) (see **Figure 4**).[13a]

Types of steroids by structures

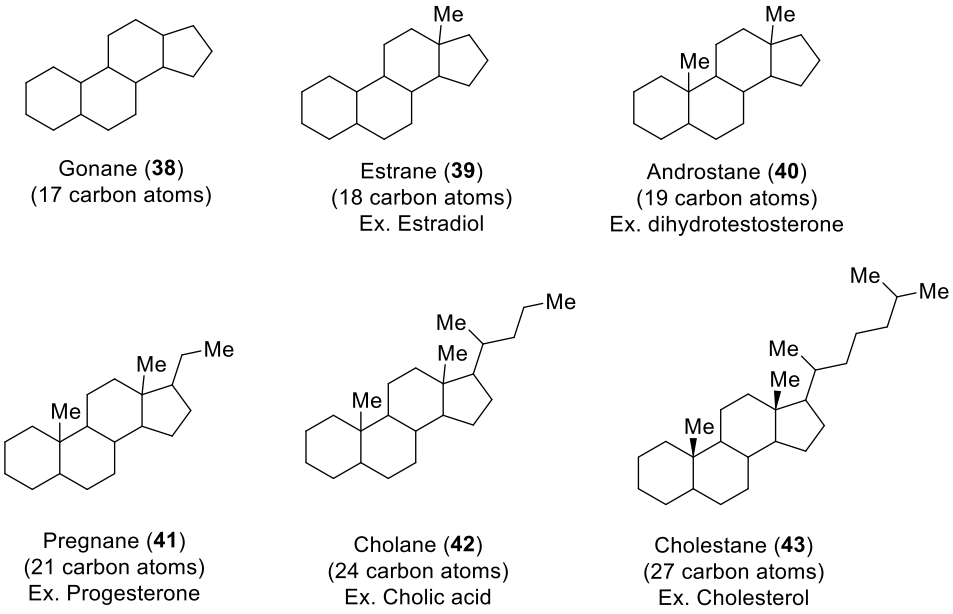

Figure 3. Categories of steroids are based on the carbon number of the backbones: gonane (**38**), estrange (**39**), androstane (**40**), pregnane (**41**), cholane (**42**), and cholestane (**43**).[12]

Steroids can be classified according to their core carbon skeletons, particularly based on the number and arrangement of carbon atoms attached to the fused ring system (see **Figure 3**).[12] The simplest structure, gonane (**38**, C17), consists of four fused rings without side chains. The addition of a single methyl group at C18 defines the estrane (**39**) class (C18), as seen in compounds like estradiol. Androstane (**40**, C19) compounds carry methyl groups at both C18 and C19; typical examples include testosterone and its metabolite dihydrotestosterone. The pregnane (**41**) class (C21) exemplified by progesterone, features a two-carbon side chain at C17. In cholane (**42**, C24), which includes bile acids such as cholic acid, a five-carbon side chain is attached at C17. Finally, cholestane (**43**, C27), the structural framework of cholesterol, contains a seven-carbon side chain at C17 and serves as the biosynthetic precursor of all other steroid classes.

Types of steroids by function

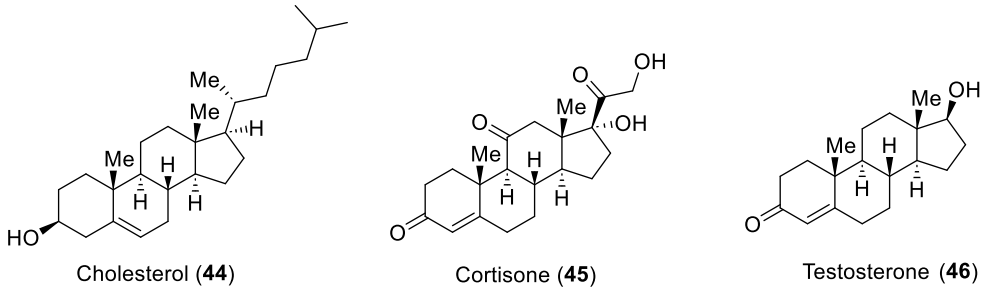

Figure 4. Well-known steroids: cholesterol, cortisone and testosterone.[12]

Steroids play essential roles in both structural and hormonal functions within the human body. Structurally, they are key components of cell membranes, such as cholesterol (**44**). Hormonally, steroids act as signaling molecules and can be classified as either catabolic, such as cortisone (**45**), which breaks down tissues, or anabolic, such as testosterone (**46**), which promotes tissue growth. Testosterone is one of the most well-known anabolic hormones. It functions as a sex hormone, and is more prevalent in males than females.[14] It contributes to muscle development and the expression of male primary and secondary sexual characteristics, including facial hair growth and voice deepening.[15]

2.1.2 Development of force-enhancing agents

Due to the ability to promote muscle mass growth, anabolic androgenic steroids (AASs) have been misused in competitive sports and bodybuilding. As a result, AASs were officially classified as prohibited substances by the World Anti-Doping Agency (WADA) in 1976.[16].

The prohibition of AAS in sports competitions has led to the emergence of synthetically modified compounds known as designer steroids. These substances are specifically designed to evade detection in routine doping tests while retaining their anabolic effects[17] One prominent example is tetrahydro gestrinone (THG), nicknamed "the clear", which was often used in combination with a testosterone-containing product called "the cream" to avoid doping detection.[18] This designer steroid entered the black market in 2003 through the *Bay Area Laboratory Co-Operative* (*BALCO*) in the United States. The case became a major scandal when it was revealed that several high-

profile athletes, including *Major League Baseball* players *Barry Bonds* and *Jason Giambi* were among *BALCO*'s clients.[19]

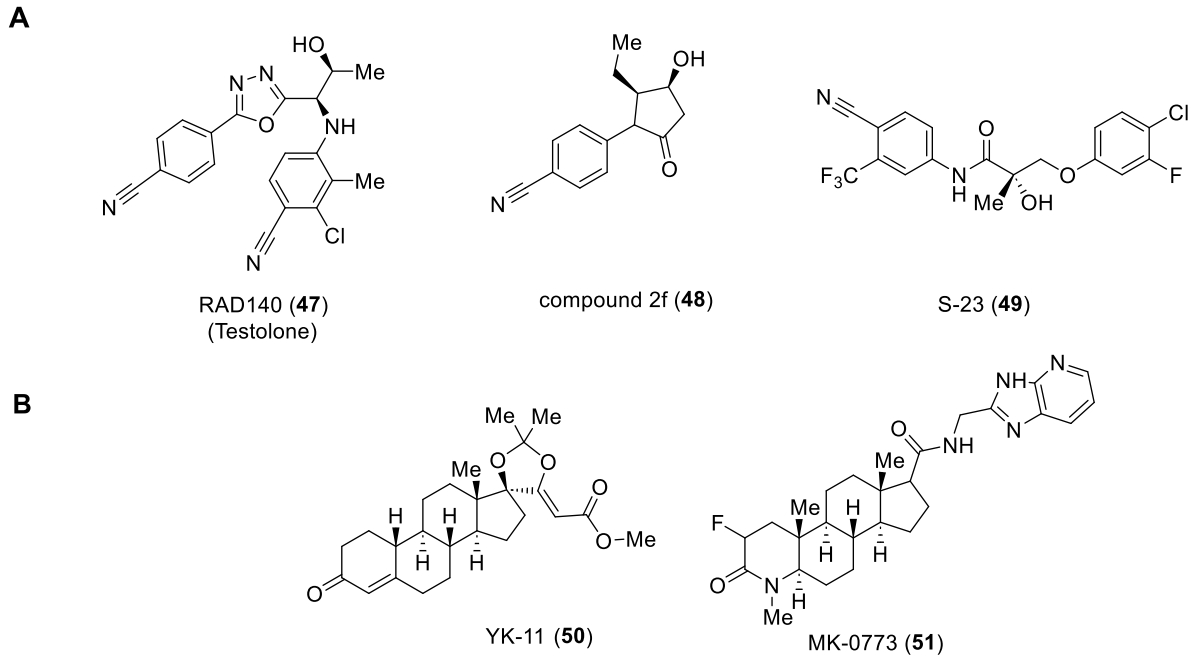

Figure 5. (A) Non-steroidal SARMs: RAD140 (**47**), 2f (**48**) and S-23 (**49**). (B) Steroidal SARMs: YK-11 (**50**) and MK-0773 (**51**). [20]

The side effects associated with the use of AAS have limited their application in medicine. Long-term use of testosterone (**46**), for instance, has been linked to an increased risk of cardiovascular events, including heart attacks, strokes, and overall mortality.[3] To mitigate these adverse effects, selective androgen receptor modulators (SARMs) were developed in 1998.[21] SARMs can be either steroidal or non-steroidal in structure. Well-known non-steroidal SARMs include RAD 140 (**47**), [20a-c] compound 2f (**48**),[20d] and S23 (**49**) (**Figure 5A**),[20e] while examples for steroidal SARMs include YK-11 (**50**) and MK0773 (**51**) (**Figure 5B**).[20f-h]

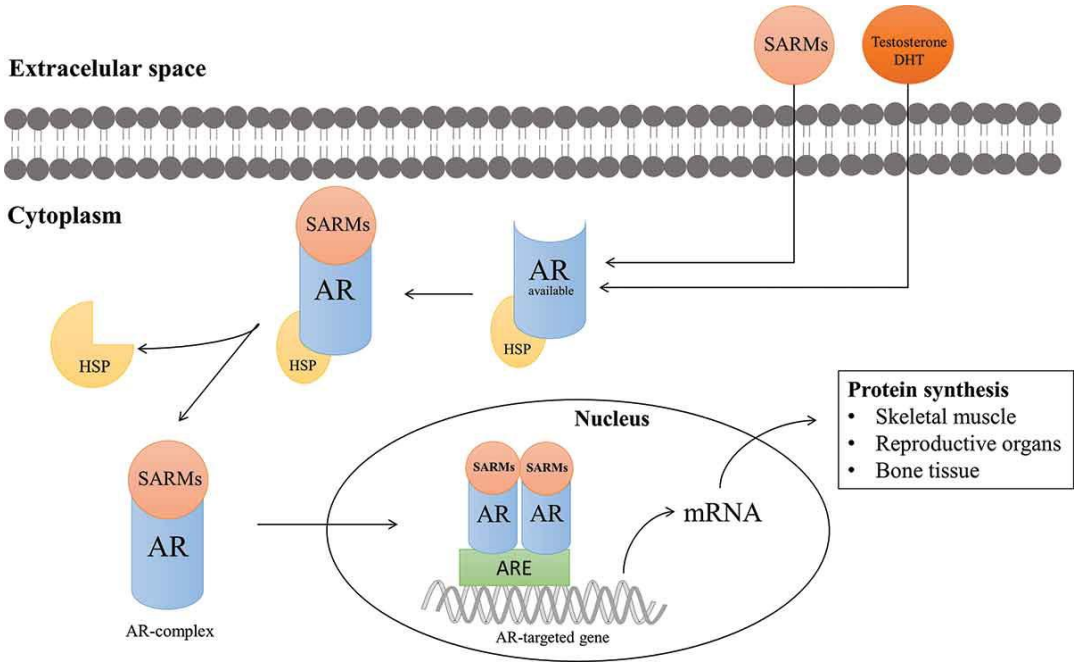

Figure 6. Mechanism of SARMs and androgen receptor to induce protein synthesis.[3b, 22]

Compared to AAS, SARMS exhibit tissue selectivity, meaning they can specifically function on muscles and bone tissues but not on other tissues, such as the prostate gland. SARMs and AASs can be administered either orally or via injection. Once in the bloodstream, these small molecules circulate by binding to specific transport proteins, such as sex hormone-binding globulin (SHBG) or albumin[23], and are subsequently delivered to target tissues (**Figure 6**).

After entering the cytoplasm, SARMs bind to the androgen receptor (AR), which is initially stabilized by heat shock proteins (HSPs). The binding of a ligand, such as testosterone or a SARM, induces a conformational change in the AR, leading to the dissociation of the HSPs and the formation of the activated AR complex. This complex then enters into the cell nucleus, where it binds to specific DNA sequences known as androgen response elements (ARE) located in the promoter regions of target genes. With the binding of co-activators (e.g., ARA70) and corepressors, the AR complex regulates the transcription of messenger RNA (messenger ribonucleic acid), ultimately promoting protein synthesis. This process drives the anabolic effects of SARMs, such as muscle and bone tissue growth.[21-22]

Several hypotheses have been proposed to explain the tissue selectivity of SARMs. One possible explanation is the distinct conformational change induced in the androgen receptor (AR) upon binding with SARMs.[24] Most SARMs are non-

steroidal,[25] for example, RAD 140 (**47**),[20b], compound 2f (**48**),[20d] and S-23 (**49**),[20e], and differ significantly in structure from natural steroidal AR ligand. Even minor structural modifications in steroidal ligands can alter their binding behaviors. Therefore, this effect potentially results in SARM-like activity. Another possible reason may be the different expression of metabolizing enzymes for SARM compared to AASs, which could influence their tissue-specific activity.[21]

The development of SARMs has raised hopes for treating muscle-related diseases and certain types of cancer, such as breast cancer. However, to date, the U.S. Food and Drug Administration (FDA) has not approved any SARM for medical use.[26] Instead of being applied therapeutically, SARMs have increasingly entered the black market and are misused similarly to AAS in competitive sports. In 2008, the World Anti-Doping Agency (WADA) officially classified SARMs as prohibited substances.[27] Doping control of SARMs remains challenging due to the availability of published data on their metabolic pathways and detection methods.

2.2 Doping control of steroidal and non-steroidal metabolites

2.2.1 Formation of steroid metabolites

According to the ADME model - A (adsorption), D (distribution), M (metabolism), and E (excretion), a drug administered either orally or via injection is transported through bloodstreams. Once distributed to various tissues, the compound undergoes metabolic transformation to increase polarity, facilitating elimination from the body via body fluids.[28] Phase I metabolism involves oxidation, reduction, and hydrolysis reactions that increase the compound's hydrophilicity. Phase II metabolism involves conjugation reactions, such as glucuronidation and sulfation, which further increase polarity.[29] Therefore, in doping control, it is essential to identify not only the parent compounds but also their metabolites in order to detect illicit substance use by the analysis of human body fluids.

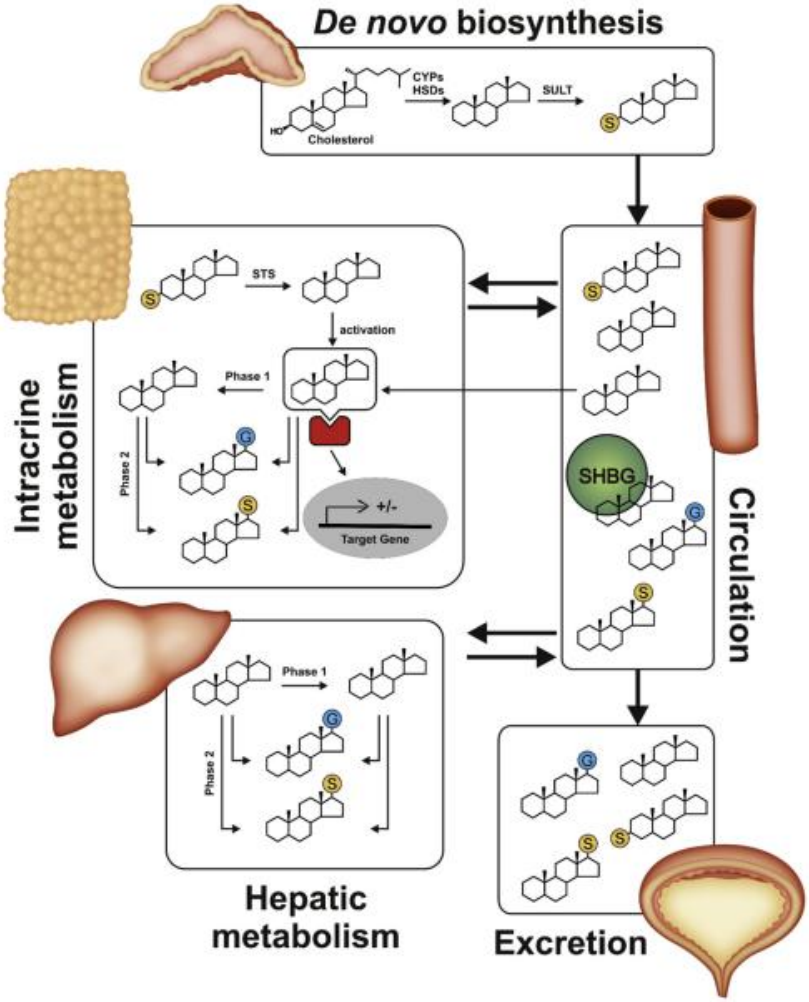

Figure 7. Metabolism pathway from biosynthesis, circulation, metabolism, and excretion, according to *Schiffer et al.*[30]

The metabolic pathway of steroids is illustrated in **Figure 7**. In the human body, C19 steroids, such as testosterone, are synthesized *de novo* in the gonads: in Leydig cells of the testicles in men[31] and in Theca cells of the ovaries in women.[32] Once synthesized, these steroids circulate in the bloodstream bound to carrier proteins such as sex hormone-binding globulin (SHBG) or albumin, which facilitate their transport to target tissues. (**Figure 7**). Steroids can undergo intracrine metabolism within cells, where they are synthesized, modified, and act within the same cell. A well-known example is the conversion of testosterone to dihydrotestosterone (DHT) by the enzyme 5*α*-reductase in tissues such as the prostate or skin.[30] For excretion, steroids are metabolized through phase I and phase II enzymatic reactions, producing more polar metabolites that are ultimately eliminated from the body.

Primary steroid metabolism occurs in the liver, predominantly by enzymes from the cytochrome P450 (CYP) family and hydroxysteroid dehydrogenases (HSDs). These two enzyme families are responsible for phase I metabolic reactions such as oxidation, reduction, and hydroxylation, which introduce or expose functional groups to increase the polarity of steroid molecules. CYP3A4 isoform within the CYP450 superfamily is especially essential for studying drug metabolism.[33] CYP3A4 is involved in the metabolism of up to 50% of drug metabolism. In addition, 30% of hepatic (liver) CYPs are CYP 3A4 isoforms.[34]

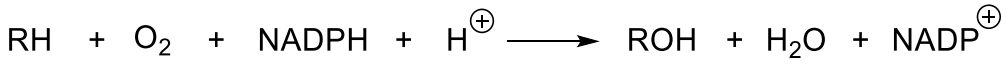

Scheme 2. Hydroxylation reaction by cytochrome P450 with O_2 and a cofactor NADPH.[35]

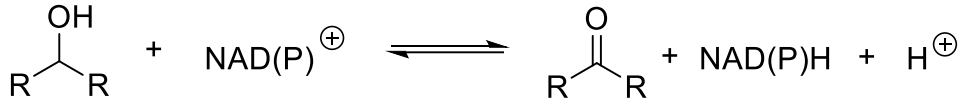

Scheme 3. Cofactor NAD+ acts as a hydrogen acceptor, and NADH is a hydrogen donor. An alcohol functional group in steroids can be oxidized to a ketone by hydroxysteroid dehydrogenases (HSDs).[35-36]

Hydroxylation during phase I metabolism, as illustrated in **Scheme 2**, requires CYP450 enzymes. These enzymes contain a heme-bound iron atom that facilitates oxygen binding and activation. NADPH acts as a crucial cofactor, enabling electron transfer during the reaction. The resulting hydroxy groups can be further oxidized to ketones by hydroxysteroid dehydrogenases (HSDs) using $NAD(P)^+$as a cofactor. Conversely, ketone-containing steroids can be reduced back to their corresponding hydroxy forms by HSDs in the presence of NAD(P)H, as shown in **Scheme 3**.[36]

Non-conjugated phase I metabolites are rapidly converted into phase II conjugated metabolites, primarily through glucuronidation or sulfation, to enhance their solubility in body fluids. Phase II metabolism, particularly glucuronidation, plays a central role in detecting androgen doping via urine analysis. In humans, glucuronidation is the predominant pathway in phase II metabolism.[35] Moreover, conjugated phase II metabolites are typically more abundant in urine than their non-conjugated phase I counterparts, especially in the case of anabolic steroids.[37] Therefore, phase II metabolites are preferred targets in doping control in urine testing.

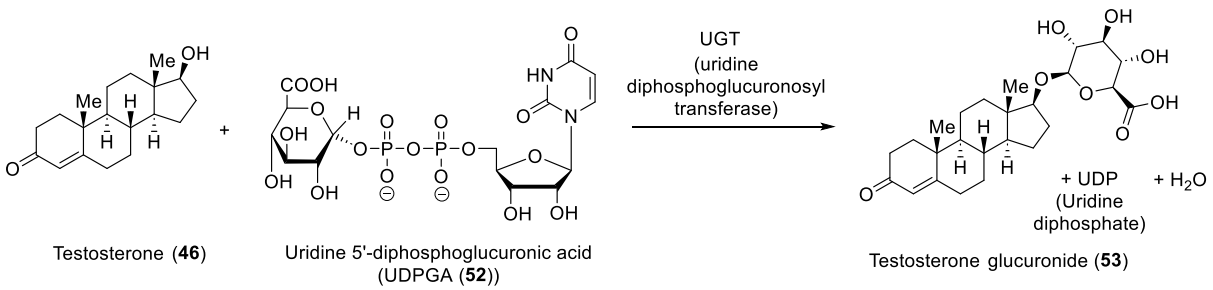

Testosterone (**46**) Uridine 5'-diphosphoglucuronic acid (UDPGA (**52**)) Testosterone glucuronide (**53**)

Scheme 4. The glucuronidation reaction of testosterone with UDPGA, which is catalyzed by UGTs (uridine diphosphoglucuronosyl-transferases).[35, 38]

Glucuronide metabolites are formed in the human body through a reaction between uridine 5'-diphosphoglucuronic acid (UDPGA (**52**)) and target molecules, catalyzed by uridine diphosphoglucuronosyltransferase (UGTs). This reaction follows an S_N2 type nucleophilic substitution mechanism, as illustrated in **Scheme 4**.[38]

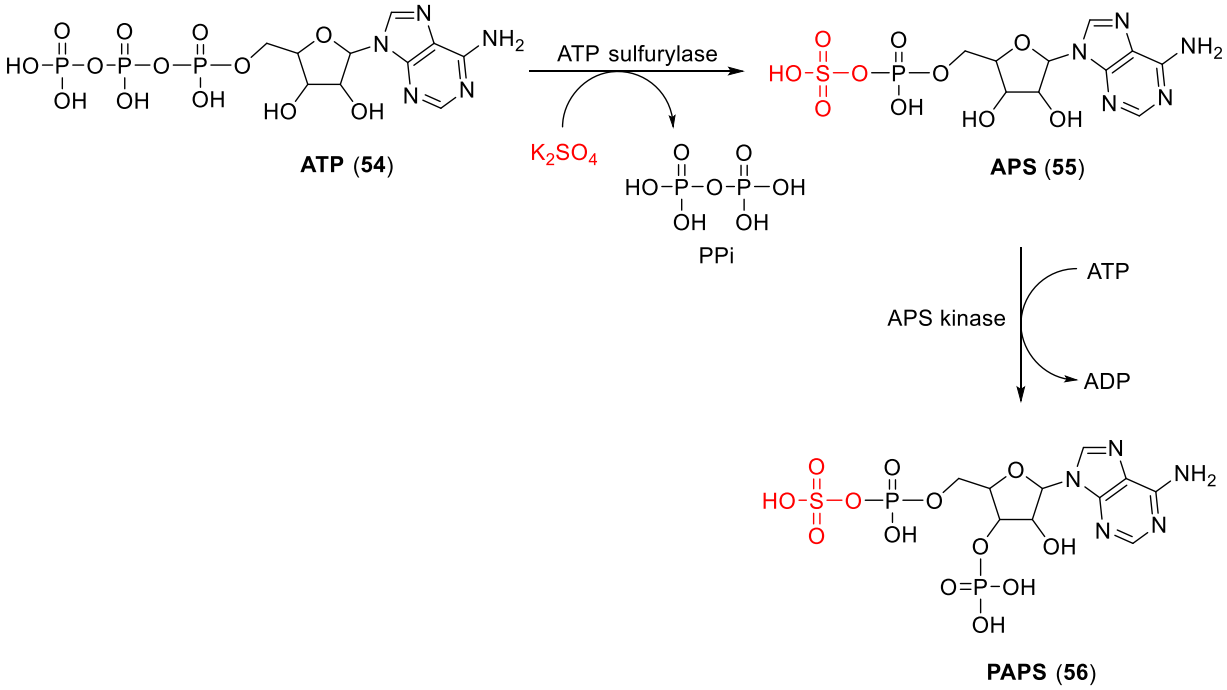

ATP (**54**) **APS** (**55**) **PAPS** (**56**)

Scheme 5. Formation of PAPS (3′-Phosphoadenosine-5′-phosphosulfate) (**56**).

$$\text{PAPS} + \text{Substrate-OH} \longrightarrow \text{Substrate-OSO}_3\text{H} + \text{PAP}$$

Scheme 6. Sulfation reaction by PAPS (3′-Phosphoadenosine-5′-phosphosulfate). [39]

In the sulfation pathway of phase II metabolism, the cofactor 3′-phosphoadenosine-5′-phosphosulfate (PAPS (**56**)) needs to be synthesized from adenosine triphosphate (ATP (**54**)).[39a] This process begins with adenosine 5'-phosphosulfate (APS (**55**))

formation by adenosine triphosphate sulfurylase (ATP sulfurylase). APS (**55**) is then phosphorylated by APS kinase to generate PAPS (**56**) (see **Scheme 5**).

Sulfotransferases catalyze the transfer of the sulfate group from PAPS to hydroxy-containing phase I metabolites, forming sulfate metabolites (see **Scheme 6**) and byproduct, 3′-phosphoadenosine 5′-phosphate (PAP).[38, 39b]

2.2.2 Doping control and analysis by GC and LC-MS

Effective doping control requires consideration of various factors that influence the types of metabolites produced. Doping substances can be administered orally, via injection, or through transdermal patches.[40] Different ways of administration affect the ratio and the types of metabolites diversely. In addition, individual variability, such as nutrition, gender, ethnicity, and biological sex, can significantly influence metabolic pathways. Therefore, studies of metabolism can be complicated.

Doping methods

The drug administration route significantly affects its therapeutic effectiveness and practical usability. Oral administration is the most common method in daily life due to its convenience. However, it often results in reduced drug concentration delivered to the target sites, as liver absorption will filter out a significant part. This impact is called the first pass effect.[41] Hypodermic injections bypass the first-pass effect, but they are less convenient and carry risks such as infection or disease transmission when non-sterile needles are used. Transdermal administration, which delivers drugs through the skin, is a novel alternative [40] that avoids the drawbacks of both oral and injectable methods. However, only a limited number of chemical compounds are suitable.

Doping samples

Various biological samples are used in doping analysis, including whole blood, serum, urine, and dried blood spot (DBS). Some chemical compounds, such as testosterone esters, can only be discovered in blood.[42] Nevertheless, traditional urine samples are still the primary sample type for doping analysis as they have some substantial advantages: Phase II metabolites from doping agents usually remain in urine, and taking urine samples is less invasive than blood samples. In addition, urine samples

provide larger volumes, which is beneficial for reanalysis. In contrast, DBS samples are limited to three A samples (initial analysis) and one or two B samples (confirmation analysis). Urine samples also offer storage advantages: they are easier to store and transport than whole blood, which requires strict temperature control during shipment, and significantly increases transportation costs.[43] Serum and urine samples are more stable than whole blood, making them more suitable for long-term storage. DBS (dried blood spot) samples were officially approved by WADA for routine doping control starting September 1, 2021, during the COVID-19 pandemic.[44] Their low costs and minimal storage requirements make them an attractive alternative, and research on DBS-based analysis is ongoing.[45] Despite these developments, urine remains the most widely used sample type in doping control.

Analysis methods

Modern doping control relies heavily on advanced analytical techniques to detect trace substances in complex biological samples. Mass spectrometry (MS) is one of the most widely used methods due to its high sensitivity, specificity, and low sample volume requirements, making it ideal for high-throughput analysis.[46] Traditional chemical analysis methods like NMR, UV-Vis, and IR spectroscopy are less suitable for analyzing complex body fluids due to their lower sensitivity, selectivity, and complexity. The current gold standard in doping control is gas chromatography (GC) or high-performance liquid chromatography (HPLC) coupling with mass spectrometry (MS). GC-MS and LC-MS are complementary rather than competing techniques. A comprehensive metabolic profile can be obtained when both methods are employed.

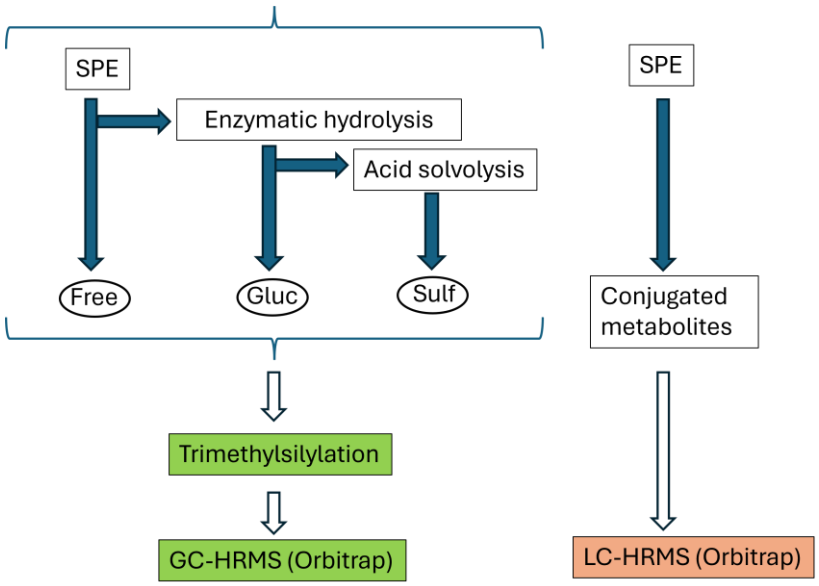

Figure 8. AAS glucuronide and sulfate metabolites in urine samples need to be hydrolyzed and derivatized (silylation) before GC-MS analysis. For LC-MS, conjugated products can be analyzed after purification from SPE. The scheme was adapted from *Putz* and *Piper et al.*[47]

Before analysis, urine samples must undergo purification (**Figure 8**). Solid-phase extraction (SPE) is a commonly used method that isolates target analytes from the complex biological matrix. For GC-MS analysis, an additional hydrolysis step is required to convert hydrophilic phase II metabolites into non-conjugated phase I metabolites, enabling their detection by GC-MS.

The purified urine samples are separated using liquid/ liquid extraction (LLE) into three fractions:

a. Free fraction: non-conjugated phase I metabolites.
b. Glucuronide fraction: hydrolyzed phase II conjugated metabolites using *β*-glucuronidase.
c. Sulfate fraction: solvolyzed phase II conjugated metabolites using acidic hydrolysis conditions.

Each fraction is dried and derivatized using trimethylsilyl (TMS) before GC-MS analysis.

In contrast, for LC-MS analysis, phase I and phase II metabolites purified by SPE can be directly diluted and analyzed, which is a more convenient workflow without hydrolysis or derivatization.

Steroid analysis with GC-EI HRMS

GC-MS and LC-MS have different advantages and disadvantages for doping control. The history of using GC-MS for steroid mixtures (cholesterol methyl ether, cholestanol methyl, and synthetic steroids analysis began in 1960s by *Horning* and *Sweeley*,[48]which is before the advent of online LC-MS coupling, which depended on the development of electrospray (ESI).[49] Compared to LC-MS, GC-MS relies on the volatility of low-molecular mass and non-polar analytes.[50] Thermal vaporization does not work with polar macromolecules, which are suited for ESI-MS and LC-MS applications.[49] Therefore, GC-MS is particularly well-suited for analyzing hydrophobic steroid molecules.

GC-EI-HRMS and LC-ESI-HRMS analysis both offer high detection sensitivity. Taking AAS analysis in liquid samples for instance, GC-EI-HRMS has a detection limit of 0.25-1.25 ng/mL,[51] while LC-ESI-HRMS/MS can present a detection limit of 0.2-20 ng/mL.[52] Nevertheless, GC-MS analysis requires a hydrolysis step to deconjugate sulfate or glucuronide metabolites. This additional sample preparation causes steroid metabolite analysis by GC-MS more time-consuming than LC-MS, which can direct detect phase II metabolites without hydrolysis workup.

However, GC-MS can provide more valuable structural information, giving profound insights into elucidating steroidal structures. The phase I metabolites of steroids are predominantly lipophilic, facilitating their ionization by electron ionization (EI) more efficiently than by electrospray ionization (ESI).[49a] Consequently, newly synthesized steroids or compounds that have not yet been fully characterized are more suitable for initial analysis by GC-MS. Furthermore, the coupling of mass spectrometry with gas chromatography showed superior resolution of epimers.[48b] As a result, GC-EI-MS remains the gold standard for comprehensive steroid analysis.

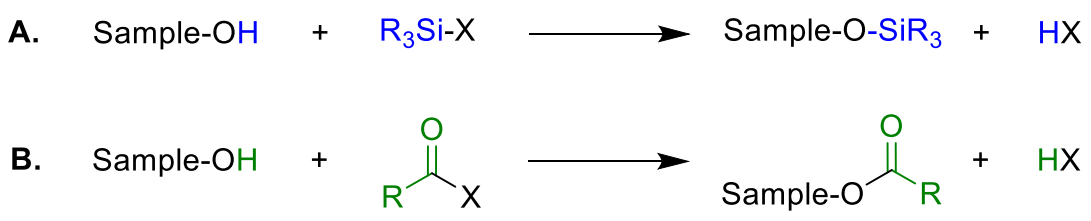

Scheme 7. (A) Silylation reaction for a hydroxy metabolite. (B) Acylation of a hydroxy metabolite.[50]

Derivatization is a critical step in enhancing the sensitivity and volatility of analytes for gas chromatography–mass spectrometry (GC-MS) analysis. It involves the chemical

modification of functional groups, such as hydroxyl, amine, or carboxyl moieties, into more volatile derivatives, typically esters or ethers (see **Scheme 7**). This transformation of functional groups improves GC-MS detection limits by increasing analyte volatility and thermal stability.[50] Some common derivatization reactions are silylation, acylation, and esterification. An additional benefit of derivatization is that it can enhance the stability of analytes by replacing labile functional groups with more stable derivatives.

However, a potential drawback of derivatization is that it can increase the number of compounds detected by GC-MS analysis. For instance, forming various trimethylsilyl (TMS) isomers during silylation reactions can complicate the interpretation of metabolic profiles and hinder accurate quantification in complex biological samples.

Steroid analysis with LC-MS

Analysis using LC has different advantages and disadvantages. The benefits of using LC-ESI MS are that the hydrophilic phase II steroid metabolites, such as glucuronides and sulfates, are readily soluble in polar solvents for LC analysis. These metabolites can be efficiently deprotonated and ionized by ESI-MS, facilitating their direct detection without hydrolysis workup.

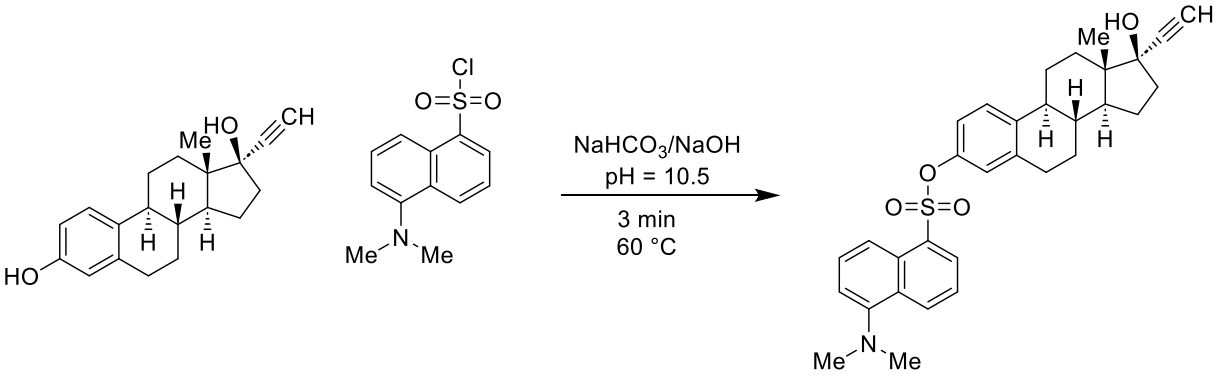

Ethinylestradiol (**57**) Dansyl chloride (**58**) 3-Dansyl-ethinylestradiol (**59**)

Scheme 8. Derivatization of ethinylestradiol by dansyl chloride.[53]

However, phase I metabolites, unconjugated and hydrophobic steroids, are less suitable to be ionized by ESI or atmospheric pressure chemical ionization (APCI) due to their low polarity. In such cases, derivatization is often necessary to improve ionization efficiency. A commonly employed derivatization reagent for LC-MS is dansyl chloride (**58**), which enhances both ionization and detection sensitivity (see **Scheme 8**).[53] However, the ability to separate diastereomers in GC can be superior than in

LC.[54] The diffusion speed in the gas phase is faster than in the liquid phase.[54] The GC columns are usually thinner and have more theoretical plates than LC-columns.[55] These factors contribute to the generally higher chromatographic resolution observed in GC-MS analyses.

Consequently, GC-MS remains the preferred method for comprehensive steroid profiling, particularly when high-resolution separation and structural elucidation are required.

Tandem MS: PRM and MRM

A mass spectrometry (MS) analyzer can operate in two primary acquisition modes: full scan mode and single ion monitoring (SIM). In full scan mode, the instrument detects a broad range of mass-to-charge (*m/z*) values, making it especially useful for identifying unknown compounds. In contrast, SIM mode monitors only specific *m/z* values, significantly increasing sensitivity and selectivity. As a result, SIM is commonly employed in targeted quantitative analysis, where precise measurement of known analytes is required.

Tandem MS

Tandem Mass Spectrometry (MS/MS) is a highly effective technique for structural elucidation of molecules, especially when combined with soft ionization techniques such as ESI. ESI delivers typically only molecular ions and only a few fragments, which deliver detailed information on the composition, when accurate ion mass analysis is performed. Tandem MS methods are developed for mass-selected ion activation and deliberately generation of structure-characteristic fragment ion. In a typical beam-type Tandem MS instrument, the first mass analyzer isolates a precursor ion with a defined mass-to-charge ratio (*m/z*). This ion is subsequently directed into a collision cell, which undergoes fragmentation via collision-induced dissociation (CID) or higher-energy collisional dissociation (HCD). The resulting product ions are then analyzed by a second mass analyzer. Only fragment ions that are sufficiently stable under the experimental conditions are detected and appear as signals in the resulting MS/MS spectrum[56], providing detailed structural information about the precursor molecule. The observed fragment ions provide critical information for the deduction of the positions of functional groups and for elucidating the overall structural composition of the molecule.

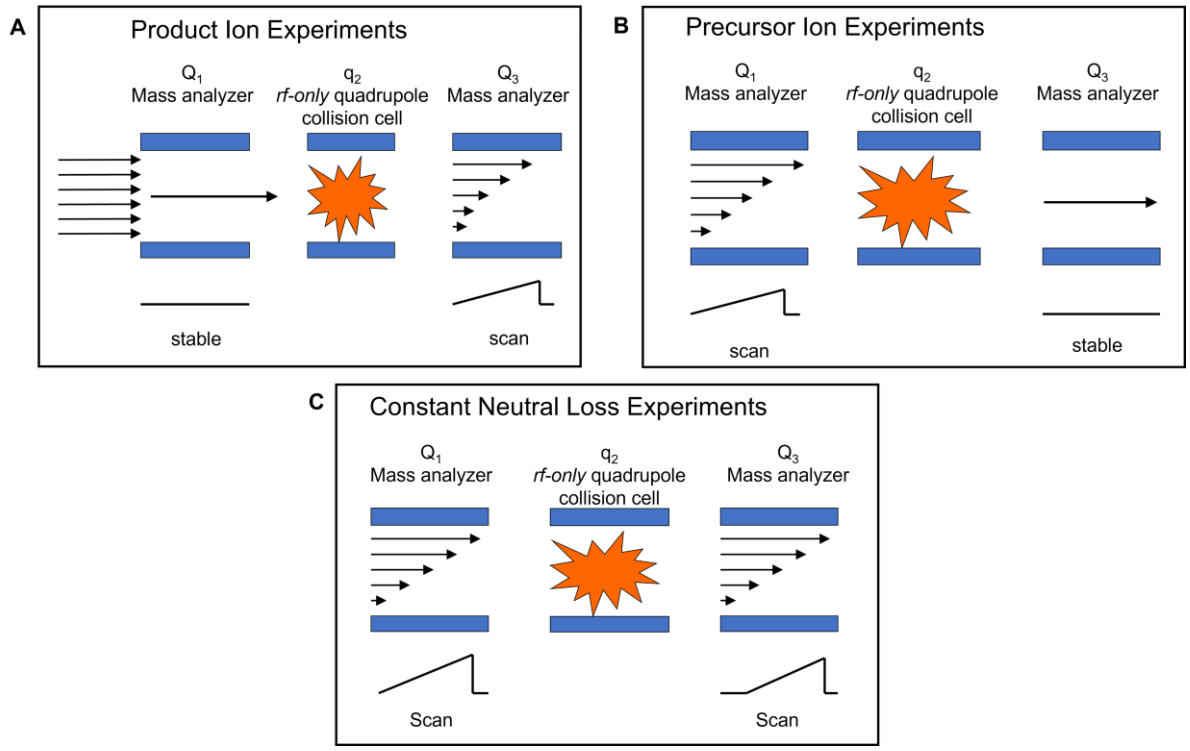

Figure 9. Scheme of a triple quadrupole mass spectrometer, showing the combination of quadrupole (Q_1), quadrupole (q_2) quadrupole (Q_3) from can be applied for different scan modes: product ion experiments (panel A), precursor ion experiments (panel B), and constant neutral Loss[49a, 57]

A widely employed instrument for tandem mass spectrometry is the triple quadrupole (QqQ) mass spectrometer. In this configuration, the first quadrupole (Q_1) serves as a mass filter, selectively transmitting precursor ions based on their mass-to-charge (*m/z*) ratio. These ions are then directed into the second quadrupole (q_2), which functions as a *rf-only* quadrupole collision cell where fragmentation is induced via collisions with an inert gas (e.g. He, Ar, N_2 etc.) and fragmentation via collision-induced dissociation (CID) is observed. The resulting product ions are subsequently analyzed by the third quadrupole (Q_3), which either scans or filters specific *m/z* values for detection **Figure 9**.[49a, 57]

For the product ion experiments (**Figure 9A**), a single precursor ion is selected in Q_1, fragmented in q_2, and all the resulting product ions are scanned in Q_3. This mode can help structure elucidation based on the fragmentation pattern.[49a, 57c] **Figure 9B** presents the precursor ion experiments, which can identify the relation between specific product ions and their precursor ions. A scan is performed in Q_1, and fragmentations occur in q_2. Only specific product ions are selected in Q_3. This technique helps investigate compounds that share common structure features, such as sulfate or glucuronide functional groups. In **Figure 9C**, constant neutral loss

experiments are illustrated. This mode detects compounds that lose the same neutral fragment in q_2. All precursor ions are separated in Q_1 and fragmented in q_2. Only product ions, which are generated by the same neutral loss, are detected by Q_3. For instance, only product ions formed by a loss of sulfuric acid from sulfate metabolites are selectively detected in this approach.

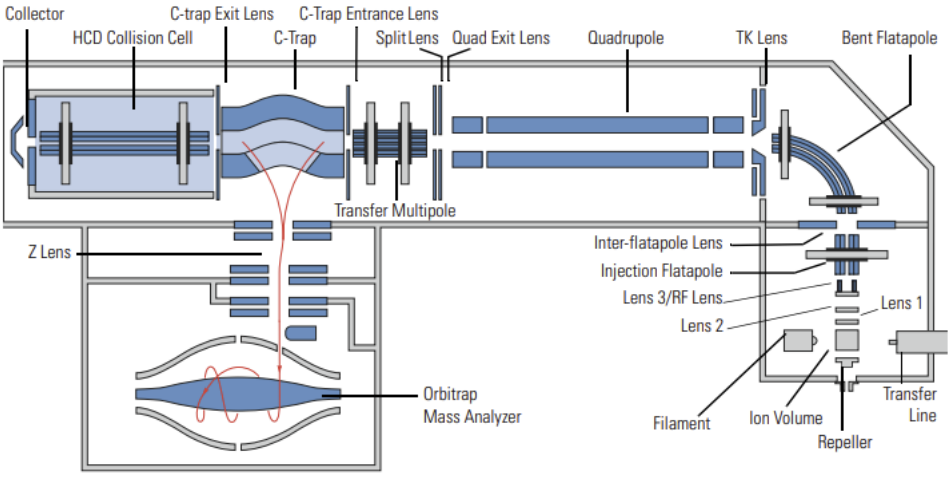

Figure 10.Q Exactive Orbitrap setup (Thermal Fisher) that can be connected with a GC at the transfer line.[58]

Due to the modest-to-low resolution capabilities of a triple quadrupole (QqQ) system, coupling it with a time-of-flight (TOF) or Orbitrap analyzer can significantly enhance mass accuracy and resolution. In **Figure 10**, the schematics of a *Q Exactive* Orbitrap are shown.[58b]

In the GC-MS orbitrap system, analytes are introduced via heated transfer lines into the ion source, where ionization typically occurs by electron impact (electron ionization, EI) using a filament which produces electrons with a kinetic energy of typically 70eV. All ions produced by EI-MS including open shell cationic molecular ions $[M]^{\bullet+}$ are directed into a bent flatapole, which can deflect neutral species and prevent their transmission into the quadrupole, therefore enhancing the signal-to-noise ratio.[58b]

The subsequent quadrupole functions as the first mass filter, exclusively transmitting the selected precursor ions within a defined *m/z* range. These ions subsequently pass through a transfer multipole, which acts as a pre-filter and guides them into the C-trap. The C-trap temporarily accumulates the selected ions before injecting them into the higher-energy collisional dissociation (HCD) cell compared to a conventional quadrupole ion trap.[49a] Within the HCD cell, ions undergo fragmentation through

collisions with an inert gas, commonly argon, under controlled energy conditions (kinetic energy range 0-100 eV).

The resulting fragment ions are then recollected in the C-trap and transferred to the Orbitrap mass analyzer, where they are subjected to high-resolution and high-accuracy *m/z* analysis. This system enables precise structural elucidation and quantification, particularly in complex biological or environmental samples.

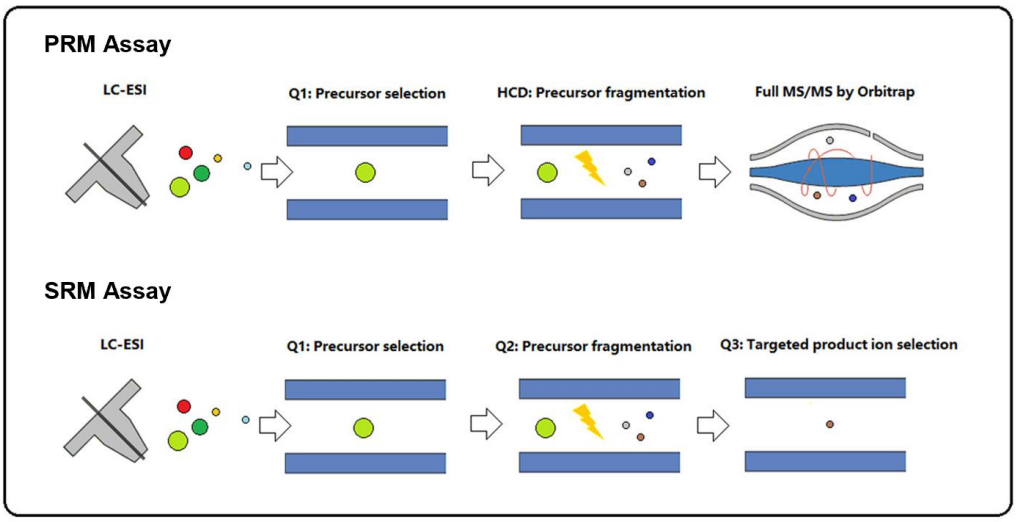

Figure 11. Representation of PRM (above) and SRM (below) methods by quadrupole-Orbitrap and triple quadrupole instruments, respectively by following and adapting a figure from *Zhou et al*.[59]

PRM (Parallel Reaction Monitoring)

Parallel reaction monitoring (PRM) is a targeted mass spectrometry (MS/MS) technique that combines high selectivity with high sensitivity, making it particularly suitable for trace-level quantification. In PRM, the first mass analyzer isolates a specific precursor ion, analogous to single ion monitoring (SIM), prior to fragmentation in the collision cell.[59] [57c] The second analyzer scans the fragmented ions. All the fragments from the precursor ions can be observed in the MS^2 spectra.

MRM (Multiple Reaction Monitoring)

MRM is another type of tandem MS analysis by monitoring a set of precursor-product pairs of single/ selected reaction monitoring (SRM). After selecting a precursor ion from the first analysis, the ions are fragmented.[59] [57c] Unlike the PRM method, a signal is only generated when precursor ions are fragmented to specific product ions after a defined neutral loss. A combined detection of stable isotope standards (with individual

mass-shifted molecular ions) and selected analyte ions makes the MRM method highly sensitive for screening and reliable for quantification (**Figure 11**) The sensitivity and selectivity (reduced chemical noise) of SRM & MRM is much higher than that of simple SIM, which recommends SRM / MRM for trace compound analysis.

2.3 Metabolite studies of xenobiotic steroid compounds

2.3.1 *In vitro* and *in vivo* metabolites studies

Different *in vitro* and *in vivo* models can be used before clinical trials to study human metabolites of xenobiotic substances. *In vitro* experiments have two advantages: They are simpler than *in vivo* animal experiments and have fewer ethical issues. The designs of the experiments and influence factors are more straightforward than those of *in vivo* models. Therefore, *in vitro* experiments are often conducted before any further animal research.

There are different methods for *in vitro* studies: application of microsomes from human tissues,[60] using S9 fraction from liver, or conducting experiments in an isolated liver containing perfusate flows.[61]

Metabolic reactions are primarily driven by the catalytic functions of hepatic enzymes, and these processes can be effectively simulated using cell-based systems or subcellular fractions.[62]

The benefit of cell culture is that all the metabolite pathways can be considered, compared to conducting subcellular experiments. Enzymes contained in mitochondria and nuclei in the cells can participate in metabolic reactions.[62]

Another type is applying subcellular fractions containing metabolism enzymes, such as S9 fraction, human liver microsomes, and cytosol. [62-63] S9 liver fraction is obtained from the liver homogenate supernatant, which has a mixture of cytosol and microsomes, under low-speed centrifugation.[64] Human liver microsomes (HLM) are derived from further high-speed ultracentrifugation of S9 fraction and resuspension of the pellet in the buffer.

Compared to HLM, sulfotransferases (SULTs) can be found in S9 fraction, which is not the case for HLM containing only uridine 5′-diphosphate glucuronosyltransferases

(UGT) and CYP, but the overall enzyme activity in HLM is higher than S9 fraction. CYPs and UGTs are enriched in HLM. In addition, there is no other enzyme competition in HLM, so quantitative metabolite analysis from the subcellular system might not show identical results from *in vivo* studies. The advantage of using the subcellular model is that they are simple to handle, but adding a cofactor for the reaction is necessary.

In vivo experiments have several advantages and potential complications that also need to be considered. For *in vivo* experiments, mice and rats are usually chosen as suitable candidates in the early stage before clinical trials. Their anatomical, physiological, and genetic properties are close to humans,[65] and their size and life span are small and short, which is more economically preferable than other big animals, like dogs, rabbits, or pigs. Rats are even more ideal than mice for doping research because their physiology is even more similar to human beings. In addition, rats have bigger body sizes, allowing for higher administration doses and more concentrated metabolites in urine samples.

In vivo experiments often give more reliable results than *in vitro* experiments because they present the full complexity of living organisms. Nevertheless, the enzymes in rats differ from those in humans.[66] Genetic factors and diets are also the reasons for different metabolisms in rats and humans. *In vivo* experiments may not give consistent results with clinical trials.

2.3.2 Chemical synthesis of steroid metabolites

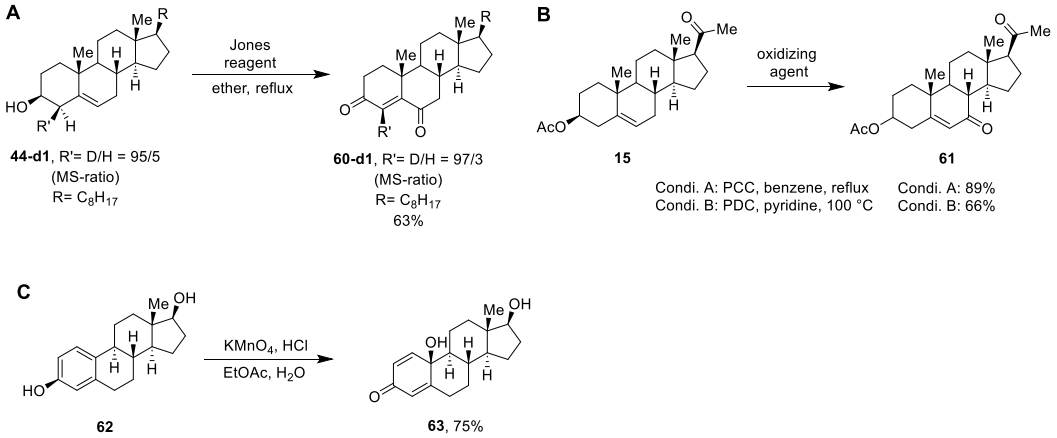

Scheme 9. (A) Steroid **44-d1** C6 oxidation reaction using Jones reagent (CrO_3, H_2SO_4) according to *Salvador* and *Hanson*.[67] (B) Synthesis of *α,β*-unsaturated C7 ketone **61** by PCC (pyridinium chlorochromate) and PDC (pyridinium dichromate).[68] (C) Oxidation of estradiol **62** by $KMnO_4$ under acidic conditions.[69]

Assigning the correct molecular structure metabolites using solely analytical methods can be challenging. MS analysis cannot fully confirm the structures of metabolites produced by small-scale bio-experiments. Therefore, a reliable approach is to synthesize specific reference compounds for comparison of analytical results to those retrieved from *in vivo* or *in vitro*.

The structure of metabolites can be affirmed by NMR and XRD analysis, for which the analytes are needed on a milligram scale. Hydroxylation is a common reaction for steroids during phase I metabolism.

Steroid ketones can be prepared at the allylic position by oxidation reagents: Jones reagents,[67] PCC (**Scheme 9A** and **B**).[68] Respective alcohols can then be generated by reduction with $NaBH_4$ or $LiAlH_4$ or double bond rearrangement with $KMnO_4$ (**Scheme 9C**).[70]

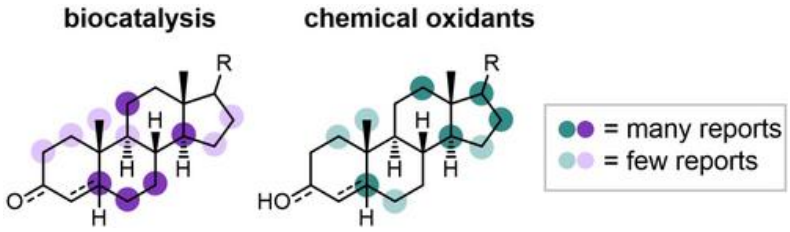

Figure 12. Common hydroxylation position by biocatalyst: CYP450 or chemical oxidants.[69b]

The steroid hydroxylation occurs at different locations depending on enzymatic or chemical preparation routes. According to literature reports, biocatalytic hydroxylation predominantly occurs in the B ring, whereas chemical oxidation concentrates on C and D rings.[69b] It gets apparent that the synthetic hydroxylation reactions show significant potential for optimization.

It turns out that one-step hydroxylation procedures are more challenging than two-step procedures via ketone intermediates followed by a reduction reaction, as the former requires activation of unreactive C-H bonds. Furthermore, the hydroxylated products are only slightly more stable than their precursors.[71]

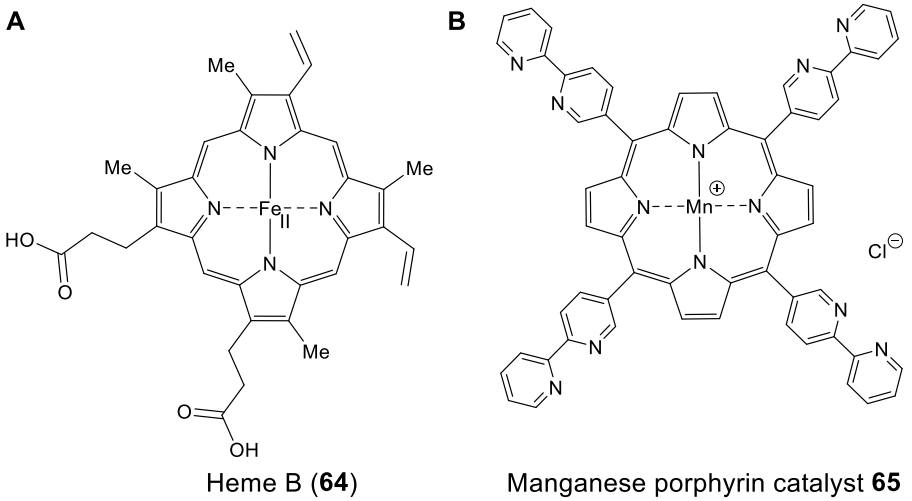

Figure 13. Structure of heme B (**64**) (left structure)[72] and the biomimetic Mn catalyst **65** (right structure) published by *Breslow et al.*[73]

Organic chemists often derive synthesis strategies from natural products and their biosynthetic mechanisms. In 2001, *Breslow et al.* employed a manganese porphyrin metal complex **65** to mimic CYP450 enzymes for the regioselective oxidation of steroids. By utilizing a Mn biomimetic catalyst **65** with various ligands, the selective hydroxylation of steroids was achieved (**Figure 13**).[73]

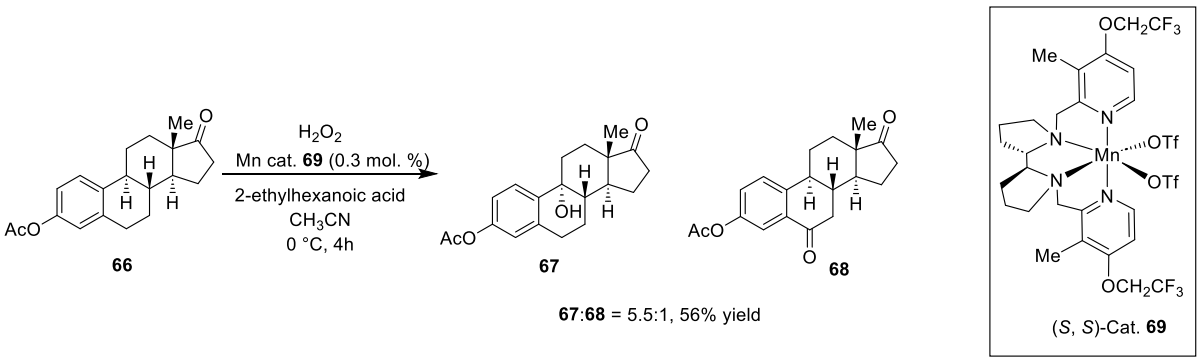

Scheme 10. Hydroxylation of estrone acetate (**66**) using chiral Mn catalyst **69** gives C9-hydroxy **67** and C6-ketone **68** products.[74]

Since 2007, non-heme catalysts have gained increasing attention for stereo-selective hydroxylation reactions.[75] Notably, the *Bryliakov* group reported a chiral Mn aminopyridine complex capable of catalyzing the stereoselective benzylic hydroxylation of estrone acetate (**66**) at the C9 position (**67**). In addition to the hydroxylated product, a ketone byproduct was also observed at the C6 position (**68**) under the same reaction conditions.[74, 76]

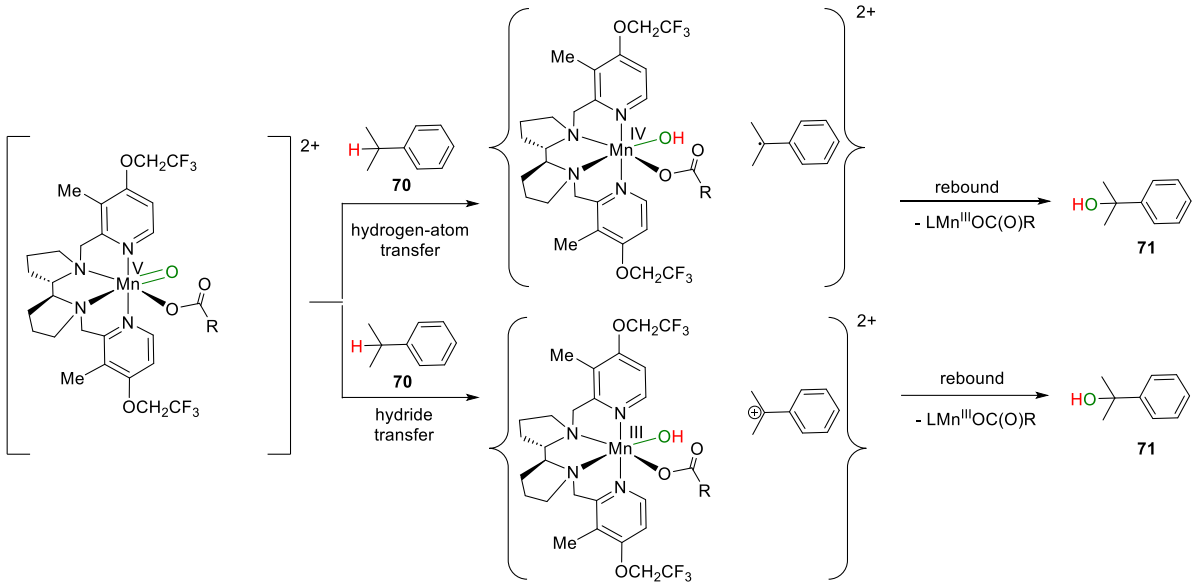

Scheme 11. A hydrogen atom transfer takes place at the benzylic position, and the Mn (V) oxo complex is reduced to the Mn (IV) hydroxide complex (top scheme). A hydride shift from a benzyl compound to the Mn (V) oxo complex can reduce the catalyst to the Mn (III) complex (bottom scheme). A rebound of a hydroxy group gives the hydroxybenzyl product.[74, 77]

The Mn (V)-oxo complex from *Bryliakov et al.* can hydroxylate benzylic carbons via two mechanistic pathways: hydrogen atom abstraction (**Scheme 11**, top) or hydride abstraction (**Scheme 11**, bottom), followed by an oxygen rebound step leading to alcohol formation. Since resonance effects stabilize a benzylic radical, the C-H bond dissociation energy is reduced at the benzylic position compared to a typical C-H bond in an alkane.

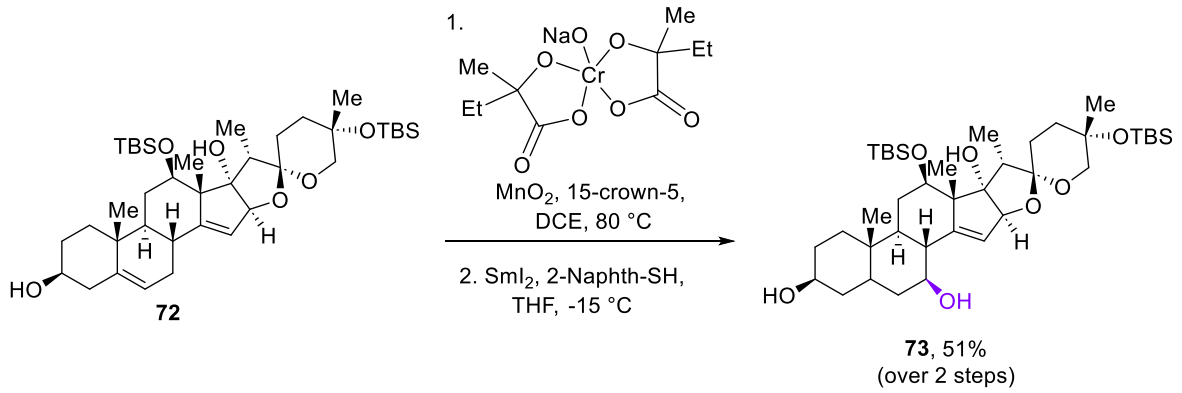

Scheme 12. Steroid **72** hydroxylation by oxochromate (Cr (V)) and MnO_2. SmI_2 was used for reduction of the enone.[78]

Besides manganese catalysts, chromium catalysts have also been proven effective for regioselective hydroxylation. *Reisman et al.* reported the first synthesis of the cytotoxic alkaloid ritterazine B[78], which involved the initial step of a C-H oxidation at the C7

position of compound **72** using Cr (V) in combination with MnO_2 as oxidants to generate an enone intermediate.[79] To enhance the solubility of the oxidizing agents in organic solvents, 15-crown-5 ether was employed. In the subsequent step, samarium (II) iodide (SmI_2) was used for selective reduction of the enone to the corresponding alcohol. The addition of 2-naphthalenethiol helped stabilize reactive intermediates at low temperatures, enabling selective reduction at C7 to afford compound **73** without affecting the C14-C15 double bond (see **Scheme 12**).

The advantage of chemical hydroxylation of steroids is the scalability which is not feasible for biosynthetic methods. However, finding the right oxidation agent and designing a catalyst for stereospecific oxidation is also challenging. The hydroxylation of steroids by chemical synthesis is still demanding and has room for development.

2.4. Synthesis and development of aromatic steroids in ring A

Steroid S42 (**1**) (structure shown in **Scheme 1**) is a synthetically derived steroidal selective androgen receptor modulator (SARM), first reported by *Uyanik* in 2006.[7] It contains an aromatic ring in the ring A structure and a ketone functional group at the C20 position. The development of this novel steroid can be traced back to research in the 1950s.

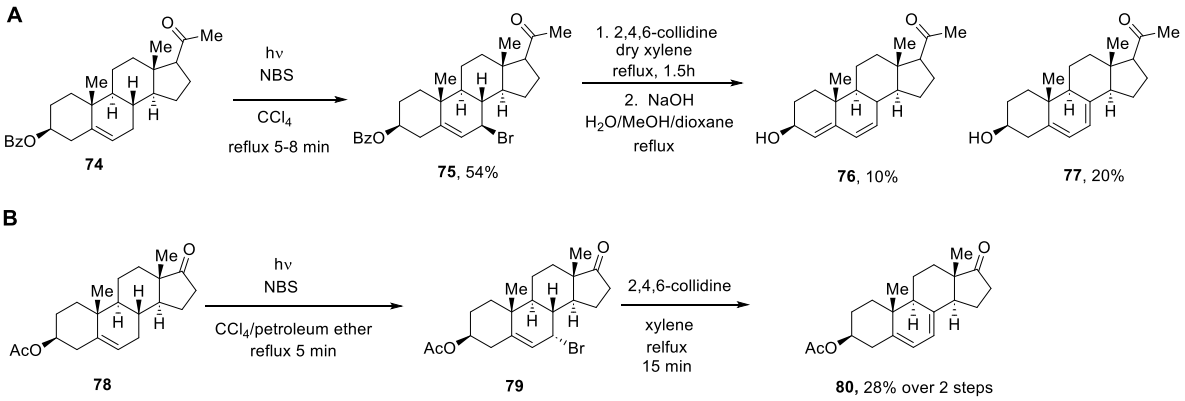

Scheme 13. (A) Synthesis of Δ5,7 and Δ4,6 steroids by bromination and dehydrobromination according to *Djerassi et al.*[80] (B) Synthesis of Δ5,7-steroids by *Wolf-Ziegler* bromination and dehydrobromination by 2,4,6-collidine according to *Antonucci et al.*[81]

In 1951, *Djerassi et al*[80] and *Antonucci et al.*[81] both published similar strategies to synthesize $\Delta^{5,7}$-steroids from Δ^{5}-steroids. *Djerassi et al* published that by application of *Wolf-Ziegler* bromination with NBS (*N*-bromosucciimide) to react with pregnenolone benzoate (**74**), a 7-bromo derivative **75** can be given (**Scheme 13A**). After

dehydrobromination with a base, 2,4,6-collidine, and saponification, $\Delta^{5,7}$ steroid **77** and $\Delta^{4,6}$ steroid **76** were discovered.

Antonucci et al. used the same strategy to treat dehydroiso-androsterone acetate (**78**) with NBS under light. After reflux in xylene with a base, 2,4,6-collidine, $\Delta^{5,7}$ androstadiene-3*β*-ol-17-one acetate (**80**) was found (**Scheme 13B**).[81]

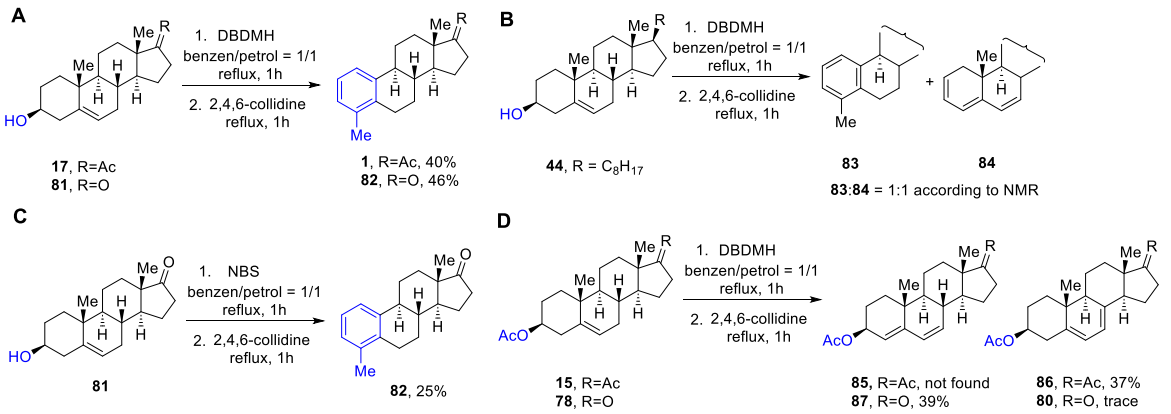

Scheme 14. (A) Dehydroiso-androsterone (**81**) and pregnenolone (**17**) were generated into aromatic steroids by brominating agent DBDMH and dehydrobrominating by 2,4, 6- collidine. (B) An aromatic product **83** and $\Delta^{2,4,6}$ triene **84** were produced from cholesterol **44** by bromination and dehydrobromination. (C) A lower yield of aromatic products was obtained from dehydroiso-androsterone (**81**) when NBS replaced DBDMH. (D) Dehydroiso-androsterone acetate (**78**) and pregnenolone acetate (**15**) did not produce aromatic products but $\Delta^{4,6}$ or $\Delta^{5,7}$ steroids after bromination and dehydrobromination. [82]

Nevertheless, when *Hanson et al.* used the same synthesis strategy to treat pregnenolone (**17**) and dehydroiso-androsterone (**81**) with another brominating agent, 1,3-dibromo-5,5-dimethylhydantoin (DBDMH), followed by reflux with 2,4,6-collidine, they discovered aromatic products **1** and **82** respectively, instead of $\Delta^{5,7}$-steroid (**Scheme 14A**).[82a, 83] Using cholesterol **44** as a starting material also afforded an aromatic product **83** and a $\Delta^{2,4,6}$ triene byproduct **84**. (**Scheme 14B**) *Hanson et al.* replaced DBDMH with NBS as a bromination agent, followed by the treatment of collidine to dehydroiso-androsterone (**81**), and showed a lower yield of aromatic product **82** (25%) (**Scheme 14C**).[82b] A lower yield from using NBS means DBDMH is a better alternative to NBS.[82]

To compare *Djerassi's* findings, *Hanson et al.* applied the same treatment to pregnenolone acetate (**15**), $\Delta^{5,7}$ -steroid **86** was successfully obtained (**Scheme 14D**), in agreement with the earlier findings of *Djerassi* in **Scheme 13A**.[83] However, $\Delta^{4,6}$

steroid **85** was not discovered. When dehydroiso-androsterone acetate (compound **78**) was used as a starting material, the major product identified was a $\Delta^{4,6}$ steroid (compound **87**) (**Scheme 14D**). Only trace amounts of the $\Delta^{5,7}$ steroid **80** were detected, which was not totally in agreement with the results reported by *Antonucci*. (**Scheme 13B**)

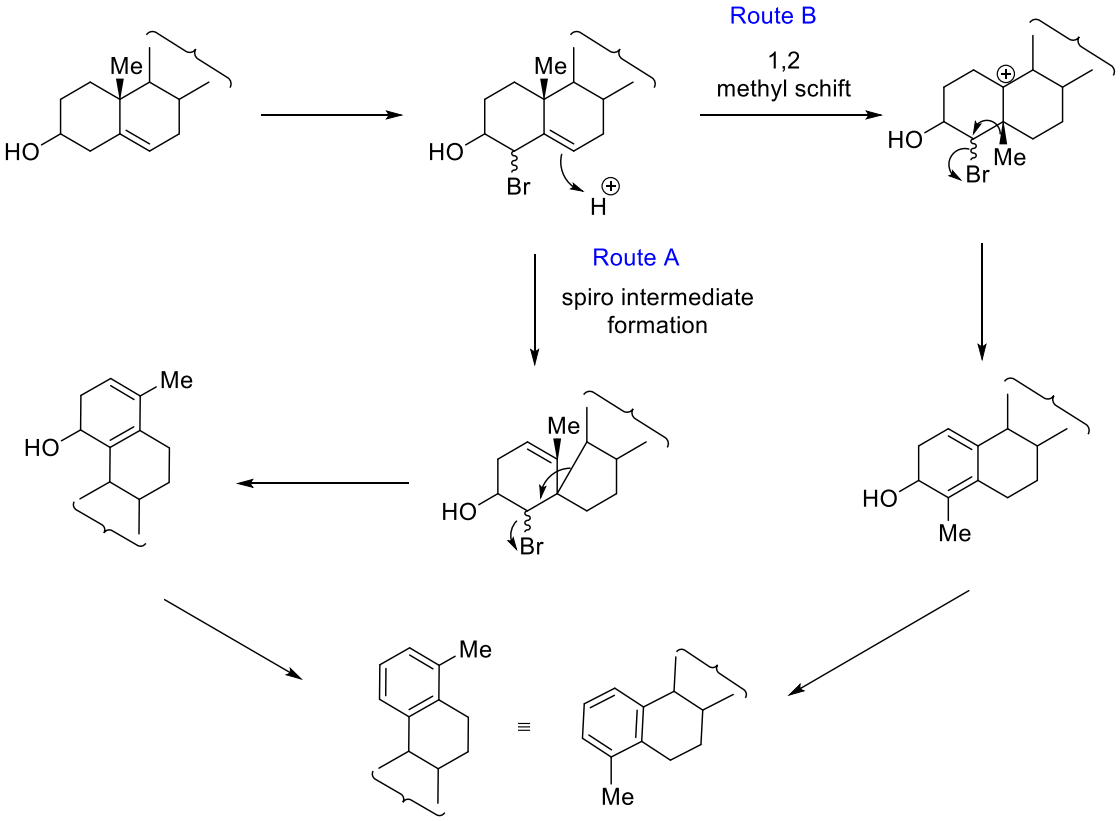

Scheme 15. Proposed aromatization reaction based on the formation of a spiro intermediate (Route A) or a 1,2 methyl shift (Route B).[84]

Hanson et al. proposed that the critical step in the aromatization mechanism of dehydroiso-androsterone **81** or pregnenolone **17** can be the formation of a spiro intermediate (**Scheme 15**, Route A) or the generation of a 1,2 methyl shift from C19 to C4 (**Scheme 15**, Route B).[84b]

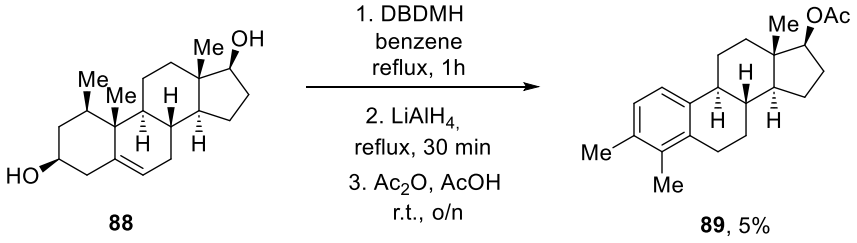

Scheme 16. Generation of 3,4 dimethyl $\Delta^{1,3,5}$ triene **89** by aromatization, reduction, and acetylation reactions of 3β,17β-dihydroxy-1β-methyandrost-5-ene (**88**).[84a]

To investigate whether a spiro intermediate or 1,2 methyl shift from C19 to C4 occurred in the reaction, 3*β*,17*β*-dihydroxy-1*β*-methyandrost-5-ene (**88**) was used for aromatization (**Scheme 16**). If a spiro intermediate were produced during the reaction, the product would be a 3,4 dimethyl $\Delta^{1,3,5}$ triene. If a 1,2 methyl shift took place from C19 to C5, the generated product would be a 1,4 dimethyl $\Delta^{1,3,5}$ triene.[84a]

The generated aromatic product was further reduced and acetylated to compare with the NMR data of the literature known as 3,4 dimethyl $\Delta^{1,3,5}$ triene acetate and 1,4 dimethyl $\Delta^{1,3,5}$ triene acetate. It was concluded that the product was 3,4 dimethyl $\Delta^{1,3,5}$ triene **89** (**Scheme 16**). Therefore, *Hanson et al.* proposed that a spiro intermediate was generated by C9-C10 bond cleavage to give the aromatic product.

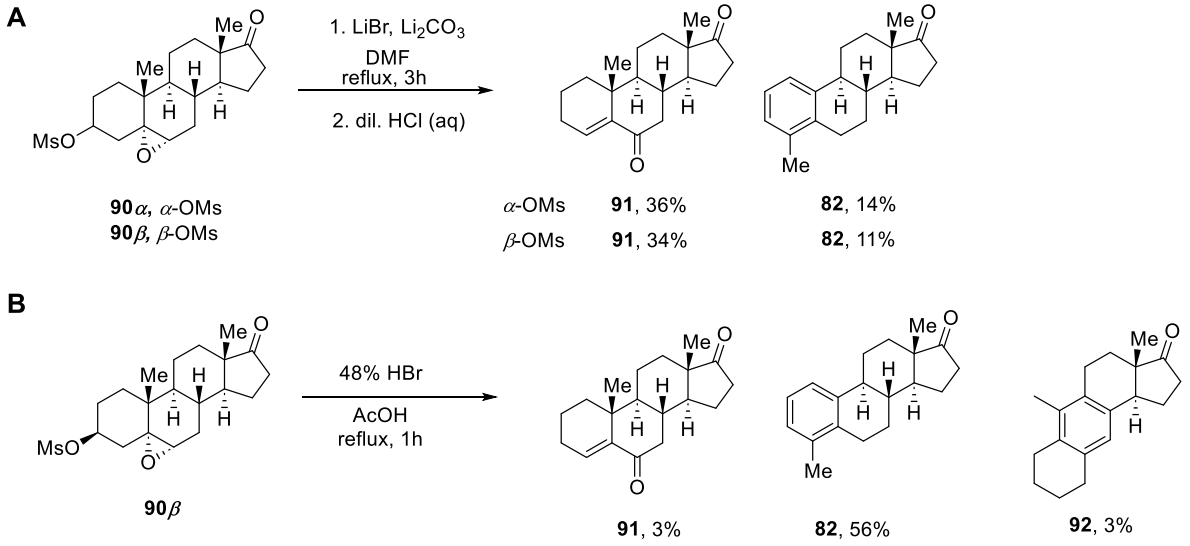

Scheme 17. Aromatization reactions by using (A) LiBr with Li_2CO_3 or (B) HBr in acetic acid.[85]

In 1972, *Hanson et al.* reported additional strategies for synthesizing aromatic steroids. Treatment of epoxide derivatives (compounds **90*α*** and **90*β***) with lithium bromide (LiBr) and lithium carbonate (Li_2CO_3), or with hydrobromic acid in glacial acetic acid, resulted in aromatization within ring A (**Scheme 17**). Notably, the reaction of the methane-sulfonate derivative of 5*α*,6*α*-epoxy-3*β*-hydroxyandrostan-17-one (**90*β***) with 48% hydrobromic acid in glacial acetic acid afforded the aromatic product **82** up to 56% (**Scheme 17B**). The authors proposed that the reaction mechanism was independent of the stereochemistry at C3, as both 3*α*- and 3*β*- methane sulfonate derivatives **90*α*** and **90*β*** yielded comparable results.[85]

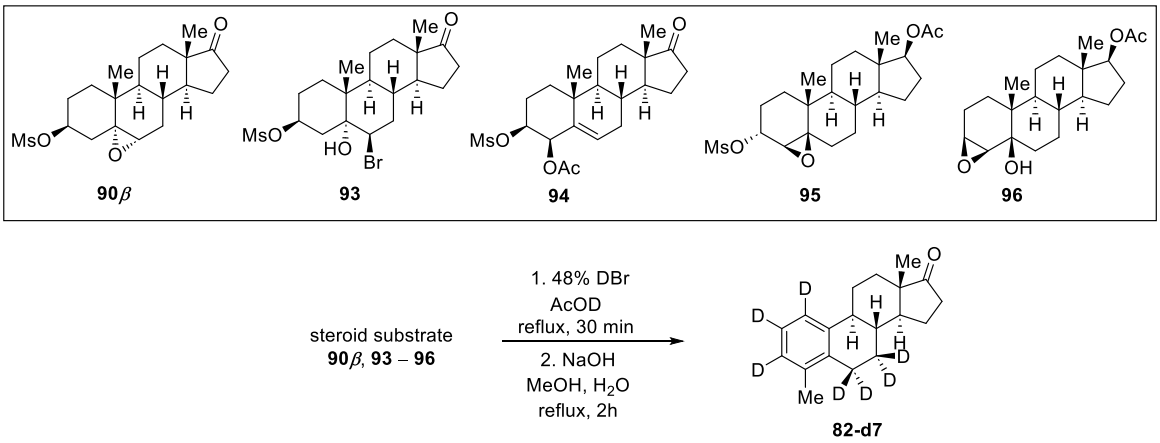

Scheme 18. Synthesis of deuterated 4-methyloestratriene with DBr and AcOD from different steroidal substrates.[86]

Hanson et al. investigated the aromatization mechanism of 5*α*,6*α*-epoxy-3*β*-mesyloxy-androstan-17-one (compound **90*β***). To elucidate the pathway, they modified the structure of dehydroiso-androsterone by introducing various functional groups to bromide **93**, acetate **94**, epoxide **95** and **96**, and employed deuterated reagents to trace hydrogen migration (see **Scheme 18**).[86]

Table 1. Deuterium ratio of different substrates. The deuterium ratio of ^{2}H-1 to ^{2}H-6 was based on 1-^{1}H ratio from ^{1}H NMR by calibration ^{1}H-18 as 3 protons. Since the proton signals of ^{1}H-7*α* and ^{1}H-7*β* overlapped with other proton signals. The deuterium ratio was calculated by ^{2}H NMR using ^{2}H-6*β* as an internal standard.[86]

Substrate	^{2}H-1	^{2}H-2	^{2}H-3	^{2}H-6*α*-	^{2}H-6*β*	^{2}H-7*α*	^{2}H-7*β*
90*β*	0.8	0.7	0.8	0.2	0.8	0.5	0.5
93	0.9	0.7	0.9	0.2	0.75	0.6	0.6
94	0.9	0.9	0.8	0.2	0.75	0.7	0.6
95	0.9	0.8	0.9	0.3	0.8	0.8	0.7
96	0.9	0.8	0.8	0.3	0.7	0.6	0.5

Deuterated hydrobromic acid and acetic acid were used to synthesize deuterium-labeled 4-methyloestratrienes, which were subsequently analyzed using ^{13}C-^{1}H (2D) NMR and ^{2}H (1D) NMR spectroscopy. The ^{2}H NMR spectra revealed deuterium incorporation at positions C1-C3, C6, C7, and C16. To resolve overlapping signals of ^{2}H at C16 and C7, the product was treated with methanolic sodium hydroxide, which selectively exchanged the deuterium at C16 back to hydrogen.

Quantitative analysis of the ^{1}H NMR spectra indicated a deuterium incorporation of approximately 70-80% at C1 to C3, and around 50% at both C7*α* and C7*β* (**Table 1**). Interestingly, deuterium incorporation at C6 was stereoselective, with approximately

80%-70% at the *β* position and only 20%-30% at the *α*-position. The high deuterium enrichment at C1 to C3 suggested the involvement of a phenyl cation intermediate in the reaction mechanism. The incorporation at C6 and C7, particularly at C6*α*, further supported the mechanistic hypothesis of the aromatization process.

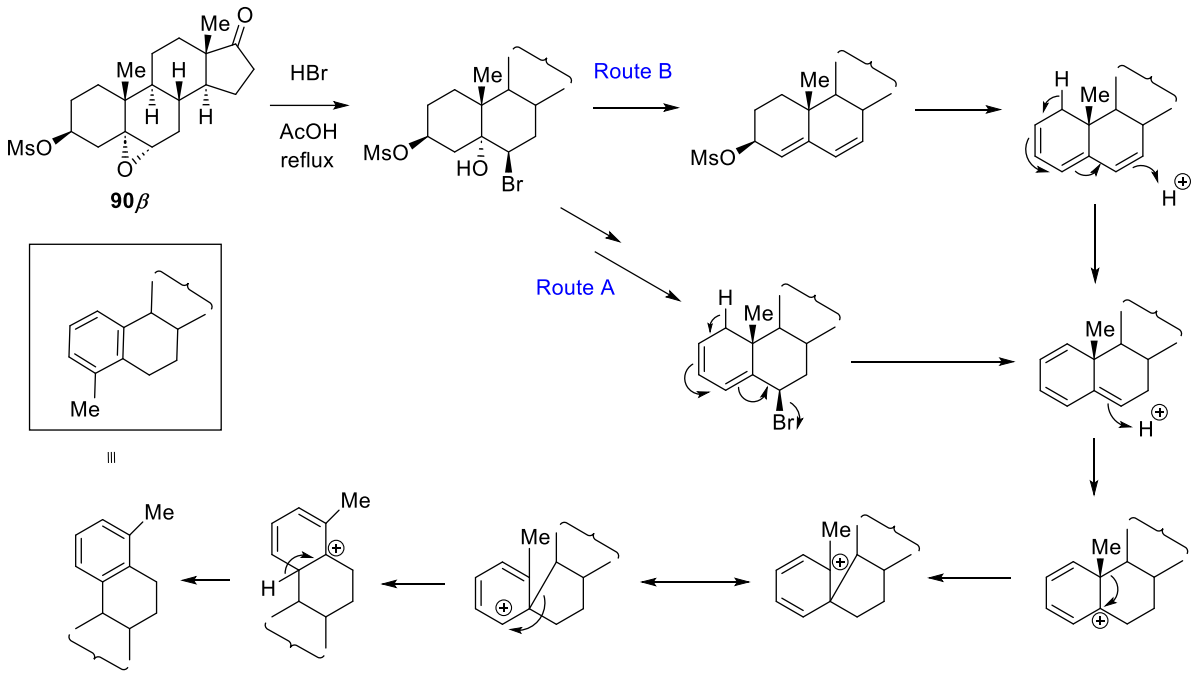

Scheme 19. Aromatization mechanism from the triene intermediate and a carbon cation.[87] [86]

Hanson et al. proposed that the aromatization mechanism converting 5*α*,6*α*-epoxy-3*β*-mesyloxyandrostan-17-one (compound **90*β***) to 4-methyloestratrienes (compound **82**) may resemble the *Westphalen–Lettré* rearrangement (**Scheme 19**).[88] The reaction condition for aromatization, hydrobromic acid in acetic acid (HBr, acetic acid) are notably similar to those used in the *Westphalen–Lettré* rearrangement, which typically involves sulfuric acid and acetic anhydride (H_2SO_4, Ac_2O) [89] In the proposed mechanism, the epoxide ring is opened via nucleophilic attack by a bromide anion, followed by elimination reactions that generate double bonds at the C2-C3 and C4-C5 positions (route A). The bromide at the C6 position can be eliminated through dehydro-bromination, yielding a $\Delta^{1,3,5}$ steroid.

The methane-sulfonyl group, being a good leaving group, facilitates the formation of a $\Delta^{2,4,6}$ triene (route B). Alternatively, elimination of the methane-sulfonic group may occur first, followed by hydrobromination, ultimately producing a $\Delta^{1,3,5}$ triene. Under acidic conditions, the resulting conjugated triene system is stabilized by resonance effects.[90] Furthermore, cleavage of the C9-C10 bond may lead to the formation of a

spiro carbocation intermediate with two conjugated double bonds. Resonance delocalization of the positive charge to C4 enables bond formation with C9, resulting in a ring flip. Final abstraction of a proton at C5 completes the formation of the aromatic A-ring.

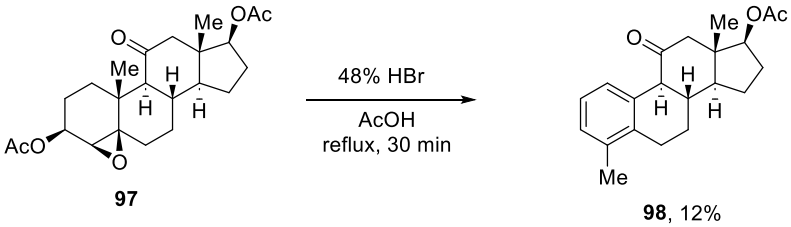

Scheme 20. The carbonyl groups at the C11 position hinder the formation of the spiro intermediate.[91]

Hanson et al observed that a carbonyl group at the C11 position in the substrate **97** led to a low yield of 17*β* acetoxy-4-methylestratrien-11-one (compound **98**).[91] It was proposed that the carbonyl group at the C11 position may interfere with the cleavage of the C9-C10 bond, thereby hindering the formation of the spiro intermediate, which was necessary for aromatization.

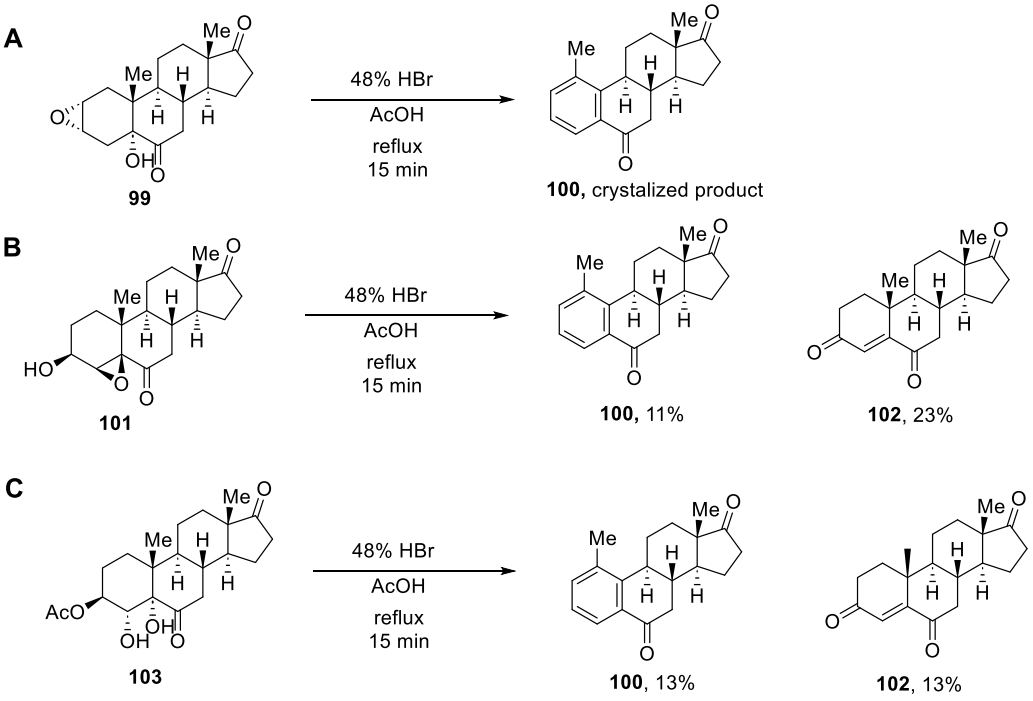

Scheme 21. Aromatization reactions were discovered using C6-carbonyl steroids as substrates and 1-methylestratrien-6-one instead of 4-methylestratrien-6-one.[91-92]

Hanson et al. also emphasized the importance of a positive charge at the C5 position for forming the spirocyclic intermediate. The presence of a functional group at C6 was

found to influence the stability of the C5 carbocation during the reaction. When steroidal substrates with a carbonyl group at the C6 position (compound **99**, **101** ,**103**) were treated with hydrogen bromide in glacial acetic acid (**Scheme 21**), 1-methylestratrien-6-one (**100**) was produced. The formation of a methyl group at C1 indicates a methyl migration from C19 to C1, without the involvement of a spirocyclic intermediate. This outcome suggests that the C5 carbocation is not sufficiently stabilized by the C6 carbonyl group, thereby preventing the formation of the spiro intermediate.

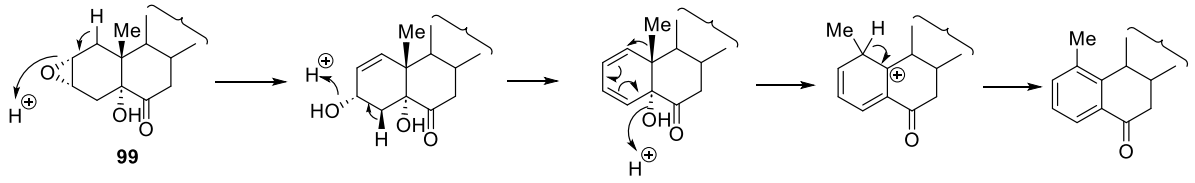

Scheme 22. Proposed mechanism of 1,2 methyl shift from C19 to C1 under acidic conditions with HBr.[92b]

The mechanism of C19 to C1 methyl migration can be explained as follows: After the epoxide ring of compound **99** was opened under acidic conditions, an elimination reaction gave $\Delta^{1,3}$ diene. A 1,2 methyl shift from C19 to C1 will produce $\Delta^{2,4}$ diene with a positive charge at C10. A proton at C1 was abstracted to give the final 1-methyl aromatic product (**Scheme 22**).

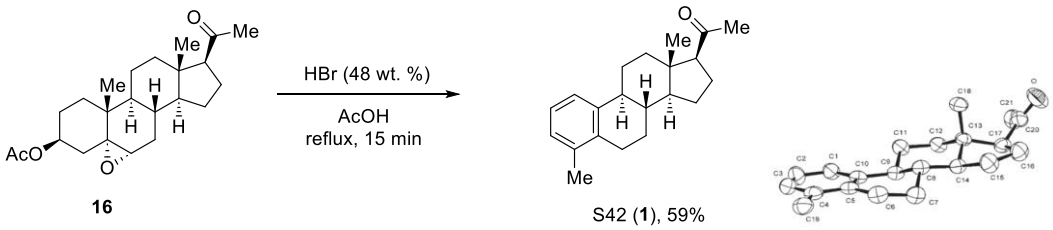

Scheme 23. Synthesis of S42 (**1**) from 3*β* acetoxy-5*α*,6*α*-epoxypregnen-20-one (**16**) with HBr in acetic acid. The structure was proved by XRD analysis.[7]

In 2006, *Hanson et al.* continued publishing ring A aromatic steroids using pregnane derivatives as precursors. The aromatic ring was also generated by bromination and hydrobromination from pregnane derivatives. One of the highlighted products, S42 (**1**), was synthesized from 3*β* acetoxy-5*α*,6*α*-epoxypregnen-20-one (**16**), and its structure was confirmed by X-ray diffraction (XRD) analysis (**Scheme 23**).[7] Notably, the yield was significantly improved when the starting material contained an epoxide moiety at the C5 and C6 positions.

S42 (**1**) was later mentioned and referenced in a publication by *Muta et al.* as a potential selective androgen receptor modulator (SARM).[9] It was shown to increase muscle mass in orchiectomized rats, demonstrating anabolic activity. S42 (**1**) was found to activate mTORC1 (mechanistic target of rapamycin complex 1), leading to enhanced phosphorylation of p70S6K (70 kDa ribosomal protein S6 kinase), a key regulator of protein synthesis in skeletal muscle. Additionally, S42 (**1**) exhibited anti-catabolic effects by inhibition of atrogin 1 (an F-box protein or Ub-protein ligase)[93] and MuRF1 (Muscle RING-finger protein-1), thereby reducing muscle degradation in cultured C2X12 myotubes.

Importantly, S42 (**1**) does not exhibit the common side effects of stimulating prostate growth, which are frequently associated with anabolic steroids such as testosterone (**46**).[9] This property suggests its potential utility in treating prostate cancer and muscle-wasting diseases.[8a, 10, 24]

In addition, S42 (**1**) may be potentially applied against breast cancer.[7] It has been shown that an aromatic ring ligand structure is critical for binding to estrogen receptors, which is an important target for suppressing cancer cell growth.[9, 94] The aromatic ring can mimic the natural ligand, estradiol, enhancing receptor binding through hydrophobicity interaction andπ-π stacking.[94] Synthetic aromatic steroids may bind to estrogen receptors but do not exhibit estrogenic activity.

Based on current medicinal investigations, S42 (**1**) may provide new opportunities for future therapeutic applications in muscle-related diseases and breast cancer. The development of S42 (**1**) highlights the significance of chemical synthesis of steroids for drug development.

3. Scientific problems

Selective androgen receptor modulators (SARMs) are listed as prohibited agents by the *World Anti-Doping Agency* (WADA).[20h] The synthesis of the novel C20-keto steroid S42 (**1**) (see **Scheme 1**) was published in 2006, and due to its anabolic properties, it can potentially be used as a doping agent in illicit sports activity.[11] To date, the metabolites of S42 (**1**) remain unidentified, and no validated analytical methods have been established for its detection in biological fluids.

The project's challenge begins with the synthesis of S42 (**1**) and the production of its deuterium-labeled isotopologues as reference compounds. The yield of the aromatization reaction is reported to be low, indicating that the current synthetic route for S42 (**1**) requires optimization. In addition, a synthetic strategy for site-specific deuterium labeling of S42 (**1**) in rings A and B should be developed to generate a potential quantitative internal standard for future analytical applications.

Subsequently, S42 (**1**) and its relevant derivatives are investigated by GC-EI-HRMS to gain fundamental understanding of their EI-MS behavior. Particularly, the electron ionization (EI) fragmentation mechanisms of S42 (**1**), of its silyl ether derivatives, and of the corresponding stable isotope-labelled reference compounds are investigated in great detail. This analytical data set is the foundation for reliable and predictable data interpretation of *in vitro* S42 (**1**) metabolism studies.

In vitro subcellular phase I and phase II metabolism experiments should be conducted and analyzed using GC-EI-HRMS^2 and LC-ESI-HRMS^2, respectively. Method development and optimization are needed to identify the metabolites and to locate oxidation positions. Furthermore, proposed metabolite structures should be synthesized and used as standard and reference compounds for confirmation of structure assignments and identification of *in vitro* metabolites of S42 (**1**).

To gain a comprehensive understanding of S42 (**1**) metabolism, not only *in vitro* but also *in vivo* experiments should be conducted. The analysis of urine samples from rats administered with S42 is expected to reveal details of a metabolism profile of realistic complexity compared to the simplified situation of *in vitro* studies.

4. Results and discussion

4.1 S42 derivatives synthesis for EI-MS fragments elucidation

4.1.1 Synthesis of S42 (**1**) and modification/ optimization of the procedures

S42 (**1**) was synthesized according to a procedure reported earlier by *Uyanik* and *Hanson et al*.[7, 86]

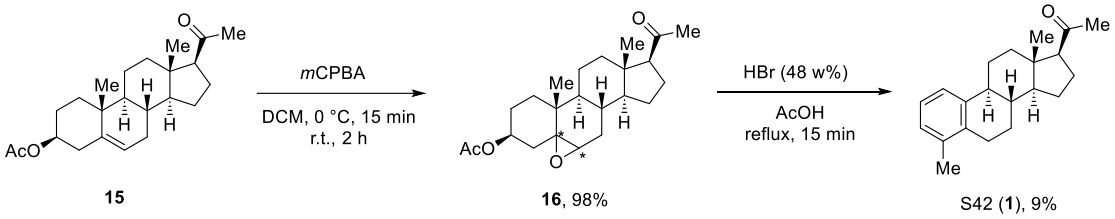

Scheme 24. S42 (**1**) synthesis starting from pregnenolone 3-acetate by epoxidation and aromatization by rearrangement as reported by *Uyanik* and *Hanson et al*.[7]

S42 (**1**) was synthesized in 2 steps from pregnenolone acetate (**15**) as a starting material (see **Scheme 24**). Pregnenolone acetate (**15**) was epoxidized by meta-chloroperoxybenzoic acid (*m*CPBA), giving a mixture of stereo isomers **16**. The following aromatization reaction was conducted in acetic acid with hydrobromic acid under reflux conditions. White precipitation can be observed in the beginning, which may be a bromination product. However, this byproduct was not further investigated. The solution quickly turned dark brown when the reflux started.

It is known that different steroid intermediates with a conjugated system were produced in the aromatization step under these conditions.[87],[86] The aromatization reaction involves deprotection of the acetyl functional group, multiple elimination steps and the generation of the spiro intermediate (mechanism see e.g. **Scheme 19**). At the same time, acetylation at C21 position may also occur. It was hard to control the aromatization reaction. Either the reaction was not complete or oxidized to a byproduct, containing a C17 acetoxy instead of an acyl group in S42 (**1**).[7]

Separation of the conjugate byproducts and S42 (**1**) is also complicated, as the byproducts have similar polarities to S42 (**1**), so their retention time is very close to each other in the GC chromatogram. Both column chromatography or normal phase HPLC could not separate the byproduct and product. The product could be isolated by multiple crystallization steps, but the purification steps could lead to low product yield.

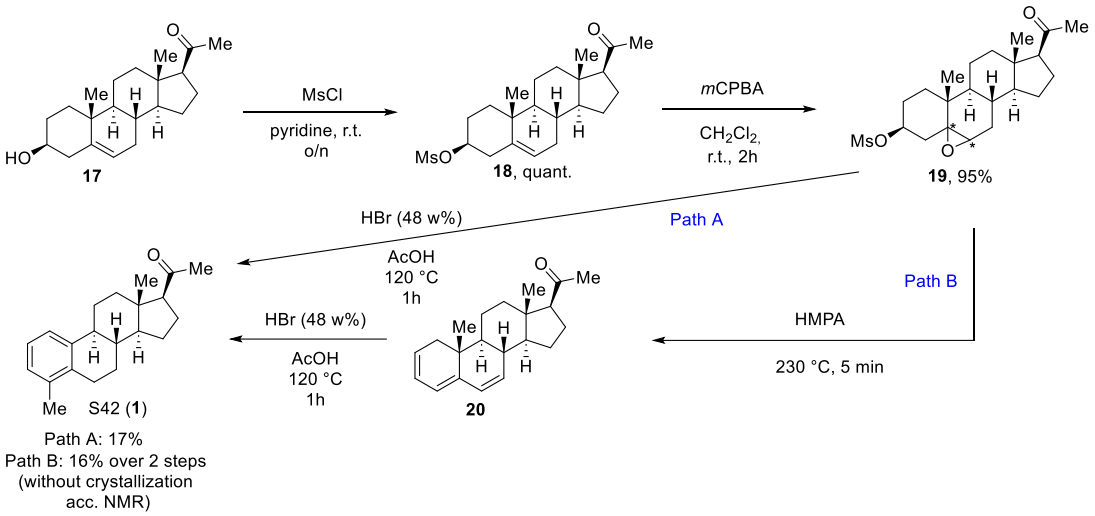

Scheme 25. Modified synthesis route to S42 (**1**) following procedures from *Hanson* (path A) [87] and *Watt* (path B)[95] respectively.

Another synthesis strategy was attempted using pregnenolone methane sulfonate (**17**) as a starting material for epoxidation and aromatization, which was presented by *Hanson et al* and *Watt et al.*[87, 95]

Pregnenolone (**17**) methane sulfonylation gave quantitative yield of compound **18** by application of methane sulfonyl chloride with pyridine as a base, which also acted as solvent in this protocol. The following synthesis route, namely epoxidation and aromatization (path A) were identical to the previously discussed route starting from pregnenolone acetate. The yield of the aromatization could be increased from 9% following the original procedure published by *Uyanik* in 2006,[7] to 17 % by exchanging the acetate at C3 with methane sulfonate. Methane sulfonate is a better leaving group than acetate. Therefore, the elimination rate increased to give a better yield.

Another modification is to perform the aromatization in two steps. The epoxide and methane sulfonyl functional groups was eliminated to $\Delta^{2,4,6}$ triene **20** in

hexamethylphosphoramide (HMPA) at 230 °C for 5 minutes.[95] Rearrangement reaction, producing $\Delta^{1,3,5}$ triene **20**, followed by the aromatization reaction could give S42 (**1**) crude with less byproducts under acidic condition with HBr in acetic acid. There were less byproducts produced in the 2-steps aromatization reaction, which simplified the purification steps. Nevertheless, HMPA is carcinogen, therefore the original one pot aromatization procedure was conducted.

4.1.2 Synthesis of hydrindane derivative **13**

The EI-MS fragmentation behavior of S42 (**1**) involves a prominent H_2O-loss reaction, likely originating from the C20 ketone moiety. A simplified C and D ring analog **13** of S42 was synthesized to check that reaction also in silico via DFT computations (See **Scheme 35**, page 54).

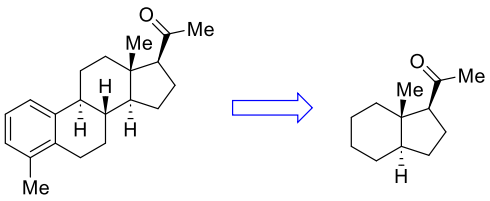

S42 (**1**) **13**

Scheme 26. The structure of S42 (**1**) was simplified to 8-methyl-1-acetyl-hydrindane **13** containing only ring C and D with the C20 ketone sidechain for independent investigation of the H_2O-loss reaction found in EI-MS.

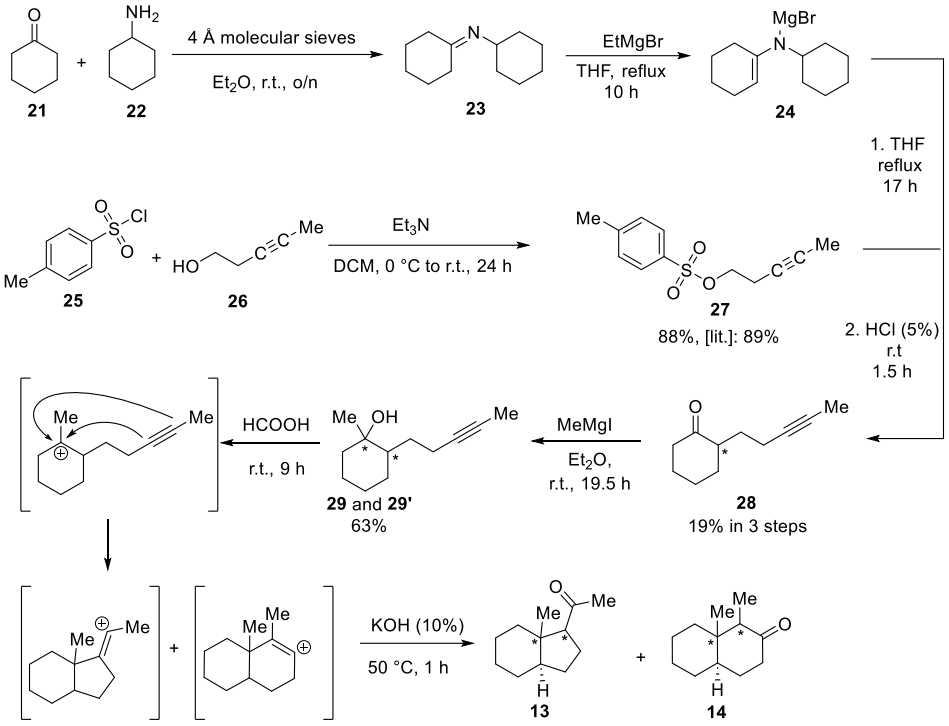

Scheme 27. Synthesis of 8-methyl-1-acetyl-hydrindane (1-(octahydro-1*H*-inden-1-yl)-1-ethanone) (**13**) used as a S42 (**1**) C,D-ring surrogate to investigate the H_2O-loss reaction in detail. The multistep synthesis yielded a mixture of the desired hydrindane derivative **13** along with the bicyclic isomer octahydro-1,8a-dimethyl-2(1*H*)-naphthalenone (**14**).[96]

The simplified steroid model of S42 (**1**), i.e. the 8-methyl-1-acetyl-hydrindane (1-(octahydro-1*H*-inden-1-yl)-1-ethanone) (**13**) was synthesized according to a procedure reported by *Lansbury et al.* (**Scheme 27**).[96-97]

Cyclohexanone (**21**) was condensed with cyclohexylamine (**22**) under inert conditions with molecular sieves overnight to give the imine compound **23**. The imine compound **23** was relative unstable, and the next step was conducted immediately after purification by *Kugelrohr* distillation.

Imine **23** was activated by a *Grignard* reagent, ethylmagnesium bromide, to react with freshly prepared sulfonate compound **27**, which was prepared by reacting 3-pentyn-1-ol (**26**) with tosyl chloride (**25**) under a basic condition. Ketone **28** was given after stirring the mixture with acid chloride for 1.5 h at r.t.

Methyl-cyclohexanol derivatives **29** and **29'** were achieved using methyl magnesium iodide. The final step was generating compound **13** and **14**. Upon the addition of acetic acid, a tertiary carbon cation was generated by a water

loss from methyl-cyclohexanol. Ring closure was achieved by alkyne nucleophilic attack on the carbocation.

Subsequently, KOH was added, and a hydroxide ion attacked the resulting positive charged double bond. Tautomerization yielded ketone products **13** and **14**, which remained as a mixture after column chromatography purification, but they could be differentiated by GC-MS analysis based on EI-fragmentation patterns.

4.1.3 Synthesis deuterium labeled S42-d7 (**1-d7**), S42-d4 (**1-d4**)

Stable isotope-labeled derivatives of S42[98] were prepared and analyzed either directly or as silyl ethers by GC-EI-HRMS to complement the results of the S42 (**1**) analysis.

TMS derivatization is routinely conducted to increase detection sensitivity.[50] Therefore, fragmentation studies of TMS derivatives of S42 are also crucial in our project.

S42-d4 (**1-d4**) synthesis

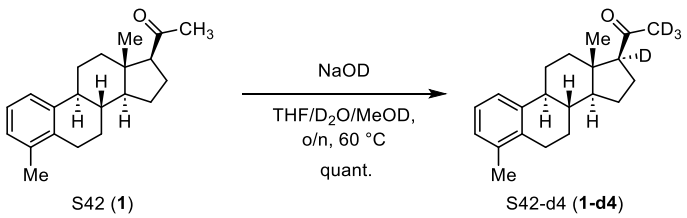

Scheme 28. Synthesis of S42-d4 (**1-d4**) by hydrogen/deuterium exchange at C17 and C21 via keto-enol tautomerization chemistry.[99]

The synthesis of S42-d4 (**1-d4**) was achieved via late stage hydrogen / deuterium exchange at C-17 and C-20 by keto-enol tautomerization chemistry in deuterated alkaline medium, as illustrated in **Scheme 28**.[99]

Deuterated water D_2O was used as a deuterium source. Since S42 (**1**) is hydrophobic and needed to be dissolved in organic tetrahydrofuran (THF) solvent, addition of extra MeOD was critical for producing a homogeneous three-solvent system for a completed deuterium labeling reaction. The reaction was monitored by GC-EI-LR-MS and NMR spectroscopy.

The deuterated products were not further purified and were directly analyzed by GC-EI-HRMS. The 8-methyl-1-acetyl-hydrindane (1-(octahydro-1*H*-inden-1-yl)-1-ethanone) (**13**) was also deuterated by this protocol for additionally GC-EI-HRMS analysis.

Since the product **1-d4** can undergo facile hydrogen deuterium exchange via keto-enol tautomerism chemistry, this isotopologue is important to study the fragmentation reactions but is not appropriate to be used in solutions as an internal standard for S42 (**1**) analysis.

S42-d7 (**1-d7**) synthesis

To avoid depletion of deuterium labels, A/B ring labeling was aimed for S42 (**1**).

Strategy A

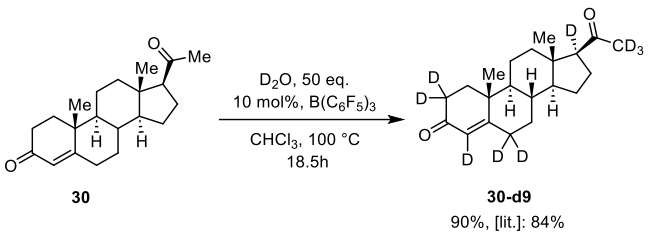

30 **30-d9**
90%, [lit.]: 84%

Scheme 29. Preparation of deuterated progesterone by D_2O and a *Lewis* acidic $B(C_6F_5)_3$.[100]

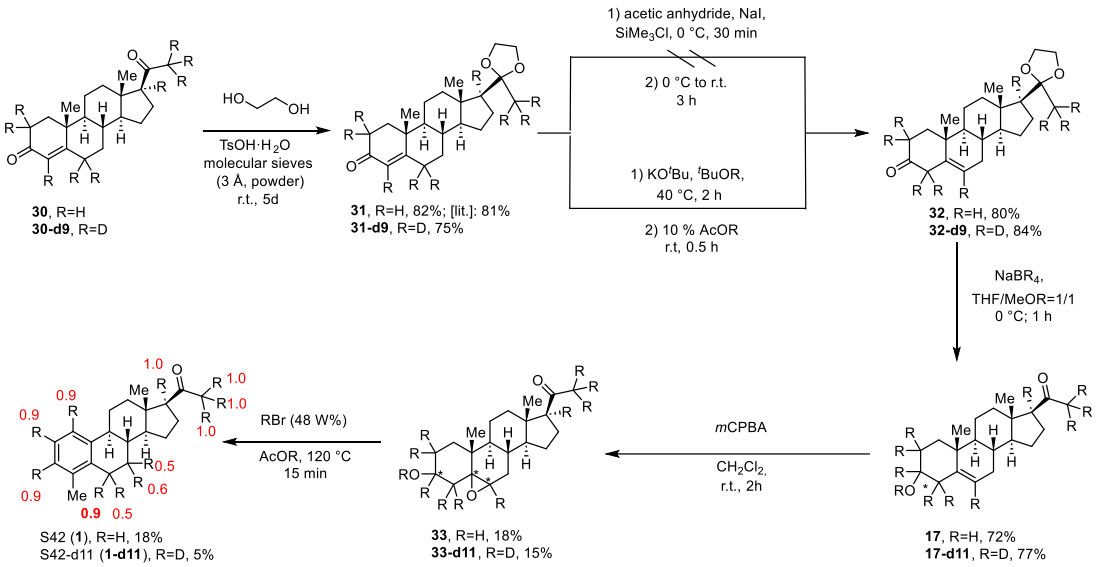

Scheme 30. S42-d11 (**1-d11**) synthesis started from progesterone. The C20 ketone group was protected by application of 1,2-ethanediol before double bond rearrangement from C4-C5 to C5-C6. A reduction reaction was conducted by $NaBD_4$ at 0 °C, which not only gave an alcohol at C3 but also deprotected the ketal functional group. After epoxidation and aromatization reaction, S42-d11 (**1-d11**) was generated. The deuteration rate (in red) was calculated by NMR calibration three proton from C18.

S42-d7 (**1-d7**) was initially planned to be synthesized from progesterone (**30**) as starting material. The hydrogen / deuterium exchange at C2, C4, C6, C17, and C21 was conducted using D_2O and a *Lewis* acidic $B(C_6F_5)_3$ according to a procedure from *Wasa et al* (**Scheme 29**).[100]

The C20 carbonyl group of compound **30** and **30-d9** was protected by 1,2-ethanediol[101] before the double bond rearrangement from C4-C5 (compound **31** and **31-d9**) to C5-C6 (**32**, **32-d9**) (**Scheme 30**). Potassium *tert*-butoxide was vital for the rearrangement reaction as a base, and deuterated *tert*-butanol served as solvent and as deuterium source.[102] The π-electron delocalization between C3 and C6 was disrupted under acidic conditions by treatment with deuterated acetic acid. The reaction mixture was added shortly after the previous step to deuterated acetic acid to avoid equilibration and back-reaction to the starting material.

The last few steps of the synthesis are firstly, reduction reaction by $NaBD_4$, secondly, epoxidation reaction by *m*CPBA and finally aromatization with DBr in AcOD according to a procedure described by *Uynik et al*.[7] The synthesis yields remained unaffected by application deuterated or non-deuterated reagents. The last two steps afforded low yields and the aromatization using DBr in AcOD

afforded only 3 mg (5% yield) S42-d11 product (**1-d11**) prior to purification. The deuteration rate at C6 and C7 was around 50% according to NMR peak integration. This synthesis strategy, especially the last two steps, should be improved. Obviously, the last two steps need to be optimized.

Strategy B

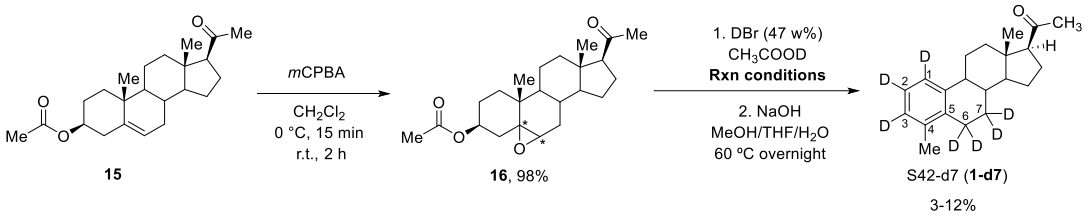

Scheme 31. The synthesis of S42-d7 (**1-d7**) can be straightforward synthesized by using deuterated agents in the aromatization step.[86] The hydrogen / deuterium exchange ratio in C7 position (around 0.2 to 0.7) is relatively lower than C1-C3 position (around 0.8 to 0.9).

Table 2 Synthesis of S42-d7 (**1-d7**). [86] Deuterium labeling ratio at each position was determined by ^{1}H-NMR, using the C18 methyl protons as an internal reference calibrated to three. The deuteration ratio was calculated as (x-y), where x and y represented normalized proton peak integrations of the non-deuterated and deuterated S42, respectively. D-6, D-6' and D-7, D-7' exhibited different chemical shifts. D-6 and D7 appeared at higher chemical shifts than D-6' and D7' in the corresponding order.

Entry	Rxn. Condition	Scale (g)	Deuteration ratio								
			D-1	D-2	D-3	D-6	D-6'	D-17	D-7	D-7'	D-21
1	120 °C, 15 min	0.6	0.8	0.8	0.6	0.5	1.2		0.7	0.4	0.4
2	120 °C, 15 min; r.t., o/n	0.6	0.8	0.8	0.5	0.6	0.4	0	0.6	0.7	0.5
3	120 °C, 30 min r.t., o/n	2	0.8	0.8	0.9	0.6	0.8	0	0.6	0.4	0
4	120 °C, 30 min r.t., 42.5 h 50 °C, 22 h		0.8	0.8	0.8	0.7	0.8	0	0.7	0.6	0
5.	120 °C, 30 min 60 °C,19 h	2	0.9	0.8	0.9	0.8	0.9	0	0.6	0.2	0
6.	r.t., 1 h 120 °C, 30 min 50 °C, 2 d	2	0.9	0.8	0.8	0.7	0.7	0	0.6	0.3	0

Another synthesis strategy of deuterated S42 at the A/B ring was achieved in three steps as illustrated in **Scheme 31**. The S42 (**1**) synthesis protocol was adapted from *Uyanik at al.* HBr and AcOH were replaced by DBr and AcOD in the respective steps.[7] This procedure is more effective and proceeds via fewer synthesis steps than strategy A. Therefore, synthesis strategy B was chosen for S42-d7 (**1-d7**) synthesis.

Reaction conditions were optimized for maximum deuteration ratios. Prolonged stirring in acidic condition proved to be beneficial and an increased deuteration ratio at D-6 and D-6' was achieved when the reaction was heated at 50 or 60 °C overnight.

The composition of deuterium labeled S42 was deduced from GC-EI-HRMS single ion monitoring (SIM) measurements and total ion counting (TIC) experiments at *m/z* 280 to 310.

SIM experiments were repeated three times and the averaged signal areas of individual ions from S42-d2 (*m/z* 298) to S42-d9 (*m/z* 305) were monitored and yielded the extent of labeling of the deuterated isotopologues present.

Full scan / total ion counting (TIC) analysis at the molecular ions at *m/z* 280 to 310 was repeated 5 times. The signal intensities of accurate ion masses from S42-d2 to S42-d9 (error lower 5 ppm) were transformed into deuteration labeling ratios. ^{13}C isotope contributions to individual ion abundances were considered to avoid intensity errors for the calculation of ^{2}H-isotopologue ratios.

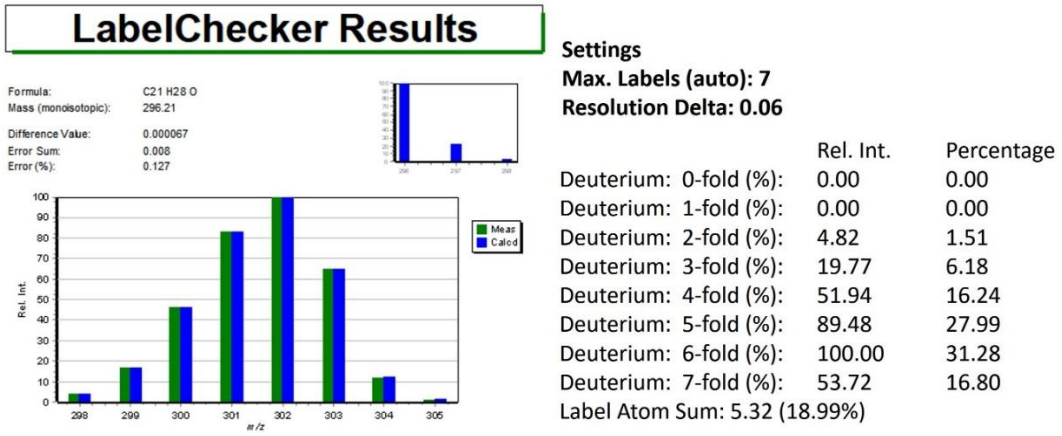

Figure 14. Simulation of an isotopic distribution of the molecular ion of synthetic S42-d7 (**1-d7**) with the *UMC V3.12.0.37* software (blue bars) and comparison with the isotopic pattern of the molecular ion of **1-d7** recorded with GC-EI-HRMS (green bars).[103] The degree of deuteration is deduced from the simulated isotopic distribution as shown.

The maximum deuterium number is seven and the percentage of compound **1-d7** containing six deuterium is close to 31%, followed by the incorporation of five deuterium atoms with 28%, seven deuteriums with 17%, and four deuteriums with 16% (**Figure 14**). To correct for the isotope effects, the isotopic

distribution was simulated with the *UMC V3.12.0.37* software based with the deuterium level values recorded in the TIC experiments.[103]

4.1.4 TMS and TBDMS derivatization S42 (**1**)

TMS and TBDMS derived S42 compounds were synthesized to examine the mass shift in their fragment ions and to investigate ion structures by GC-EI-HRMS.

TMS/TBDMS derivatization of S42

Trimethyl silyl ether derivative synthesis of the analytes (**1-C20-TMS** and **1-C17-TMS(*E*/*Z*)**) were achieved by two different procedures summarized in **Scheme 32**.[98a, 104]

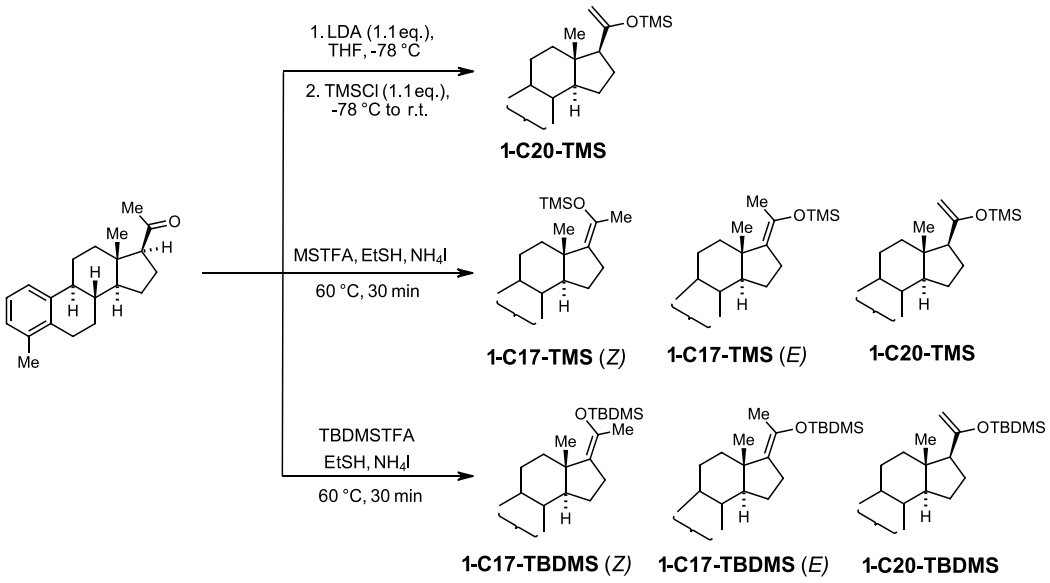

Scheme 32. Preparation of TMS-ether derivatives of S42 (**1-C17-TMS(*Z*)**; **1-C17-TMS(*E*)**; **1-C20-TMS**) by either lithium diisopropyl amine (LDA) and chloro(trimethyl)silane (TMSCl) treatment, or by using a mixture of *N*-methyl-*N*-trimethylsilyl-trifluoroacetamide (MSTFA)/ ammonium iodide (NH_4I)/ ethanethiol (EtSH).[98a, 98c] TBDMS-ether derivatives of S42 (**1-C17-TBDMS(*Z*)**; **1-C17-TBDMS(*E*)**; **1-C20-TBDMS**) were generated by replacing MSTFA with TBDMSTFA. However, the assignment of the absolute configuration of the *E* or *Z* diastereomers of the **1-C17-TMS** and the **1-C17-TBDMS** derivatives could not be achieved via GC-EI-HRMS as their respective EI-HRMS spectra are not distinguishable

Compound **1-C20-TMS** was initially synthesized by *Dr. Tobias Wilczek* before the start of this project. A strong base, lithium isopropyl amide (LDA) was used to generate an enolate at S42(**1**) (**Scheme 32**, top) under inert conditions. For

silylation, trimethylsilyl chloride (TMSCl), was added and the **1-C20-TMS** product was generated by a S_N2 attack by the enolate. Structure confirmation of the C20-TMS derivative was achieved by observing protons at the C20-C21 double bond in the ^1H NMR spectrum.

TMS derivatization by LDA under inert condition is impractical for routine analysis involving large sample sizes, so a derivatization mixture of *N*-methyl-*N*-trimethylsilyl-trifluoroacetamide (MSTFA)/ ammonium iodide (NH_4I) / ethanethiol (EtSH) was more commonly applied (see **Scheme 32**, middle). A purified dried samples will be TMS derivatized by mixing with the derivatizing agent mentioned above and heating at 60 °C for 30 min.[98a, 98c]

MSTFA first reacted with ammonium iodide to produce trimethyl iodide (TMSI), a reactive derivatization agent (see **Scheme 32**, middle). Ethanethiol was an agent to react with iodine, that formed from decomposition of TMSI. Byproducts diethyl disulfide and hydrogen iodide were generated during derivatization.[104b] Therefore, the reactive iodine was consumed to prevent its interaction with steroids S42 (**1**).

Preparation of S42-TBDMS (*tert*-butyldimethylsilyl) (**1-C20-TBDMS** and **1-C17-TBDMS(*E*/*Z*)**) was accomplished with *N*-methyl-*N*-*tert*-butyl-dimethylsilyl-trifluoroacetamide (TBDMSTFA) instead of *N*-methyl-*N*-trimethylsilyl-trifluoroacetamide (MSTFA) (see **Scheme 32**, bottom). Ammonium iodide could not be completely dissolved in TBDMSTFA, which results in less concentrated *tert*-butyldimethylsilyl iodide (TBDMSI) in the derivatization agent. This procedure is not commonly used in routine doping sample preparation.

Using LDA and TMSCl can generate **1-C20-TMS** stereo selectively because the bulky base, LDA, abstract the hydrogens at C20 more easily than at C17 to produce the enolate, reacting with TMSCl.

Mixture of *N*-methyl-*N*-trimethylsilyl-trifluoroacetamide (MSTFA)/ ammonium iodide (NH_4I) / ethanethiol (EtSH) produce TMSI, which is more reactive than TMSCl, but all three TMS products:**1-C17-TMS(*Z*)**; **1-C17-TMS(*E*)**; **1-C20-TMS** will be given.

TMS/TBDMS derivatization of S42-d4 (**1-d4**)

We note that the synthesis of S42-d4-TMS (**1-d4-TMS**) led to a mixture of S42-d3/d2/d1-TMS isotopologues (**1-d1-C20-TMS**; **1-d2-C20-TMS**; **1-d3-C17-TMS(*E*/*Z*)**) as **Scheme 33**.

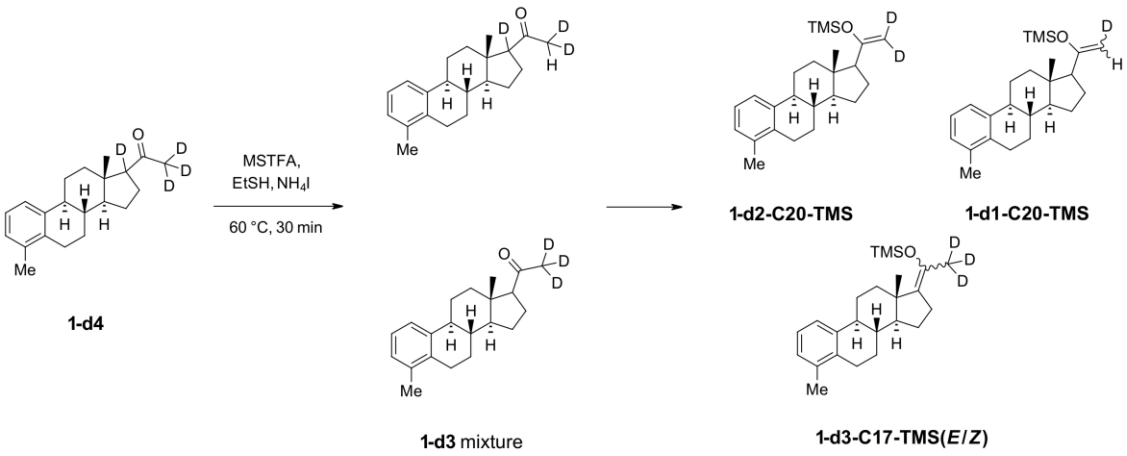

Scheme 33. Preparation of TMS-ether derivatives of S42-d4 (**1-d4**) with a mixture of MSTFA/NH_4I/EtSH. Deuterium/hydrogen back exchange to S42-d3 (**1-d3**) was detected to take place in the silylation reaction mixture. The resulting mixture of S42-d1 to d3 isotopologues was characterized with GC-EI-HRMS.

Hydrogen iodide, which was produced as a byproduct in the mixture of the derivatization agent, was suspected to be responsible for the deuterium-hydrogen back exchange of S42-d4 (**1-d4**) before TMS. The resulting mixture of d1-, d2-, and d3-TMS derivatives of S42 (**1-d1-C20-TMS**; **1-d2-C20-TMS**; **1-d3-C17-TMS(*E*/*Z*)**) were separated and individually analyzed by GC-EI-HRMS (see **Scheme 33**). However, the assignment of the absolute configuration of the *E* or *Z* diastereomers of **1-d3-C17** could not be achieved via GC-EI-HRMS as their EI-HRMS spectra are not distinguishable.

A similar phenomenon was found with TMS and TBDMS derivatized S42 (**1**). The assignment of the absolute configuration of the individual silylated diastereomers **1-C17-TMS(*E*)**, **1-C17-TMS(*Z*)** and **1-C17-TBDMS(*E*)** **1-C17-TBDMS(*Z*)** (see **Scheme 32**) was not possible via GC-EI-HRMS. We therefore rely on the characteristic elution behavior, *i.e.* the individual retention times, and the EI-HRMS spectra for structure assignments of the isomers.

4.1.5 Mechanism studies of S42 (**1**) by GC-EI-MS

Analysis of S42 (**1**) by GC-EI HRMS

A detailed studies of S42 (**1**) fragmentation pattern in EI-MS is an important precondition for the investigation of complex S42 metabolites.

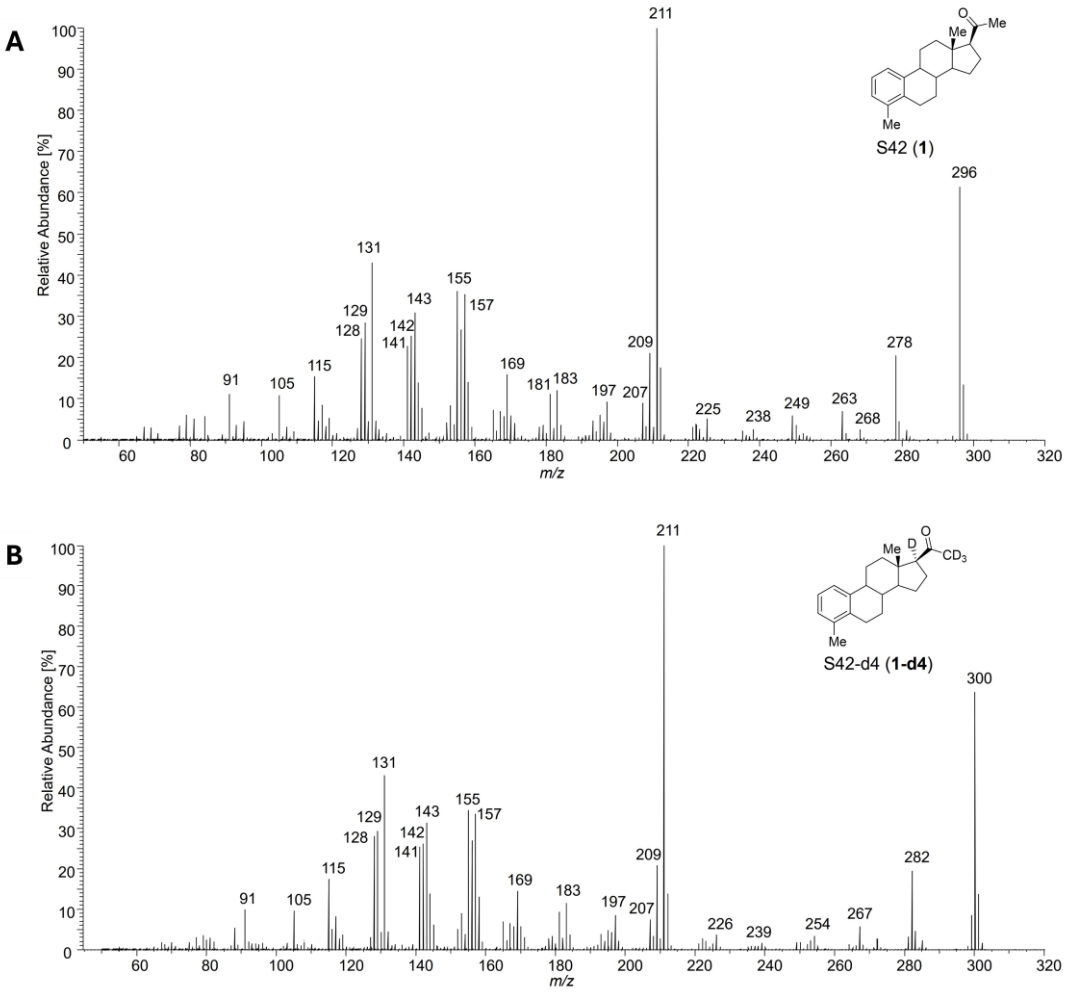

Figure 15. (A) GC-EI-HRMS spectra of S42 (1) (see **Table 3** for accurate ion masses and compositions). (B) GC-EI-HRMS spectra of S42-d4 (**1-d4**). The samples were analyzed at University of Cologne. A characteristic mass shift of 4 Da werefound in the GC-EI-HRMS spectrum of S42-d4 compared to the one of S42: ions at *m/z* 296 shifted to 300; *m/z* 278 to 282; *m/z* 263 to 267; *m/z* 249 to 250.

The fragmentation pathways observed in the EI-HRMS spectrum of S42 (**1**) (see **Figure 15**, **Scheme 34** to **Scheme 40**) and their interpretation along with the structure assignments therefore rests on the broad knowledge available on GC-EI-HRMS of steroids.[96, 105]

The EI-MS spectrum of S42 (**1**) exhibits the radical molecular ion $[M]^{+\bullet}$ at *m/z* 296 along with a number of significant fragment ions, at *m/z* 278, 263, 157, 155, 131, as shown in **Figure 15A**. All relevant ion masses are determined with GC-EI-HRMS. The accurate ion mass determination allows the identification of the molecular compositions, which underpin straight-forward structure assignments as listed in **Table 3**.

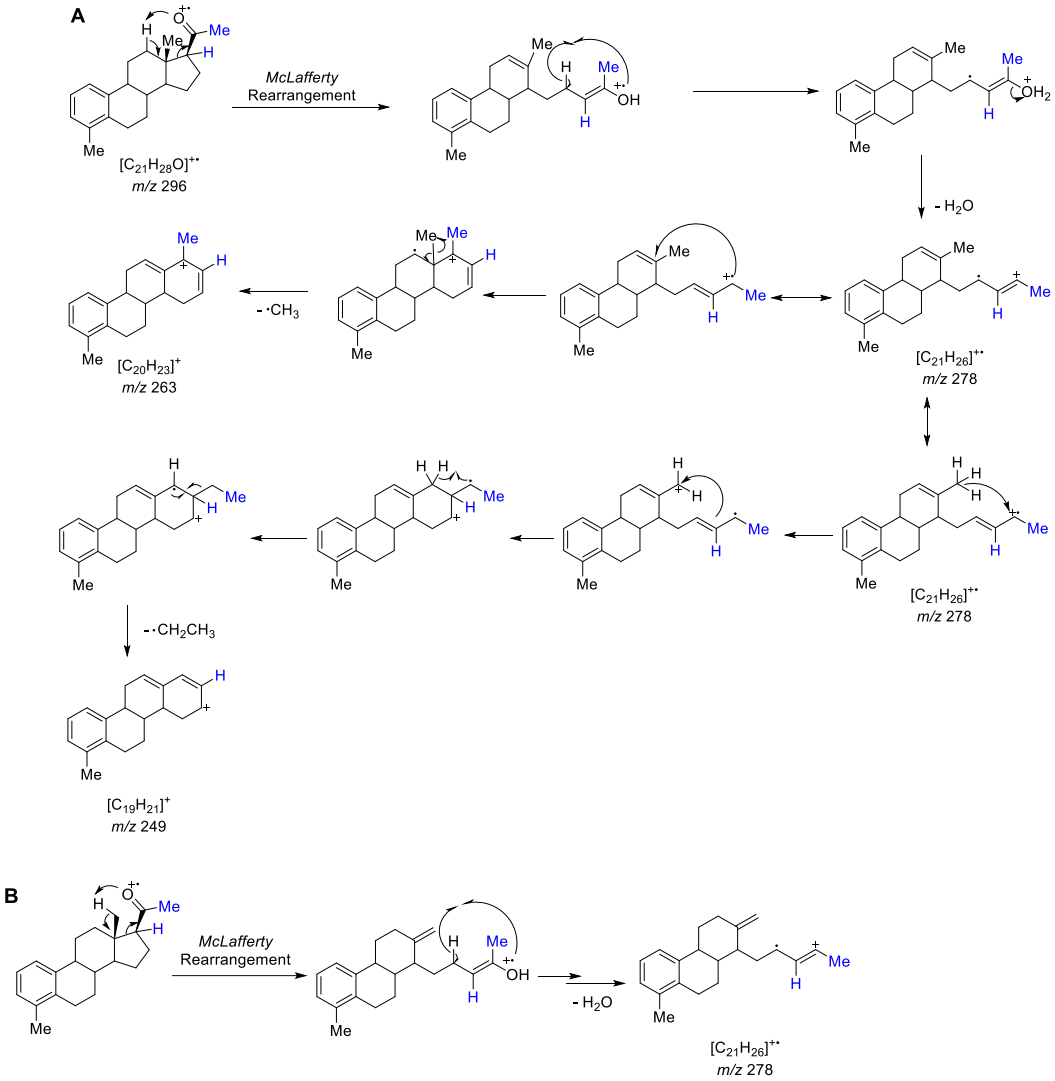

Scheme 34. Suggested reaction sequence of the molecular radical cation of S42 (**1**) at *m/z* 296 leading to the allylic fragment ion at *m/z* 278 upon water loss. Subsequent methyl, or ethyl radical loss (Δm 15 Da or 29 Da) delivers the allylic fragment ions at *m/z* 263 and at *m/z* 249, respectively. Accurate ion masses are provided in **Table 3**. Atoms in blue were labeled by deuterium in S42-d4 (**1-d4**).

To investigate the mechanism of the water-loss, generating an ion at *m/z* 278 and especially to clarify the origin of the hydrogens expelled with the water molecule in EI-HRMS of S42 (**1**), we performed H/D exchange in the condensed phase at carbons C17 and C21 and analyzed S42-d4 (**1-d4**) with GC-EI-HRMS.

The unambiguous loss of H_2O from the molecular ions of S42-d4 (**1-d4**) and S42-d3 (**1-d3**) evidenced that the hydrogens at C17 and C21 are not involved (compare **Figure 15A** with **B**).

Apparently, there are a few γ-hydrogens within reach of the carbonyl oxygen which can be transferred in a *McLafferty* rearrangement reaction as illustrated in **Scheme 34**.[105a, 105b, 106]

Hydrogens in γ-position to the carbonyl oxygen are available at the C12 methylene group in ring C (**Scheme 34A**), and at the C18 methyl group (**Scheme 34B**) as discussed and studied earlier by *Djerassi*.[96] Afterwards, or concerted with the first step, a *β*-fragmentation opens ring D and a second hydrogen e.g. from C16 is transferred to pave the way for the ultimate release of water and the formation of the $[C_{21}H_{26}]^{+\bullet}$ ion at *m/z* 278 (*m/z* 282 from compound **1-d4**).

Starting from the ion at *m/z* 278 the formation of the allylic fragment ion $[C_{20}H_{23}]^+$ at *m/z* 263 (*m/z* 267 from compound **1-d4**) is rationalized upon ring closure and loss of the C18 methyl radical as shown in **Scheme 34A**. The analogous reaction in S42-d3 (**1-d3**) and S42-d4 (**1-d4**) shifts the mass of the respective product ion to *m/z* 267 and *m/z* 266, supporting the mechanism shown above (**Scheme 34B**).

Besides the formation of the ion $[C_{20}H_{23}]^+$ at *m/z* 263, we envisage a similar formation of the low abundant fragment ion $[C_{19}H_{21}]^+$ at *m/z* 249 (**Scheme 34A**) via hydride shift from methyl group at C18, hydrogen atom shift followed by the ring closure reaction and ultimate loss of an ethyl radical ($^{\bullet}C_2H_5$, Δm 29 Da) from *m/z* 278 (**Figure 15A**)). An analogous fragment ion is found in the EI-MS spectrum of S42-d4 (**1-d4**) mass shifted by one unit to *m/z* 250, albeit with very low abundance (**Scheme 34B**).

Additionally, a series of low-abundant signals corresponding to, for example, $[C_{19}H_{21}]^+$ at *m/z* 249 (**Figure 15A**) and to $[C_{19}H_{17}{}^2H_4]^+$ at *m/z* 253 (**Figure 15B**), which document extensive H/D scrambling of *m/z* 282 (**Figure 15B**), that is, the water-loss product of the d4-isotopologue at *m/z* 300 (compare to *m/z* 278 in (**Figure 15A**). Finally, the fragment ions $[C_{19}H_{23}]^+$ at *m/z* 251, $[C_{19}H_{22}{}^2H]^+$ at

m/z 252, and $[C_{19}H_{18}{}^{2}H_4]^{+\bullet}$ at *m/z* 254 stem from different formation pathways (**Figure 15B**).

Table 3. Ions found in the EI-HRMS Spectrum of S42 (**1**) presented in **Figure 15A**.

S42 ($C_{21}H_{28}O$)	Nominal mass [Da]	Composition	Theo. mass [Da]	Accurate ion mass measured [Da]	Error (ppm)
$[M]^{+\bullet}$	296	$[C_{21}H_{28}O]^{+\bullet}$	296.2135	296.2132	-0.89
$[M-H_2O]^{+\bullet}$	278	$[C_{21}H_{26}]^{+\bullet}$	278.2029	278.2027	-0.77
$[M-H_2O-Me^{\bullet}]^{+}$	263	$[C_{20}H_{23}]^{+}$	263.1794	263.1793	-0.31
	249	$[C_{19}H_{21}]^{+}$	249.1638	249.1636	-0.14
	238	$[C_{18}H_{22}]^{+\bullet}$	238.1716	238.1715	-0.06
	225	$[C_{17}H_{21}]^{+}$	225.1638	225.1636	-0.57
	211	$[C_{16}H_{19}]^{+}$	211.1481	211.1479	-1.16
	209	$[C_{16}H_{17}]^{+}$	209.1325	209.1323	-0.66
	169	$[C_{13}H_{13}]^{+}$	169.1012	169.1010	-0.94
	157	$[C_{12}H_{13}]^{+}$	157.1012	157.1010	-1.35
	156	$[C_{12}H_{12}]^{+}$	156.0934	156.0932	-1.20
	155	$[C_{12}H_{11}]^{+}$	155.0855	155.0854	-0.90
	143	$[C_{11}H_{11}]^{+}$	143.0855	143.0854	-0.58
	131	$[C_{10}H_{11}]^{+}$	131.0855	131.0855	-0.23
	115	$[C_9H_7]^{+}$	115.0542	115.0542	-0.41

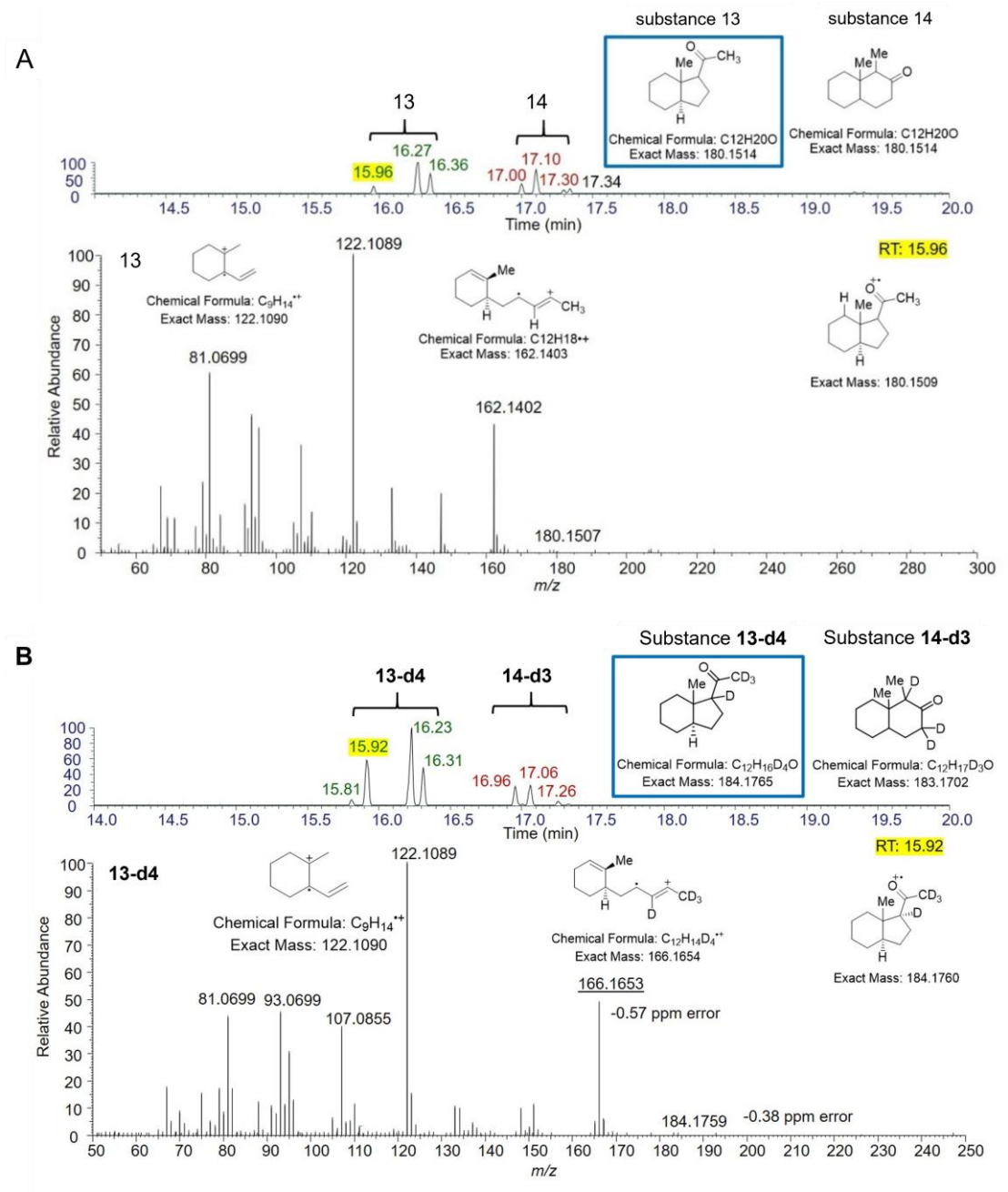

Figure 16 (A) GC-EI-HRMS analysis of isomers of compounds **13** at a retention time of 15.96 min. (B) GC-EI-HRMS and spectrum of deuterated **13-d4** at a retention time of RT: 15.92 min. Three isomers of **13** are three isomers of **13-d4** were presented (RT: 15.96, 16.27 and 16.36 min). All isomers have similar EI-HRMS spectra.

Additionally, the GC-EI-HRMS analysis of freshly synthesized 8-methyl-1-acetyl-hydrindane (**13**) and of its d4 derivative, labeled with ^{2}H at C1 and C12 delivered results additionally validating the mechanistic assumptions by observation of ions at *m/z* 162 and *m/z* 166 from compound **13** and **13-d4**.[96]

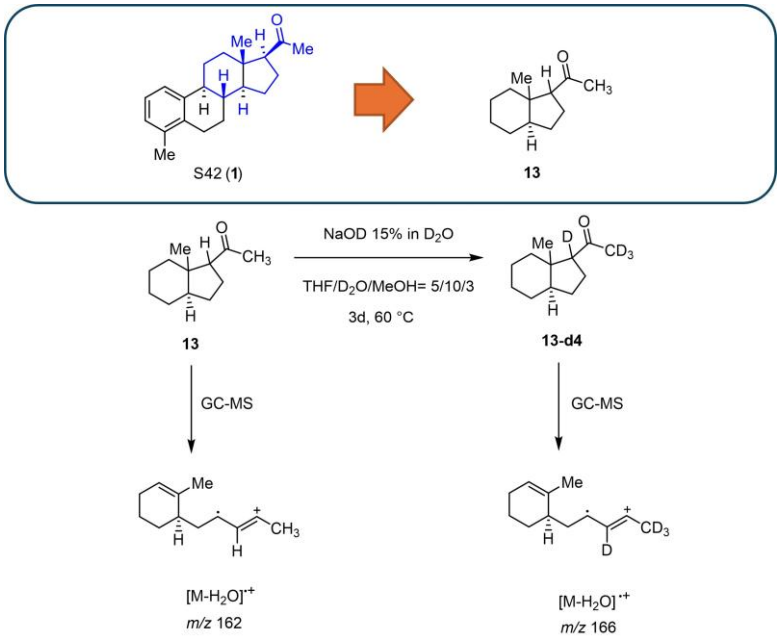

Scheme 35. S42 (**1**) structure simplification and deuteration of GC-MS analysis. The 4-ring structure was simplified to a hydride derivative (**13**) to study the mechanism of water loss by GC-EI-HRMS.

Table 4. Literature mass spectra of deuterated hydrindane derivative **13** adapted from *Djerassi et al.*[6] The result of the deuterated derivative at the acetyl functional group fits our experimental outcome.

Structure	D percentage (%)		[M]+• [Da]	Δm	Water loss product ion [Da]
	d_0	100	180	18	162
	d_3	99>	183	20 19 18	163 (~20%) 164 (~40%) 165 (~40%)
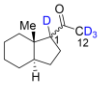	d_4 d_3 d_2	89 7 4	184	18	166
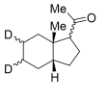	d_2 d_1 d_3	83 13 4	182	19 18	163 164
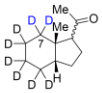	d_8 d_7 d_9	82 12 6	188	20 19 18	168 (~15%) 169 (~60%) 170 (~25%)

Further confirmation of the depicted reaction pathways was drawn from exhaustive work by *Djerassi* with 9 different deuterium-labeled hydrindane derivatives.[96] A loss of D_2O was found when C4-7 and C10 were labeled with deuterium.

The H_2O-loss reaction in 8-methyl-1-acetyl-hydrindane (**13**) was complemented by preliminary DFT computations, which also indicated that both pathways in **Scheme 34A** and **B** are possible and energetically feasible.[107]

GC-EI-HRMS analysis of S42 (**1**) and of S42 isotopologues (**1-d3**, **1-d4**, **1-d7**)

The GC-EI-HRMS spectra of S42 (**1**), S42-d4 (**1-d4**) and S42-d7 (**1-d7**) mixture are dominated by the prominent fragment ion at *m/z* 211, and *m/z* 217 respectively (**Figure 17A, B** and **C**) which results from D-ring cleavage. More than one reaction pathway is conceivable to explain the formation of the C-ring cyclohexene structures of $[C_{16}H_{19}]^+$ isomers, found at *m/z* 211 as shown in **Scheme 36A** and **B**.

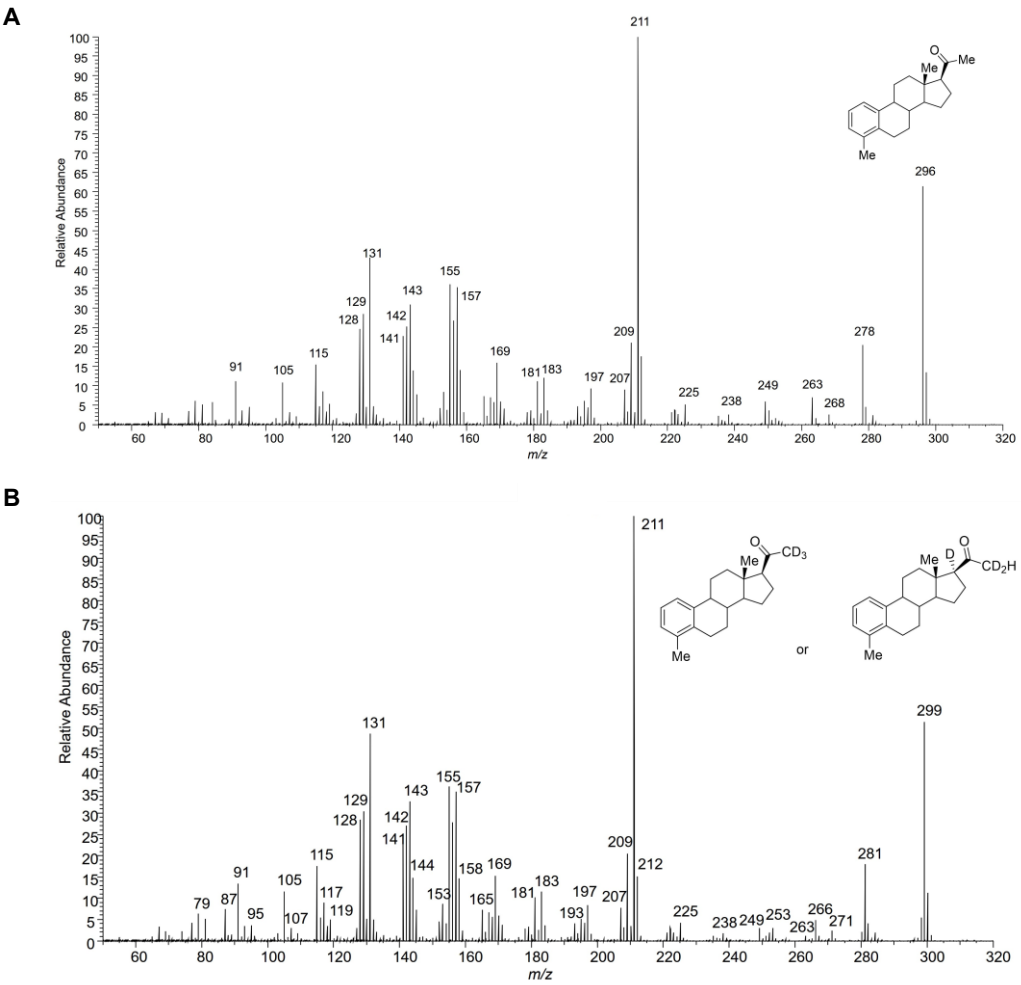

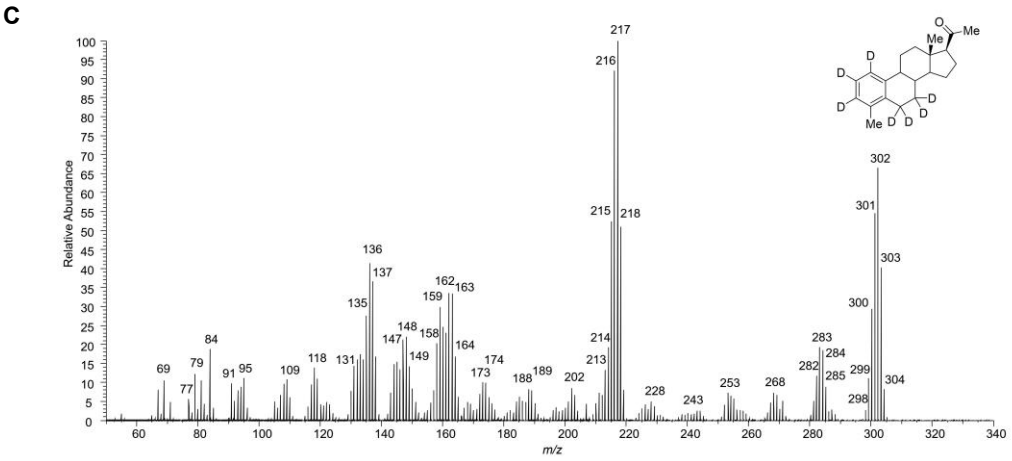

Figure 17. GC-EI-HRMS spectra of S42 (**1**) (**Figure A**), of S42-d3 (**1-d3**) (**Figure B**), and of the A,B-ring labeled S42-d7 (**1-d7**) (**Figure C**). In this synthetic product, **1-d7**, a maximum number of seven deuterium atoms are presented.

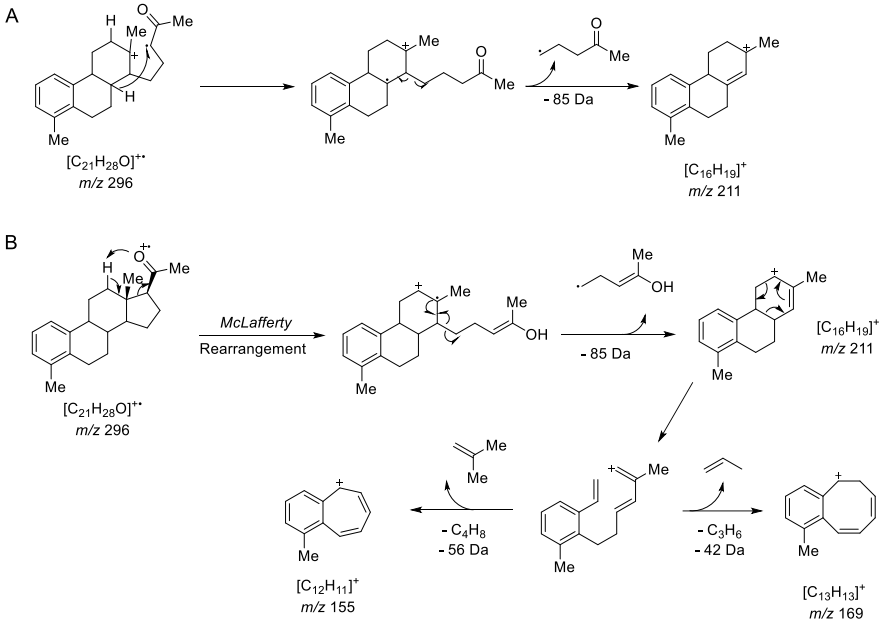

Scheme 36. Fragmentation reaction sequences of the molecular ion of steroid S42 (**1**) at *m/z* 296. (a) Formation of fragment ion at *m/z* 211. (b) Alternative formation mechanism to fragment ions at *m/z* 211, 155 and 169. Accurate ion masses are provided in **Table 3**.

First, we propose an isomeric molecular ion, ionized at the sigma bond between C13 and C17, which loses the 2-pentanonyl radical ($^{\bullet}C_5H_9O$, Δm 85 Da) after hydrogen rearrangement as shown (**Scheme 36A**). Second, an initial *McLafferty* rearrangement reaction opens the D-ring followed by the loss of the enol moiety as a radical ($^{\bullet}C_5H_9O$, Δm 85 Da) (**Scheme 36B**).[49a, 105a, 105b] The ion at *m/z* 211 is central for the following reactions involving *retro-Diels-*

Alder reactions, *RDA*[49a, 105a, 105b] followed by intramolecular ring closure and olefin loss (propene, Δm 42 Da or isobutene, Δm 56 Da).

The resonance stabilization favors the formation of the bicyclic product ion structures of $[C_{12}H_{11}]^+$ at *m/z* 155 and of $[C_{13}H_{13}]^+$ at *m/z* 169 at dispense of an entropic penalty for the ring closure reaction (**Scheme 36B**).

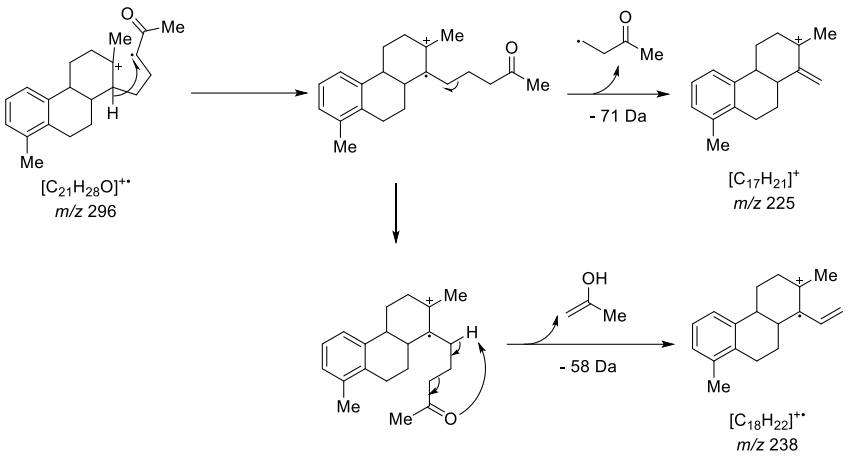

Scheme 37. Fragmentation reaction sequences of the molecular ion of steroid S42 (**1**) at *m/z* 296. Formation of fragment ions at *m/z* 238 and 225. Accurate ion masses are provided in **Table 3**.

The ionization of the sigma bond between C13 and C17 opens ring D in the molecular ion of S42 (**1**), a pathway described earlier for 20-keto steroids (**Scheme 37**). [49a, 105a, 105b, 106, 108] This process leads to the formation of the fragment ions at *m/z* 238 (loss of propen-2-ol; Δm 58 Da) and at *m/z* 225 (loss of 2-butanonyl radical $^{\bullet}C_4H_7O$; Δm 71 Da).

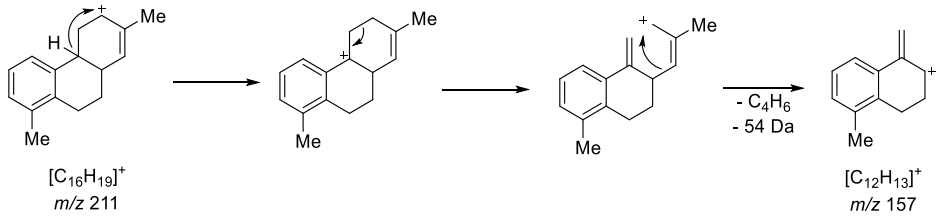

Scheme 38. Fragmentation reaction sequences of the molecular ion of steroid S42 (**1**) at *m/z* 296. Formation of fragment ion at *m/z* 157. Accurate ion masses are provided in **Table 3**.

Finally, it is reasonable to assume that the important ion $[C_{12}H_{13}]^+$ at *m/z* 157 may originate from *m/z* 211 by loss of C_4H_6 (**Scheme 38**). All named fragment ions retain the A and B ring system of S42 (**1**) and are therefore insensitive to

the deuterium labels at C-17 and C-21, as documented in the EI-MS spectrum of S42-d3 (**1-d3**) and S42-d4 (**1-d4**) (**Figure 17B** and **Figure 15B**).

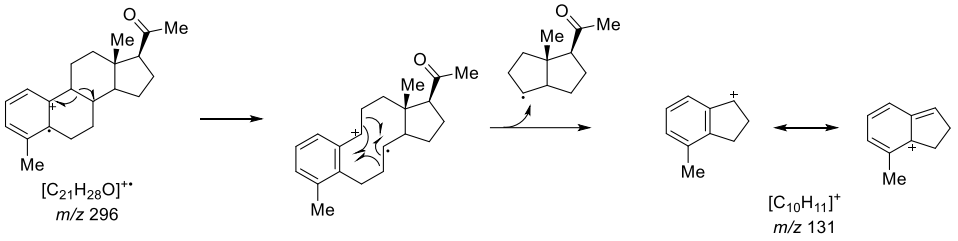

Scheme 39. Fragmentation reaction sequences of the molecular ion of steroid S42 (**1**) at *m/z* 296. (e) Formation of fragment ion at *m/z* 131.[105a] Accurate ion masses are provided in **Table 3**.

Additionally, we attribute the reaction sequence shown in **Scheme 39** starting from an A-ring ionized molecular ion of S42 (**1**), a subsequent loss of the C,D-ring system as a radical, ultimately leading to the resonance stabilized 4-methyl-indanylium cation at *m/z* 131. This reaction considers that the ion at *m/z* 131 is observed also in the EI mass spectrum of the S42-C20 enol-TMS ether (**1-C20-TMS**) in which the ion at *m/z* 211 is absent (**Figure 18B**).

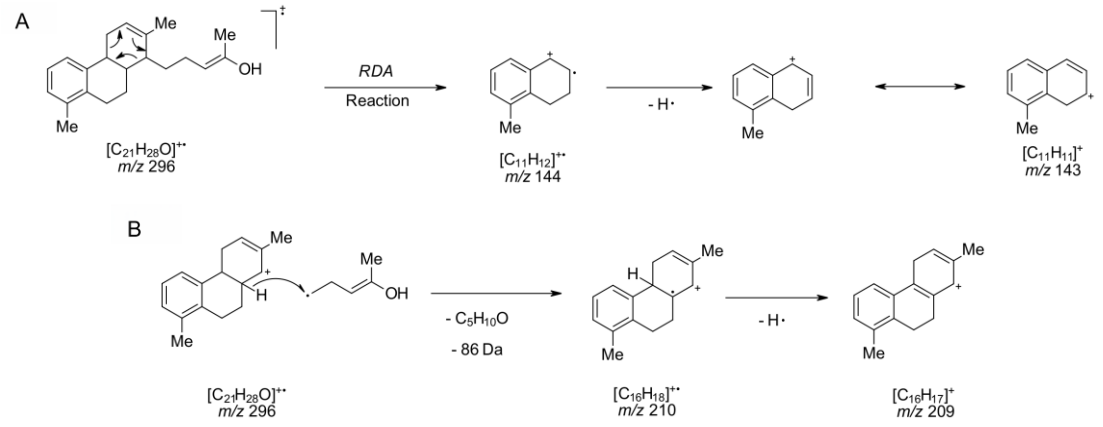

Scheme 40 *RDA* reaction of the rearranged radical molecular ion of S42 (**1**) at *m/z* 296 leading ultimately to the A,B-ring fragment ion $[C_{11}H_{11}]^+$ at *m/z* 143 found in the GC-EI-HRMS spectrum shown **Figure 15A**. The side-chain cleavage and subsequent hydrogen atom transfer generates the resonance stabilized fragment ion $[C_{16}H_{17}]^+$ at *m/z* 209. Accurate ion masses are provided in **Table 3**.

Finally, the A,B-ring fragment at *m/z* 143 can be formed via a *retro Diels-Alder* (*RAD*) reaction of the radical molecular ion as shown in **Scheme 40A**. Similarly, a side-chain cleavage followed by a hydrogen atom transfer generates the resonance stabilized fragment ion $[C_{16}H_{17}]^+$ at *m/z* 209 (**Scheme 40B**).

It is remarkable that the radical cationic intermediates at *m/z* 144 and *m/z* 210 formed by the initial neutral loss reactions described in **Scheme 40** are not found with prominent abundance in the GC-EI-HRMS spectrum of S42 (**1**). Confirmation for this mechanistic understanding rests on the fact that these ions are not mass-shifted in the spectra of and S42-d4 (**1-d4**) and S42-d3 (**1-d3**) (**Figure 15B** and **Figure 17**).

4.1.6 GC-EI-HRMS analysis of TMS derived S42 derivatives

The understanding of TMS derived S42 fragment ions is the base for analysis TMS derived S42 metabolites in the future. The fragmentation patterns of **1-C20-TMS** and **1-C17-TMS(*E*/*Z*)** are different.

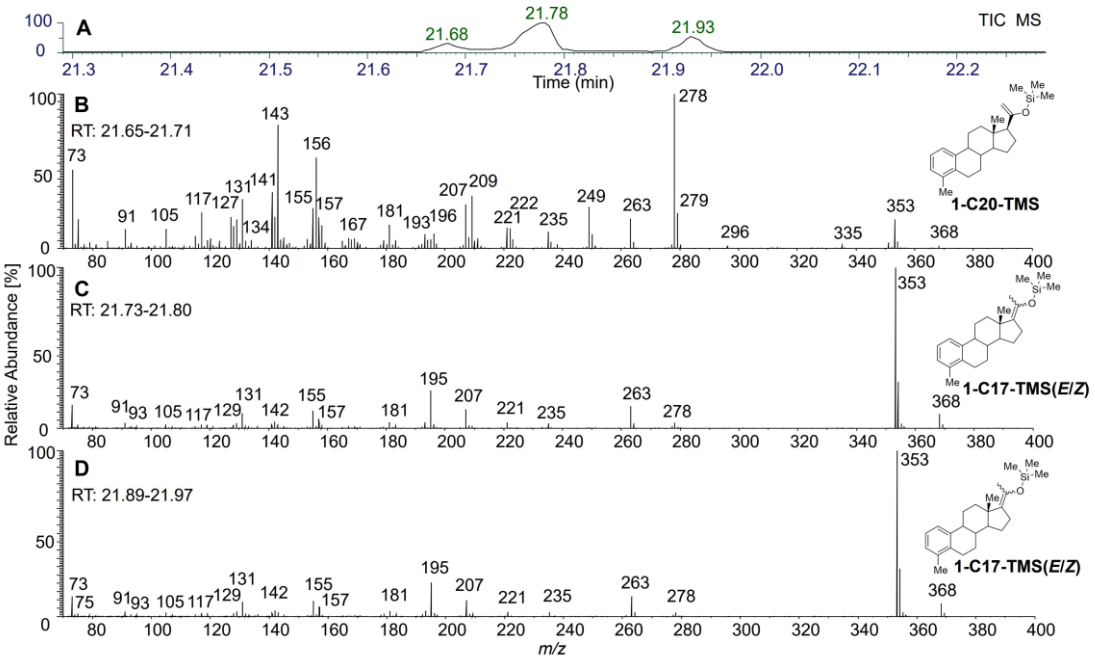

Figure 18. GC-EI-HRMS analysis of silylated steroid S42-TMS isomers yielded from treatment of S42 (**1**) by using MSTFA/ NH_4I / EtSH mixture. (A) All three different S42-enol-TMS ether isomers are separated by GC. (B) GC-EI-HRMS of a C20 enol-TMS ether of S42 (**1-C20-TMS**). (C) GC-EI-HRMS of a C17 enol-TMS ether of S42 (**1-C17-TMS(*E*/*Z*)**). (D) GC-EI-HRMS of the diastereomer of the C17 enol-TMS ether of S42 (**1-C17-TMS(*E*/*Z*)**) analyzed in (C). The samples were analyzed at the University of Cologne.

EI-MS fragmentation pattern of **1-C20-TMS**

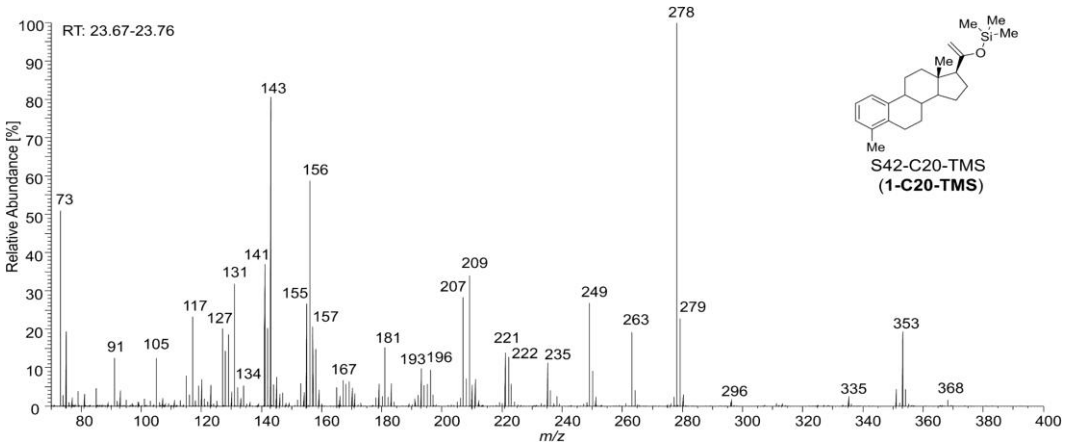

Figure 19. GC-EI-HRMS spectrum of the **1-C20-TMS** derivative found in the TIC at RT: 23.70 min with a GC temperature program: 100(5)-10-320(5) (analyzed at the University of Cologne).

We identify typical enol TMS ether derivative (**1-C20-TMS**) reaction pathways to the important fragment ions at *m/z* 353 (methyl radical loss), at *m/z* 278 (loss of trimethyl silanol), and formation of $[(CH_3)_3Si]^+$ at *m/z* 73 (**Table 5**).[98a, 98b, 104, 109]

Table 5. Ions found in the EI-HRMS spectrum of the C-20 enol-TMS ether derivative of S42 (**1-C20-TMS**) presented in **Figures 18B** and **19**. The sample was analyzed at the German Sport University Cologne.

S42-C20-TMS ($C_{24}H_{36}OSi$)	Nominal mass [Da]	Composition	Theo. Mass [Da]	Accurate ion mass measured [Da]	Error (ppm)
$[M]^{+\bullet}$	368	$[C_{24}H_{36}OSi]^{+\bullet}$	368.2529	368.2529	0.00
$[M\text{-}Me^{\bullet}]^+$	353	$[C_{23}H_{33}OSi]^+$	353.2295	353.2298	0.87
$[M\text{-}TMSOH]^{+\bullet}$	278	$[C_{21}H_{26}]^{+\bullet}$	278.2029	278.2029	0.02
$[M\text{-}TMSOH\text{-}Me^{\bullet}]^+$	263	$[C_{20}H_{23}]^+$	263.1794	263.1795	0.03
$[M\text{-}TMSOH\text{-}C_2H_5^{\bullet}]^+$	249	$[C_{19}H_{21}]^+$	249.1638	249.1638	-0.01
	235	$[C_{18}H_{19}]^+$	235.1481	235.1481	-0.03
	222	$[C_{17}H_{18}]^+$	222.1403	222.1405	0.17
	209	$[C_{16}H_{17}]^+$	209.1325	209.1324	-0.04
	207	$[C_{16}H_{15}]^+$	207.1168	207.1168	0.00
	193	$[C_{15}H_{13}]^+$	193.1012	193.1010	-0.17
	181	$[C_{14}H_{13}]^+$	181.1012	181.1011	-0.13
	157	$[C_8H_{17}OSi]^+$	157.1043	157.1043	-0.05
	157	$[C_{12}H_{13}]^+$	157.1012	157.1010	-0.14
	156	$[C_8H_{16}OSi]^{+\bullet}$	156.0965	156.0964	-0.05
	156	$[C_{12}H_{12}]^{+\bullet}$	156.0934	156.0933	-0.02
	155	$[C_{12}H_{11}]^+$	155.0855	155.0855	-0.05
	143	$[C_7H_{15}OSi]^+$	143.0887	143.0886	-0.07
	141	$[C_7H_{13}OSi]^+$	141.0730	141.0730	-0.03
	131	$[C_{10}H_{11}]^+$	131.0855	131.0856	0.06
	117	$[C_5H_{13}OSi]^+$	117.0730	117.0730	0.00
	105	$[C_8H_9]^+$	105.0699	105.0699	0.06
	91	$[C_7H_7]^+$	91.0542	91.0543	0.07
	75	$[C_2H_7O\ Si]^+$	75.0261	75.0261	0.05
	73	$[C_3H_9Si]^+$	73.0468	73.0469	0.05

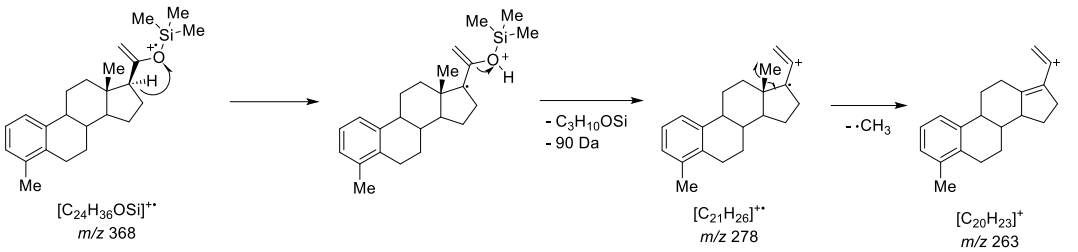

Scheme 41. Prominent fragmentation pathways of the molecular ion at *m/z* 368 observed in the GC-EI-HRMS spectrum of the C-20 enol-TMS ether of S42 (**1-C20-TMS**) depicted in **Figure 19**. Formation of fragment ions at *m/z* 278 and *m/z* 263. Accurate ion masses are provided in **Table 5**.

Apparently, the structure of the ion $[C_{21}H_{26}]^{+\bullet}$ at *m/z* 278 formed from the S42 C-20 enol-TMS ether (**1-C20-TMS**) differs from the $[C_{21}H_{26}]^{+\bullet}$ ions accessible from the molecular radical cation $[M]^{+\bullet}$ of S42 (**1**) (compare **Scheme 34** with **Scheme 41**).

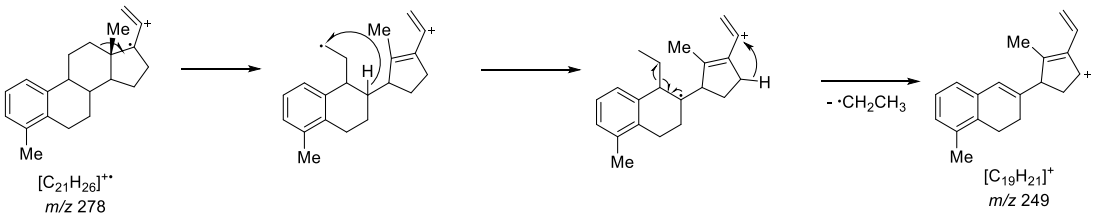

Scheme 42. Fragmentation pathway of the ion at *m/z* 278 explaining the ethyl radical loss and the formation of fragment ion at *m/z* 249 observed in GC-EI-HRMS of the C-20 enol-TMS ether of S42 (**1-C20-TMS**) in **Figure 18**. Accurate ion masses are provided in **Table 5**.

An ethyl radical loss $\bullet CH_2CH_3$ (Δm 29 Da) from a C-ring fragmentation of the ion at *m/z* 278 explains to the formation of fragment ion at *m/z* 249 as illustrated in **Scheme 42**.

Based on this finding, differences in the two EI-HRMS spectra of S42 (**1**) and **1-C20-TMS** are rationalized. Especially, the absence of the ion at *m/z* 211 in **Figure 19** is significant and correlates with the substantially reduced abundance of the ions at *m/z* 155, 157, and at *m/z* 169 which are all present in **Figure 15** (see also **Scheme 36B** and **Scheme 38**).

Interestingly, two isobaric fragment ions are identified at *m/z* 157 in the EI-HRMS data of the molecular ions of S42 enol-TMS ether isomers (**1-C20-TMS**, **1-C17-TMS(*E*/*Z*)**), *i.e.* $[C_{12}H_{13}]^+$ and $[C_8H_{17}O_{28}Si]^+$ (see **Table 5**, **6** and **Figure A46**, **Figure A47**, and **Figure A48** in the Appendix).

Close inspection of the EI-HRMS data at *m/z* 156 reveals that more than one species is present in the spectrum of **1-C20-TMS** (compare **Figure A45** in the Appendix) which are not observed in the EI mass spectra of the C-17 enol TMS ether isomers (**1-C17-TMS(*E*/*Z*)**)(**Figure 18B,C** ,and **D**). Besides the abundant ion $[C_{12}H_{12}]^{+\bullet}$ at *m/z* 156.0933 (as listed in **Table 5**), we also separately detect $[C_8H_{16}O_{28}Si]^{+\bullet}$ at *m/z* 156.0963 with minor intensity (see **Figure A45** in the Appendix). The latter results from D-ring fragmentation, whereas the ultimate formation of the $[C_{12}H_{12}]^{+\bullet}$ is not further rationalized.

The formation of a bicyclic fragment $[C_{10}H_{11}]^{+}$ at *m/z* 131 is independent of the formation of the intermediate ion at *m/z* 211 and is consequently found in both EI-HRMS spectra (compare **Figure 15A** and **Figure 19**).

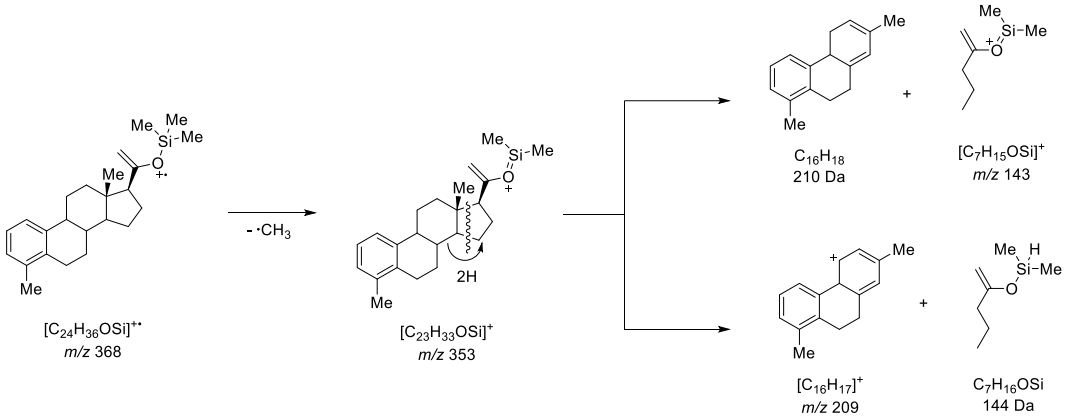

Scheme 43. Prominent fragmentation pathways of the molecular ion at *m/z* 368 observed in the GC-EI-HRMS spectrum of the C-20 enol-TMS ether of S42 (**1-C20-TMS**) depicted in **Figure 19**. (a) Formation of fragment ions at *m/z* 143 and *m/z* 209. (b) Formation of fragment ions at *m/z* 278 and *m/z* 263. Accurate ion masses are provided in **Table 5**.

Additionally, a D-ring fragmentation of **1-C20-TMS**, accompanied with a shift of 2 hydrogens observed at the ion at *m/z* 353 explains the formation of the abundant ions $[C_7H_{15}OSi]^{+}$ and $[C_{16}H_{17}]^{+}$ at *m/z* 143 and 209 by the loss of the complementary neutrals (see **Scheme 43**).[98b, 105a, 108b]

Finally, the ion at *m/z* 143 found in the EI-HR mass spectrum of the C-20 enol-TMS ether S42 derivative (**1-C20-TMS**) (**Figure 19**), contains silicon, *i.e.* $[C_7H_{15}OSi]^{+}$ (**Scheme 43**) and differs insofar from the isobaric ion formed from the molecular radical cation $[M]^{+\bullet}$ of S42 (**1**) (see **Figure 17A** and **Scheme 40A**),

which is $[C_{11}H_{11}]^+$ according to the accurate ion mass measurements (compare **Table 3** and **Table 5**.

GC-EI-HRMS analysis of S42-C17-TMS(*E*/*Z*)

The two spectra of **1-C17-TMS(*E*)** and **1-C17-TMS(*Z*)** are virtually identical, and cannot be differentiated by GC-MS. It is remarkable that the abundance of the fragment ion at *m/z* 278 ion is substantially reduced in the EI-HRMS spectra of the two S42 C-17 enol TMS ether diastereomers (**1-C17-TMS(*E*/*Z*)**) (**Figure 18C** and **D**, **Figure 20**) compared to the spectrum of the C20 enol-TMS ether isomer (**1-C20-TMS**) in **Figure 18B.**

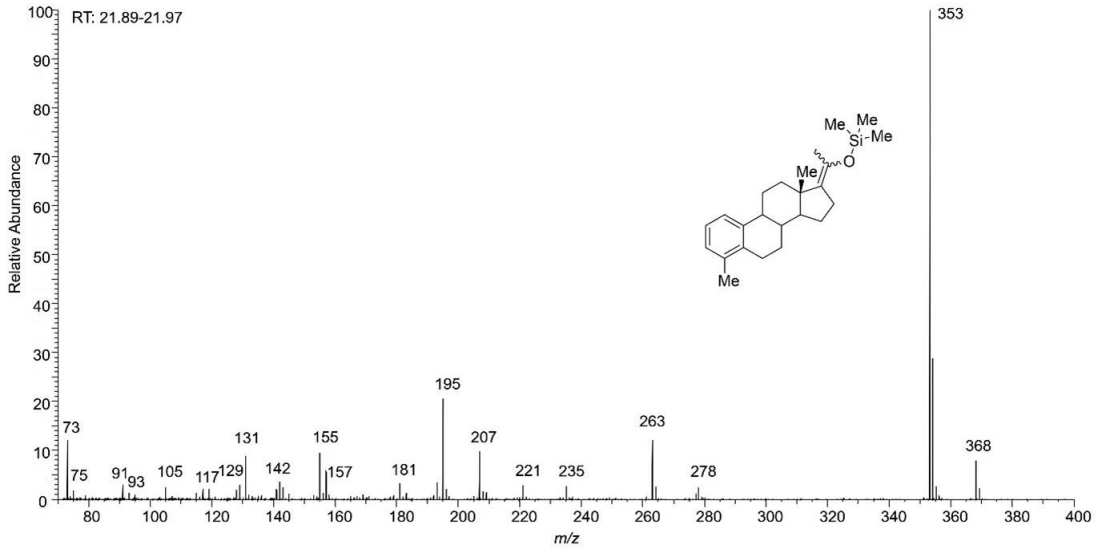

Figure 20. GC-EI-HRMS analysis and spectrum of **1-C17-TMS(*E*/*Z*).** The spectrum refers to fraction at RT: 21.78 min. The sample was analyzed at the University of Cologne with a GC temperature program of 120(5)-10-320(5).

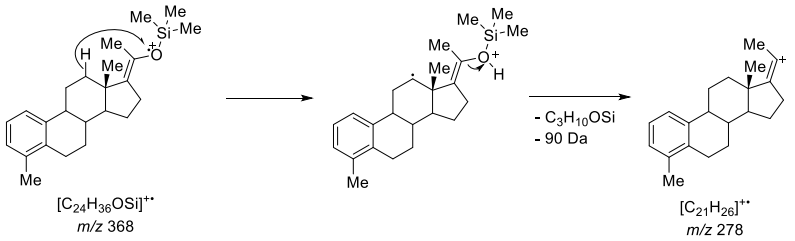

Scheme 44. Formation and fragmentation pathway to the **1-C17-TMS(*E*/*Z*)** fragment ion at *m/z* 278. A hydrogen can be rearranged from C12.

This finding suggests that the hydrogen from C17 of **1-C20-TMS** is crucial for the formation of the ion at *m/z* 278 and preferably transferred as shown in

Scheme 41. Instead a hydrogen can be rearranged from C12 as shown for the d3 isotopologues of the S42-C17 TMS diastereomers (**1-C17-TMS(*E*/*Z*)** and **1-**d3-C17-TMS(*E*/*Z*)) (compare **Figure 20** with **Figure 21C**, **Scheme 44** and **Scheme 46**).

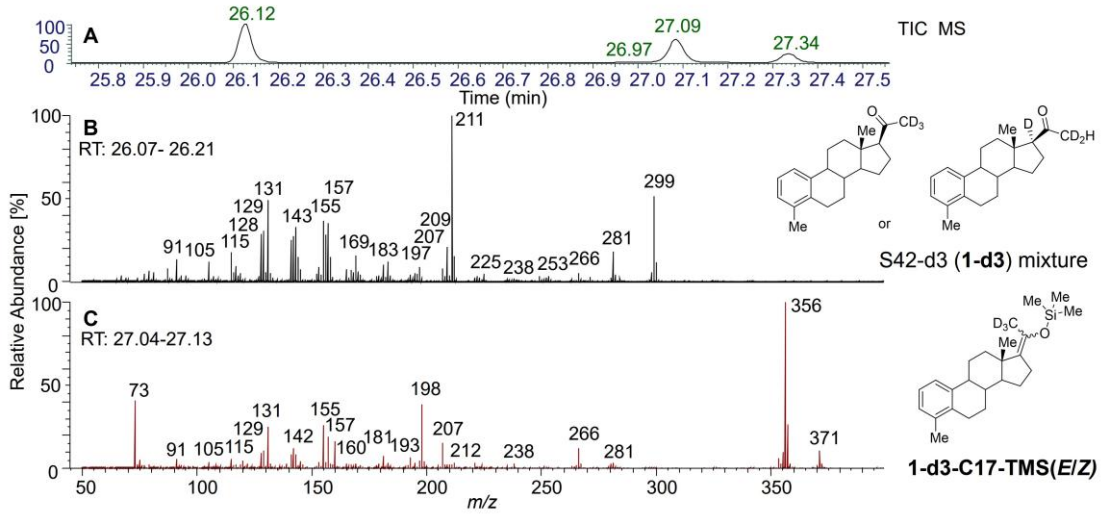

Figure 21. GC-EI-HRMS analysis of a S42-d3 (**1-d3**) compared with a S42-d3-C17 enol TMS derivative (**1-d3-C17-TMS(*E*/*Z*)**). (A) The GC separation indicates 4 components and the EI-HRMS spectra evidence the presence of a large portion of unreacted S42-d3 (**1-d3**) (RT: 26.12 min) besides three deuterated S42-enol TMS ether derivatives (RT: 26.97, 27.09, 27.34 min). (B) Mass spectrum of S42-d3 (**1-d3**). (C) Mass spectrum of S42-d3-C17 enol TMS derivative (**1-d3-C17-TMS(*E*/*Z*)**). Details of the GC temperature program, the stationary phase and the GC-EI-HRMS results of the other two S42-d1/3-TMS isomers (**1-d3-C17-TMS(*E*/*Z*)**; **1-d1-C20-TMS**; **1-d1-C20-TMS**) are provided in the Experimental part. The sample was analyzed at University of Cologne.

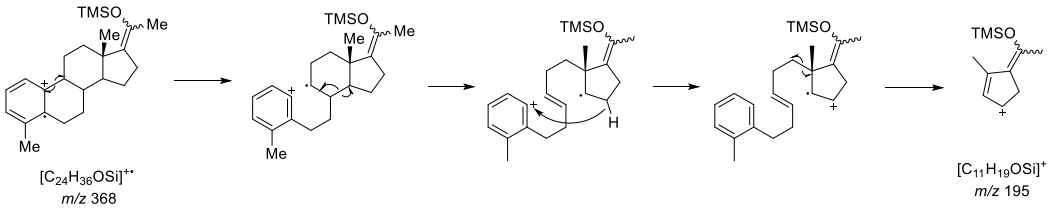

Scheme 45. The D ring fragmentation pathway observed in the GC-EI-HRMS spectra of both C-17 enol-TMS ether of S42 (1-C17-TMS(*E*/*Z*)) leading to the significant silicon containing fragment ion $[C_{11}H_{19}OSi]^+$ at *m/z* 195 as observed in **Figure 20**.[19,26] Accurate ion masses are provided in **Table 3**.

Significant for the EI-HRMS spectra of the two S42 C-17 enol-TMS ether diastereomers (**1-C17-TMS(*E*/*Z*)**) is a prominent ion $[C_{11}H_{19}OSi]^+$ at *m/z* 195 (**Scheme 45**) which is generated via a reaction sequence starting from an A-ring ionized molecular ion as **Scheme 45** illustrates (see **Table 6** for accurate ion mass of *m/z* 195).

Table 6. Ions found in the EI-HRMS spectrum of the S42 C-17 enol-TMS ether derivative of S42 (1-C17-TMS(*E*/*Z*)) presented in **Figure 18C** and **D**. The sample was analyzed at German Sport University Cologne.

S42-C17-TMS ($C_{24}H_{36}OSi$)	Nominal mass [Da]	Composition	Theo. Mass [Da]	Accurate ion mass measured [Da]	Error (ppm)
$[M]^{+\bullet}$	368	$[C_{24}H_{36}OSi]^{+\bullet}$	368.2530	368.2533	0.29
$[M\text{-}Me^{\bullet}]^{+}$	353	$[C_{23}H_{33}OSi]^{+}$	353.2295	353.2300	0.45
$[M\text{-}TMSOH\text{-}Me^{\bullet}]^{+}$	263	$[C_{20}H_{23}]^{+}$	263.1794	263.1798	0.38
$[M\text{-}TMSOH\text{-}C_3H_7^{\bullet}]^{+}$	235	$[C_{18}H_{19}]^{+}$	235.1481	235.1483	0.18
	221	$[C_{17}H_{17}]^{+}$	221.1325	221.1323	-0.19
	209	$[C_{12}H_{21}OSi]^{+}$	209.1356	209.1357	0.06
	207	$[C_{16}H_{15}]^{+}$	207.1168	207.1169	0.06
	195	$[C_{11}H_{19}OSi]^{+}$	195.1200	195.1202	0.21
	193	$[C_{15}H_{13}]^{+}$	193.1012	193.1010	-0.17
	181	$[C_{14}H_{13}]^{+}$	181.1012	181.1012	-0.01
	157	$[C_8H_{17}OSi]^{+}$	157.1043	157.1044	0.06
	157	$[C_{12}H_{13}]^{+}$	157.1012	157.1012	0.02
	155	$[C_{12}H_{11}]^{+}$	155.0855	155.0856	0.03
	142	$[C_{11}H_{10}]^{+}$	142.0777	142.0778	0.11
	131	$[C_{10}H_{11}]^{+}$	131.0855	131.0856	0.10
	105	$[C_8H_9]^{+}$	105.0699	105.0700	0.16
	91	$[C_7H_7]^{+}$	91.0542	91.0544	0.13
	75	$[C_2H_7OSi]^{+}$	75.0261	75.0262	0.12
	73	$[C_3H_9Si]^{+}$	73.0468	73.0469	0.10

GC-EI-HRMS analysis of S42-TBDMS

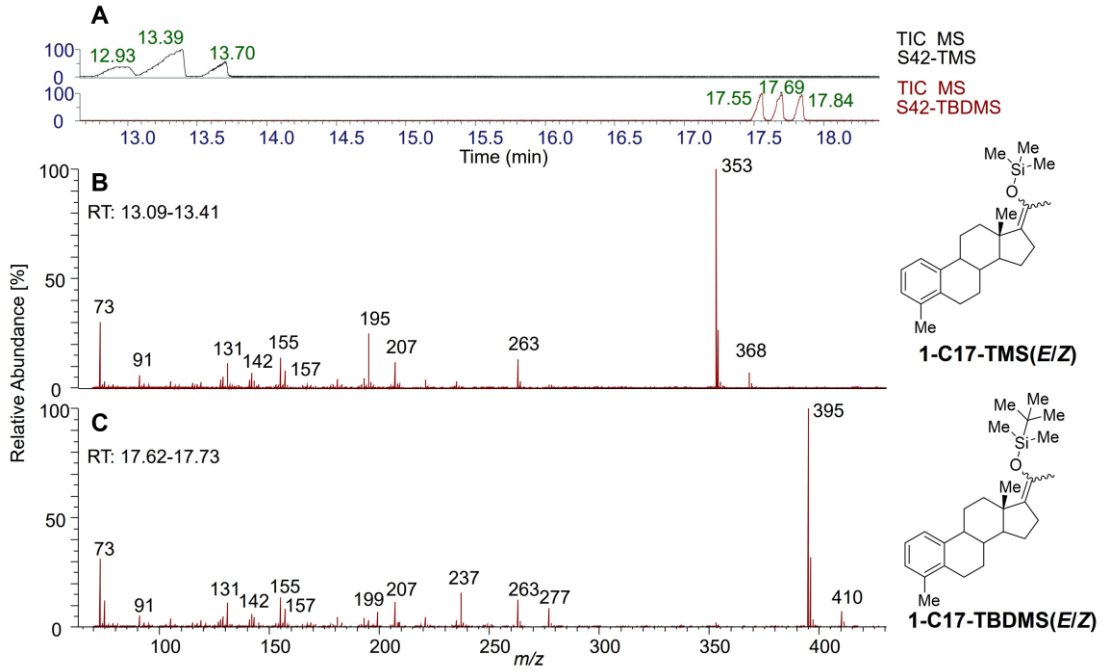

Figure 22. Comparison of GC-EI-HRMS results obtained for S42 C-17 enol-TMS ether (**1-C17-TMS(*E*/*Z*)**) and S42 C17 enol S42-TBDMS (**1-C17-TBDMS(*E*/*Z*)**). (A) Upper traces total ion currents TICs documenting the separation of the three isomers. (B) Spectrum of substance **1-C17-TMS(*E*/*Z*)**. (c) Spectrum of substance **1-C17-TBDMS(*E*/*Z*)**. (GC-EI-HRMS results of the two pairs of TMS and TBDMS isomers are provided in the Appendix: **Figure A49** to **Figure A53**. Temperature program and other details of the GC separations are provided). The samples were analyzed at German Sport University Cologne.

The comparison of the GC-EI-HRMS results obtained for S42-TMS (**1-C20-TMS**, **1-C17-TMS(*E*/*Z*)**) with S42-TBDMS ether isomers (**1-C20-TBDMS**, **1-C17-TBDMS(*E*/*Z*)**) clearly confirms the origin and the structure of the fragment ions as discussed above (compare **Figure 22**, see also **Figure A49** to **Figure A53** in the Appendix).

An exemplary case is the mass shifted D-ring fragment ion $[C_{11}H_{19}OSi]^+$ at *m/z* 195 of the S42 C17 enol-TMS ether (**1-C17-TMS(*E*/*Z*)**) (**Figure 22**) by 42 Da to *m/z* 237 in the spectrum of the S42 C17 enol-TBDMS ether (**1-C17-TBDMS(*E*/*Z*)**) (**Figure 22C**). Besides the correct accurate ion mass this result is strong evidence for the D-ring fragment structure assignment.

Additionally, we find that the signal at *m/z* 157 in the EI-HRMS spectrum of the S42-TBDMS ether isomers (**1-C17-TBDMS(*E*/*Z*)**) evidences the exclusive presence of the hydrocarbon species $[C_{12}H_{13}]^+$. The isobaric silicon containing ion $[C_8H_{17}O^{28}Si]^+$ at *m/z* 157 which is additionally present in the EI-HRMS spectrum of the S42 enol-TMS ether ions (**1-C17-TMS(*E*/*Z*)**) is shifted in the spectrum of **1-C17-TBDMS(*E*/*Z*)** to *m/z* 199 (compare **Table 6**, **Figure 22** and **Figure A52** and **Figure A53** in the Appendix).

GC-EI-HRMS analysis of S42-d3-TMS isotopologues

The GC-EI-HRMS analysis of S42-d3-C17 enol-TMS ether (**1-d3-C17-TMS(*E*/*Z*)**) (**Figure 23B**) is also fully consistent with the fragment ion structures outlaid above for the silyl ether derivatives as **Figure 23B** and **Scheme 46** illustrate.

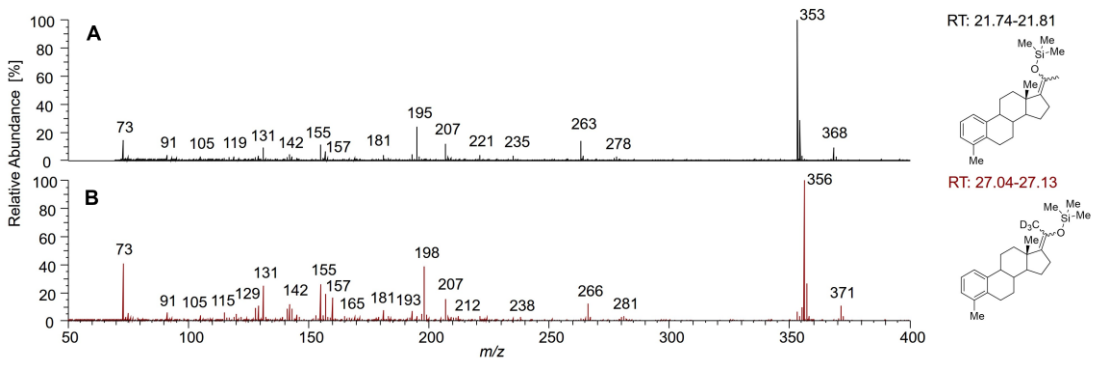

Figure 23. GC-EI-MS spectra of **1-C17-TMS(*E*/*Z*)** and a S42-d3-C17 enol TMS derivative (**1-d3-C17-TMS(*E*/*Z*)**). The sample was analyzed at University of Cologne.

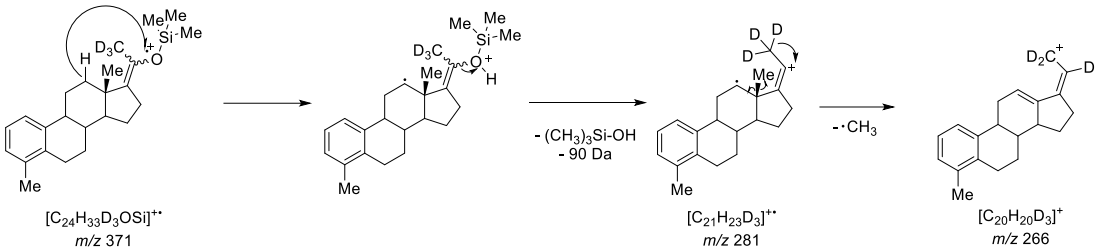

Scheme 46. Formation and fragmentation pathway to the d3 labeled fragment ion at *m/z* 281 and subsequently that of *m/z* 266 found in the GC-EI-HRMS spectrum of the C17 enol-TMS ether (**1-d3-C17-TMS(*E*/*Z*)**) shown in **Figure 23**.

In the spectrum of the S42-d3 C17 enol-TMS ether (**1-d3-C17-TMS(*E*/*Z*)**, the characteristic D-ring fragment ion $[C_{11}H_{19}OSi]^+$ at *m/z* 195 (see **Scheme 46** and **Figure 23A**), is mass shifted by 3 Da to *m/z* 198 $[C_{11}{}^1H_{16}{}^2H_3OSi]^+$ (see **Figure 23B**), evidencing trifold deuterium labeling at C21. The loss of a methyl radical $^{\bullet}CH_3$ from the TMS moiety conserves the three deuterium labels at terminal carbon C21 and leads to the most abundant fragment ion at *m/z* 356 in the spectrum of the S42-d3-C17 enol-TMS ether (**1-d3-C17-TMS(*E*/*Z*)**).

However, the observation of the $[C_{12}H_{11}]^+$ and $[C_{12}H_{13}]^+$ fragment ions at *m/z* 155 and 157 found in the EI-HRMS spectra of both S42-d3 C17 enol-TMS ether isomers (**1-d3-C17-TMS(*E*/*Z*)**) (**Figure 23B** and **Figure A49** to **Figure A51** in the Appendix) can also be interpreted as an indication for an alternative formation pathway without involvement of the intermediate ion at *m/z* 211 (compare **Scheme 38**), which is absent in **Figure 18B**, **C** and **D**.

The ion $[M\text{-}TMSOH]^{+\bullet}$ was discovered at *m/z* 281 (**Figure 23B**). Loss of TMSOH instead of TMSOD indirectly supports our assumption that the migrated hydrogen lost with TMSOH originates from C12 (**Scheme 46**). The subsequent loss of a methyl radical delivers the resonance-stabilized even electron ion at *m/z* 266.

GC-EI-HRMS of S42-d7-C17-TMS (*E*/*Z*)

The GC-EI-HRMS analysis of the A,B-ring labeled S42-d7-TMS derivative (**1-d7-C20-TMS**, **1-d7-C17-TMS(*E*/*Z*)**) concludes the study with additional evidence for the ion structure assignments (**Figure A54** in the Appendix).

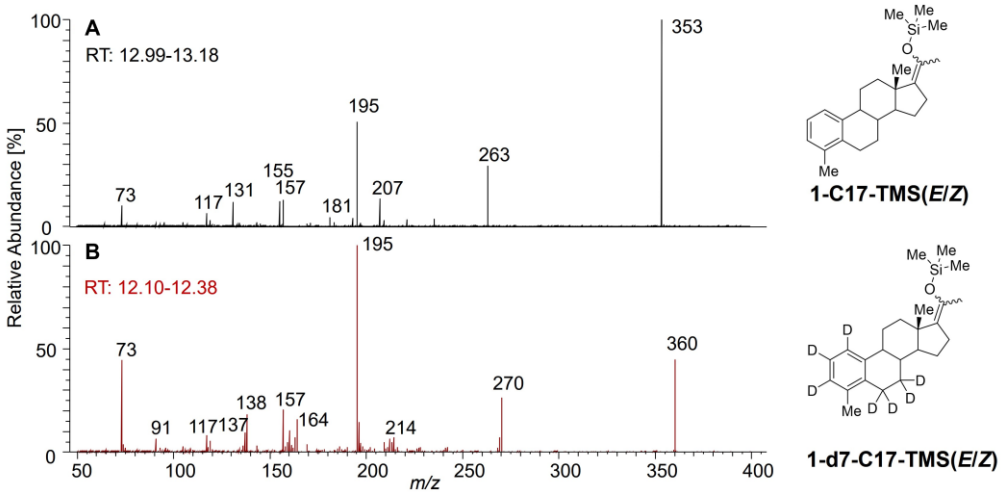

Figure 24. GC-EI-MS^2-product ion spectra of mass selected molecular ions of the S42 C17 enol-TMS-ether (**1-C17-TMS(*E*/*Z*)**) at *m/z* 368 and of S42-d7 C17 enol-TMS-ether (**1-d7-C17-TMS(*E*/*Z*)**) at *m/z* 375 performed in the HCD collision cell of a *GC-Q Exactive Orbitrap* instrument. (A) EI MS^2 spectrum of **1-C17-TMS(*E*/*Z*)**. (B) EI MS^2 spectrum of **1-d7-C17-TMS(*E*/*Z*)**. The samples were analyzed at German Sport University Cologne. Accurate ion masses are provided in **Table 7** and **Table 8**.

Table 7. Product ions observed in the MS^2-product ion spectrum of the mass selected molecular ion of the S42 C-17 enol-TMS-ether (**1-C17-TMS(*E*/*Z*)**) at *m/z* 368. The sample was analyzed at German Sport University Cologne.

MS^2 S42-C17-TMS ($C_{24}H_{36}OSi$)	Nominal mass [Da]	Composition	Theo. Mass [Da]	Accurate ion mass measured [Da]	Error (ppm)
$[M\text{-}Me^{\bullet}]^+$	353	$[C_{23}H_{33}OSi]^+$	353.2295	353.2300	0.43
$[M\text{-}TMSOH\text{-}Me^{\bullet}]^+$	263	$[C_{20}H_{23}]^+$	263.1794	263.1798	0.42
$[M\text{-}C_{12}H_{15}^{\bullet}]^+$	209	$[C_{12}H_{21}OSi]^+$	209.1356	209.1365	0.86
	207	$[C_{16}H_{15}]^+$	207.1168	207.1170	0.20
	195	$[C_{11}H_{19}OSi]^+$	195.1200	195.1202	0.27
	181	$[C_{14}H_{13}]^+$	181.1012	181.1012	0.03
	171	$[C_{13}H_{15}]^+$	171.1168	171.1169	0.06
	169	$[C_9H_{17}OSi]^+$	169.1043	169.1047	0.39
	157	$[C_8H_{17}OSi]^+$	157.1043	157.1046	0.28
	157	$[C_{12}H_{13}]^+$	157.1012	157.1014	0.18
	156	$[C_{12}H_{12}]^{+\bullet}$	156.0934	156.0935	0.20
	155	$[C_{12}H_{11}]^+$	155.0855	155.0857	0.17
	145	$[C_{11}H_{13}]^+$	145.1012	145.1013	0.14
	143	$[C_7H_{15}OSi]^+$	143.0887	143.0889	0.23
	143	$[C_{11}H_{11}]^+$	143.0855	143.0857	0.22
	131	$[C_{10}H_{11}]^+$	131.0855	131.0857	0.19
	117	$[C_5H_{13}OSi]^+$	117.0730	117.0732	0.19
	73	$[C_3H_9Si]^+$	73.0468	73.0469	0.10

Table 8. Product ions observed in the MS^2-product ion spectrum of mass selected molecular ions of the S42-d7 C-17 enol-TMS ether (**1-d7-C17-TMS(*E*/*Z*)**) at *m/z* 375. The sample was analyzed at German Sport University Cologne.

MS^2 S42-d7-TMS ($C_{24}H_{29}D_7OSi$)	Nominal mass [Da]	Composition	Theo. mass [Da]	Accurate ion mass measured [Da]	Error (ppm)
$[M\text{-}Me^{\bullet}]^+$	360	$[C_{23}H_{26}D_7OSi]^+$	360.2735	360.2737	0.23
$[M\text{-}TMSOH\text{-}Me^{\bullet}]^+$	270	$[C_{20}H_{16}D_7]^+$	270.2234	270.2239	0.51
$[M\text{-}C_8H_{21}OSi^{\bullet}]^+$	214	$[C_{16}H_8D_7]^+$	214.1608	214.1614	0.67
$[M\text{-}C_8H_{19}DOSi^{\bullet}]^+$		$[C_{16}H_{10}D_6]^+$	214.1623		-0.87
	212	$[C_{16}H_{10}D_5]^+$	212.1482	212.1488	0.56
	209	$[C_{12}H_{21}OSi]^+$	209.1356	209.1358	0.20
	195	$[C_{11}H_{19}OSi]^+$	195.1200	195.1203	0.29
	169	$[C_9H_{17}OSi]^+$	169.1043	169.1045	0.16
	164	$[C_{12}H_6D_7]^+$	164.1451	164.1424	-2.69
	160	$[C_{12}H_6D_5]^+$	160.1169	160.1172	0.25
	157	$[C_8H_{17}OSi]^+$	157.1043	157.1045	0.18
	143	$[C_7H_{15}OSi]^+$	143.0887	143.0888	0.18
	138	$[C_{10}H_4D_7]^+$	138.1295	138.1296	0.16
	137	$[C_{10}H_5D_6]^+$	137.1232	137.1234	0.18
	117	$[C_5H_{13}OSi]^+$	117.0730	117.0732	0.20
	73	$[C_3H_9Si]^+$	73.0468	73.0470	0.15

To further scrutinize the fragmentation pathways we conducted EI-MS^2 product ion experiments of the molecular ion of S42 C17 enol-TMS-ether (**1-C17-TMS(*E*/*Z*)**) and the one of the S42-d7-C17-enol-TMS-ether derivative (**1-d7-C17-TMS(*E*/*Z*)**) by collision induced dissociation in a multipole collision cell (HCD, CID) with accurate ion mass determination as presented in (see also **Figure 24**, **Table 7** and **Table 8**).[49a]

The significant mass shift of 7 Da found in selected fragment ions is in complete agreement with the fragment ion structure proposals presented. This holds true for the fragment ions stemming from trimethyl silanol loss from the TMS moiety at ring D (**Scheme 44** and **Scheme 45**).

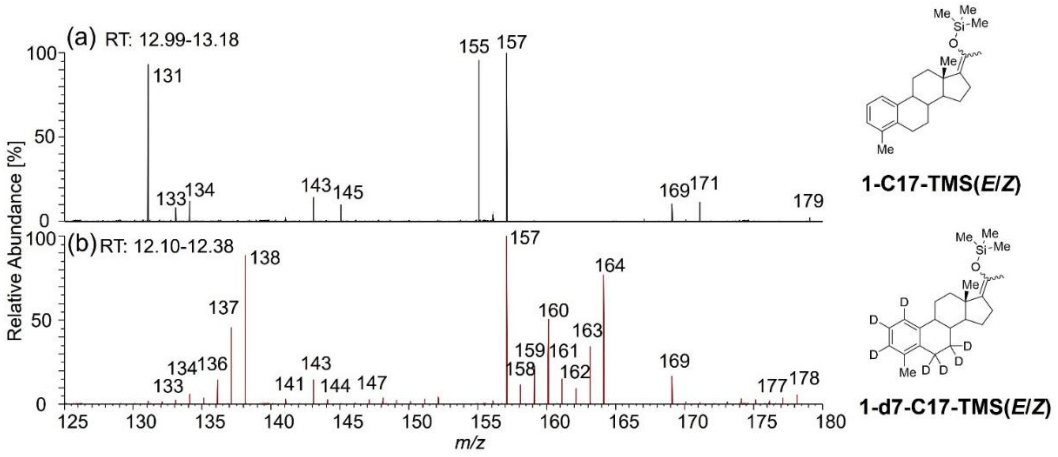

Figure 25. Close-up of the mass range *m/z* 125 to *m/z* 180 of the GC-EI MS^2-product ion spectra of mass selected molecular ions of the S42 C-17 enol-TMS-ether (**1-C17-TMS(*E*/*Z*)**) and of S42-D7 C-17 enol-TMS-ether (**1-d7-C17-TMS(*E*/*Z*)**) shown in **Figure 7**. (a) MS^2 spectrum of **1-C17-TMS(*E*/*Z*)**. (b) MS^2 spectrum of **1-d7-C17-TMS(*E*/*Z*)**. The samples were analyzed at the German Sport University Cologne.

All ions containing the steroid A,B-ring system, e.g. $[C_{10}H_{11}]^+$ at *m/z* 131, $[C_{12}H_{13}]^+$ at *m/z* 157, and $[C_{20}H_{23}]^+$ at *m/z* 263 are shifted accordingly to *m/z* 138, 164, and 270 (**Figure 24** and **Figure 25**, compare **Scheme 38** and **Scheme 39**), while the silicon containing fragment ion $[C_{11}H_{19}OSi]^+$ at *m/z* 195 is found in both spectra of **Figure 24** without any mass shift (compare **Scheme 45**). The observation of the ion at *m/z* 157 in the product ion spectrum of the molecular ion of S42-d7 C17 enol-TMS-ether derivative (**1-C17-TMS(*E*/*Z*)**) shown in **Figure 25A** and **Figure 25B**) indicates the presence of a D-ring fragment $[C_8H_{17}OSi]^+$, while the ion at *m/z* 160 in **Figure 25B** results from a d5 isotopologue of the ion $[C_{12}{}^1H_{11}]^+$ at *m/z* 155 found in **Figure 25A**. The latter ion is mass shifted by 5 Da to *m/z* 160 and is found with the composition $[C_{12}{}^1H_6{}^2H_5]^+$ in **Figure 25B**.

4.1.7 GC-EI-HRMS investigations of S42 (**1**) and of synthetic derivatives

A comprehensive GC-EI-HRMS examination of the synthetic 20-keto-steroid S42 (**1**) was conducted. A GC-EI-HRMS study of an array of silyl derivatives as well as of selectively labelled isotopologues of S42 delivered a compendious insight into the fragmentation behavior of the new steroid S42 (**1**). In an exemplary case study, we carefully examined the water-loss reaction found in

the EI-MS spectrum of S42 (**1**). As clearly evidenced γ-positioned hydrogens at either C12 or C18 of S42 (**1**) are rearranged to the carbonyl oxygen in a *McLafferty*-type rearrangement reaction which precedes the ultimate water-loss and the formation of the respective product ion at *m/z* 278. Furthermore, we deduce fragmentation patterns of the respective molecular ions and propose product ion formation mechanisms on the basis of accurate ion mass measurements of all relevant ions as well as by comparison with GC-EI-HRMS data of selectively ^{2}H-labelled derivatives. Furthermore, synthetic TMS and TBDMS derivatives of S42 (**1**) were included in our GC-EI-HRMS study. Concluding, we present an extensive and fundamental GC-EI-HRMS data set to serve as a firm basis for the development of selective and sensitive detection protocols for application in forensic detection of this new compound.

4.2 S42-C20/C6/C7-OH synthesis and investigation

Before performing the *in vitro* experiments, the phase I metabolism was simulated by *BioTransformer 3.0* (https://biotransformer.ca/) developed by *Wishart et al.,* which indicated a high probability for hydroxylation at the steroidal A-, B- and D-rings of S42 (**1**).[110] Accordingly, three hydroxylated S42 derivatives at ring D and B were synthesized: S42-C20-OH (**2**), S42-C6ß-OH (**3**) and S42-C7α-OH (**4**) as reference materials (see **Scheme 47**). The synthesis of the mono-hydroxylated S42 derivatives **2-4** was accomplished employing established synthetic routes.[111],[101]

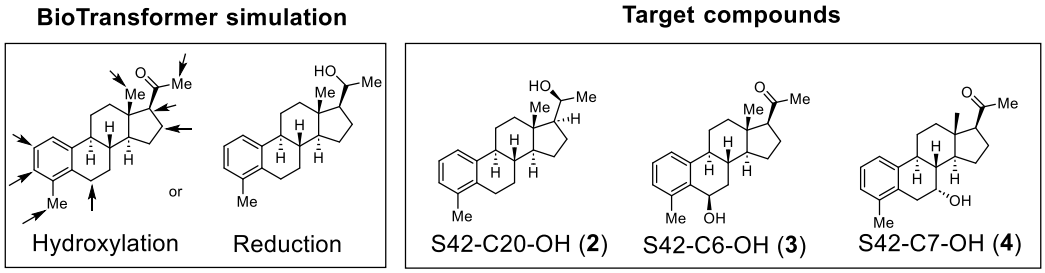

Scheme 47. *BioTransformer 3.0* (https://biotransformer.ca/) proposed the hydroxylated and reduced position of S42 (**1**).[110] At the same time, the hydroxylation position at C6 and C7 were proposed based on the later phase I *in vitro* metabolism experiment (**section 4.3**). According to the simulation and the *in vitro* phase I experiment, the target compounds S42-C20-OH (**2**), S42-C6ß-OH (**3**) were aimed to be synthesized.

4.2.1 Synthesis of S42- C20/C6/C7-OH

Synthesis of S42-C20-OH (**2**)

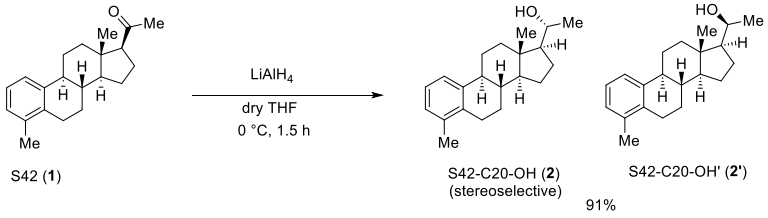

Scheme 48. Synthesis of S42-C20-OH (**2**) and S42-C20-OH' (**2'**) from S42 (**1**) by reduction with $LiAlH_4$.[101]

Stereoselective synthesis of S42-C20-OH (**2**) was accomplished by application of $LiAlH_4$, according to a protocol from *MacNevin et al.*[101] The configuration of S42-C20-OH (**2**) was confirmed by crystallization and XRD analysis.

Compound **2** was TMS derivatized and analyzed by GC-EI-MS, compared with the analysis results from the *in vitro* phase I experiments.

Synthesis of S42-C6ß-OH (**3**)

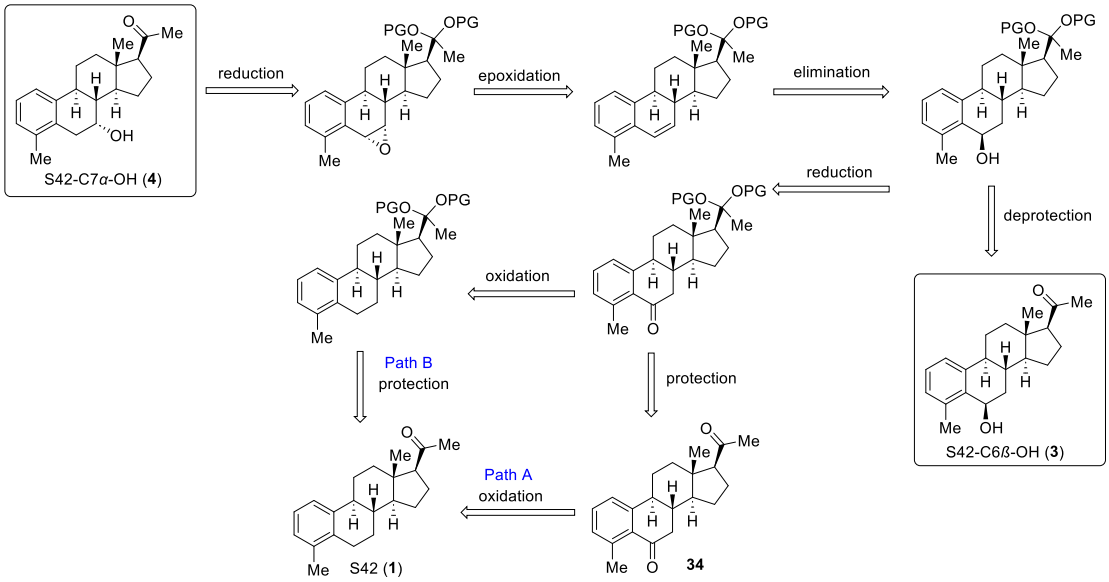

Scheme 49. Retro-synthesis plane of S42-C6ß-mono-OH (**3**) and S42-C7α-mono-OH (**4**) from S42 (**1**).

The retrosynthesis of S42-C6ß-mono-OH (**3**) and S42-C7α-mono-OH (**4**) are derived from the synthesis strategy reported by *Neto et al.*[111] The first step could be either benzylic oxidation (Path A) or C20 ketone protection (Path B). However, the ketal protection group is sensitive to moisture and acidic conditions, so initial oxidation (Path A) eliminates any concerns towards the acidity of oxidation reagents. Initial protection at C20 (Path B) necessitates selective ketone protection at either C20 or C6.

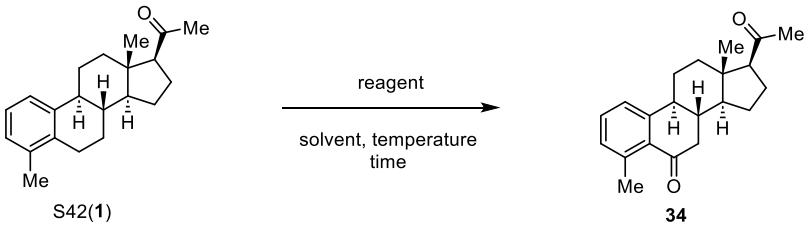

Scheme 50. Benzylic oxidation reactions were conducted to produce a C6 ketone **34**.

Table 9. Different oxidative agents were tested at small scale to synthesize a C6 ketone **34**.

Entry	Reagent	Solvent	Temp. (°C)	Time (h)	Yield	GC-EI-LRMS
1	CrO_3	AcOH/H_2O	r.t.	28	n.a.	n.a.
2	$KMnO_4$	benzene	85	3	trace (more byproducts)	RT=17.15 *m/z* =310
3	PCC/Celite	toluene	135	5	no full conversion	RT=18.013 *m/z* =310
4	PCC/Celite	benzene	90	8	37%	RT=18.013 *m/z* =310

Three different oxidative agents, CrO_3, $KMnO_4$, and pyridinium chlorochromate (PCC) were tested. It was found that PCC was most effective for benzylic oxidation to give product **34** with a yield of 37% (**Table 9**, entry 4). Celite was added with PCC to absorb tarry byproducts from PCC to maintain a homogeneous reaction mixture.[112]

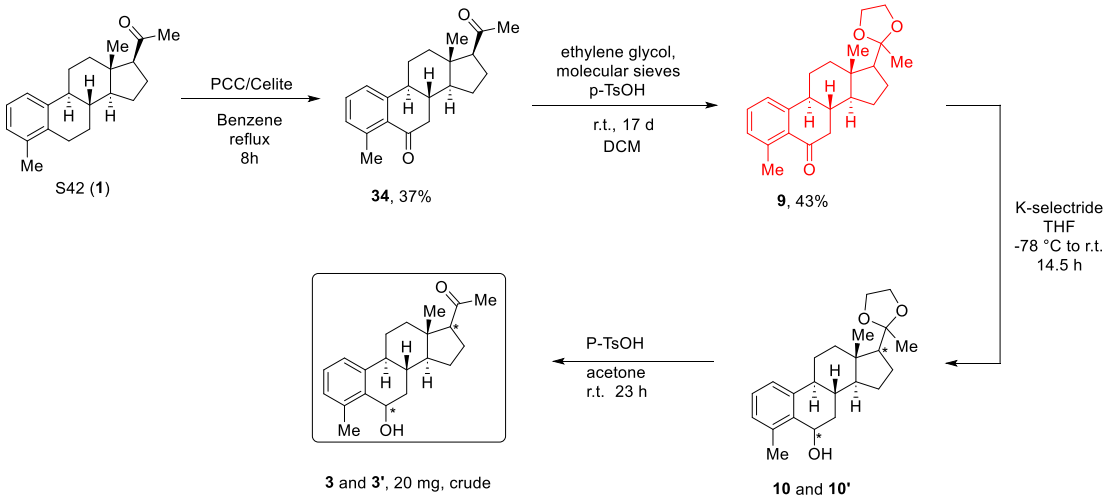

Scheme 51. Preliminary S42-C6-OH (**3** and **3'**) synthesis strategy. The procedure to produce compound **9** could not be reproduced.

The C6-ketone was successfully generated by PCC oxidation and underwent C20 selective protection in mild conditions at r.t. for 17 days to avoid any ketal formation at C6 position. The protected derivative **9** was reduced by K-selectride, which was a stereoselective reducing agent and C20-ketal **10** was deprotected to form a crude in 20 mg scale. The stereo structure was not confirmed by XRD analysis in this scale. It was attempted to repeat the reaction in larger scale; however successful synthesis could not be reproduced due to

overprotection at both C6 and C20 ketones. In addition, K-selektride was not an efficient reducing agent. Therefore, a different synthesis strategy of S42-C6*β*-OH (**3**) was developed according to pathway A sketched in **Scheme 49**.

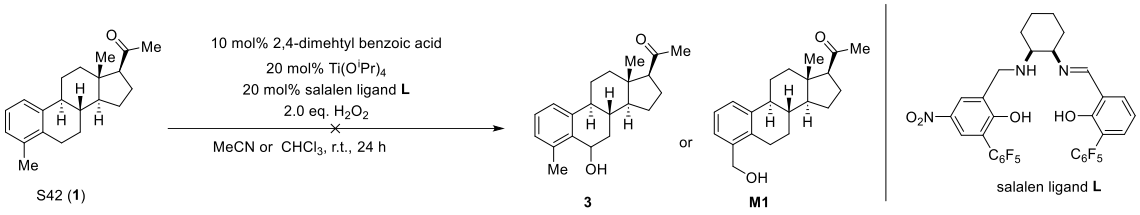

Scheme 52. The benzylic hydroxylation reaction failed by using Ti(O^{i}Pr)$_4$ catalyst with salalen ligand **L** that was developed by *Dr. Christina Wartmann*.[113]

Hydroxylation reaction at C6 position was attempted with the procedure and the titanium catalyst from *Wartmann et al*.[113] It is reported that this reaction works the best in acetonitrile, but acetonitrile could not totally dissolve the S42 (**1**) substrate. Therefore, the solvent was changed to $CHCl_3$. Unfortunately, both attempts failed.

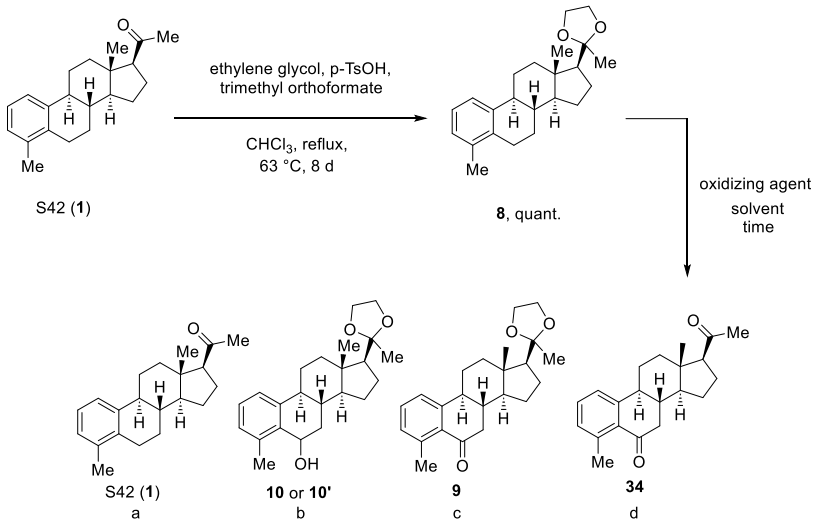

Scheme 53. Screening benzylic oxidation of C20 protected S42 (**1**) with different oxidizing agents.

Table 10 Screening of benzylic oxidation reaction by PCC, PDC/^{t}BuOOH, CrO_3/ 3,5-dimethyl pyrazole (DMP) under different conditions.

Entry	Oxidizing reagent	Temp. and time	Salt	Mixture ratio (GC-MS) a:b:c:d
1	PCC/celite	90 ºC, 10 h	NaOAc	0:0:0:1
2	PDC, *tert*-butyl hydroperoxide	10 to 25 ºC, o/n	-	2:3:5:0
3	PDC, *tert*-butyl hydroperoxide	10 to 25 ºC, o/n	NaOAc	0:1:1:0
4	PDC, *tert*-butyl hydroperoxide	10 to 25 ºC, o/n	NaOAc	trace after column chromatography (500 mg scale)
5	CrO_3/DMP	-14 ºC, 2 h	-	Only SM
6	CrO_3/DMP	0 ºC, 2 h r.t. o/n	NaOAc	SM and 1:0:2:3 (0:0:1:1.2 after column) Yield: 19%

The synthesis strategy was changed to first perform the protection and then the oxidation to avoid overprotection at both C6 and C20 ketone sites. PCC was not ideal for this purpose because PPC is an acidic oxidizing agent, which needs substantial heating to 92 °C to work. This harsh condition, however, led to deprotection of the C20 ketal group during oxidation (**Table 10**, entry 1). Therefore, the less acidic pyridinium dichromate (PDC) with NaOAc as a buffer salt was used instead to avoid deprotection and produce product **34** /(d) (see **Scheme 53**).[114] Unfortunately, only traces of products **10** or **10**' /(b) and **9** /(c) were generated, which were lost after column chromatography (**Table 10**, entry 4). Finally, the CrO_3/ 3,5-dimethyl pyrazole (DMP) was applied for oxidation at r.t. overnight (**Table 10**, entry 6). These reagents produced a mixture of the product, byproduct and precursor, but preparative column chromatography on silica gel allowed separation.

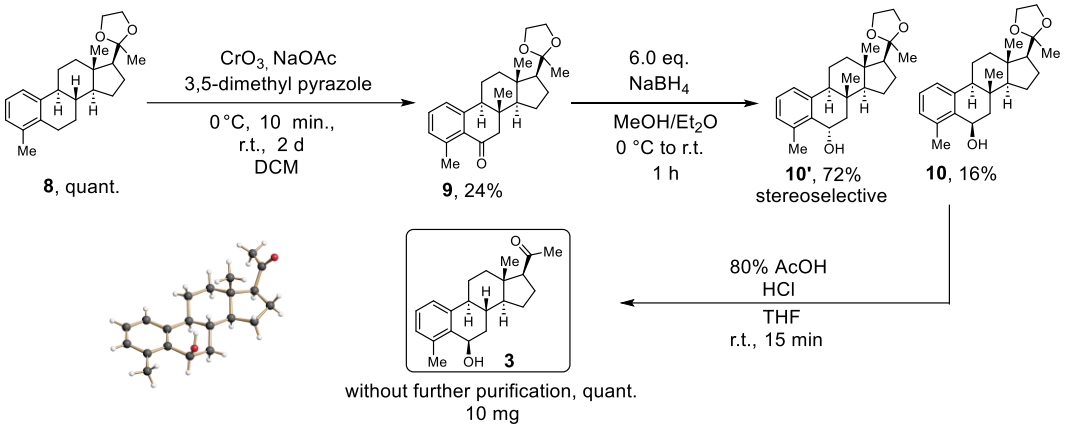

Scheme 54. Synthesis of S42-C6*β* (**3**)-OH by adapting the synthesis strategy from *Neto et al*.[111]

Final reduction reaction with $NaBH_4$, yielded the C20 protected *α* (stereoselective) and *β* epimers (**10** and **10'**) which were separated via column chromatography. Deprotection reaction under acidic conditions at r.t. generated S42-C6*β*-OH (**3**). The structure of the product was confirmed by XRD analysis.

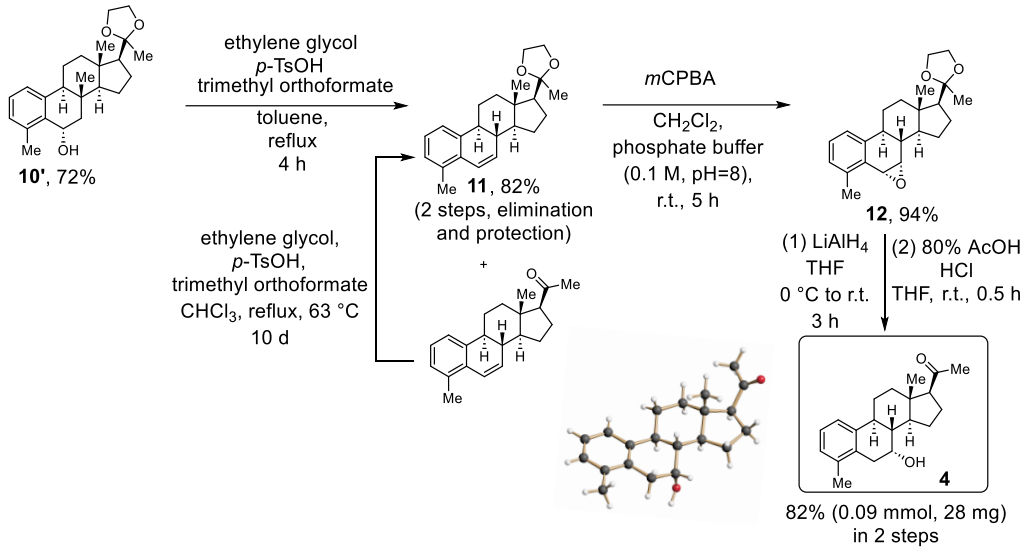

Scheme 55. Synthesis of S42-C7*α*-OH (**4**) from protected S42-C6*α*-OH (**1**), according to a synthetic strategy reported by *Neto et al*.[111]

The protected C6*β*-OH (**10'**) underwent elimination reaction to generate double bond at C6-C7. In the reaction, extra ethylene glycol, catalyst *p*-TsOH and trimethyl orthoformate were added to prevent C20 ketal deprotection. Since the deprotection reaction still occurred, C20 carbonyl group protection was repeated and a 2-step reaction yielded 82% of the compound **11**. Selective epoxidation was performed by *m*CPBA at pH=8. After reduction reaction with $LiAlH_4$ and C20 ketal protection, the target product S42-C7*β*-OH (**4**) was

accessible. It was fully characterized spectroscopically and via XRD crystallography.[111]

The synthesized hydroxyl S42 derivatives: S42-C20-OH (**2**), S42-C6ß-OH (**3**), and S42-C7α-OH (**4**) could be used as reference materials for comparing the results of *in vitro* and even *in vivo* experiments.

4.2.2 Characterization S42- C20/C6/C7-OH by GC-EI-HRMS

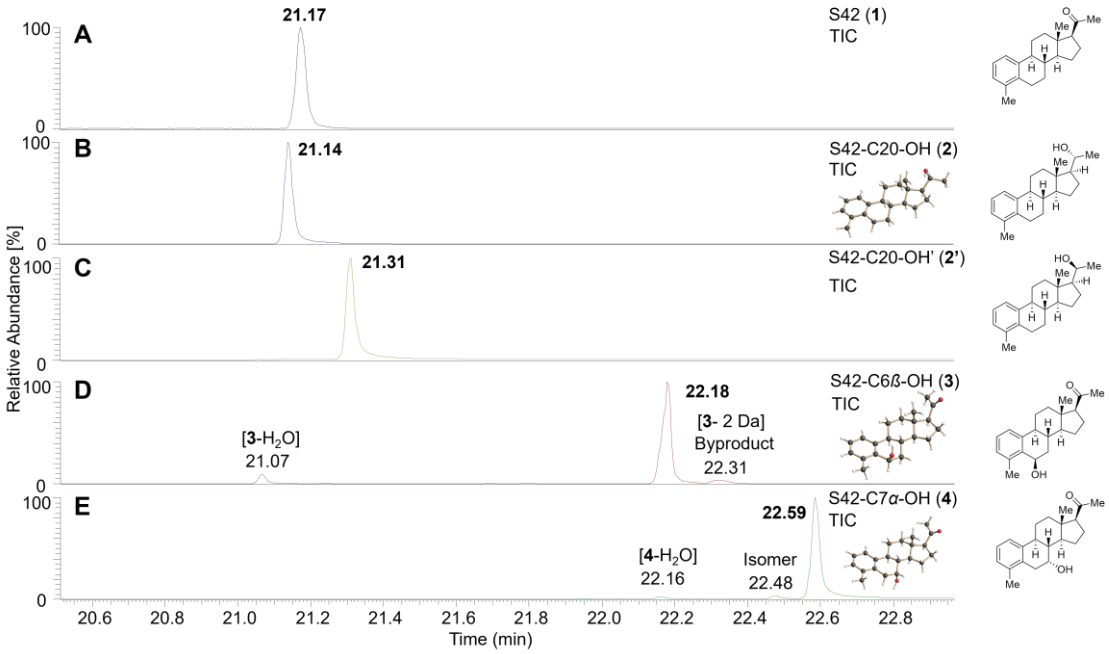

Figure 26. Total ion chromatograms (TIC) of S42 (**1**), S42-C20-OH (**2**) and (**2'**), S42-C6ß-OH (**3**) and S42-C7α-OH (**4**). Structures in panel B, D and E are deduced from X-ray crystallography. In panel D, a C6-C7 S42 olefine was found at RT: 21.07 min, while a byproduct was observed at RT: 22.31 min (Spectra of these byproducts are in the **Appendix 9.3.3**).

All synthetic hydroxyl S42 derivatives **2-4** were analyzed by GC-EI-HRMS. The chromatograms, MS spectra and the proposed fragment ions were compared as **Figure 26** and **Figure 27** illustrate.

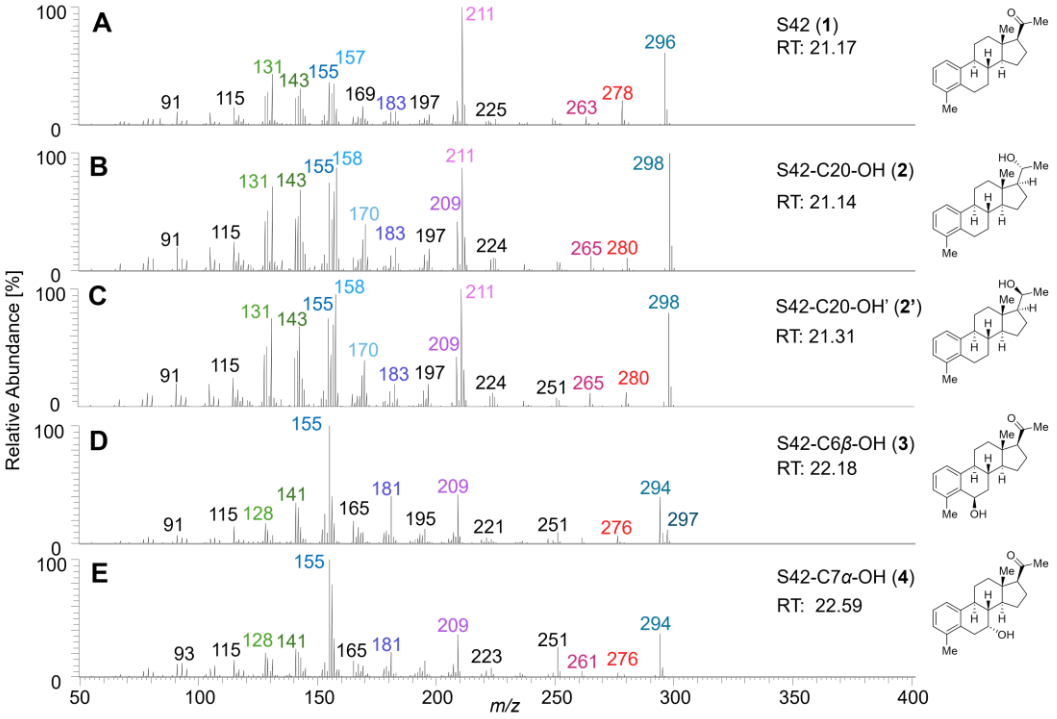

Figure 27. GC-EI HR mass spectra of S42 (**1**) in panel A, S42-C20-OH (**2 and 2'**) in panels B and C, S42-C6ß-OH (**3**) in panel D, and S42-C7*α*-OH (**4**) in panel E.

The EI HR MS spectra of the two epimers of S42-C20-OH (**2**) and (**2'**) show identical spectra (**Figure 27B** and **C**). However, the crystal structure of S42-C20-OH (**2**) allows the assignment of the absolute configuration at C20 as shown in **Figure 26B**. The fragmentation patterns of analytes **2** and **2'** are related to those found in the MS spectrum of S42 (**1**) (**Figure 27A**); compare **Figure 27**, panels A with B and C. Significant fragments of S42-C20-OH (**2**) can be derived from those of S42 (**1**) (See **Section 4.1.5**) as shown in **Figure 28** (panels **A** and **B&C**).[115]

The water-loss reaction of the molecular ion of S42 (**1**) leading to the fragment ion at *m/z* 278 (**Figure 28A**) is also found in the EI mass spectra of **2** and **2'** (here leading to the ion at *m/z* 280, **Figure 28B&C**). The subsequent loss of the C18-methyl group is suggested to deliver the closed-shell fragment ion at *m/z* 265 (see **Figure 27B** and **C** and ions in **Figure 28B&C**).

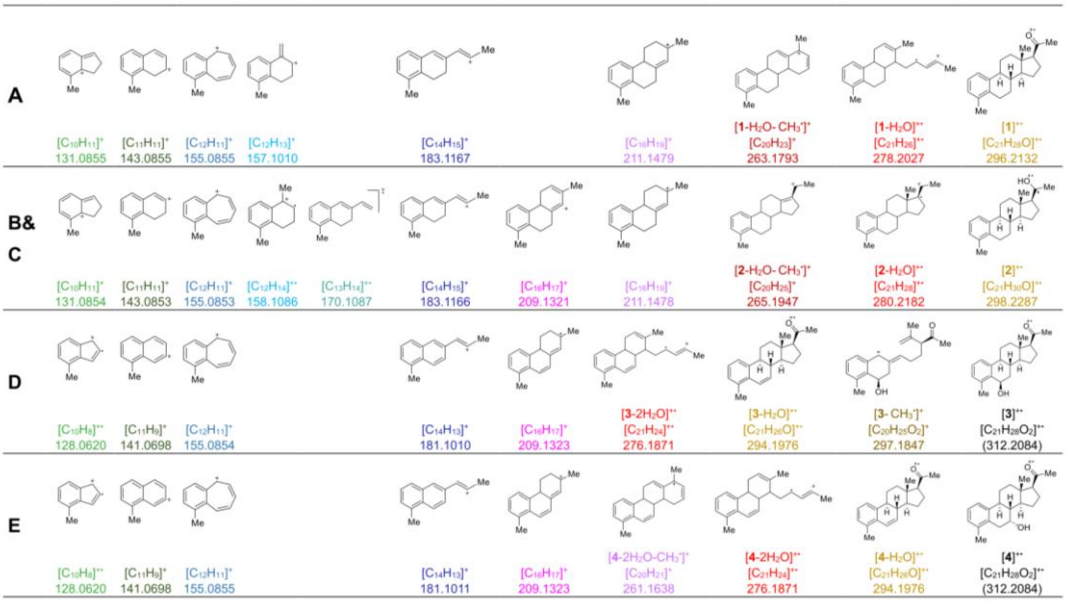

Figure 28. Ion structures suggested in accordance with the composition deduced from the accurate ion masses measured from S42 (**1**) in panel A, S42-C20-OH (**2**) and (**2'**) in panel B and C, S42-C6ß-OH (**3**) in panel D and S42-C7*α*-OH (**4**) in panel E, obtained from the GC-EI HR mass spectra presented in **Figure 27**. Accurate ion masses are presented in **Table A1** to **Table A4** in Appendix.

The ions at *m/z* 211 and *m/z* 209 are proposed to originate from D-ring fragmentation, followed by the formation of A,B-ring fragments at *m/z* 155, 143 and 131, which are found in the EI-HR MS data of S42 (**1**) and in those of the S42-C20-OH compounds (**2** and **2'**) (**Figure 28A** and **B&C**). The radical cationic ion of the steroidal A,B-ring system at *m/z* 158 observed in the spectra of both S42-C20-OH analytes (**2**) and (**2'**) (**Figure 27**, **Figure 26B** and **C**) represents a distinctive difference from the spectrum of S42 (**1**) (**Figure 27A**).

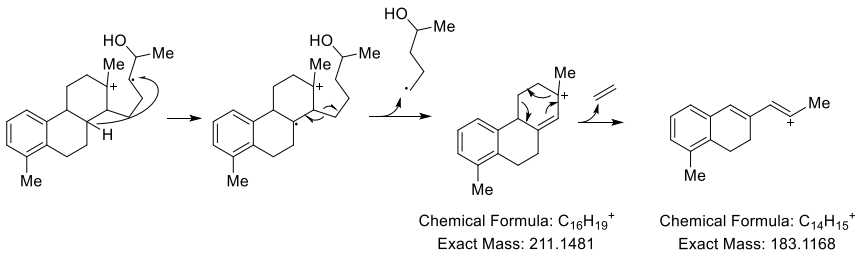

Scheme 56. EI-MS Fragmentation pathway with an initial cleavage of the C13-C17 bond, followed by a radical loss and a *retro-Diels Alder* (*RDA*) reaction, ultimately leading to the fragment ion at *m/z* 183 from S42-C20-OH (**2** and **2'**).

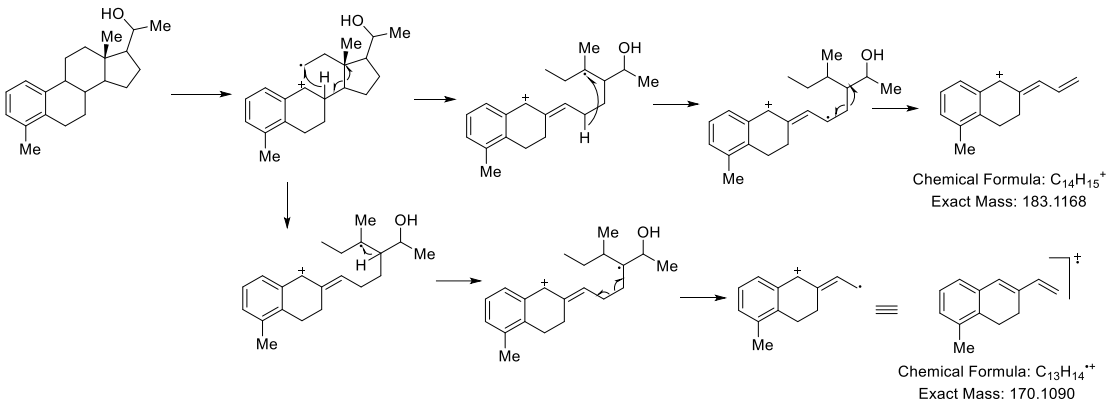

Scheme 57. Alternative EI-MS fragmentation pathway with an initial benzylic cleavage, hydrogen atom migration steps, and ultimate bond cleavage reactions leading to the ions at *m/z* 183 and *m/z* 170 from S42-C20-OH (**2** and **2'**).

Additionally, the EI spectra of both S42-C20-OH analytes (**2** and **2'**, see **Figure 27B** and **C**) show fragment ions at *m/z* 183 and at *m/z* 170. We propose fragmentation pathways to explain the formation of the latter ions in **Scheme 56** and **Scheme 57**.[105c, 116]

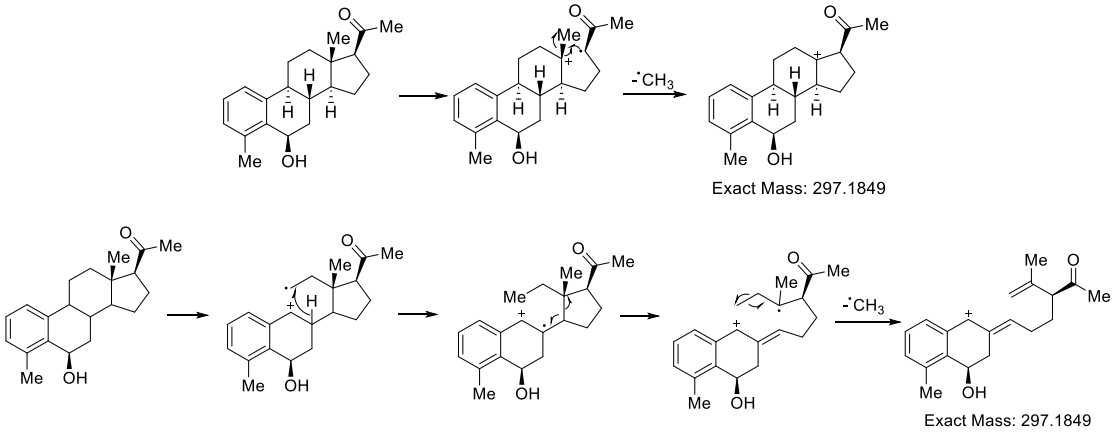

Scheme 58. Proposed fragmentation pathways for the elimination of a methyl radical $^{\bullet}CH_3$ from the molecular ion S42-C6ß-OH (**3**) according to *Djerassi* and *Budzikiewicz*.[105c, 116] The [**3**-$^{\bullet}CH_3$]$^{+}$ is found at *m/z* 297 in the GC-EI-HRMS spectrum of **3** as shown in **Figure 27D**.

Next, the GC-EI HR MS spectrum of S42-C6*ß*-OH (**3**) was investigated (see **Figure 27D**). First of all, the absence of the radical cationic molecular ion [**3**]$^{+\bullet}$ of S42-C6*ß*-OH (**3**) at *m/z* 312 in the EI mass spectrum (see **Figure 27D**) was noted. Instead, ions resulting from the loss of a methyl group [**3**-$^{\bullet}CH_3$]$^{+}$ at *m/z* 297 and a water molecule [**3**-H_2O]$^{+\bullet}$ at *m/z* 294 are found with highest *m/z* value (see **Figure 28D**).

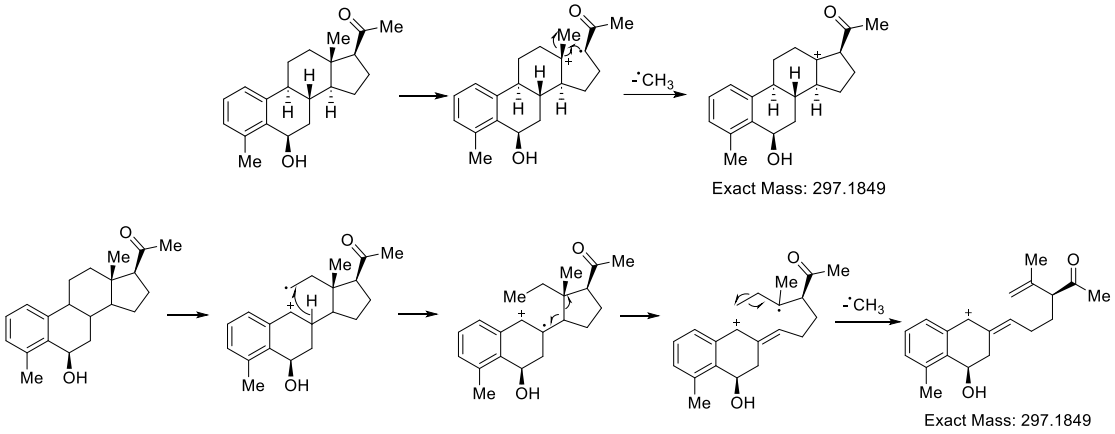

Scheme 59. Proposed fragmentation pathways for the elimination of a methyl radical $^{\bullet}CH_3$ from the molecular ion S42-C6ß-OH (**3**) according to *Djerassi* and *Budzikiewicz*.[105c, 116] The [**3**-$^{\bullet}CH_3$]$^+$ is found at *m/z* 297 in the GC-EI-HRMS spectrum of **3** as shown in **Figure27D**.

The elimination reaction of the methyl group of the S42 derivative can be explained along the lines discussed by *Djerassi* and *Budzikiewicz*.[105c, 116] Accordingly, the CH_3-residue located at C18 or a methyl group comprising carbon C11 can be lost as illustrated in **Scheme 59**. The loss of the C21 methyl group is not considered here, as an initial *α*-cleavage at C20-C21 would produce a fragile acylium ion [**3**-$^{\bullet}CH_3$]$^+$ destabilized by the facilitated subsequent loss of carbon monoxide.[105a, 117] The absence of an elimination of the C21-linked methyl group in EI MS data of other 20-keto steroids like pregnan-20-one and *D*-homopregnan-20-one rests on this rationale.[116]

Finally, the GC-EI HR MS spectrum of S42-C7*α*-OH (**4**) was investigated (see **Figure 27E** and **Figure 28E**). Largely, the spectrum of analyte **4** is indistinguishable from the one of analyte **3**. Only the absence of the product ion at *m/z* 297 representing the loss of the methyl group in the spectrum of the C6 isomer (**3**) is noted, as documented in **Figure 27E**.

4.2.3 GC-EI-HRMS analysis of TMS derivatives of S42- C20/C6/C7-OH

The hydroxylated S42 derivatives S42-C20-OH (**2**, **2'**), S42-C6*ß*-OH (**3**), S42-C7*α*-OH (**4**) were further derivatized to the trimethyl silyl (TMS) ethers **5, 5', 6(C17-TMS)**, isomers (**7(C20-TMS)**, and **7(C17-TMS)** respectively (SIC traces presented in **Figure 29**). The singly TMS-derivatized S42-C20-OH epimers (**5,**

RT: 21.65 min in **Figure 29**, panel A; **5'**, RT: 21.76 min in **Figure 29,** panel B) were separately analyzed. The series of GC-EI-HRMS data are presented in **Figure 29** to **Figure 31**.

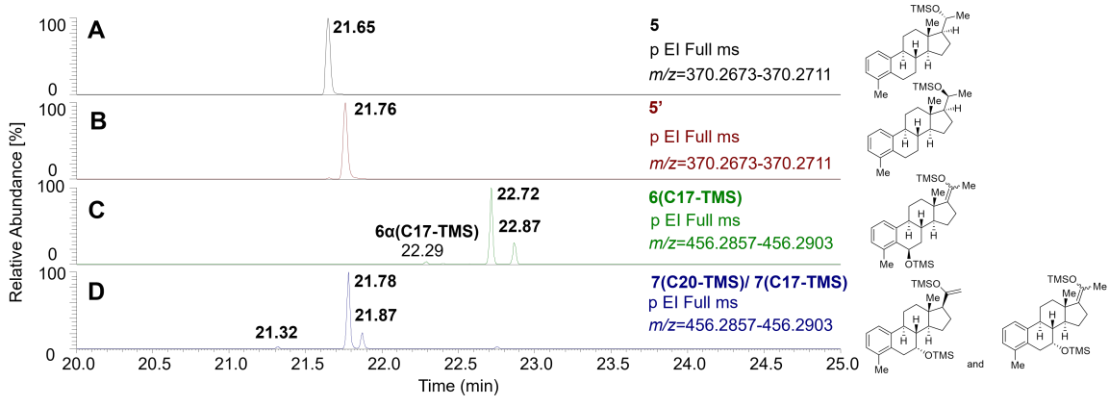

Figure 29. Extracted ion chromatograms of the molecular ions of S42-TMS derivatives evidenced the formation of diastereomers (**5** & **5'**; **6(C17-TMS)** and isomers (**7(C20-TMS)** & **7(C17-TMS)**) mixtures. Panel A and B: TMS derivatized S42-C20-OH epimers (**5** and **5'**), Panel C: doubly TMS derivatized S42-C6*ß*-OH epimers (**6(C17-TMS)** and **6'(C17-TMS)**, Panel D: S42-C7*α*-OH isomers (**7(C20-TMS)**, **7(C17-TMS)** and **7'(C17-TMS)**.

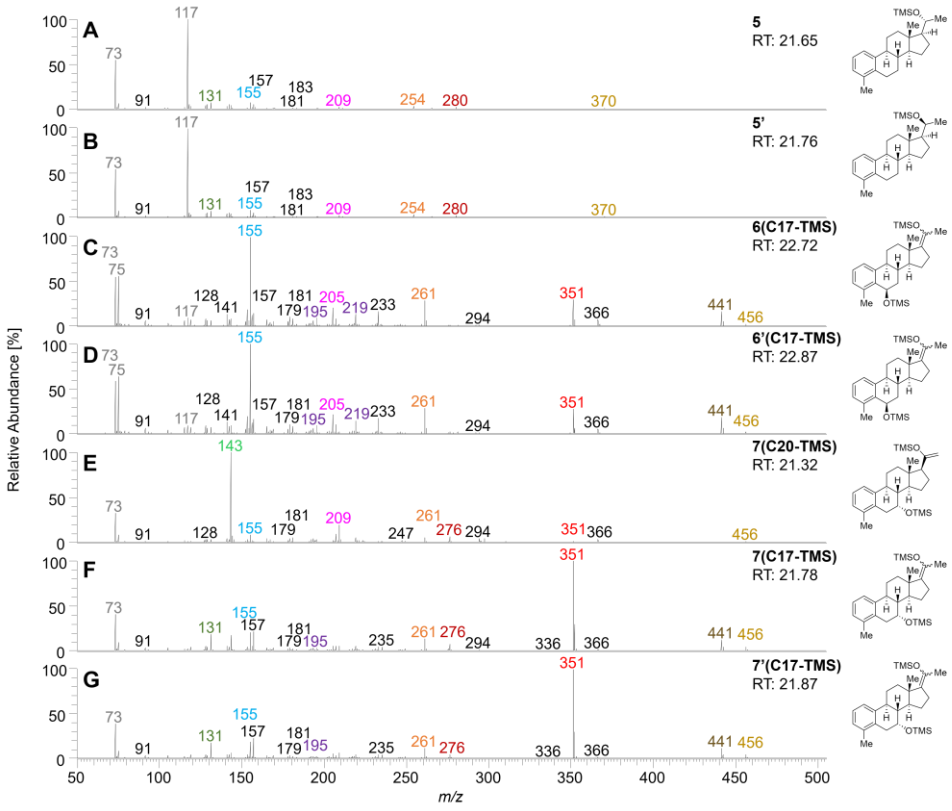

Figure 30. GC-EI HR MS Spectra of TMS-derivatized S42-C20-OH, S42-C6ß-OH, S42-C7*α*-OH (**5, 5', 6(C17-TMS), 6'(C17-TMS), 7(C20-TMS), 7(C17-TMS)** and **7'(C17-TMS)**). The isomer **6(C20-TMS)** was found in the GC-EI- HRMS data analyzed at German Sport University Cologne in **Figure A63** in Appendix).

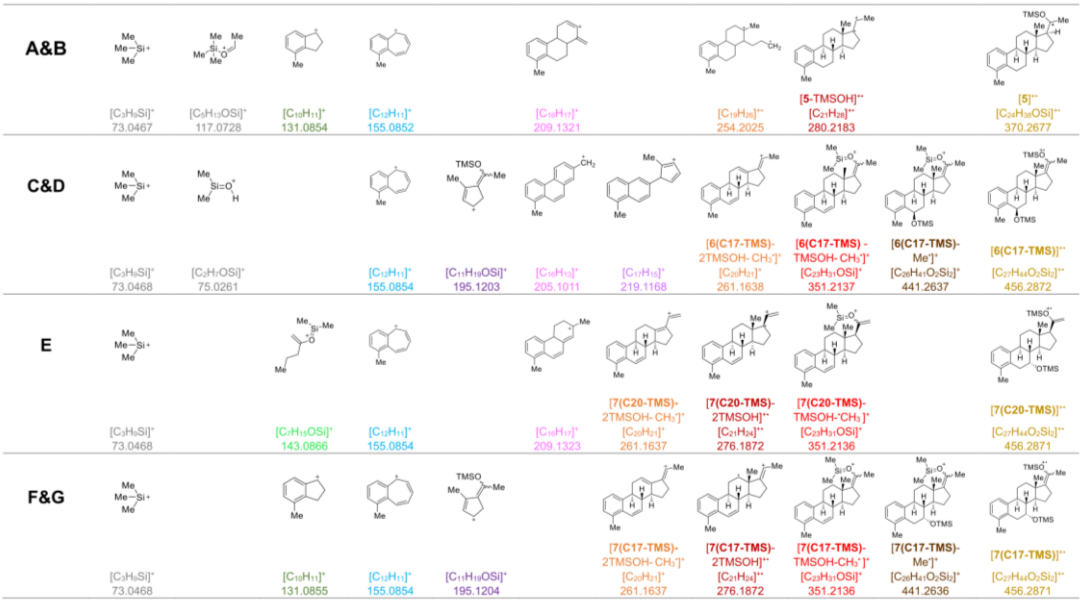

Figure 31. Ion structures according to the composition deduced from the accurate ion masses measured from TMS derivatized S42-C20-OH (**5** and **5'** in panel A and B), S42-C6ß-OH (**6(C17-TMS)** and **6'(C17-TMS)** in panel C and D) and S42-C7*α*-OH (**7(C20-TMS)**, **7(C17-TMS)** and **7'(C17-TMS)** in panel E, F and G) found in the GC-EI-HRMS data presented in **Figure 30**.

Interpretation of the GC-EI-HRMS spectra of S42-C20-OH derivatives **5** and **5'**

The GC-EI HR MS spectra of the singly TMS-derivatized S42-C20-OH epimers (**5** and **5'**) are virtually identical as documented in **Figure 30A** and **B**. The molecular ions are found with low abundance at *m/z* 370 and the loss of trimethyl silanol TMSOH (90 Da) explains the formation of the fragment ion at *m/z* 280 (**Figure 31A&B**), isobaric to the water-loss product ions found in **Figure 27B**, **C** and **Figure 28B**, **3C**. The EI HR mass spectra of **5** and **5'** are dominated by the pronounced ions at *m/z* 73 and *m/z* 117 which evidence the TMS group at position C20 in the two analytes **2** and **2' (Figure 30A** and **B)**.

Interpretation the GC-EI-HRMS spectra of S42-C6ß-OH derivatives **6(C17-TMS)** and **6'(C17-TMS)**

S42-C6ß-OH (**3**) turned out to be unstable under the reaction conditions of the TMS-derivatization (MSTFA/NH_4I/EtSH) which led to the formation of byproducts which were fractionated as documented in the selected ion chromatogram of the respective molecular ion mass at *m/z* 456 (see **Figure**

30C). E.g. an unsaturated water-loss product of S42-C6ß-OH (**3**) with a molecular ion [**3** -H_2O]$^{+\bullet}$ at *m/z* 366 was detected by GC-EI-HRMS (see **Figure A59 to Figure A62** in the Appendix for further details).

Two TMS-S42-C6ß-OH diastereomers (**6(C17-TMS)** in **Figure 29C**; **6'(C17-TMS)** in **Figure 29D**) were identified. The assignment of the C17-TMS-regio isomers of TMS-S42-C6ß-OH (**6(C17-TMS)**) rests on the observation of the D-ring fragment [$C_{11}H_{19}OSi$]$^+$ at *m/z* 195 (see **Scheme 45**) and the prominent A,B-ring fragment ion [$C_{12}H_{11}$]$^+$ at *m/z* 155, whereas the C20-TMS regio isomer of TMS-S42-C7α-OH (**7(C20-TMS)** in **Figure 29E**) was assigned on the basis of the dominant signal of the respective D-ring fragment [$C_7H_{15}OSi$]$^+$ at *m/z* 143 (see **Scheme 43**).

These assumptions are derived from the evaluation of a previous comprehensive investigation of S42 (**1**) and its TMS derivatives.[115] The GC-EI HRMS spectra of **6(C17-TMS)** in **Figure 30C** and **6'(C17-TMS)** in **Figure 30D** are very similar. The mass spectra presented **Figure 30C** and **D** document a methyl-radical loss leading to the fragment ion at *m/z* 441, generated from the molecular ion at *m/z* 456. Furthermore, product ions attributed to TMSOH-loss (Δm = 90 Da) explain the ions at *m/z* 366 and *m/z* 351, in which the latter ion suggested in the formation of a C6,C7-double bond in the B-ring.

Interpretation of the GC-EI-HRMS spectra of S42-C7α-OH derivatives **7(C20-TMS)**, **7(C17-TMS)** and **7'(C17-TMS)**

Prominent TMS-derivatized isomers of S42-C7α-OH (**4**) are identified: the regio isomers (7(C20-TMS) in **Figure 30E** and 7(C17-TMS) in **Figure 30F**, as well as the epimer of the latter 7'(C17-TMS) in **Figure 30G**. The evaluation of the GC-EI HR mass spectrum shown in **Figure 30F** is less straightforward, as the spectrum exhibits the C17-TMS diagnostic D-ring fragments [$C_{11}H_{19}OSi$]$^+$ at *m/z* 195 and [$C_8H_{17}OSi$]$^+$ at *m/z* 157, but also exhibits an [$C_7H_{15}OSi$]$^+$ ion at *m/z* 143, albeit with low to medium abundance (**Table A6** and **Table A7** in the Appendix).

More remarkable is that the spectrum in **Figure 30F** and **G** differ significantly from the other ones in **Figure 30** as the ion at *m/z* 351 dominates these spectra.

This finding can be related to the TMSOH-loss from C7, yielding the C6,C7-double bond in ring B in the open-shell ion at *m/z* 366. A subsequent methyl-radical loss from the C17-TMS group generates the prominent ion at *m/z* 351 (**Figure 31**), which is obviously very stable and is observed with high abundance in the EI-MS spectrum in **Figure 30F**.

Apparently, the isobaric ion at *m/z* 351 in **Figure 30E** resulting from the analogous fragmentation sequence of the C20-TMS moiety is much less stable and is therefore found with only minimal abundance (cf. **Figure 30E** with **F**). These considerations led to the conclusion that the spectrum in **Figure 30F** belongs to **7(C17-TMS)**.

From the observations of MS spectra of compounds **2**, **3**, and **4** above, the hydroxy groups at **C6** and **C7** appear to be relatively unstable. The molecular ion peaks of compounds **3** and **4** were relatively weak and were not clearly observed. A water loss is suggested to be favored, resulting in a double bond at C6-C7, which is a stable conjugate system.
A similar phenomenal was also observed in the TMS derivatives of compound **3** and **4**. The ion peak $[M\text{-}TMSOH\text{-}Me^{\cdot}]^{+}$ is significantly more intense than the molecular ion, supporting the tendency of formation the double bond at C6-C7.

In addition, the ion *m/z* 143 and 195 from the D ring were also observed in the MS spectra. Notably, the ion at *m/z* 155 was constantly found in all MS spectra of the synthesized derivatives. The ion at *m/z* 155 may be a diagnostic fragment for investigation S42 metabolites using GC-EI-HRMS.

4.3 *In vitro* studies applied with HLM and S9

In vitro metabolism experiments of S42 (**1**) were conducted together with the deuterated S42-d7 (**1-d7**) isotopologue in parallel experiments.[115] For the *in vitro* study, the S9 enzyme fraction and human liver microsomes (HLM) were used.[118] The samples were purified by SPE extraction, dried and TMS derivatized before GC-EI-HR-MS/MS (Orbitrap) analysis.

4.3.1 Method setup for GC-EI-HRMS analysis

The molecular ion masses of phase I metabolites of S42 (**1**) were calculated and respective single ion current traces were selected and monitored by GC-EI-HRMS (Orbitrap) in the full scan mode.

To securely prevent spectra-overlays of simultaneously eluting compounds resulting of insufficient GC-separation present in the *in vitro* experiments, MS^2-product ion spectra of the S42 molecular ion species were conducted. The MS^2-product ion experiments yielded reliable data sets to further investigate specific fragmentation pathways of the molecular ions of S42 phase I metabolites. Mono-, bis-, and tris-hydroxylated S42 derivatives were identified as TMS-derivatives.

Close inspection of the MS data of the *in vitro* experiments showed that neither the retention times of the TMS-derivatized reference analytes S42-C20-OH (**5**), S42-C6*ß*-OH (**6(C17-TMS)**), and S42-C7*α*-OH (**7(C20-TMS)** and **7(C17-TMS)**) nor the qualitative analysis of their EI HR MS data matched the results that were found in the TMS-derivatized metabolites of the *in vitro* experiments. Accordingly, we concluded that S42-C20-OH (**2**), S42-C6*ß*-OH (**3**), and S42-C7*α*-OH (**4**) were not formed in the *in vitro* experiments of S42 (**1**).

Despite that, at least 8 different TMS-derived phase I S42 metabolites were successfully identified and their structures were elucidated with GC-EI HR.[119] The structure elucidation of individual S42 metabolites was based on GC separation (single ion current analysis of the molecular ions), interpretation of the MS^2-product ion spectra of the molecular ions and the parallel examination of a specifically ^2H-labeled S42 derivative (**1-d7**) fed in the *in vitro* experiments. Significant mass shifts of the molecular ions and important fragment ions was the basis for a largely straightforward analysis of the data and allowed the location of the hydroxy functional groups to individual steroidal rings. Additional product ion experiments of selected ions were conducted to further scrutinize ion structure proposals and fragmentation mechanisms.

4.3.2 *In vitro* S42-mono-OH metabolites **M1a**, **M1b** and **M1c** investigated by GC-EI-HRMS

Three TMS derivatized S42-mono-OH isomers (**M1a**, **M1b** and **M1c)** of a mono-hydroxylated S42 metabolite were identified on the basis of their accurate ion mass (see **Figure 32A** and **B**) and the characteristic fragmentation patterns in the GC-EI HR mass spectra (see **Figure 32C**, **D** and **Figure 33C** and **D**).

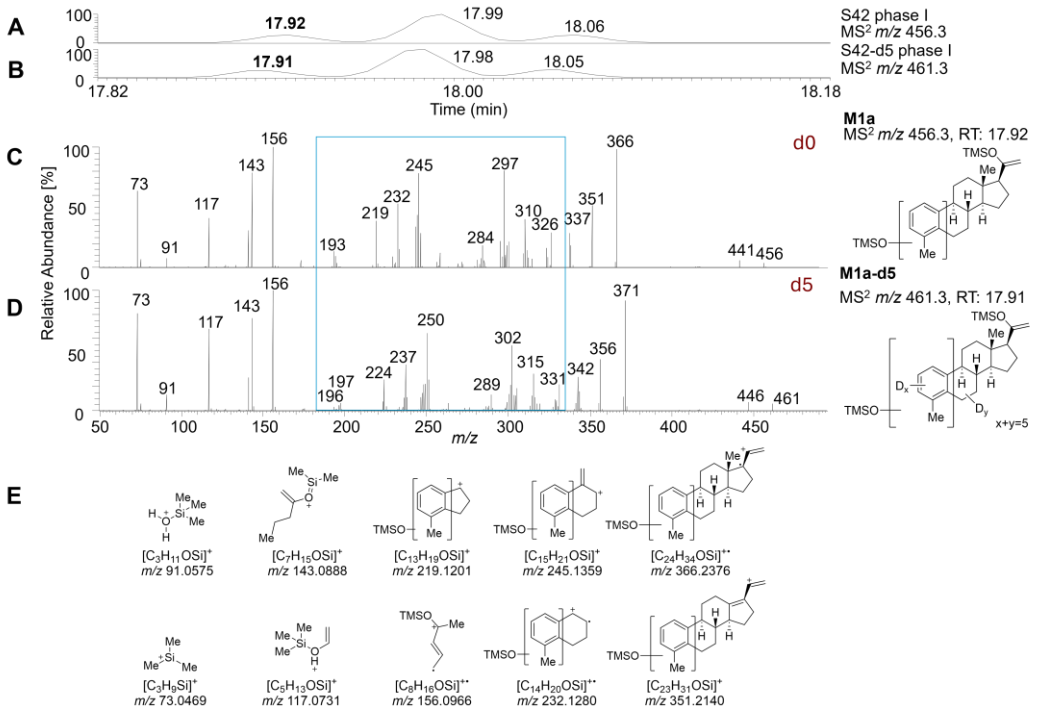

Figure 32. Extracted SICs of the molecular ions of the TMS derivatized S42-mono-OH metabolites at *m/z* 456 and *m/z* 461 (panel A and B). MS^2-product ion mass spectra of the molecular ions of the **M1a** at *m/z* 456 (RT: 17.92 min) and **M1a-d5** at *m/z* 461 (RT: 17.91 min) metabolites (panel C and D). Ion structures of significant fragment ions are included in panel E.

One C20-TMS isomer (**M1a**, RT: 17.92) and two C17-TMS isomers (**M1b**, RT: 17.99 and **M1c**, RT: 18.06) were assigned on the basis of the observation of the already highlighted diagnostic fragment ions, *i.e.* the D-ring fragment ions at *m/z* 143 indicating C20-TMS (see **Figure 32**) and the respective ion at *m/z* 195 indicating C17-TMS isomers of S42 (see **Figure 33**).

The silicon-containing fragment ions in the lower *m/z* range (*m/z* 73 and 117) are stemming from D-ring fragmentations as they are not mass shifted in the spectrum of the labeled isotopologue (see **Figure 32** and **Figure 33**). The position of the TMS-ether moiety (C_3H_8OSi Δm 88 Da) can be located to the

A,B-rings as the respective A,B-ring fragment ions found in the EI-HR MS spectrum of the S42-C20-TMS derivatives are characteristically shifted by 88 Da. The respective ions are observed at *m/z* 219 (131 + 88 Da), *m/z* 232 (144 + 88 Da), *m/z* 245 (157 + 88 Da), and *m/z* 297 (209+88 Da). All of these ions are characteristically mass shifted by 5 Da in the EI-HR MS spectrum of the d5-isotopologue (see **Figure 32C** and **D**).

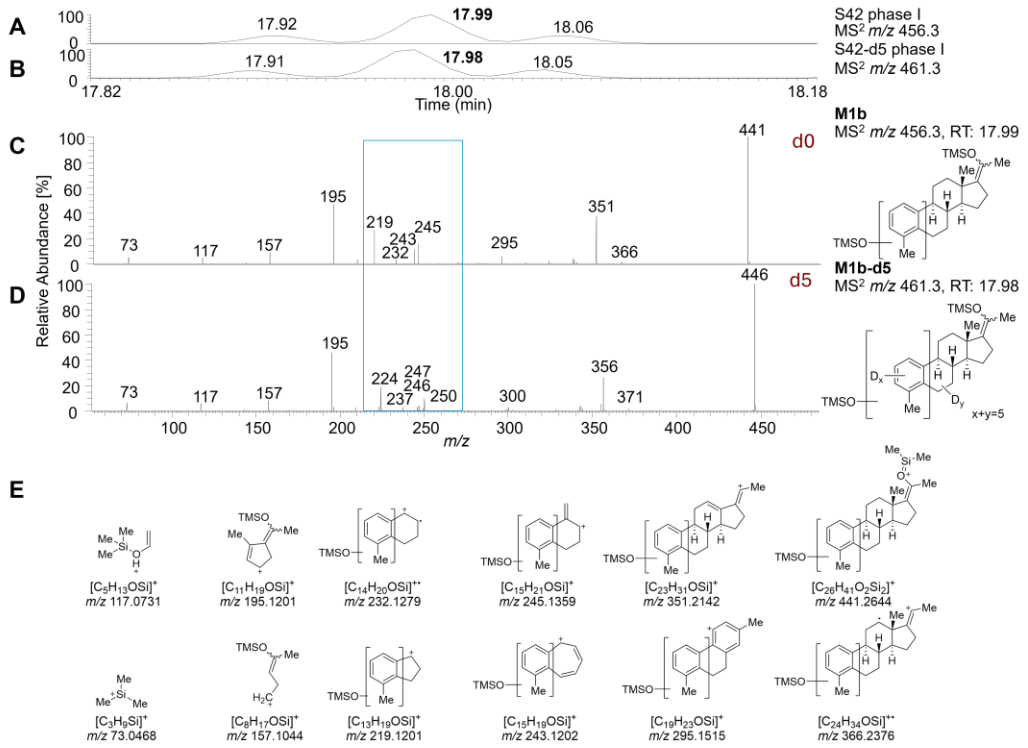

Figure 33. Extracted single ion currents (SICs) of the molecular ions of the TMS derivatized S42-mono-OH metabolites at *m/z* 456 and *m/z* 461 (panel A and B). MS^2-product ion mass spectra of the molecular ions of **M1b** at *m/z* 456 (RT: 17.99 min) and **M1b-d5** at *m/z* 461 (RT: 17.98 min) metabolites (panel C and D). Ion structures of significant fragment ions are included in panel E.

Similarly, the almost identical GC-EI HR mass spectra of the C17-TMS isomers **M1b** and **M1c** exhibit shifted fragment ions at *m/z* 295 (207 + 88 Da), 245 (157+ 88 Da), 243 (155 + 88 Da), 219 (131 + 88 Da) leading to the same assumption (see **Figure 33**).

Localization of the hydroxyl group in metabolites **M1a**, **M1b** and **M1c**

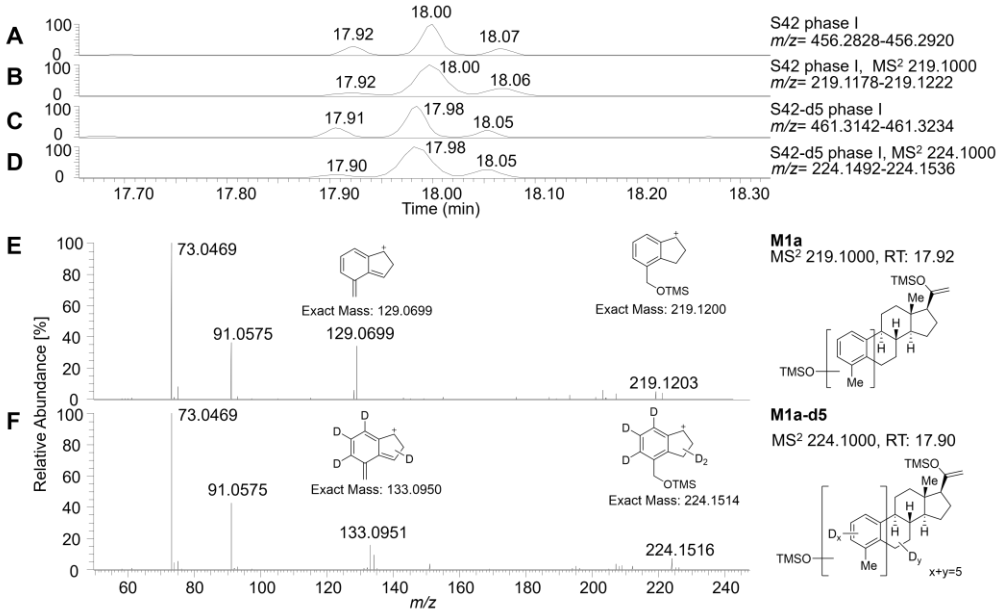

Figure 34. Extracted SICs of the characteristic fragment ions of the TMS derivatized S42-mono-OH metabolites at *m/z* 456 (panel A), *m/z* 219 (panel B), *m/z* 461(d5) (panel C) and *m/z* 224 (d5) (panel D). MS^2-product ion experiments of the ions at *m/z* 219 (131+88 Da) (d0), of *m/z* 224 (131+88+5 Da) (d5) of **M1a** and of **M1a-d5**, respectively (panel E and F). MS^2-product ion mass spectra of metabolites **M1b**, **M1c**, **M1b-d5** and **M1c-d5** deliver similar results; data not shown.

On the basis of the collected MS data, we assume that the phase I hydroxylation in compounds **M1a**, **M1b** and **M1c** can be ring A benzylic alcohol. This conclusion rests on the following considerations.

Firstly, A/B-ring fragment ions of all three S42-derivatives **M1a**, **M1b**, **M1c** decorated with a TMSO functional group were characteristically mass-shifted in the EI HR MS spectra of the deuterated derivatives **M1a-d5**, **M1b-d5** and **M1c-d5** (see **Figure 32D** and **Figure 33D**). Additionally, the indicative D-ring fragment ions at *m/z* 143 ($[C_7H_{15}OSi]^+$), and at *m/z* 195 ($[C_{11}H_{19}OSi]^+$) were found in the MS^2-spectra of the non- and deuterated molecular ions, clearly excluding any D-ring hydroxylation.

Furthermore, the mismatch of the *in vitro* metabolite mass spectra with the MS data collected of the reference analytes S42-C6-OH and S42-C7-OH (cf. **Figure 30**) excluded a B-ring hydroxylation as result of the *in vitro* metabolism. In conclusion, these findings point towards an A-ring oxidation of S42, which

lead upon silylation to the formation of the set of isomeric **M1a**, **M1b** and **M1c** S42 derivatives, documenting a phase I metabolism pathway also found for estrogen and estrone.[120]

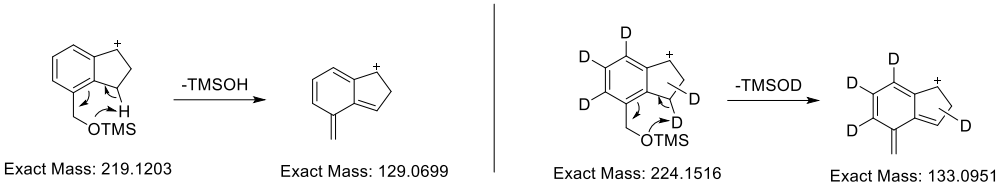

Scheme 60. Charge-remote fragmentation pathway of the TMSOH/D-loss of *m/z* 219 and its d5-isotopologue at *m/z* 224 via a 6-membered transition state.

Finally, the characteristic loss of trimethyl silanol (Δm of 90 Da; TMSOH) and of TMOD (Δm of 91 Da) of the ^{2}H-labelled isotopologues, indicated the benzylic hydroxylation at C19 and renders the formation of phenolic OH groups at either C2 or C3 unlikely (see **Figure 34**). The TMSOH-loss (Δm of 90 Da), observed in the product ion mass spectra of the respective A/B-ring fragments at *m/z* 219 (d0) → *m/z* 129, can proceed via a 6-membered transition state as shown in **Scheme 60A** TMSOD-loss is found in the MS^2-spectrum of the analogous d5-ion at *m/z* 224 → *m/z* 133 (Δm of 91 Da)(see **Figure 34**).

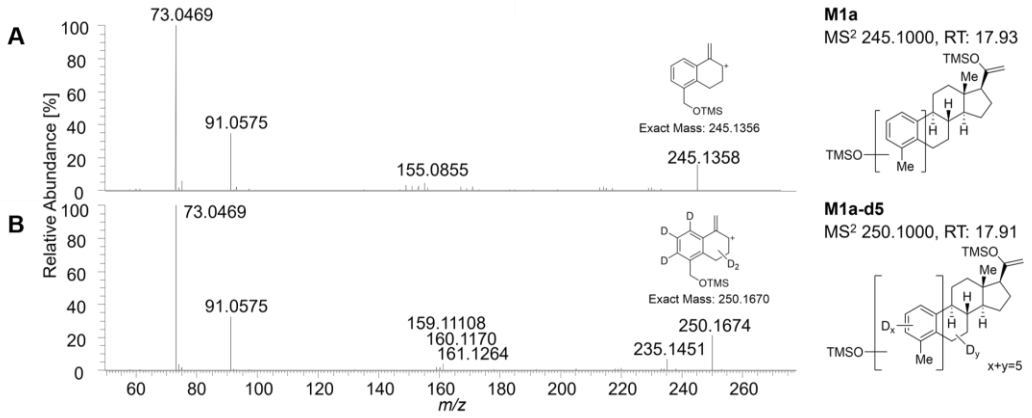

Figure 35. Extracted single ion currents SIC of the characteristic fragment ions of the TMS derivatized S42-mono-OH metabolites **M1a** and **M1a-d5** at *m/z* 245 and *m/z* 250 (panel B and D). MS^2-product ion experiments of the ions at *m/z* 245 (157+88 Da) (d0), of *m/z* 250 (157+88+5 Da) (d5) of **M1a** and of **M1a-d5**, respectively (panel E and F). MS^2-product ion mass spectra of metabolites **M1b**, **M1c**, **M1b-d5** and **M1c-d5** deliver similar results; data not shown.

Similar results were collected for the A/B-ring fragments at *m/z* 245 (d0) and *m/z* 250 (d5) as **Figure 35** documents. In line with these assumptions and considerations, MS^2-experiments of the ions at *m/z* 243 of **M1a, M1b** and **M1c**

did not show any TMSOH-loss (**Figure 36**). This finding is in accordance with the proposed bicyclic ion structure with a double bond at C6-C7 position, preventing a TMSOH elimination.

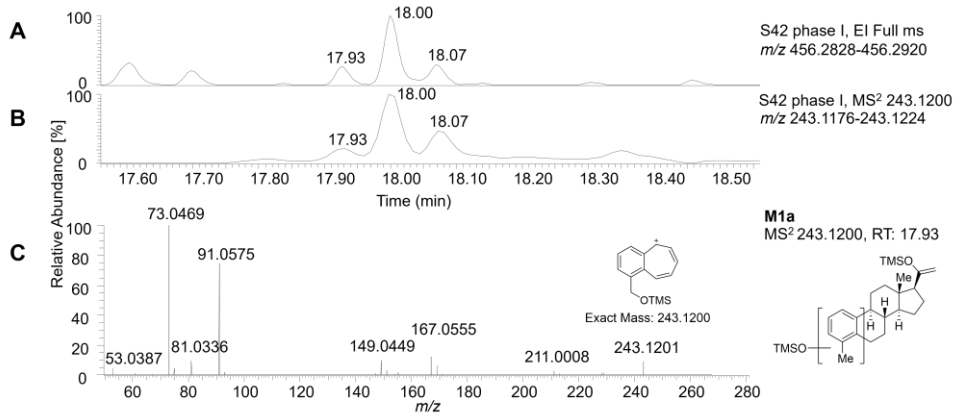

Figure 36. Extracted single ion currents SIC of the molecular ion at *m/z* 456 (panel A) and the characteristic fragment ion of the TMS derivatized S42-mono-OH metabolites **M1a** at *m/z* 243 (panel B). MS^2-product ion experiment of the ion at *m/z* 243 (d0) of **M1a** (panel C). MS^2-product ion mass spectra of metabolites **M1b** and **M1c** deliver similar results; data not shown.

In conclusion we assume that the three isomeric TMS derivatives **M1a-M1c** carry an OTMS group at benzylic position and stem from one benzyl mono-hydroxylated S42 metabolite.

4.3.3 *In vitro* S42-bis-OH metabolites: **M2a, M2b, M2c** and **M2d** investigated by GC-EI-HRMS

Bis-hydroxylated metabolites of S42 (**M2a-M2c**) formed in the *in vitro* experiments were identified according to their calculated molecular ion masses (GC-EI HR MS) at *m/z* 544 along with deuterated d6-isotopologues (**M2a-d6** to **M2d-d6**) at *m/z* 550. GC separation was documented by the respective SIC traces. The structure elucidation of the detected bis-hydroxy-metabolites was accomplished on the basis of the MS^2-product ion mass spectra of the respective molecular ions.

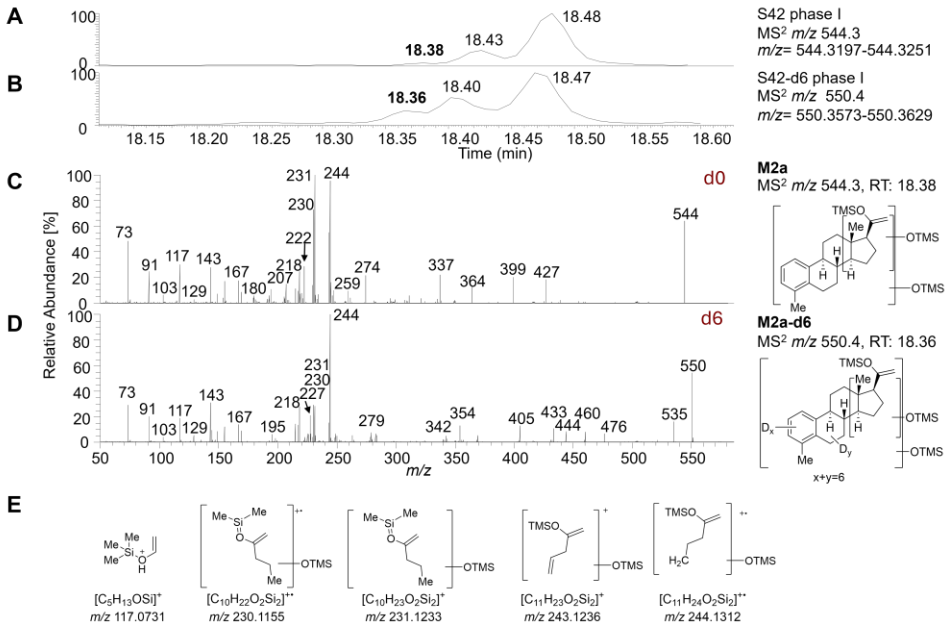

Figure 37. Extracted single ion currents SIC of the molecular ions of the TMS derivatized S42-bis-OH metabolites **M2a** and **M2a-d6** at *m/z* 544 and *m/z* 550 (panel A and B). MS^2-product ion mass spectra of the molecular ions of the **M2a** (RT: 18.38 min) and **M2a-d6** metabolites (RT: 18.36 min) (panel C and D). Ion structures of significant fragment ions are included in panel E.

In the MS^2-product ion mass spectrum of the molecular ion of **M2a** at *m/z* 544 shown in **Figure 37**, characteristically mass-shifted D-ring fragment ions are found at *m/z* 244 $[C_{11}H_{24}O_2Si_2]^{+\bullet}$ ($C_8H_{16}OSi$ + 88 Da), at *m/z* 231 $[C_{10}H_{23}O_2Si_2]^+$ ($C_7H_{15}OSi$ + 88 Da), and at *m/z* 230 $[C_{10}H_{22}O_2Si_2]^{+\bullet}$ ($C_7H_{14}OSi$ + 88 Da) (with C_3H_8OSi = 88 Da) suggesting an OTMS functionalization in the D-ring. These pronounced ions were also observed in the mass spectrum of the A,B-ring deuterated metabolite **M2a-d6** (see **Figure 37D**), hinting towards the formation of a C20-TMS isomer and an unchanged steroidal A/B ring system.

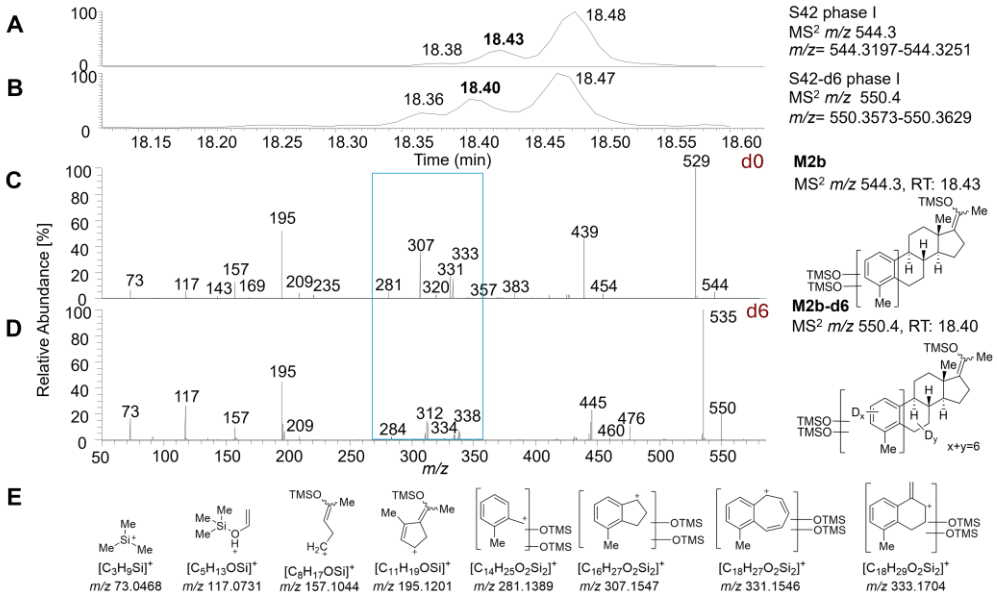

Figure 38. Extracted single ion currents SIC of the molecular ions of the TMS derivatized S42-bis-OH metabolites **M2b** and **M2b-d6** at *m/z* 544 and *m/z* 550. MS^2-product ion mass spectra of the molecular ions of the **M2b** (RT: 18.43 min) and **M2b-d6** metabolites (RT: 18.40 min). Ion structures of significant fragment ions are included in panel E.

In the MS^2 product ion mass spectrum of the molecular ion of metabolite **M2b**, the prominent formation of the D-ring fragment ion at *m/z* 195 $[C_{11}H_{19}OSi]^+$ indicates the presence of a C17-TMS moiety (see **Figure 38C**). The significant ion at *m/z* 195 is not mass shifted in the spectrum of the **M2b-d6** isotopologue confirming this assumption (see **Figure 38D**).

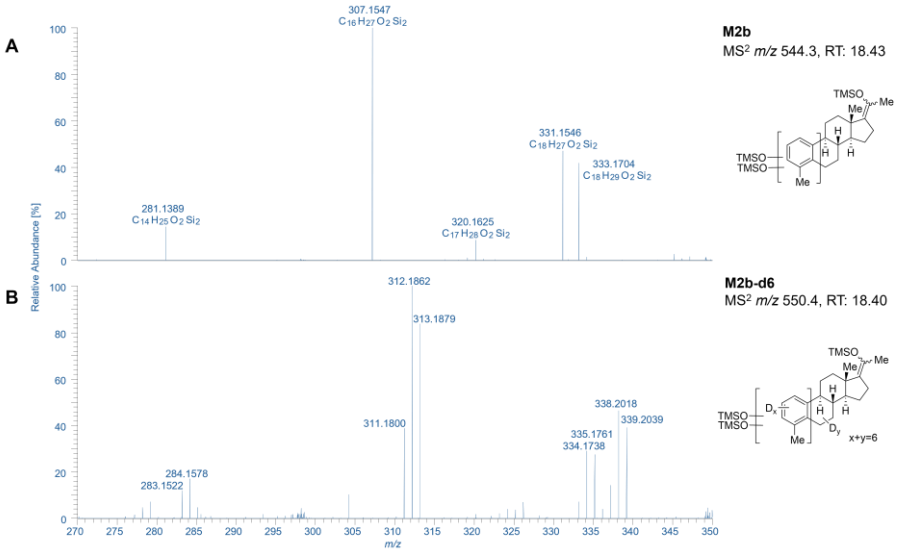

Figure 39. Sections of the MS^2-product ion mass spectra (*m/z* 270-350) of the molecular ions of the **M2b** at *m/z* 544 (RT: 18.43 min) and **M2b-d6** at *m/z* 550 (RT: 18.40 min) metabolites highlighting the characteristic mass-shifts in the product ions of **M2b-d6**.

The indicative fragment ions of **M2b** at *m/z* 333 $[C_{18}H_{29}O_2Si_2]^+$, at *m/z* 331 $[C_{18}H_{27}O_2Si_2]^+$ and at *m/z* 307 $[C_{16}H_{27}O_2Si_2]^+$ originate from characteristic A,B-ring fragments ($[C_{12}H_{13}]^+$ at *m/z* 157, $[C_{12}H_{11}]^+$ at *m/z* 155, $[C_{10}H_{11}]^+$ at *m/z* 131) now mass shifted by 176 Da corresponding to the mass of two OTMS moieties attached to the A-ring (with C_3H_8OSi = 88 Da).

These ions are characteristically mass-shifted in the spectrum of the A,B-ring deuterated metabolite **M2b-d6** (see **Figure 38D** and **Figure 39**), indicating the presence of two OTMS moieties in the A,B ring system of **M2b**.

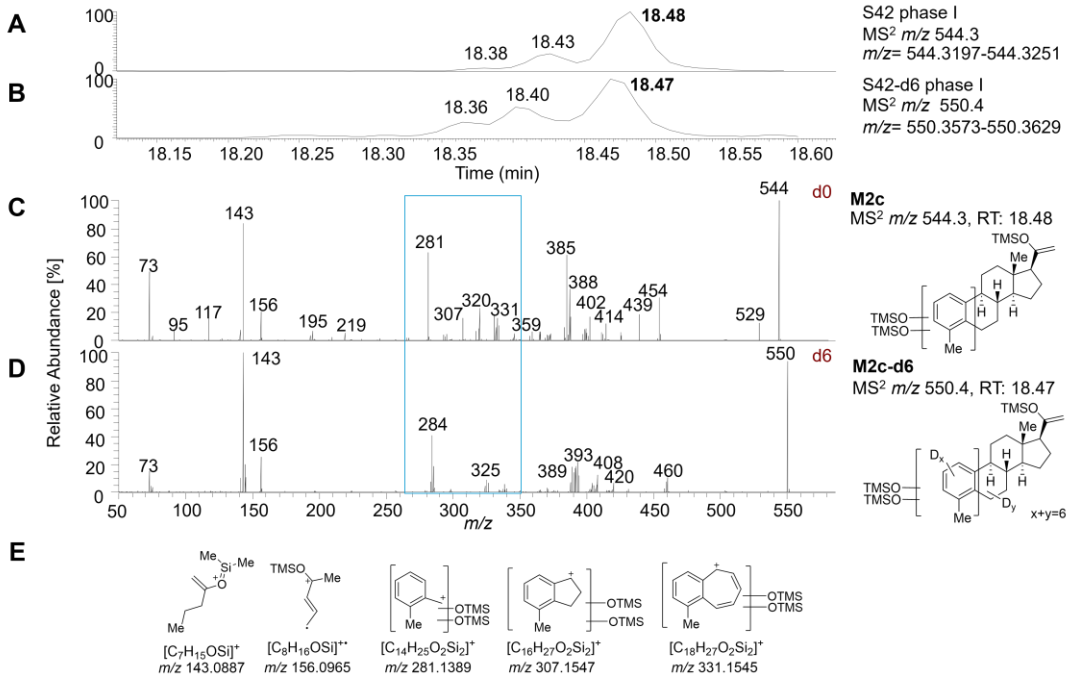

Figure 40. Extracted single ion currents SIC of the molecular ions of the TMS derivatized S42-bis-OH metabolites **M2c** and **M2c-d6** at *m/z* 544 and *m/z* 550 (panel A and B). MS^2-product ion mass spectra of the molecular ions of the **M2c** (RT: 18.48 min) and **M2c-d6** metabolites (RT: 18.47 min) (panel C and D). Ion structures of significant fragment ions are included in panel E.

In the MS^2 product ion mass spectrum of the molecular ion of the metabolite **M2c**, the abundant signals at *m/z* 143.0888 and *m/z* 156.0965 were noted, which point towards the C20-TMS-ion structure (see **Figure 40**).[115] The significant fragment ion signal at *m/z* 281 $[C_{14}H_{25}O_2Si_2]^+$, *i.e.* a benzylic fragment ion, mass shifted by the presence of two OTMS groups, is observed in the respective MS^2-product ion mass spectrum of the d6-isotopologue **M2c-d6** to *m/z* 284 (d3), indicating A,B-ring substitution (cf. **Figure 40C,D**). The trimethyl silanol TMSOH loss (Δm 90 Da) is found in the MS^2 product ion mass

spectra of the molecular ions of **M2c** at *m/z* 454 and of the deuterated isotopologue **M2c-d6** at *m/z* 460, indicating a TMSOH loss from the C20 position to the product ions at *m/z* 454 and at *m/z* 460.

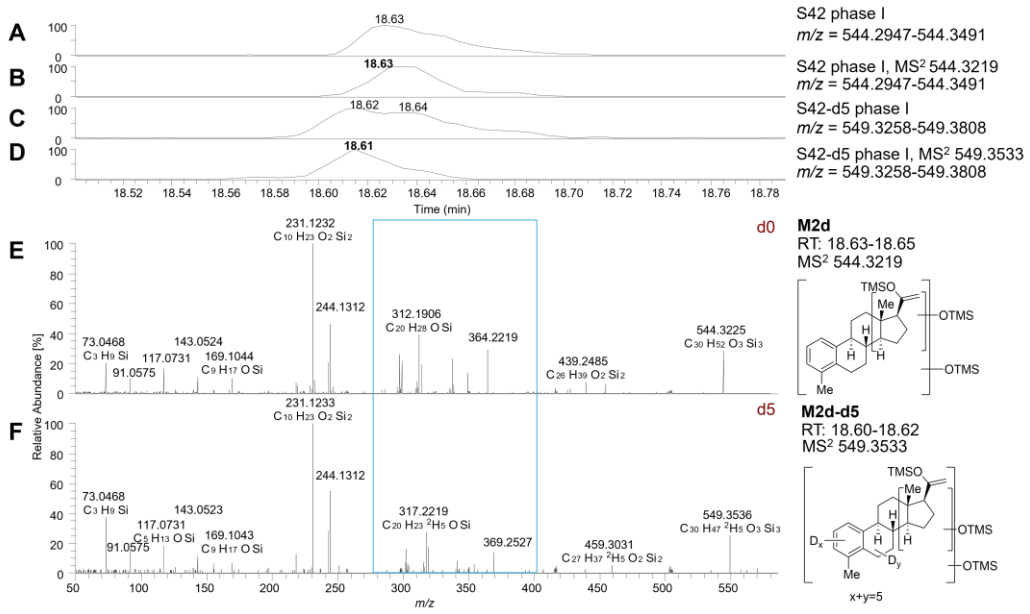

Figure 41. Extracted SIC of the molecular ions of metabolites **M2d** and **M2d-d5** at *m/z* 544 and *m/z* 549 (panel B; panel D). MS^2-product ion mass spectra of the molecular ions of the **M2d** (RT 18.63 min) and **M2d-d5** metabolites (RT 18.61 min) (panel E and F). A new GC column was used, so the retention time of **M2d** was shifted from 18.66 min to 18.63 min. The major signal of the fragment ion $[C_{10}H_{23}O_2Si_2]^+$ at *m/z* 231 indicates a D-ring hydroxylation in metabolite **M2d**.

In the MS^2-product ion mass spectrum of the molecular ion of **M2d** at *m/z* 544, characteristically mass-shifted D-ring fragment ions are found at *m/z* 244 $[C_{11}H_{24}O_2Si_2]^{+\bullet}$ ($C_8H_{16}OSi$+88 Da) and at *m/z* 231 $[C_{10}H_{23}O_2Si_2]^+$ ($C_7H_{15}OSi$+88 Da) as evidenced in **Figure 41**. These pronounced ions were also observed in the mass spectrum of the A,B-ring deuterated metabolite M2d-d5, which suggests the formation of a C20-TMS isomer. (cf. **Figure 41E** with **F**).

4.3.4 *In vitro* S42-tris-OH metabolites **M3a, M3b** and **M3c** investigated by GC-EI-HRMS

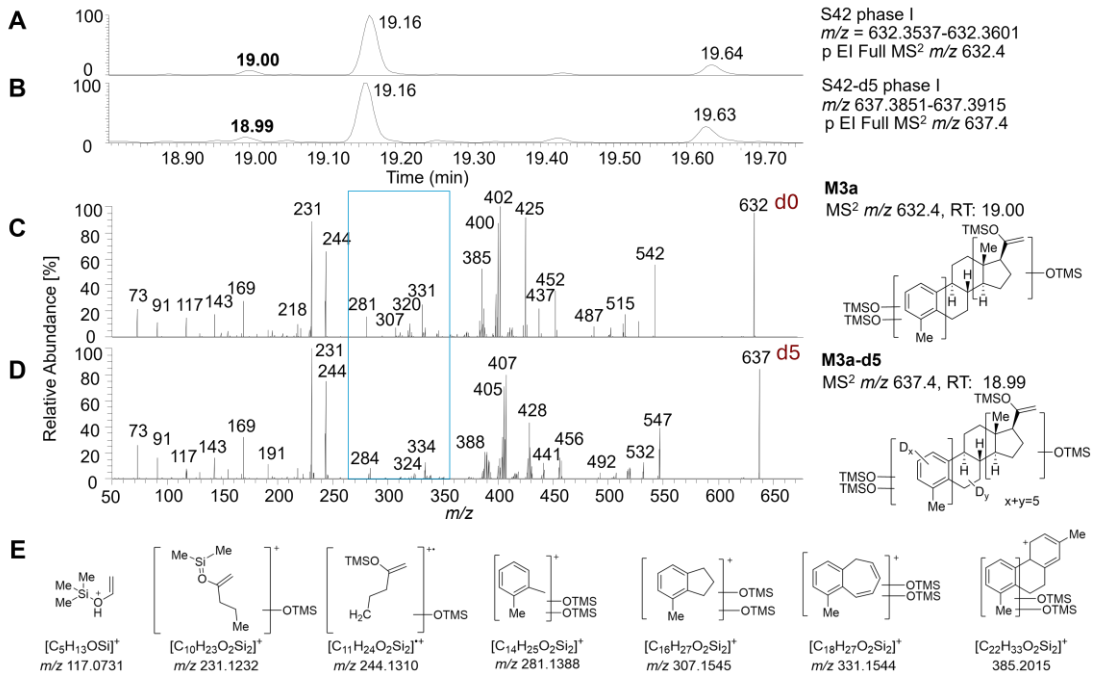

Figure 42. Extracted single ion currents SIC of the molecular ions of the TMS derivatized S42-tris-OH metabolites **M3a** and **M3a-d5** at *m/z* 632 and *m/z* 637 (panel A and B). MS^2-product ion mass spectra of the molecular ions of the **M3a** (RT: 19.00 min) and **M3a-d5** metabolites (RT: 18.99 min) (panel C and D). Ion structures of significant fragment ions are included in panel E.

The MS^2-product ion mass spectrum of the molecular ion of TMS-derivatized S42-tris-OH metabolite **M3a** at *m/z* 632 shows the prominent fragment ions $[C_{10}H_{23}O_2Si_2]^+$ at *m/z* 231 and $[C_{11}H_{24}O_2Si_2]^{+\bullet}$ at *m/z* 244 which indicates the formation of the C20-TMS substructure (see **Figure 42C**). These ions are not influenced by the presence of deuterium labelling in rings A and B as the spectrum of the deuterated metabolite **M3a-d5** documents (cf. **Figure 42C** and **D**). These findings indicate a D-ring hydroxylation in analogy to the observations and conclusions made for the **M2a** and **M2d** metabolites.

The fragment ion at *m/z* 281 $[C_{14}H_{25}O_2Si_2]^+$ of **M3a** is shifted to *m/z* 284 in the MS^2-product ion mass spectrum of the molecular ion of **M3a-d5** (see **Figure 42D**). This observation implies the presence of two hydroxy groups at the steroidal A,B-ring system investigated here as TMS derivatives (cf. discussion of **M2c**). This assumption is additionally confirmed by the presence of the

characteristic fragment ions at *m/z* 331, at *m/z* 320, and at *m/z* 307 (see **Figure 38**, cf. discussion of **M2b**).

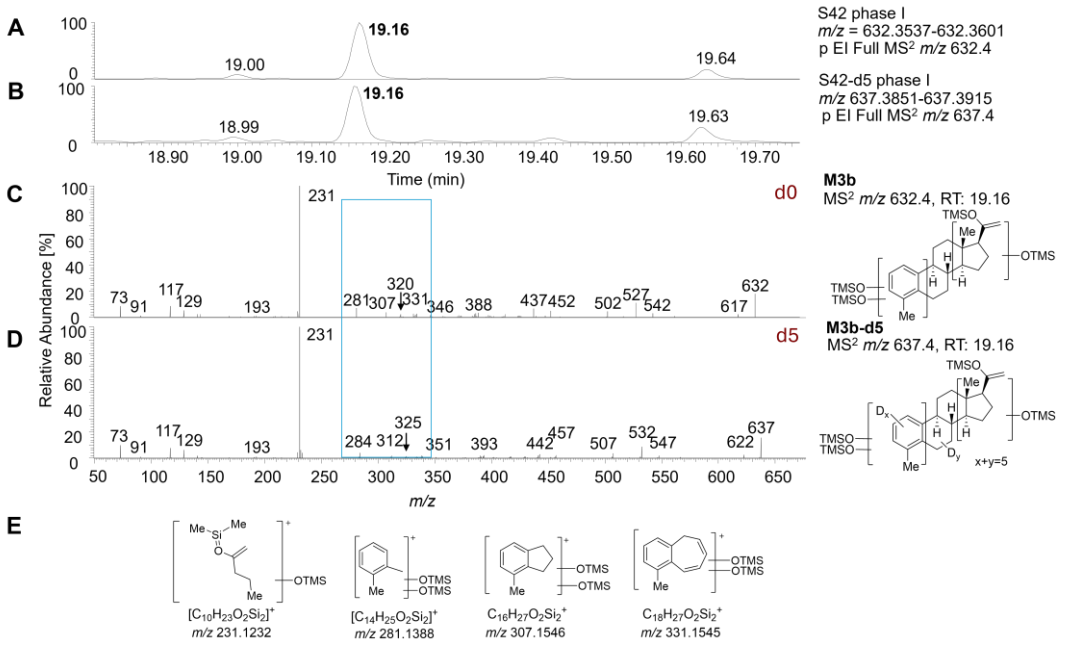

Figure 43: Extracted SIC of the molecular ions of the TMS derivatized S42-bis-OH metabolites **M3b** and **M3b-d5** at *m/z* 632 and *m/z* 637 (panel A and B). MS^2-product ion mass spectra of the molecular ions of the **M3b** (RT: 19.16 min) and **M3b-d5** metabolites (RT: 19.16 min) (panel C and D). Ion structures of significant fragment ions are included in panel E.

Metabolite **M3b** can be identified to be a C20-TMS isomer with one hydroxy group at ring D of the steroidal scaffold on the basis of the observation of the significant ion $[C_{10}H_{23}O_2Si_2]^+$ at *m/z* 231 found in the MS^2-product ion mass spectrum, which is not mass shifted in the spectrum of **M3b-d5** (see **Figure 43C** and **D**). Again, the formation of the ions at *m/z* 281, at *m/z* 307, at *m/z* 320, and at *m/z* 331 are evidences for the presence of two hydroxy groups attached to the A,B-ring system of metabolite **M3b** (cf. discussion of metabolites **M3a** and **M2b**).

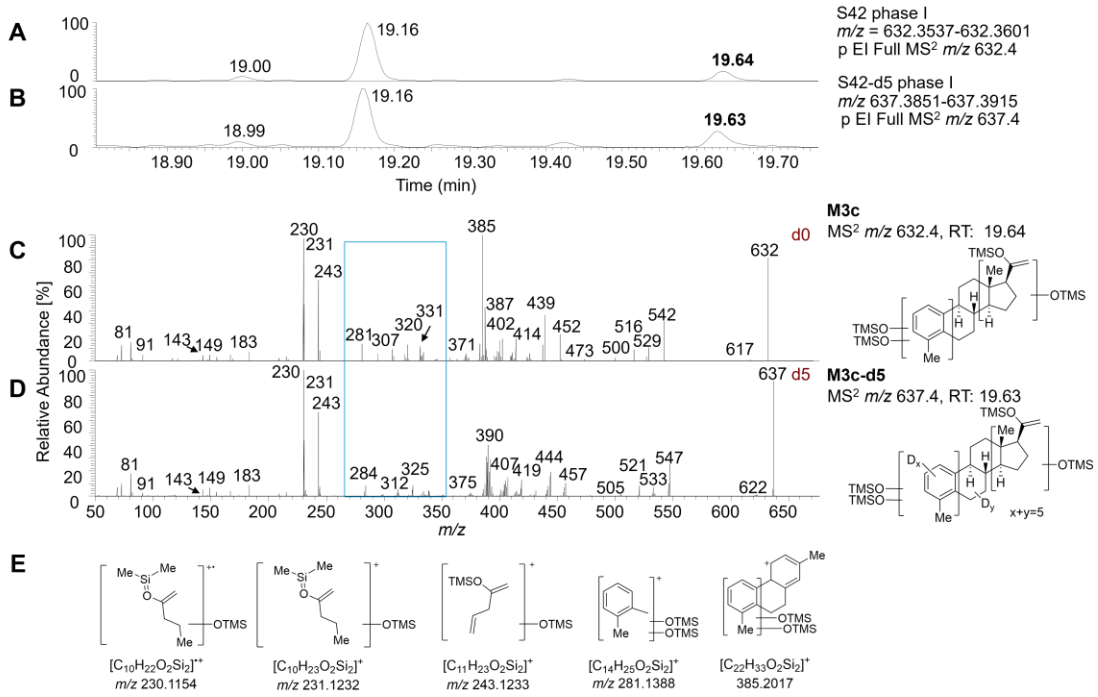

Figure 44. Extracted SIC of the molecular ions of the TMS derivatized S42-tris-OH metabolites **M3c** and **M3c-d5** at *m/z* 632 and *m/z* 637 (panel A and B). MS^2-product ion mass spectra of the molecular ions of the **M3c** (RT: 19.64 min) and **M3c-d5** metabolites (RT: 19.63 min) (panel C and D). Ion structures of significant fragment ions are included in panel E.

The interpretation of the MS^2-product ion mass spectrum of metabolite **M3c** led to similar assumptions as presented for **M3a** (see **Figure 44C**). The MS^2-product ion mass spectrum of **M3c** shows characteristic fragment ions at *m/z* 281 (105 + 88 x 2 Da), *m/z* 307 (131 + 88 x 2 Da), *m/z* 320 (144 + 88 x 2 Da) and at *m/z* 331 (155 + 88 x 2 Da) indicating the presence of two hydroxy groups located at the A,B-ring system (C_3H_8OSi; Δm 88 Da). These ions are observed mass-shifted in the MS^2-product ion mass spectrum of the respective **M3c-d5** metabolite (see **Figure 44D**).

Besides, significant D-ring fragments at *m/z* 231(143 + 88 Da) and at *m/z* 230 (142 + 88 Da) were detected in both spectra of **M3c** and of **M3c-d5**. Interestingly, an $[C_{11}H_{23}O_2Si_2]^+$ ion at *m/z* 243 is found in this case, whereas in the MS^2-product ion mass spectrum of the isomeric C20-TMS metabolite **M3a** an ion at *m/z* 244 is found (cf. **Figure 42**). This could be an indication of an influence of the OTMS moiety at ring D on the fragmentation pathways of the C20-TMS isomer **M3c**.

4.3.5 Analysis of additional *in vitro* metabolites **M4** and **M5** investigated by GC-EI-HRMS

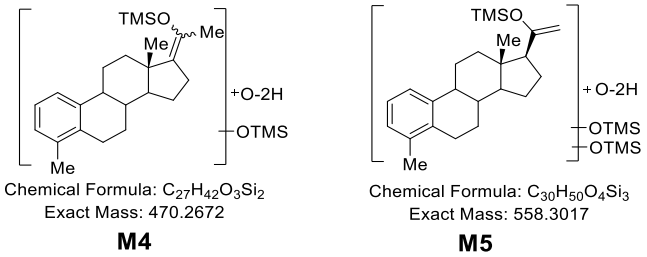

Figure 45. Metabolite structures of TMS-derivatized **M4** and **M5** deduced from the GC-EI-HRMS data.

Finally, 2 additional metabolites were detected in trace amounts with respective molecular ions at *m/z* 470 and at *m/z* 558 (**Figure 45**). The diagnostic fragment ions at *m/z* 195 and at *m/z* 231(143 + 88 Da) were instrumental to identify C-17 and C20-TMS isomers.

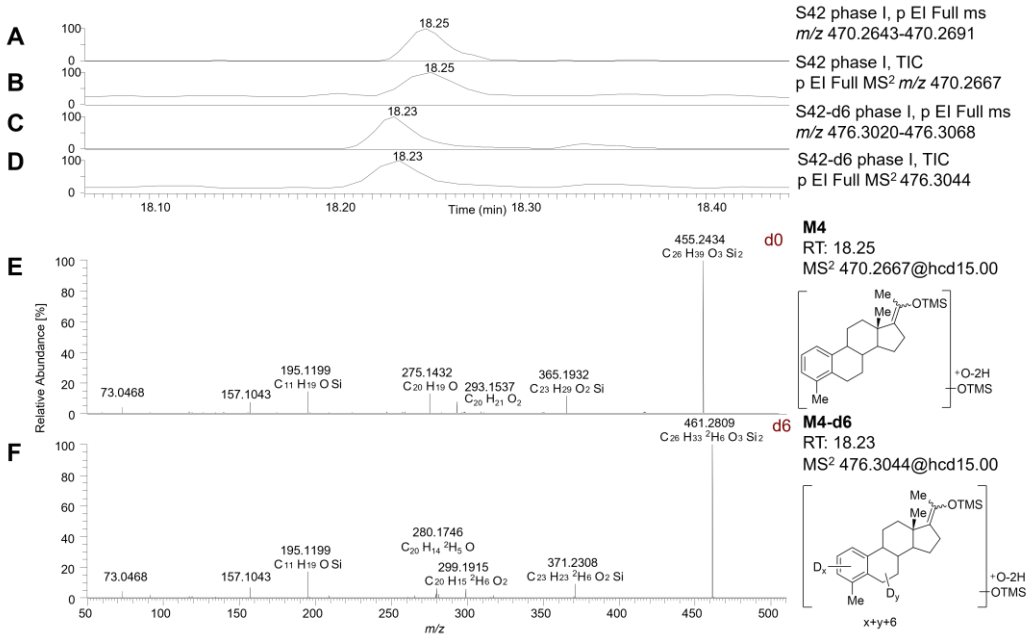

Figure 46. Extracted single ion current SIC of the molecular ion $[C_{27}H_{42}O_3Si_2]^{+\bullet}$ of the TMS derivatized S42-metabolite **M4** at *m/z* 470 and **M4-d6** at *m/z* 461 (panel B and D). The composition of the molecular ion points towards an additional oxidation (+O -2H) potentially documenting a S42-keto-derivative. MS^2-product ion mass spectra of the **M4** metabolite exhibits the diagnostic fragment ion at *m/z* 195 indicating the formation of a C17-TMS derivative (panel E). A retention time shift of **M4** from 18.27 min to 18.25 min was registered upon the use of a new GC column.

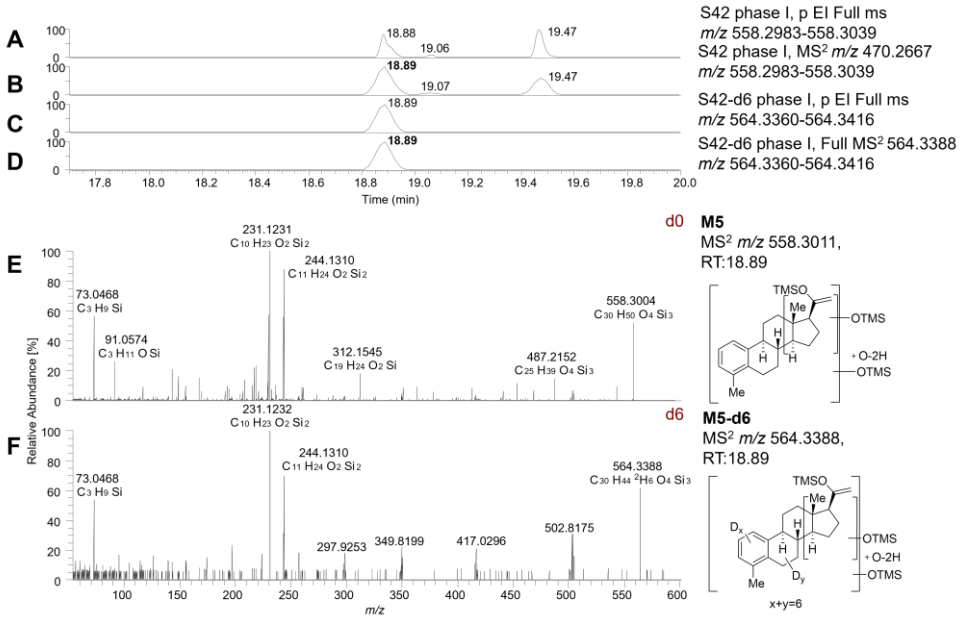

Figure 47. Extracted single ion current SIC of the molecular ion $[C_{30}H_{50}O_4Si_3]^{+\bullet}$ of the TMS derivatized S42-metabolite **M5** at *m/z* 558 and **M5-d6** at *m/z* 564 (panel B and D). The composition of the molecular ion points towards an additional oxidation (+O-2H) potentially documenting a S42-keto-derivative. MS^2-product ion mass spectra of the **M5** and **M5-d6** metabolite exhibit the diagnostic fragment ion at *m/z* 231 and 244 indicating the formation of a C17-TMS derivative (panel E and F). The old GC column was replaced by a new one, but the retention time shifting of **M5** was not observed.

4.3.6 Conclusions of the analysis of the phase I metabolites from *in vitro* experiments of S42 (**1**)

In vitro phase I metabolism experiments of S42 (**1**) and S42-d7 (**1-d7**) with HLM and S9 were conducted and analyzed by GC-EI-HRMS. Eight different TMS-derivatives from S42 hydroxylated metabolites were reliably identified (**Scheme 61**).

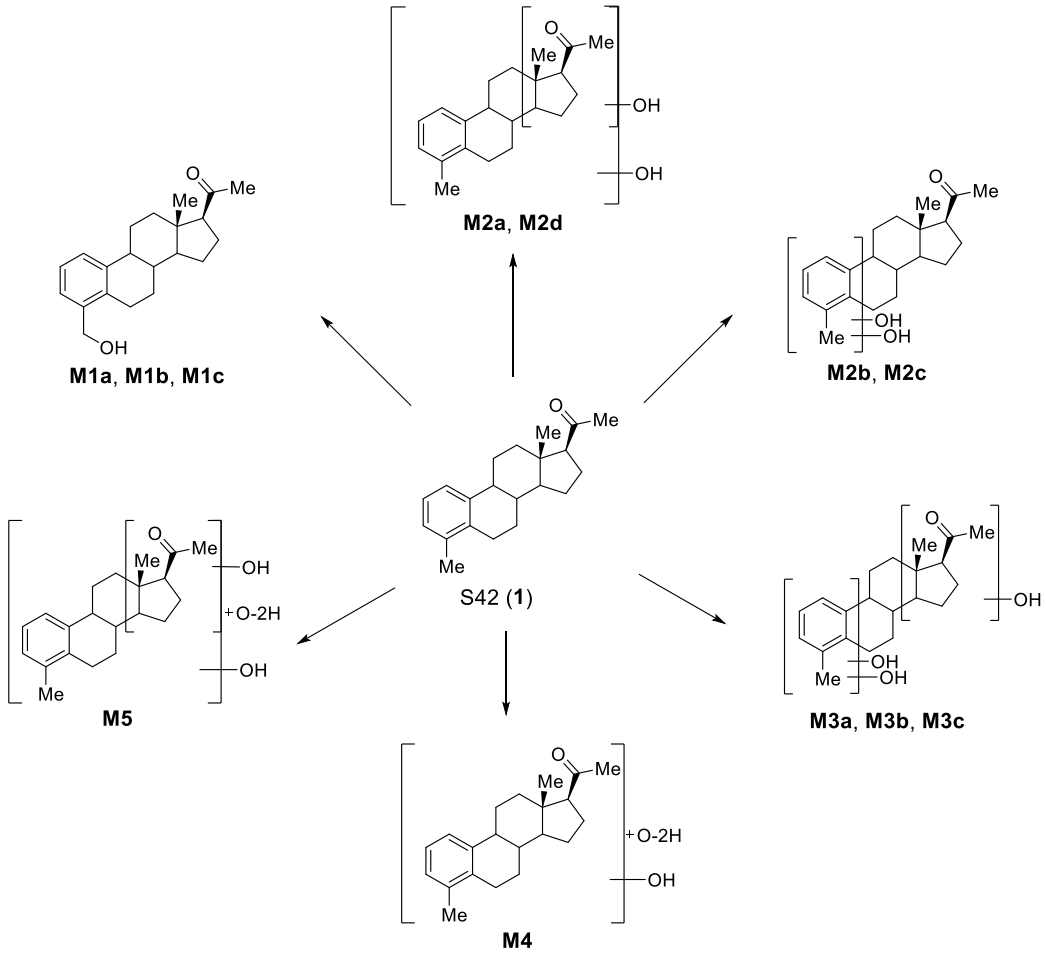

Scheme 61. Metabolite structures identified in the *in vitro* study of S42 -based on data obtained from GC-EI-HRMS^2 experiments.

Table 11. Phase I metabolites of S42 generated by *in vitro* transformation with HLM and S9 fraction. *The relative abundance was determined by the peak area from the extracted ion chromatograms.

Metabolite	Molecular ion composition	Identified hydroxylation site/s	Molecular ion mass [Da]	Identified TMS isomer	Rel. abundance
Mono hydroxylated S42					
M1a	$[C_{27}H_{44}O_2Si_2]^{+\bullet}$	A-ring benzylic OH	456.2875	C20-TMS	+++
M1b	$[C_{27}H_{44}O_2Si_2]^{+\bullet}$	A-ring benzylic OH	456.2878	C17-TMS	++++
M1c	$[C_{27}H_{44}O_2Si_2]^{+\bullet}$	A-ring benzylic OH	456.2876	C17-TMS	+++
Bis hydroxylated S42					
M2a	$[C_{30}H_{52}O_3Si_3]^{+\bullet}$	D-ring	544.3225	C20-TMS	+
M2b	$[C_{30}H_{52}O_3Si_3]^{+\bullet}$	A,B-ring	544.3233	C17-TMS	+++
M2c	$[C_{30}H_{52}O_3Si_3]^{+\bullet}$	A,B-ring	544.3228	C20-TMS	++
M2d	$[C_{30}H_{52}O_3Si_3]^{+\bullet}$	D-ring	544.3225	C20-TMS	++
Tris hydroxylated S42					
M3a	$[C_{33}H_{60}O_4Si_4]^{+\bullet}$	A,B & D-ring	632.3589	C20-TMS	+
M3b	$[C_{33}H_{60}O_4Si_4]^{+\bullet}$	A,B & D-ring	632.3586	C20-TMS	+++
M3c	$[C_{33}H_{60}O_4Si_4]^{+\bullet}$	A,B & D-ring	632.3588	C20-TMS	+
oxygenated S42					
M4	$[C_{27}H_{42}O_3Si_2]^{+\bullet}$	-	470.2666	C17-TMS	++
M5	$[C_{30}H_{50}O_4Si_3]^{+\bullet}$	-	558.3004	C20-TMS	+

The mono-hydroxylated S42 metabolite characterized on the basis of the GC-EI HR MS analysis of three isomeric TMS derivatives (**M1a**, **M1b**, and **M1c**) is identified to have a benzylic alcohol functionality in ring A (**Scheme 61**) This conclusion can be drawn on the basis of the characteristic mass shifts found in the respective A,B-ring fragment ions of ^{2}H-labeled metabolites **M1a-d5**, **M1b-d5**, and **M1c-d5** and in comparison with the EI HR MS data of S42-C6*ß*-OH (**3**), S42-C7*α*-OH (**4**).

The analyses of the bis-hydroxylated S42 metabolites yielded extensive structural insights on a set of four isomeric TMS-S42 derivatives (**M2a**, **M2b**, **M2c**, and **M2d)** However, the respective GC-EI HR MS and MS^2-product ion mass spectra do not allow a conclusive assignment to either a single or more than one metabolite structures. The structural similarities of **M2a** and **M2d** as well as of **M2b** and **M2c** were found but the results do not allow an unambiguous judgment and an unequivocal structure assignment.

Furthermore, three tris-hydroxylated S42 metabolites **M3a**, **M3b**, and **M3c** were identified and investigated on the basis of GC-EI-MS and MS^2-product ion spectra Finally, two additional oxidized S42 metabolites **M4** and **M5** were

identified in trace amounts on the basis of MS^2-product ion mass spectra. The EI HR mass spectra of the analytes **M4** and **M5** indicate an additional oxidation site, potentially the formation of an oxo-function in these S42 biotransformation products.

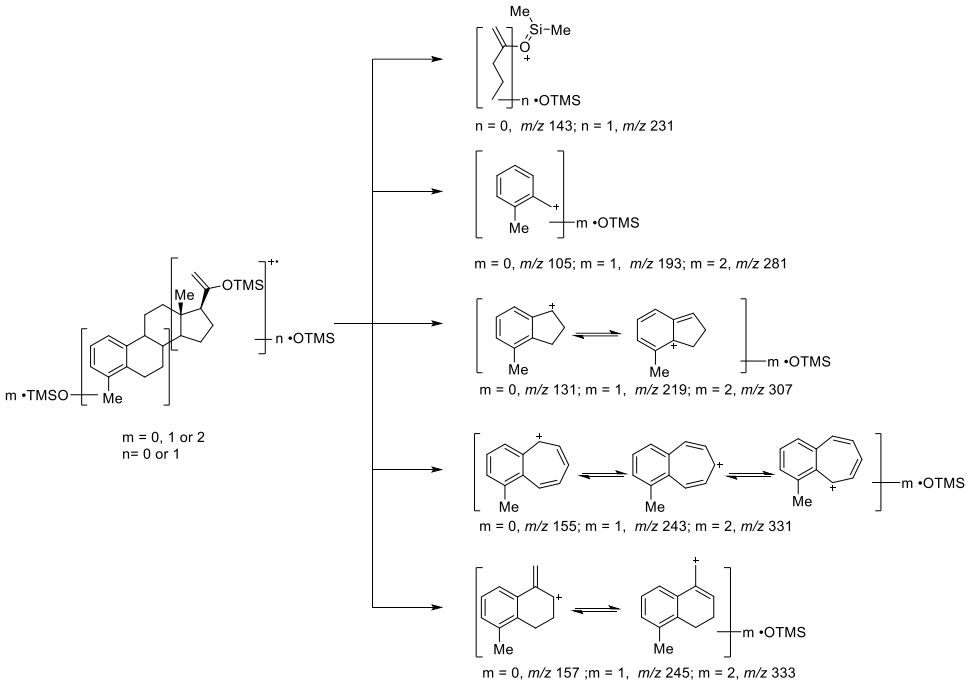

Scheme 62. Proposed ion structures of significant fragment ions that were found in GC-EI-MS^2 spectra. The precursor ions were the respective molecular ions of TMS-derivatized S42 *in vitro* metabolites.

Generally, characteristically mass-shifted fragment ions indicate the presence of TMS functionalities (88 Da) in the respective steroid sub-structure (**Scheme 62**). For example, the ion series at *m/z* 281 (105 + 88 x 2 Da), *m/z* 307 (131 + 88 x 2 Da), *m/z* 320 (144 + 88 x 2 Da), *m/z* 331 (155 + 88 x 2 Da), and *m/z* 333 (157 + 88 x 2 Da) indicated double hydroxylation at ring A based on the TMS-related mass-shifts; while the indicative fragment ions at *m/z* 230 (142 + 88 Da), at *m/z* 231 (143 + 88 Da), and at *m/z* 244 (156 + 88 Da) suggested hydroxylation at ring D for the same reasons.

This study provides fundamental analytical data for further studies on the metabolic transformation of synthetic 20-keto steroids like S42 (**1**). The observed fragments from the *in vitro* phase I metabolites may be found in *in vivo* samples as well.

4.3.7 *In vitro* phase II metabolism of S42 (**1**) analyzed by LC-ESI-HRMS

Phase II metabolites are usually more abundant than phase I metabolites in urine.[37, 121] The conjugation reactions enhance the metabolites' polarity and solubility in urine, allowing them to be excreted in urine. Therefore, phase II metabolites are the preferred targets for urine doping control. Due to the high polarity, phase II metabolites are better suited for LC-ESI-HRMS while phase I metabolites, which are less polar, are more compatible for GC-EI-HRMS analysis.

Sample preparation

Aliquots from the phase I reaction mixture were taken for glucuronidation and sulfation to study phase II conjugation. Uridine-5′-diphosphoglucuronic acid (UDPGA) was applied as a glucuronidation agent. The common sulfation method utilizes 3'-phosphoadenosine-5'-phosphosulfate (PAPS). In this study, PAPS was substituted with a cost-effective mixture of ATP, Na_2SO_4, and $MgCl_2$, which yielded higher conjugation efficiency in the literature.[122]

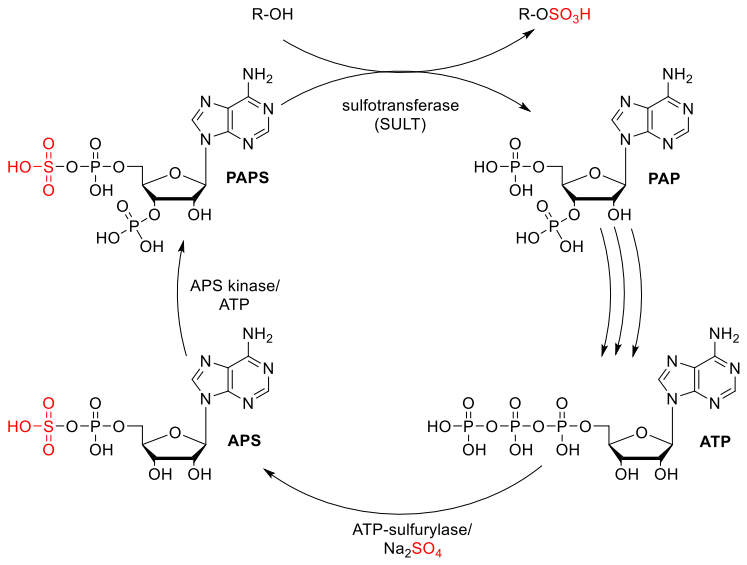

Scheme 63. Formation of PAPS by using ATP and Na_2SO_4 with S9 fraction according to *Weththasinghe et al*.[122]

Furthermore, additional human liver microsomes (HLM), enzyme S9 fraction, and the cofactor NADPH were added. The phase II reaction included two

additional reagents, alamethicin and *D*-saccharic acid-1,4-lactone (SL). The inclusion of the pore-forming peptide alamethicin in the phase II reaction has been shown to enhance conjugation rates.[123] Alamethicin improves substrate accessibility to enzymes by disrupting the membrane diffusion barrier between substrate and enzyme. D-saccharic acid-1,4-lactone (SL) acts as a *β*-glucuronidase inhibitor to prevent degradation of glucuronide conjugates.[124]

After incubation at 37 °C for 24 hours, the reaction was stopped by the addition of cold acetonitrile, then centrifuged, transferred, and dried for LC-ESI-HRMS analysis.[20b] Due to the hydrophilic property of the conjugated metabolites, LC-ESI-HRMS in negative ion mode was performed for most sensitive phase II metabolite detection without derivatization. Based on in silico predictions from *BioTransformer*, the phase I metabolites that were found from previous experiments (**Section 4.3.6**) were anticipated to undergo conjugation with either glucuronic acid or sulfate groups. The extracted ion chromatograms (EICs) from the full MS analysis were then screened for signals corresponding to the expected exact masses, using a mass accuracy threshold of 5 ppm.

LC-HRMS/MS analysis of *in vitro* phase II metabolites of S42

Signals identified in full scan acquisition mode were further analyzed using LC-ESI-HRMS^2 PRM experiments to identify diagnostic product ions indicative of glucuronide or sulfate conjugation (see **Figure 11**).

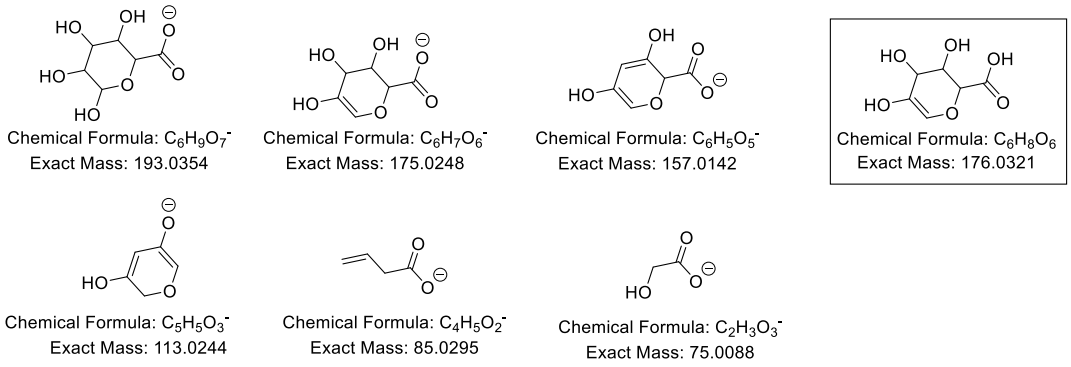

Scheme 64. Common fragments at *m/z* 193, 175, 157, 113, 85, and 75 from glucuronide metabolites by MS^2 experiments in negative mode. A neutral loss of 176 Da will produce an ion at *m/z* $[M\text{-}H\text{-}C_6H_8O_6]^-$.[125]

For glucuronide metabolites, common product ions were observed at *m/z* 193, 175, 157, and 113, corresponding to characteristic glucuronide cleavage patterns (see **Scheme 64**). Additional minor fragments at *m/z* 85 and *m/z* 75 were also occasionally detected. A neutral loss of 176 Da ($C_6H_8O_6$), which is most likely assigned the dehydrated glucuronic acid residue, is identified as a characteristic dissociation pathway for glucuronide metabolites investigated. [125] This neutral loss provides an effective screening method for glucuronide adducts and serves as first evidence for the presence of glucuronide-conjugated metabolites.

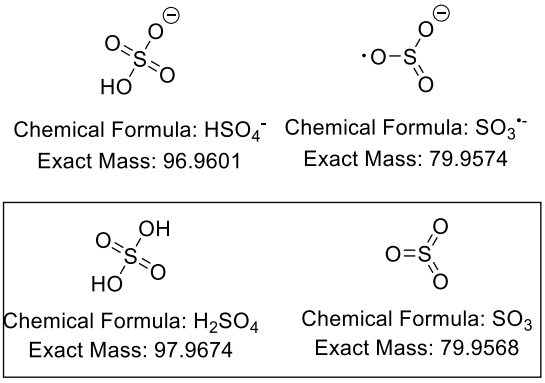

Scheme 65. Common fragments at *m/z* 97 and 80 from sulfate metabolites by MS^2 experiments in negative ionization mode. Neutral loss of 98 Da or 80 Da will produce ions at *m/z* $[M\text{-}H\text{-}H_2SO_4]^-$ and $[M\text{-}H\text{-}SO_3]^-$ respectively.[126]

The confirmatory product ions for sulfate-conjugated metabolites in the MS^2 spectra were observed at *m/z* 97 and 80, corresponding to characteristic sulfate-related fragments (SO_4^- and $SO_3^{\bullet-}$, respectively) (**Scheme 65**). Additionally, neutral losses of 98 Da (H_2SO_4) and 80 Da (SO_3) from the precursor ion forming product ions at *m/z* $[M–H–H_2SO_4]^-$ and $[M–H–SO_3]^-$, respectively. These fragmentation patterns provide strong evidence for the presence of sulfate conjugates, consistent with findings by *Fitzgerald et al*.[126]

Qualitative analysis of *in vitro* phase II metabolites of S42

Based on EICs and MS^2 data, both glucuronide and sulfate metabolites were successfully identified. The relative ratios of different metabolites were determined by the signal area ratio. For that approach the signal areas of the metabolites were divided by the area of the internal standard (testosterone

glucuronide-d3 added with known concentration) from the EICs in the full mass analysis.

Although the matrix in the sample may induce ion suppression when comparing metabolite ratios in full MS analysis, the relatively high concentrations of the conjugated metabolites and the minimal salt and matrix under simplified *in vitro* conditions provide a good reliability of this comparative analysis.

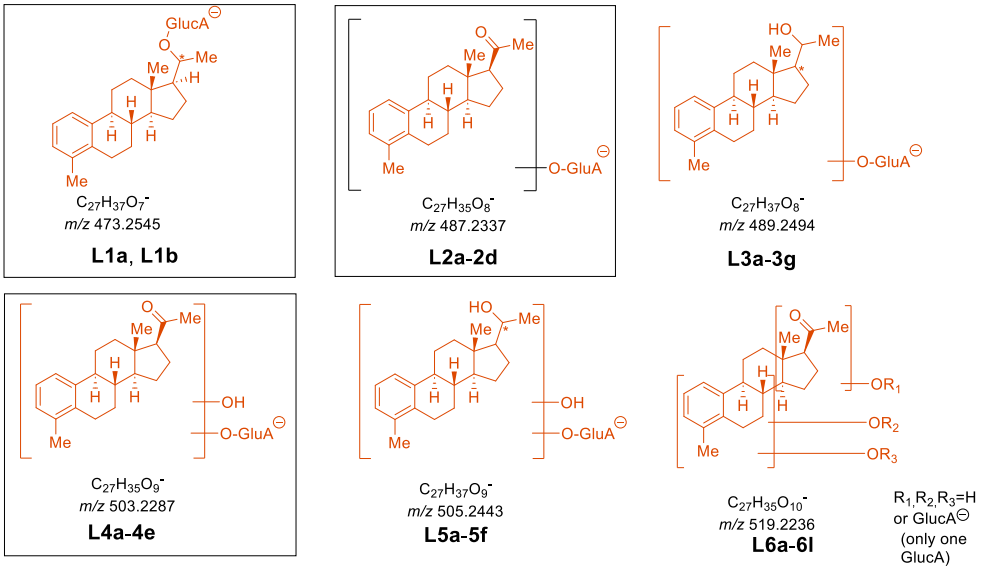

Scheme 66. Ionized glucuronide metabolites (negative mode) detected by LC-ESI-HR-MS.The major glucuronide-conjugated metabolites identified were **L1a**, **L2c**, **L4a**, and **L4b**. These correspond to the glucuronidation products of reduced S42 (**L1a**, *m/z* 473), S42-mono-OH (**L2c**, *m/z* 487), and S42-bis-OH (**L4a**, **L4b**, *m/z* 503). Additional minor metabolites were detected at *m/z* 489 (reduced S42-mono-O-GlucA), 505 (reduced S42-mono-O-GlucA+OH), and 519 (S42-mono-O-GlucA+2OH), with lower intensities.

It was identified that the major metabolites are the glucuronide-conjugated products from reduced S42 (**L1a**, *m/z* 473), S42-mono-OH (**L2c**, *m/z* 487), and S42-bis-OH (**L4a**, **L4b**, *m/z* 503). Additional metabolites with lower concentrations were found including reduced S42-mono-O-GlucA (**L3a-L3g**, *m/z* 489), reduced S42-mono-O-GlucA+OH (**L5a-L5g**, *m/z* 505), and S42-mono-O-GlucA+2OH (**L6a-L6l**, *m/z* 519). Only low levels of sulfated products from S42-mono-OH (**L7a**, **L7b**, *m/z* 391), reduced S42 (**L8a**, **L8b**, *m/z* 393), and S42-bis-OH (**L9a**, *m/z* 407) were detected.

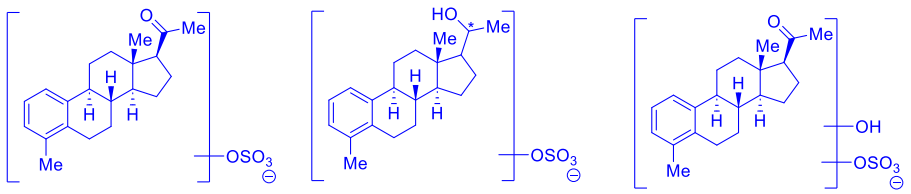

Scheme 67. Ionized sulfate metabolites (negative mode) from *in vitro* phase II experiments analyzed by LC-ESI-HRMS^2 (Orbitrap). Only low intensity of sulfated products (**L7a-L9a**) was discovered: conjugates derived from S42-mono-OH (**L7a**, **L7b**, *m/z* 391), reduced S42 (**L8a**, **L8b**, *m/z* 393), and S42-bis-OH (**L9a**, *m/z* 407).

Comparative results from *in vitro* phase I and phase II

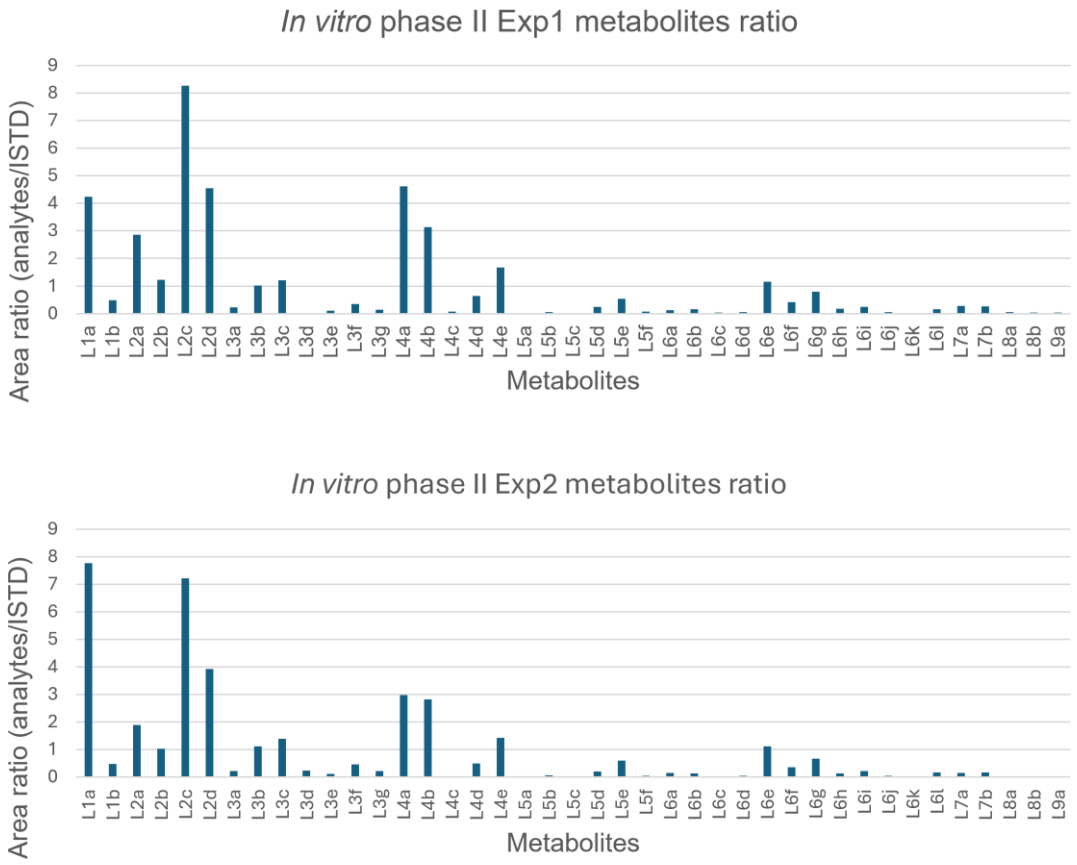

Figure 48. *In vitro* phase II metabolite profiles from two independent samples (A and B). They show the same trends and types of glucuronide and sulfate metabolites. The area ratios of glucuronide metabolites (**L1a-L6l**) were much higher than the sulfate metabolites (**L7a-L9a**).

The metabolic patterns observed in the two independently prepared samples by the same method were consistent, demonstrating reproducible glucuronidation and sulfation profiles (see **Figure 48A** and **B**). The experiments

Exp1 and Exp2 showed that glucuronide conjugates (**L1a**–**L6l**) were significantly more abundant than sulfate conjugates (**L7a**–**L9a**). Among the glucuronide products, metabolites derived from S42-mono-OH (**L2a–L2d**) and S42-bis-OH (**L4a**–**L4e**) were particularly prominent. Several triple-oxidized glucuronide species (**L6a**–**L6l**) were also detected but appeared at much lower intensities.

Metabolites with reduced C20-keto functionality (**L1a-1b**, **L3a-3g**, **L5a-5f**) were detected based on the mass shift of 2 Da (**Scheme 66**). Interestingly, the intensity of the reduced glucuronide metabolite **L1a** was comparable to **L2c**, that was derived from S42-mono-OH (**Figure 48**). The results suggest that respective metabolite formation, *i.e.* reduction pathways, occurred during the phase II experiment.[127] In fact, the metabolites **L1a-1b** are glucuronide conjugates of the identical synthetic S42-C20-OH compound (**2**), which was not detected in the *in vitro* phase I experiments analyzed by GC-EI-HRMS. One possible explanation could be the ionization efficiency of compound **2** in EI-MS. In contrast, sulfate conjugates of S42-mono-OH (**L7a**–**L7b**) were found in smaller quantities, reinforcing the predominance of glucuronidation in this system.

These findings from phase II *in vitro* studies are consistent with phase I results. In phase II, the glucuronidation and sulfation reaction occurred to S42-mono-OH, S42-bis-OH, or S42-tirs-OH, that were detected by the GC-EI-HRMS. Glucuronide formation was more favorable over sulfation. This trend is consistent with phase II metabolic patterns of structurally related steroids such as testosterone, epitestosterone, androsterone, and etiocholanolone reported in the literature.[37]

Origin of reduced metabolites in the *in vitro* phase II study

The detection of molecular ions of reduced S42 metabolites at *m/z* 473 (**L1a**–**L1b**), 489 (**L3a**–**L3g**), and 505 (**L5a**–**L5f**) indicates a respective formation on the *in vitro* phase II level (**Scheme 66**), as these ions were absent in the previous phase I study by GC-EI-HRMS. This finding may be related to the different detection sensitivity and selectivity in LC-ESI-HRMS and GC-EI-

HRMS methods, but can also be an artefact from reduction of phase I metabolites during *in vitro* incubation with the reaction mixture for phase II metabolite formation.[127]

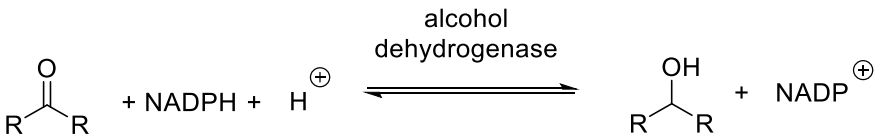

Scheme 68. Oxidation and reduction reactions by alcohol dehydrogenase are reversible and influenced by the cofactors concentration and substrate availability.[128]

In particular, it is plausible that both reduction and re-oxidation reactions occurred in the phase I system, with cytochrome P450 enzymes and alcohol dehydrogenase in the S9 fraction and the presence of NADPH as a cofactor (see **Scheme 67**).

In the phase II experiments, additional NADPH was introduced, which could have shifted the oxidation equilibrium toward the reduction pathway.[128] In addition, the competition between glucuronidation and sulfation reactions may have further influenced this shift, consistent with *Le Chatelier*'s Principle.

Metabolite's structure elucidation based on phase I and phase II experiments

The enhanced sensitivity of LC-ESI-HRMS (Orbitrap) also contributed to detecting trace amounts of triply oxidized metabolites which weren't observed in the GC-EI-HRMS (Orbitrap) approach. Possibly, triply hydroxylated metabolites (**L6e**-**6g**) show enhanced ionization properties compared to the mono- and bis-hydroxylated S42 derivatives in (-)ESI-MS analysis. LC-MS allowed the identification of a set of new metabolites with molecular ions at *m/z* 489 (**L3a**–**L3g**) and 505 (**L5a**–**L5f**). Furthermore, the enzymatic systems employed in phase I and phase II in vitro experiments, could have continued the phase I oxidation reaction, thereby generating additional tris-hydroxylated precursors available for conjugation. Despite the increased complexity of metabolites, most observed products remained single- or bis-oxidized species, aligning with the phase I data acquired earlier.

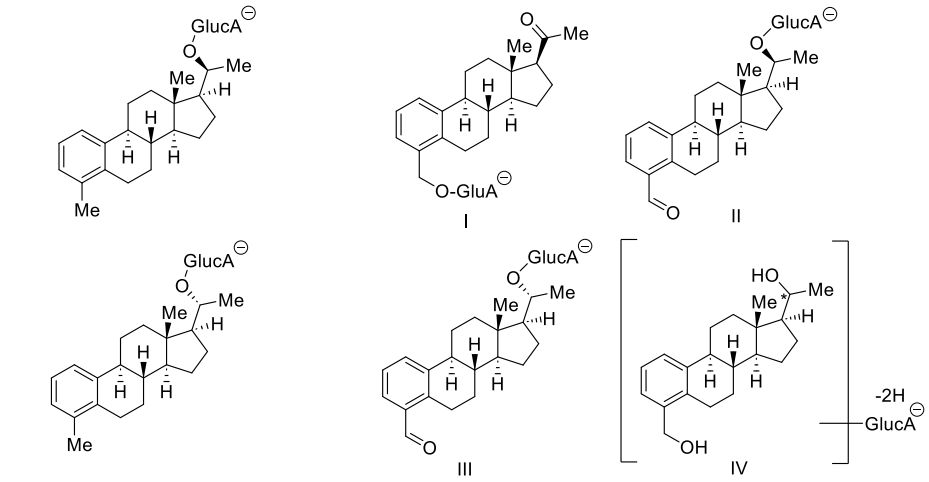

Chemical Formula: $C_{27}H_{37}O_7^-$
Exact Mass: 473.2545
L1a, **L1b**

Chemical Formula: $C_{27}H_{35}O_8^-$
Exact Mass: 487.2337
L2a-2d

Scheme 69. Proposed metabolite ion structures of abundant phase II metabolites: **L1a**, **L1b**; **L2a**, **L2b**, **L2c** and **L2d**. Ion structure IV contains a double bond, but the exact position is not determined and is indicated by a loss of two hydrogen atoms.

Because MS^2 dissociation in LC-MS primarily cleaves conjugated groups like glucuronide or sulfate, localizing exact oxidation sites is challenging. Based on the findings of the phase I experiments, oxidation sites are likely to be the A, B, or D rings in the steroid skeleton. The reduction products **L1a** and **L1b**, which were not observed previously, are hypothesized to result from the reduction of the C20 ketone group in S42 (**1**), forming glucuronic ester epimers (epimers, see **Scheme 69**).

In the phase I experiments, TMS-derivatized S42-mono-OH metabolites (**M1a**–**M1b**) were identified as hydroxyl derivatives in the C4 methyl group. The results of the phase I experiment indicate that glucuronidation may have occurred at the benzylic alcohol position (compound I, see **Scheme 69**). Further oxidation of the benzylic alcohol could produce a benzaldehyde intermediate. When the intermediate undergoes a reduction reaction at the C20 ketone group, this may lead to the formation of compound II and compound III. Compound IV is likely a product containing two hydroxy groups and one double bond without knowing the exact position. The double bond was indicated by a loss of two hydrogen atoms in **Scheme 69**.

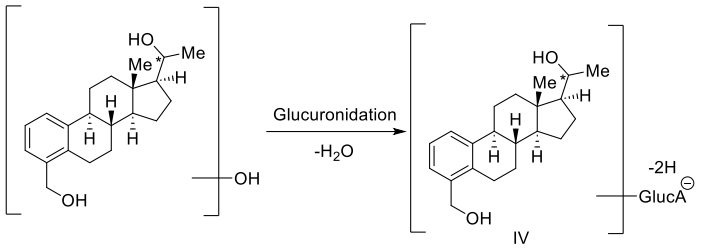

Scheme 70. A water elimination reaction from reduced S42-bis-OH and glucuronidation may give compound IV. The double bond position is not determined and is indicated by a loss of two hydrogen atoms.

Compound IV may be derived from S42-bis-OH through stepwise reactions involving the reduction of the C20 ketone to a secondary alcohol, followed by glucuronidation and an elimination reaction. The elimination step likely forms a double bond within the steroid ring system, ultimately yielding compound IV (see **Scheme 70**).

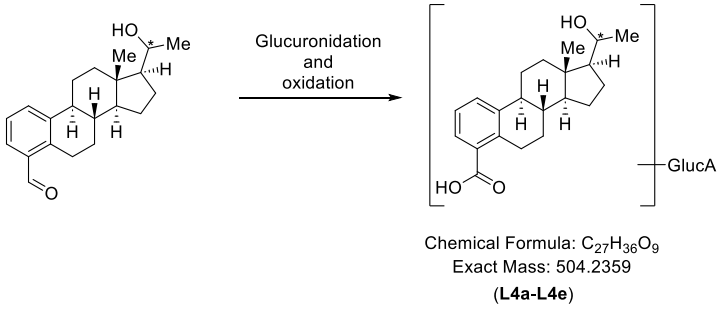

Scheme 71. Hypothesized structures of **L4a**-**L4e** from oxidation of benzaldehyde to benzylic acid derivatives and glucuronidation.

Further oxidation of the unstable aldehyde intermediates could produce benzoic acid derivatives, which may correspond to **L4a**–**L4e**, as shown in **Scheme 71**. Literature reports have shown the formation of a benzoic acid through stepwise oxidation of benzylic alcohols and aldehydes.[129]

4.4 *In vivo* animal studies of S42 (**1**): rat model

Compared to simplified *in vitro* assays using human liver microsomes (HLM) and the S9 fraction, *in vivo* animal studies offer a more complex and physiologically relevant view of metabolic pathways. To investigate the metabolism of S42 (**1**) *in vivo*, the *CER* Group in Belgium administered the compound to six male rats (average weight 276 ± 12 g). Blank urine samples were collected on day 1 prior to the administration of S42 (**1**). Subsequent urine samples were collected daily from day 2 through day 8.

Urine samples from Rats 1 and 2 were analyzed by GC-EI-HRMS (Orbitrap), using a targeted parallel reaction monitoring (PRM) mode. Samples from Rats 2 to 4 were analyzed by GC-EI-LRMS (triple quadrupole) using multiple reaction monitoring (MRM) to enhance detection sensitivity. Urine sample preparation for GC-MS analysis comprised enzymatic and acid-catalyzed hydrolysis of phase II-conjugates followed by trimethyl silylation (TMS) to improve volatility and sensitivity. For LC-MS analysis, urine samples from all six rats were cleared by centrifugation and analyzed subsequently without any front-end derivatization step.

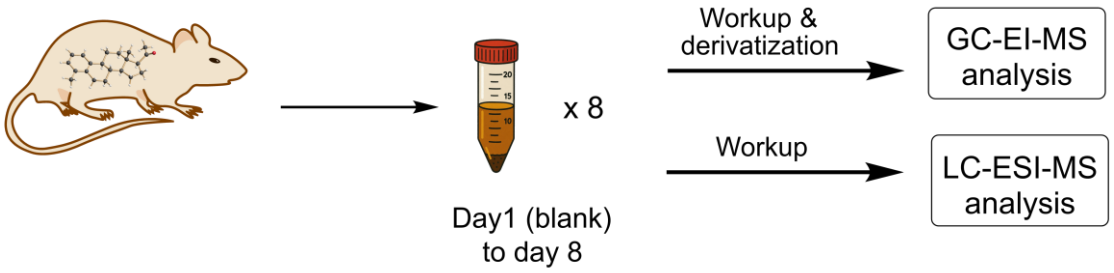

Scheme 72. Overviews of the S42 (**1**) administration in male rats and urine collection for eight consecutive days, followed by analysis via GC-EI-HR/LRMS and LC-ESI-HRMS. Image of the urine sample was produced by *ChatGPT*.[130]

4.4.1 Sample workup before GC-MS analysis

Since GC-MS is more suitable for analyzing hydrophobic compounds, glucuronide and sulfate conjugates required enzymatic and acid-catalyzed deconjugation to reduce polarity before trimethylsilyl (TMS) derivatization of the set of resulting phase I metabolites.

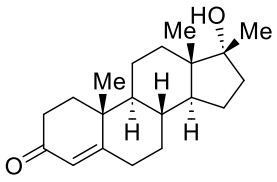

Methyltestosterone (**103**)

Scheme 73. Structure of methyltestosterone used as an internal standard (ISTD) in rat urine sample analysis.

Rat urine samples were purified using a combination of solid-phase extraction (SPE) and liquid-liquid extraction (LLE) to isolate both non-conjugated phase I metabolites (free fraction) and conjugated phase II metabolites (glucuronides and sulfates fractions). The initial SPE purification step used a C18 cartridge to concentrate samples and to remove salt and matrix impurities and minimize microbial interference, which is critical for the preservation of the internal standard methyltestosterone.[131] Methyltestosterone is commonly used due to its structural similarity to anabolic androgenic steroids (AAS) and comparable physicochemical characteristics.

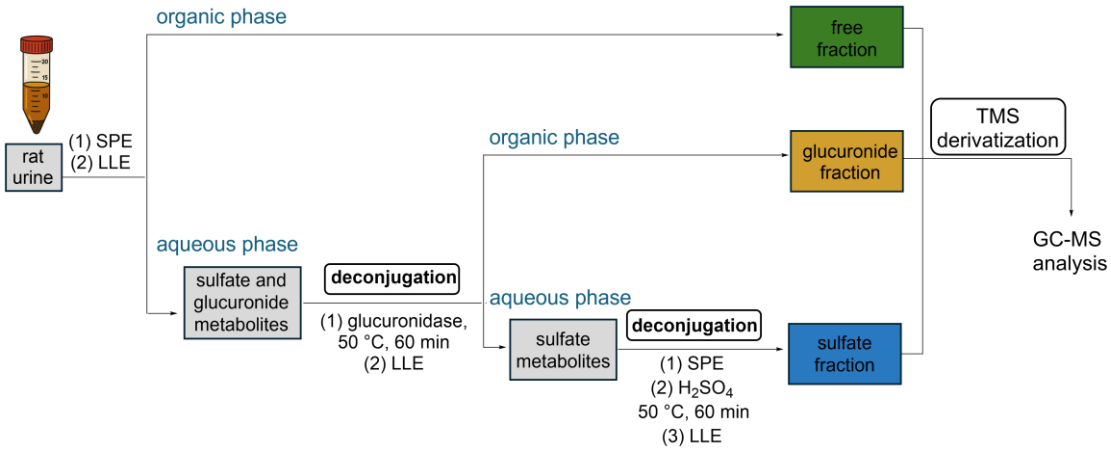

Scheme 74. Sample preparation is conducted according to the procedures of *Putz*, *Piper*, and *Thevis*.[47] The free fraction was separated after SPE and LLE. Conjugated glucuronide and sulfate metabolites underwent hydrolysis to yield hydroxy derivatives suitable for GC-MS analysis. Image of the urine sample was produced by ChatGPT.[130]

Following SPE, samples were dried and reconstituted for liquid/liquid extraction (LLE) using methyl *tert*-butyl ether (MTBE) and phosphate buffer (**Scheme 74**). The non-conjugated (free) phase I metabolites were extracted into the organic phase, while glucuronide and sulfate conjugates remained in the aqueous phase.

Glucuronide conjugates were hydrolyzed using *β*-glucuronidase and then subjected to a second LLE to isolate the liberated hydroxy metabolites in the organic layer. Enzymatic hydrolysis was stopped by adding 20% aqueous potassium carbonate (K_2CO_3). These samples were purified by an additional SPE step, followed by sulfuric acid solvolysis and a final LLE to extract formerly sulfated metabolites. All processed fractions (free, deconjugated glucuronide and deconjugated sulfate) were dried, and TMS derivatized before GC-EI-MS analysis.

4.4.2 PRM analysis by GC-EI-HRMS (Orbitrap)

Overview of metabolite investigation by PRM method

GC-EI-HRMS (Orbitrap) was employed to characterize S42 metabolites in rat urine. Conventional 70-50 eV electron ionization (EI) imparts a substantial amount of activation energy on the molecular ions which therefore show typically extensive fragmentation reactions leading to the formation of characteristic fragment ions that are instrumental for structure elucidation. In the much more gentle electrospray ionization (ESI) cooled molecular ions are formed and only minimal fragment formation is observed.

Urine samples from Rat 1 (days 1 to 8) were analyzed via full-scan GC-EI-HRMS following TMS derivatization. Based on previous *in vitro* data and *BioTransformer* (https://biotransformer.ca/) predictions,[110] specific molecular ions were selected for monitoring in the extracted ion chromatograms, particularly within the retention window of 17.0–19.5 minutes. When both $[M]^{+\bullet}$ and $[M-Me^{\bullet}]^{+}$ signals were detected within a five-ppm mass error, MS^2 (PRM) experiments were then conducted to reduce matrix interference and provide information about their product ions.

TMS-derivatized mono-, bis- and tris-hydroxylated metabolites were observed, consistent with the earlier *in vitro* experiments. However, since only non-deuterated S42 was administered *in vivo*, the assignment of hydroxylation position was interpreted solely from high-resolution MS^2 data and previous structural knowledge from *in vitro* experiments. Notably, TMS derivatization can

complicate MS interpretation, especially when distinguishing between ketone products and hydroxylated compounds with extra double bonds.

Several fragment ions (*m/z* 193.1043 and 281.1388) correspond to multiple constitutional isomers originating from TMS groups on the A/B or D rings. In contrast, ions such as *m/z* 307.1544 and 331.1554 are characteristic of A/B ring fragmentation. In *in vitro* MS^2 data, the co-appearance of *m/z* 281, 307, 331, and 333 supports the oxidation at A/B rings. Therefore, high-resolution MS^2 is indispensable for assigning oxidation positions in S42 metabolites.

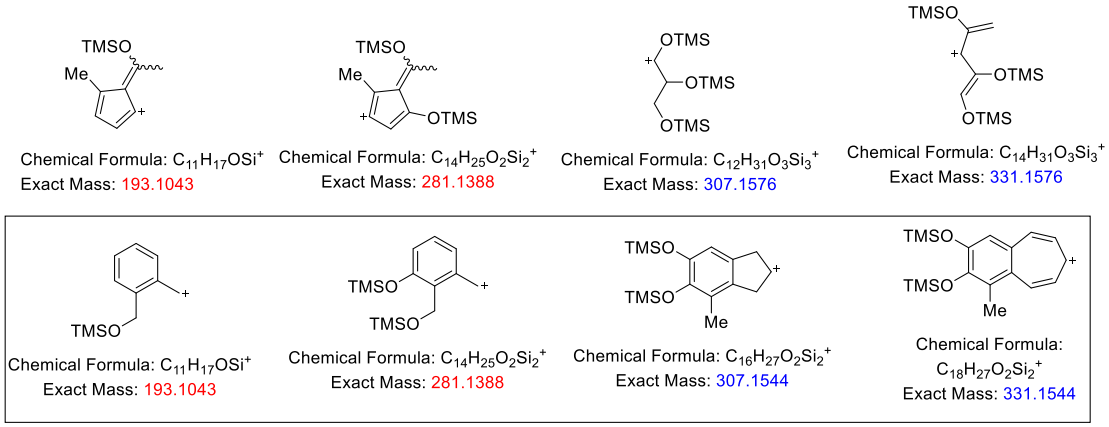

Scheme 75. Possible TMSO fragments at *m/z* 193 and 281 can be from A/B, or D rings. The positions of the TMSO groups were unknown. The ions at *m/z* 307.1544 and 331.1554 should be from the A/B ring.

GC-EI-PRM analysis of urine samples collected from Rat 1

Identification of mono-hydroxylated metabolites (*m/z* 450–456)

Mono-hydroxylated metabolites of S42 were detected across a retention time window of 18.21–18.82 minutes. Most of these species were present in the sulfate fraction, although some ions were also observed in the free fraction. (**Scheme 76**) Notably, metabolites at *m/z* 450 (**R1_M1a** – **R1_M1e**) were detected in the free fraction and may arise as fragment ions from parent species at *m/z* 540 due to their identical retention times.

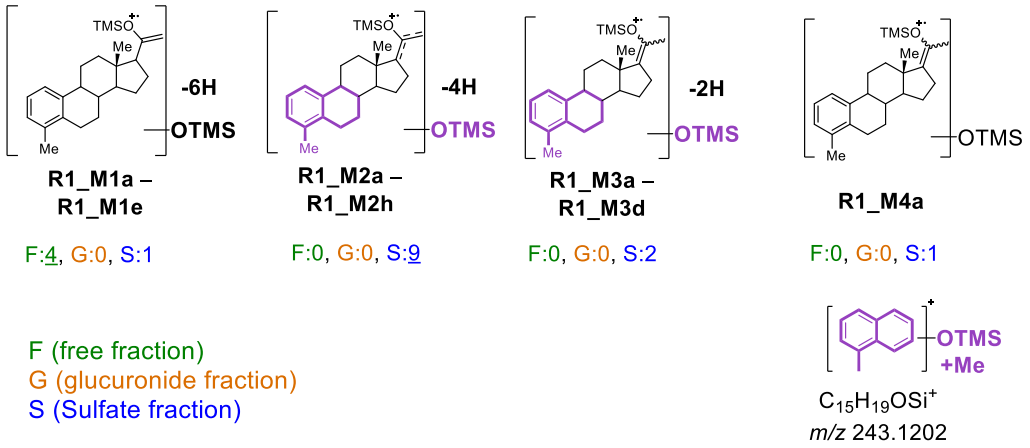

Scheme 76. S42-mono-OH derivatives found in urine samples of Rat 1 by GC-EI-HRMS (Orbitrap). **R1_M1b**, **R1_M1c**, **R1_M2b**, **R1_M2c**, **and R1_M2g** may be derived from S42-bis-OH derivative. The double bonds exact positions are not determined in the metabolites and is indicated by a loss of two hydrogen atoms.

A similar finding was observed with *m/z* 452 (**R1_M2a** – **R1_M2h**) in the sulfate fraction, which could be derived from the fragmentation of a *m/z* 542 precursor. Coelution patterns were observed in extracted ion chromatograms. Because these ions share retention times with known bis-hydroxylated metabolites, it is challenging to determine whether they represent different hydroxylated species or are simply $[M-TMSOH]^+$ fragments of more oxidized parent ions.

The presence of product ions,$[M\text{-}Me^{\bullet}]^+$ and $[M\text{-}Me^{\bullet}\text{-}TMSOH]^+$ were discovered in most precursor ions at *m/z* 435, 345 (from *m/z* 450); *m/z* 437 and 347 (from *m/z* 452); *m/z* 439 and 349 (from *m/z* 454); *m/z* 351 (from *m/z* 456).

MS^2 spectra for *m/z* 452 and 454 consistently detected *m/z* 243, a diagnostic ion suggestive of A/B ring oxidation. The oxidation position is supported by earlier *in vitro* data

Table 12. Mono-hydroxylated metabolites of S42 found in free, glucuronide and sulfate fractions in urine samples of Rat 1 on day 2. The signals (in red) of *m/z* 450 and 452 may be fragmented ions from other molecular ions at *m/z* 540 and 542 respectively (see **Table 15**).

	Rat 1		GC T program: 185(0)-3-234(0)-40-310(2) ISTD: Methyltestosterone RT:14.12 (RT 18-20 min not influence)			
Metabolites	Theo. mass [Da]	Precursor ion composition	RT			Product ions (*m/z*)
			Free	Glucuronide	Sulfate	
S42-mono-OH-6H (**R1_M1a** - **R1_M1e**)	450.2405	$[C_{27}H_{38}O_2Si_2]^{+\bullet}$	18.37, 18.60, 18.64, 18.76 (**R1_M1a** - **R1_M1d**)	n.a.	18.21 (**R1_M1e**)	435, 345
S42-mono-OH-4H (**R1_M2a** - **R1_M2h**)	452.2561	$[C_{27}H_{40}O_2Si_2]^{+\bullet}$	n.a.	n.a.	18.05, 18.27, 18.32, 18.53, 18.63, 18.70, 18.73, 18.81 (**R1_M2a** - **R1_M2h)**	437, 347, 243
S42-mono-OH-2H (**R1_M3a** - **R1_M3d**)	454.2718	$[C_{27}H_{42}O_2Si_2]^{+\bullet}$	n.a.	n.a.	17.83, 17.89, 18.76, 18.82 (**R1_M3a** - **R1_N3d**)	439, 349, 243
S42-mono-OH (**R1_M4a**)	456.2874	$[C_{27}H_{44}O_2Si_2]^{+\bullet}$	n.a.	n.a.	17.72 (**R1_M4a**)	351, 244, 117

High-resolution MS^2 spectra for *m/z* 452 (**R1_M2a** – **R1_M2h**) revealed consistent signals at *m/z* 193.1043 and 196.1278, which correspond to possible TMS-ether fragments from either the C17 or C20 positions at the D ring.

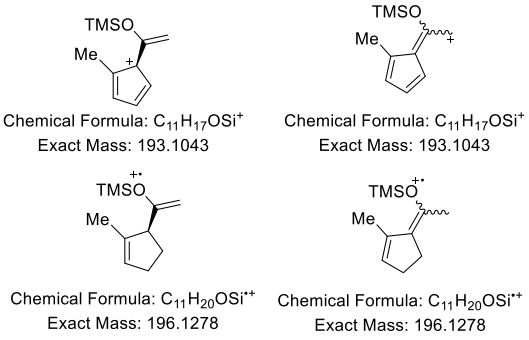

Scheme 77. Proposed structures for *m/z* 193 and 196 fragment ions may be C20 or C17-TMS isomers from mono-OH precursors or degradation of bis-OH species.

It was observed that the peaks at *m/z* 196, *m/z* 193, and *m/z* 195 correspond in their extracted ion chromatograms. The ion at *m/z* 193 could be generated

when a new double bond at the D ring formed during the hydrolysis workup or analysis.

Identification of bis-hydroxylated metabolites (*m/z* 540–544)

Bis-hydroxylated metabolites of S42 were identified across the free, glucuronide, and sulfate fractions in Rat 1 urine collected on day 2. The GC-EI-HRMS chromatogram presents these compounds in retention times between 18.22 and 18.72 minutes. Three different molecular ions were observed at: *m/z* 540 (**R1_M5a** – **R1_M5d**), 542 (**R1_M6a** – **R1_M6f**) and 544 (**R1_M7a** – **R1_M7d**).

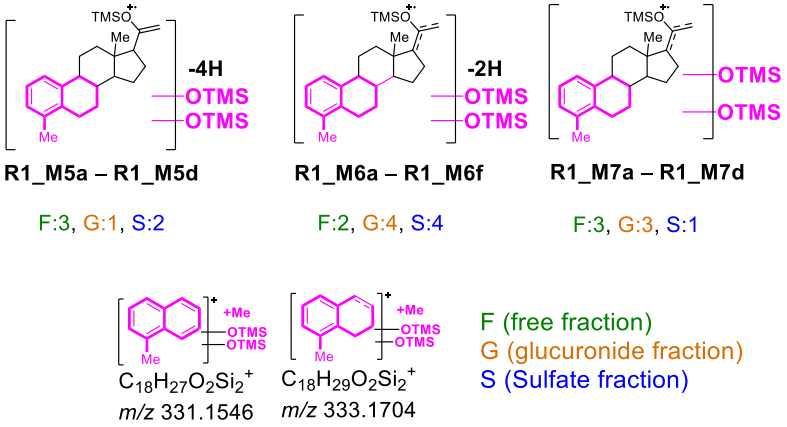

Scheme 78. S42-bis-OH derivatives found in urine samples of Rat 1 by GC-EI-HRMS (Orbitrap). The double bonds exact positions are not determined in the metabolites and is indicated by a loss of two hydrogen atoms.

These ion masses correspond to metabolites with two oxygen atoms and up to two double bonds (likely hydroxyl groups with double bonds or ketone groups), confirmed by their MS^2 product ions. The most prominent bis-OH derivatives were **R1_M5b** (*m/z* 540, RT 18.61 min) and **R1_M7a** (*m/z* 544, RT 18.22 min), both detected in the free fraction.

Their product ions at *m/z* 281, 307, and 331 were found to be similar to the *in vitro* experiment results, indicating oxidation position at the A and B rings. Ions at *m/z* 143 and 195 hinted at derivatization at the C17 and C20 positions, respectively.

Many bis-OH metabolites detected in the free fraction were also identified in the glucuronide and sulfate fractions, with matching retention times and fragmentation profiles. This observation supports the theory that phase I

hydroxylated compounds undergo phase II conjugation, presenting an incomplete metabolic conversion.

Table 13. S42-bis-OH derivatives found in Rat 1 urine on day 2.

	Rat 1		GC T program: 185(0)-3-234(0)-40-310(2) ISTD: Methyltestosterone RT:14.11			
Metabolites	Nominal mass [Da]	Molecular ion composition	RT (*m/z*) F	G	S	MS^2 product ions (*m/z*)
S42-bis-OH-4H (**R1_M5a** - **R1_M5d**)	540.2906	$[C_{30}H_{48}O_{33}Si_3]^{+\bullet}$	18.23 (**R1_M5a**) 18.61, (**R1_M5b**) 18.65 (**R1_M5c**)	18.79 (**R1_M5d**)	18.61 (**R1_M5b'**) 18.64 (**R1_M5c'**)	525, 435, 345, 331, 143/195
S42-bis-OH-2H (**R1_M6a** - **R1_M6f**)	542.3062	$[C_{30}H_{50}O_3Si_3]^{+\bullet}$	18.30 (**R1_M6a**) 18.72 (**R1_M6b**)	18.30 (**R1_M6a'**) 18.32 (**R1_M6c**) 18.55 (**R1_M6d**) 18.72 (**R1_M6b'**)	18.27 (**R1_M6e**) 18.32 (**R1_M6c'**) 18.68 (**R1_M6f**) 18.72 (**R1_M6b''**)	527, 333, 331, 281, 143/195
S42-bis-OH (**R1_M7a** - **R1_M7d**)	544.3219	$[C_{30}H_{52}O_3Si_3]^{+\bullet}$	18.22 (**R1_M7a**) 18.27 (**R1_M7b**) 18.48 (**R1_M7c**)	18.22 (**R1_M7a'**) 18.27 (**R1_M7b'**) 18.48 (**R1_M7c'**)	(18.27) (**R1_M7b''**) 18.46 (**R1_M7d**)	333, 331, 307, 281, 195/143

Identification of tris-hydroxylated metabolites (*m/z* 630, 632)

Tris-hydroxylated derivatives of S42 were identified predominantly in the free and glucuronide fractions of Rat 1 urine samples collected on day 2. These metabolites eluted between 18.90 and 19.40 minutes in the GC-EI-HRMS chromatogram. Molecular ions were observed at *m/z* 630 (S42-tris-OH-2H, **R1_M8a** – **R1_M8e**) and *m/z* 632 (S42-tris-OH, **R1_M9a** – **R1_M9b**). The most intense signals originated from **R1_M8a** in free fraction and **R1_M8a'** in glucuronide fraction, both at RT 18.93 min.

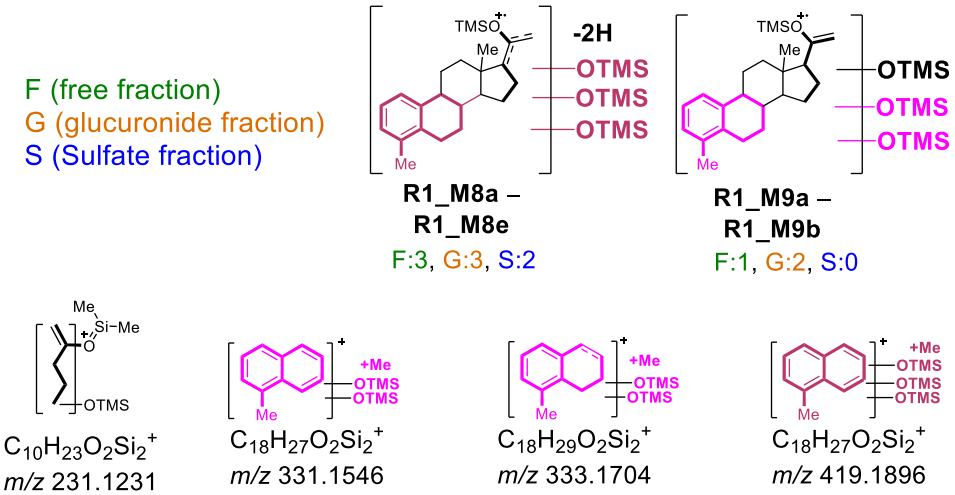

Scheme 79. S42-tris-OH derivatives were discovered in Rat 1 urine on day 2. Hydroxylation at the D ring and A/B ring was hypothesized by detecting ions at *m/z* 231, and *m/z* 331, 333, and 419 in MS^2 spectra, with TMSO groups contributing characteristic *m/z* 143, 155, 157 + n x 88 Da shifts (n = 1 - 3).

A new key diagnostic fragment ion at *m/z* 419 was consistently observed in the MS^2 spectra of **R1_M8a** and **R1_M8a'** (see **Table 14**). This fragment corresponds to *m/z* 155 + 3 x 88 Da (TMSO functional groups), suggesting all three hydroxy groups are located at A, B ring system.

The product ions at *m/z* 331 (155 + 2 × 88 Da) and *m/z* 307 (131 + 2 × 88 Da), observed in both **R1_M9a** and **R1_M9b**, indicate the presence of two hydroxyl groups derivatized with TMS on the A, B ring system. The fragment ion at *m/z* 231 (143 + 88 Da) also suggests a third hydroxyl group at the D ring. These fragmentation signatures closely match the results in *in vitro* phase I MS^2 spectra of S42-tris-OH derivatives, supporting structural consistency across *in vitro* and *in vivo* models.

Table 14. S42-tris-OH derivatives were discovered in Rat 1 urine on day 2.

Rat 1			GC T program: 185(0)-3-234(0)-40-310(2) ISTD: Methyltestosterone RT:14.11			
Types	Theo. mass [Da]	Molecular ion composition	RT F	RT G	RT S	MS^2 product ions from rat samples (*m/z*)
S42-tris-OH-2H (**R1_M8a** - **R1_M8e**)	630.3407	$[C_{33}H_{58}O_4Si_4]^{+\bullet}$	18.93 (**R1_M8a**) 19.11 (**R1_M8b**) 19.17 (**R1_M8c**)	18.93 (**R1_M8a'**) 18.99 (**R1_M8d**) 19.10 (**R1_M8b'**)	n.a. 18.98 (**R1_M8d'**) 19.21 (**R1-M8e**)	331, 231 525, 419, 331, 195
S42-tris-OH (**R1_M9a** - **R1_M9b**)	632.3563	$[C_{33}H_{60}O_4Si_4]^{+\bullet}$	(19.06) (**R1_M9a**) 19.40 (**R1_M9b**)	19.05 (**R1_M9a'**) 19.40 (**R1_M9b'**)	n.a. n.a. n.a.	331, 307, 231

Comparison of the metabolite profile found in urine of Rat 1 and in the *in vitro* phase I study

A comparison between *in vitro* and *in vivo* (rat) metabolism models of S42 reveals notable differences in oxidative biotransformation and conjugation patterns. The primary metabolites in the *in vitro* phase I experiments were mono-hydroxylated species. However, in urine samples from Rat 1, particularly those collected on Days 2 and 3, the dominant metabolites identified in the free and glucuronide fractions were bis- and tris-hydroxylated compounds. In contrast, the sulfate fraction predominantly contains mono-hydroxylated metabolites.

Analysis of the MS² spectra revealed key diagnostic fragment ions at *m/z* 231, 243, 331, and 419. These ions are essential for elucidating the oxidation positions on the S42 backbone. Fragment ions at *m/z* 231 (143 + 88 Da) and 243 (155 + 88 Da) typically indicate oxidation at the D ring and A/B rings, respectively. The ion at *m/z* 331 (155 + 2 × 88 Da) corresponds to two TMSO-derivatized hydroxyl groups at the A/B ring. A novel peak at *m/z* 419 (155 + 3 × 88 Da) strongly indicates tris-hydroxylation at the A/B rings. All of these fragments, except *m/z* 419, were previously detected in the *in vitro* data, providing a solid basis for comparison and structural interpretation.

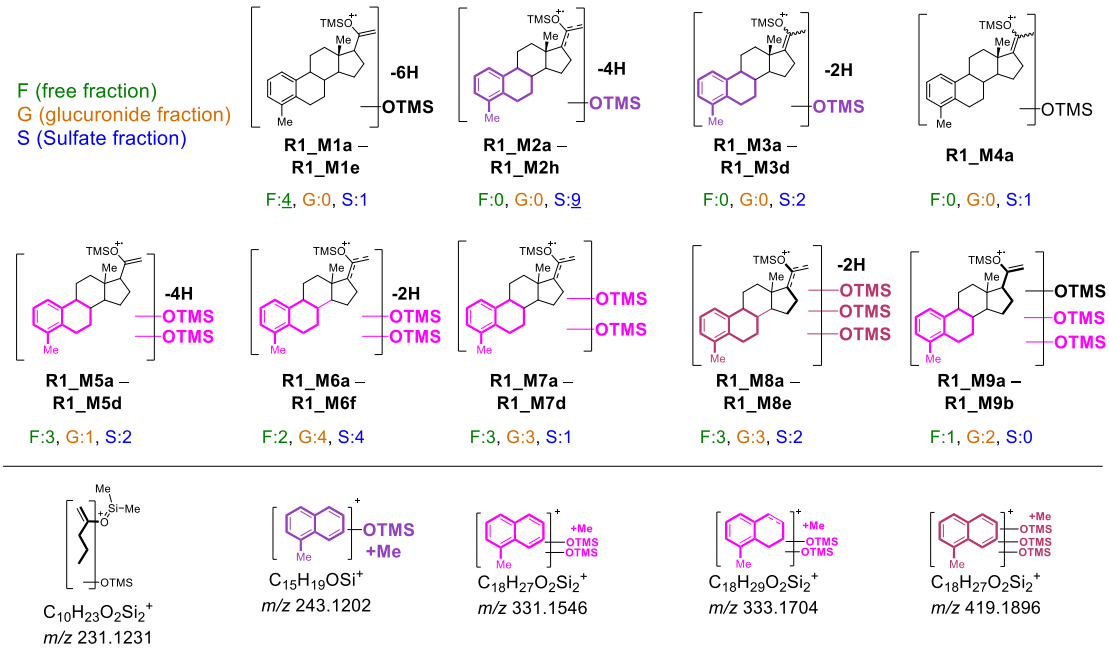

Scheme 80. Illustration of the TMS-derivatized metabolites detected in the urine of Rat 1. Fragment ions at *m/z* 231, 243, 331, and 419 were consistently observed across the free, glucuronide, and sulfate fractions. In the free fraction, a fragment ion at *m/z* 450 likely originated from a parent ion at *m/z* 540, based on their identical retention times in the extracted chromatograms. Similarly, *m/z* 452 is likely derived from *m/z* 542 in the sulfate fraction.

As illustrated in **Scheme 80**, the fragment ions mentioned above were consistently found across all three sample types: free, glucuronide, and sulfate fractions. Importantly, in the free fraction, an ion at *m/z* 450 was observed at the same retention time as a precursor ion at *m/z* 540 (see **Table 15**). This coelution suggests that *m/z* 450 is not a molecular ion but a fragment ion ($[M-TMSOH]^{+\bullet}$) of the bis-hydroxylated metabolite at *m/z* 540. A similar phenomenon was found in the sulfate fraction, where *m/z* 452 coeluted with *m/z* 542. Full-scan and MS^2 analysis suggested that *m/z* 450 and 452 are fragment ions originating from TMS-dehydration of precursor ions at *m/z* 540 and 542, respectively.

It is interesting to compare rat and *in vitro* metabolism models. The major *in vitro* phase I metabolite is a mono-hydroxylate product. For Rat 1 samples, the free and glucuronide fractions were identified as bis- or tris-hydroxylated derivatives. In contrast, the sulfate fraction mainly contained mono-hydroxylated metabolites. These compounds were primarily detected in samples from Day 2 and Day 3.

In addition, many metabolites observed in the free fraction were also detected in the glucuronide and sulfate fractions with matching molecular ion masses, retention times, and fragmentation profiles. This observation supports a sequential metabolic pathway where phase I hydroxylated metabolites become substrates for phase II conjugation reactions. The identical metabolite patterns and retention time in conjugated and non-conjugated fractions confirm that hydroxylation precedes glucuronidation or sulfation. Therefore, the rat metabolism data shows that S42 (**1**) undergoes multiple oxidations followed by conjugation, highlighting a more complex metabolic pathway from the *in vivo* model than the *in vitro* model.

Table 15. Metabolites identified from Rat 1 urine samples were analyzed using GC-EI-HR-MS (Orbitrap) with HCD at 20 eV. The bis-hydroxylated metabolite S42-bis-OH appeared at 18.48 minutes (in bold) and exhibited a fragmentation pattern and retention behavior closely aligned with the *in vitro* phase I experiments. Importantly, metabolites with identical molecular ions and retention times (underlined) were consistently observed across the free, glucuronide, and sulfate fractions. Notably, fragment ions detected at *m/z* 450 and 452 were found to share retention times (in red) with parent ions at *m/z* 540 and 542, respectively. * Results not from the same *in vitro* experiment.

Rat 1				T program: 185(0)-3-234(0)-40-310(2) ISTD: Methyltestosterone RT:14.12 → 14.81 (RT 18-20 min not influence)					
Types	Metabolites	Theo. mass [Da]	Molecular ion composition	RT			MS^2 product ions from rat samples (*m/z*)		Hypothesized oxidation position
				F	G	S	In vitro phase I		
S42-mono-OH-6H	**R1_M1a - R1_M1e**	450.2405	$[C_{27}H_{38}O_2Si_2]^{+\bullet}$	18.37, 18.60, 18.64, 18.76	n.a.	18.21	n.a.	435, 345	n.a.
S42-mono-OH-4H	**R1_M2a - R1_M2h**	452.2561	$[C_{27}H_{40}O_2Si_2]^{+\bullet}$	n.a.	n.a.	18.05, 18.27, 18.32, 18.53, 18.63, 18.70, 18.73, 18.81	n.a.	437, 347, 243	A, B ring
S42-mono-OH-2H	**R1_M3a - R1_M3d**	454.2718	$[C_{27}H_{42}O_2Si_2]^{+\bullet}$	n.a.	n.a.	17.83, 17.89, 18.76, 18.82	n.a.	439, 349, 243	A, B ring
S42-mono-OH	**R1_M4a**	456.2874	$[C_{27}H_{44}O_2Si_2]^{+\bullet}$	n.a.	n.a.	17.72	17.88, 17.96, 18.03	351, 244, 117	n.a.
S42-bis-OH-4H	**R1_M5a - R1_M5d**	540.2906	$[C_{30}H_{48}O_{33}Si_3]^{+\bullet}$	18.23, 18.61, 18.65	18.79	18.61, 18.64	n.a.	435, 345, 331	A, B ring
S42-bis-OH-2H	**R1_M6a - R1_M6f**	542.3062	$[C_{30}H_{50}O_3Si_3]^{+\bullet}$	18.30, 18.72	18.30, 18.32, 18.55, 18.72	18.27, 18.32, 18.68, 18.72	n.a.	527, 333, 331, 281	A, B ring
S42-bis-OH	**R1_M7a - R1_M7d**	544.3219	$[C_{30}H_{52}O_3Si_3]^{+\bullet}$	18.22, 18.27, **18.48**	18.22, 18.27, **18.48**	(18.27), 18.46	18.37, 18.41, **18.47**, 18.63	333, 331, 307, 281	A, B ring
S42-tris-OH-2H	**R1_M8a - R1_M8e**	630.3407	$[C_{33}H_{58}O_4Si_4]^{+\bullet}$	18.93, 19.11, 19.17	18.93, 18.99, 19.10	18.98, 19.21	n.a.	525, 419, 331; 331, 231	A, B ring; A,B and D ring;
S42-tris-OH	**R1_M9a - R1_M9b**	632.3563	$[C_{33}H_{60}O_4Si_4]^{+\bullet}$	(19.06), 19.40	19.05, 19.40	n.a.	*19.00, 19.15, 19.64	331, 307, 231	A, B and D ring

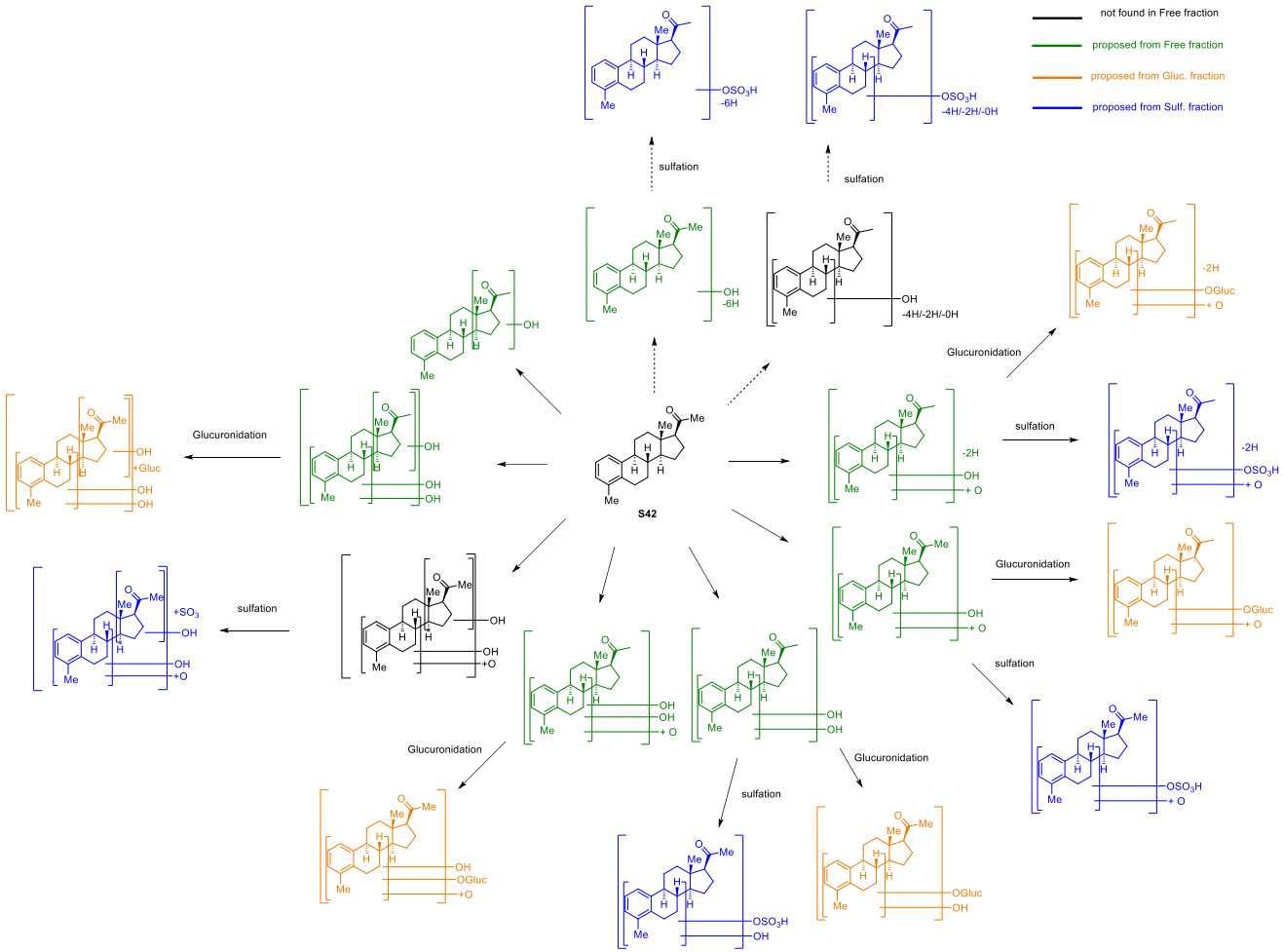

Scheme 81. Proposed metabolite structures found in urine collected from Rat 1. GC-EI-HRMS/MS analysis after phase II adduct hydrolysis and TMS derivatization.

Comparative analysis of urine samples collected from Rats 1 and 2

Rat 2 samples on day 1 and day 2 were analyzed by GC-MS (Orbitrap) to determine whether the metabolites profile from Rat 2 is similar to samples from Rat 1. Due to biological variation and therefore differences in excretion patterns from individuals can be expected. The data here only showed the preliminary results of S42 rat metabolites and more data is needed to confirm the findings.

Although several derivatives from Rat 1 and Rat 2 showed similar MS^2 fragmentation patterns and aligned retention times, they cannot be definitively confirmed as the same metabolites due to the coelution problem and instrument-related retention time shifts.

Nevertheless, the observed metabolites identified in the urine samples of Rat 2 are similar to those found in the urine of Rat 1. In Rat 1 samples, the S42-tris-OH-2H (*m/z* 630) had a high intensity in the free and glucuronide fraction, while S42-mono-OH-4H (*m/z* 452) is more abundant in the sulfate fraction. In Rat 2, less S42-mono-OH-4H derivative (*m/z* 452) was observed. Our focus was comparing the presence and abundance of S42-mono-OH derivatives (*m/z* 450, 452, 454), S42-bis-OH derivatives (*m/z* 540, 542, 544), and S42-tris-OH derivatives (*m/z* 630, 632).

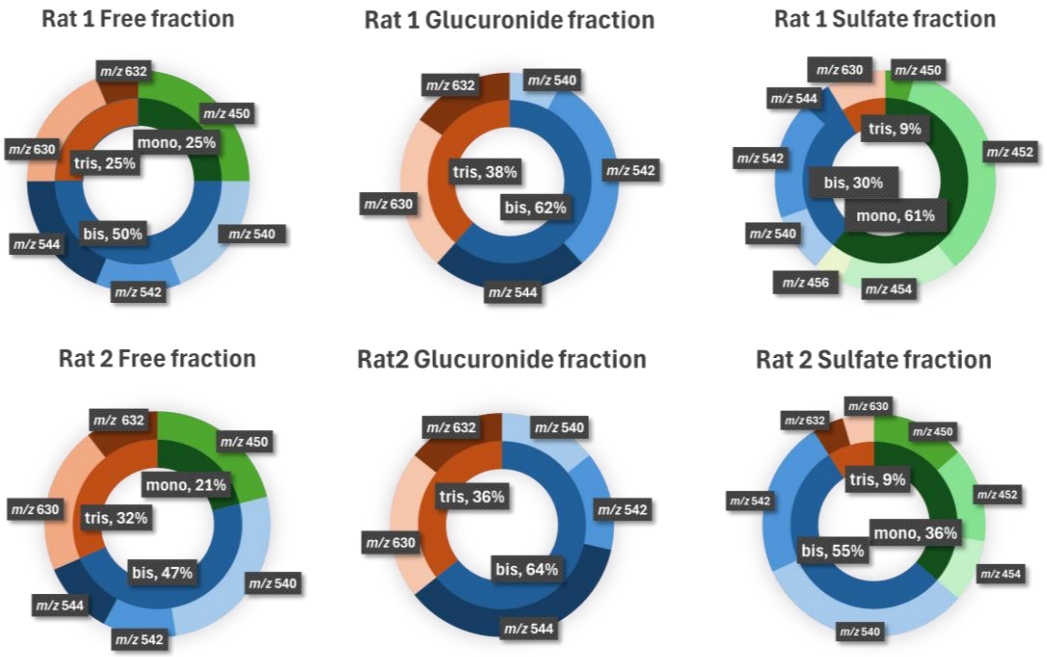

Figure 49. Percentage of different metabolites on day 2 in free, glucuronide, and sulfate fractions from Rat 1 and Rat 2.

In the free fraction, similar patterns were observed for both Rat 1 and Rat 2. All three metabolite categories were detected: S42-mono-OH, -bis-OH, and -tris-OH derivatives. S42-bis-OH derivatives dominate approximately 50%, while S42-tris-OH and S42-mono-OH derivatives represent about 30% and 20%, respectively.

In the glucuronide fraction, the profiles of both rats were also highly comparable. Only S42-bis-OH (around 60%) and S42-tris-OH (around 40%) derivatives were present. Mono-hydroxylated derivatives were not detected in either of the two rats.

In contrast, the sulfate fraction differed distinctly between Rat 1 and Rat 2. In Rat 1, S42-mono-OH derivatives were predominant (61%), followed by S42-bis-OH (30%) and S42-tris-OH (9%). In Rat 2, the primary metabolites were S42-bis-OH derivatives (55%), with mono-OH (36%) and tris-OH (9%) present in smaller proportions.

These results suggest that phase II sulfation may differ between the two animals. In Rat 1, sulfate conjugation primarily involved mono-hydroxylated metabolites, while Rat 2 primarily presented bis-hydroxylated metabolites.

Table 16. Ions at *m/z* 450 and *m/z* 540 were both discovered at the same retention time by Orbitrap and quadrupole analysis.

Nominal mass (*m/z*)	Chemical composition	Orbitrap Rt (min) (after 2.5 weeks)
450	$C_{27}H_{38}O_2Si_2^{\bullet+}$	18.40, 18.73, 18.88
540	$C_{30}H_{48}O_3Si_3^{\bullet+}$	18.39, 18.72, 18.88, 18.81, 18.98, 19.18, 19.27
452	$C_{27}H_{40}O_2Si_2^{\bullet+}$	18.41, 18.45, 18.50, 18.92
454	$C_{27}H_{42}O_2Si_2^{\bullet+}$	18.45, 18.94
542	$C_{30}H_{50}O_3Si_3^{\bullet+}$	18.41, 18.45,18.50, 18.91, 18.87
544	$C_{30}H_{52}O_3Si_3^{\bullet+}$	n.a.

From another perspective, it is also possible that the sulfate metabolites decomposed before the MS^2 experiment in the Rat 1 sample. In the sulfate fraction in Rat 2, the retention time of metabolite at *m/z* 540 and *m/z* 450 were the same. Additionally, *m/z* 450, 452, 454, and 542 showed similar retention times. This phenomenon is also observed in the analysis of GC-EI-LRMS (triple quadrupole) (see **Section 4.4.1**).

One possible explanation is that during ionization, S42-bis-OH ([M]$^{+\bullet}$) derivatives may undergo elimination of a TMSOH group (−90 Da), resulting in more stable fragment ions that resemble S42-mono-OH derivatives ([M − TMSOH]$^{+\bullet}$). This phenomenon would explain the concurrent presence of *m/z* 450 and 540, or 452 and 542, at the same retention times. Nevertheless, it is challenging to know whether the two different compounds coeluted at the same retention time or a produced fragmented ion is much more concentrated than its molecular ion.

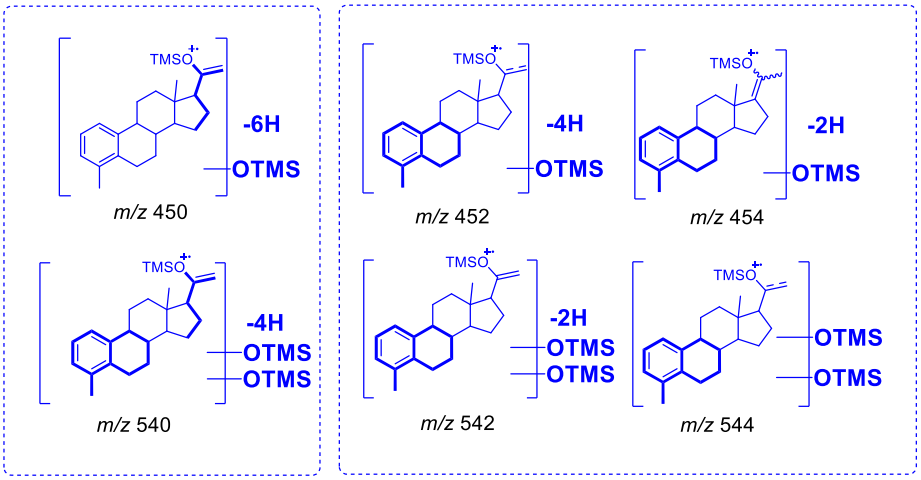

Scheme 82. Structures of ions sharing the same retention time in the chromatogram. The double bonds exact positions are not determined in the metabolites and are indicated by a loss of two hydrogen atoms.

This finding suggests that the hydrolyzed sulfate metabolites were not very stable.[132] From the previous synthesis results, GC-MS analysis of TMS-derivatized S42-C6-OH and S42-C7-OH revealed the formation of double bonds at the C6–C7 position. If the hydroxy position is at C6 or C7, an additional double bond may be formed during either TMS derivatization or sample injection with heat. These findings strongly suggest that S42 metabolite samples should be analyzed immediately after derivatization.

4.4.3 Low resolution GC-EI-MS (triple quadrupole) MRM experiments

PRM experiments using GC-MS (Orbitrap) are crucial for structure elucidation, but only three to four precursor ions can be included in a PRM experiment. Detailed MS^2 spectra allows structure assignment, but PRM experiments are inefficient for routine doping control purposes. MRM experiments by GC-EI-LRMS (triple quadrupole) can help reduce matrix effects for sensitive, quantitative analysis. In this approach more precursor-product ion transitions can be included per run than in the Orbitrap

instrument, making it more suitable for routine monitoring of previously characterized metabolites.

Comparative validation of GC-EI-LRMS with GC-EI-HRMS for the analysis of S42 *in vitro* metabolites

Before analyzing the more complex metabolic profile of the rat urine samples, *in vitro* phase I metabolism studies were conducted with a set of MRM experiments by GC-EI-LRMS (QqQ (triple quadrupole)). This preliminary analysis allowed us to investigate the retention time window and fragmentation characteristics of S42 metabolites, providing valuable information for interpreting *in vivo* data.

Although both the Orbitrap and triple quadrupole instruments employed the same GC columns, the retention times of metabolites shifted. **Table 17** summarizes the retention time shifts observed between the GC-Orbitrap (HCD: 20 eV) and the triple quadrupole MS (CID: 20 eV or 8 eV)

Table 17. Retention time comparison of *in vitro* metabolites between GC-Orbitrap (HCD 20 eV) and triple quadrupole MS. (CID 20 eV for ISTD, **M1a**-**M1c**, **M2a**-**M2b**; CID 8 eV for **M3a**-**M3b**, **M4**, and **M5**).

	In vitro phase I Exp			
Metabolites	Molecular ion (*m/z*)	GC-Orbitrap-PRM (RT)	GC-QqQ MRM (RT)	Transitions MRM (*m/z*)
	ISTD: MT (methyltestosterone)	14.81 (after column change)	14.39	301.3→169.1 446.3→301.3
M1a - **M1c**	456.2874	17.88, 17.96, 18.03	17.74, 17.82, 17.90	456.3→195.2 456.3→245.1 456.3→351.2
M2a – **M2d**	544.3219	18.35, 18.41, 18.47, 18.65	18.20, 18.22, 18.28, 18.51	544.3→231.1 544.3→244.1 544.3→307.1 544.3→439.2
M3a, **M3b**	632.3563	19.00, 19.15	19.00	632.3→231.1 632.3→331.1 632.3→542.3
M4	470.2667	18.25	18.13	470.2→195.1 470.2→455.2
M5	558.3004	18.89	18.73	558.3→231.1 558.3→244.1

The triple quadrupole machine is a low-resolution mass spectrometer, providing mass measurements roughly accurate to two decimals, with a mass tolerance of ±0.7 u. As a result, coeluting isobaric ions selected by the first quadrupole may can originate from different molecular species having the same nominal mass. A similar phenomenon can occur in the third quadrupole, where product ions with identical nominal masses are

detected following fragmentation in the second quadrupole. Therefore, comparing the results with blank samples and the coordinated high resolution mass spectra obtained from GC-HRMS (Orbitrap) is important.

A particularly noteworthy observation occurred in the MRM traces at RT 18.12 minutes in the chromatogram of the transitions at *m/z* 456 to 195 (**Figure 50**, left). The peak at 18.12 min was detected along with **M1a**, **M1b**, and **M1c**. However, the signal did not belong to a S42-mono-OH derivative as expected, but it could be attributed to an oxygenated compound S42-mono-OH+O-2H, previously identified metabolite **M4** (see **Figure 45**, page 101). In the MS^2 spectrum obtained from the Orbitrap analysis, **M4** contained a molecular ion at *m/z* 470, with significant fragment ions at *m/z* 455 ($[M-Me^{\bullet}]^+$), and 195, which explained the detection in the MRM experiment.

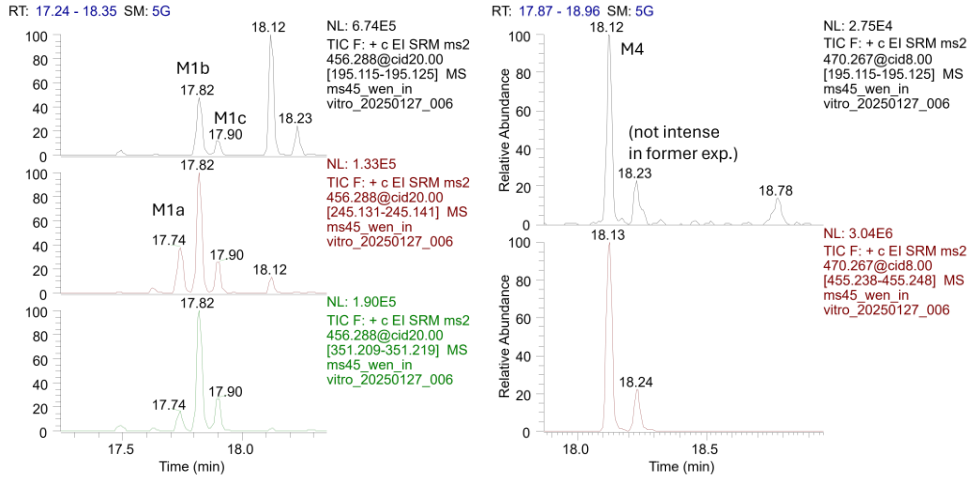

Figure 50. Chromatograms of MRM experiment of different *in vitro* metabolites **M1a**, **M1b**, **M1c** (left) and **M4** (right).

This finding emphasizes the need to interpret MRM results with PRM (targeted MS^2) data to distinguish overlapping signals, especially when coeluting isomers are present within narrow retention windows.

The investigated TMS derivatized *in vitro* sample had aged within three and half months and was likely undergoing decomposition. Analysis of an aged sample may explain the absence of detectable transition ions from **M3a** in the triple quadrupole data. **M4** and **M5** could be identified in the MRM experiment, which was consistent with the GC-EI-HRMS analysis.

Comparative validation of GC-EI-LRMS with GC-EI-HRMS MRM methods for the S42 metabolic screening of urine collected from Rat 2

Urine samples from Rat 2 were analyzed using both GC-EI-HRMS (Orbitrap) and GC-EI-LRMS (QqQ (triple quadrupole)). This section focusses on the targeted screening of S42-derived metabolites in urine collected from Rat 2 using the multiple reaction monitoring (MRM) method on a triple quadrupole mass spectrometer with CID at 20 eV (routinely used CID collision energy). The analytical goal was to identify S42-mono-, bis-, and tris-OH metabolites across the free, glucuronide, and sulfate fractions.

A series of mono- and bis-OH metabolites were detected in sulfate fraction. Notably, metabolites with nominal mass at *m/z* 450 (S42-mono-OH-6H) and *m/z* 540 (S42-bis-OH-4H) presented coeluting peaks at 18.29 min and 18.61 min, respectively. The ions at *m/z* 450 can be water-loss olefins from metabolites at *m/z* 540. Similarly, ions at *m/z* 452, 454, 542, and 544 were detected at close retention times between 18.30 and 18.39 minutes. This finding was also observed in Orbitrap-based PRM analysis. This observation suggested that the ions discovered for mono-hydroxylated metabolites with at *m/z* 450, 452, and 454, may originate from bis-hydroxylated metabolite at *m/z* 540, 542, and 544 in the Rat 1 samples.

Table 18. Comparison of the retention times RT of the metabolites from the sulfate fraction from Rat 2 urine on day 2, analyzed by the GC-EI-QqQ/ Orbitrap MS machine.

Nominal mass *(m/z)*	Chemical composition	GC-EI-LRMS (QqQ) RT (min)	GC-EI-HRMS (Orbitrap) RT (min)
450	$C_{27}H_{38}O_2Si_2^{\bullet+}$	18.29, 18.61	18.40, 18.73, 18.88
540	$C_{30}H_{48}O_3Si_3^{\bullet+}$	18.29, 18.61	18.39, 18.72, 18.88, 18.81, 18.98, 19.18, 19.27
452	$C_{27}H_{40}O_2Si_2^{\bullet+}$	18.30, 18.34, 18.38, 18.66	18.41, 18.45, 18.50, 18.92
454	$C_{27}H_{42}O_2Si_2^{\bullet+}$	18.30, 18.34, 18.39	18.45, 18.94
542	$C_{30}H_{50}O_3Si_3^{\bullet+}$	18.30, 18.34, 18.39, 18.79	18.41,18.50, 18.91, 18.45, 18.87
544	$C_{30}H_{52}O_3Si_3^{\bullet+}$	18.30, 18.34, 18.39	-

While *m/z* 544 was observed exclusively in the MRM experiments on the QqQ instrument, it was not detected in Orbitrap PRM mode. This observation may be due to the higher sensitivity in MRM mode or the degradation of unstable compounds before the delayed Orbitrap analysis. In contrast, the Orbitrap machine identified more isobaric metabolites with molecular ion mass at *m/z* 540 than the triple quadrupole machine (see **Table 18**), which may also result from degradation.

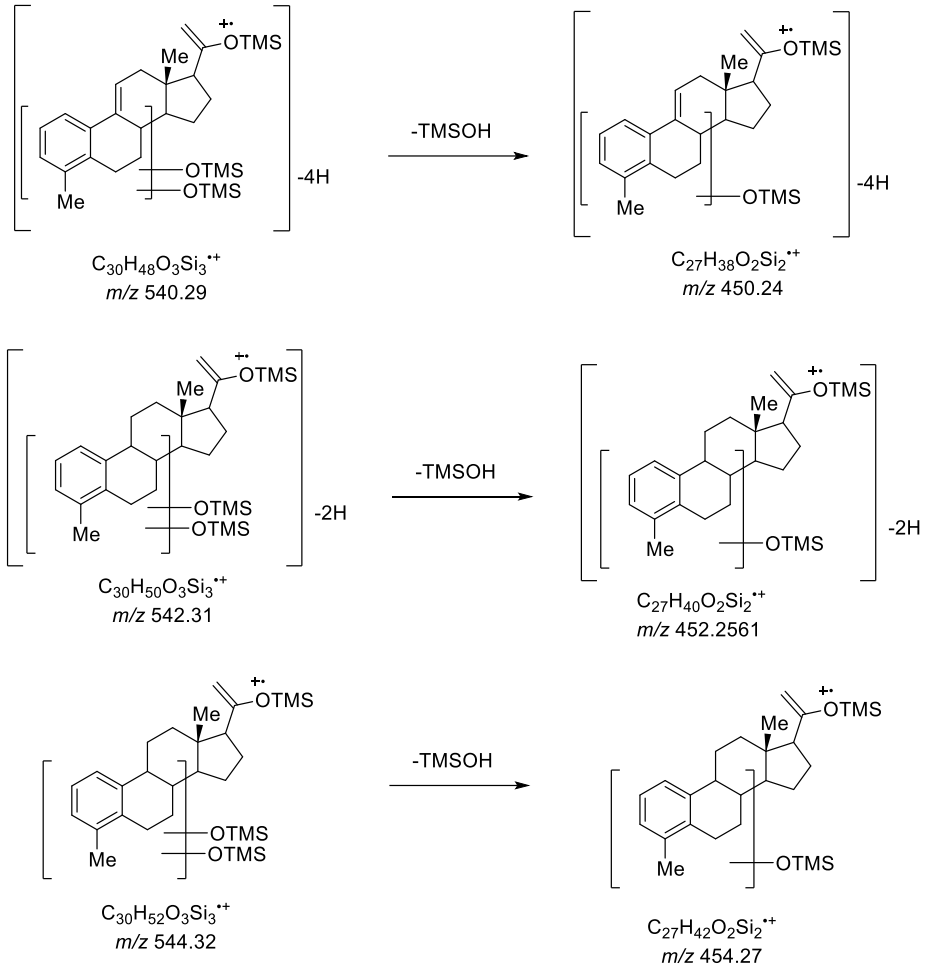

Scheme 83. Neutral loss of TMSOH from *m/z* 540, 542, and 544 gives product ions at *m/z* 450, 452, and 454, respectively, all sharing the identical retention time RT with the respective precursors in the MRM experiments.

It is hypothesized that some molecular ions assigned to S42-mono-OH derivatives (e.g., *m/z* 450, 452) may actually originate from the loss of TMSOH (−90 Da) from S42-bis-OH precursors such as *m/z* 540 or 542. This neutral loss could generate abundant $[M-TMSOH]^{+\bullet}$ fragments, explaining the identical retention times of these ions (see **Scheme 83**). Different hydrolysis conditions applied to glucuronides (enzyme-based) and sulfates (acidic) may also affect metabolite stability and detection. The acidic conditions used for hydrolysis of sulfate conjugates might promote TMSOH loss or thermal degradation, leading to abundant $[M-TMSOH]^{+\bullet}$ product ion formation within the sulfate fraction.

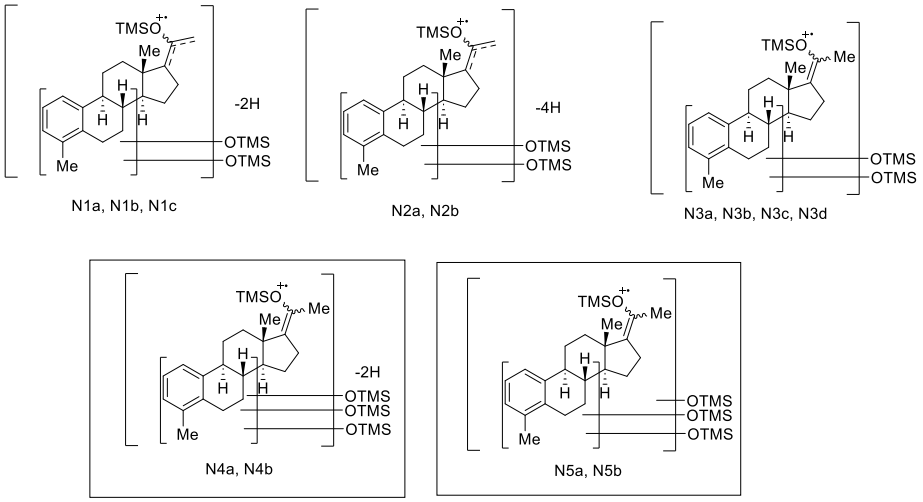

Scheme 84. Abundant TMS derivatized metabolites observed by GC-EI-LRMS (triple quadrupole) using MRM experiments: S42-bis-OH-4H (*m/z* 540), S42-bis-OH (*m/z* 544), S42-tris-OH (*m/z* 630) and S42-tris-OH (*m/z* 632). Metabolites N4a and N5b found in the glucuronide fraction are most abundant.

Significantly, the metabolite distribution patterns varied between the three fractions. Bis-hydroxylated derivatives were most abundant in the sulfate (S) fraction, whereas tris-hydroxylated metabolites dominated in free (F) and glucuronide (G) fractions. Based on diagnostic product ions *m/z* 231, 307, 331, and 419, the oxidation sites were assigned primarily to the A/B rings of the S42 scaffold (**Scheme 84**).

Table 19. TMS derivatized S42 metabolites (*m/z* 540, 544, 630, 632) from Rat 2 were screened on day 2 using MRM transitions across all urine fractions. Only specific transitions (CID 20 eV) were used to determine peak area and relative intensity (in bold).

Metabolites	Nom. mass (*m/z*)	RT (min)						Transitions (*m/z*)
		Free	Glucuronide			Sulfate		
ISTD (MT)	446	14.44	14.43			14.39		301.3→169.1 **446.3→301.3**
S42-bis-OH-4H (**N2a-N2b**)	540				18.29 (**N2a**)		18.61 (**N2b**)	**540.3→435.2** 540.3→345.1 540.3→331.1
S42-bis-OH-2H (**N1a-N1c**)	542				18.30 (**N1a**)	18.34 (**N1b**)	18.39 (**N1c**)	**542.3→437.2** 542.3→331.1 542.3→333.1
S42-bis-OH (**N3a-N3d**)	544	18.29 (**N3a**)	18.29 (**N3a**)	18.55 (**N3b**)	18.28 (**N3a**)	18.34 (**N3c**)	18.38 (**N3d**)	544,3→307.1 544.3→**195.1** 544.3→ 331.1 (F, G)
S42-tris-OH (**N4a- N4b**)	630	18.99 (**N4a**)	18.99 (**N4a**)	19.16 (**N4b**)				**630.3→ 419.1** 630.3→195.1 630.3→ 525.2 (G)
S42-bis-OH-2H (**N5a-N5b**)	632		18.79 (**N5a**)	19.00 (**N5b**)				632.3→419.1 **632.3→231.1** 632.3→437.2 **632.3→527.2**

From a semi-quantitative perspective, the area ratio of analyte to ISTD (methyltestosterone) was calculated for each metabolite in each fraction. In the sulfate fraction, only bis- and tris-OH metabolites were considered for semi-quantitation due to the ambiguous results from S42-mono-OH, which may originate from in-source fragmentation of S42-bis-OH derivatives.

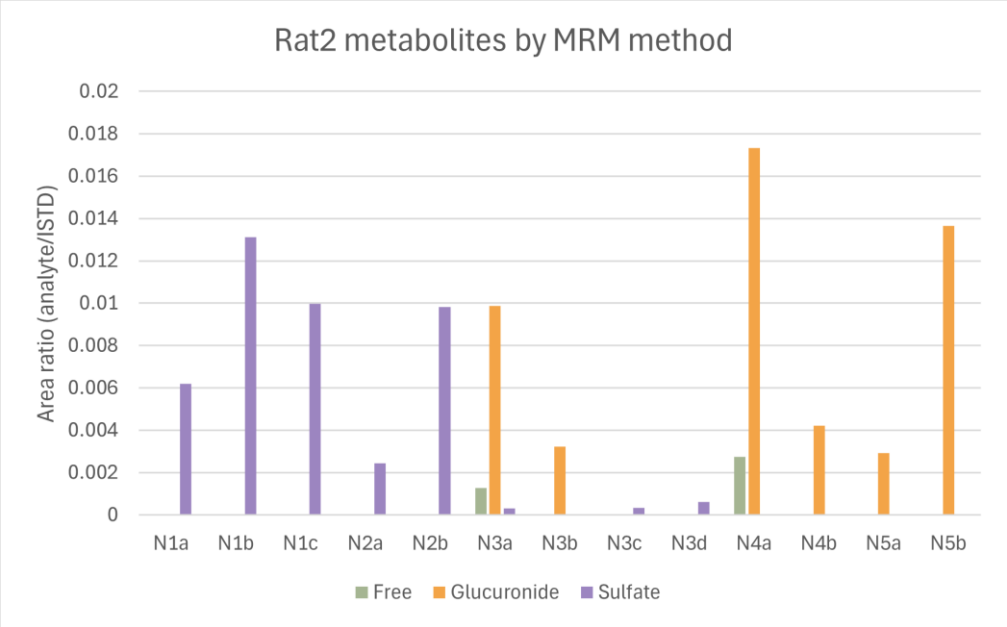

Figure 51. Rat 2 metabolites ratio in free, glucuronide, and sulfate fractions.

The metabolite profile found in the Rat 2 urine (**Figure 51**) reveals a conjugation preference: glucuronides dominate among tris- and bis-OH derivatives (notably **N3a**, **N4b**, and **N5b**), while sulfate conjugation mainly targets bis-OH derivatives (**N1b**, **N1c**, **N2b**). The free fraction showed relatively low concentrations of S42 metabolites. One exception is N3a (S42-bis-OH). In addition, **N4a** (S42-tris-OH-2H) was found in free and glucuronide fractions with a consistent retention time of 18.99 min, showing glucuronide as a primary phase II conjugate from S42-tris-OH-2H.

Overall, the MRM-based analysis by triple quadrupole mass spectrometry proved to be highly efficient for screening Rat 2 metabolites. The results not only match those from GC-EI-HRMS Orbitrap experiments but also provide higher sensitivity for detecting trace metabolites such as *m/z* 544. These findings highlight the analytical complementarity of these two instrumental approaches and the significance of careful interpretation of fragment ions to distinguish between true metabolites and derived species.

Qualitative MRM with GC-EI-LRMS of urine samples collected from Rat 3 and Rat 4

The number of targeted ions in the MRM (multiple reaction monitoring) method was reduced, and the injection volume was increased from 2 µL to 3 µL to enhance sensitivity in the analysis of Rat 3 and Rat 4 urine samples. The collision-induced energies (20, 25, 30 eV) of different transition ions were modified.

Due to previous findings from the analysis of urine of Rat 2, where the degradation of labile compounds was observed after 2.5 weeks, all urine samples of Rats 3 and 4 were analyzed immediately after sample preparation in order to minimize the decomposition of metabolites.

Table 20. Summary of the retention times and optimized transitions from metabolites in the Rat 3 and Rat 4 urine samples. The concentration of metabolites was highest on day 2. Only specific transitions were used to determine peak area and relative intensity (in bold).

Metabolites	Nom. mass (*m/z*)	RT (min)						Transitions (*m/z*)	Collision energies (eV)
		Free		Glucuronide		Sulfate			
		Rat 3	Rat 4	Rat 3	Rat 4	Rat 3	Rat 4		
ISTD (MT)	446	14.40	14.44	14.42	14.44	14.41	14.44	301.3→169.1 **446.3→301.3**	20 20
S42-bis-OH-4H (**N2a-N2b**)	540					18.29, 18.60 **N2a**, **N2b**	18.30, 18.65 **N2a**	540.2→525.2 **540.2→435.2** 540.2→345.1 540.2→331.1	20 20 20 30
S42-bis-OH (**N3a-N3d**)	544	18.28, 18.55 **N3a**, **N3b**	18.30, 19.56 **N3a**, **N3b**	18.28, 18.55 **N3a**, **N3b**	18.29, 18.57 **N3a**, **N3b**	18.29, 18.33, 18.39 **N3a**, **N3c**, **N3d**	18.31, 18.34, 18.39 **N3a**, **N3c**, **N3d**	544.3→529.3 544.3→439.2 544.3→331.1 544.3→307.1 **544.3→195.1**	25 25 30 30 20
S42-tris-OH-2H (**N4a-N4b**)	630	18.98, 19.16 **N4a**, **N4b**	18.99, 19.16 **N4a**, **N4b**	18.98, 19.16 **N4a**, **N4b**	18.99, 19.16 **N4a**, **N4b**			630.3→525.2 **630.3→419.1** 630.3→331.1 630.3→195.1	25 20 30 20
S42-tris-OH (**N5a-N5b**)	632	18.78, 19.00 **N5a**, **N5b**	18.80, 19.00 **N5a**, **N5b**	18.78, 19.00 **N5a**, **N5b**	18.80 19.01 **N5b**	19.00 **N5b**	19.00 **N5b**	**632.3→527.2** (RT 18.78 min) 632.3→419.1 **632.3→231.1** (RT 19.00 min) 632.3→195.1	20 20 25 20

The targeted metabolites in this screening included hydroxylated S42 derivatives: S42-bis-OH-4H (*m/z* 540: **N2a**, **N2b**), S42-bis-OH (*m/z* 544: **N3a**–**N3d**), S42-tris-OH-2H

(*m/z* 630: **N4a**, **N4b**), and S42-tris-OH (*m/z* 632: **N5a**, **N5b**) according to the findings from samples of Rat 2. Most metabolites were discovered on day 2 and day 3.

The metabolite profiles of the Rat 3 and Rat 4 individuals were compared by the ratio of the metabolite signal area divided by the one of the internal standard (methyltestosterone). Since free, glucuronide, and sulfate fractions were prepared and analyzed separately, the area ratios are presented independently, and the signal intensities were compared in a relative manner.

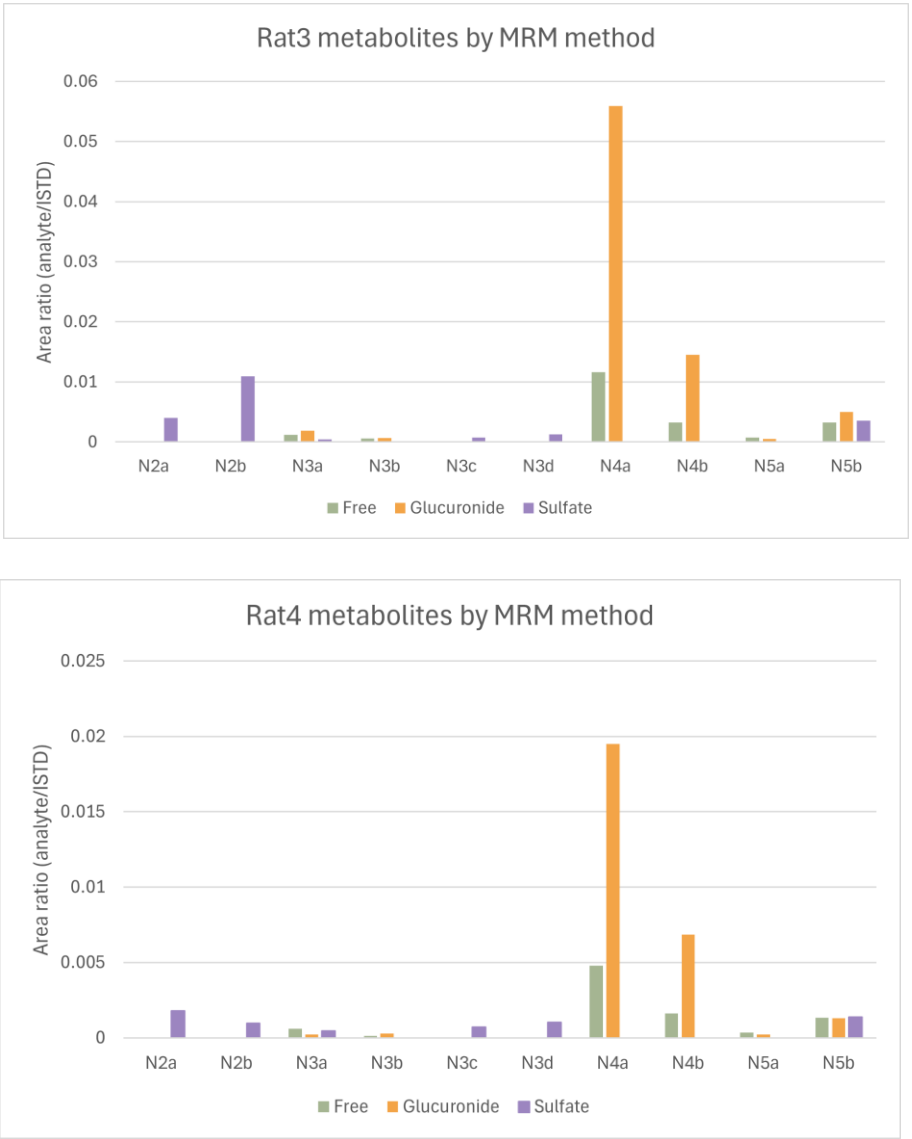

Figure 52. Analytes intensities in Rat 3 and Rat 4 using the same MRM method.

The results yielded from Rat 3 and Rat 4 showed distinct differences in overall metabolite intensities. Unfortunately, technical problems reduced the sensitivity of the measurements of the Rat 4 samples (ion source contamination). Hence, the signal intensities of all the metabolites detected in Rat 4 samples were substantially

decreased. However, the overall trends and the metabolite distribution remained similar for Rat 3 and Rat 4.

Metabolite **N4a** (S42-Tris-OH-2H) has a stronger intensity than other metabolites in the glucuronide fraction. **N4b** (S42-Tris-OH) was the second most abundant metabolite in the glucuronide fraction. Metabolite **N4a** (S42-Tris-OH-2H) was also found in the free fraction. Bis-hydroxylated metabolites were more concentrated in the sulfate fraction. These results agree with the analysis from Rat 2 samples.

4.4.4 Summary of the GC-MS analyses of rat urine

Combination of high-resolution GC-EI-HRMS (Orbitrap) and low-resolution GC-EI-LRMS (triple quadrupole) methods enabled comprehensive metabolic profiling of S42 in rat urine. Day 2 and day 3 post-dosing samples revealed the most abundant metabolite excretion.

Across all four rats investigated, tris-hydroxylated metabolites were more abundant in the glucuronide fraction and in the free fraction. In contrast, mono- and bis-hydroxylated derivatives were more commonly observed in the sulfate fraction. However, potential EI-MS fragmentation or chemical degradation during sample preparation and storage, especially under acidic conditions for sulfate hydrolysis or TMS derivatization, may have led to artefact formation and alterations. As a result, S42-bis-OH metabolites are observed as S42-mono-OH derivatives. This finding was particularly evident in Rat 2, where the Orbitrap and triple quadrupole analyses showed close retention times for *m/z* 450 and 540 and *m/z* 452 and 542.

The high-resolution Orbitrap-MS provided information about the product ions with an error lower than 5 ppm through PRM analysis mode. Characteristic product ions at *m/z* 243, 307, 331, and 419 were consistently observed in metabolites. These ions supported hydroxylation at the A and B rings of the steroid system. Additional fragments at *m/z* 143, 195, and 231 indicated potential modifications at the respective D ring. These diagnostic ions were crucial for knowing the oxidation position and assignment of TMS-C17 or -C20 isomers.[115]

Triple quadrupole MS in MRM mode enhanced detection sensitivity and throughput, allowing a more effective S42 screening of urine samples collected from Rats 2 to 4. The acquired results were consistent with high-resolution Orbitrap data.

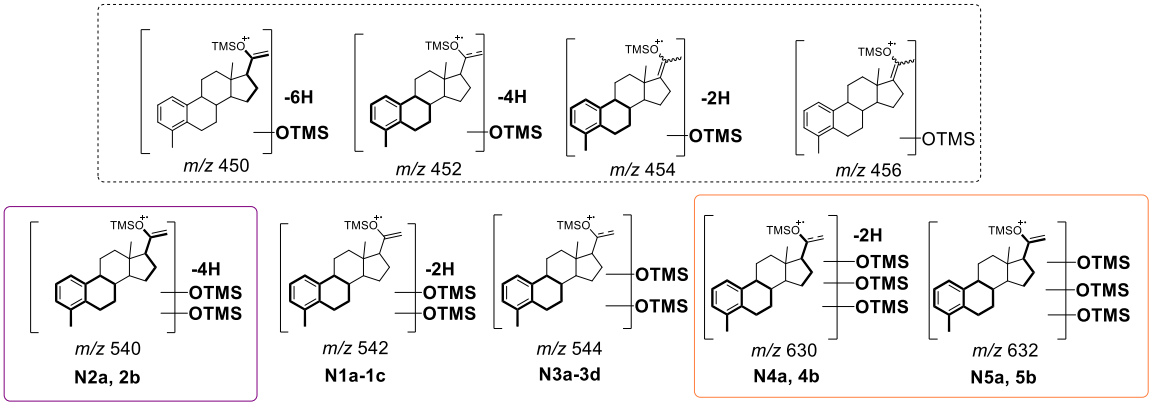

Scheme 85. The most abundant TMS-derivatized metabolites in glucuronide fraction are **N4a**, **N4b**, following **N5a** and **N5b**. **N2a** and **N2b** were more abundant in the sulfate fraction than in the free fraction.

Significantly, in both Rats 3 and 4, metabolites **N4a** and **N4b** (tris-OH derivatives at *m/z* 630 and 632) showed the highest intensity in the glucuronide fraction, which is consistent with the observation in Rat 1 and Rat 2 (see **Scheme 85**). Metabolites **N2a** and **N2b** (bis-OH derivatives at *m/z* 540) were most abundant in the sulfate fraction in Rat 2 - Rat 4. The metabolism profiles are consistent across biological replicates.

4.4.5 S42 high resolution LC-ESI-MS/MS PRM experiments

S42 phase II metabolites were also analyzed in rat urine using LC-ESI-HR-MS/MS (Orbitrap). This method can directly detect glucuronide and sulfate conjugates without hydrolysis or derivatization for sample preparation. Electrospray ionization (ESI), as a soft ionization technique, maintains the precursor ions and minimizes fragmentation during full-scan MS acquisition.[49b] Therefore, LC-ESI-MS is complementary to GC-EI-MS, providing a broader coverage of metabolite profiles due to its compatibility with polar and thermally labile compounds.

LC-ESI-MS/MS analysis methods

Dr. Felicitas Wagener conducted LC method development, sample preparation, and injections and provided us with the analysis data. Rat urine samples (50 µL each) were centrifuged and analyzed directly without further purification. Testosterone-glucuronide-d3, androsterone-glucuronide-d5, and testosterone sulfate-d3 were added as internal standards.

The analysis yielded the identification of glucuronide and sulfate conjugates derived from bis- and tris-hydroxylated S42 metabolites. More sulfate metabolites than glucuronides were detected. In MS^2 experiments, diagnostic product ions were observed at *m/z* 175 and 113 for glucuronide fragments and *m/z* 97 and 80 for sulfate fragments, confirming the metabolite identities (see **Scheme 64**, page 107).

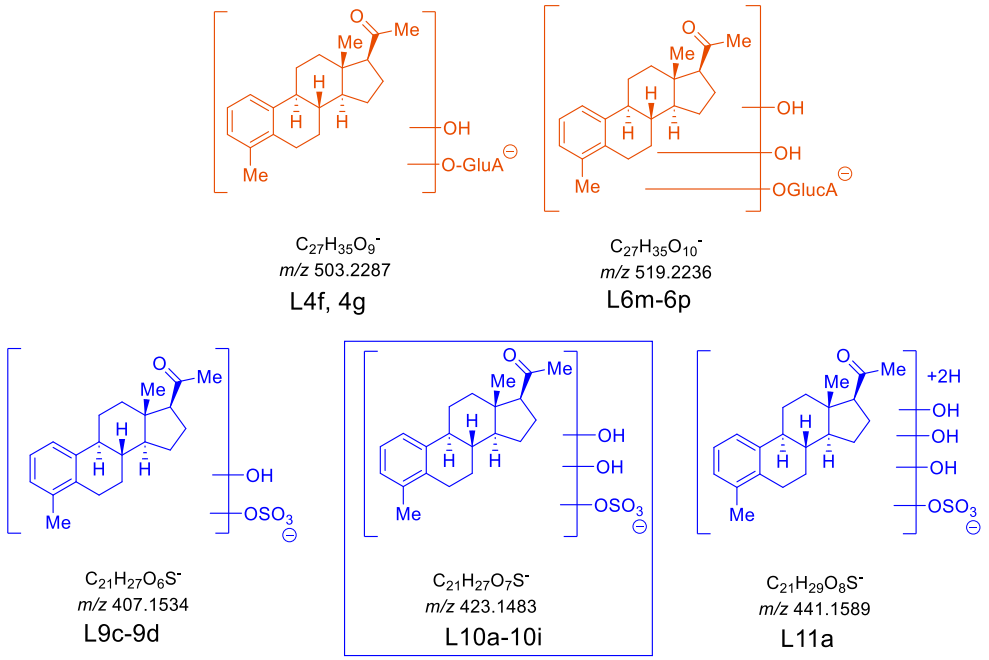

Scheme 86. Discovered glucuronide and sulfate metabolites in rat urine samples on day 2.

Semi-quantitative analysis and ion selection with LC-ESI-MS/MS

Metabolite quantification was based on extracted ion chromatograms (EICs) targeting specific product ions from PRM mode. The intensities of the glucuronide and sulfate metabolites were compared separately because the ionization and fragmentation energies of sulfate and glucuronide products varied.

For glucuronide metabolites, the peak area at *m/z* 113 was normalized to the peak area of the internal standard, testosterone-glucuronide-d3 at *m/z* 113 (see **Scheme 64**, page 107). For sulfate metabolites, the peak area at *m/z* 80 was compared against testosterone sulfate-d3 at *m/z* 80 (see **Scheme 65**, page 108).

Only metabolites generating the selected product ions (*m/z* 113 or 80) were included in the intensity comparisons to reduce errors from choosing different product ions. Although *m/z* 96 was frequently observed in some metabolites. It was excluded due to severe coelution, likely caused by matrix effects from the unpurified urine samples.

The ion corresponding to $[M–C_6H_7O_6]^-$ (loss of 176 Da) was detected in the rat metabolites but not consistently observed in all the glucuronide metabolites from *in vitro* experiments. Differences in fragment ion patterns may be attributed to the glucuronide conjugation in different functional groups, such as benzylic or acylic.[133] The ion at *m/z* 113 was found to be an intense and significant signal for area ratio calculation.

Metabolites found in urine sample of Rats 1 – 6 with LC-ESI-MS/MS

The metabolic profiles of all six rat samples were consistent. The primary glucuronide conjugates originated from S42-bis-OH (**L4g**) and S42-tris-OH (**L6m**–**L6p**).

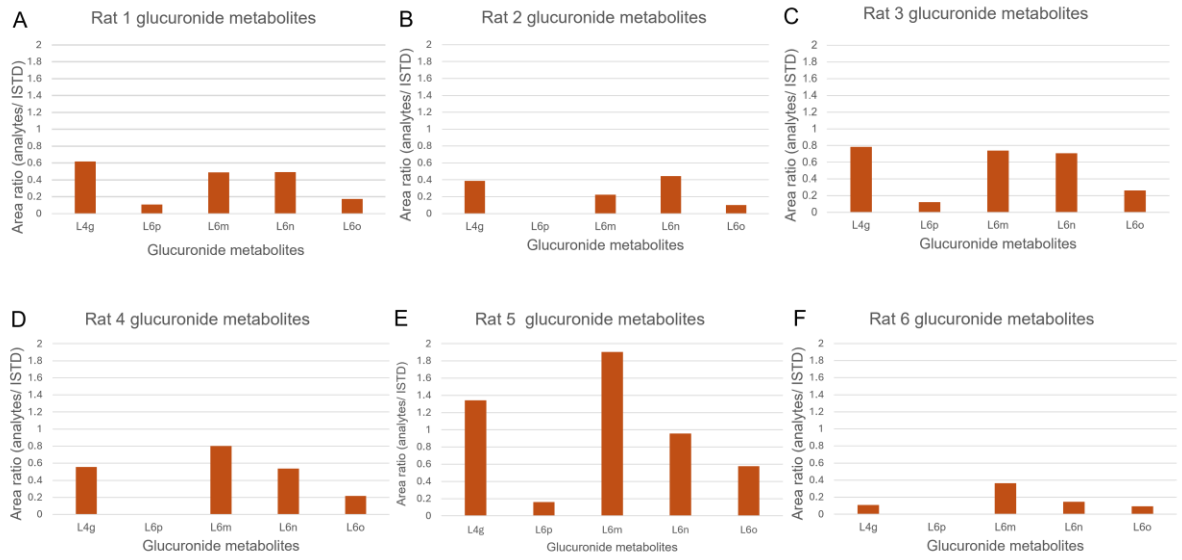

Figure 53. Area ratio at *m/z* 113 from metabolites and internal standard (ISTD). Only metabolites with a product ion at *m/z* 113 were included for intensity comparison. The number of different glucuronide metabolites from S42-tris-OH (**L6m-L6p**) is higher than from S42-bis-OH (**L4g**).

More sulfate metabolites were detected. They were derived from S42-bis-OH (**L9c-L9d**), S42-tris-OH (**L10a-10i**) and even S42-tetra-OH (**L11a**) (see **Scheme 86**). Among these sulfate metabolites, **L10g** exhibited a notably high peak intensity with an area ratio exceeding 12 in the PRM experiments. In contrast, other sulfate metabolites had area ratios below 2.

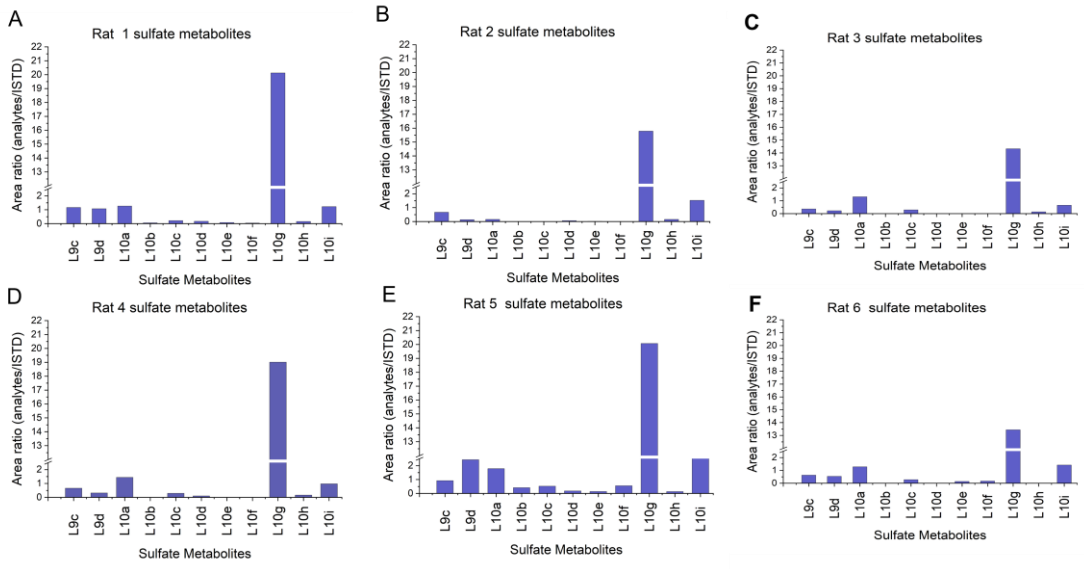

Figure 54. Area ratio at *m/z* 80 from sulfate metabolites and internal standard (ISTD). Only metabolites with a product ion at *m/z* 80 were included for intensity comparison. Metabolite **L10g** has a much higher area ratio than other sulfate metabolites from Rat 1 to Rat 6.

Nevertheless, we can not conclusively claim that **L10g** is the most abundant metabolite since the peak intensity is influenced by its chemical structure, degradation, pH value,[134] flow rate, and matrix effects. Especially sulfate conjugates are generally more acidic than glucuronide conjugates and therefore easier to be ionized by ESI-MS in negative ion mode.[135]

The rat urine samples were not further purified prior to LC-MS analysis, which can lead to different results from purified samples. In addition, sulfate metabolite intensity from S42-tris-OH was surprisingly low by the GC-MS analysis. The results from GC-MS and LC-MS are not consistent. A simple potential explanation is the significantly higher sensitivity of LC/MS in negative mode for sulfated metabolites.

To improve metabolite recovery and detection, urine samples from Rats 2 - 4 were processed using C18 solid-phase extraction, followed by drying and reconstitution. The intensity of the metabolite signals increased significantly, especially for glucuronide conjugates, and a greater number of sulfate metabolites were detected. S42 rat metabolites were found in MS^2 experiments from direct injections, but a modified purification approach is needed to detect all the metabolites in rat urine for a comprehensive metabolic profile. Application of ion exchange cartridges (*HR-XA* or *HR-XC*) for SPE purification could be a potential method for improving the recovery of metabolites.

S42 phase II metabolites can be analyzed by LC-ESI-HRMS without prior hydrolysis, allowing direct detection of sulfate and glucuronide conjugates. This approach avoids chemical decomposition during enzymatic or chemical deconjugation steps for the GC-EI-LR/HRMS analysis. In addition, there is no necessity for derivatization, which is commonly required for GC-EI-LR/HRMS analysis, and it avoids the issue of dehydration or TMSO elimination reaction, especially of sulfate conjugates.

4.4.6 General comparison of S42 (**1**) *in vitro* and *in vivo* metabolic studies acquired with different methods

For an evaluation of the results a comparison of the metabolic profiles found with LC-ESI-HRMS^2 from rat urines and from *in vitro* (HLM and S9) experiments is needed. The *in vitro* experiments using human enzymes may present results more closely aligned with human metabolic pathways than *in vivo* rat experiments. Nevertheless, the preparation of *in vivo* urine samples, which contain salts and matrix components, can resemble processing clinical human urine samples more closely.

S42 *In vitro* metabolites detected with various methods

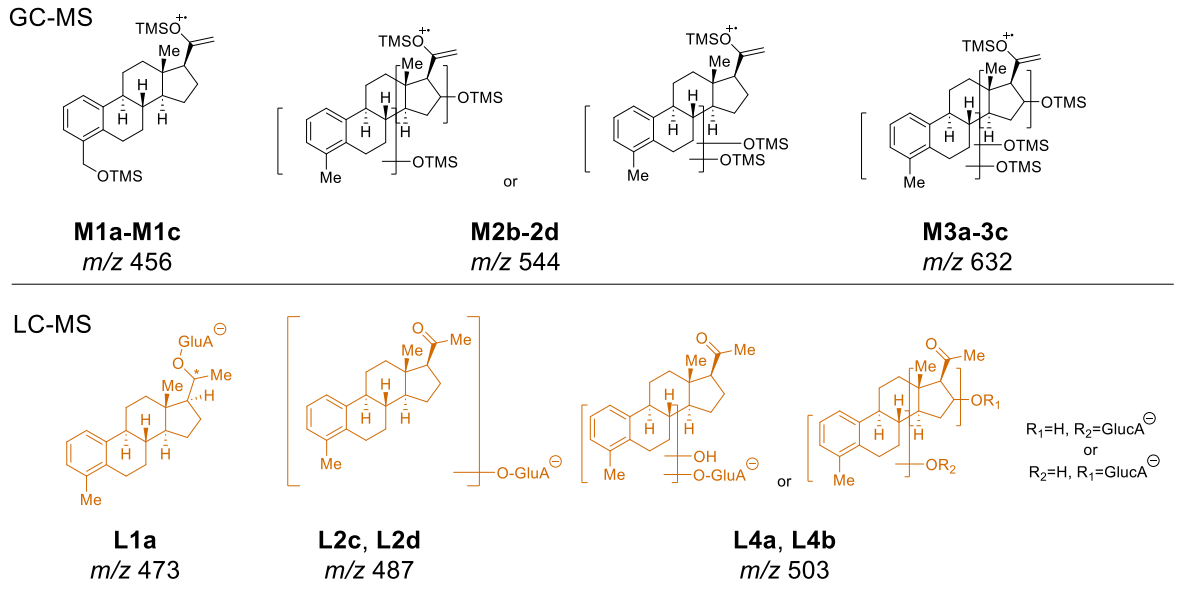

Scheme 87. Major *in vitro* phase I TMS analogs and phase II TMS molecular ions were hypothesized using GC-MS and LC-MS analysis, respectively.

According to the *in vitro* phase I and phase II samples analyzed by GC-MS and LC-MS, respectively. It is known that the primary phase I metabolites are S42-mono-OH

(**M1a**-**M1c**), S42-bis-OH (**M2a**-**M2d**) and S42-tri-OH (**M3a**-**M3c**). The primary phase II products are the glucuronide conjugates of S42-mono-OH (**L2c**, **L2d**), S42-mono-OH-2H (**L1a**), and S42-bis-OH (**L4a**, **L4b**). Consistent results were found in phase I and phase II *in vitro* experiments, suggesting that mono hydroxylation or reduction followed by glucuronidation, is the main metabolism pathway in humans.

In vivo metabolites

Rat urine metabolite analysis by LC-MS does not agree with the results found in the metabolic study analyzed with GC-MS. The complexity of detecting metabolites increases from the simplified *in vitro* model to the *in vivo* model due to matrix effects, lower concentrations of metabolites, and the necessity of multiple purification steps.

The analysis of the GC-MS results turned out to be challenging due to the formation of three TMS isomers for each metabolite after derivatization. Further decomposition of unstable derivates, cleaving TMSOH generating additional byproducts.

PRM experiments presented metabolites from Rat 1 urine from GC-HR-MS (Orbitrap). S42-bis-OH and S42-tris-OH derivatives were discovered in the free and the glucuronide fractions. A series of S42-mono-OH derivatives with low abundance were discovered in the sulfate fraction. These trends in the free and glucuronide fraction from Rat 1 urine samples match Rat 2 urine samples. However, in the sulfate fraction of Rat 2 samples, a small number of multiple S42-bis-OH peaks were detected instead of the S42-mono-OH peaks in the Rat 1 samples. The intense peaks of $[M]^{+\bullet}$ and [M-90 Da]$^{+\bullet}$ (e.g., *m/z* 544 and *m/z* 454, respectively) have the same retention time in the EICs.

It is possible that the metabolites in the sulfate fraction are not stable as the elimination reaction of TMSOH can occur easily, which is common in TMS derivatized steroid analysis by GC-EI-MS, and decomposition happens in the sulfate fraction in the Rat 1 urine after 2 weeks (compare **Section 4.4.2**). Another possibility is that S42-bis-OH existed in the sulfate fraction of both animals, but it is only intense enough to see S42-bis-OH derivatives in the sulfate fraction from Rat 2. The above reason may explain the different results from Rat 1 and Rat 2.

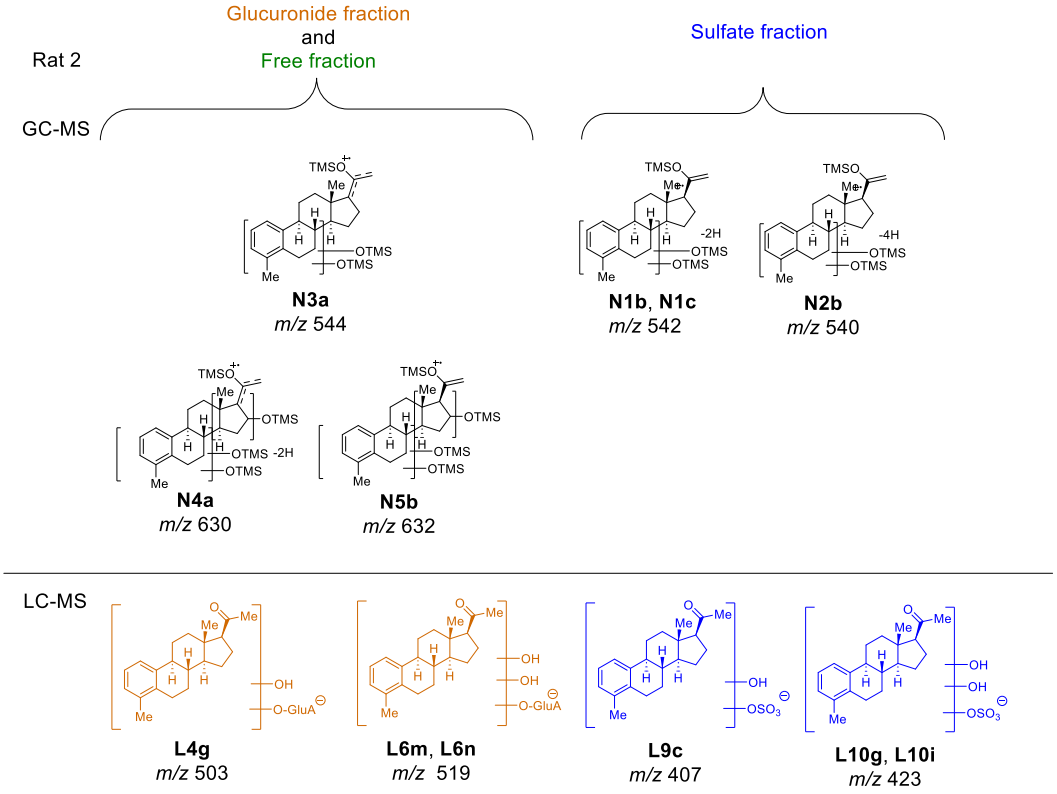

Scheme 88. LC-MS and GC-MS analysis of Rat 2 samples presented primary molecular ions. TMS-derived sulfate metabolites may not be stable, and an elimination reaction may occur. The positions of generated double bonds are not determined and are indicated by a loss of two or four hydrogen atoms.

Analysis of Rat 2 samples using a triple quadrupole showed the low intensity of precursor ions from **N3a** (S42-bis-OH), **N4a** (S42-tris-OH-2H), and **N5b** (S42-tris-OH) in the free fraction (see **Scheme 88**). Metabolites **N4a** and **M5b** were found with highest abundance in the glucuronide fractions. **N1b**, **N1c** (S42-bis-OH-2H) and **N2b** (S42-bis-OH-4H) were more concentrated in the sulfate fractions. Metabolite **N5b** (S42-tris-OH) was only detected in freshly prepared samples from Rat 3 and Rat 4 with low intensity in the sulfate fractions.

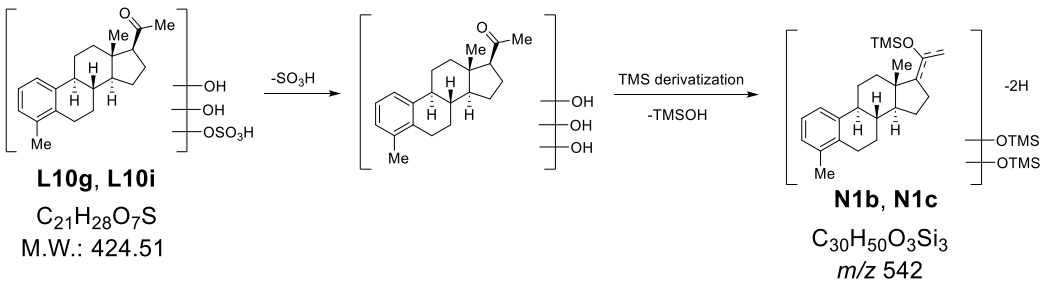

Scheme 89. Metabolites **L10g** and **L10i** were solvolyzed to eliminate the sulfate group. An extra double bond was generated during the hydrolysis and derivatization reaction. The GC-MS detected product ions **N1b** and **N1c** with an extra double bond. The position of the generated double bond is not determined and is indicated by a loss of two hydrogen atoms.

Compared to the results from LC-ESI-MS, glucuronide from S42-bis-OH (**L4g**) and S42-tris-OH (**L6m** and **L6n**) were the major products (see **Scheme 87**). No metabolite with an extra double bond, which was frequently observed in GC-MS analyses, was found in the metabolites analyzed by LC-MS. It is possible that metabolites **N1b**-**N1c** (S42-bis-OH-2H) and **N4a** (TMS-derived S42-tris-OH-2H), identified in GC-MS, originated from conjugated products by losing TMSOH as a neutral. The sulfate metabolites **L10g** and **L10i** appear to show a loss of a TMSOH molecule due to hydrolysis, as the TMS-products **N1b** and **N1c** were discovered by GC-MS analysis (see **Scheme 88**).

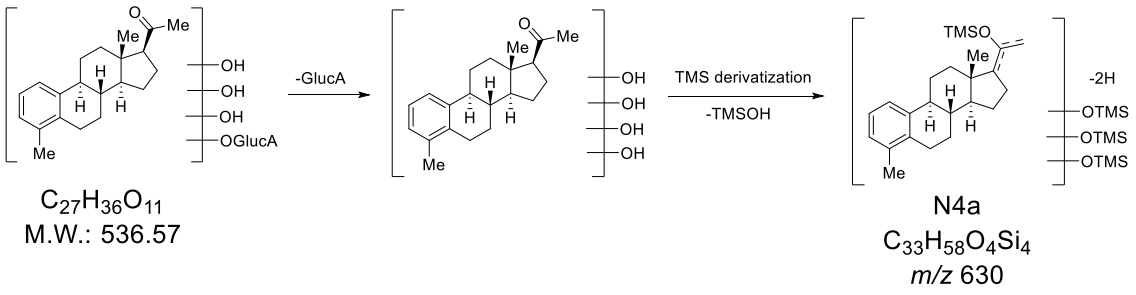

Scheme 90. Metabolite **N4a** may originate from a glucuronide product of S42-tetra-OH. Formation of a double bond can occur during derivatization and sample injection.

During GC analysis, the metabolite **N4a** found in the glucuronide fraction is likely derived from S42-tetra-OH by hydrolysis and TMS derivatization. An abundant signal at RT 5.21 min was found in the extracted ion chromatogram of *m/z* 535.2185 in the full MS analysis of Rat 1 to Rat 6 urine samples of day 2. Two peaks were also discovered in the *in vitro* phase II samples in the extracted chromatogram at *m/z* 535.2185 from full MS analysis. However, this compound was not considered in the PRM experiment due to the time constraints in the study and should be investigated in the future.

Final assessment of the S42 *in vitro* and *in vivo* studies

Glucuronide adducts of S42 mono-OH were found to be the significant products from phase II *in vitro* experiments, while sulfate and glucuronide metabolites of S42 bis-/tris-OH phase I metabolites dominate in rat urine samples collected from *in vivo* experiments.

Previous research indicates that rats or mice tend to produce metabolites with multiple hydroxy functional groups during bile acid synthesis and metabolism.[136] Differences in rat and human models may be a reason for different trends in these two sets of experiments. However, the oxidation positions may be similar. In GC-EI-MS/MS spectra of *in vitro* and *in vivo* samples, the fragmentation products *m/z* 243, 307, 331, 333 can be found, and the ion at *m/z* 195 or 231 is especially standing out. These fragments will greatly help future investigations of the human S42 (**1**) metabolites and their oxidation positions.

Screening for S42 (**1**) sulfate metabolites by GC-MS is certainly not the ideal method due to the elevated analyte polarity and complex derivatization chemistry including artefact formation. Metabolite screenings by LC-MS from biological models is recommended. The benefit of using GC-MS is that PRM experiments could investigate the oxidation position in non-conjugated products. The hydrolyzed glucuronide metabolites could be monitored by GC-EI-HR-MS/MS (Orbitrap) or even GC-EI-LR-MS/MS (triple quadrupole) with increased sensitivity.

5. Summary

In this study, the investigation of *in vitro* and *in vivo* metabolites of a novel steroidal SARM S42 (**1**) was successfully achieved by chemical synthesis and GC/LC-MS methods.

SARM S42 (**1**) and its deuterated derivatives S42-d7 (**1-d7**) and S42-d4 (**1-d4**) were successfully synthesized. Potential S42 (**1**) phase I metabolites were prognosticated *in silico* indicating a high probability of hydroxylation at the steroidal A-, B-, and D-rings.[110] Accordingly, three hydroxylated S42 derivatives were synthesized as. the reference compounds for GC-EI-HRMS analysis.[111] S42-C20-OH (**2**), S42-C6*ß*-OH (**3**), and S42-C7*α*-OH (**4**) were found to be essential for a reliable and correct structure elucidation and assignment of S42 (**1**) metabolites collected from *in vitro* and *in vivo* experiments.

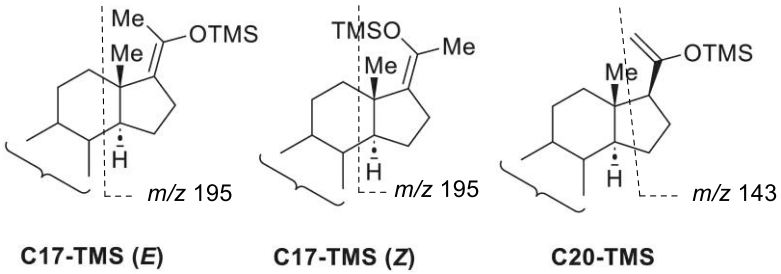

Scheme 91. Structures of C17-TMS (*E*), C17-TMS (*Z*), and C20-TMS isomers, showing distinctive fragments at *m/z* 195 and 143**.**

As a firm basis for further studies, the fundamental fragmentation behavior of S42 (**1**) and of its TMS silyl ether derivatives in GC-EI-HRMS was thoroughly examined. Especially, the unique water-loss reaction of S42 (**1**) was identified to proceed via a *McLafferty*-type rearrangement of γ-positioned hydrogens at either C12 or C18 to form a characteristic product ion at *m/z* 278. The comparative GC-EI-HRMS investigation of S42-TMS and TBDMS derivatives implied that C17-TMS isomers and C20-TMS isomers can be distinguished on the basis of characteristic and indicative fragment ions at *m/z* 195 and 143, stemming from D ring fragmentation processes observed in respective MS spectra (**Scheme 91**).

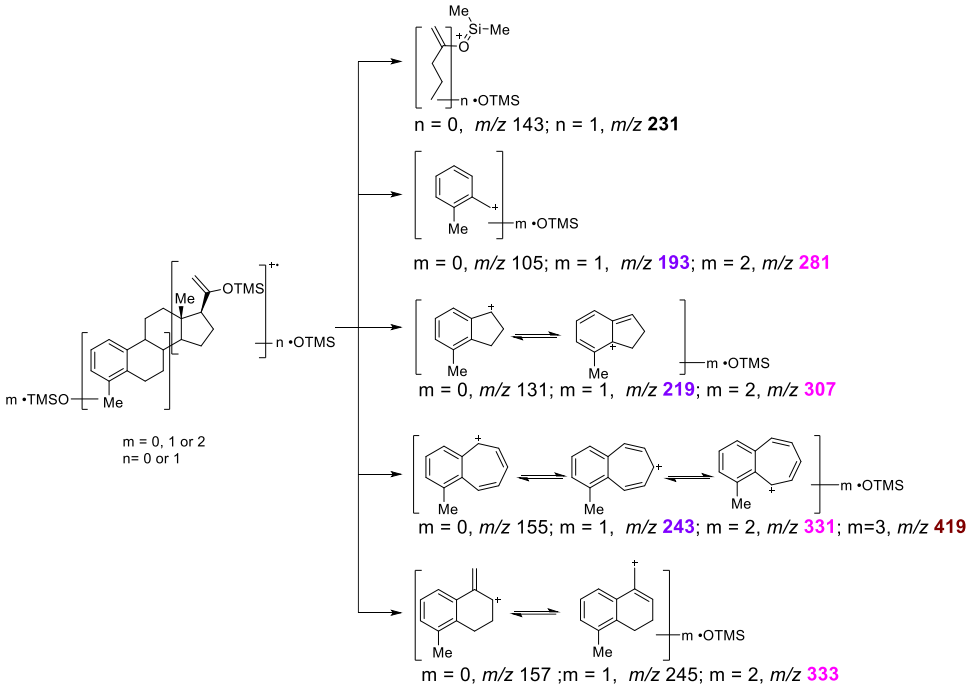

Scheme 92. Corresponding structure with additional TMSO groups at *m/z* 143, 105, 131, 155, and 157 from GC-EI-MS^2 spectra.

Characteristically mass-shifted fragment ions indicate the presence of TMS functionalities (88 Da) in the respective steroid sub-structure, which were found from the GC-MS^2 analysis of both *in vitro* and *in vivo* metabolites. The ion series at *m/z* 243 (155 + 88 x 1 Da), *m/z* 331 (155 + 88 x 2 Da), *m/z* 419 (155 + 88 x 3 Da) indicated single, double or even triple hydroxylation at ring A and B, based on the TMS-related mass-shifts. The indicative fragment ions at *m/z* 231 (143 + 88 Da) suggested hydroxylation at ring D for the same reasons. These characteristic ions are important for metabolite structure elucidations and semi-qualitative studies by GC-MS analysis.

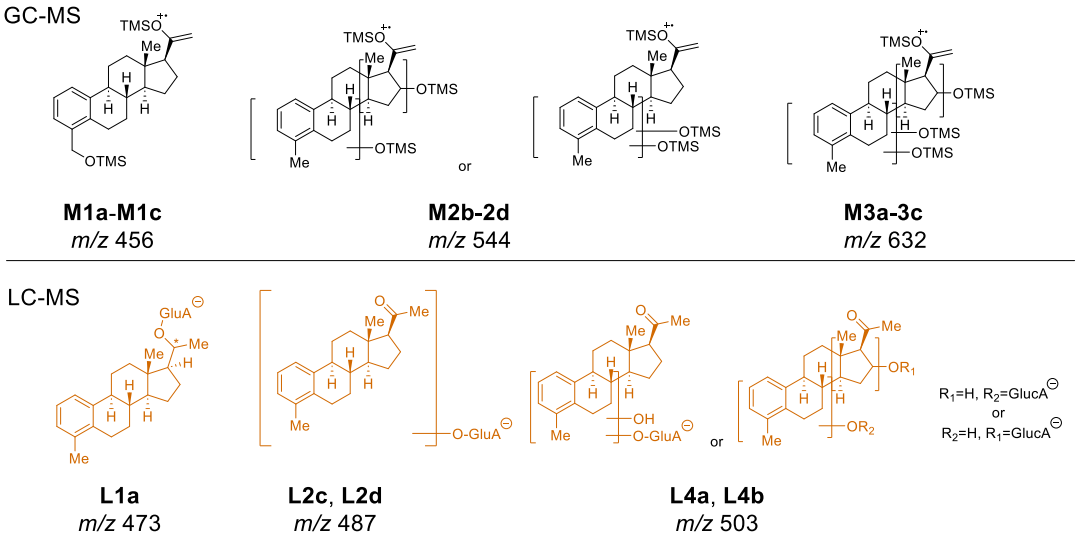

Scheme 93. Major *in vitro* S42 metabolites. Top: Phase I TMS analogs analyzed by GC-EI-HRMS. **M1a-M1b** showed abundant signals in the gas EICs. Bottom: phase II glucuronide conjugates analyzed by means of LC-ESI-HRMS; structures were hypothesized based on the phase I results. **L1a, L2c** and **L2d** showed abundant signals in the liquid EICs.

In vitro phase I metabolites of S42 (**1**) and S42-d7 (**1-d7**) and the related phase II metabolites were analyzed by GC-EI-HRMS/MS and LC-ESI-HRMS/MS, respectively. The main metabolic pathways of phase I and phase II transformations, i.e. mono-hydroxylation or reduction, followed by glucuronidation, were clearly identified. Furthermore, the GC-EI-HRMS study of phase I metabolites allowed a straight-forward identification of the hydroxyl functionality located in the benzylic position of ring A in major metabolites **M1a-c** (see **chapter 4.3.2**).

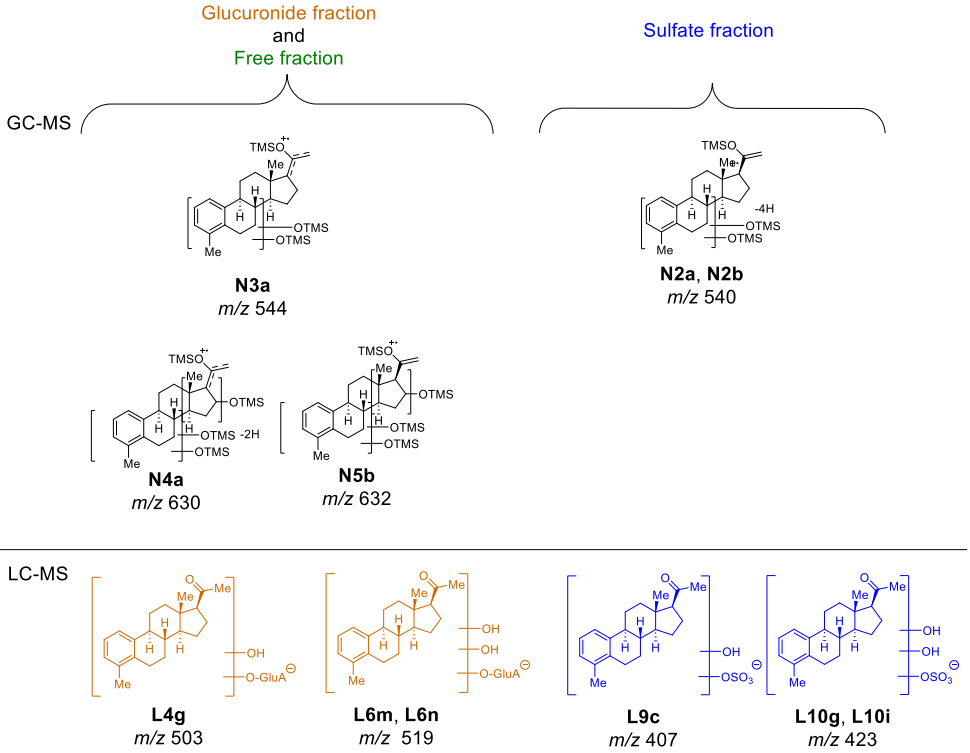

Scheme 94. Major *in vivo* S42 rat metabolites. Top: TMS analogs analyzed by GC-MS (Rat 1 - 4). **N4a** and **N4b** showed abundant signals in the EICs. TMS-derived sulfate metabolites may not be stable, and an elimination reaction may occur. Bottom: phase II glucuronide conjugates analyzed by means of LC-MS (Rat 1-6). **L10g** showed high intense peaks in the EICs.

The *in vivo* study was conducted with 6 male rats and urine samples were collected over a period of 8 days after S42 uptake. PRM experiments were conducted by GC/LC-HRMS (Orbitrap) for metabolite structure elucidation, while MRM experiments were performed by GC-EI-LRMS (triple quadrupole) for semi-quantitative characterization. Major excretion of S42 metabolites were found in urine samples from days 2 and 3. The multidimensional analyses document that hydrolysis conditions in the sulfate fraction promoted alterations of the phase II metabolites. In particular the elimination of TMSOH of phase I TMS derivatives prior to GC-MS analysis led to inconsistencies between GC-MS and LC-MS results. According to the GC-MS data, the primary glucuronide metabolites were the triply hydroxylated derivatives **N4a** and **N5b**, along with **L6m** and **L6n**, which were detected in LC-MS. However, bis-hydroxylated derivatives **N2b**, the primary sulfate metabolite by GC-MS analysis, did not correspond to the most intense sulfate peak from **L10g** by LC-MS analysis.

6. Outlook

Extensive *in vitro* and *in vivo* metabolism studies of S42 (**1**) were conducted in this work. The *in vitro* phase I studies of S42 with HLM and S9 enzyme fraction indicate that a major S42 oxidation product is a C4 benzylic alcohol derivative based on the analysis of the TMS analogues **M1a**, **M1b** and **M1c**. Besides the collection of clear instrumental-analytic evidence, only a chemically synthesized analogue can completely confirm the assumption. The respective target molecule **M1** could be synthesized from estrone for subsequent GC-EI-HRMS analysis (**Scheme 95**).

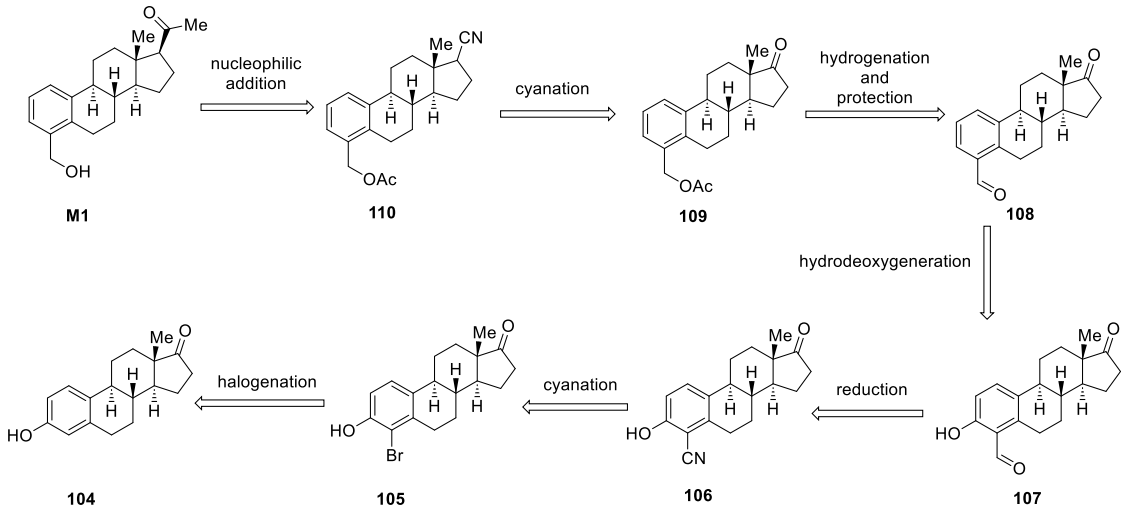

Scheme 95. Retrosynthesis of S42 C4-methoxy compound **M1** from estrone (**104**).[137]

A possible retrosynthesis involves halogenating estrone (**104**) at the C4 position, followed by cyanation and reduction of the nitrile to generate aldehyde **107**.[137a] A hydrodeoxygenation reaction can be applied to remove the hydroxy group at C3, generating compound **108**.[137b] After hydrogenation to form a benzylic alcohol and protection, the C17 ketone **109** can be transformed to a cyanide **110** and substituted by an acetyl functional group to give **M1**. Besides target compound **M1**, S42 derivatives with hydroxy groups in ring C and ring D can also be achieved by chemical synthesis.[69b] The synthesized target compounds can be used as reference materials to compare with S42 (**1**) metabolite from *in vitro* and *in vivo* studies.

An alternative to chemical synthesis might be to produce S42 metabolites in bulk scale by an electrochemical flow-through cell reaction as performed in the *Kast* lab at the University of Münster.[138] The generated S42-mono-OH in bulk scale can be purified and analyzed by NMR to solve its structure.

Furthermore, S42 metabolites could also be generated by organs on a chip (OOC) of S42 (**1**).[20b] On the perspective of *in vivo* experiments, administering S42 (**1**) and S42-d7 (**1-d7**) to humanized mice could generate more realistic results.

The steroid S42 (**1**) showed SARM properties and is certainly of interest for illicit performance enhancement purposes in sports doping. The extensive collection of fundamental data on S42 and its metabolism provides a firm basis for the development of sensitive, selective and effective S42 screening method for routine doping urine sample controls.

7. Experimental section

7.1. Materials

7.1.1 Chemicals and glassware

Steroids synthesis

For the synthesis of S42 (**1**) and its derivatives, pregnenolone and pregnenolone acetate were purchased from *TCI* (Eschborn, Germany). All other reagents were obtained from *Sigma Aldrich* (Steinheim, Germany) or *Thermo Scientific* (Geel, Belgium). or provided by *Dr. Tobias Wilczek* and *Dr. Christina Wartmann*. The solvents, ethyl acetate (EtOAc), and cyclohexane (*c*Hex) were distilled before use.

All glassware for reactions was dried in an oven at 75 °C. *Schlenk* tubes or *Schlenk* flasks that connected to a *Schlenk* line were dried by a heat gun before they were used for reactions. Glass volumetric pipettes were dried only at an ambient temperature.

In Vitro experiments

Chemicals KH_2PO_4, *D*-Saccharic acid-1,4-lactone (SL), uridine-5′-diphosphoglucuronic acid (UDPGA), and $MgCl_2$ were purchased from *Sigma Aldrich* (St. Louis, MO, USA). Formic acid (FA), S9 fraction and HLM (human liver microsome) were obtained from *Thermo Scientific* (Bremen, Germany). Na_2HPO_4, nicotinamide adenine dinucleotide phosphate (NADPH), methanol (MeOH), acetonitrile (ACN), ethanethiol, and ammonium iodide (NH_4I) were obtained from *Merck* (Darmstadt, Germany). Adenosine triphosphate (ATP) and Na_2SO_4 were ordered from Carl ROTH (Karlsruhe, Germany). Alamethicin was purchased from Enzo Life Sciences (Farmingdale, NY, USA). *N*-methyl-*N*-trimethylsilyl trifluoroacetamide (MSTFA) was from *Chemische Fabrik Karl Bucher* (Waldstetten, Germany). Ultrapure water was generated with a Barnstead GenPure xCAD Plus from *Thermo Scientific*. The Chromabond HLB (60 µm, 3 mL/60 mg) and (500 mg, 6 mL) cartridges were used for solid-phase extraction (SPE), *Macherey-Nagel* (Düren, Germany).

Rat urine analysis

All solvents and reagents were analytical grades for the workup and the analysis. *Tert*-butyl methyl ether (TBME), methanol (MeOH), ethyl acetate (EtOAc), ethanethiol, ammonium iodide (NH_4I), and acetonitrile (ACN) were from *Merck* (Darmstadt, Germany). Sulfuric acid, and glacial acetic acid were from *Sigma Aldrich*. *N*-methyl-N-trimethylsilyltrifluoroacetamide (MSTFA) for silylation was obtained from *Chemische Fabrik Karl Bucher* (Waldstetten, Germany). The *β*-glucuronidase from *Escherichia coli* for hydrolysis reaction was purchased from *Roche Diagnostics GmbH* (Mannheim, Germany). Solid phase extraction (SPE) cartridges *Chromabond*® C18 (500 mg, 6 mL) were acquired from *Macherey & Nagel* (Düren, Germany).

7.1.2 Equipment and analytical methods

NMR spectroscopy

NMR spectra were measured at a *Bruker Avance II*. ^{1}H NMR spectra were measured at a frequency of 500 or 300 MHz. The assignments were carried out using ^{13}C NMR at a frequency of 75 or 126 MHz. The chemical shift δ and the coupling constant *J* are indicated in ppm and Hz respectively.

The multiplicity is classified as singlet (s), doublet (d), triplet (t), doublet of doublet (dd), triplet of triplet (tt) and multiplet (m). The solvent used in this experimental project is deuterated chloroform ($CDCl_3$ = 99.8%, TMS = 0.03%).

The calibration of spectrum is based on the solvent peak or TMS (tetramethyl silane). In ^{1}H NMR, the residual solvent signal of $CDCl_3$ is at 7.26 ppm, while in ^{13}C-NMR, a solvent signal of $CDCl_3$ is at 77.0 ppm.

FT-IR

Infrared spectra were measured by a *Shimadzu IR Affinity-1* FT-IR spectrometer with ATR (attenuated total reflection) technique. The frequency of each peak was shown in cm^{-1} and the peaks were labeled as weak (w), medium (m), strong (s) and broad (br).

Thin layer chromatography

Thin film plates *ALUGRAM Xtra SIL G/UV254* which were manufactured by *Macherey-Nagel* were used. Each thin film consisted of 0.2 mm thickness of silica and fluorescence indicator for UV light analysis. Oxidation dye, phosphomolybdic acid (PMA) in ethanol solution, was used for further analysis of TLC plates.

Column chromatography

Standard silica 60 from *Macherey-Nagel* was used with the particle size from 0.035-0.070 mm and pore size of 60 Å. Pressure was applied during the packing and running process.

Melting point detection

Melting points were determined by heating up packed compounds in a *Mettler Toledo MP50* digital melting point system in open glass capillaries. The transformation from solid state to liquid state was observed through a camera by use of light transmission.

GC-EI LR-MS at University of Cologne

GC-EI LR MS analysis was attained by *Agilent 7890A GC*-System with a *5975C Inert XL MSD* detector and a *7693 autosampler*. The capillary column was *HP HP-5 MS* crosslinked silicon gum (30 m × 0.25 mm, 0.25 µm film thickness) with hydrogen carrier gas at a flow rate of 2 mL min^{-1}.

For analysis of the synthesis compound, oven method 50(5)-20-280(10) (50 °C for 5 min, increasing 20 °C min^{-1} to 280 °C for 10 min) was used with 1 µL injection volume. The compound was identified by the specific molecular mass.

GC-EI HR-MS (Orbitrap) at University of Cologne

A *Thermo Scientific™ Exactive™ GC Orbitrap™ GC-MS* system instrument (*TriPlus RSH Autosampler*, *TRACE 1300 Series GC*, *Exactive GC-Orbitrap MS*, *Thermo Fisher Scientific*) was used for GC-EI-HRMS, supplied with He gas as mobile GC phase and was operated at a routinely used resolution of 60,000 FWHM. The capillary column, TG-5SILMS (length 30 m × diameter 0.25 mm, 0.25 µm film thickness, 5% diphenyl/

95% dimethyl- polysiloxane) from Thermo Scientific was used for all measurements. A sample volume of 1 µL was injected into the GC with a split flow of 12.0 mL/min, a purge flow of 5.0 mL/min, and a carrier helium gas flow of 1.2 mL/min at an inlet temperature of 300 °C.

Three GC oven temperature programs were used: 50(5)-10-270(5), 100(5)-10-320(5), 120(5)-10-320(5) or 220(20)-20-280(10). EI-MS conditions: ion source temperature was set to 250 °C, the emission current is set at 50 µA, and the electron energy was 70 eV, and the spectra were acquired over a mass range of *m/z* 50-550. Accurate ion mass measurements were conducted with external calibration with perfluoro-tributylmine as standard.

For S42-d7 (**1-d7**) analysis,[115] a resolution of 120,000 or 60,000 was used. The oven temperature program is 220(20)-20-280(10). For TIC (total ion chromatogram) mode, a measuring range of *m/z* 280-310 was used, while for SIM (selected ion monitoring) mode, *m/z* 296.21, 297.22, 298.23, 299.23, 300.24, 301.24, 302.25, 303.26, 304.26, 305.26 and 306.27 were selected at RT: 18-20 min with a width of 0.6 or 0.9 *m/z*.

GC-EI HR-MS (Orbitrap) at the German Sport University Cologne

A *Thermo Scientific™ Q Exactive™ GC Orbitrap™ GC-MS/MS* system (*Thermo Fisher Scientific*) was used for GC-EI HR MS, supplied with He gas as mobile GC phase and was operated at a routinely used resolution of 60,000 FWHM. A *19091A-008*, *HP-ULTRA-1* (length 17 m × diameter 0.20 mm, 0.11 µm film thickness, 7-inch format, 100% dimethylpolysiloxane) (*Agilent*) GC column was used. A sample volume of 2 µL was injected into the GC with a split flow of 8.0 mL/min or 7.0 mL/min, a purge flow of 5.0 mL/min. Helium was employed as GC mobile phase with a constant pressure of 17 psi. And a flow rate of 1.2 mL/min. The GC inlet temperature was set to 300 °C. A new GC column replaced the old one during this project. Nevertheless, the retention time of metabolites did not largely shift.

The mass spectrometer acquired data in full scan mode with a scan range from *m/z* 70 to 700 at a resolution of 60,000. Daily mass calibration using perfluorotributylamine of the instrument yielded mass accuracy in the range ± 5 ppm. The mass error from an average spectrum was automatically calculated by *Xcalibur Qual Browser* from *Thermo Scientific.*

The GC temperature program 185(0)-3-234(0)-40-310(5) was used. The ion source temperature was 250 °C, the emission current was set to 50 µA, and the electron energy of 50 eV was used for EI-MS. The mass range of *m/z* 70–700 was used. The collision energy of HCD (higher-energy collisional dissociation) was 15 or 20 eV for PRM (parallel reaction monitoring) experiments. The selected deuterated precursor ions (ex. **M1a-d5**, **M1b-d5**, **M1c-d5**) for MS^2 experiments were decided according to the abundance in the mixture of **1-d7** metabolites.

GC-EI LR-MS (Triple quadrupole) at the German Sport University Cologne

Thermo TSQ8000 Evo coupled to a *Trace GC 1310* (*ThermoFisher*, Bremen, Germany) was used. Injections were performed in split mode with a split ratio of 1:15 at 300 °C by employing a *Thermospray SSL Injector Module* (*ThermoFisher*, Bremen, Germany). The ion source temperature was set at 250 °C and the electron energy was set at 70 eV: The injection volume was 3 µL and the GC column was *19091A-008*, *HP-ULTRA-1* (length 17 m × diameter 0.20 mm, 0.11 µm film thickness, 7-inch format, 100% dimethylpolysiloxane) (*Agilent*). The GC temperature program 185(0)-3-234(0)-40-310(5) was used as the GC-EI-HRMS (Orbitrap). Helium was employed as carrier gas with a constant pressure of 17 psi. The collision energy was listed in the table in discussion parts.

LC-ESI HR-MS (Orbitrap) at the German Sport University Cologne

LC-MS analysis was conducted by a Vanquish UHPLC system coupled with an *Orbitrap Exploris 480* mass spectrometer, both from *Thermo Fisher* (Bremen, Germany). The HPLC system was equipped with *EC 4/2 Nucleodur C-18 Pyramid* 3 µm pre-column from *Macherey-Nagel* (Düren, Germany) and a *Poroshell 120 EC-C18* column (3.0 × 50 mm, 2.7 µm) from Agilent (Santa Clara, CA, USA)

Ammonium acetate (5mM, pH4.5) was used as eluent A and MeOH was applied as eluent B. For the analysis, 5 µl of the sample were injected into the LC system with a flow rate of 300 µl/min. A total run time of 35 min. With a constant flow of 300 µl/min, the gradient started with 30% B over 1 min, increased to 60% B within 22 min, 70% B within 2 min, 75% within 3 min, 100% within 2 min and held for 2 min. The re-equilibration allowed the gradient to go back to the starting conditions of 30% B over 3 min.

The full-scan experiments were conducted with a resolution of 30,000 FWHM and a scan range of *m*/*z* 80–800. HRMS/MS experiments were used in parallel reaction monitoring mode with a resolution of 30,000 FWHM with an isolation window of *m*/*z* 1. Only negative ionization mode was performed using a heated ESI source with −3500 V and a vaporizer temperature set at 300 °C. Nitrogen was applied as collision gas and generated using a *CMC* nitrogen generator (Eschborn, Germany). The MS was calibrated weekly with the calibration solution provided by *Thermo Scientific*.

The normalized collision energies were optimized and listed below: using 30% for *m/z* 489.2494, 503.2287, 487.2337, 505.2443, and 519.2236; 45% for *m/z* 466.2526, 470.2808, 391.1585, 407.1534, 393.1741, 423.1483, 441.1589, and 443.1745, 473.2545; 60% for *m/z* 370.1773.

X-ray crystallography

All crystal structure measurements and analysis were performed and assigned by *Dr. Jörg Neudoerfl*, Department of Chemistry, University of Cologne, Greinstraße 6, D-50939, Cologne, Germany. The measurement was carried out by using *Bruker D8 Venture diffractometer* applied with a copper micro focus tube. *Photon III M14* was utilized as a detector and *Program Apex 3* assisted the measurement and data analysis. The structure solution was performed with *SHELXT*. For refining the structure, *Shelxl* was applied. Details on the crystallographic analysis are found with the general analytical data sets of the new compounds.

7.1.3 General software and AI tools

The GC-MS and LC-MS data analysis were conducted by *Xcalibur Qual Browser* or *Freestyle* from *Thermo Fishcer. Scientific*. The NMR spectra were analyzed by *Bruker Topspin 4.0.9* data program. Charts and diagrams were produced by *Excel* and *Origin.* Grammar and word choice were edited by *Grammarly,*[139] and *Copilot*[140]*. ChatGPT*[130] was used for preparing outlines, listing word choice, and producing pictures. *Perplexity*[141] was used for literature searching.

7.2 Steroid S42 (**1**) and derivatives synthesis

7.2.1 Synthesis and characterization of compound **16**

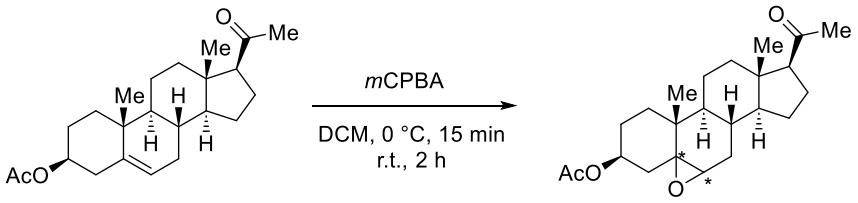

15 **16**, 98%

According to the synthesis procedure from *Uyanik et al.*[7], pregnenolone acetate (5-pregnen-3*β*-ol-20-on-acetat) (**15**) (10.0 g, 27.9 mmol, 1.0 eq.) was dissolved in DCM (1.06 L) in a round bottom flask and cooled portion-wise to 0 °C. Subsequently, 70% *m*CPBA (3-chloroperbenzoic acid) (10.3 g, 41.8 mmol, 1.5 eq.) was added portion-wise. The reaction mixture was stirred at 0 °C for 15 min and warmed to ambient temperature. After the reaction was stirred at r.t. for 2 h, the reaction mixture was quenched by sat. Na_2SO_3 (aq.) solution and stirred at ambient temperature. The organic phase was separated, washed by sat. $NaHCO_3$ (aq.) and brine. The solution was dried over Na_2SO_4, filtered, and concentrated under reduced pressure. The crude product was purified by column chromatography on silica (*c*Hex/EtOAc = 4/1) to yield a white solid (10.2 g, 27.3 mmol, 98%).

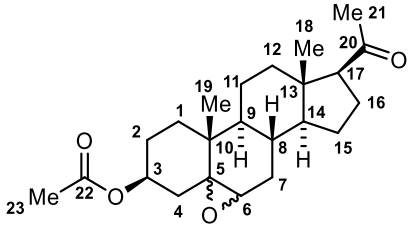

Appearance:	white solid.
Chemical Formula:	$C_{23}H_{34}O_4$.
Molecular Weight:	374.5210
Yield:	98% (10.2 g, 27.3 mmol).
R_f:	0.38 (*c*Hex:EtOAc = 2:1).
m_p:	159.7 °C.
^{1}H-NMR:	(500 MHz, $CDCl_3$, mixture of diasteromers, protons from a minor diasteromer is marked as H*. The ratio is 84:16 by NMR integrals) δ [ppm]: 4.98–4.92 (m, 0.84 H, H-3α), 4.80–4.74 (m, 0.16 H, H*-3α), 3.09 (d, 0.16H, H*-6β), 2.90 (d, 0.84 H, H-6α), 2.52–2.47 (m, 1 H, H-17), 2.19–2.12 (m, 2H, H-4), 2.10 (s, 3H, H-21), 2.03-1.92 (m, 6H, H-23, H-7, H-7', H-14), 1.76-1.11 (m, 14H, H-1, H-1', H-2, H-2', H-8, H-9. H-11, H-11', H-12, H-12', H-15, H-15', H-16, H-16'), 1.08 (s, 2.6H, H-19), 1.01(s, 0.4H, H*-19), 0.60 (s, 0.5H, H*-18), 0.56 (s, 2.5H, H-18').

^{13}C-NMR: (75 MHz, $CDCl_3$, mixture of diasteromers, protons from a minor diasteromer is marked as C*) δ [ppm]: 209.5 (C-20), 170.3 (C-22), 71.2 (C-3), 65.1 (C-5), 63.3 (C-6*) 63.2 (C-17), 58.9 (C-6), 56.9, 56.2, 43.9, 42.3, 38.7, 38.4, 37.9, 36.7, 36.0, 35.0, 32.3, 32.0, 32.1, 31.5 (C-21), 31.4, 29.7, 28.5, 27.1, 24.2, 22.7, 21.9, 21.3 (C-23), 20.6, 17.01 (C-19'), 15.8 (C-19), 13.2 (C-18) 13.1 (C-18*).

IR (ATR): $\tilde{\nu}$ [cm^{-1}] = 2940 (m), 2974 (w), 1732 (s), 1701 (s), 1472 (w), 1437 (w), 1358 (m), 1238 (vs), 1032 (s), 961 (w), 870 (w), 731 (w).

7.2.2 Synthesis and characterization of compound **18**

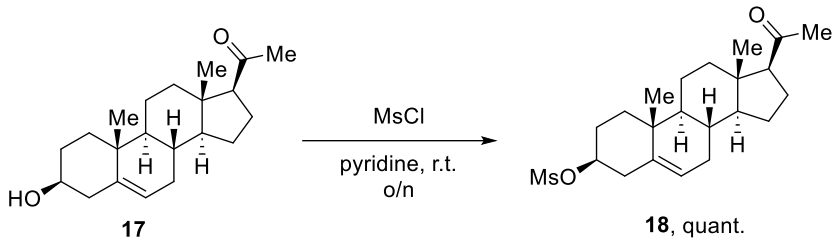

17 **18**, quant.

According to the published synthesis procedure,[142] pregnenolone (**17**) (6.0 g, 19.0 mmol, 1.0 eq.) was dissolved in dried pyridine (19 mL) in a dried *schlenk* flask under inert conditions, followed by addition of methyl sulfonyl chloride (1.8 mL, 22.8 mmol, 1.2 eq.). The reaction mixture was stirred at r.t. overnight. The reaction mixture was stopped by an addition of con. HCl (360 mL) diluted in H_2O (360 mL) and stirred for 60 min.

The white solid was filtered, washed by H_2O, dissolved in DCM, dried over Na_2SO_4, filtered off, and concentrated under reduced pressure. The product was obtained as light yellow solid (7.4 g, 18.8 mmol, quant.).

Appearance: white yellow solid.

Chemical Formula: $C_{22}H_{34}O_4S$

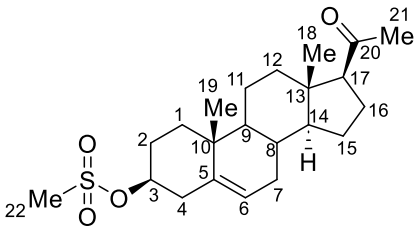

Molecular Weight: 394.5710

Yield: quant.
(7.4 g, 18.8 mmol).

R_f: 0.56 (*c*Hex:EtOAc = 2:1).

m_p: 124.4 °C.

^{1}H-NMR: (500 MHz, $CDCl_3$) δ [ppm]: 5.43−5.42 (m, 1H, H-6), 4.57− 4.50 (m, 1H, H-3), 3.01 (s, 3H, H-22), 2.55−2.47 (m, 3H, H-4, H-17), 2.23−2.15 (m, 1H, H-16), 2.15 (s, 3H, H-21), 2.07−1.99 (m, 3H, H-2, H-7, H-15), 1.92 (m, 1H, H-1), 1.85−1.76 (m, 1H, H-2), 1.73−1.60 (m, 3H, H-11, H-12, H-16'), 1.55−1.42

(m, 4H, H-7, H-8, H-11', H-15'), 1.28−1.21 (m, 1H, H-12'), 1.18-1.13 (m, 2H, H-1, H-14), 1.02 (s, 3H, H-19), 1.00−0.97 (m, 1H, H-9), 0.63 (s, 3H, H-18).

^{13}C-NMR: (126 MHz, $CDCl_3$, C-10 is ambiguous) δ [ppm]: 209.5 (C-20), 138.7 (C-5), 123.5 (C-6), 81.8 (C-3), 63.6 (C-17), 56.7 (C-14), 49.8 (C-9), 43.9 (C-13), 39.1 (C-4), 38.8 (C-22), 38.7 (C-15), 36.9 (C-1), 36.4 (C-7), 31.7 (C-8), 31.5 (C-21), 28.9 (C-2), 24.4 (C-12), 22.8 (C-16), 21.0 (C-11), 19.2 (C-19), 13.2 (C-18).

IR (ATR): $\tilde{\nu}$ [cm^{-1}] = 3942.50 − 3446,79 (br), 2966.52 (m), 2931.80 (m), 2902.87 (m), 2873.94 (m), 2852.72 (m), 2378.23 (w), 2349.30 (w), 2310.72 (w), 1734.01 (w), 1691.57 (s), 1473.62 (w), 1436.97 (w), 1384.89 (w), 1346.31 (s), 1172,72 (s), 1134.14 (m), 962.48 (m), 943.19 (s), 891.11 (m), 860.25 (s), 844.82 (s), 810.10 (m), 798.53 (m), 754.17 (m).

GC-EI-LRMS t_R= 16.84 min, *m/z* 298 $[M]^{\bullet+}$.

7.2.3 Synthesis and characterization of compound **19**

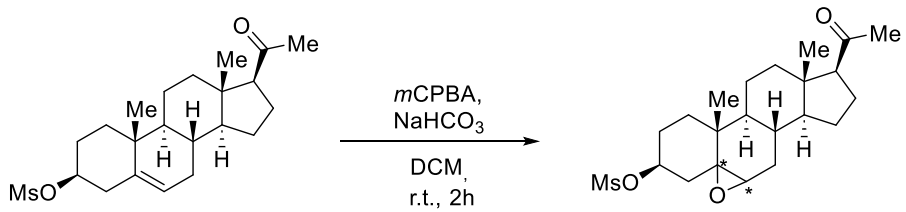

18 **19**, 95%

According to the synthesis procedure from *Uyanik et al.*,[7] pregnenolone methanesulfonate (**18**) (7.4 g, 18.7 mmol, 1.0 eq.) was dissolved in dried DCM (562 mL), followed by addition of $NaHCO_3$ (6.3 g, 75.0 mmol, 4.0 eq.) in a round bottom flask. Subsequently, 70% *m*CPBA (3-chloroperbenzoic acid) (9.2 g, 37.5 mmol, 2.0 eq.) was added portion-wise. The reaction mixture was stirred at r.t. for 2 h, before it was quenched by sat. $Na_2S_2O_3$ (aq.) solution and stirred at ambient temperature for 60 min. The organic phase was separated, washed by sat. $NaHCO_3$ (aq.) and brine. The solution was dried over Na_2SO_4, filtered, and concentrated under reduced pressure. The crude product was purified by column chromatography on silica (*c*Hex/EtOAc = 2/1) to yield a white solid (7.4 g, 17.8 mmol, 95%).

Appearance: white solid.

Chemical Formula: $C_{22}H_{34}O_5S$.

Molecular Weight: 410.5690

Yield:	95% (7.4 g, 17.8 mmol).
R_f:	0.14 (*c*Hex:EtOAc = 2:1).
m_p:	145.5 °C.

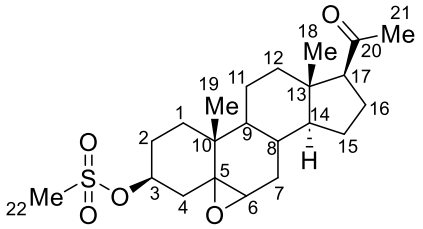

^{1}H-NMR:	(500 MHz, $CDCl_3$) δ [ppm]: 4.86–4.80 (m, 1H, H-3), 2.99 (s, 3H, H-22), 2.94 (d, *J* = 4.4 Hz ,1H, H-6) 2.50 (t, *J* = 9.0 Hz, 1H, H-17), 2.38-2.33 (m, 1H, H-4), 2.19–2.12 (m, 2H, H-2, H-15), 2.10 (s, 3H, H-21), 2.01-1.92 (m, 2H, H-7, H-15'), 1.92-1.85 (m, 1H, H-1), 1.78-1.74 (m, 1H, H-11), 1.70-1.60 (m, 2H, H-2, H-16), 1.54-1.25 (m, 8H, H-1', H-4', H-7', H-8, H-9, H-11',H-12, H-12'), 1.21-1.10 (m, 2H, H-14, H-16'), 1.08 (s, 3H, H-19), 0.56 (s, 3H, H-18).
^{13}C-NMR:	(75 MHz, $CDCl_3$) δ [ppm]: 209.4 (C-20), 79.5 (C-3), 65.0 (C-5), 63.3 (C-17) 59.1 (C-6), 56.9 (C-14), 43.9 (C13), 42.4 (C-9), 38.5 (C-22), 38.4 (C-7), 37.3 (C-4), 34.8 (C-10), 32.2 (C-11), 31.5 (C-21), 29.8 (C-8), 28.6 (C-1), 28.5 (C-15), 24.2 (C-16), 22.7 (C-2), 20.6 (C-12), 15.8 (C-19), 13.2 (C-18).
IR (ATR):	$\tilde{\nu}$ [cm^{-1}] = 2980 (m), 2937 (m), 1697 (s), 1473 (w), 1431 (w), 1382 (w), 1355 (w), 1325 (s), 1232 (w), 1195 (w), 1163 (s), 1130 (w), 983 (w), 929 (s), 908 (s), 866 (s), 817 (m), 779 (m), 748 (m), 719 (w), 690 (w).

7.2.4 Synthesis and characterization of S42 **(1)**

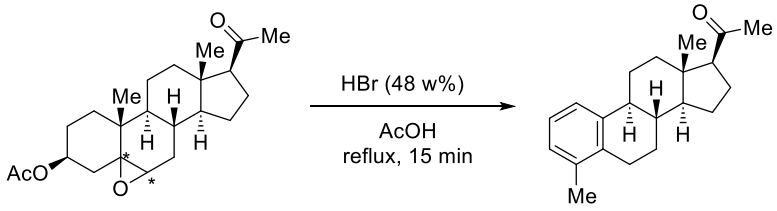

16 S42 (**1**), 9%

According to the synthesis procedure from *Uyanik et al.*[7], 3ß-acetoxy-5,6-epoxypregnan-20-one (**16**) (1.00 g, 2.68 mmol, 1.0 eq.) was dissolved in acetic acid (9 mL) in a 2-necked round bottom flask. Subsequently, 48 w% HBr (2.46 mL) were added. The reaction mixture was stirred to reflux for 15 min. After the reaction was cooled to r.t., the reaction mixture was slowly added into sat. $NaHCO_3$ (aq.). Further $NaHCO_3$ was added until no bubbles formed, and the pH was neutral. The reaction mixture was extracted three times with EtOAc, washed with sat. $NaHCO_3$ (aq.), dried over Na_2SO_4, filtered off, and concentrated under reduced pressure. The crude product was purified by column chromatography on silica (*c*Hex/EtOAc = 29/1) to give a mixture of blue oil and white crystals. After recrystallization from pentane and cyclohexane, the

product was obtained as white needles (71 mg, 0.24 mmol, 9%).

* Compound **19** produced S42 (**1**) with a yield of 17% under the same reaction conditions with a reaction time for 60 min.

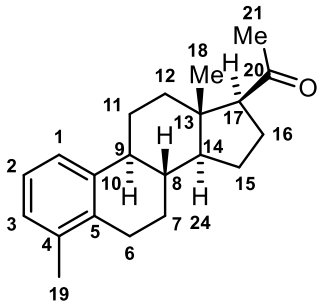

Appearance:	white crystals.
Chemical Formula:	$C_{21}H_{28}O$.
Molecular Weight:	296.4540
Yield:	9% (71 mg, 0.24 mmol).
R_f:	0.7 (*c*Hex:EtOAc = 2:1).
m_p:	168.0-169.0 °C.
^{1}H-NMR:	(500 MHz, $CDCl_3$) δ [ppm]: 7.19 (d, *J* = 7.8 Hz, 1H, H-1), 7.08 (t, *J* = 7.6 Hz, 1H, H-2), 7.01 (d, *J* = 7.4 Hz, 1H, H-3), 2.78 (dd, *J* = 17.1, 5.6 Hz, 1H, H-6), 2.67 – 2.60 (m, 2H, H-6', H-17), 2.57 – 2.37 (m, 1H, H-11), 2.37 – 2.27 (m, 1H, H-9), 2.27 – 2.18 (m, 4H, H-16, H-19), 2.20 – 2.17 (m, 1H, H-12), 2.16 (s, 3H, H-21), 2.01 – 1.97 (m, 1H, H-7), 1.84 – 1.79 (m, 1H, H-15), 1.75 – 1.63 (m, 2H, H-12', H-16'), 1.58 – 1.49 (m, 1H, H-11'), 1.44 – 1.29 (m, 4H, H-7', H-8, H-14, H-15'), 0.65 (s, 3H, H-18).
^{13}C-NMR:	(126 MHz, $CDCl_3$) δ [ppm]: 209.5 (C-20), 140.0 (C-10), 136.4 (C-4), 135.1 (C-5), 127.3 (C-3), 125.3 (C-2), 123.0 (C-1), 63.8 (C-17), 55.8 (C-14), 44.4 (C-9), 44.2 (C-13), 39.1 (C-12), 37.8 (C-8), 31.5 (C-21), 27.7 (C-7), 27.1 (C-6), 26.7 (C-11), 24.1 (C-15), 22.9 (C-16), 19.8 (C-19), 13.3 (C-18).
IR:	$\tilde{\upsilon}$ [cm^{-1}]: 2936 (m), 2869 (w), 2824 (w), 1681 (w), 1645 (w), 1601 (w), 1471 (w), 1453 (w), 1443 (w), 1419 (w), 1380 (w), 1361 (w), 1321 (w), 1296 (m), 1251 (s), 1237 (m), 1176 (w), 1125 (w), 1090 (w), 1072 (w), 1044 (m), 1017 (m), 1009 (m), 961 (w), 950 (w), 872 (m), 841 (s), 804 (s), 778 (m), 756 (m), 742 (s), 707 (w), 696 (w), 646 (w), 607 (w), 570 (w), 552 (w), 517 (w).
GC-EI-LRMS	t_R= 16.50 min, *m/z* 296.2 $[M]^{\bullet+}$.
GC-EI-HRMS	t_R= 28.17 min, *m/z* 296.2129 $[M]^{\bullet+}$.

7.2.5 Synthesis and characterization of S42-d4 (**1-d4**)[99]

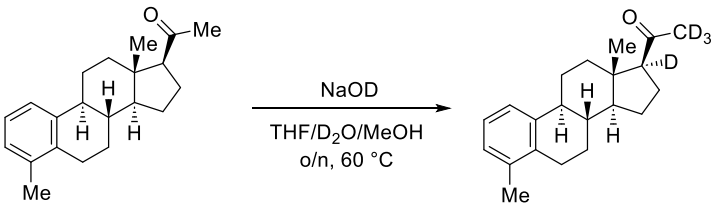

S42 (**1**) **1-d4**, quant.

To a dried *Schlenk* flask was added S42 (**1**) (20 mg, 0.07 mmol, 1.0 eq.) in dry THF (600 µL), NaOD (40% in D_2O, 30 µL), D_2O (450 µL) and MeOD (120 µL).[99] The white suspension was stirred at 60 °C overnight and the reaction progress was monitored by GC-MS. After the pH was adjusted to neutral by addition of AcOD (9% in D_2O), the mixture was extracted by EtOAc three times, dried over Na_2SO_4, filtered, and concentrated under reduced pressure. The solid was triturated by *n*-hexane and gave a white solid with a quantitative yield.

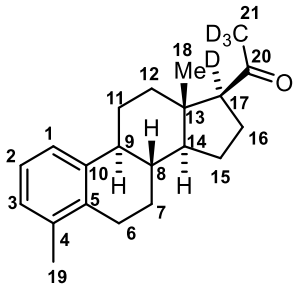

Appearance:	White solid.
Chemical Formula:	$C_{21}H_{24}D_4O$.
Molecular Weight:	300.4784
Yield:	Quantitative (20 mg).
R_f:	0.7 (CyHex:EtOAc = 10:1).
^{1}H-NMR:	(500 MHz, $CDCl_3$) δ [ppm]: 7.19 (d, *J* = 7.8 Hz, 1H, H-1), 7.08 (t, *J* = 7.5 Hz, 1H, H-2), 7.01 (d, *J* = 7.4 Hz, 1H, H-3), 2.78 (dd, *J* = 17.4, 5.6 Hz, 1H, H-6), 2.68 – 2.60 (m, 1H, H-6'), 2.41 – 2.35 (m, 1H, H-11), 2.35 – 2.31 (m, 1H, H-9), 2.25 – 2.19 (m, 4H, H-16, H-19), 2.19 – 2.14 (m, 1H, H-12), 2.01 – 1.97 (m, 1H, H-7), 1.84 – 1.78 (m, 1H, H-15), 1.73 – 1.63 (m, 2H, H-12', H-16'), 1.59 – 1.49 (m, 1H, H-11'), 1.46 – 1.28 (m, 4H, H-7', H-8, H-14, H-15'), 0.65 (s, 3H, H-18).
^{13}C-NMR:	126 MHz, $CDCl_3$) δ [ppm]: 140.0 (C-10), 136.5 (C-4), 135.1 (C-5), 127.4 (C-3), 125.4 (C-2), 123.0 (C-1), 55.9 (C-14), 44.4 (C-9), 44.2 (C-13), 39.0 (C-12), 37.9 (C-8), 27.8 (C-7), 27.2 (C-6), 26.8 (C-11), 24.2 (C-15), 22.8 (C-16), 19.8 (C-19), 13.4 (C-18).
IR:	$\tilde{\upsilon}$ [cm^{-1}]: 3676 (w), 3224 (w), 2969 (s), 2923 (s), 2092 (m), 2112 (w), 1923 (w), 1694 (m), 1670 (m), 1620 (w), 1543 (w), 1472 (w), 1451 (m), 1407 (m), 1381 (m), 1261 (m), 1229 (m), 1221 (m), 1189 (w), 1159 (w), 1137 (w), 1067 (s), 1051 (s), 1027 (m), 957 (w), 945 (w), 870 (m), 799 (m), 779 (m), 738 (m), 635 (w), 571 (w), 542 (w), 527 (w), 511 (w).
GC-EI-LRMS	t_R = 17.10 min, *m/z* 300.2 $[M]^{\bullet+}$.
GC-EI-HRMS	t_R = 23.02 min, *m/z* 300.2386 $[M]^{\bullet+}$.

7.2.6 Synthesis and characterization S42-d7 (**1-d7**)

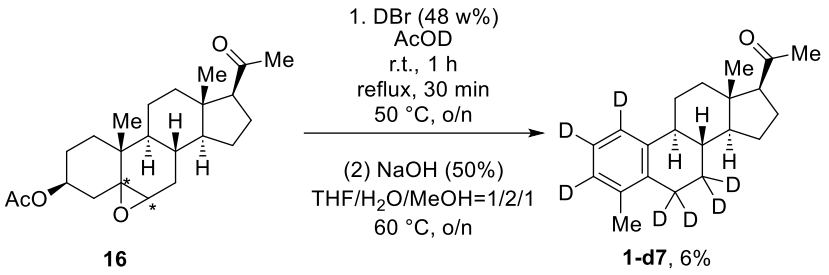

Adapting the synthesis procedure from *Uyanik et al.*[7], 3ß-acetoxy-*5,* 6-epoxypregnan-20-one (**16**) (2.00 g, 5.34 mmol, 1.0 eq.) was dissolved in deuterated acetic acid (12 mL) in a dried 2-necked round bottom flask under inert conditions. Subsequently, 48% DBr (4 mL) was added. The reaction mixture was stirred at r.t for 1h and heated to reflux for 30 min. Then, the reaction mixture was stirred at 50 °C overnight. After the reaction was cooled to r.t., the mixture was slowly added into sat. $NaHCO_3$ (aq.). $NaHCO_3$ was added to the solution until no bubbles formed, and the pH was 7. The reaction mixture was extracted with DCM four times, washed with $NaHCO_3$ (aq.), dried over Na_2SO_4, filtered and concentrated under reduced pressure.

The crude product was dissolved in a mixture of THF (12 mL), H_2O (24 mL) and MeOH (12 mL) followed by an addition of 50% NaOH (aq.) (2 mL). After stirring at 60 °C overnight, the mixture was neutralized with 10% AcOH. The reaction mixture was extracted with EtOAc three times, dried over Na_2SO_4, filtered and concentrated under reduced pressure. The crude product was further purified by column chromatography on silica (*c*Hex/EtOAc = 29/1) to give a mixture of blue oil and white crystals. After recrystallization from pentane and cyclohexane, the product was obtained as white needle-like crystals (93 mg, 0.31 mmol, 6%).

Appearance:	White crystals**.**
Chemical Formula:	$C_{21}H_{21}D_7O$.
Molecular Weight:	303.4967
Yield:	6% (93 mg, 0.31 mmol).
R_f:	0.55 (*c*Hex:EtOAc = 2:1).
m_p:	162-165 °C.

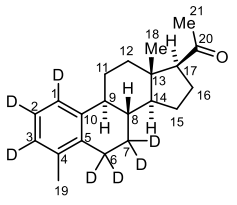

^{1}H-NMR:	(500 MHz, CD_2Cl_2) δ [ppm]: 7.16 (m, 0.16H, H-1), 7.04 (m, 0.19H, H-2), 6.97 (m, 0.16H, H-3), 2.74 (m, 0.35H, H-6), 2.62 (m, 1.29H, H-6', H-17), 2.41-2.36 (m, 1H, H-11), 2.34 – 2.25 (m, 1H, H-9), 2.22 (s, 3H, H-19), 2.19-2.14 (m, 2H, H-12, H-16), 2.12 (s, 3H, H-21), 2.00 – 1.95 (m, 0.3H, H-7), 1.84-.178 (m, 1H, H-15), 1.73 – 1.63 (m, 2H, H-12', H-16'), 1.54 – 1.46 (m, 1H, H-11'), 1.43 – 1.27 (m, 3.6H, H-7', H-8, H-14, H-15', 0.63 (s, 3H, H-18).
^{2}H-NMR:	(77 MHz, CD_2Cl_2) δ [ppm]: 7.26-6.95 (D-1, D-2, D-3), 2.74 (D-6), 2.60 (D-6'), 1.96 (D-7), 1.36 (D-7').
^{13}C-NMR:	(126 MHz, CD_2Cl_2) δ [ppm]: 209.3 (C-20), 140.5 (m, C-10), 136.7 (m, C-5), 135.5 (m, C-4), 127.4 (m, C-3), 125.3 (m, C-2), 123.2 (m, C-1), 64.1 (C-17), 56.2 (m, C-14), 44.7 (m, C-9), 44.5 (C-13), 39.4 (C-12), 38.2 (m, C-8), 38.1 (m, C-8), 31.7 (C-21), 27.2 (m, C-11), 24.5 (C-15), 23.2 (C-16), 19.9 (m, C-19), 19.8 (m, C-19'), 13.5 (C-18)
IR:	$\tilde{\upsilon}$ [cm^{-1}]: 2957 (w), 2945 (w), 2916 (m), 2862 (w), 1697 (s), 1560 (w), 1470 (w), 1447 (m), 1425 (w), 1381 (m), 1348 (s), 1248 (m), 1213 (m), 1182 (m), 1159 (m), 1026 (w), 800 (w), 691 (w), 658 (m), 644 (m), 610 (m), 577(s), 559 (s)
GC-EI-HRMS	t_R = 18.68 min, *m/z* 303.2563 (d7), 302.2505 (d6), 301.2446 (d5), 300.2364 (d4) $[M]^{\bullet+}$. (Temp: 220(20)-20-280(10))

7.2.7 Synthesis and characterization of compounds **2** and **2'**

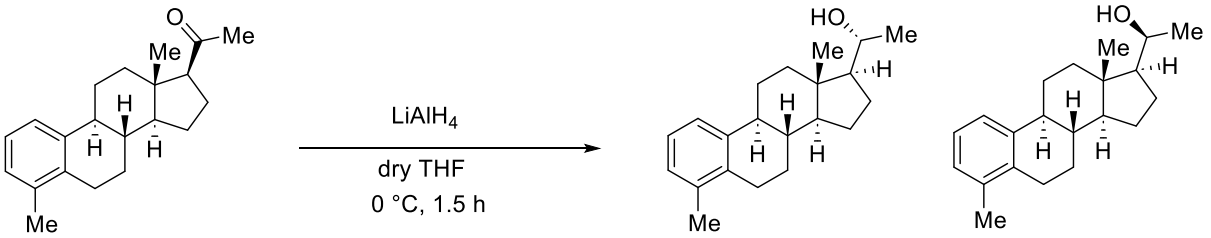

S42 (**1**)

S42-C20-OH (**2**) (stereoselective)

S42-C20-OH' (**2'**)

2 : **2'** = 0.76 : 0.24
(acc. NMR and separated fractions)
91% (overall yield)

According to the synthesis procedure from *MacNevin et al.*,[101] steroid S42 (**1**) (50 mg, 0.17 mmol, 1.0 eq.) was dissolved in dry THF (1.5 mL) in a dried *Schlenk* tube connected to a *Schenk* line under an inert condition. Subsequently, $LiAlH_4$ (95%) (15 mg, 0.34 mmol, 2.0 eq.) was added. The reaction mixture was stirred at 0 °C for 1.5 h, then the reaction was quenched by sat. Rochelle salt (potassium sodium tartrate tetrahydrate). The mixture was extracted with Et_2O three times, washed with brine, dried over Na_2SO_4, filtered off, and concentrated under reduced pressure. The

crude product was purified by column chromatography on silica (*c*Hex/EtOAc = 5/1) to give a mixture of epimers (46 mg, 0.15 mmol, 91%).

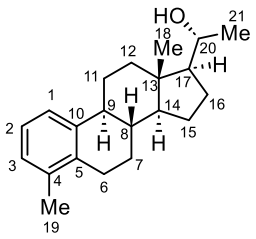

Appearance:	White solid**.**
Chemical Formula:	$C_{21}H_{30}O$
Molecular Weight:	298.4700 g/mol.
Yield:	91% (46 mg, 0.15 mmol).
R_f:	0.5 (*c*Hex:EtOAc = 2:1)
^{1}H-NMR:	(500 MHz, $CDCl_3$) δ [ppm]: 7.20 (d, *J* = 7.8 Hz, 1H, H-1), 7.07 (t, *J* = 7.6 Hz, 1H, H-2), 7.00 (d, *J* = 7.4 Hz, 1H, H-3), 3.80-3.74 (m, 1H, H-20), 2.77 (dd, *J* = 5.7 Hz, 17.1 Hz,1H, H-6), 2.67-2.60 (m, 1H, H-6'), 2.34-2.26 (m, 2H, H-9, H-16), 2.23-2.19 (m, 4H, H-15, H-19), 1.99-1.95 (m, 1H, H-7), 1.79-1.70 (m, 2H, H-11, H-12), 1.55-1.51 (m,1H, H-16'), 1.49-1.46 (m, 1H, H-15'), 1.44-1.32 (m, 3H, H-7', H-8, H-17), 1.28-1.19 (m, 3H, H-11', H-12', H-14), 1.17 (d, *J* = 6.1 Hz, 3H, H-21), 0.79 (s, 3H, H-18).
^{13}C-NMR:	(75 MHz, $CDCl_3$) δ [ppm]: 140.7 (C-10), 136.5 (C-5), 135.3 (C-4), 127.4 (C-3), 125.4 (C-2), 123.3 (C-1), 70.7 (C-20), 58.8 (C-17) , 55.3 (C-14), 44.7 (C-9), 42.8 (C-13), 40.3 (C-16), 37.9 (C-8), 28.0 (C-7), 27.3 (C-6), 27.1 (*c*Hex), 26.9 (C-15), 25.9 (C-12), 24.4 (C-11), 23.8 (C-21), 20.0 (C-19), 12.6 (C-18).
IR:	$\tilde{\upsilon}$ [cm^{-1}]: 3600-3200 (br), 2937.59 (s), 2916.37 (s), 2864.29 (s), 2818.00 (w), 1583.56 (w), 1471.69 (m), 2456.26 (m), 1419. 61 (w), 1398.39 (w), 1371.39 (m), 1338.60 (w), 1296.16 (w), 1276.88 (w), 1261.45 (w), 1251.80 (w), 1215.15 (w), 1178.51 (w), 1153.43 (w), 1112.93 (m), 1089.78 (s), 1076.28 (s), 1049.28 (w), 1028.06 (w), 1001.06 (m), 970.19 (s), 933.55 (w), 918.12 (w), 887.26 (m), 866.04 (m), 865.47 (m), 833.25 (w), 802.39 (m), 779.24 (s), 738.74 (s), 692.44 (w), 657.73 (w), 651.94 (w), 630.72 (w), 603.72 (w).
GC-EI LR MS:	t_R= 17.14 min, *m/z* 298.3 ($[M]^{+\bullet}$).
GC-EI HR MS:	t_R= 21.14 min, *m/z* 298.2286 ($[M]^{+\bullet}$).

7.2.8 Synthesis and characterization of compound **8**

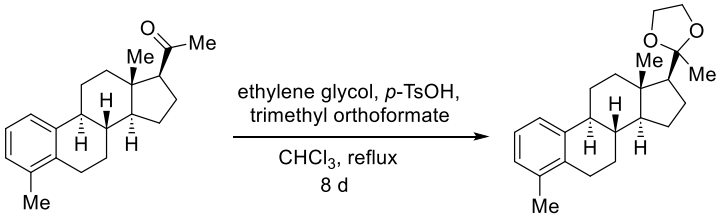

S42 (**1**) **8**, 99%

Steroid S42 (**1**) (1003 mg, 3.38 mmol, 1.0 eq.) was dissolved in dry $CHCl_3$ (10 mL) in a 2-necked round bottom flask attached to a condenser under an inert condition.[111] Subsequently, ethylene glycol (0.94 mL, 16.91 mmol, 5.0 eq.), triethyl orthoformate (0.37 mL, 3.38 mmol, 1.0 eq.), and *p*-toluene sulfonic acid monohydrate (32 mg, 0.17 mmol, 0.05 eq.) were added. The reaction mixture was refluxed for 8 days. Extra ethylene glycol (0.94 mL, 16.91 mmol, 5.0 eq.) and trimethyl orthoformate (0.37 mL, 3.38 mmol, 1.0 eq.) were added on day 4 and day 7 respectively.

After the reaction was cooled to r.t., the reaction mixture was quenched by sat. $K_2CO_{3\,(aq.)}$. The reaction mixture was extracted three times by DCM, dried over Na_2SO_4, filtered off, and concentrated under reduced pressure. The crude product was purified by column chromatography on silica (*c*Hex/EtOAc = 5/1) to give a white solid (1140 mg, 3.35 mmol, 99%).

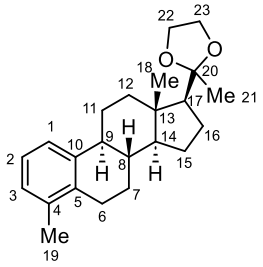

Appearance:	White solid
Chemical Formula:	$C_{23}H_{32}O_2$
Molecular Weight:	340.5070 g/mol.
Yield:	99% (1140 mg, 3.35 mmol).
R_f:	0.31 (*cHex*:EtOAc = 10:1).
m_p:	126-130°C.
^{1}H-NMR:	(500 MHz, $CDCl_3$) δ [ppm]: 7.19 (d, *J* = 7.7 Hz, 1H, H-1), 7.07 (t, *J* = 7.6 Hz,1H, H-2), 6.99 (d, *J* = 7.3 Hz ,1H, H-3), 4.03-3.86 (m, 4H, H-22, H-23), 2.79-2.74 (m, 1H, H-6), 2.67-2.60 (m, 1H, H-6'), 2.31-2.22 (m, 2H, H11, H-9), 2.21 (s, 3H, H-19), 2.20-2.15 (m, 1H, H-12), 2.02-1.96 (m, 1H, H-7), 1.91-1.88 (m, 1H, H-17), 1.81-1.73 (m, 3H, H-15, H-16, H-16'), 1.56-1.46 (m, 1H, H-11'), 1.45-1.33 (m, 3H, H-12', H-14, H-7'), 1.33 (s, 3H, H-21), 1.28-1.22 (m, 2H, H-15', H-8), 0.79 (s, 3H, H-18).
^{13}C-NMR:	(126 MHz, $CDCl_3$) δ [ppm]: 140.6 (C-10), 136.3 (C-4), 135.2 (C-5), 127.2 (C-3), 125.2 (C-2), 123.0 (C-1), 111.9 (C-20), 65.2 (C-23), 63.2 (C-22), 58.4 (C-17), 55.5 (C-8), 44.5 (C-9), 42.1 (C-13), 39.7 (C-12), 37.3 (C-14), 27.7 (C-7), 27.2 (C-6), 26.6 (C-11), 24.6 (C-21), 23.5 (H-15), 23.1 (H-16), 19.8 (C-19), 13.0 (C-18).
IR:	$\tilde{\upsilon}$ [cm^{-1}]: 2974.23 (s), 2931.80 (s), 2872.91 (s), 1583.56 (w), 1471.69 (m), 1454.33 (m), 1369.46 (m), 1290.38 (w), 1261.45 (w), 1246.02 (m), 1219.01 (m),1180.44 (w), 1161.15 (w), 1143.79 (m), 1085.92 (m), 1066.64 (s), 1049.28 (s), 948.89 (m), 912.33 (w), 833.40 (m), 862.18 (w), 883.40 (m), 862.18 (m), 840.96 (w), 827.46 (w), 804.32 (m), 777.31 (s), 694.37 (w).
GC-EI LR MS:	t_R= 17.61 min, *m/z* 325.2 ([M-Me$^•$]$^+$).

GC-EI HR MS: t_R= 22.85 min, *m/z* 325.2156 ([M-Me•]$^+$).

7.2.9 Synthesis and characterization of compound **9**

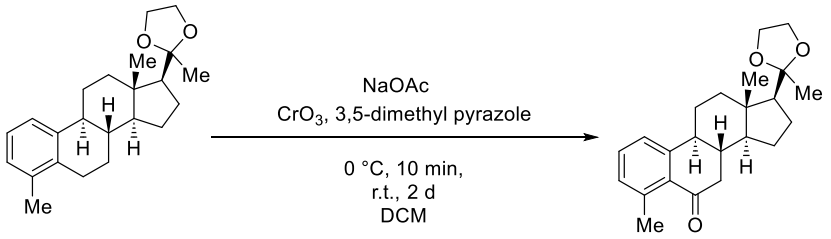

8 **9**, 24%

Adapting the synthesis procedure from *Li et al.*,[7] CrO_3 (2310 mg, 23.10 mmol, 10.0 eq.) was dissolved in dry DCM (10 mL) in a *Schlenk* tube under an inert condition. The system was cooled down to 0 ºC before adding 3,5- dimethyl pyrazole (2221 mg, 23.10 mmol, 10.0 eq.). The dark solution was stirred at r.t. for 15 min and cooled down to 0 ºC. Compound **8** (785 mg, 2.31 mmol, 1.0 eq.) was dissolved in $CHCl_3$ (14 mL) in another *Schlenk* tube and added to the reaction mixture. The mixture was stirred at 0 ºC for 10 min in an ice bath. NaOAc (1895 mg, 23.10 mmol, 10.0 eq.) was added and the solution was stirred at r.t. for 2 days, during which the reaction was not completed according to TLC or GC-EI LR MS analysis, but the unprotected starting material was observed.

The crude mixture was filtered over a fritted glass funnel filled with short-packed silica and the filtered mixture was concentrated and purified by column chromatography on silica (*c*Hex/EtOAc = 5/1) to give a white solid (197 mg, 0.56 mmol, 24%).

Appearance:	White solid.
Chemical Formula:	$C_{23}H_{30}O_3$
Molecular Weight:	354.4900 g/mol.
Yield:	24% (197 mg, 0.56 mmol).
R_f:	0.31 (*c*Hex:EtOAc = 5:1).
m_p:	128-130°C.

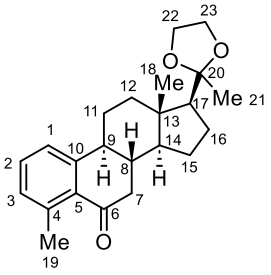

^{1}H-NMR:	(500 MHz, $CDCl_3$) δ [ppm]: 7. 36 (t, *J* = 7.7 Hz, 1H, H-2), 7.29 (d, *J* = 7.7 Hz,1H, H-1), 7.11 (d, *J* = 7.5 Hz, 1H, H-3), 4.04-3.86 (m, 4H, H-22, H-23), 2.73 (dd, *J* = 4.1 Hz, 17.2 Hz, 1H, H-7), 2.64 (s, 3H, H-19), 2.48-2.42 (m, 1H, H-8), 2.33-2.28 (m, 1H, H-11), 2.27-2.16 (m, 2H, H-7', H-16), 1.93-1.84 (m, 2H, H-17, H-9), 1.84-1.77 (m, 2H, H-12, H-12'), 1.75-1.62 (m, 2H, H-15, H-11'), 1.49-1.43 (m, 1H, H-16'), 1.37-1.31 (m, 4H, H-21, H-14), 1.25-1.17 (m, 1H, H-15'), 0.84 (s, 3H, H-18).
^{13}C-NMR:	(126 MHz, $CDCl_3$) δ [ppm]: 200.1 (C-6), 148.3 (C-10), 141.2 (C-4), 132.2 (C-2), 131.3 (C-5), 130.4 (C-3), 122.9 (C-1), 111.7 (C-20), 65.1 (C-23), 63.2 (C-22), 58.0 (C-17), 55.5 (C-14), 46.1 (C-7), 43.4 (C-8), 41.9 (C-13), 39.1 (H-16), 38.4 (C-9), 26.0 (C-11), 24.5 (C-21), 23.4 (C-19), 23.2 (C-15), 23.0 (C-12), 12.8 (C-18).
IR:	$\tilde{\upsilon}$ [cm^{-1}]: 2931.80 (m), 2872.01 (m), 1670.35 (s), 1589.34 (w), 1539.20 (w), 1506.41 (w), 1465.90 (w), 1417.68 (w), 1369.46 (m), 1338.60 (w), 1292.31 (w), 1263.37 (m), 1240.23 (m), 1215.15 (m), 1178.51 (w), 1153.43 (w), 1109.07 (w), 1089.78 (w), 1080.14 (w), 1058.92 (s), 1039.63 (s), 966.34 (w), 947.05 (m), 933.55 (w), 894.97 (w), 887.26 (w), 860.25 (m), 831.32 (m), 804.32 (m), 794.67 (w), 775.38 (m), 750.31 (m), 732.95 (w), 723.31 (w), 704.02 (w), 680.87 (w), 665.44 (w), 657.73 (w), 644.22 (w).
GC-EI LR MS:	t_R = 18.72 min, *m/z* 339.2 ([M-Me•]$^+$).
GC-EI HR MS:	t_R = 24.10 min, *m/z* 339.1952 ([M-Me•]$^+$).

7.2.10 Synthesis and characterization of compounds **10** and **10'**

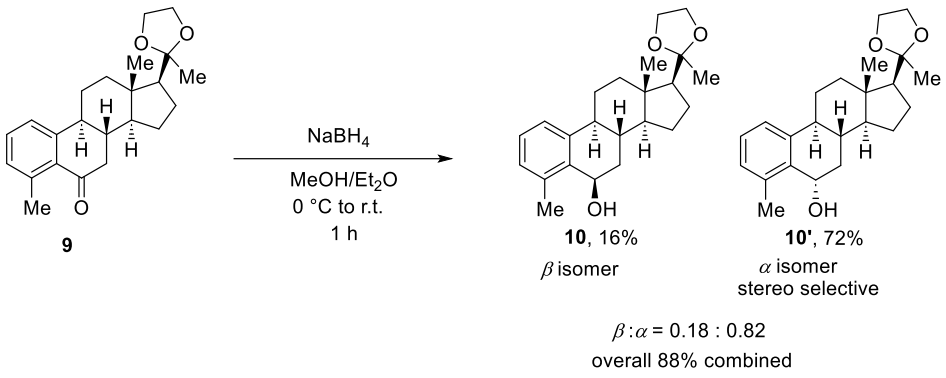

In a dried *Schlenk* tube, compound **9** (88 mg, 0.25 mmol, 1.0 eq.) was added and dissolved in dry MeOH (1.7 mL) and dry Et_2O (0.6 mL) under an inert condition.[111] The mixture was cooled down to 0 ºC in an ice bath. A white suspension was formed and $NaBH_4$ (118 mg, 3.08 mmol, 6.0 eq., 98%) was added slowly in small portions. The mixture was then stirred at r.t. for 1 h. The mixture was concentrated under reduced pressure, quenched by adding H_2O, extracted by DCM three times, dried over Na_2SO_4, filtered off, and concentrated under reduced pressure. The crude was purified

by column chromatography on silica (*c*Hex/EtOAc = 6/1) and this gave separate isomer products (14 mg, 0.04 mmol, 16%; 64 mg, 0.18 mmol, 72%).

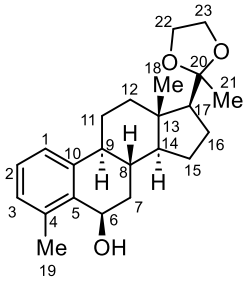

Appearance: White solid.

Chemical Formula: $C_{23}H_{32}O_3$

Molecular Weight: 356.5060 g/mol.

Yield: 16% (14 mg, 0.04 mmol).

R_f: 0.2 (*c*Hex:EtOAc = 5 :1).

^{1}H-NMR: (500 MHz, $CDCl_3$) δ [ppm]: 7.22 (d, *J* = 7.8 Hz, 1H, H-1), 7.17 (t, *J* = 7.6Hz, 1H, H-2), 7.07 (d, *J* = 7.3 Hz, 1H, H-3), 4.93 (s, 1H, H-6), 4.04-3.86 (m, 4H, H-22, H-23), 2.47 (s, 3H, H-19), 2.34-2.28 (m, 1H, H-15), 2.23-2.19 (m, 1H, H-11), 2.17-2.13 (m, 1H, H-9), 2.11-2.08 (m, 1H, H-7), 1.92-1,88 (m, 1H, H-17), 1.82-1.73 (m, 4H, H-8, H-12, H-12', H-16), 1.57-1.49 (m, 2H, H-7', H-15'), 1.45-1.39 (m, 1H, H-11'), 1.33 (s, 3H, H-21), 1.31-1.25 (m, 2H, H-14, H-16'), 0.84 (s, 3H, H-18).

^{13}C-NMR: (126 MHz, $CDCl_3$) δ [ppm]: 140.7 (C-10), 138.3 (C-4), 135.6 (C-5), 128.5 (C-3), 127.8 (C-2), 123.2 (C-1), 111.9 (C-20), 65.2 (C-23), 64.9 (C-6) ,63.2 (C-22), 58.3 (C-17), 55.0 (C-14), 45.0 (C-9), 42.3 (C-13), 39.7 (C-11), 37.1 (C-7), 31.7 (C-8), 26.2 (C-15), 24.6 (C-21), 23.3 (C-16), 23.1 (C-12), 19.0 (C-19), 13.1 (C-18).

IR: $\tilde{\upsilon}$ [cm^{-1}]: 3600-3400 (bp), 2966.52 (m), 2939.52 (s), 2881.65 (s), 1581.63 (w), 1473.62 (m), 1433.11 (m), 1371.39 (s), 1259.52 (m), 1244.09 (m), 1217.08 (s), 1193.94 (s), 1163.93 (m), 1151.50 (m), 1134.14 (m), 1089.78 (m), 1064.71(m), 1047.35 (s), 1039.63 (s), 1016.49 (s), 974.05 (m), 948.89 (s), 900.76 (s), 883.40 (m), 852.54 (m), 829.39 (m), 783.10 (s), 740.67 (s), 732.95 (s), 686.66 (w), 626.87 (w).

GC-EI-LRMS: t_R= 17.41 min, *m/z* 338.2 ($[M-H_2O]^{\bullet+}$).

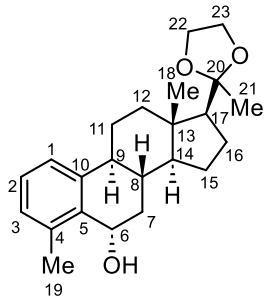

Appearance: White solid.

Chemical Formula: $C_{23}H_{32}O_3$

Molecular Weight: 356.5060 g/mol.

Yield: 72% (64 mg, 0.18 mmol).

R_f: 0.14 (*c*Hex:EtOAc =5 :1).

^{1}H-NMR: (500 MHz, $CDCl_3$) δ [ppm]: 7.17-7.13 (m, 2H, H-1, H-2), 7.07-7.05 (m, 1H, H-3), 5.13-5.06 (m, 1H, H-6), 4.03-3.86 (m, 4H, H-22, H-23), 2.48-2.41 (m, 4H, H-12, H-19), 2.41-2.36 (m, 1H, H-9), 2.26-2.17 (m, 2H, H-7, H-11), 1.91-1.87 (m, 1H, H-17), 1.87-1.73 (m, 3H, H-15, H-15', H-16), 1.54-1.38 (m, 5H, H-7', H-8, H-11', H-

12', OH), 1.32 (s, 3H, H-21), 1.31-1.27 (m, 1H, H-14), 1.27-1.17 (m, 1H, H-16'), 0.76 (s, 3H, H-18).

^{13}C-NMR: (126 MHz, $CDCl_3$) δ [ppm]: 142.3 (C-10), 138.0 (C-4), 136.8 (C-5), 128. 8 (C-3), 127.4 (C-2), 122.7 (C-1), 111.90 (C-20), 67.5 (C-6), 65.1 (C-23), 63.2 (C-22), 58.2 (C-17), 55.4 (C-14), 43.6 (C-9), 41.9 (C-13), 39.5 (C-12), 39.3 (C-7), 37.7 (C-8), 26.5 (C-11), 24.6 (C-21), 23.5 (C-16), 23.0 (C-15), 20.3 (C-19), 12.8 (C-18).

GC-EI-LRMS: t_R= 17.66 min, *m/z* 338.3 ($[M-H_2O]^{\bullet+}$).

7.2.11 Synthesis and characterization of compound **3**

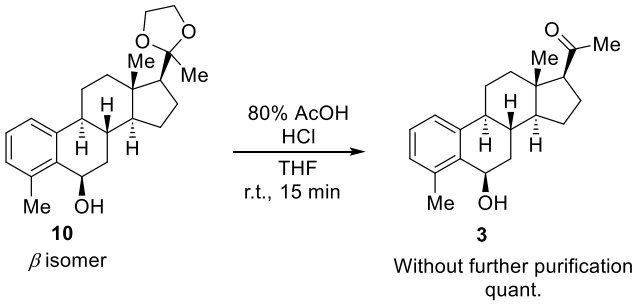

Compound **10** (11 mg, 0.03 mmol, 1.0 eq.) was dissolved in THF (0.5 mL) and $AcOH_{(aq.)}$ (80%, 0.5 mL) with one drop of HCl and stirred at r.t. for 15 min. The reaction was quenched by an addition of sat. $NaHCO_3$ (aq.). The crude was concentrated under reduced pressure and added H_2O (0.5 mL) for extraction with DCM three times. The organic phase was dried over Na_2SO_4, filtered off, and concentrated under reduced pressure to give a white solid (10 mg, 0.03 mmol, quant.).

Appearance: White solid.

Chemical Formula: $C_{21}H_{28}O_2$

Molecular Weight: 312.4530 g/mol.

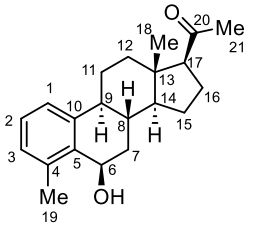

Yield: quant. (10 mg, 0.03 mmol).

R_f: 0.14 (*c*Hex:EtOAc = 5:1).

m_p 139-141°C.
(Start to decompose and turn red solid)

^{1}H-NMR:	(500 MHz, $CDCl_3$) δ [ppm]: 7.23-7.17 (m, 2H, H-1, H-2), 7.08 (d, *J* = 7.2 Hz, 1H, H-3), 4.95-4.94 (m, 1H, H-6), 2.62 (t, *J* = 9.2 Hz, 1H, H-17), 2.47 (s, 3H, H-19), 2.43-2.39 (m, 1H, H-11), 2.28-2.17 (m, 3H, H-8, H-12, H-16), 2.16 (s, 3H, H-21), 2.10 (m, 1H, H-7), 1.85-1.76 (m, 2H, H-9, H-15), 1.75-1.71 (m, 1H, H-16'), 1.69-1.61 (m, 3H, OH, H-12' and H_2O), 1.59-1.51 (m, 2H, H-7', H-11'), 1.46-1.34 (m, 2H, H-14, H-15'), 0.70 (s, 3H, H-18).
^{13}C-NMR:	(126 MHz, $CDCl_3$) δ [ppm]: 209.4 (C-20), 140.1 (C-10), 138.3 (C-4), 135.5 (C-5), 128.7 (C-3), 127.9 (C-2), 123.2 (C-1), 64.7 (C-6), 63.8 (C-17), 55.3 (C-14), 44.9 (C-8), 44.4 (C-13), 39.0 (C-12), 37.0 (C-7), 32.2 (C-9), 31.5 (C-21), 26.3 (C-11), 23.9 (C-15), 22.9 (C-16), 19.0 (C-19), 13.4 (C-18).
IR:	$\tilde{\upsilon}$ [cm^{-1}]: 3608.81-3170.97 (br), 3061.03 (w), 2926.01 (s), 2875.86 (m), 2848.86 (m), 1732.08 (m), 1699.29 (s), 1585.49 (w), 1558.48 (w), 1506.41 (w), 1471.69 (m), 1435.04 (w), 1417.68 (w), 1384.89 (m), 1355.96 (m), 1261.45 (m), 1228.66 (m), 1195.87 (m), 1174.65 (m), 1151.5 (w), 1136.07 (w), 1126.43 (w), 1089.78 (m), 1037.7 (m), 1016.49 (m), 950.91 (w), 933.55 (w), 918.12 (w), 881.47 (w), 862.18 (w), 800.46 (m), 783.1 (s), 738.74 (s), 702.09 (w), 646.15 (w).
GC-EI-LRMS:	t_R= 17.148 min, *m/z* 297.2 ([M-Me•]$^+$).
GC-EI-HRMS:	t_R= 22.18 min, *m/z* 297.1847 ([M-Me•]$^+$).

Formation of byproducts:

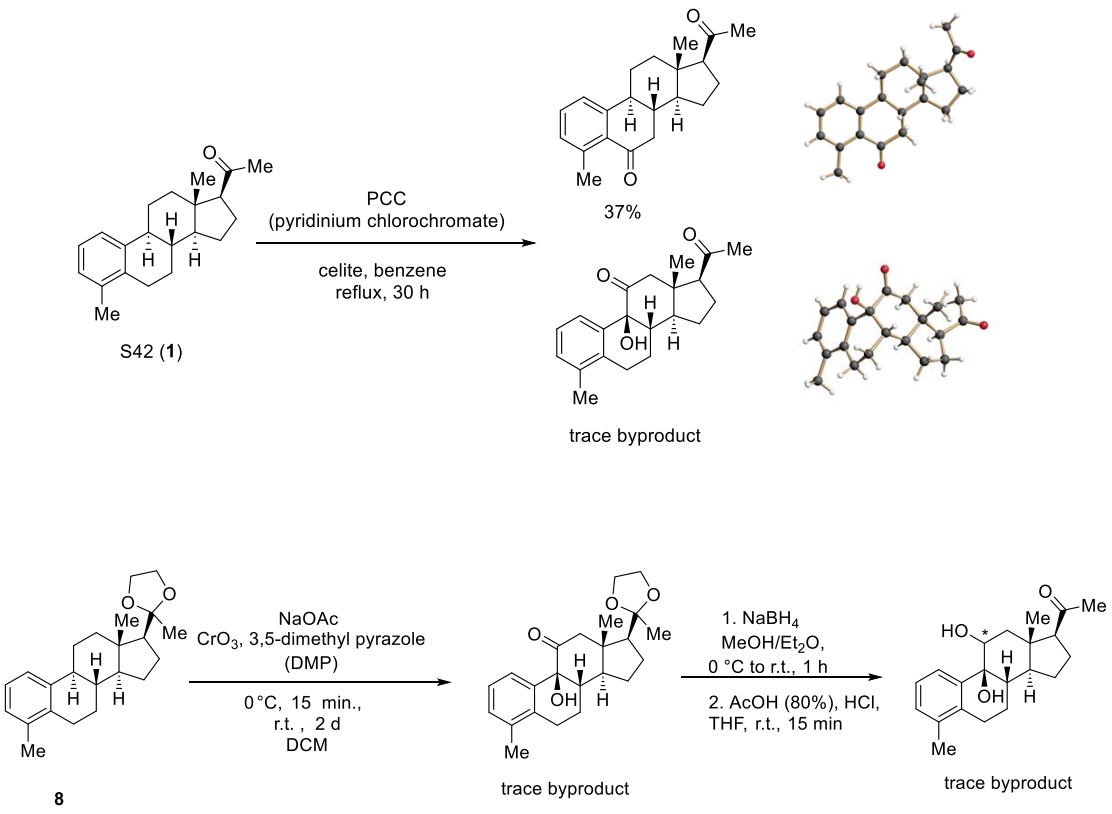

From the oxidation reaction with PCC/celite, a byproduct was found, and the structure was discovered by XRD analysis. We proposed that the trace protected byproduct could be produced during the synthesis of compound **3.** After reduction and deprotection reaction, a small amount of the byproduct S42-C9, C11-bis-OH may be generated and was mixed with compound **3**. The ion peak $[M\text{-}H_2O]^{+\bullet}$ was discovered by the GC-MS analysis.

7.2.12 Synthesis and characterization of compound **11**

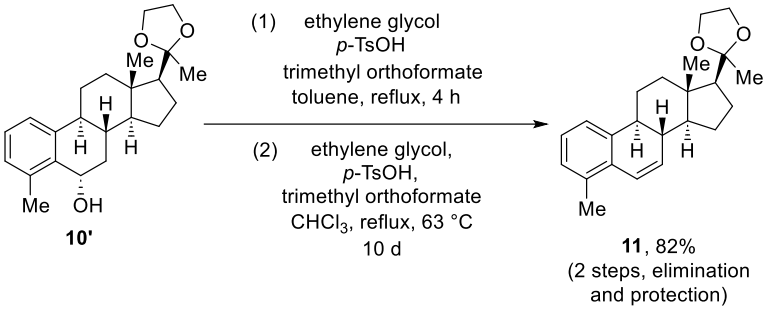

In a dried 3-necked flask equipped with a condenser, compound **10'** (62 mg, 0.17 mmol, 1.0 eq.) was added and dissolved in dry toluene (3 mL) under inert conditions.[111] Ethylene glycol (10 µL, 0.18 mmol, 1.1 eq.), trimethyl orthoformate (38 µL, 0.35 mmol, 2.1 eq.), and *p*-toluene sulfonic acid monohydrate (5 mg, 0.03 mmol, 0.2 eq.) were added subsequently. The mixture was heated to reflux for 4 h. After the mixture was cooled down to r.t., $Na_2CO_{3\,(aq.)}$ was added to quench the reaction. The aqueous phase was separated and extracted with DCM three times. The combined organic phases were washed with brine, dried over Na_2SO_4, filtered off, and concentrated under reduced pressure. The crude product was purified by column chromatography on silica (*c*Hex/EtOAc = 8/1), which gave both protected and deprotected products.

To protect the carbonyl group at C20 again, the mixture of protected and deprotected products was added to a dried 3-necked flask charged with a condenser and dissolved in $CHCl_3$ (2 mL). *P*-toluene sulfonic acid monohydrate (10 mg, 0.01 mmol, 0.06 eq.), ethylene glycol (77 µL, 1.39 mmol, 8.2 eq.) and trimethyl orthoformate (61 µL, 0.55 mmol, 3.0 eq.) were added to the flask. The mixture was stirred at 63 ºC for 10 days. The reaction was monitored by thin-layer column chromatography. Extra ethylene glycol (77 µL, 1.39 mmol, 8.2 eq.) and trimethyl orthoformate (61 µL, 0.55

mmol, 3.2 eq.) were added on day 8. The reaction was quenched by sat. $K_2CO_{3\,(aq.)}$. The mixture was extracted by DCM three times, dried over Na_2SO_4, filtered off, and concentrated under reduced pressure. The crude was purified by column chromatography on silica (*c*Hex/EtOAc = 10/1), which gives only protected products (48 mg, 0.14 mmol, 82%).

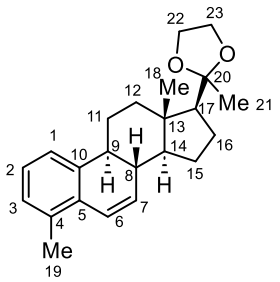

Appearance:	White solid.
Chemical Formula:	$C_{23}H_{30}O_2$
Molecular Weight:	338.4910 g/mol.
Yield:	82% (48 mg, 0.14 mmol).
R_f:	0.46 (*c*Hex:EtOAc = 5:1).
m_p:	116-119°C.
^{1}H-NMR:	(500 MHz, $CDCl_3$) δ [ppm]: 7.12-7.07 (m, 2H, H-1, H-2), 7.01 (d, *J* = 6.6 Hz ,1H, H-3), 6.68 (dd, 1H, *J* = 2.7 Hz, 9.8 Hz, H-6), 6.05 (dd, *J* = 1.8 Hz, 9.8 Hz ,1H, H-7), 4.03-3.86 (m, 4H, H-22, H-23), 2.36-2.31 (m, 4H, H-19, H-9), 2.22-2.19 (m, 1H, H-15), 2.15-2.05 (m, 2H, H-11, H-8), 1.94-1.88 (m, 2H, H-12, H-17), 1.86-1.72 (m, 3H, H-16, H-16', H-11'), 1.48-1.42 (m, 1H, H-14), 1.39-1.36 (m, 1H, H-15'), 1.33 (s, 3H, H-21), 1.31-1.22 (m, 1H, H-12'), 0.79 (s, 3H, H-18).
^{13}C-NMR:	(126 MHz, $CDCl_3$) δ [ppm]: 139.5 (C-10), 133.1 (C-7), 132.8 (C-4), 132.4 (C-5), 128.0 (C-3), 126.6 (C-1), 124.3 (C-6), 121.1 (C-2), 111.8 (C-20), 65.1 (C-23), 63.2 (C-22), 58.1 (C-17), 53.6 (C-14), 42.7 (C-13), 42.6 (C-9), 39.0 (C-15), 37.2 (C-8), 24.6 (C-11), 24.4 (C-21), 23.4 (C-12), 23.0 (C-16), 19.2 (C-19), 12.7 (C-18).
IR:	$\tilde{\upsilon}$ [cm^{-1}]: 2924.09 (m), 2897.08 (m), 2875.86 (m), 2854.65 (m), 2794.85 (m), 1465.90 (m), 1446.61 (m), 1417.68 (w), 1386.82 (w), 1369.46 (m), 1294.24 (w), 1259.52 (w), 1247.94 (m), 1219.01 (m), 1197.79 (w), 1186.22 (w), 1163.08 (m), 1147.65 (m), 1128.36 (w), 1105.21 (w), 1082.07 (m), 1064.71 (s), 1056.99 (s), 1037.70 (s), 1022.27 (m), 997.20 (w), 968.27 (w), 952.84 (m), 925.83 (w), 898.83 (w), 862.18 (s), 840.96 (w), 829.39 (w), 812.03 (w), 798.53 (w), 779.24 (s), 759.95 (s), 725.23 (w), 704.02 (m), 677.01 (m), 650.01 (w), 632.65 (w), 603.72 (w).
GC-EI-LRMS:	t_R= 17.65 min, *m/z* 338.2 ($[M]^{\bullet+}$).
GC-EI-HRMS:	t_R= 22.91 min, *m/z* 338.2238 ($[M]^{\bullet+}$), 323.2002 ($[M\text{-}Me^{\bullet}]^{+}$).

7.2.13 Synthesis and characterization of compound **12**

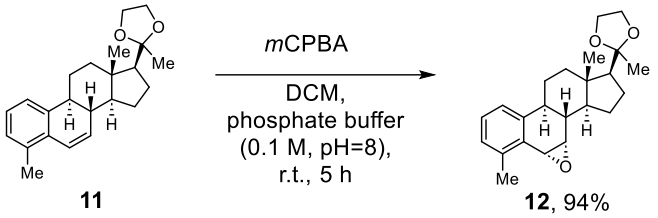

11 **12**, 94%

In a round-bottom flask, compound **11** (20 mg, 0.06 mmol, 1.0 eq.) was added and dissolved in DCM (1.5 mL) and phosphate buffer (1.2 mL, 0.1 M, pH=8).[111] After the reaction was cooled down to 0 ºC, *m*CPBA (13 mg, 0.06 mmol, 1.0 eq., 77%) was added. The heterogenous solution was stirred vigorously at r.t. for 5 h. The organic layer was separated and quenched by sat. $Na_2S_2O_{3(aq.)}$. After the mixture was stirred at r.t. for 15 min, the organic phase was separated, washed with brine, dried over $MgSO_4$, filtered off and concentrated under reduced pressure. The crude was purified by column chromatography on silica (*c*Hex/EtOAc = 10/1) to give a white solid (20 mg, 0.056 mmol, 94%).

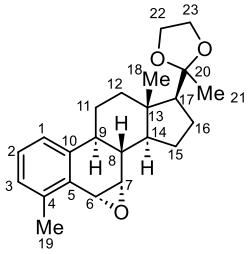

Appearance:	White solid.
Chemical Formula:	$C_{23}H_{30}O_3$
Molecular Weight:	354.4900 g/mol.
Yield:	94% (20 mg, 0.056 mmol).
R_f:	0.31 (*c*Hex:EtOAc = 5:1).
^{1}H-NMR:	(500 MHz, $CDCl_3$) δ [ppm]: 7.17 (t, *J* = 7.6 Hz, 1H, H-2), 7.10 (d, *J* = 7.7 Hz, 1H, H-1), 7.04 (d, *J* = 7.5 Hz, 1H, H-3), 4.18 (d, *J* = 4.5 Hz, 1H, H-6), 4.04-3.86 (m, 4H, H-22, H-23), 3.55 (d, 1H, *J* = 4.5 Hz, H-7), 2.50 (s, 3H, H-19), 2.49-2.43 (m, 1H, H-8), 2.23-2.17 (m, 2H, H-11, H-12), 2.07-1.98 (m, 1H, H-15), 1.98-1.93 (m, 1H, H-17), 1.92-1.80 (m, 2H, H-16, H-16'), 1.68-1.53 (m, 3H, H-11', H-9, H-14), 1.44-1.35 (m, 2H, H-12', H-15'), 1.34 (s, 3H, H-21), 0.81 (s, 3H, H-18).
^{13}C-NMR:	(126 MHz, $CDCl_3$) δ [ppm]: 140.6 (C-10), 137.5 (C-4), 130.2 (C-5), 128.4 (C-3), 127.9 (C-2),122.1 (C-1), 111.9 (C-20), 65.3 (C-23), 63.3 (C-22), 58.0 (C-17), 56.5 (C-7), 52.5 (C-14), 49.9 (C-6), 42.9 (C-13), 39.0 (C-12), 36.5, (C-8), 36.4 (C-9), 24.7 (C-21), 24.6 (C-11), 23.9 (C-15), 23.3 (C-16), 19.3 (C-19), 12.7 (C-18).
IR:	$\tilde{\upsilon}$ [cm^{-1}]: 2976.16 (s), 2941.44 (s), 2877.79 (s), 2362.80 (w), 2312.65 (w), 1591.27 (m), 1558.48 (w), 1539.20 (w), 1475.54 (m), 1448.54 (w), 1417.68 (w), 1369.46 (m), 1338.60 (w), 1296.16 (w), 1261.45 (m), 1242.16 (w), 1222.87 (m), 1184.29 (m), 1165.00 (m), 1145.72 (m), 1122.57 (m), 1083.99 (m), 1066.64 (s), 1047.35 (s),

975.98 (w), 948.98 (m), 923.90 (w), 893.04 (s), 875.68 (m), 860.25 (m), 833.25 (w), 815.89 (s), 781.17 (m), 761.88 (s), 734.88 (m), 704.02 (w), 615.29 (s).

7.2.14 Synthesis and characterization of compound **4**

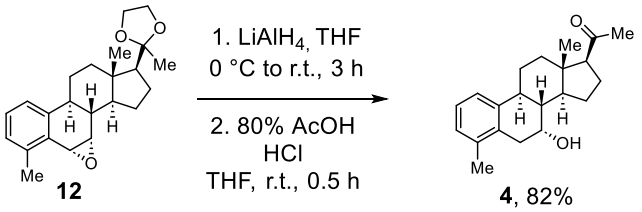

In a dried *Schlenk* tube, compound **12** (39 mg, 0.11 mmol, 1.0 eq.) was dissolved in dry THF (0.4 mL) under an inert condition.[111] The mixture was cooled down to 0 ºC in an ice bath and $LiAlH_4$ (9 mg, 0.24 mmol, 2.2 eq.) was added. The mixture was then stirred at r.t. for 3 h. The reaction was quenched by the addition of sat. potassium sodium tartrate tetrahydrate$_{(aq.)}$ slowly until no bubbles formed. To the crude product was added EtOAc (2 mL) and HCl (4 mL, 5%) together, and stirred at r.t. for 0.5 h and neutralized by 0.5 M $NaOH_{(aq.)}$. The mixture was extracted with EtOAc four times, dried over Na_2SO_4, filtered off, and concentrated under reduced pressure.

To deprotect the cyclic acetal functional group, the crude was dissolved in THF (10 mL), AcOH (10 mL, 80%) and one drop of conc. HCl. After stirring at r.t. for 0.5 h, the mixture was concentrated, diluted in H_2O, extracted by DCM four times, dried over Na_2SO_4, filtered off and concentrated under reduced pressure. The crude was purified by column chromatography on silica (*c*Hex/EtOAc = 5/1) and this afforded a white solid (28 mg, 0.09 mmol, 82%).

Appearance:	White solid.
Chemical Formula:	$C_{21}H_{28}O_2$
Molecular Weight:	312.4530 g/mol.
Yield:	82% (28 mg, 0.09 mmol).
R_f:	0.23 (*c*Hex:EtOAc = 5:1).
m_p:	163-168°C. (Start to decompose).

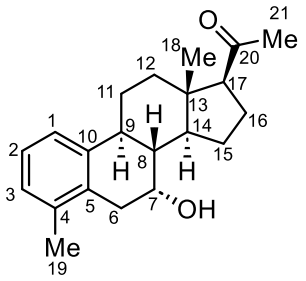

^{1}H-NMR:	(500 MHz, $CDCl_3$) δ [ppm]: 7.22 (d, *J* = 7.9 Hz, 1H, H-1), 7.11 (t, *J* = 7.6 Hz, 1H, H-2), 7.03 (d, *J* = 7.3 Hz, 1H, H-3), 4.21 (m, 1H, H-7), 2.93-2.81(m, 2H, H-6, H-6'), 2.76 (m, 1H, H-9), 2.65 (t, *J* = 9.2 Hz, 1H, H-17), 2.51-2.47 (m, 1H, H-11), 2.28-2.22 (m, 1H, H-16), 2.22 (s, 3H, H-19), 2.18-2.13 (m, 4H, H-21, H-12), 1.92-1.85 (m, 1H, H-15), 1.78-1.64 (m, 3H, H-12', H-14, H-16'), 1.62-1.53 (m, 2H, H-11', OH), 1.49 (t, 11 Hz, 1H, H-8), 1.37-1.28 (m, 1H, H-15'), 0.63 (s, 3H, H-18).
^{13}C-NMR:	(126 MHz, $CDCl_3$) δ [ppm]: 209.5 (C-20), 139.0 (C-10), 137.1 (C-4), 131.6 (C-5), 127.7 (C-3), 125.9 (C-2), 123.2 (C-1), 66.1 (C-7), 63.8 (C-17), 51.2 (C-14), 44.3 (C-13), 41.5 (C-8), 38.9 (C-12), 36.4 (C-6), 35.6 (C-9), 31.5 (C-21), 26.7 (C-11), 23.6 (C-15), 22.9 (C-16), 19.9 (C-19), 13.2 (C-18).
IR:	$\tilde{\upsilon}$ [cm^{-1}]: 3523.95-3365.78 (br) 2964.59 (w), 2947.23 (w), 2916.37 (m), 2877.79 (m), 2864.29 (w), 1683.86 (s), 1558.48 (w), 1539.20 (w), 1506.41 (w), 1471.69 (m), 1448.54 (m), 1406.11 (m), 1381.03 (m), 1357.89 (m), 1340.53 (m), 1290.38 (w), 1257.59 (w), 1211.30 (s), 1180.44 (s), 1165.00 (w), 1151.50 (w), 1111.00 (w), 1093.64 (m), 1066.64 (m), 1053.13 (w), 1039.63 (w), 1024.20 (m), 979.84 (w), 962.48 (w), 947.05 (w), 933.55 (w), 920.05 (w), 881.47 (m), 869.90 (w), 837.11 (w), 783.10 (s), 767.67 (m), 727.16 (s), 696.30 (m), 659.66 (w), 644.22 (w), 632.65 (w), 624.94 (w)
GC-EI-LRMS:	t_R= 17.46 min, *m/z* 294.2 ($[M-H_2O]^{\bullet+}$).
GC-EI-HRMS:	t_R= 22.59 min, *m/z* 294.1976 ($[M-H_2O]^{\bullet+}$).

7.2.15 General TMS and TBDMS derivatization methods

For TMS derivatization in a small scale, a mixture of reagent was prepared. A stock solution was prepared by mixing MSTFA (*N*-methyl-*N*-(trimethylsilyl) trifluoracetamide), ethanethiol and ammonium iodide in the ratio of 100 (µL)/ 3 (µL)/ 2 (mg).[143] The mixture was heated at 60 °C until ammonium iodide was dissolved. The stock solution was diluted by a factor of 10 in MSTFA as a derivatization working agent.

A dried compound (compound **1**, **1-d4**, **1-d7**, **2**, **2', 3**, **4, 13** respectively, 1 mg) was heated with the derivatization agent (1 mL) at 60 °C for 30 min in a dried tube. The sample was diluted by a factor of 20 in DCM and transferred to a GC vial for GC-EI HR MS analysis at the University of Cologne. For synthesis of TBDMS derivatives, MSTFA was replaced by TBDMSTFA.

7.2.16 Synthesis and characterization S42-C20-TMS (**1-C20-TMS**)

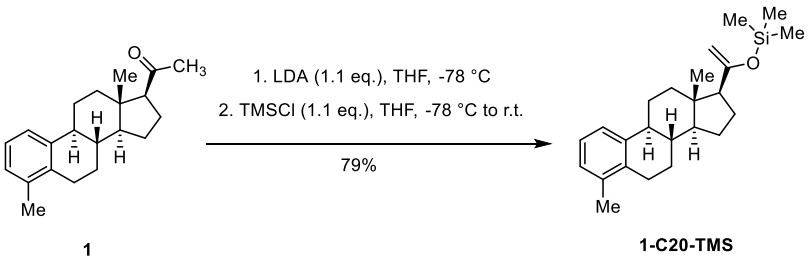

This experiment was conducted by *Dr. Tobias Wilczek*. A flame-dried *Schlenk*-tube was charged with THF (0.06 ml) and diisopropylamine (0.04 ml, 0.28 mmol, 2.0 eq.). The solution was cooled to -78 °C, *n*-butyllithium (0.15 mmol, 1.2 eq.) was added and the reaction mixture was stirred for 15 min. Then, the steroid S42 (**1**) (39 mg, 0.13 mmol, 1.0 eq.) was added and the reaction mixture was stirred for further 15 min at -78 °C before *trimethylsilyl chloride* (TMSCl) (20.0 µL, 0.15 mmol, 1.2 eq.) was added. The reaction mixture was stirred at -78 °C for further 15 min and then it was warmed to r.t. After full conversion of the starting material via GC-MS analysis, the solvent was evaporated under reduced pressure. The remaining solids were extracted with pentane, the suspension was filtered and the filtrate was evaporated under reduced pressure. The product 1-C20-TMS was obtained as a white solid in a yield of 79 % (39 mg, 0.11 mmol).

Appearance:	White solid.
Chemical Formula:	$C_{24}H_{36}OSi$
Molecular Weight:	368.6360
Yield:	79 % (39 mg, 0.11 mmol).
m_p:	94.0-95.0 °C.

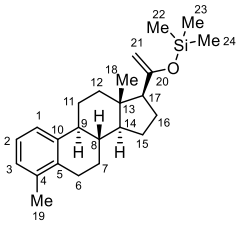

^{1}H-NMR: (500 MHz, CDCl3)) *δ* [ppm]: 7.20 (d, *J* = 7.8 Hz, 1H, H-1), 7.07 (t, *J* = 7.6 Hz, 1H, H-2), 7.00 (d, *J* = 7.3 Hz, 1H, H-3), 4.08 (d, *J* = 17.7 Hz, 2H, H- 21), 2.79 – 2.75 (m, 1H, H-6), 2.67 – 2.60 (m, 1H, H-6'), 2.34 – 2.24 (m, 2H, H- 9, H-11), 2.21 (s, 3H, H-19), 2.13 – 2.07 (m, 2H, H-12, H-17), 2.00 – 1.96 (m, 1H, H-7), 1.81 – 1.73 (m, 3H, H-15, H-15', H-16), 1.50 – 1.48 (m, 1H, H-11'), 1.40 – 1.24 (m, 5H, H-7', H-8, H-12', H-14, H-16'), 0.64 (s, 3H, H- 18), 0.22 (s, 9H, H-22, H-23, H-24).

^{13}C-NMR: (126 MHz, $CDCl_3$) *δ* [ppm]: 160.1 (C-20), 140.7 (C-10), 136.3 (C-4), 135.2 (C-5), 127.2 (C-3), 125.2 (C-2), 123.1 (C-1), 89.6 (C-21), 56.4 (C-17); 55.0 (C-14), 44.7 (C-9), 43.3 (C-13), 38.8 (C-12), 38.1 (C-8), 27.8 (C-7), 27.2

(C-6), 26.9 (C-11), 24.6 (C-15), 24.0 (C-16), 19.8 (C-19), 12.8 (C-18), 0.18 (C-22, C-23, C-24).

IR: $\tilde{\upsilon}$ [cm^{-1}]: 2936 (m), 2869 (w), 2824 (w), 1681 (w), 1645 (w), 1601 (w), 1471 (w), 1453 (w), 1443 (w), 1419 (w), 1380 (w), 1361 (w), 1321 (w), 1296 (m), 1251 (s), 1237 (m), 1176 (w), 1125 (w), 1090 (w), 1072 (w), 1044 (m), 1017 (m), 1009 (m), 961 (w), 950 (w), 872 (m), 841 (s), 804 (s), 778 (m), 756 (m), 742 (s), 707 (w), 696 (w), 646 (w), 607 (w), 570 (w), 552 (w), 517 (w).

GC-EI-HRMS t_R = 23.70 min, *m/z* 368.2526 $[M]^{\bullet+}$, 353.2291 $[M\text{-}Me^{\bullet}]^{+}$. (Temp: 100(5)-10-320(5))

7.3 Hydrindane derivative **13** synthesis

7.3.1 Synthesis and characterization of compound **27**

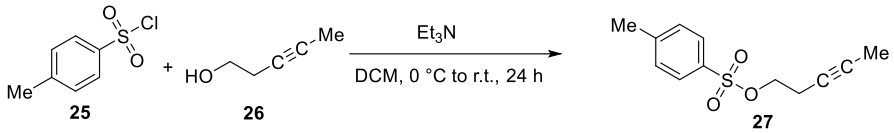

By adapting the synthesis procedure from Lansbury *et. al*.[144], 3-pentyn-1-ol (**26**) (59 mmol, 5.4 mL, 1.0 eq.) and TosCl (**25**) (11.3 g, 59.4 mmol, 1.0 eq.) were dissolved in dry DCM (89 mL) in a dried *Schlenk* flask. Et_3N (95.1 mmol, 13.3 mL, 1.6 eq.) was added at 0 °C. The mixture was stirred at ambient temperature for 24 h and quenched by an addition of water. The mixture was extracted with DCM three times, washed with brine, dried over Na_2SO_4, filtered, and concentrated under reduced pressure. The crude product was purified by column chromatography (*c*Hex/EtOAc = 9:1) which afforded a slightly yellow oil (12.5 g, 52.5 mmol, 88%).

Appearance:	Slightly yellow oil.
Chemical Formula:	$C_{12}H_{14}O_3S$
Molecular Weight:	238.3010
Yield:	88% (12.5 g, 52.5 mmol).
R_f:	0.27 (*c*Hex:EtOAc = 5:1)
^{1}H-NMR:	(300 MHz, $CDCl_3$) δ [ppm]: 7.82 (m, 2H, H-7), 7.37 (d, *J* = 4.5 Hz, 2H, H-8), 4.07 (t, *J* = 7.2 Hz, 2H, H-1), 2.53-2.47 (m, 2H, H-2), 2.47 (s, 3H, H-10), 1.73 (t, *J* = 2.6 Hz, 3H, H-5).
^{13}C-NMR:	(75 MHz, $CDCl_3$) δ [ppm]: 144.8 (C-6), 132.9 (C-9), 129.8 (C-8), 127.9 (C-7), 78.2 (C-3), 73.1 (C-4), 68.2 (C-1), 21.6 (C-10), 19.6 (C- 2), 3.4 (C-5).
IR:	$\tilde{\upsilon}$ [cm^{-1}]: 2970 (w), 2914 (w), 1597 (m), 1458 (w), 1356 (s), 1308 (w), 1292 (w), 1188 (s), 1175 (s), 1096 (s), 1020 (w), 970 (s), 899 (s), 845 (s), 814 (s), 762 (s), 704 (w), 662 (s).
GC-EI-LRMS	t_R = 13.86 min, *m/z* 196.0 $[M]^{\bullet+}$.

7.3.2 Synthesis and characterization of compound **28**

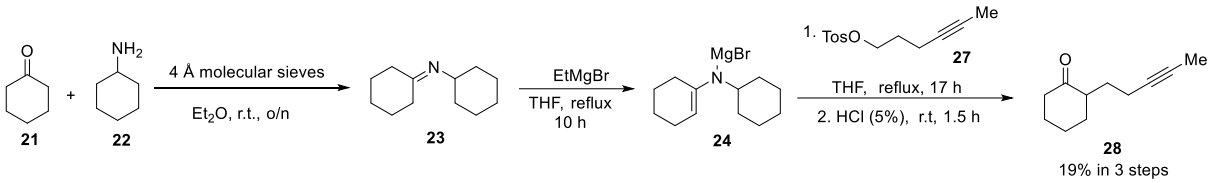

According to the synthesis procedure from *Lansbury et. al.*[144], cyclohexanone (**21**) (31 mmol, 3.2 mL, 1.0 eq.) and cyclohexylamine (**22**) (31 mmol, 3.5 mL,1.0 eq.) were added in a dried *Schlenk* flask under inert conditions, followed by addition of dried molecular sieves (4 Å). Afterward, dry diethyl ether (22 mL) was added and the mixture was stirred at ambient temperature overnight. The reaction was stopped by filtering off the solid and the liquid phase was concentrated under reduced pressure. The crude was purified by using a *Kugelrohr* distillation apparatus under 0.80 mbar at 100 ºC to 110 ºC.

EtMgBr (5.9 mL, 18.8 mmol, 1.125 eq.) was dissolved in dry THF (50 mL) in a dried *Schlenk* flask, which appeared as a slightly red solution. Then, the reaction mixture was slowly added to the flask. The reaction was heated to reflux for 10 h. After the mixture was cooled to r.t., 3-pentyn-1-ol, 1-(4-methyl benzenesulfonate) (**27**) (4.33 g, 18.2 mmol, 1.0 eq.) was added. The mixture was heated to reflux for 17 h and an orange suspension was observed. The mixture was slowly dropped into HCl (5%) and stirred at room temperature for 1.5 h for hydrolysis, resulting in a clear solution. The mixture was extracted with Et_2O three times, dried with Na_2SO_4, filtered off, and concentrated under reduced pressure. After column chromatography (*c*Hex/EtOAc = 1:5) as a purification method, a yellow oil was obtained with a yield of 19% (973 mg, 5.90 mmol) was given.

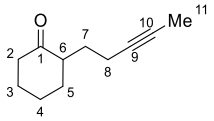

Appearance:	Yellow oil.
Chemical Formula:	$C_{11}H_{16}O$.
Molecular Weight:	164.2480
Yield:	19% (973 mg, 5.90 mmol).
R_f:	0.4 (*c*Hex/EtOAc = 5:1).
^{1}H-NMR:	(300 MHz, $CDCl_3$) δ [ppm]: 2.52-2.41 (m, 1H, H-6), 2.40-2.27 (m, 2H, H-2), 2.23-2.14 (m, 2H, H-8), 2.15-2.06 (m, 1H, H-5), 2.05-1.93 (m, 2H, H-3, H-4), 1.91-1.83 (m, 1H, H-7), 1.77 (t, 3H, J = 2.6 Hz, H-11), 1.74–1.62 (m, 2H, H-3', H-7'), 1.42–1.27 (m, 2H, H-4', H-5').

^{13}C-NMR:	(75 MHz, $CDCl_3$) δ [ppm]: 213.0 (C-1), 78.7 (C-9), 75.8 (C- 10), 49.2 (C-6), 42.2 (C-2), 33.9 (C-8), 28.7 (C-5), 28.1 (C- 3), 25.1 (C-4), 16.4 (C-7), 3.5 (C-11).
IR:	$\tilde{\upsilon}$ [cm^{-1}]: 2930 (m), 2860 (m), 2357 (w), 1707 (s), 1558 (w), 1506 (w), 1449 (m), 1364 (m), 1339 (m), 1314 (w), 1177 (m), 1128 (m), 1090 (w), 1042 (w), 993 (w).
GC-EI-LRMS	t_R = 10.91 min, *m/z* 164.1 $[M]^{\bullet+}$.

7.3.3 Synthesis and characterization of compound **29** and **29'**

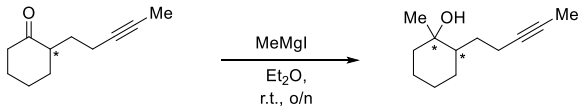

28 **29** and **29'**, 63%

According to the synthesis procedure from *Lansbury et. al*.[144], a dried *Schlenk* flask was charged with 2-(3-pentynyl)cyclohexanone (**28**) (5.9 mmol, 1.0 mL,1.0 eq.) and Et_2O (4 mL). MeMgI (18 mmol, 5.9 mL, 3.0 eq.) was added and the solution was stirred at r.t. for o/n. The reaction mixture was quenched by an addition of sat. $NH_4Cl_{(aq.)}$. The mixture was extracted with Et_2O three times, washed with brine, dried over Na_2SO_4, filtered off and concentrated under reduced pressure. The crude product was further purified by column chromatography (*c*Hex/EtOAc = 5:1 to 2:1), which gave a yellow oil of a mixture of diastereomers in a yield of 63% (674 mg, 3.74 mmol).

The separated pure fractions from column chromatography purification were analyzed by NMR respectively.

Appearance:	Yellow oil.
Chemical Formula:	$C_{12}H_{20}O$.
Molecular Weight:	180.2910
Yield:	63% (674 mg, 3.74 mmol)(mixture of diastereomers).
R_f:	0.20 and 0.16 (*c*Hex/EtOAc = 5:1).
^{1}H-NMR:	(500 MHz, $CDCl_3$) δ [ppm]: Isomer **29**: 2.28-2.20 (m, 1H, H-8), 2.10-2.02 (m, 1H, H-8'), 1.88-1.79 (m, 1H, H-2), 1.78 (t, *J* = 2.6 Hz, 3H, H-11), 1.72-1.66 (m, 1H, H-5), 1.66-1.60 (m, 2H, H-3, H-4), 1.55-1.49 (m, 2H, H-4', H- 13), 1.43-1.33 (m, 1H, H-3'), 1.33-1.25 (m, 2H, H-6, H-2'), 1.22-1.15 (m, 6H, H-12, H-7, H-5') Isomer **29'**: 2.30-2.22 (m, 1H, H-8), 2.22-2.05 (m, 1H, H-8'), 1.93-1.86 (m, 1H, H-2), 1.79 (t, *J* = 2.9 Hz, 3H, H-11), 1.78-1.74 (m, 1H, H-5), 1.73-1.69 (m, 1H, H-3), 1.69-1.61 (m, 2H, H-4, H-7), 1.44-1.27 (m, 4H, H-3', H-4', H-6, H-13), 1.26-1.13 (m, 2H, H-2', H-7'), 1.09 (s, 3H, H-12), 1.02-0.93 (m, 1H, H-5').
^{13}C-NMR:	(75 MHz, $CDCl_3$) δ [ppm]: Isomer **29**: 79.3 (C-9), 75.5 (C-10), 71.4 (C-1), 44.6 (C-6), 40.3 (C-2), 28.8 (C-7), 28.7 (C-12), 26.8 (C-5), 25.6 (C-4), 21.9 (C-3), 16.9 (C-8), 3.5 (C-11). Isomer **29'** (C1, C-9 and C-10 are ambiguous): 47.2 (C-6), 42.2 (C-2), 29.2 (C-7), 28.8 (C-5), 25.4 (C-4), 24.0 (C-3), 21.1 (C-12), 17.3 (C-8), 3.5 (C-11).
IR: **WEN-II-ALE-008**	$\tilde{\upsilon}$ [cm^{-1}]: 3600-3200 (b), 2922 (s), 2857 (s), 2361 (m), 1717 (w), 1558 (w), 1506 (w), 1447 (m), 1437 (m), 1373 (m), 1364 (m), 1339 (w), 1250 (w), 1155 (m), 1128 (m), 1103 (m), 1055 (w), 982 (m), 843 (w), 920 (m), 847 (m), 799 (w).
GC-EI-LRMS	t_R = 11.14 min, *m/z* 180.3, t_R = 11.26, *m/z* 180.0 $[M]^{\bullet+}$.
GC-EI-HRMS	t_R = 16.50 min, *m/z* 179.1426, 165.1270; t_R = 16.71 min, *m/z* 179.1426, 165.1270. (Temp: 50(5)-10-270(5))

7.3.4 Synthesis and characterization of hydrindane derivatives **13** and ccompound **14**

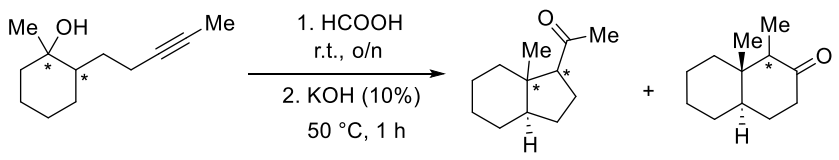

29 and **29'** **13** **14**

78%

According to the synthesis procedure from *Lansbury et. al*.[144], the mixture of diastereomers of methyl-2-(3-pentynyl)cyclohexanol (**29** and **29'**) (450 mg, 2.50 mmol, 1.0 eq.) was mixed with HCOOH (5.8 mL) and stirred at r.t. overnight, the addition of water resulted in the formation of a white suspension. After the mixture was stirred at r.t. for a further 30 min, it was extracted with Et_2O three times, dried over Na_2SO_4, filtered off and concentrated under reduced pressure, after which a dark yellow oil formed. To the crude product was added KOH (10%, 13.7 mL) and the mixture was stirred at 50 °C for 1h. Then, water was added into the reaction mixture and the aqueous phase was extracted with Et_2O three times, dried over Na_2SO_4, filtered, and concentrated under reduced pressure. Column chromatography (*c*Hex/EtOAc = 15:1) afforded a yellow oil of two structural isomers with a yield of 78% (353 mg, 1.96 mmol).

Appearance:	Yellow oil.
Chemical Formula:	$C_{12}H_{20}O$.
Molecular Weight:	180.2910
Yield:	78% (353 mg, 1.96 mmol).
R_f:	0.55, 0.45 (*c*Hex/EtOAc = 10:1).

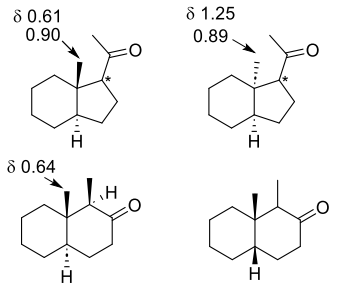

^{1}H-NMR:	(500 MHz, $CDCl_3$) (mixture of isomers) δ [ppm]: angular methyl singlets at 1.25, 0.89, 0.64, 0.61
IR:	$\tilde{\upsilon}$ [cm^{-1}]: 2926 (s), 2859 (m), 2363 (w), 1942 (w), 1869 (w), 1792 (w), 1749 (w), 1701 (s), 1653 (m), 1558 (m), 1522 (w), 1506 (m), 1449 (w), 1356 (m), 1159 (m), 608 (w).
GC-EI-HRMS	t_R = 15.96 min, *m/z* 180.1507 $[M]^{\bullet+}$ t_R = 16.27 min, *m/z* 180.1504 $[M]^{\bullet+}$; t_R = 16.36 min, *m/z* 180.1505 $[M]^{\bullet+}$; t_R = 17.00 min, *m/z* 180.1506 $[M]^{\bullet+}$; t_R = 17.10 min, *m/z* 180.1506 $[M]^{\bullet+}$; t_R = 17.30 min, *m/z* 180.1505 $[M]^{\bullet+}$.

7.3.5 Hydrogen deuterium exchange by keto/enol tautomerization [99]

In a dried *Schlenk* flask was added compound **13** and **14** (50 mg, 0.277 mmol, 1.0 eq.) and dissolved in MeOD (0.3 mL), THF (0.5 mL) and D_2O (1 mL), followed by addition of 15% NaOD (aq.) (200 µL).[99] The mixture was stirred at 60 °C for 3 d and the reaction progress was controlled by GC-MS analysis. The reaction was quenched by addition of CH_3COOD (9% in D_2O) and extracted three times with Et_2O, dried over Na_2SO_4, filtered off, and concentrated under reduced pressure. The solid was triturated with hexane (2×0.5 mL). The product was directly analyzed by GC-MS and NMR.

7.4 *In vitro* phase I and phase II studies

7.4.1 *In vitro* phase I metabolism

S42 (**1**)/S42-d7 (**1-d7**) samples with enzymes were prepared in duplicates, followed by one S42 (**1**)/ S42-d7 (**1-d7**) sample without enzymes and one without S42 (**1**)/ S42-d7(**1-d7**) substrate[118]. The total sample volume of each sample is 500 µL. For samples without enzymes, the volume of enzymes solution was replaced by a phosphate buffer.

Stock solution of S42 (**1**) / S42-d7 (**1-d7**) with a concentration of 1 mg/mL in MeOH was prepared in a glass tube. This stock solution of S42 (**1**)/ S42-d7 (**1-d7**) (338 nmol, 100 µL, 1 mg/mL) was added into an *Eppendorf* LoBind® tube (2 mL) and the solvent was evaporated to dryness to be further reconstituted and vortexed with phosphate buffer (370 µL, 50 mM phosphate buffer containing 5 mM $MgCl_2$, pH 7.4). Freshly prepared NADPH solution (100 µL, 50 mM in phosphate buffer), S9 fraction (15 µL, 20 µg/µL) and HLM (15 µL, 20 µg/µL) were added according to the stated order. All samples had an overall sample volume of 500 µL. The mixture was incubated at 37 °C at 400 rpm for 24 h. The reactions were terminated by adding ice-cold MeCN (1.5 mL), vortexed, and cooled to 0 °C in an ice bath. After the samples were centrifuged at 17,000 x g for 2 min, the supernatant was transferred to new *Eppendorf* tubes and concentrated under vacuum for 2.5 h at 45 °C. Samples were reconstituted in H_2O (900 µL) and MeCN (100 µL) for the SPE (HLB (60 µm), 60 mg, 3 mL) cartridge which was first conditioned by MeOH (3 mL) and then H_2O (3 mL). After the samples were loaded on the SPE cartridge, H_2O (1 mL) was added for washing and the substrate was eluted with MeOH (1 mL). The solvent was evaporated to dryness and the dry residues were derivatized by a mixture of NH_4I/MSTFA/EtSH (100 µL) at 60 °C for 30 min before GC-EI HR MS orbitrap analysis at the German Sport University Cologne.[115]

7.4.2 *In vitro* phase II metabolism

Phase II metabolism experiments were conducted subsequently by repeating phase I experiments with higher sample concentrations.[20b, 145]

S42 (**1**)/ S42-d7 (**1-d7**) (338 nmol, 100 µL, 1 mg/mL) was added into an E*ppendorf* LoBind® tube (2 mL) and the solvent was evaporated to dryness to be further reconstituted and vortexed with *in vitro* phosphate buffer (120 µL, 50 mM

phosphate buffer containing 5 mM $MgCl_2$, pH 7.4). Freshly prepared NADPH solution (100 µL, 50 mM in phosphate buffer), S9 fraction (15 µL, 20 µg/µL) and HLM (15 µL, 20 µg/µL) were added according to the stated order. For samples without enzymes, the volume of enzymes solution was replaced by a phosphate buffer

After phase I samples were incubated at 37°C for 21 h, phase I aliquot (20 µL) from each sample, except substrate blank sample, was added to E*ppendorf* LoBind® tubes containing dried alamethicin (5 µg, 1µL, 5 mg/mL). To the samples for phase II experiments were subsequently added phosphate buffer (80 µL, 50 mM phosphate buffer containing 5 mM $MgCl_2$, pH 7.4), freshly prepared NADPH solution (20 µL, 50 mM in phosphate buffer), UDPGA (20µL, 50 mM), *D*-saccharic acid-1,4-lactone (SL) (20µL, 50 mM), sulfate solution* (20µL), S9 fraction (10 µL, 20 µg/µL) and HLM (10 µL, 20 µg/µL) for a total volume of 200 µL. For samples without enzymes, or without substrate, the volume of enzymes or substrate solution was replaced by a phosphate buffer. The samples were incubated at 37 °C, 400 rpm for 20.5 h. Reactions were stopped by the addition of cold MeCN (600 µL), vortexed, and cooled to 0 °C in an ice bath for 15 min. After the samples were centrifuged at 17,000 x g for 2 min, the supernatant was transferred to new E*ppendorf* tubes and concentrated under vacuum for 2.5 h at 45 °C. Internal standard** (10 uL) was added before samples were diluted in solvent (90 uL, MeOH/ NH_4Ac buffer = 30/70) for LC-MS analysis.

*Sulfate solution was prepared freshly by mixing ATP (64 µL, 500 mM), Na_2SO_4 (80 µL, 200 mM), $MgCl_2 \cdot 6H_2O$ (11.4 µL, 2 M) in phosphate buffer (44.6 µL).

**Internal standard was a mixture of d3-testosterone-gucuronide (0.1 µg/µL), d5-androsterone-glucuronide (0.1 µg/µL), d3-testosteronte-sulfate (1 µg/µL) in a solvent of MeCN/H_2O=1/1.

7.5 Rat urine workup and analysis

7.5.1 GC-MS sample preparation

All samples for GC-MS analysis were hydrolyzed enzymatically or chemically and separated into free, glucuronide, and sulfate fractions.[143, 146] The purification procedure was from Piper and coworkers.[146a]

Free fractions:

Rat urine sample (5 mL) fortified with methyl testosterone as an internal standard (20 µl, 20 ng/µl in MeOH) and transferred to a C18 cartridge, which was previously conditioned with MeOH (2 mL) and H_2O (2 mL). After washing the cartridge with H_2O (2 mL), S42 metabolites were eluted by MeOH (3 x 1 mL). The collected MeOH solution was evaporated and reconstituted in phosphate buffer (2 mL, 0.2M, pH 7), and vortexed. Then TBME (5 mL) was added, and the sample was shaken for 5 min before centrifugation for 5 min. The organic layer was transferred to a new test tube, evaporated to dryness and derivatized by standard derivatization agent (100 µl, MSTFA/NH_4I/ethanethiol = 1000/2/3 (v:w:v) at 60 °C for 30 min before GC-MS analysis.

Glucuronide fractions

The separated aqueous layer was fortified with methyl testosterone (20 µl, 20 ng/µl in MeOH) and added *β*-glucuronidase (100 µl) before the sample was incubated at 50 °C for 60 min. The hydrolysis reaction was stopped by addition of potassium carbonate buffer (1mL, 20%, pH 10), before addition of TBME (5 mL), shaken for 5 min, and centrifuged using Program 3 for 5 min. The organic layer was transferred to a new test tube, evaporated to dryness and derivatized by standard derivatization agent (100 µl, MSTFA/NH_4I/ethanethiol = 1000/2/3 (v:w:v)) at 60 °C for 30 min before GC-MS analysis.

Sulfate fractions

The remaining aqueous layer from the liquid liquid extraction was neutralized by adding glacial acetic acid (100 µl) slowly, till no CO_2 bubbles were generated during vortex. The sample was again fortified with methyl testosterone (20 µl, 20 ng/µl in MeOH) and the sample was transferred to a C18 cartridge, which was previously conditioned with MeOH (2 mL) and H_2O (2 mL). After washing with H_2O (2 mL) and eluting with MeOH (1mL X 3), the collected MeOH solution was evaporated and reconstituted in diluted sulfuric acid in EtOAc (2.5 mL, H_2SO_4/EtOAc = 2 µL/1 mL). The sample was vortexed and heated at 50 °C for 60 min. After the sample was cooled down to room temperature, NaOH in MeOH (0.5 mL, 1 M) was added and the solution was evaporated. The generated solid was redissolved in H_2O (5 mL) and TBME (5 mL), shaken for 5 min,

and centrifuged using Program 3 for 5 min. The organic layer was transferred to a new test tube, evaporated to dryness and derivatized by standard derivatization agent (100 µl, MSTFA/NH_4I/ethanethiol = 1000/2/3 (v:w:v)) at 60 °C for 30 min before GC-MS analysis.

7.5.2 LC-MS sample preparation

The LC-MS instrument methods and all rat urine LC-MS sample preparation for LC-MS direct injection were developed by *Dr. Felicitas Wagener.*

Internal standard** (5 µl) was added to a rat urine sample (45 µl), centrifuged at 1800 x g, and the supernatant was added to a LC-vial for analysis.

**Internal standard was a mixture of testosterone-gucuronide-d3 (0.1 µg/µL), androsterone-glucuronide-d5 (0.1 µg/µL), testosteronte-sulfate-d3 (1 µg/µL) in a solvent of MeCN/H_2O=1/1.

8. References

[1] Z. Wenbo, Z. Yan, *J. Multidiscip. Healthc.* **2023**, 4293-4305.
[2] A. Goldman, S. Basaria, *Mol. Cell. Endocrinol.* **2018**, *464*, 46-55.
[3] a) M. L. Eisenberg, S. Li, D. Herder, D. J. Lamb, L. I. Lipshultz, *International journal of impotence research* **2015**, *27*, 46-48; b) G. D. Albano, F. Amico, G. Cocimano, A. Liberto, F. Maglietta, M. Esposito, G. L. Rosi, N. Di Nunno, M. Salerno, A. Montana, *Healthcare (Basel)* **2021**, *9* (1), 97.
[4] D. J. Handelsman, *Medical journal of Australia* **2006**, *185*, 436-439
[5] a) WADA, *World Anti-Doping Code International Standard Prohibited List 2024*, World Anti-Doping Agency, Montreal, Quebec, Canada, 2023.; b) M. Thevis, T. Kuuranne, H. Geyer, *Drug Test. Anal.* **2024,** *16*, 5-29.
[6] R. Narayanan, C. C. Coss, J. T. Dalton, *Mol. Cell. Endocrinol.* **2018**, *465*, 134-142.
[7] C. Uyanik, A. Malay, J. R. Hanson, P. B. Hitchcock, S. Tiryakioglu, *J. Chem. Res.* **2006**, *2006*, 417-419.
[8] a) L. Min, T. Yanase, T. Tanaka, W. Fan, M. Nomura, H. Kawate, T. Okabe, R. Takayanagi, H. Nawata, *Endocrinology* **2009**, *150*, 5606-5616; b) X. Zhang, Z. Sui, *Expert Opin. Drug Discov.* **2013**, *8*, 191-218.
[9] Y. Muta, T. Tanaka, Y. Hamaguchi, N. Hamanoue, R. Motonaga, M. Tanabe, T. Nomiyama, H. Nawata, T. Yanase, *Biochem Biophys. Rep.* **2019**, *17*, 177-181.
[10] T. Kawanami, T. Tanaka, Y. Hamaguchi, T. Nomiyama, H. Nawata, T. Yanase, *Endocrinology* **2018**, *159*, 1774-1792.
[11] M. Thevis, K. Walpurgis, A. Thomas, *Anal. Chem.* **2020**, *92*, 506-523.
[12] A. Kasal, in *Steroid Analysis* (Eds.: H. L. J. Makin, D. B. Gower), Springer Netherlands, Dordrecht, **2010**, pp. 1-25.
[13] a) G. Moss, *Pure Appl. Chem.* **1989**, *61*, 1783-1822; b) IUPAC Commission on the Nomenclature of Organic Chemistry and IUPAC-IUB Commission on Biochemical Nomenclature, *Pure Appl. Chem.*, **1972**, *31* (1-2), 283-322
[14] D. J. Handelsman, A. L. Hirschberg, S. Bermon, *Endocrine reviews* **2018**, *39*, 803-829.
[15] a) S. Inui, S. Itami, *Experimental dermatology* **2013**, *22*, 168-171; b) Y. Bensoussan, J. Anderson, *Clin. Case Rep.* **2019**, *7*, 1067.
[16] K. Fitch, *Clinical Medicine* **2012**, *12*, 257-260.
[17] B. D. Anawalt, *J. Clin. Endocrinol. Metab.* **2019**, *104*, 2490-2500.
[18] a) R. Kazlauskas, in *Doping in Sports: Biochemical Principles, Effects and Analysis* (Eds.: D. Thieme, P. Hemmersbach), Springer Berlin Heidelberg, Berlin, Heidelberg, **2010**, pp. 155-185; b) L. Gheddar, A. Ameline, J.-S. Raul, P. Kintz, *Tox. Anal. Clin.* **2019**, *31*, 293-297.
[19] N. C. Athey, M. Bouchard, in *Advances in Research on Illicit Networks*, Routledge, **2016**, pp. 98-119.
[20] a) C. P. Miller, M. Shomali, C. R. Lyttle, L. S. L. O'Dea, H. Herendeen, K. Gallacher, D. Paquin, D. R. Compton, B. Sahoo, S. A. Kerrigan, *ACS Med. Chem. Lett.* **2011**, *2*, 124-129; b) F. Wagener, N. Naumann, V. Göldner, C. Görgens, S. Guddat, U. Karst, M. Thevis, *Anal Bioanal Chem.* **2023**, *415*, 5657-5669; c) F. Wagener, L. Euler, C. Görgens, S. Guddat, M. Thevis, *Metabolites* **2022**, *12*, 666; d) T. Möller, H.-C. Wen, N. Naumann, O. Krug, M. Thevis, *Molecules* **2023**, *28*, 5541; e) M. Thevis, E. Gerace, A. Thomas, S. Beuck, H. Geyer, N. Schlörer, J. D. Kearbey, J. T. Dalton, W. Schänzer, *Drug Test. Anal.* **2010**, *2*, 589-598; f) M. Thevis, T. Piper, J. Dib, A. Lagojda, D. Kühne, L. Packschies, H. Geyer, W. Schänzer, *Rapid Commun. Mass Spectrom.* **2017**, *31*, 1175-1183; g) A. Lagojda, D. Kuehne, O. Krug, A. Thomas, T. Wigger, U. Karst, W. Schänzer, M. Thevis, *Eur. J. Mass Spectrom.* **2016**, *22*, 49-59; h) M. Thevis, W. Schänzer, *Mol. Cell. Endocrinol.* **2018**, *464*, 34-45.
[21] J. T. Dalton, *Br. J. Clin. Pharmacol.* **2017**, *83*, 2131-2133.
[22] G. W. P. D. Fonseca, E. Dworatzek, N. Ebner, S. Von Haehling, *Expert Opin. Investig. Drugs.* **2020**, *29*, 881-891.
[23] H. L. Makin, D. Gower, *Steroid analysis*, Springer Science & Business Media, **2010**.
[24] A. R. Christiansen, L. I. Lipshultz, J. M. Hotaling, A. W. Pastuszak, *Transl Androl Urol.* **2020**, *9*, 135-148.
[25] S. Bhasin, V. Krishnan, T. W. Storer, M. Steiner, A. S. Dobs, *J. Gerontol. A Biol. Sci. Med. Sci.* **2023**, *78* (S1) S25-S31.
[26] J. D. Vignali, K. C. Pak, H. R. Beverley, J. P. DeLuca, J. W. Downs, A. T. Kress, B. W. Sadowski, D. J. Selig, *J. Xenobiot.* **2023**, *13*, 218-236.
[27] M. Thevis, H. Geyer, M. Kamber, W. Schänzer, *Drug Test. Anal.* **2009**, *1*, 387-392.
[28] S. K. Balani, G. T. Miwa, L.-S. Gan, J.-T. Wu, F. W. Lee, *Curr. Top. Med. Chem.* **2005**, *5*, 1033-1038.
[29] S. Phang-Lyn, V. A. Llerena, Biochemistry, Biotransformation, StatPearls, Treasure Island, Florida, **2023**
[30] L. Schiffer, W. Arlt, K.-H. Storbeck, *Mol. Cell. Endocrinol.* **2018**, *465*, 4-26.
[31] B. R. Zirkin, V. Papadopoulos, *Biol. Reprod.* **2018**, *99*, 101-111.
[32] V. L. Nelson, K.-n. Qin, R. L. Rosenfield, J. R. Wood, T. M. Penning, R. S. Legro, J. F. Strauss III, J. M. McAllister, *J. Clin. Endocrinol. Metab.* **2001**, *86*, 5925-5933.
[33] J. Owens, *Nat. Rev. Drug Discov.* **2004**, *3*, 736-736.
[34] S. A. Wrighton, E. G. Schuetz, K. E. Thummel, D. D. Shen, K. R. Korzekwa, P. B. Watkins, *Drug Metab. Rev.* **2000**, *32*, 339-361.
[35] A. T. Kicman, in *Doping in Sports: Biochemical Principles, Effects and Analysis* (Eds.: D. Thieme, P. Hemmersbach), Springer Berlin Heidelberg, Berlin, Heidelberg, **2010**, pp. 25-64.
[36] T. M. Penning, *J. Steroid Biochem.* **2011**, *125*, 46-56.
[37] G. Forsdahl, K. Zanitzer, D. Erceg, G. Gmeiner, *Steroids* **2020**, *157*, 108614.

[38] T. Kuuranne, in *Doping in Sports: Biochemical Principles, Effects and Analysis* (Eds.: D. Thieme, P. Hemmersbach), Springer Berlin Heidelberg, Berlin, Heidelberg, **2010**, pp. 65-75.
[39] a) D. T. Monterrey, R. Benito-Arenas, J. Revuelta, E. García-Junceda, *Front. Bioeng. Biotechnol.* **2023**, *11*, 1099924; b) J. Xu, Y. Chen, L. Li, Z. Li, C. Wang, T. Zhou, W. Lu, *J. Pharm. Biomed. Anal.* **2012**, *62*, 182-186.
[40] L. Gessner, M. Thevis, M. A. Rothschild, M. Jübner, *Drug Test. Anal.* **2022**, *14*, 1744-1761.
[41] G. Lippi, M. Franchini, G. Banfi, *Mini-Rev. Med. Chem.* **2011**, *11*, 362-373.
[42] G. Forsdahl, D. Erceg, T. Geisendorfer, M. Turkalj, D. Plavec, M. Thevis, L. Tretzel, G. Gmeiner, *Drug Test. Anal.* **2015**, *7*, 983-989.
[43] J. B. Vaught, *Cancer Epidemiol. Biomarkers Prev.* **2006**, *15*, 1582-1584.
[44] M. Thevis, T. Kuuranne, A. Thomas, H. Geyer, *Drug Test. Anal.* **2021**, *13*, 505-509.
[45] a) T. Lange, A. Thomas, K. Walpurgis, M. Thevis, *Anal Bioanal Chem.* **2020**, *412*, 3765-3777; b) A. M. Garzinsky, A. Thomas, S. Guddat, C. Görgens, J. Dib, M. Thevis, *Biomed. Chromatogr.* **2023**, *37*, e5633.
[46] B. Gray, K. Lubbock, C. Love, E. Ryder, S. Hudson, J. Scarth, *Drug Test. Anal.*
[47] M. Putz, T. Piper, M. Thevis, *Front. Chem.* **2020**, *8*, 435.
[48] a) C. Sweeley, E. C. Horning, *Nature* **1960**, *187*, 144-145; b) M. Zendjabil, Z. Chellouai, O. Abbou, *Ann. Endocrinol., 77*, Elsevier, **2016**, 43-48.
[49] a) J. H. Gross, *Mass spectrometry: a textbook*, Springer Science & Business Media, **2006**; b) J. B. Fenn, M. Mann, C. K. Meng, S. F. Wong, C. M. Whitehouse, *Science* **1989**, *246*, 64-71.
[50] D. C. Turner, M. Schäfer, S. Lancaster, I. Janmohamed, A. Gachanja, J. Creasey, *Gas Chromatography–Mass Spectrometry: How Do I Get the Best Results?*, Royal society of Chemistry, **2019**.
[51] W. Abushareeda, M. Tienstra, A. Lommen, M. Blokland, S. Sterk, S. Kraiem, P. Horvatovich, M. Nielen, M. Al-Maadheed, C. Georgakopoulos, *Rapid Commun. Mass Spectrom.* **2018**, *32*, 2055-2064.
[52] J. H. Lee, E. J. Jung, H. J. Ham, Y. J. Yang, N. S. Kim, H. I. Kim, S. Y. Baek, *Rapid Commun. Mass Spectrom.* **2022**, *36*, e9334.
[53] M. R. Anari, R. Bakhtiar, B. Zhu, S. Huskey, R. B. Franklin, D. C. Evans, *Anal. Chem.* **2002**, *74*, 4136-4144.
[54] L. R. Snyder, J. J. Kirkland, J. W. Dolan, *Introduction to modern liquid chromatography*, John Wiley & Sons, **2011**.
[55] a) R. Mametov, I.-A. Ratiu, F. Monedeiro, T. Ligor, B. Buszewski, *Crit. Rev. Anal. Chem.* **2021**, *51*, 150-173; b) M. Novotny, *Anal. Chem.* **1981**, *53*, 1294A-1308A.
[56] H. Nakata, *Mass Spectrom.* **2019**, *8*, A0074-A0074.
[57] a) F. W. McLafferty, *Science* **1981**, *214*, 280-287; b) G. L. Glish, D. J. Burinsky, *J. Am. Soc. Mass Spectrom.* **2008**, *19*, 161-172; c) M. C. McMaster, *GC/MS - A Practical User's Guide*, 2nd. ed., John Wiley & Sons, Inc, New Jersey, **2008**.
[58] a) J. Eiler, J. Cesar, L. Chimiak, B. Dallas, K. Grice, J. Griep-Raming, D. Juchelka, N. Kitchen, M. Lloyd, A. Makarov, *Int. J. Mass spectrom.* **2017**, *422*, 126-142; b) Thermo Fisher Scientific, *Q Exactive GC Mass Spectrometer Software Manual*, Revision B, 2015.
[59] J. Zhou, H. Liu, Y. Liu, J. Liu, X. Zhao, Y. Yin, *Anal. Chem.* **2016**, *88*, 4478-4486.
[60] K. M. Knights, D. M. Stresser, J. O. Miners, C. L. Crespi, *Curr. Protoc. Pharmacol.* **2016**, *74*, 7.8. 1-7.8. 24.
[61] I. J. Schurink, J. Willemse, M. M. Verstegen, L. J. van Der Laan, J. de Jonge, *Hepatol.* **2020**, *72*, 1485-1487.
[62] S. A. Wrighton, B. J. Ring, M. Vandenbranden, *Toxicol. Pathol.* **1995**, *23*, 199-208.
[63] J. C. Lipscomb, T. S. Poet, *Pharmacol. Ther.* **2008**, *118*, 82-103.
[64] D. Medina, B. Omanakuttan, R. Nguyen, E. Alwarsh, C. Walgama, *Metabolites* **2024**, *14*, 429.
[65] a) J. Ruberte, P. N. Schofield, J. P. Sundberg, A. Rodriguez-Baeza, A. Carretero, C. McKerlie, *Mamm. Genome* **2023**, *34*, 389-407; b) R. Iwanaga, D. J. Orlicky, J. Arnett, M. K. Guess, K. J. Hurt, K. A. Connell, *Int Urogynecol J.* **2016**, *27*, 1697-1704.
[66] I. Taneja, K. Karsauliya, M. Rashid, A. K. Sonkar, K. S. R. Raju, S. K. Singh, M. Das, M. Wahajuddin, S. P. Singh, *Food Chem. Toxicol.* **2018**, *111*, 94-101.
[67] B. A. Šolaja, D. R. Milić, L. I. Došen-Mićović, *Steroids* **1994**, *59*, 330-334.
[68] E. J. Parish, T.-Y. Wei, *Synth. Commun.* **1987**, *17*, 1227-1233.
[69] a) L. Lista, P. Manini, A. Napolitano, A. Pezzella, M. d'Ischia, *Steroids* **2006**, *71*, 670-673; b) H. Abas, P. Blencowe, J. L. Brookfield, L. A. Harwood, *Chem. Eur. J.* **2023**, *29*, e202301066.
[70] J. A. Salvador, J. R. Hanson, *J. Chem. Res.* **2004**, *2004*, 513-516.
[71] J. B. Johnston, H. Ouellet, L. M. Podust, P. R. O. de Montellano, *Arch. Biochem. Biophys.* **2011**, *507*, 86-94.
[72] T. L. Poulos, *Chem. Rev.* **2014**, *114*, 3919-3962.
[73] S. Belvedere, R. Breslow, *Bioorg. Chem.* **2001**, *29*, 321-331.
[74] R. V. Ottenbacher, E. P. Talsi, T. V. Rybalova, K. P. Bryliakov, *ChemCatChem* **2018**, *10*, 5323-5330.
[75] M. S. Chen, M. C. White, *Science* **2007**, *318*, 783-787.
[76] R. V. Ottenbacher, E. P. Talsi, K. P. Bryliakov, *Molecules* **2016**, *21*, 1454.
[77] E. P. Talsi, D. G. Samsonenko, R. V. Ottenbacher, K. P. Bryliakov, *ChemCatChem* **2017**, *9*, 4580-4586.
[78] Y. Nakayama, M. R. Maser, T. Okita, A. V. Dubrovskiy, T. L. Campbell, S. E. Reisman, *J. Am. Chem. Soc.* **2021**, *143*, 4187-4192.
[79] a) M. Krumpolc, J. Rocek, *Inorg. Chem.* **1985**, *24*, 617-621; b) R. W. Huigens, B. R. Brummel, S. Tenneti, A. T. Garrison, T. Xiao, *Molecules* **2022**, *27*, 1112.

[80] C. Djerassi, J. Romo, G. Rosenkranz, *J. Org. Chem.* **1951**, *16*, 754-760.
[81] R. Antonucci, S. Bernstein, D. Giancola, K. J. Sax, *J. Org. Chem.* **1951**, *16*, 1126-1133.
[82] a) J. Hanson, T. Organ, *J. Chem. Soc. C Org.* **1970**, 513-515; b) J. R. Hanson, T. D. Organ, *J. Chem. Soc. C Org.* **1970**, 513.
[83] M. Rappoldt, P. Westerhof, *Recl. Trav. Chim. Pays-Bas.* **1961**, *80*, 43-46.
[84] a) J. Hanson, T. Organ, *J. Chem. Soc. D.* **1970**, 1052-1052; b) J. Hanson, *J. Chem. Res. Synop.* **1999**, 200-201.
[85] A. Ogilvie, J. Hanson, *J. Chem. Soc., Perkin Trans. 1* **1972**, 1981-1983.
[86] J. R. Hanson, P. B. Reese, I. H. Sadler, *J. Chem. Soc., Perkin Trans. 1* **1984**, 2937-2939.
[87] J. R. Hanson, P. B. Reese, *Tetrahedron Lett.* **1983**, *24*, 3405-3408.
[88] S. G. Knights, J. R. Hanson, *J. Chem. Res.* **2004**, *2004*, 830-831.
[89] J. R. Hanson, L. Yang-Zhi, *J. Chem. Soc., Perkin Trans. 1* **1984**, 2173.
[90] J. Blunt, A. Fischer, M. Hartshorn, F. Jones, D. Kirk, S. Yoong, *Tetrahedron* **1965**, *21*, 1567-1580.
[91] D. Baldwin, J. Hanson, *J. Chem. Soc., Perkin Trans. 1* **1972**, 1889-1891.
[92] a) D. Baldwin, J. R. Hanson, A. M. Holtom, *J. Chem. Soc., Perkin Trans. 1* **1973**, 2687-2691; b) J. Hanson, H. Shapter, *J. Chem. Soc., Perkin Trans. 1* **1972**, 1445-1447.
[93] M. D. Gomes, S. H. Lecker, R. T. Jagoe, A. Navon, A. L. Goldberg, *Proc. Natl. Acad. Sci.* **2001**, *98*, 14440-14445.
[94] G. M. Anstead, K. E. Carlson, J. A. Katzenellenbogen, *Steroids* **1997**, *62*, 268-303.
[95] I. Stoilov, R. Shetty, J. St. Pyrek, S. L. Smith, W. J. Layton, D. S. Watt, *j. Org. Chem.* **1994**, *59*, 926-928.
[96] B. Zeeh, G. Jones, C. Djerassi, *Chem. Ber.* **1968**, *101*, 1018-1034.
[97] P. T. Lansbury, T. R. Demmin, G. E. Dubois, V. R. Haddon, *J. Am. Chem. Soc.* **1975**, *97*, 394-403.
[98] a) J. M. Halket, V. G. Zaikin, *Eur. J. Mass Spectrom.* **2004**, *10*, 1-19; b) D. J. Harvey, P. Vouros, *Mass Spectrom. Rev.* **2020**, *39*, 105-211; c) V. Zaikin, J. M. Halket, *A handbook of derivatives for mass spectrometry*, IM publications, **2009**.
[99] P. Grocholska, R. Bachor, *Molecules* **2021**, *26*, 2989.
[100] Y. Chang, T. Myers, M. Wasa, *Adv. Synth. Catal.* **2020**, *362*, 360-364.
[101] C. J. Macnevin, F. Atif, I. Sayeed, D. G. Stein, D. C. Liotta, *J. Med. Chem.* **2009**, *52*, 6012-6023.
[102] H. J. Ringold, S. K. Malhotra, *Tetrahedron Lett.* **1962**, *3*, 669-672.
[103] The computer software UMC (Universal Mass Calculator) was used to [simulate isotope patterns, evaluate the degree of deuteration/labelling, evaluate elemental compositions]. UMC V3.14.0.47, Dr. Matthias C. Letzel, Universtität Münster, Org.-Chem. Institut, Germany. https://www.uni-muenster.de/Chemie.oc/ms/downloads.html
[104] a) P. Woollard, *Biol. Mass Spectrom.* **1983**, *10*, 143-154; b) J. Segura, R. Ventura, C. Jurado, *J. Chromatogr. B, Biomed. Appl.* **1998**, *713*, 61-90.
[105] a) H. Budzikiewicz, C. Djerassi, D. H. Williams, *Structure Elucidation of Natural Products by Mass Spectrometry - Vol. II: Steroids, Terpenoids, Sugars, and Miscellanous Classes.*, Holden-Day Inc, **1964**; b) F. W. McLafferty, *Mass spectrometry of organic ions*, Elsevier, **2012**; c) H. Budzikiewicz, *Biochemical Applications of Mass Spectrometry*, Wiley Interscience, **1972**.
[106] H. Budzikiewicz, C. Djerassi, and D. H. Williams, *Structure Elucidation of Natural Products by Mass Spectrometry—Vol. II: Steroids, Terpenoids, Sugars, and Miscellanous Classes*, Holden-Day Inc, **1964.**
[107] M. Vermeer, Bachelor Thesis, University of Cologne **2022**.
[108] a) L. Tokes, R. T. Lalonde, C. Djerassi, *J. Org. Chem.* **1967**, *32*, 1020-1029; b) G. J. L. Tókes, and Carl Djerassi, *J. Am. Chem. Soc.* **1968**, *90*, 5465-5477.
[109] J. Diekman, C. Djerassi, *Mass Spectrometry of Some Trimethylsilyl Ethers* **1966**, *32*, 1005-1012.
[110] a) Y. Djoumbou-Feunang, J. Fiamoncini, A. Gil-de-la-Fuente, R. Greiner, C. Manach, D. S. Wishart, *J. Cheminform.* **2019**, *11*; b) D. S. Wishart, S. Tian, D. Allen, H. P. Eponine Oler, V. W.Lui, V. Gautam, Y. Djoumbou-Feunang, R. Greiner, T. O. Metz, *Nucleic Acids Res.* **2022**, *50*.
[111] C. Neto, M. C. Oliveira, L. Gano, F. Marques, T. Yasuda, T. Thiemann, T. Kniess, I. Santos, *Steroids* **2012**, *77*, 1123-1132.
[112] a) A. R. Bressette, L. C. Glover Iv, *Synlett* **2004**, *2004*, 738-740; b) F. A. Luzzio, R. W. Fitch, W. J. Moore, K. J. Mudd, *J. Chem. Educ.* **1999**, *76*, 974; c) S. Mons, L. Lebeau, C. Mioskowski, *Synth. Commun.* **1998**, *28*, 213-218.
[113] C. Wartmann, S. Nandi, J. M. Neudorfl, A. Berkessel, *Angew. Chem. Int. Ed. Engl.* **2023**, *62*, e202306584.
[114] J. Shet, V. Desai, S. Tilve, *Synthesis* **2004**, *2004*, 1859-1863.
[115] H.-C. Wen, T. Wilczek, J.-M. Neudörfl, F. Wagener, T. Piper, M. Thevis, M. Schäfer, *J. Mass Spectrom.* **2024**, *59*, e5077.
[116] S. Popov, G. Eadon, C. Djerassi, *J. Org. Chem.* **1972**, *37*, 155-165.
[117] B. Paizs, S. Suhai, *Mass Spectrom. Rev.* **2004**, *24*, 508-548.
[118] T. Kuuranne, A. Leinonen, W. Schänzer, M. Kamber, R. Kostiainen, M. Thevis, *Drug Metab. Dispos.* **2008**, *36*, 571-581.
[119] H. C. Wen, F. Wagener, T. Piper, J. Neudörfl, M. Thevis, M. Schäfer, *Drug Test. Anal.* **2025**.
[120] a) S. M. Ervin, Hao Li, L. Lim, L. R. Roberts, X. Liang, S. Mani, X. M. R. Redinbo, *J. Biol. Chem.* **2019**, *294*, 18586-18599; b) B. T. Zhu, A. H.Conney, *Carcinog.*, *19*, 1-27.
[121] D. E. Davis Jr, K. L. Leaptrot, D. C. Koomen, J. C. May, G. d. A. Cavalcanti, M. C. Padilha, H. M. Pereira, J. A. McLean, *Anal. Chem.* **2021**, *93*, 10990-10998.
[122] S. A. Weththasinghe, C. C. Waller, H. L. Fam, B. J. Stevenson, A. T. Cawley, M. D. McLeod, *Drug Test. Anal.* **2018**, *10*, 330-339.

[123] M. Vollmer, M. Klingebiel, S. Rohn, R. Maul, *In Vitro Toxicol.* **2017**, *39*, 111-118.
[124] T. Kuuranne, A. Leinonen, M. Thevis, W. Schänzer, K. Pystynen, R. Kostiainen, in *Recent advances in doping analysis (14): proceedings of the Manfred Donike workshop, 24th Cologne Workshop on Dope Analysis. Cologne: Sportverlag Strauß ; 4th to 9th June 2006, Sportverl. Strauß.,* **2006**, pp. 161-168.
[125] C. Johnson, E. Karlsson, S. Sarda, L. Iddon, M. Iqbal, X. Meng, J. Harding, A. Stachulski, J. Nicholson, I. Wilson, *Xenobiotica* **2010**, *40*, 9-23.
[126] C. C. Fitzgerald, R. Hedman, D. R. Uduwela, B. Paszerbovics, A. J. Carroll, T. Neeman, A. Cawley, L. Brooker, M. D. McLeod, *Front. Mol. Biosci.* **2022**, *9*, 829511.
[127] T. Iyanagi, *Int. Rev. Cytol.* **2007**, *260*, 35-112.
[128] L. Hitschler, L. S. Nissen, M. Kuntz, M. Basen, *Biotechnol. biofuels* **2021**, *14*, 1-17.
[129] a) N. Tamie, W. Rui-Sheng, *Int. J. Biochem.* **1994**, *26*, 1333-1340; b) H. Kim, R. Wang, E. Elovaara, H. Raunio, O. Pelkonen, T. Aoyama, H. Vainio, T. NAKAJIMA*, *Xenobiotica* **1997**, *27*, 657-665.
[130] OpenAI., 2024-2025 ed., 2024, https://chatgpt.com/
[131] C. Schweizer Grundisch, N. Baume, M. Saugy, *Drug Test. Anal.* **2014**, *6*, 1170-1173.
[132] M. Thevis, *Mass spectrometry in sports drug testing: characterization of prohibited substances and doping control analytical assays*, John Wiley & Sons, **2010**.
[133] a) Z. Han, E. K. Tangni, J. Diana Di Mavungu, L. Vanhaecke, S. De Saeger, A. Wu, A. Callebaut, *Toxins* **2013**, *5*, 2671-2685; b) K. Levsen, H.-M. Schiebel, B. Behnke, R. Dötzer, W. Dreher, M. Elend, H. Thiele, *J. Chromatogr. A* **2005**, *1067*, 55-72.
[134] W. Schänzer, *Clin. Chem.* **1996**, *42*, 1001-1020.
[135] a) H. Keski-Hynnilä, R. Andersin, L. Luukkanen, J. Taskinen, R. Kostiainen, *J. Chromatogr. A* **1998**, *794*, 75-83; b) J. Caslavska, B. Jung, W. Thormann, *Electrophoresis* **2011**, *32*, 1760-1764.
[136] D. Zheng, K. Ge, C. Qu, T. Sun, J. Wang, W. Jia, A. Zhao, *Commun. Biol.* **2024**, *7*, 641.
[137] a) Y. Liu, B. Kim, S. D. Taylor, *J. Org. Chem.* **2007**, *72*, 8824-8830; b) X.-Y. Wang, J. Leng, S.-M. Wang, A. M. Asiri, H. M. Marwani, H.-L. Qin, *Tetrahedron Lett.* **2017**, *58*, 2340-2343.
[138] V. Göldner, J. Fangmeyer, U. Karst, *Drug Test. Anal.* **2022**, *14*, 262-268.
[139] *Grammarly Inc., 2024-2025 ed., 2025, https://www.grammarly.com/*
[140] *Microsoft. (2025). Copilot in Microsoft Word (AI assistant)*
[141] Perplexity. (2025). Perplexity.ai (AI Chatbot), https://www.perplexity.ai/
[142] X. J. Gu, Chengyu; Qiu, Wenwei; Gao, Wei*, Process for configuration inversion of 3-hydroxy group in steroids,* CN108864237 A, **2018**.
[143] U. Mareck, H. Geyer, G. Opfermann, M. Thevis, W. Schänzer, *J. Mass Spectrom.* **2008**, *43*, 877-891.
[144] Peter T. Lansbury, Timothy R. Demmin, Grant E. Dubois, V. R. Haddon, *Journal of the American Chemical Society* **1975**, *97*, 394-403.
[145] a) T. Kuuranne, A. Leinonen, W. Schänzer, M. Kamber, R. Kostiainen, M. Thevis, *Drug Metab. Dispos.* **2008**, *36*, 571-581; b) C. C. Waller, A. Cawley, S. A. Weththasinghe, L. McClure, C. Suann, E. Suann, E. Sutherland, E. Cooper, A. Heather, M. D. McLeod, *Drug Test. Anal.* **2020**, *12*, 752-762.
[146] a) T. Piper, G. Fußhöller, M. Thevis, *Metabolites* **2024**, *14*, 141; b) M. Thevis, G. Fußhöller, W. Schänzer, *Drug Test. Anal.* **2011**, *3*, 777-783.

9. Appendix

9.1 List of abbreviations

AAS	anabolic androgenic steroid
Ac	acetyl
CID	collision-induced dissociation
*c*Hex	cyclohexane
CYPs	cytochromes
DBDMH	1,3-dibromo-5,5-dimethylhydantoin
DBS	dried blood spot
DCM	dichloromethane
DMSO	dimethyl sulfoxide
DNA	deoxyribonucleic acid
Et_2O	diethyl ether
EtOAc	ethyl acetate
EI	electrospray ionization
E	epitestosterone
ESI-MS	electrospray ionization mass spectrometry
EIC	extracted ion chromatogram
eq.	equivalent
et al.	et alteri
GC- MS	gas chromatography–mass spectrometry
GlucA	glucuronic acid
h	hour
HCD	Higher-energy collisional dissociation
HLM	human liver microsomes
HMPA	hexamethylphosphoramide
HR-MS	high resolution mass spectrometry
Hz	hertz
IR	infrared spectroscopy
IUPAC	International Union of Pure and Applied Chemistry
min	minute

MRM	multiple reaction monitoring
Me	methyl
MeOH	methanol
MeCN	acetonitrile
MS	mass spectrometry
MSTFA	*N*-Methyl-*N*-trimethylsilyl-trifluoroacetamide
MT	methyltestosterone
MTBE	methyl-*tert*-butyl ether
n.a.	not applicable
NADH	nicotinamide adenine dinucleotide
NADPH	nicotinamide adenine dinucleotide phosphate
NBS	*N*-bromosuccinimide
NMR	nuclear magnetic resonance
PAPS	3′-Phosphoadenosine-5′-phosphosulfate
Ph	phenyl
PRM	parallel reaction monitoring
QqQ	triple quadrupole
R_f	retention factor
RT	retention time
SARM	selective androgen receptor modulator
SL	*D*-saccharic acid-1,4-lactone (SL)
SIC	single ion current
SIM	single ion monitoring
SPE	solid-phase extraction
SULT	sulfotransferases
^{t}Bu	*tert*-butyl
TBDMSTFA	*N*-*tert*-butyldimethylsilyl-*N*-methyltrifluoroacetamide
T	testosterone
Theor.	theoretical
THF	tetrahydrofuran
TLC	thin layer chromatography
TMS	trimethylsilyl

UDPGA	uridine diphosphate glucuronic acid
UGT	uridine diphospho-glucuronosyltransferase
WADA	World Anti-Doping Agency

9.2. NMR spectra

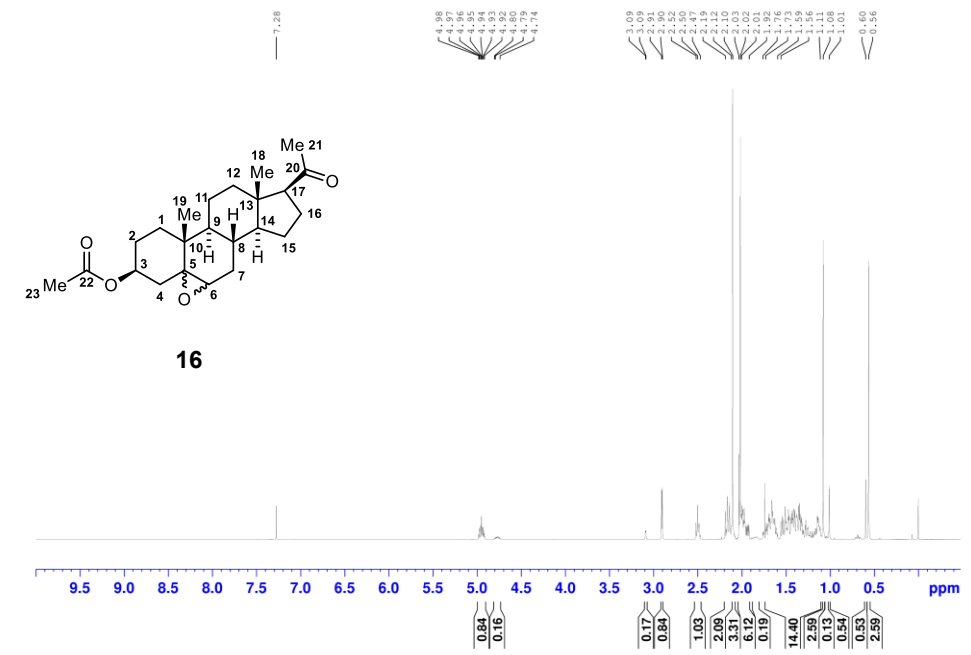

Figure A1. ^{1}H NMR (500 MHz, $CDCl_3$) spectrum of 3ß-acetoxy-5,6-epoxypregnan-20-one (**16**).

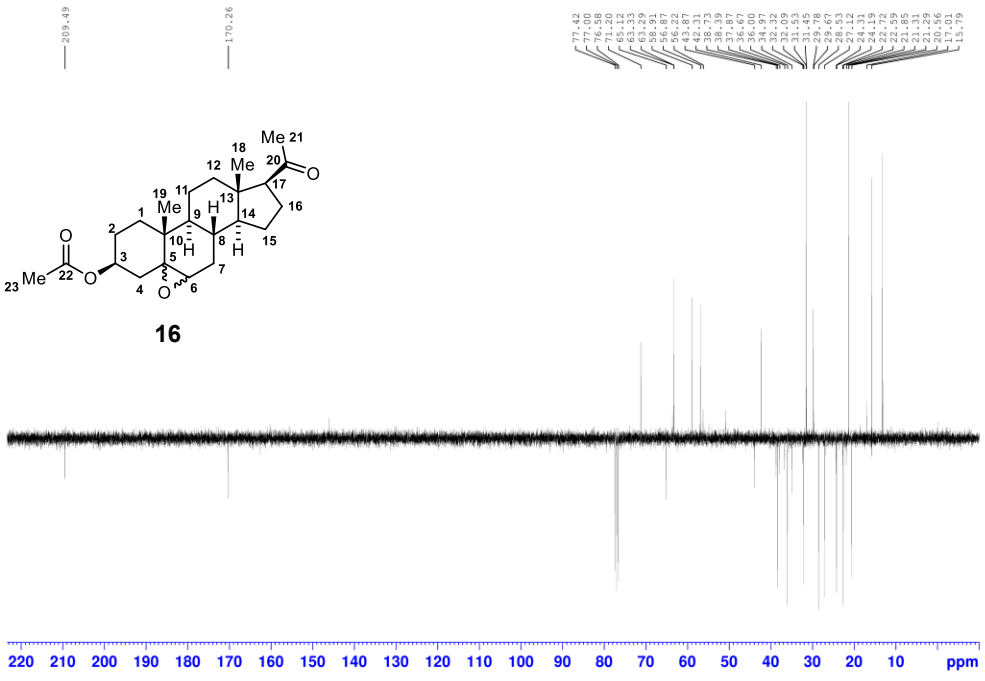

Figure A2. ^{13}C NMR spectrum (75 MHz, $CDCl_3$) of 3ß-acetoxy-5,6-epoxypregnan-20-one (**16**).

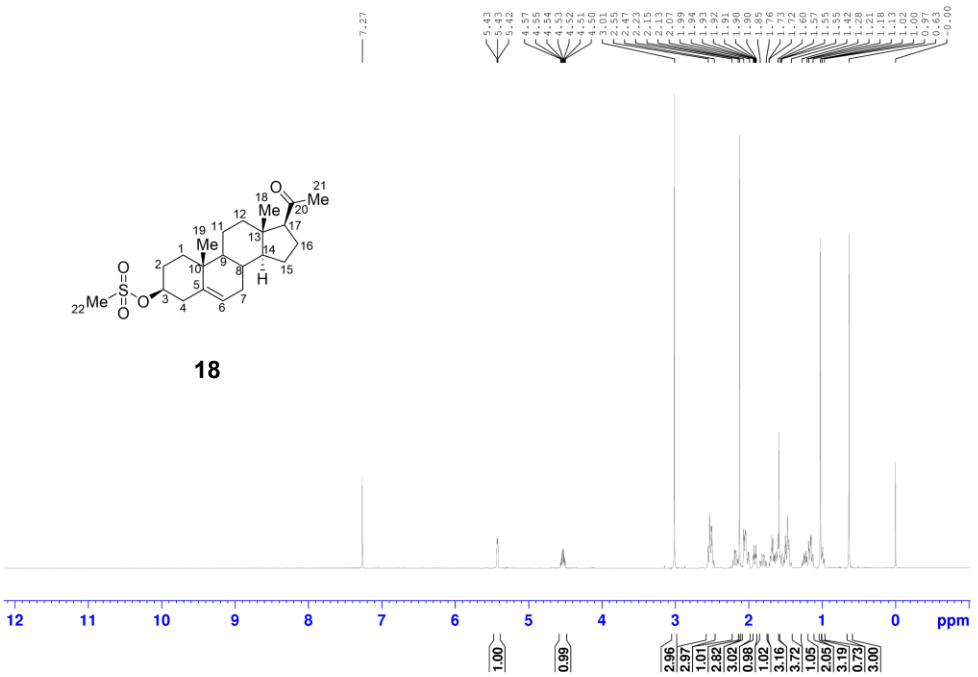

Figure A3. ^{1}H NMR (500 MHz, $CDCl_3$) spectrum of pregn-5-en-20-one, 3*β*-hydroxy-, methane-sulfonate (**18**).

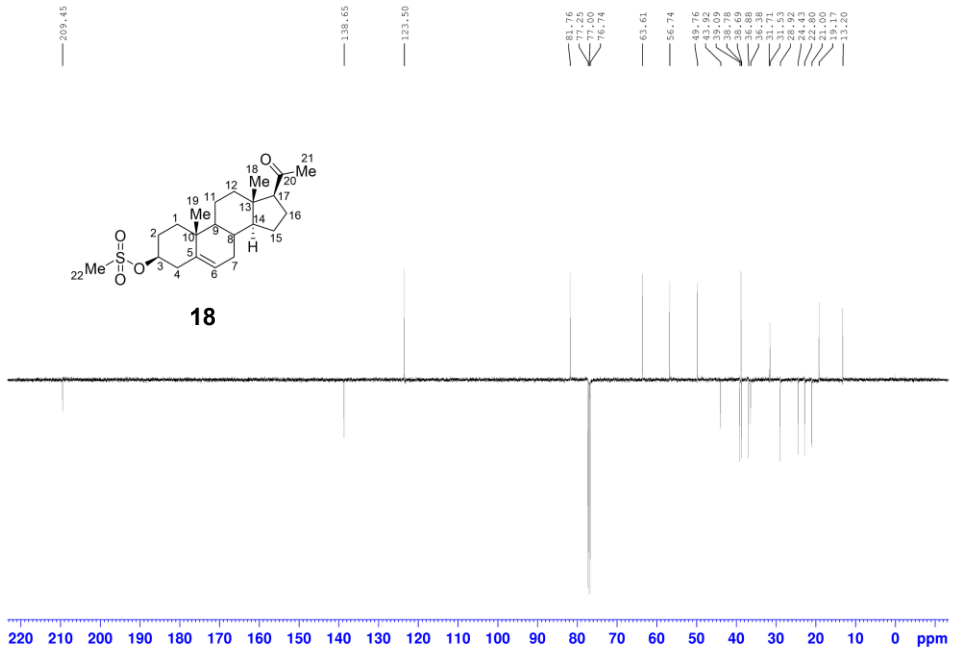

Figure A4. ^{13}C NMR spectrum (126 MHz, $CDCl_3$) spectrum of pregn-5-en-20-one, 3*β*-hydroxy-, methane-sulfonate (**18**).

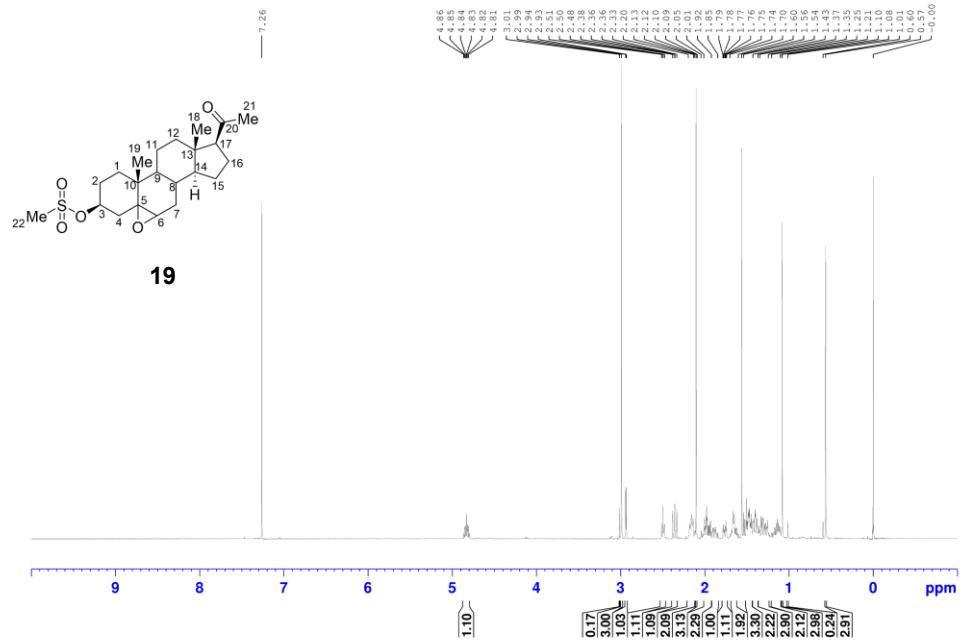

Figure A5. ^{1}H NMR (500 MHz, $CDCl_3$) spectrum of (3*β*,5*α*,6*α*)-5,6-epoxy-3-[(methylsulfonyl)oxy]pregnan-20-one (**19**).

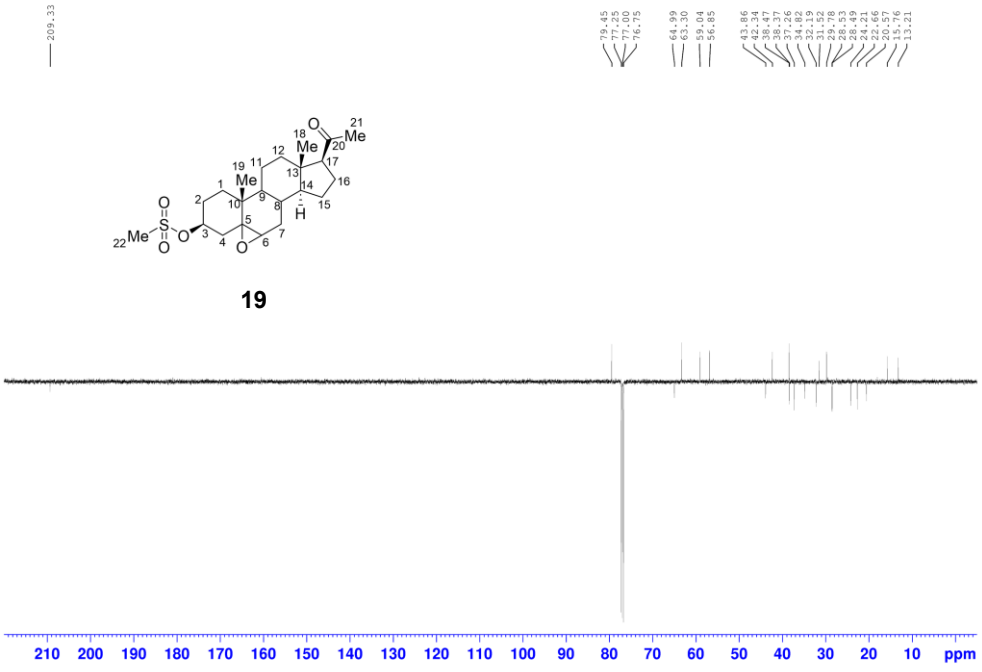

Figure A6. ^{13}C NMR spectrum (126 MHz, $CDCl_3$) spectrum of (3*β*)-5,6-epoxy-3-[(methylsulfonyl)oxy]pregnan-20-one (**19**).

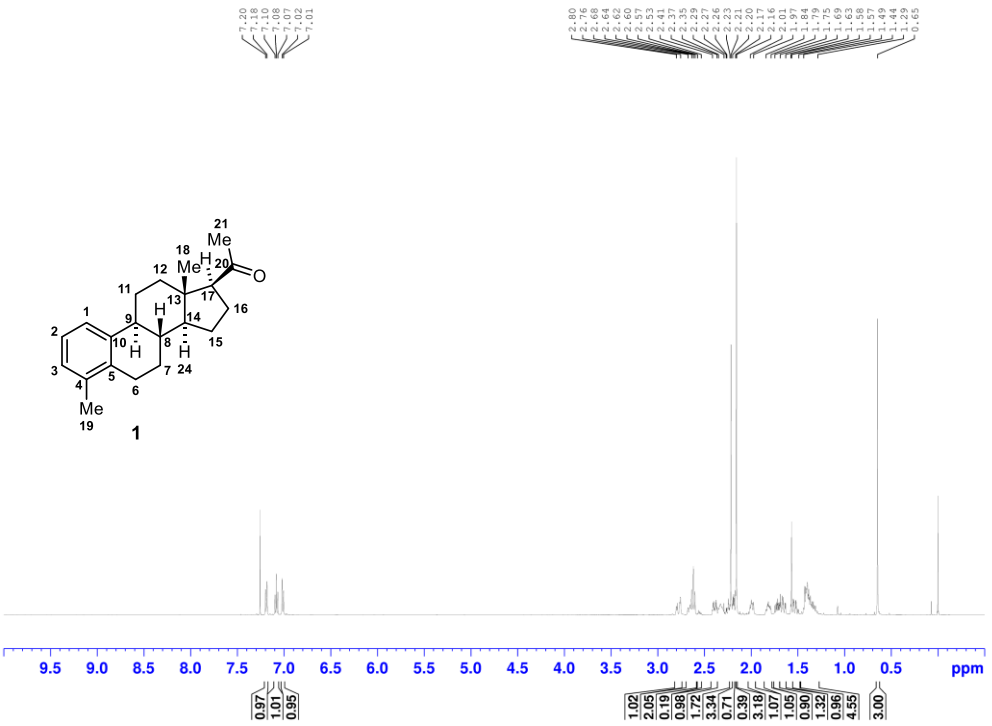

Figure A7. ^{1}H NMR (500 MHz, $CDCl_3$) spectrum of S42 (**1**).

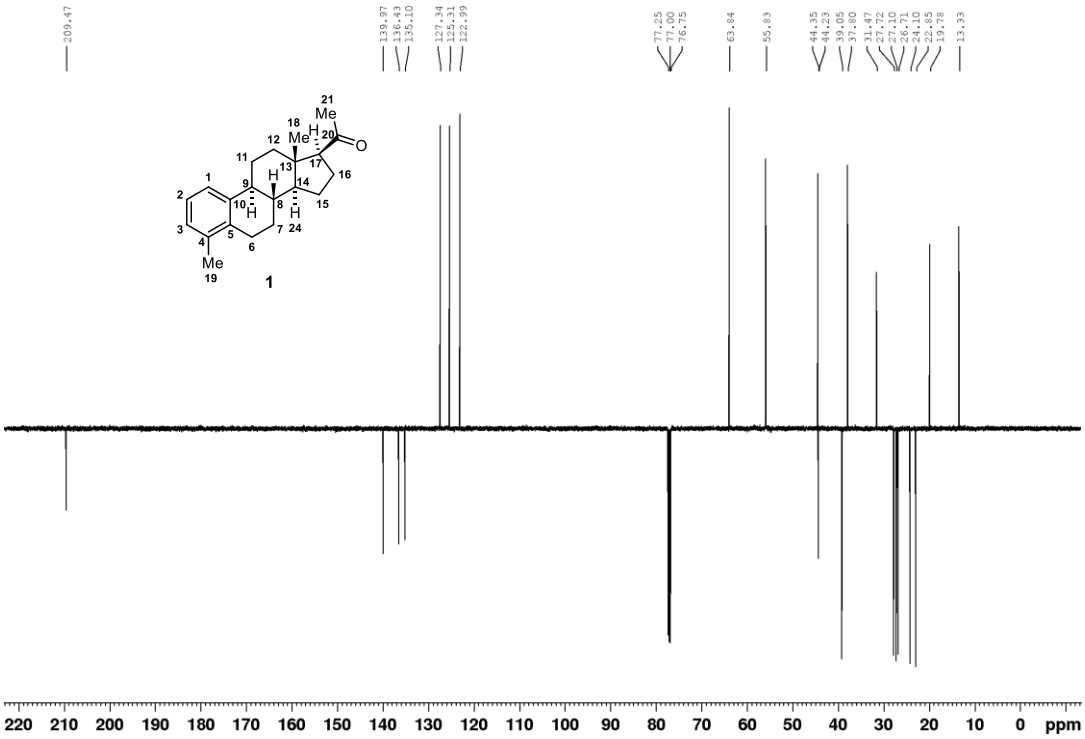

Figure A8. ^{13}C NMR (126 MHz, $CDCl_3$) spectrum of S42 (**1**).

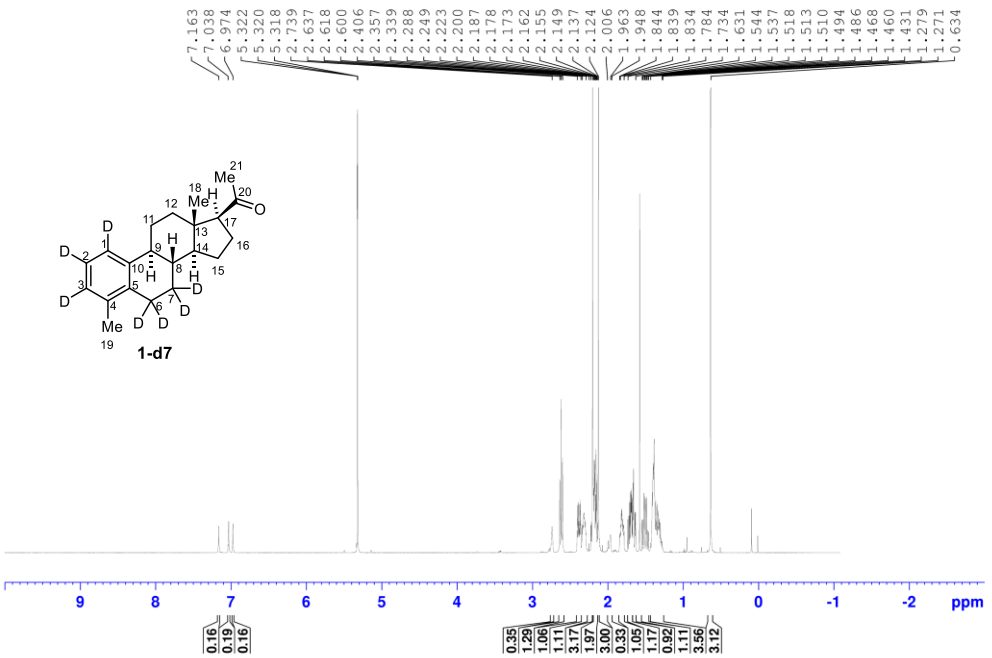

Figure A9. ^{1}H NMR spectrum (500 MHz, CD_2Cl_2) of S42-d7 (**1-d7**).

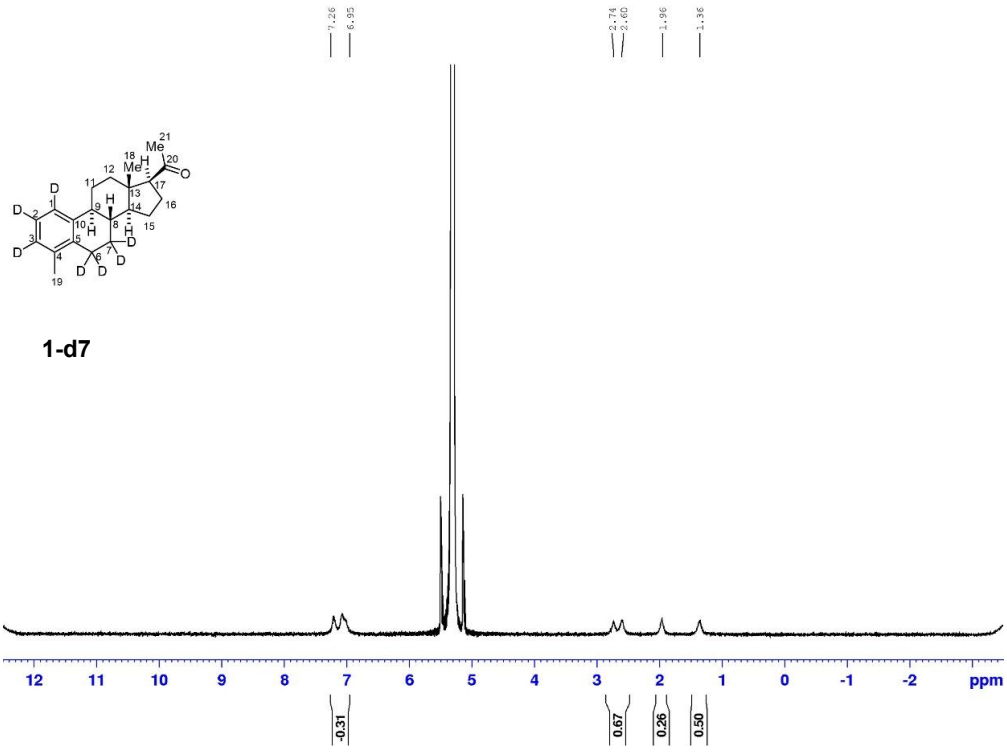

Figure A10. ^{2}H NMR spectrum (77 MHz, CD_2Cl_2) of S42-d7 (**1-d7**).

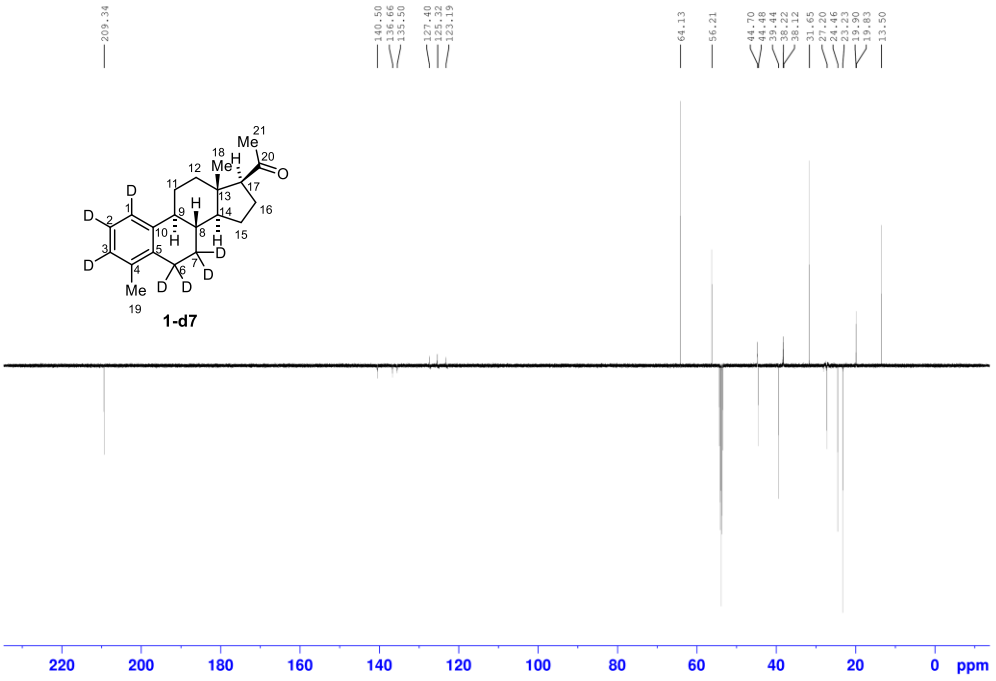

Figure A11. ^{13}C NMR spectrum (126 MHz, CD_2Cl_2) of S42-d7 (**1-d7**).

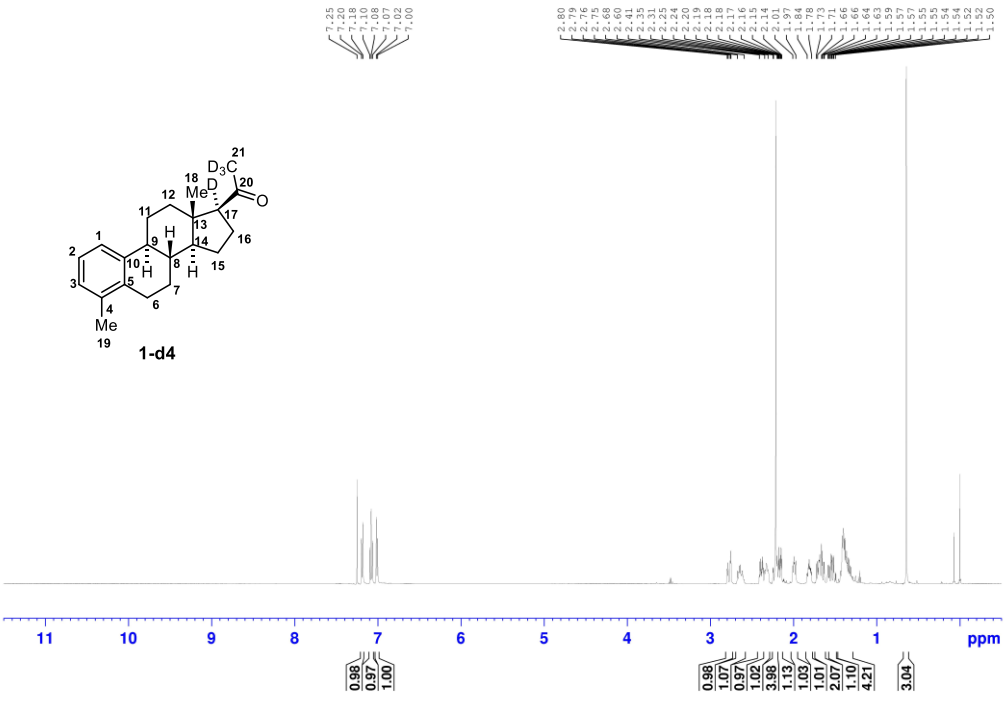

Figure A12. ^{1}H NMR (500 MHz, $CDCl_3$) spectrum of S42-d4 (**1-d4**).

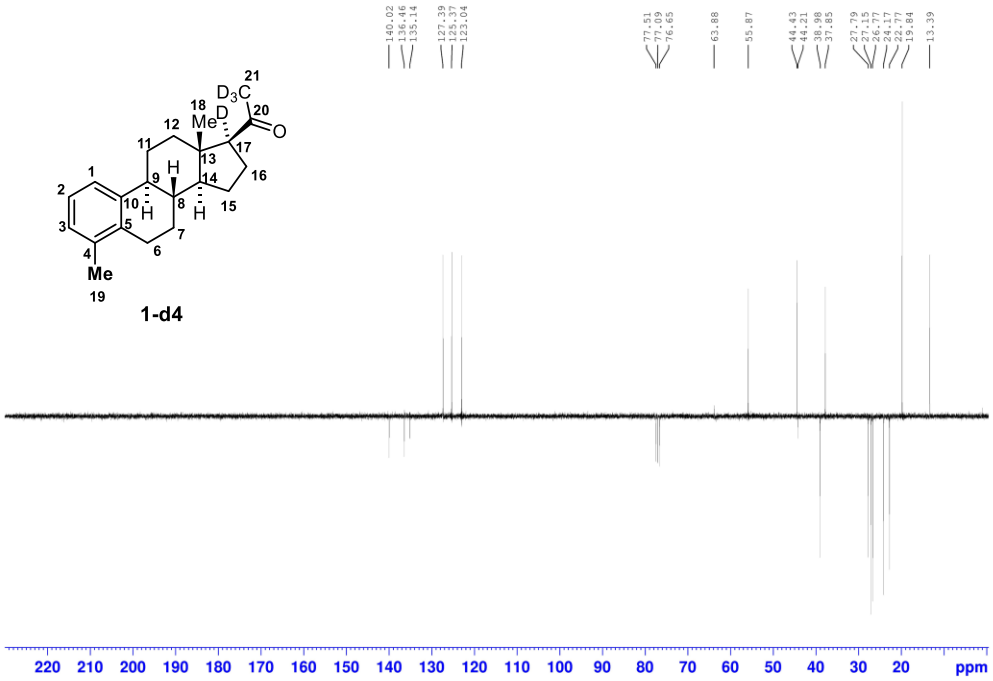

Figure A13. ^{13}C NMR (75 MHz, $CDCl_3$) spectrum of S42-d4 (**1-d4**).

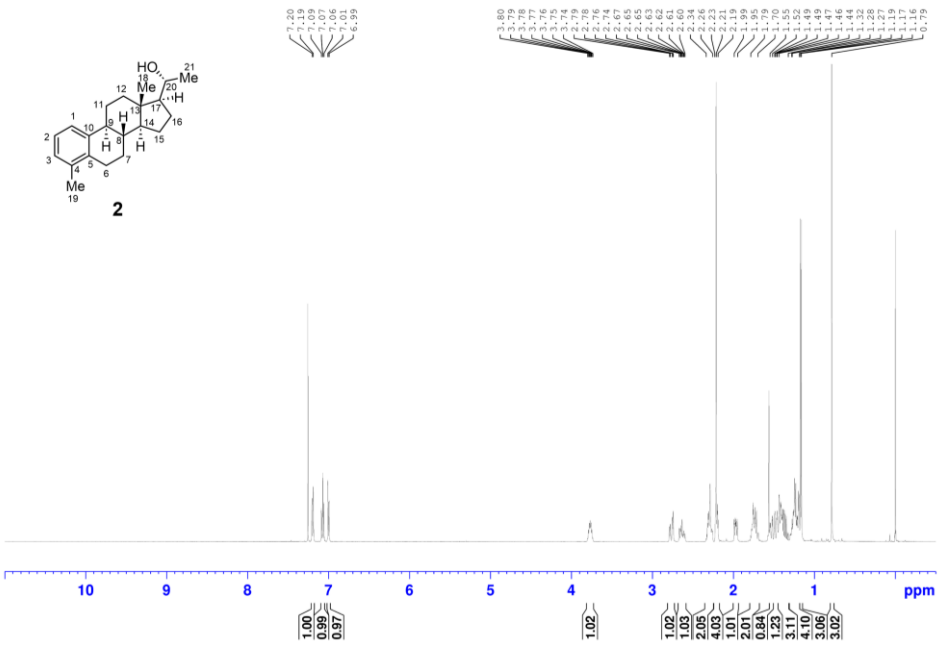

Figure A14. ^{1}H NMR (500 MHz, $CDCl_3$) spectrum of compound **2**.

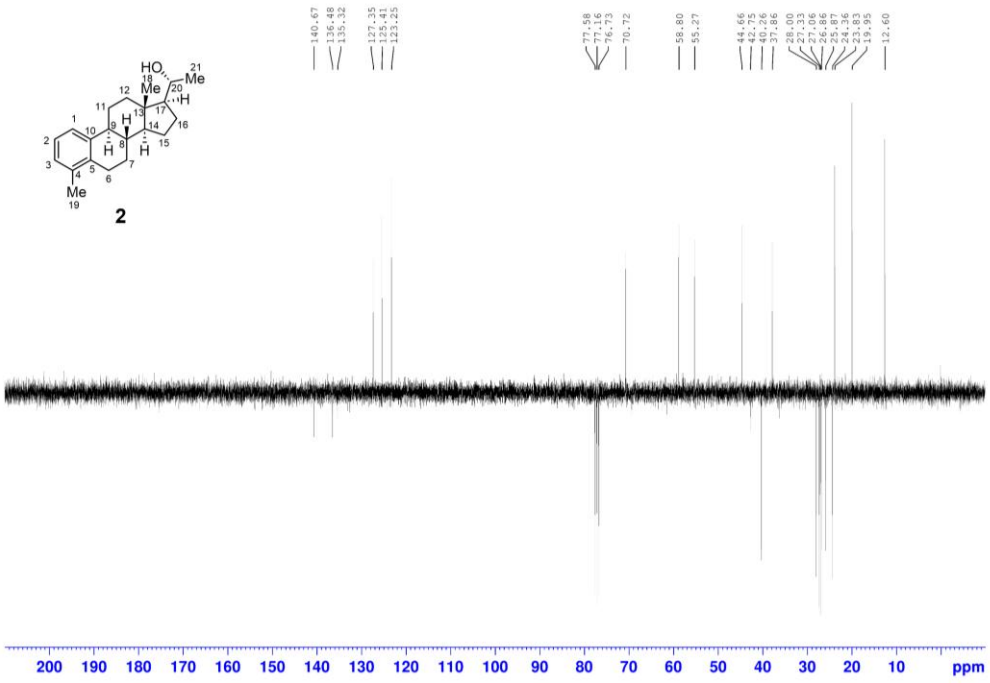

Figure A15. ^{13}C NMR (75 MHz, $CDCl_3$) spectrum of compound **2**.

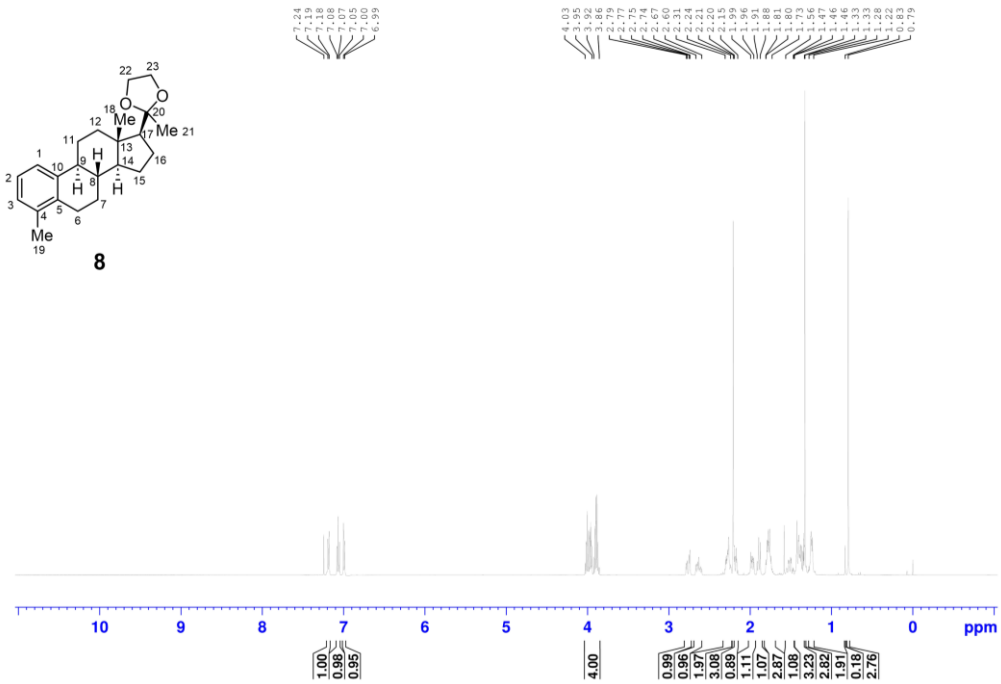

Figure A16. ^{1}H NMR (500 MHz, $CDCl_3$) spectrum of compound **8**.

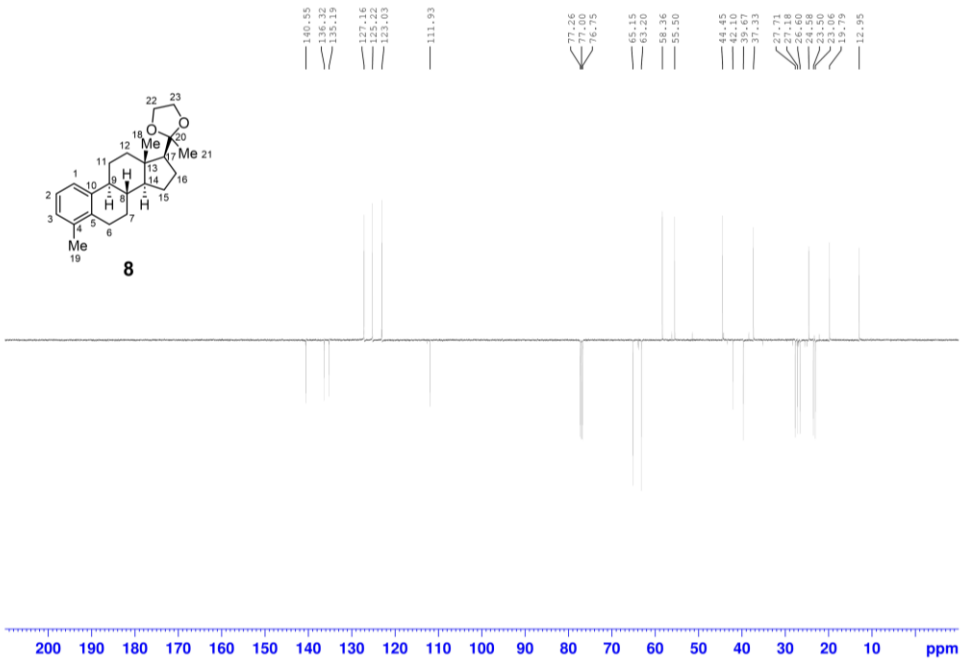

Figure A17. ^{13}C NMR (126 MHz, $CDCl_3$) spectrum of compound **8**.

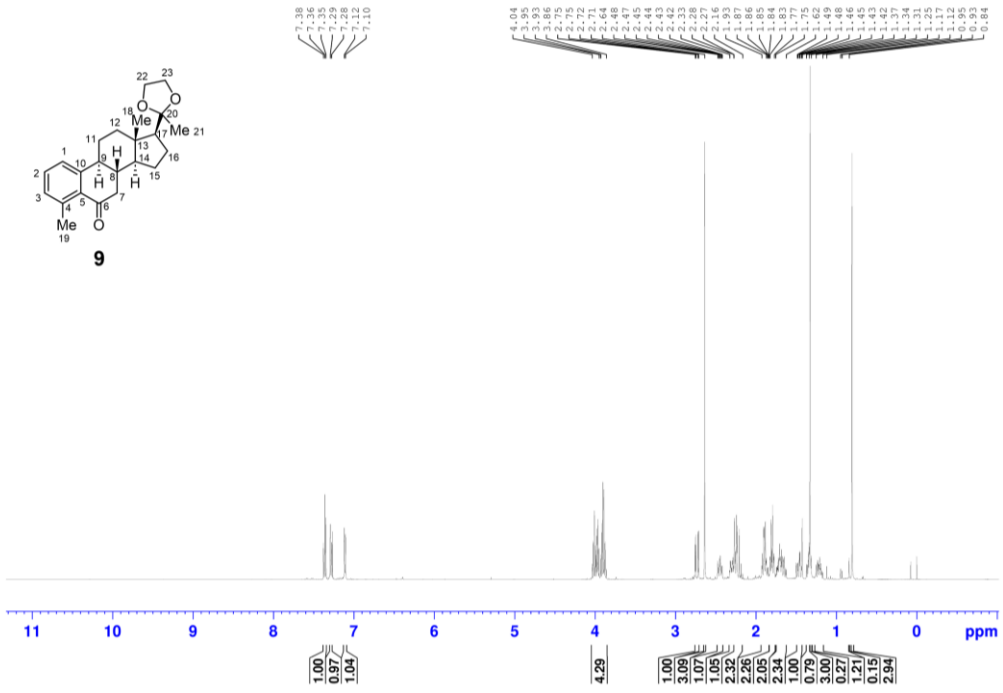

Figure A18. ^{1}H NMR (500 MHz, $CDCl_3$) spectrum of compound **9**.

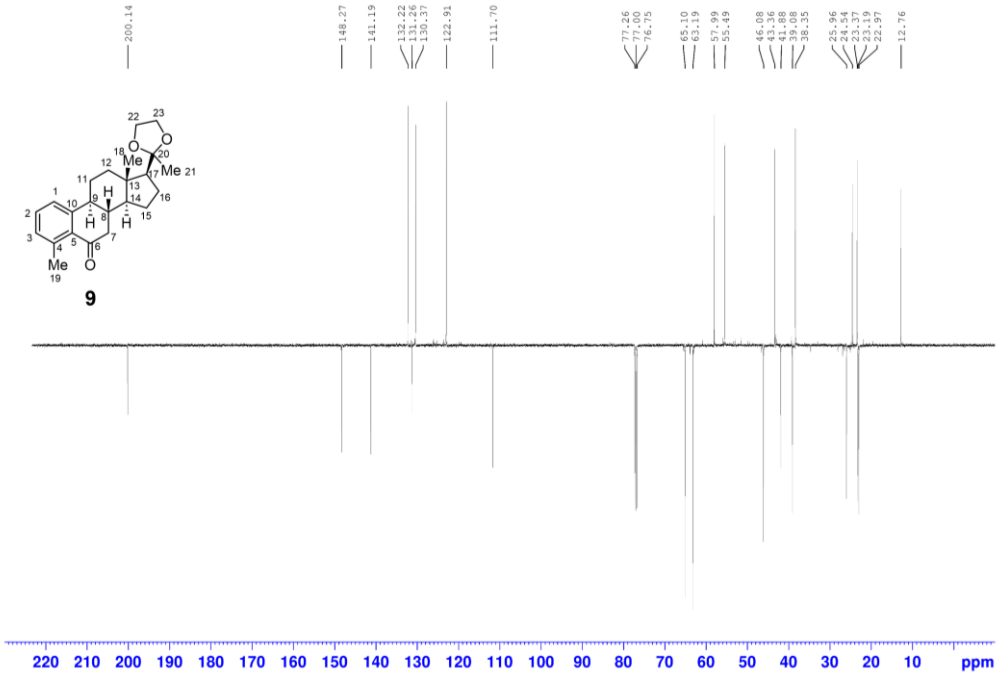

Figure A19. ^{13}C NMR (126 MHz, $CDCl_3$) spectrum of compound **9**.

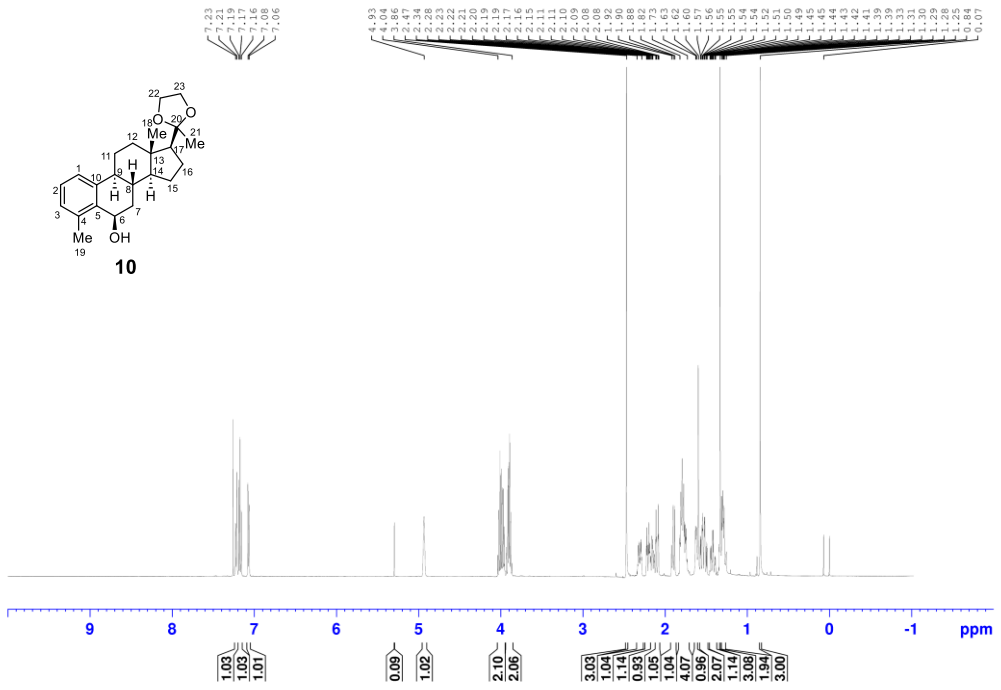

Figure A20. ^{1}H NMR (500 MHz, $CDCl_3$) spectrum of compound **10**. A solvent peak from CH_2Cl_2.was found at 5.3 ppm.

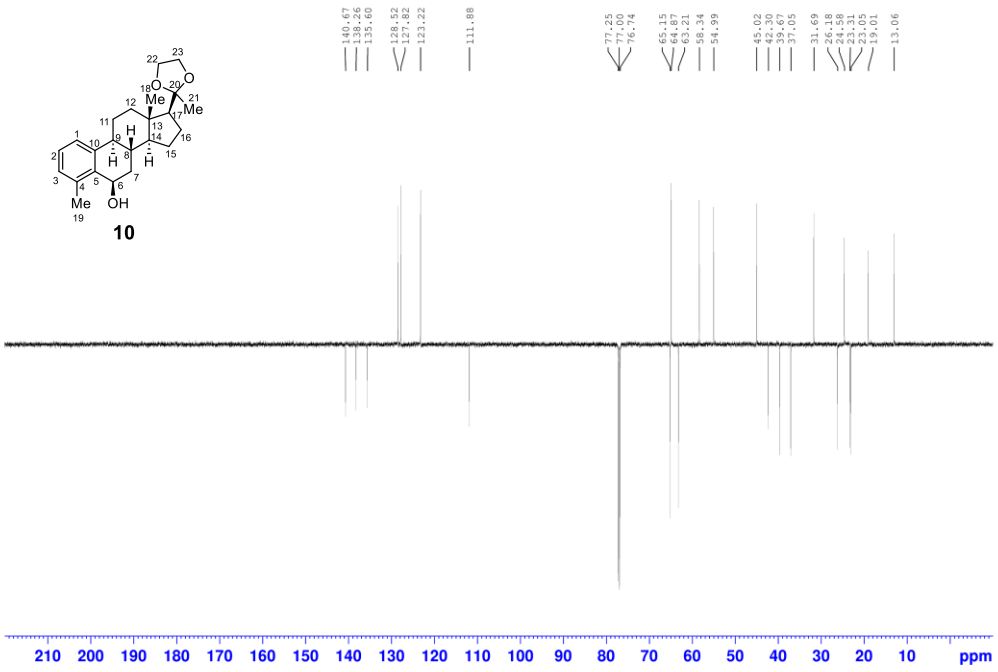

Figure A21. ^{13}C NMR (126 MHz, $CDCl_3$) spectrum of compound **10**.

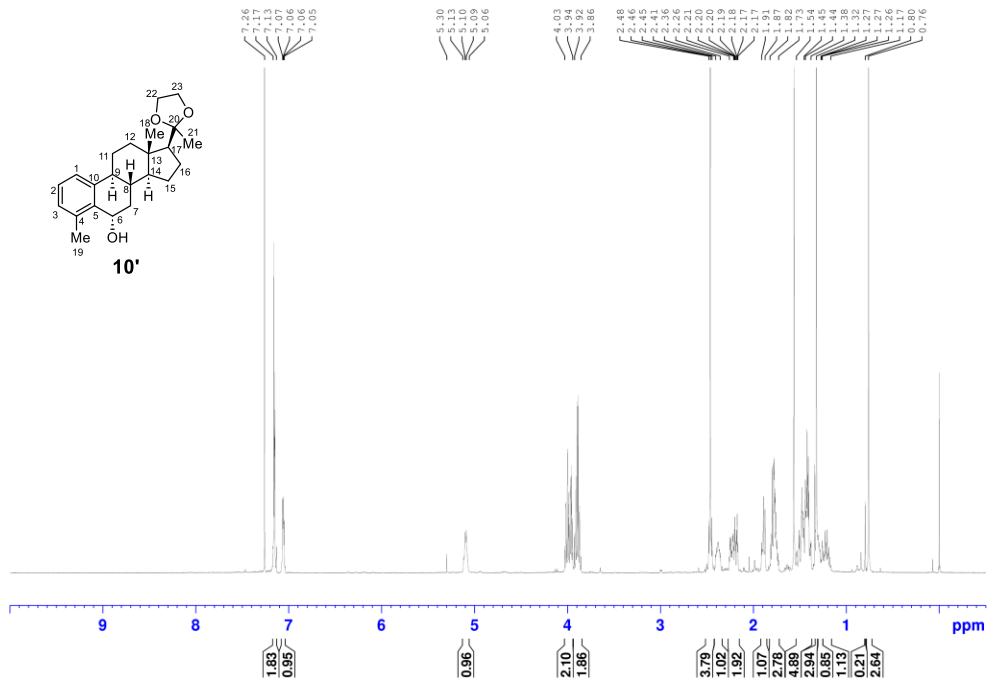

Figure A22. ^{1}H NMR (500 MHz, $CDCl_3$) spectrum of compound **10'**. A solvent peak from CH_2Cl_2.was found at 5.3 ppm.

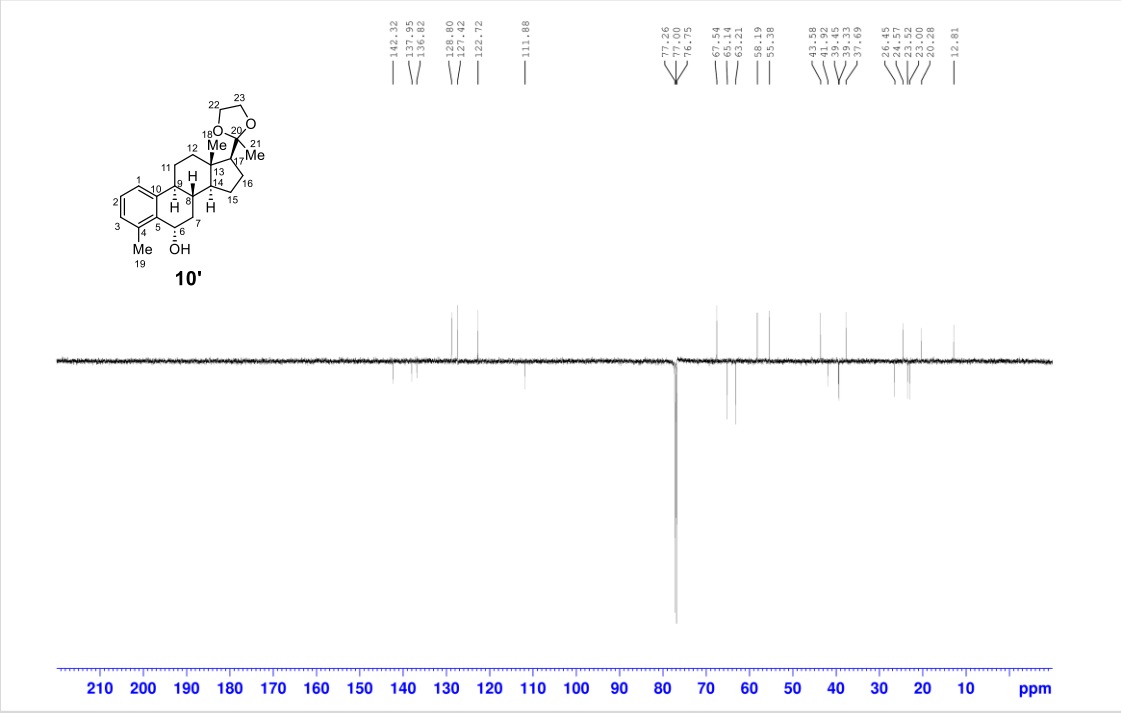

Figure A23. ^{13}C NMR (126 MHz, $CDCl_3$) spectrum of compound **10'**.

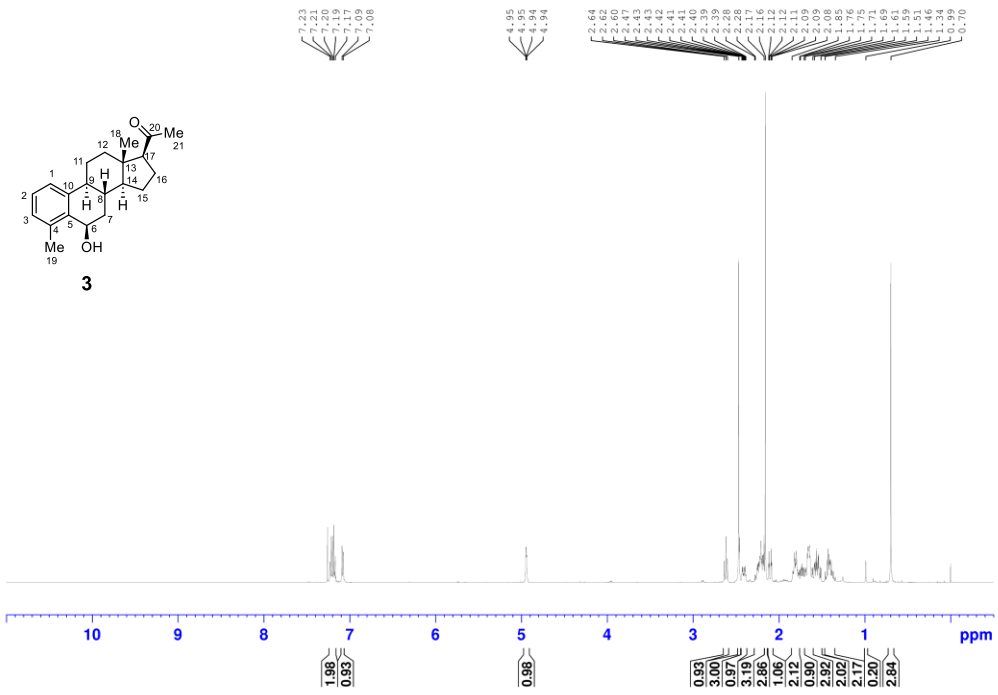

Figure A24. ^{1}H NMR (500 MHz, $CDCl_3$) spectrum of compound **3**.

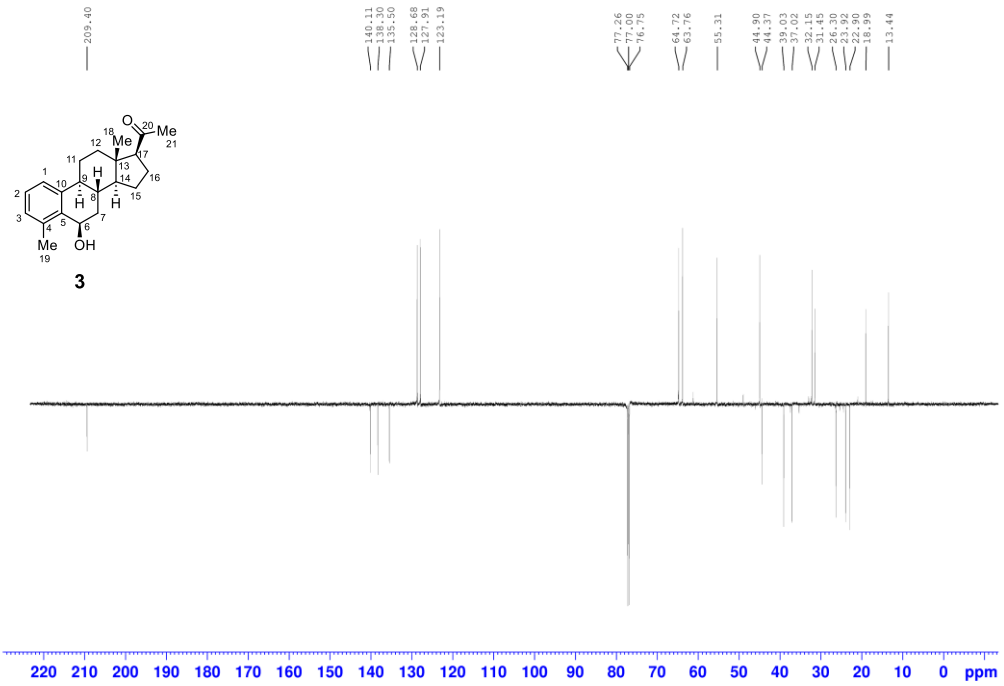

Figure A25. ^{13}C NMR (126 MHz, $CDCl_3$) spectrum of compound **3**.

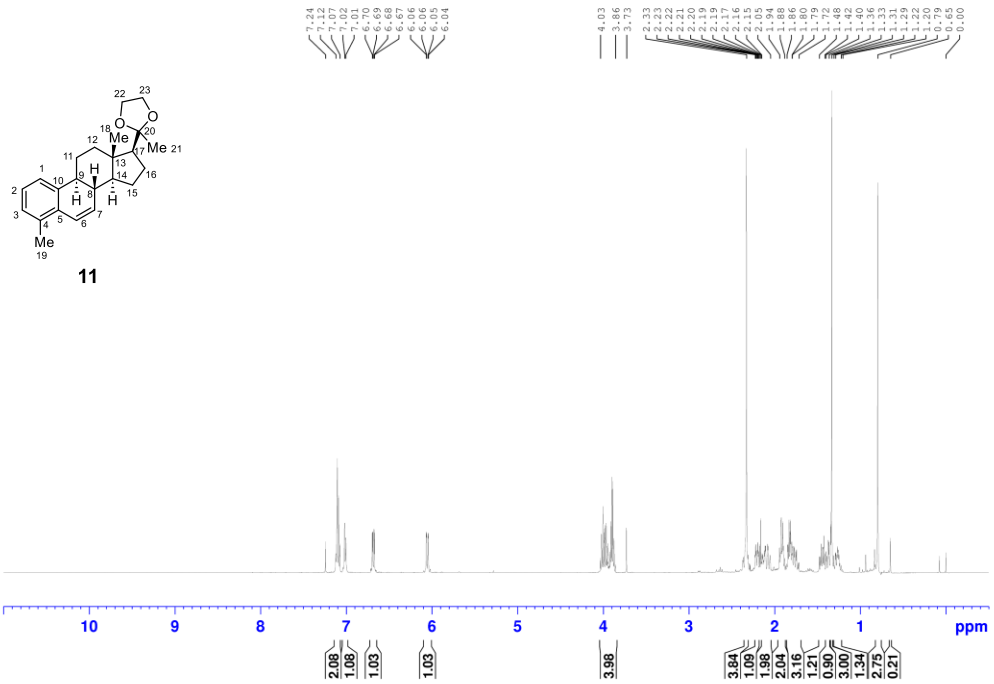

Figure A26. ^{1}H NMR (500 MHz, $CDCl_3$) spectrum of compound **11**.

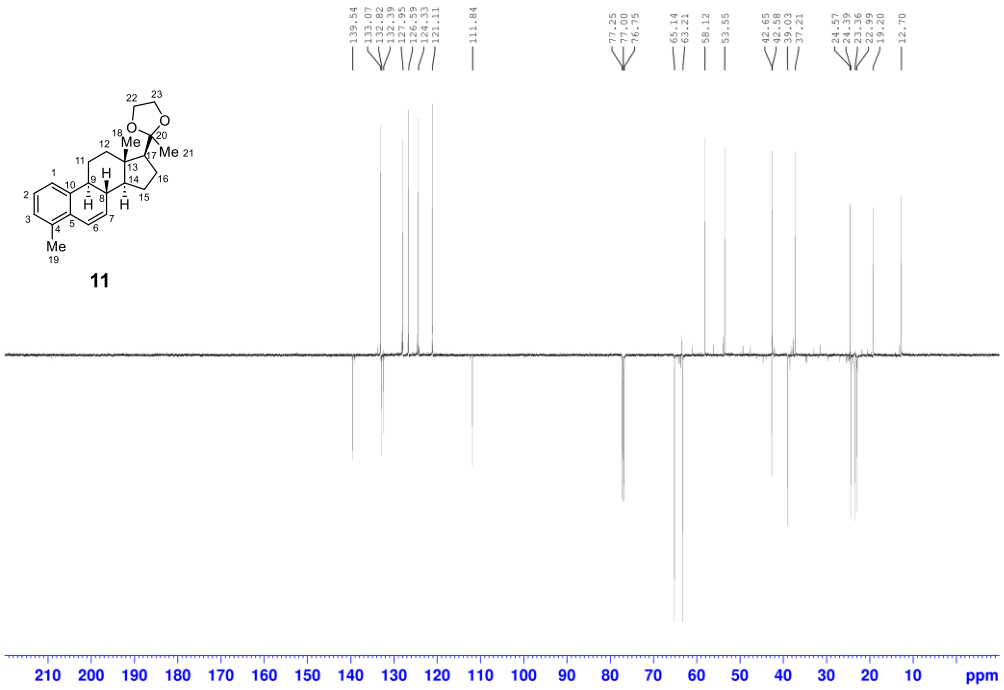

Figure A27. ^{13}C NMR (126 MHz, $CDCl_3$) spectrum of compound **11**.

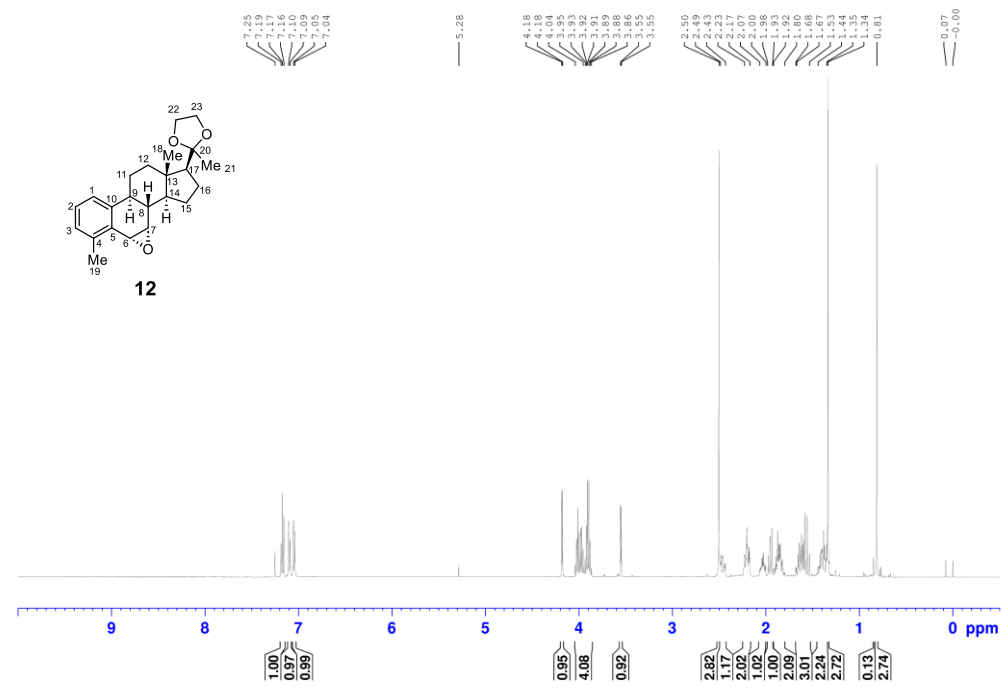

Figure A28. ^{1}H NMR (500 MHz, $CDCl_3$) spectrum of compound **12**. A solvent peak from CH_2Cl_2.was found at 5.3 ppm.

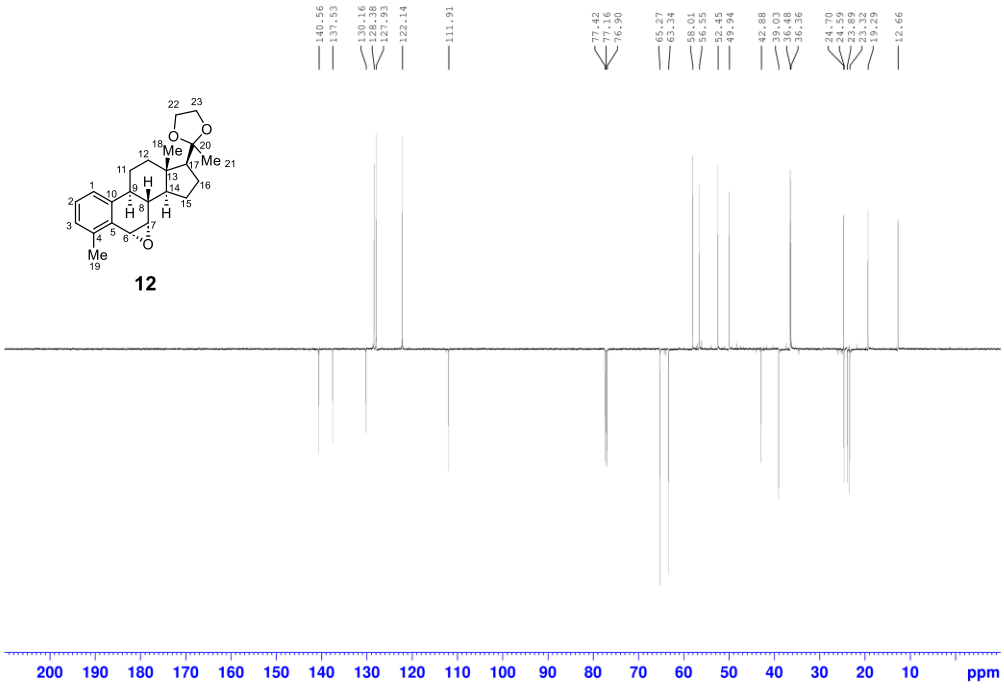

Figure A29. ^{13}C NMR (126 MHz, $CDCl_3$) spectrum of compound **12**.

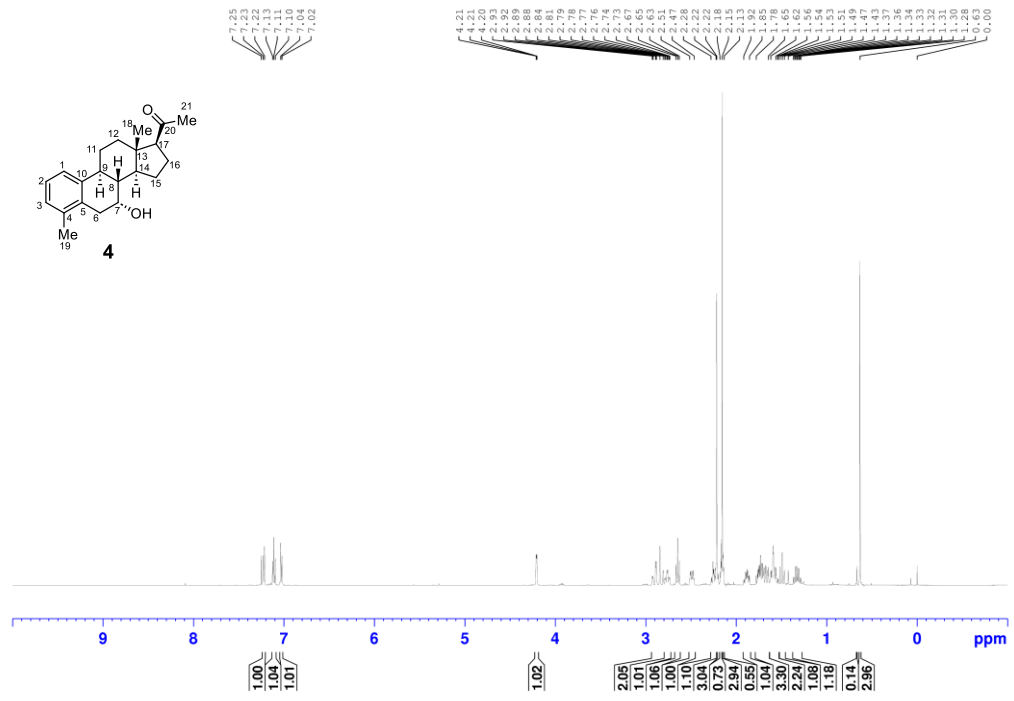

Figure A30. ^{1}H NMR (500 MHz, $CDCl_3$) spectrum of compound **4**.

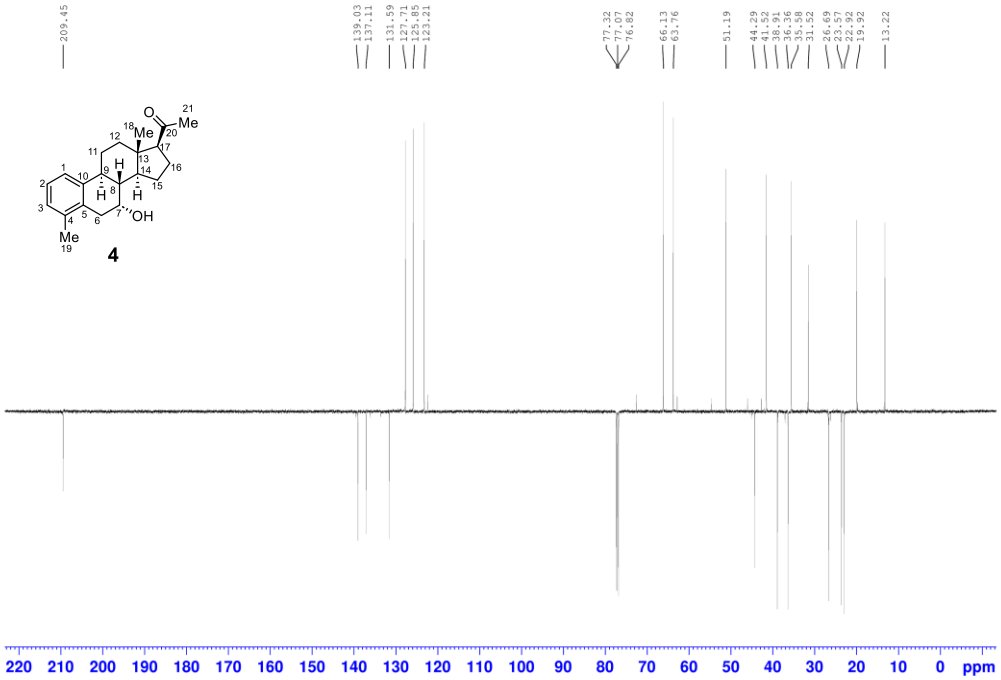

Figure A31. ^{13}C NMR (126 MHz, $CDCl_3$) spectrum of compound **4**.

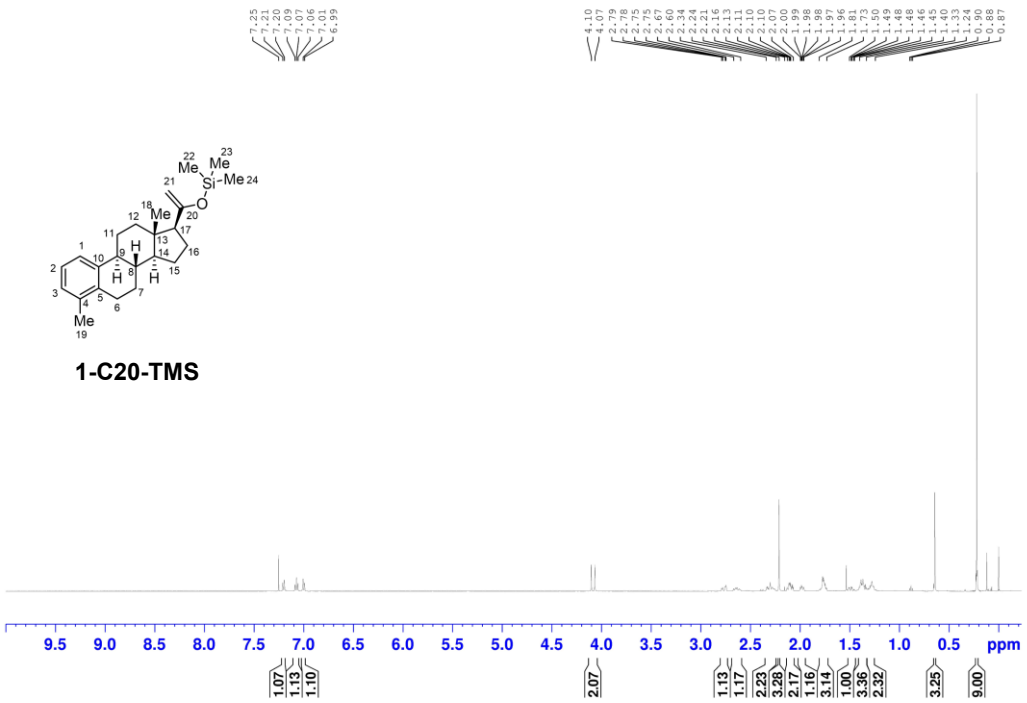

Figure A32. 1H NMR (500 MHz, CDCl3) spectrum of S42-C20-TMS (**1-C20-TMS**).

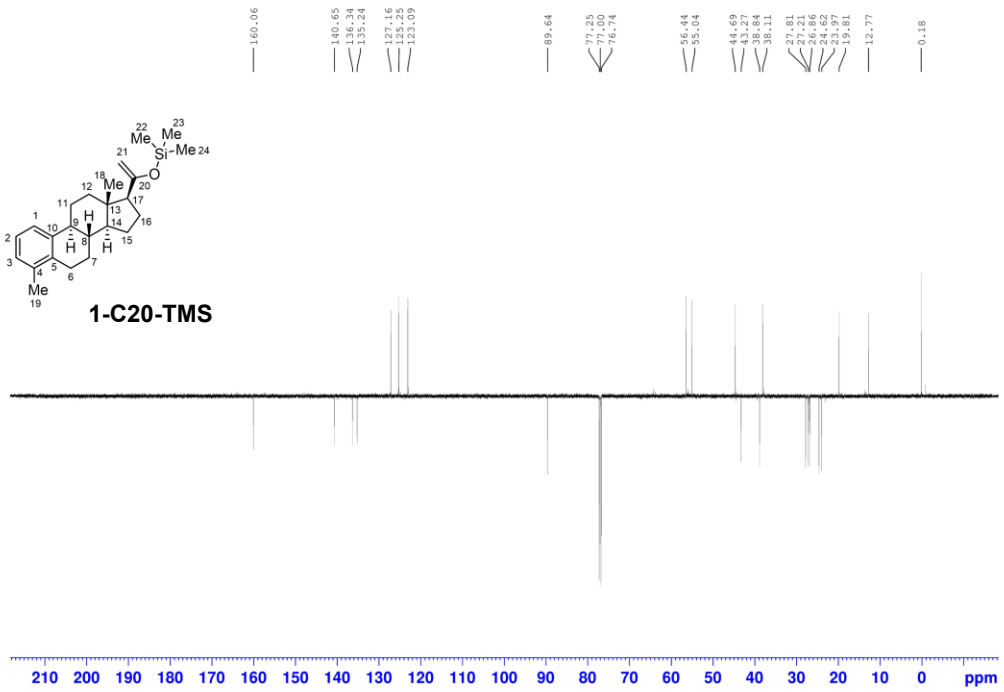

Figure A33. ^{13}C NMR (126 MHz, CDCl3) spectrum of S42-C20-TMS (**1-C20-TMS**).

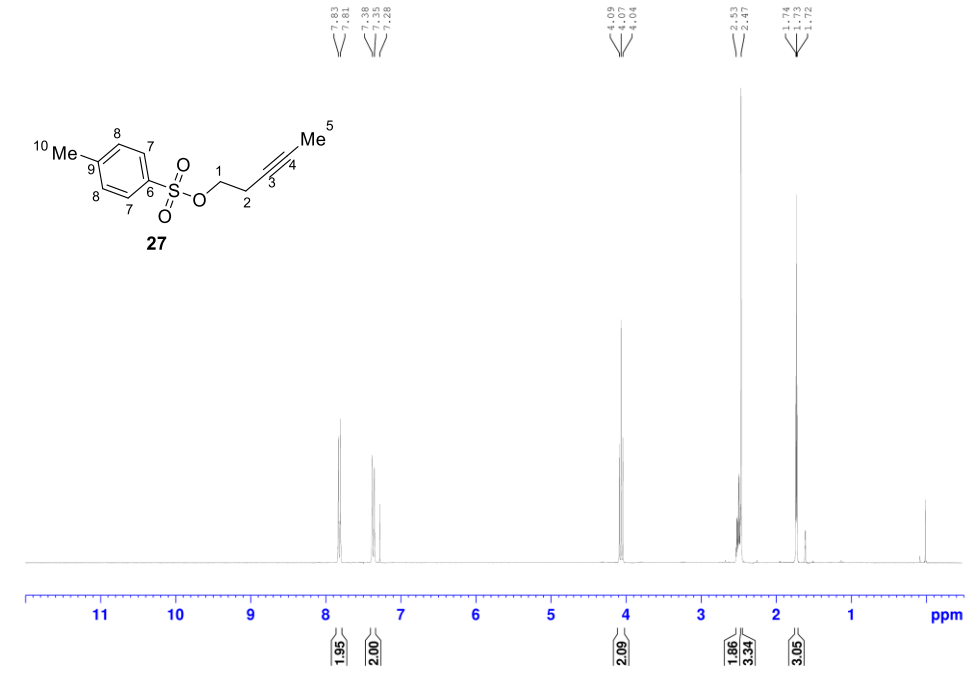

Figure A34. ^{1}H NMR (300 MHz, $CDCl_3$) spectrum of 3-pentyn-1-ol, 1-(4-methylbenzenesulfonate) (**27**).

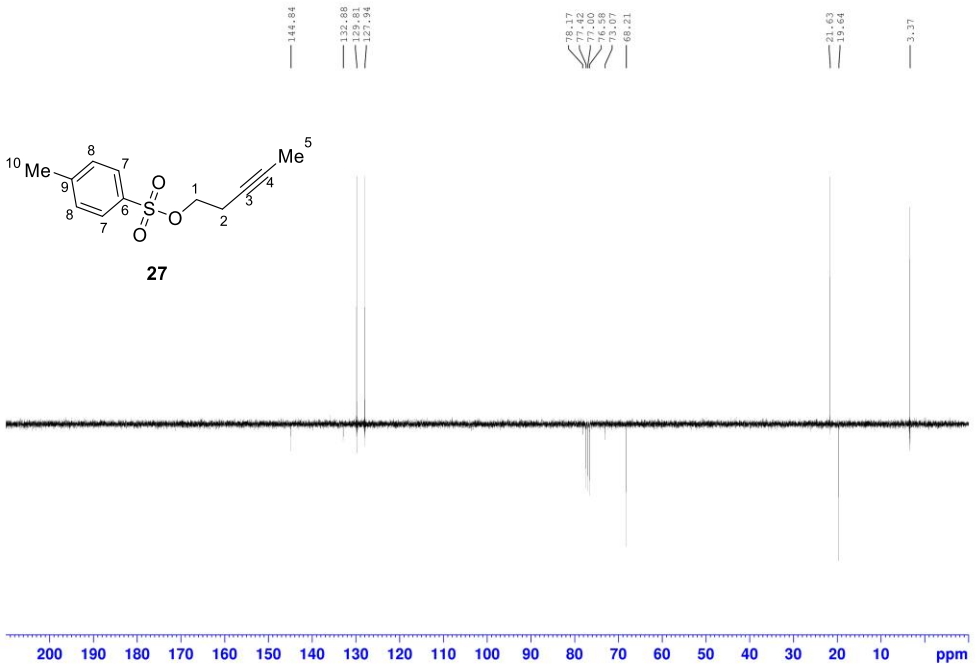

27

Figure A35. ^{13}C NMR spectrum (75 MHz, $CDCl_3$) of 3-pentyn-1-ol, 1-(4-methylbenzenesulfonate) (**27**).

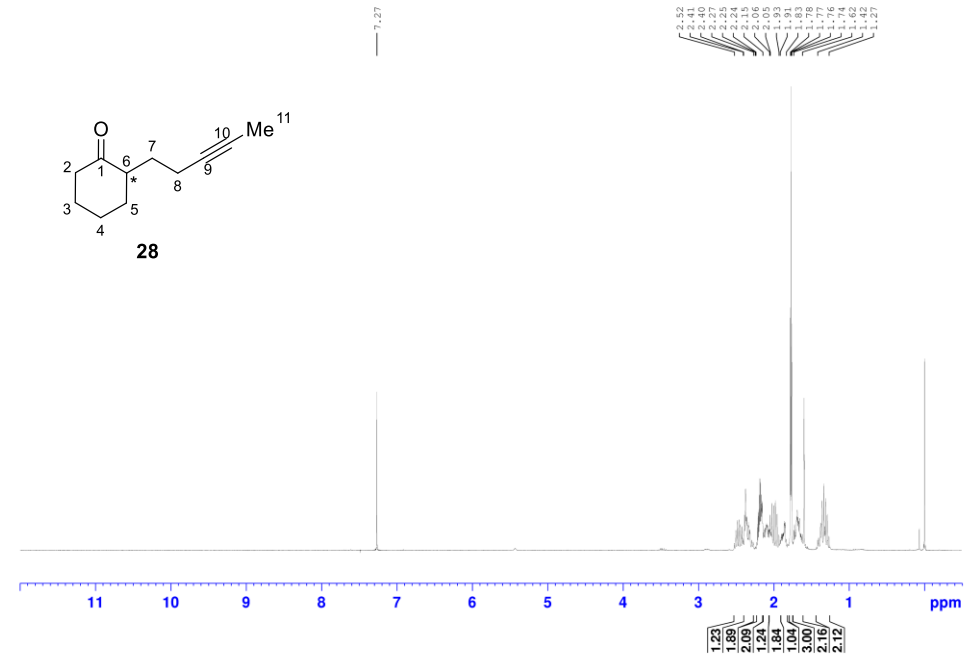

28

Figure A36. ^{1}H NMR (300 MHz, $CDCl_3$) spectrum of 2-(3-pentynyl)cyclohexanone (**28**).

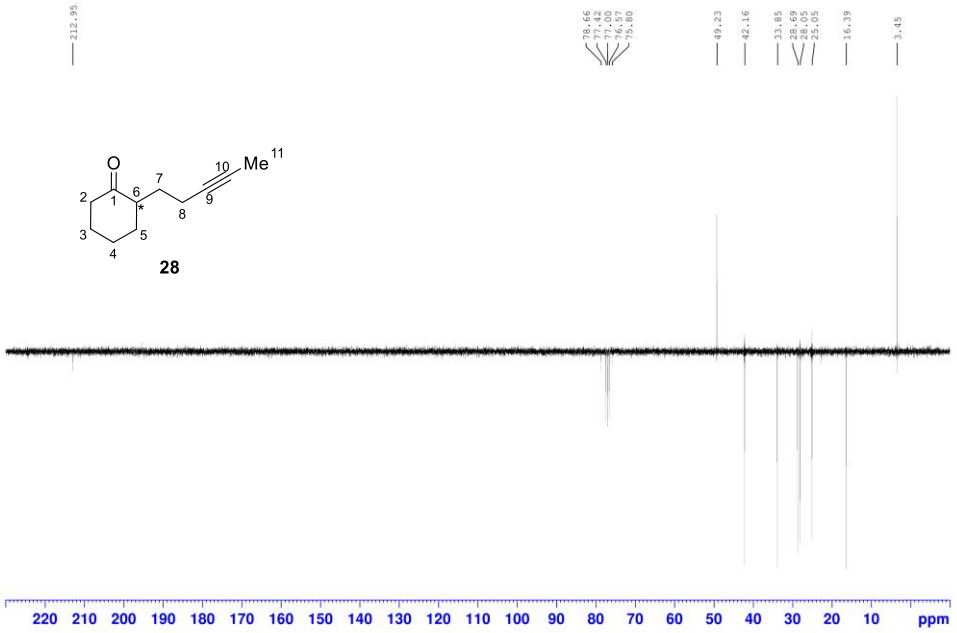

Figure A37 ^{13}C NMR spectrum (75 MHz, $CDCl_3$) of 2-(3-pentynyl)cyclohexanone (**28**).

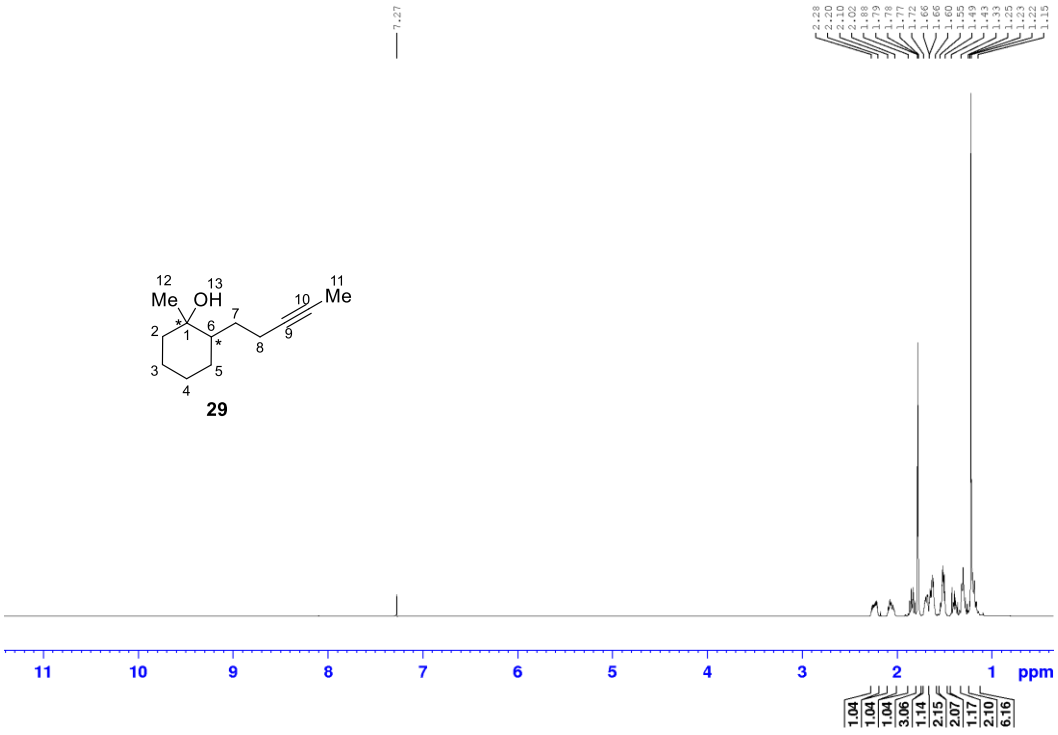

Figure A38. ^{1}H NMR (500 MHz, $CDCl_3$) spectrum of methyl-2-(3-pentynyl)cyclohexanol isomer **29**.

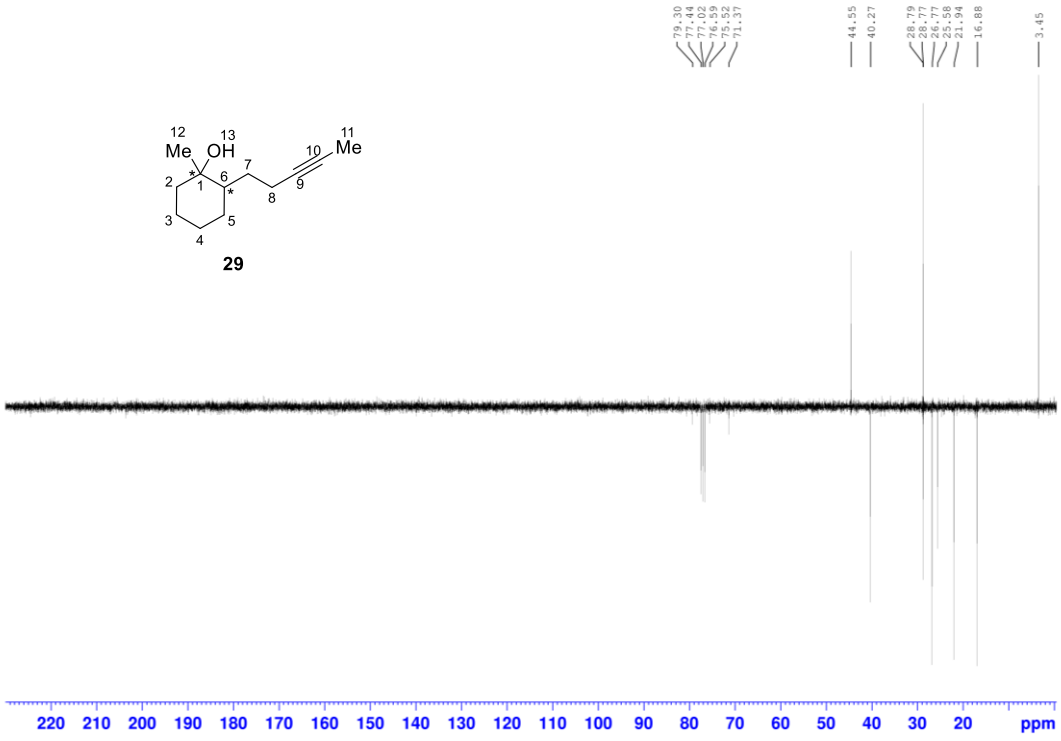

Figure A39. ^{13}C NMR (75 MHz, $CDCl_3$) spectrum of methyl-2-(3-pentynyl)cyclohexanol isomer **29**.

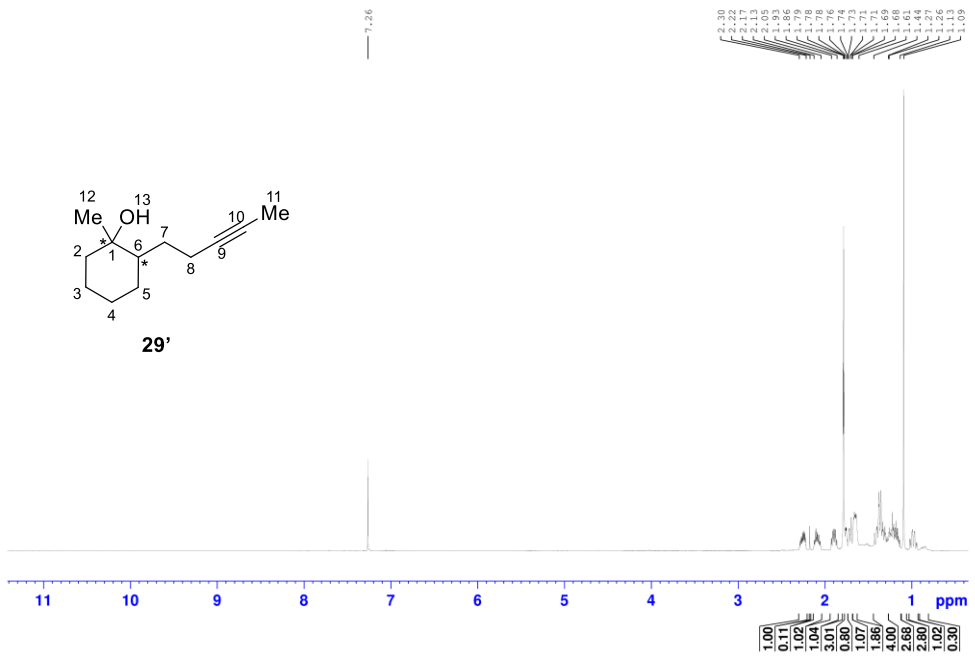

Figure A40. ^{1}H NMR (500 MHz, $CDCl_3$) spectrum of methyl-2-(3-pentynyl)cyclohexanol isomer (**29**').

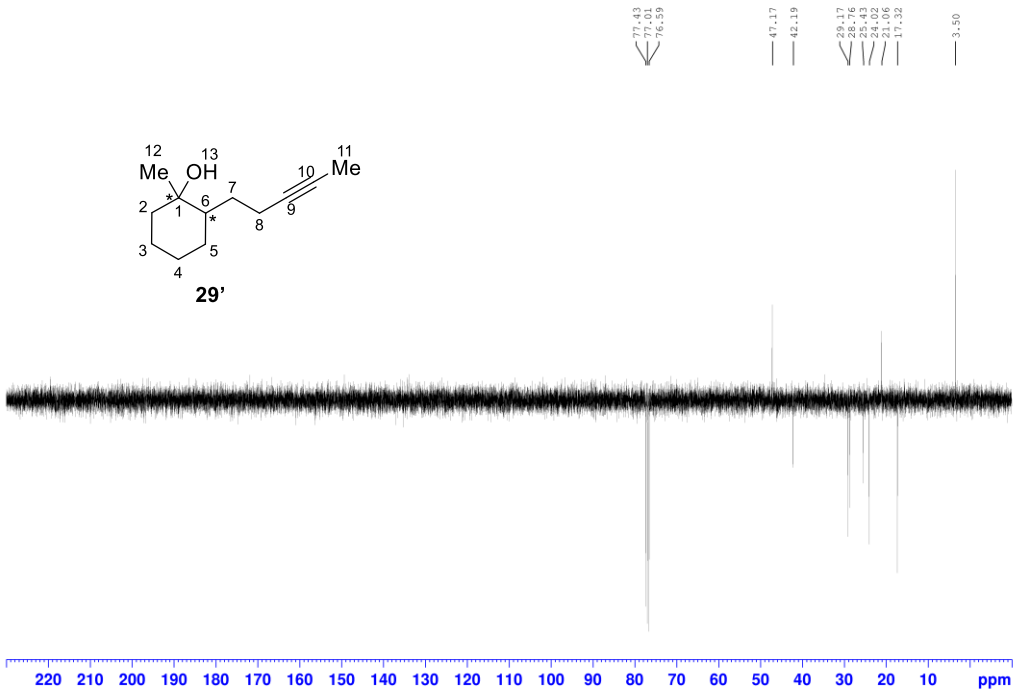

Figure A 41. ^{13}C NMR (75 MHz, $CDCl_3$) spectrum of methyl-2-(3-pentynyl)cyclohexanol isomer (**29**').

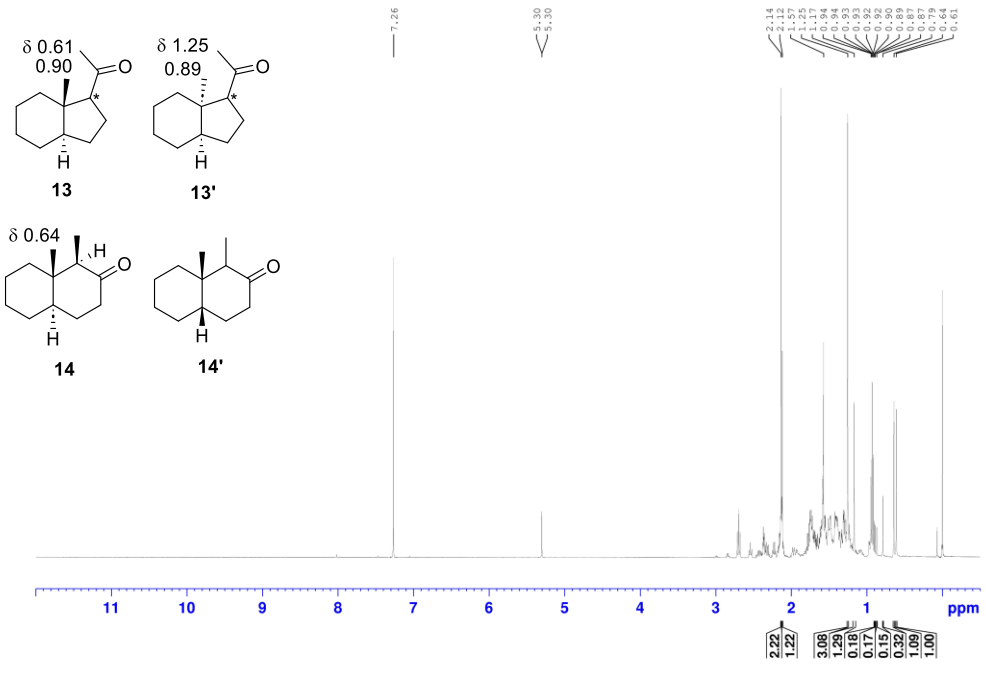

Figure A42. ^{1}H NMR (500 MHz, $CDCl_3$) spectrum of hydrindane derivatives **13, 13'** and substance **14, 14'** mixture.

9.3. MS data

9.3.1 Chromatograms and MS spectra of compound **14**

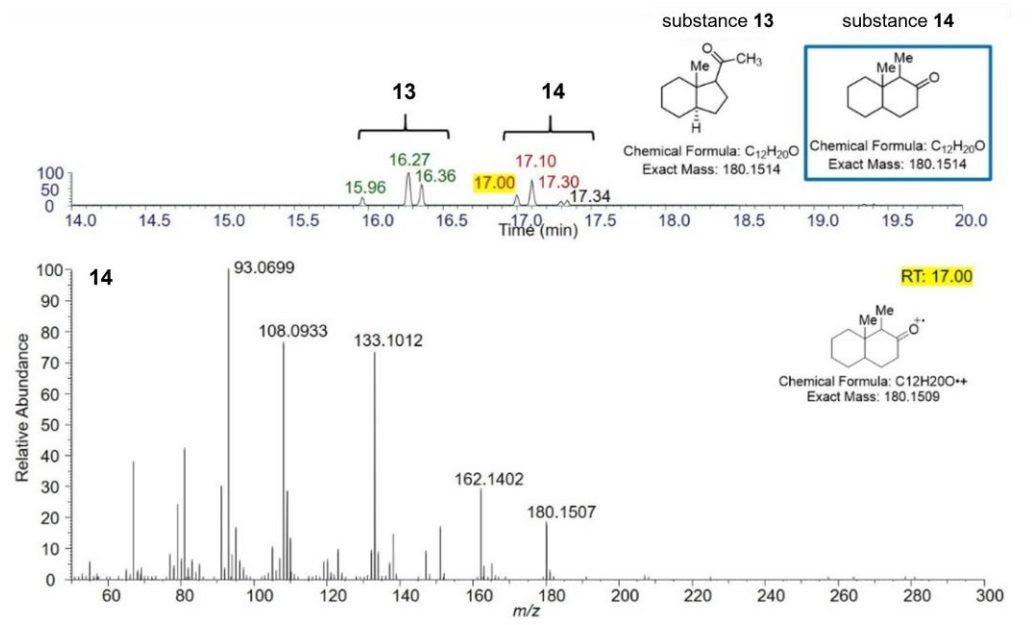

Figure A43. Chromatograms and spectrum of 1-methyloctahydro-2(1H)-one (**14**). The spectrum shows the substance at a retention time of 17.00 min. The peaks from fraction of substances **14** (RT: 17.00, 17.10 and 17.30 min) have similar spectra. The sample was analyzed at the University of Cologne.

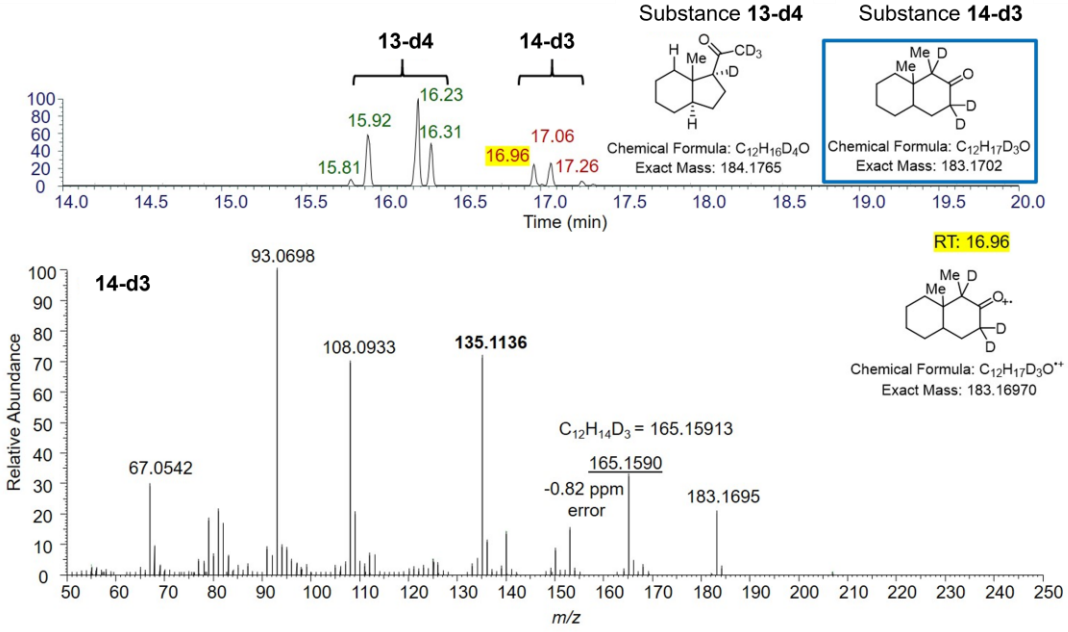

Figure A44. GC-EI-HRMS analysis and spectrum of deuterated 1-methyloctahydro-2(1H)-one (**14-d3**). The analyte is detected at a retention time of 16.96 min. The fractions of isomers of **14-d3** (RT= 16.96, 17.06, and 17.26) have similar EI-HRMS spectra.

9.3.2 Chromatograms and MS spectra of silylated S42 (**1**)

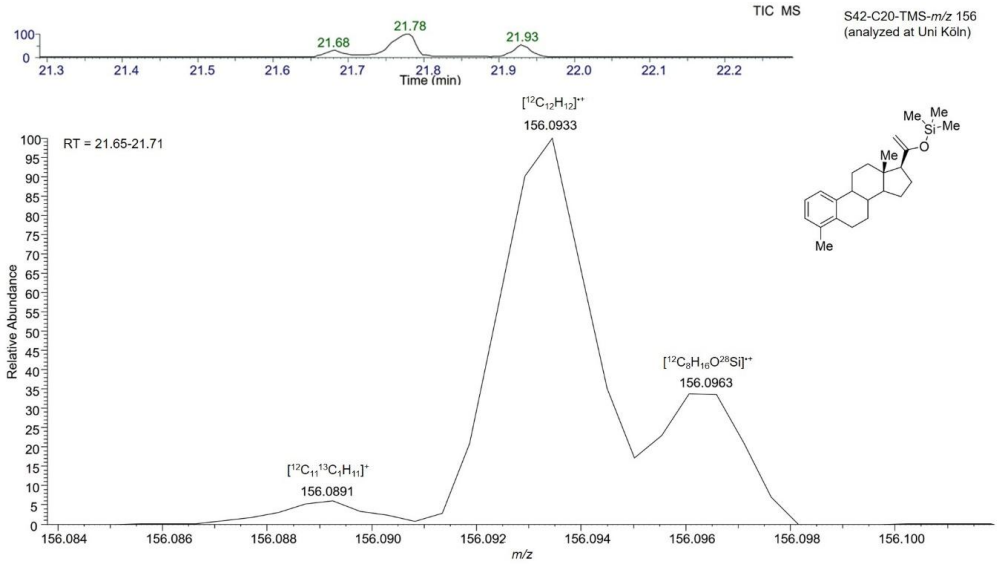

Figure A45. Section of the GC-EI-HRMS spectrum of S42-C20-TMS (**1-C20-TMS**) (RT: 21.68 min) at *m/z* 156. The sample was analyzed at the University of Cologne with a temperature program of 120(5)-10-320(5).

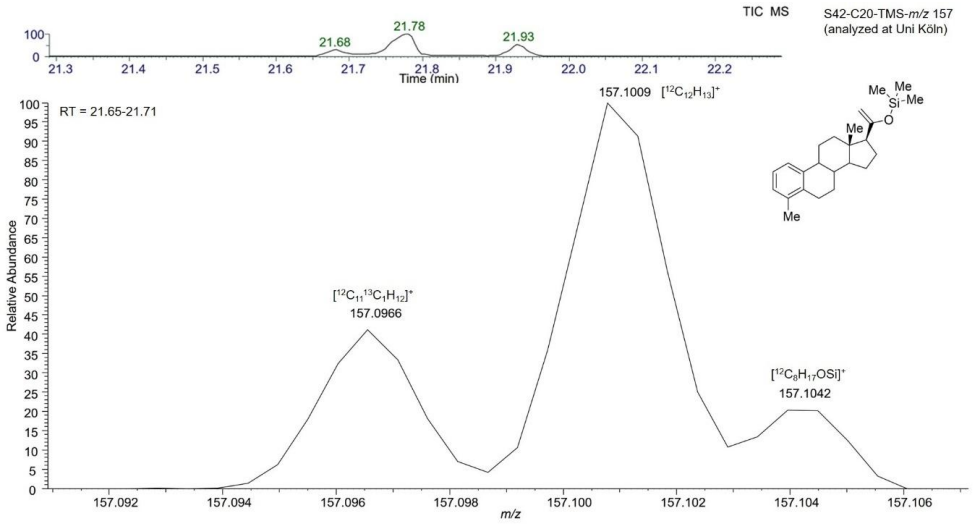

Figure A46. Section of the GC-EI-HRMS spectrum of S42-C20-TMS (**1-C20-TMS**) (RT=21.68) at *m/z* 157. The sample was analyzed at the University of Cologne with a temperature program of 120(5)-10-320(5).

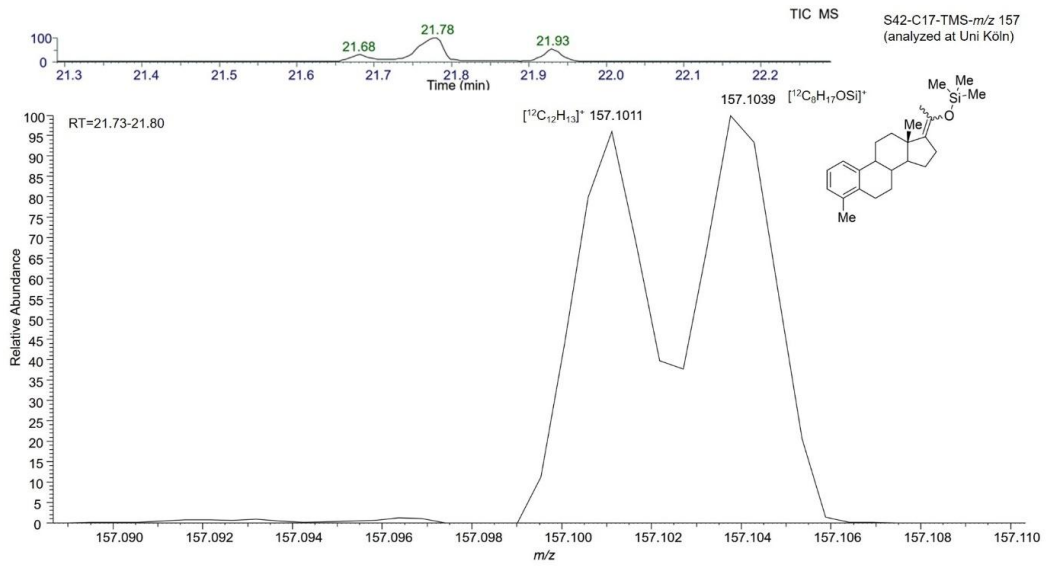

Figure A47. Section of the GC-EI-HRMS spectrum of S42-C17-TMS (**1-C17-TMS(*E*/*Z*)**) (RT=21.78) at *m/z* 157. The sample was analyzed at the University of Cologne with a temperature program of 120(5)-10-320(5).

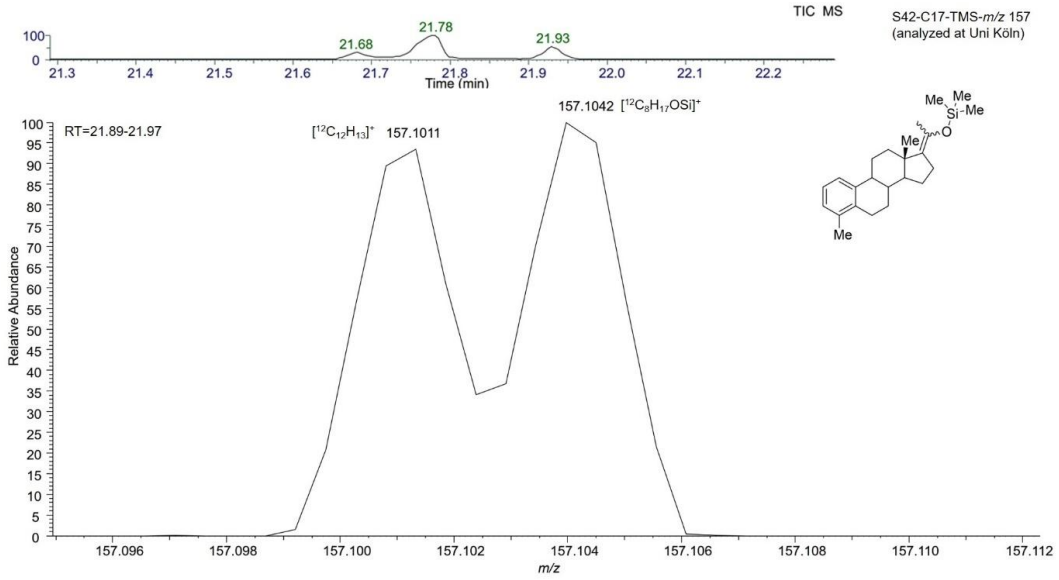

Figure A48. Section of the GC-EI-HRMS spectrum of S42-C17-TMS **(1-C17-TMS(*E*/*Z*))** (RT=21.93) at *m/z* 157. The sample was analyzed at the University of Cologne with a temperature program of 120(5)-10-320(5).

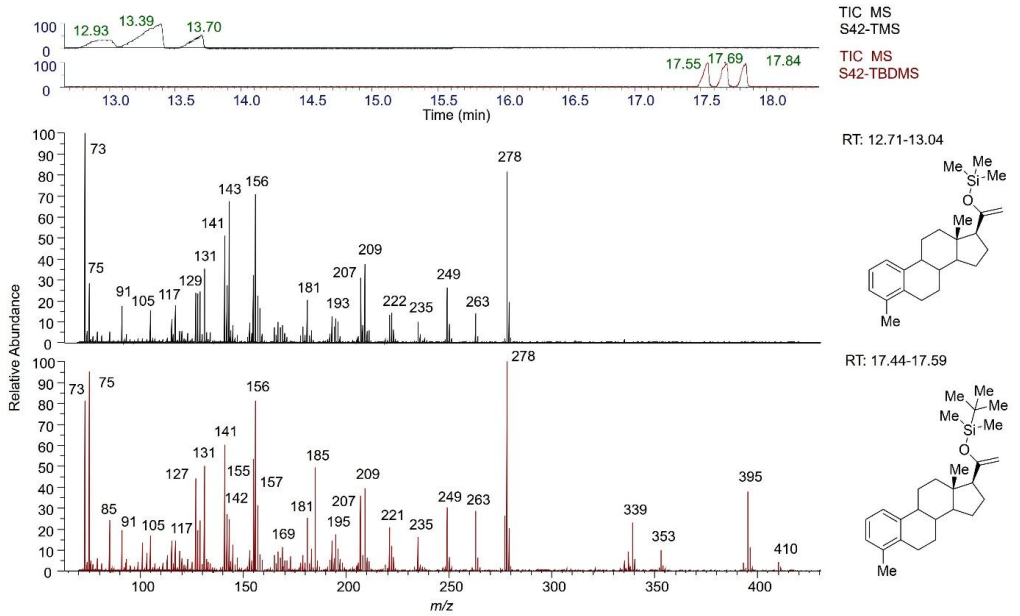

Figure A49. Comparison of GC-EI-HRMS results obtained for S42 C-20 enol-TMS ether (**1-C20-TMS**) and S42 C-20 enol S42-TBDMS (**1-C20-TBDMS**). The TIC traces document the separation of the three isomers. The samples were analyzed at German Sport University Cologne with a temperature program: 185(0)-3-234(0)-40-310(2) and a flow rate of 8.0 mL/min.

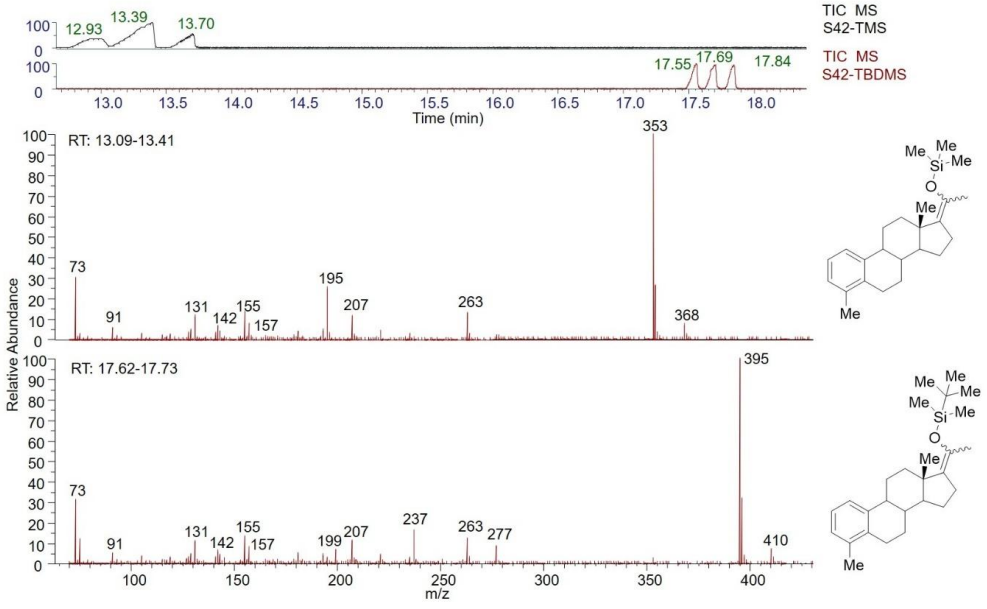

Figure A50. Comparison of GC-EI-HRMS results obtained for S42 C-17 enol-TMS ether (**1-C17-TMS(*E*/*Z*)**) and S42 C-17 enol S42-TBDMS (**1-C17-TBDMS(*E*/*Z*)**). The TIC traces document the separation of the three isomers. The samples were analyzed at German Sport University Cologne with a temperature program: 185(0)-3-234(0)-40-310(2) and a flow rate of 8.0 mL/min.

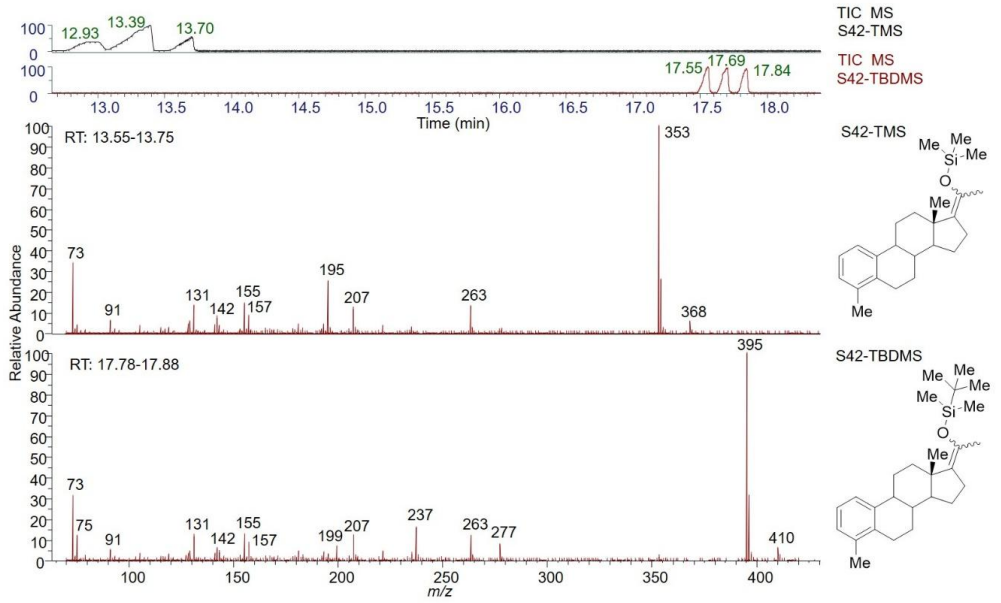

Figure A51. Comparison of GC-EI-HRMS results obtained for S42 C-17 enol-TMS ether isomer (**1-C17-TMS(*E*/*Z*)**) and S42 C-17 enol S42-TBDMS ether isomer (**1-C17-TBDMS(*E*/*Z*)**). The TIC traces document the separation of the three isomers. The samples were analyzed at German Sport University Cologne with a temperature program: 185(0)-3-234(0)-40-310(2) and a flow rate of 8.0 mL/min.

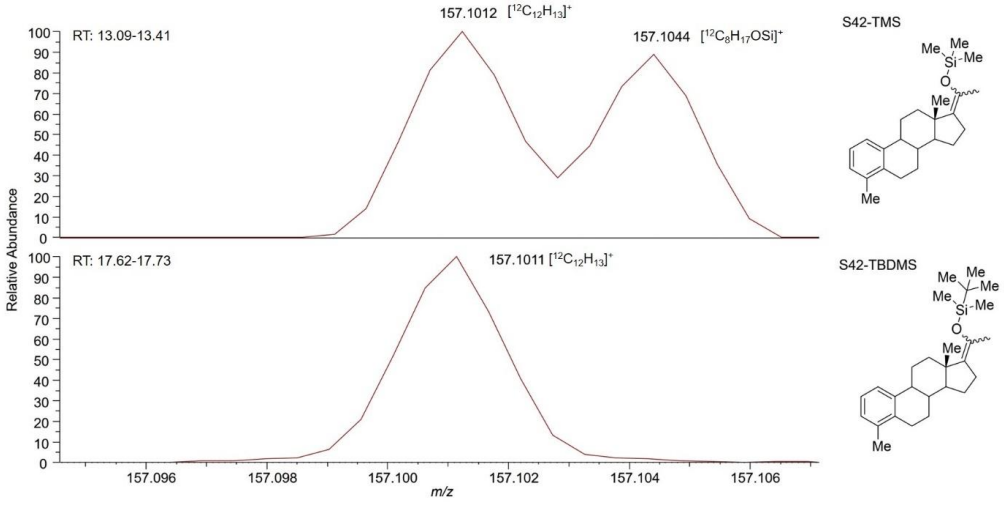

Figure A52. Comparison of GC-EI-HRMS results obtained for S42 C-17 enol-TMS ether (**1-C17-TMS(*E*/*Z*),** RT: 13.39) and S42 C-17 enol S42-TBDMS (**1-C17-TBDMS(*E*/*Z*)**, RT: 17.69) at *m/z* 157. The samples were analyzed at German Sport University Cologne with a temperature program: 185(0)-3-234(0)-40-310(2) and a flow rate of 8.0 mL/min.

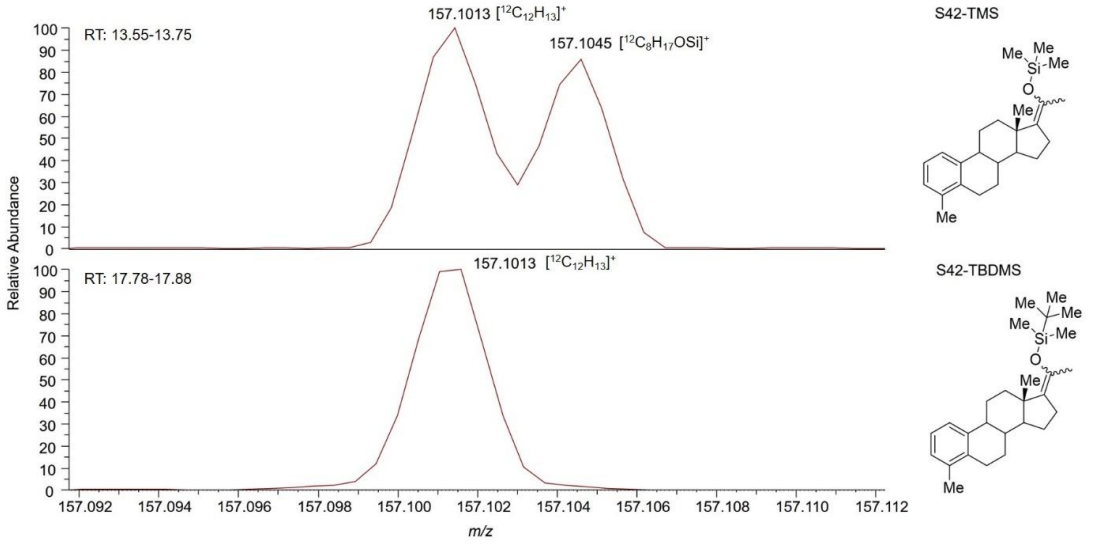

Figure A53. Comparison of GC-EI-HRMS results obtained for S42 C-17 enol-TMS ether isomer (**1-C17-TMS(*E*/*Z*)**, **R**T: 13.70) and S42 C-17 enol S42-TBDMS ether isomer (**1-C17-TBDMS(*E*/*Z*)**, RT: 17.84) at *m/z* 157. The samples were analyzed at German Sport University Cologne with a temperature program: 185(0)-3-234(0)-40-310(2) and a flow rate of 8.0 mL/min.

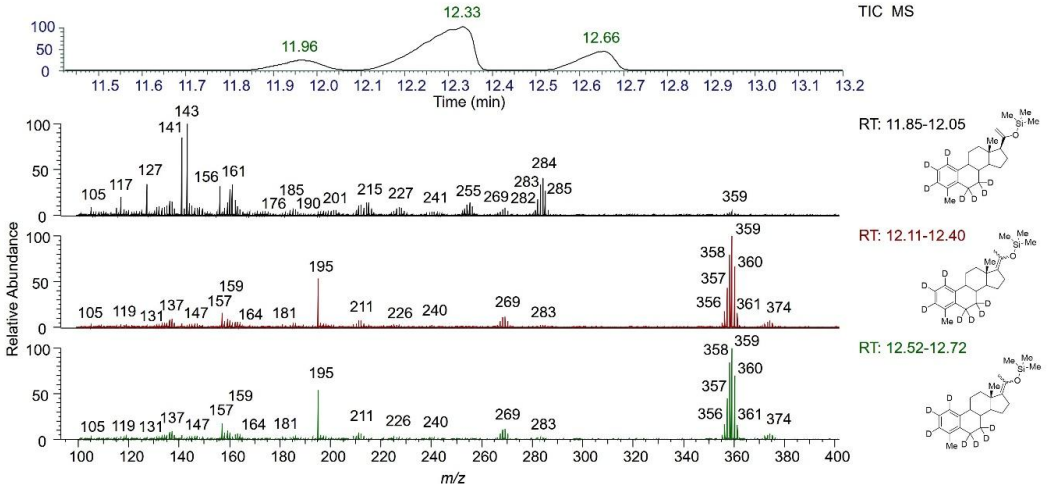

Figure A54. S42-d7-TMS (**1-d7-C20-TMS**, **1-d7-C17-TMS(*E*/*Z*)** from top to bottom) chromatogram and spectra. The sample was analyzed at German Sport University of Cologne with a temperature program of 185(0)-3-234(0)-40-310(2).

Table A1. Accurate ion masses from the GC-EI HR MS data of compound **2**.

RT: 21.14					
compound 2	Nominal mass [Da]	Composition	Theo. Mass [Da]	Accurate ion mass measured [Da]	Error [ppm]
$[M]^{+\bullet}$	298	$C_{21}H_{30}O$	298.2291	298.2287	-0.42
$[M\text{-}H_2O]^{+\bullet}$	280	$C_{21}H_{28}$	280.2186	280.2182	-0.36
$[M\text{-}H_2O\text{-}CH_3^{\bullet}]^{+}$	265	$C_{20}H_{25}$	265.1951	265.1947	-0.35
	251	$C_{19}H_{23}$	251.1794	251.1792	-0.27
	224	$C_{17}H_{20}$	224.1560	224.1558	-0.16
	211	$C_{16}H_{19}$	211.1481	211.1478	-0.38
	209	$C_{16}H_{17}$	209.1325	209.1321	-0.34
	197	$C_{15}H_{17}$	197.1325	197.1322	-0.30
	183	$C_{14}H_{15}$	183.1168	183.1165	-0.32
	170	$C_{13}H_{14}$	170.1090	170.1087	-0.32
	158	$C_{12}H_{14}$	158.1090	158.1086	-0.36
	157	$C_{12}H_{13}$	157.1012	157.1009	-0.27
	156	$C_{12}H_{12}$	156.0934	156.0931	-0.25
	155	$C_{12}H_{11}$	155.0855	155.0853	-0.26
	143	$C_{11}H_{11}$	143.0855	143.0853	-0.18
	131	$C_{10}H_{11}$	131.0855	131.0854	-0.13
	115	C_9H_7	115.0542	115.0541	-0.13
	91	C_7H_7	91.0542	91.0542	-0.08

Table A2. Accurate ion masses from the GC-EI HR MS data of compound **2'**.

RT: 21.31					
compound **2'**	Nominal mass [Da]	Composition	Theo. Mass [Da]	Accurate ion mass measured [Da]	Error [ppm]
$[M]^{+\bullet}$	298	$C_{21}H_{30}O$	298.2291	298.2287	-0.38
$[M\text{-}H_2O]^{+\bullet}$	280	$C_{21}H_{28}$	280.2186	280.2183	-0.28
$[M\text{-}H_2O\text{-}CH_3^{\bullet}]^{+}$	265	$C_{20}H_{25}$	265.1951	265.1948	-0.29
	251	$C_{19}H_{23}$	251.1794	251.1792	-0.21
	224	$C_{17}H_{20}$	224.1560	224.1558	-0.12
	211	$C_{16}H_{19}$	211.1481	211.1478	-0.33
	209	$C_{16}H_{17}$	209.1325	209.1322	-0.29
	207	$C_{16}H_{15}$	207.1168	207.1165	-0.28
	197	$C_{15}H_{17}$	197.1325	197.1322	-0.24
	183	$C_{14}H_{15}$	183.1168	183.1166	-0.26
	170	$C_{13}H_{14}$	170.1090	170.1087	-0.28
	158	$C_{12}H_{14}$	158.1090	158.1087	-0.32
	157	$C_{12}H_{13}$	157.1012	157.1009	-0.24
	156	$C_{12}H_{12}$	156.0934	156.0931	-0.21
	155	$C_{12}H_{11}$	155.0855	155.0853	-0.22
	143	$C_{11}H_{11}$	143.0855	143.0854	-0.15
	142	$C_{11}H_{10}$	142.0777	142.0776	-0.14
	141	$C_{11}H_9$	141.0699	141.0698	-0.1
	131	$C_{10}H_{11}$	131.0855	131.0854	-0.11
	129	$C_{10}H_9$	129.0699	129.0658	-4.11
	128	$C_{10}H_8$	128.0621	128.0619	-0.12
	115	C_9H_7	115.0542	115.0541	-0.09
	91	C_7H_7	91.0542	91.0542	0

Table A3. Accurate ion masses from the GC-EI HR MS data of compound **3**.

RT: 22.18 compound **3**	Nominal mass [Da]	Composition	Theo. Mass [Da]	Accurate ion mass measured [Da]	Error [ppm]
$[M\text{-}CH_3^{\bullet}]^+$	297	$C_{20}H_{25}O_2$	297.1849	297.1847	-0.75
$[M\text{-}H_2O]^{+\bullet}$	294	$C_{21}H_{26}O$	294.1978	294.1976	-0.80
$[M\text{-}2H_2O]^{+\bullet}$	276	$C_{21}H_{24}$	276.1873	276.1871	-0.66
$[M\text{-}2H_2O\text{-}CH_3^{\bullet}]^+$	251	$C_{19}H_{23}$	251.1794	251.1794	0
	221	$C_{17}H_{17}$	221.1325	221.1324	-0.21
	209	$C_{16}H_{17}$	209.1325	209.1323	-0.82
	195	$C_{15}H_{15}$	195.1168	195.1167	-0.88
	181	$C_{14}H_{13}$	181.1012	181.1010	-1.03
	165	$C_{13}H_9$	165.0699	165.0698	-0.75
	157	$C_{12}H_{13}$	157.1012	157.1010	-1.16
	156	$C_{12}H_{12}$	156.0934	156.0931	-1.35
	155	$C_{12}H_{11}$	155.0855	155.0854	-0.8
	141	$C_{11}H_9$	141.0699	141.0698	-0.25
	129	$C_{10}H_9$	129.0699	129.0698	-0.35
	128	$C_{10}H_8$	128.0621	128.0620	-0.11
	115	C_9H_7	115.0542	115.0542	0

Table A4. Accurate ion masses from the GC-EI HR MS data of compound **4**.

RT: 22.59 compound **4**	Nominal mass [Da]	Composition	Theo. Mass [Da]	Accurate ion mass measured [Da]	Error [ppm]
$[M\text{-}H_2O]^{+\bullet}$	294	$C_{21}H_{26}O$	294.1978	294.1976	-0.64
$[M\text{-}2H_2O]^{+\bullet}$	276	$C_{21}H_{24}$	276.1873	276.1871	-0.52
$[M\text{-}2H_2O\text{-}CH_3^{\bullet}]^+$	261	$C_{20}H_{21}$	261.1638	261.1638	0
$[M\text{-}^{\bullet}C_2H_3O]^+$	251	$C_{19}H_{23}$	251.1794	251.1794	0
	223	$C_{17}H_{19}$	223.1481	223.1481	0
	209	$C_{16}H_{17}$	209.1325	209.1323	-0.76
	207	$C_{16}H_{15}$	207.1168	207.1167	-0.59
	195	$C_{15}H_{15}$	195.1168	195.1167	-0.60
	181	$C_{14}H_{13}$	181.1012	181.1011	-0.58
	165	$C_{13}H_9$	165.0699	165.0698	-0.72
	157	$C_{12}H_{13}$	157.1012	157.1010	-1.27
	156	$C_{12}H_{12}$	156.0934	156.0931	-1.63
	155	$C_{12}H_{11}$	155.0855	155.0855	0
	143	$C_{11}H_{11}$	143.0855	143.0855	0
	141	$C_{11}H_9$	141.0699	141.0698	-0.22
	131	$C_{10}H_{11}$	131.0855	131.0855	0
	128	$C_{10}H_8$	128.0621	128.0620	-0.04
	115	C_9H_7	115.0542	115.0542	0
	107	C_8H_{11}	107.0855	107.0855	0
	95	C_7H_{11}	95.0855	95.0855	0
	93	C_7H_9	93.0699	93.0699	0
	91	C_7H_7	91.0542	91.0543	0.30
	77	C_6H_5	77.0386	77.0386	0
	67	C_5H_7	67.0542	67.0542	0

9.3.3 Chromatograms and MS spectra of non-silylated and silylated compound **3** and **4**

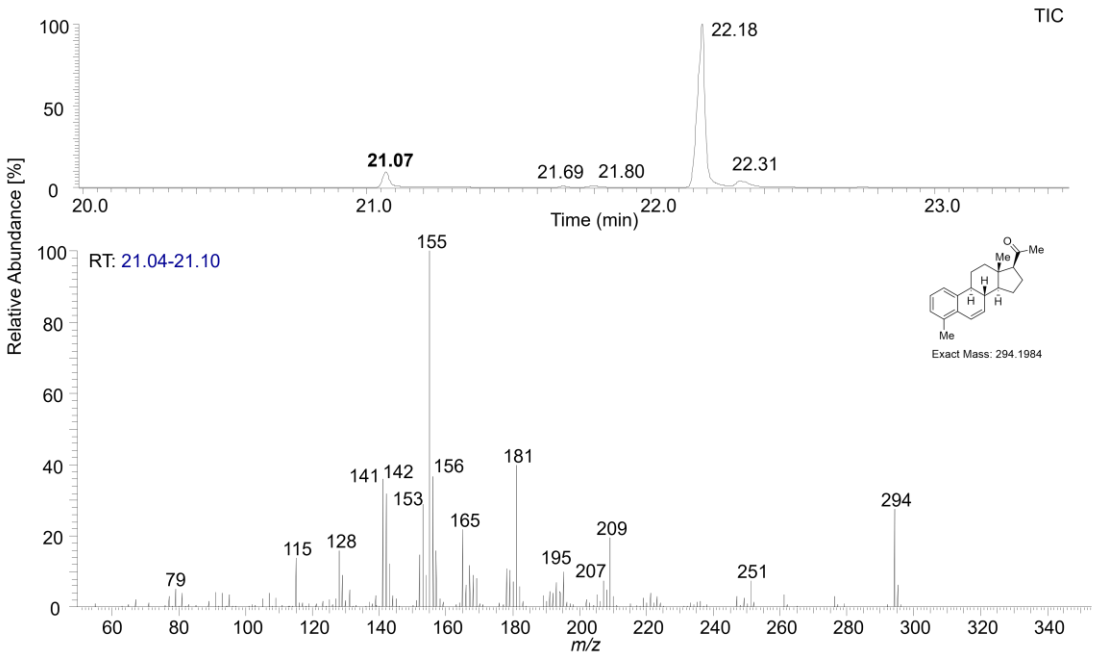

Figure A55.Water-loss delivered of compound **3** produced an olefine product at retention time at 21.07 minutes (analyzed at University of Cologne).

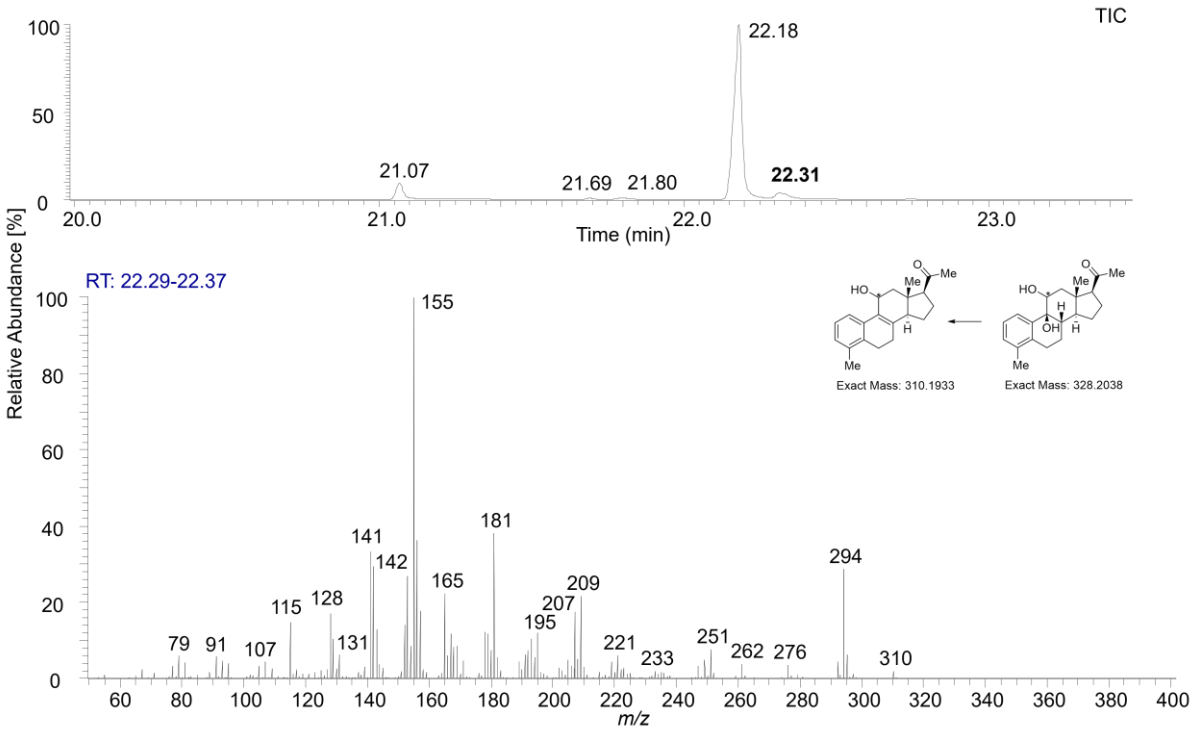

Figure A56. GC total ion current and EI mass spectrum of the byproduct of compound **3** resulting from reduction and water-loss.

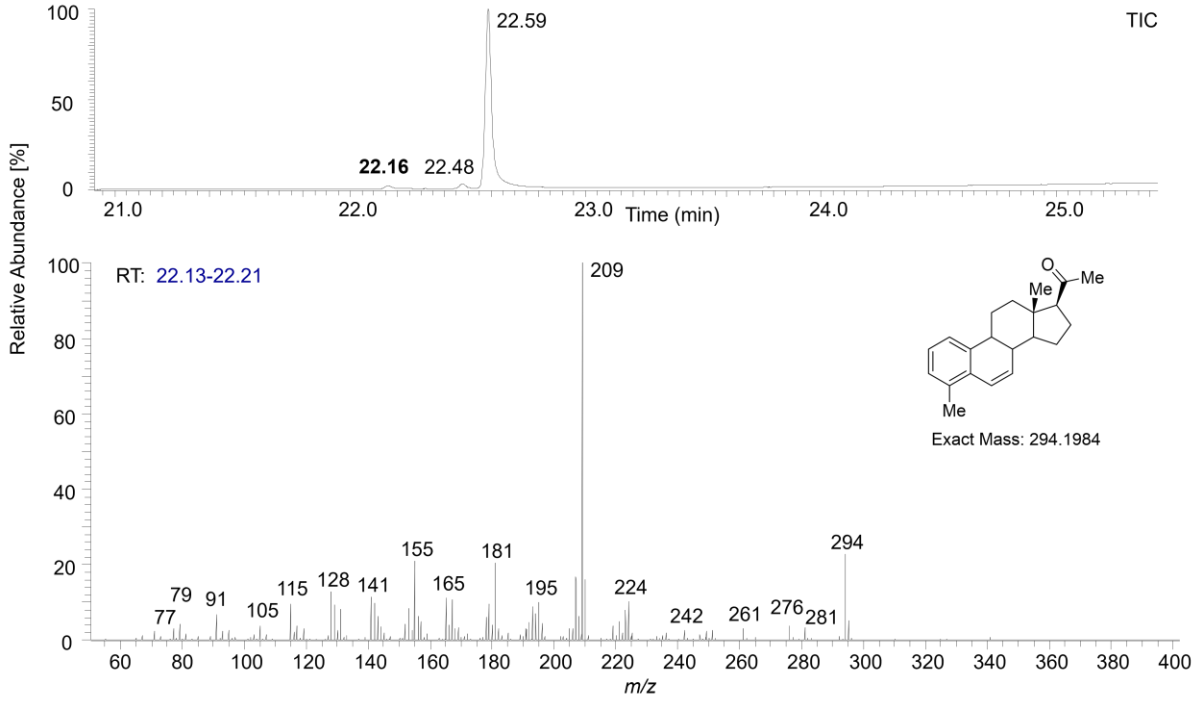

Figure A57. GC total ion current and EI mass spectrum of an olefin byproduct that was generated from compound **4**.

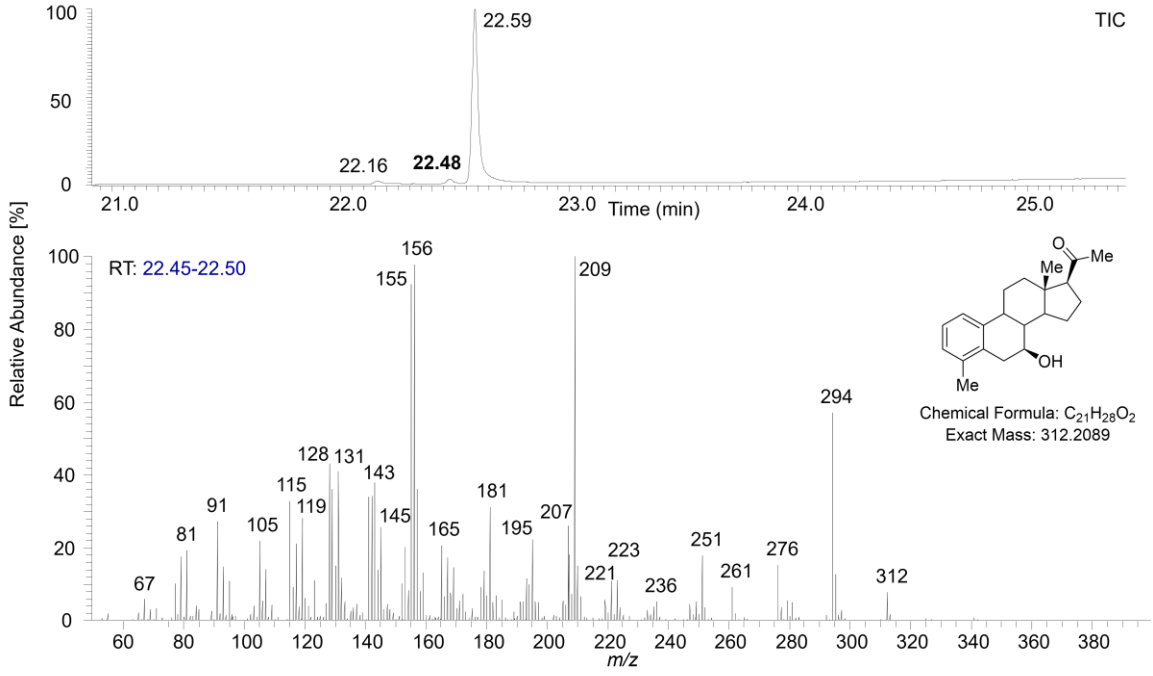

Figure A58. A minor signal at RT: 22.48 in the total ion current chromatogram of compound **4** indicates the formation of a byproduct in trace amounts. This byproduct was proposed to be a diastereomer of substance **4**.

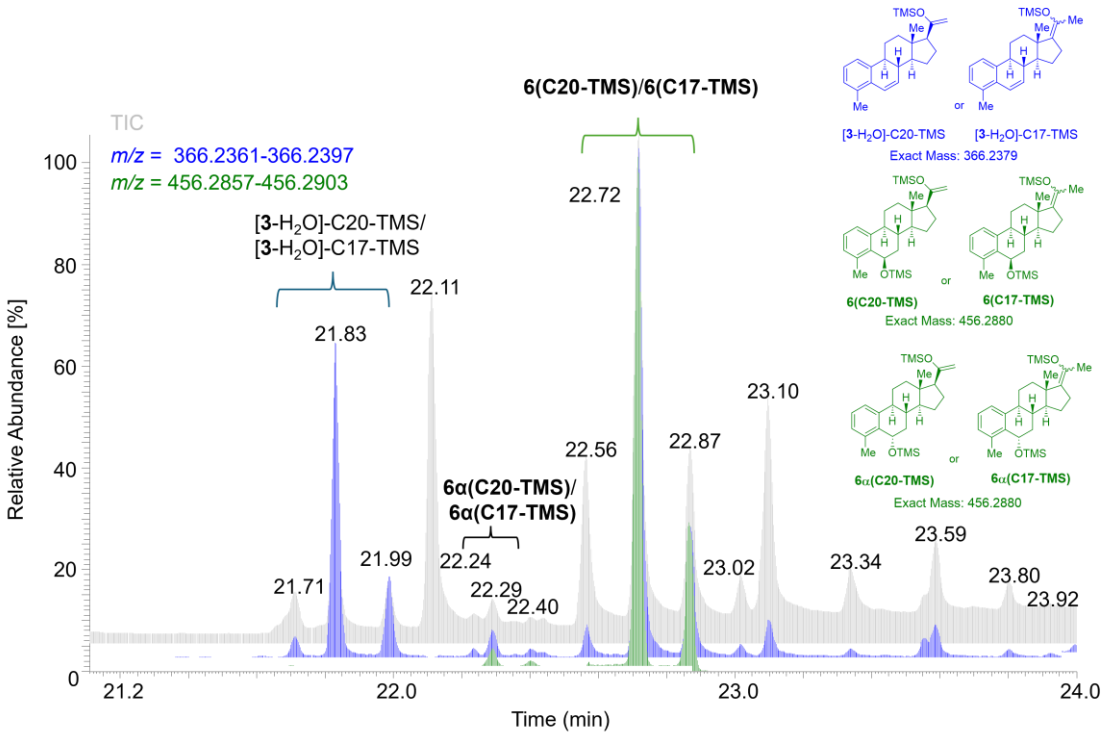

Figure A59. Total ion and single ion current chromatograms of TMS-derivatized products of compound 3. The mixture contained **6(C20-TMS)**, **6(C17-TMS)**, **6'(C17-TMS)** (structures in green) and TMS-derivatized water-loss products, i.e. olefins (structures in blue).

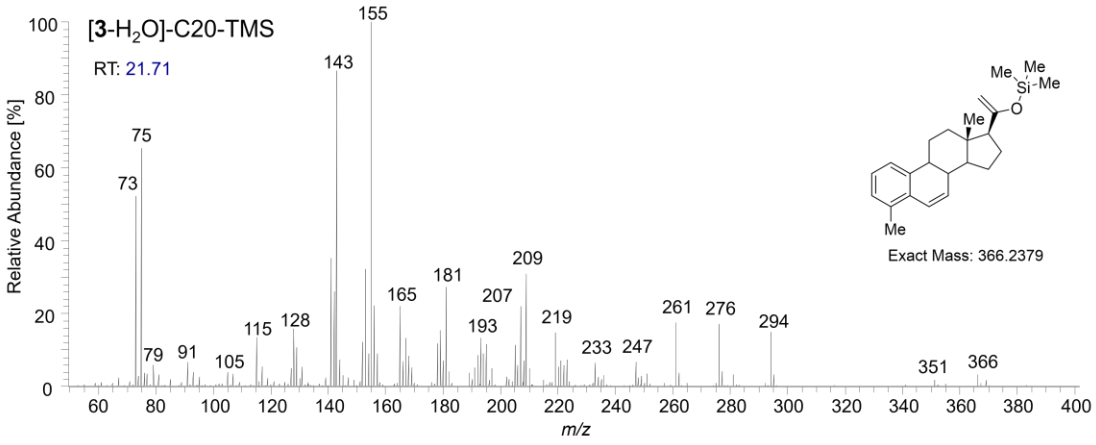

Figure A60. GC-EI MS spectrum of [**3**-H_2O]-C20-TMS. The signal at *m/z* 143 from the D-ring structure indicates the C20-TMS sub-structure isomer.

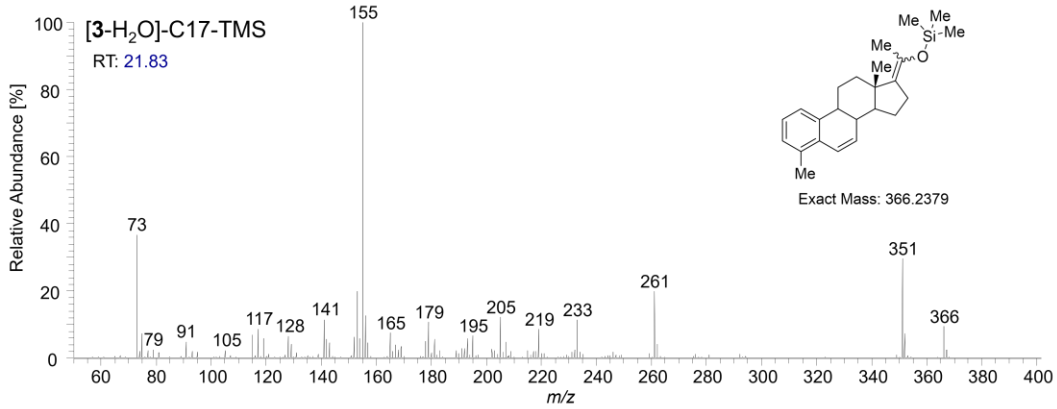

Figure A61. GC-EI MS spectrum of [**3**-H_2O] -C17-TMS. The signal at *m/z* 195 from the D-ring structure indicates the C17-TMS sub-structure isomer.

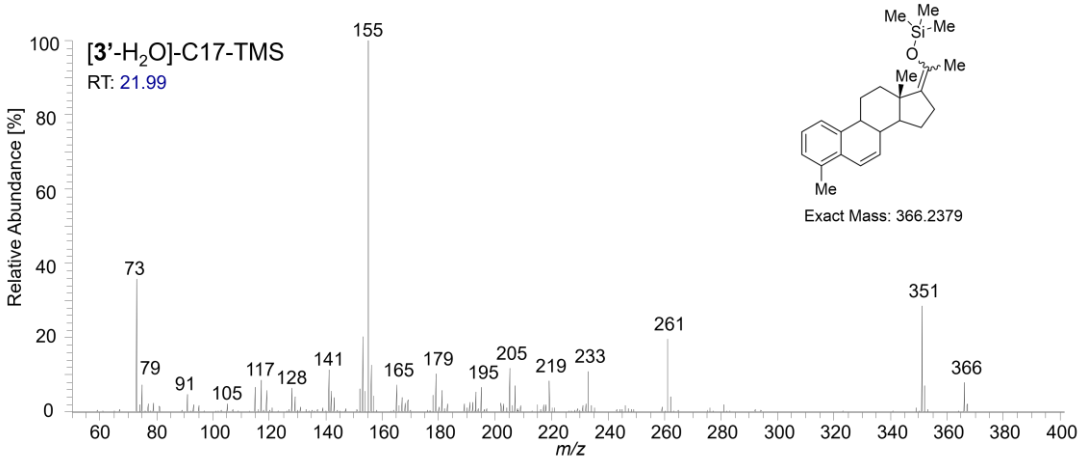

Figure A62. GC-EI MS spectrum of [**3'**-H_2O]-C17-TMS. The signal at *m/z* 195 from the D-ring structure indicates the C17-TMS sub-structure isomer.

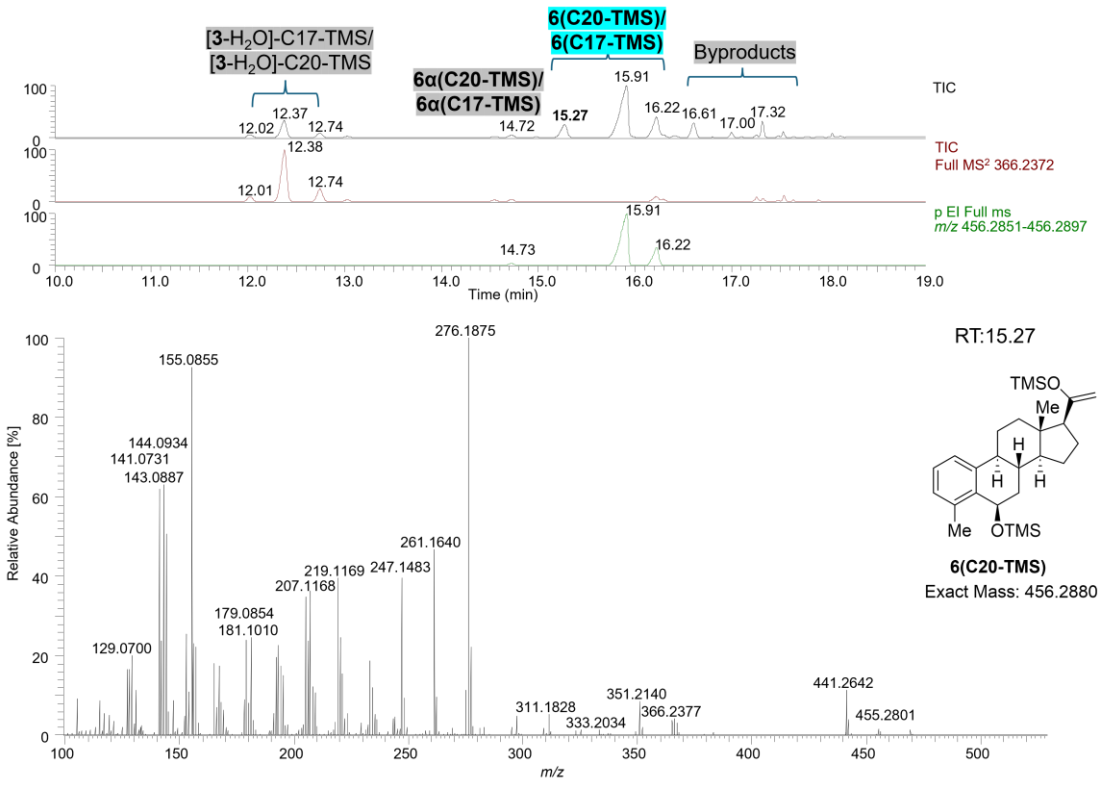

Figure A63. Total ion current chromatogram, single ion current chromatogram and GC-EI mass spectrum of compound **6(C20-TMS)** along with byproducts analyzed at German Sport University Cologne.

Table A5. Accurate ion masses from the GC-EI HR MS data of compound **7(C20-TMS)**. The ion at *m/z* 143.0886 indicates it is a C20-TMS isomer.

RT: 21.32 **7(C20-TMS)**	Nominal mass [Da]	Composition	Theo. Mass [Da]	Accurate ion mass measured [Da]	Error [ppm]
$[M]^{+\bullet}$	456	$C_{27}H_{44}O_2Si_2$	456.2874	456.2871	-0.70
$[M\text{-}CH_3^{\bullet}]^+$	441	$C_{26}H_{41}O_2Si_2$	441.2640	441.2634	-1.22
$[M\text{-TMSOH}]^{+\bullet}$	366	$C_{24}H_{34}OSi$	366.2373	366.2370	-0.32
$[M\text{-TMSOH-}CH_3^{\bullet}]^+$	351	$C_{23}H_{31}OSi$	351.2139	351.2136	-0.27
	297	$C_{19}H_{25}OSi$	297.1669	297.1667	-0.17
	294	$C_{21}H_{26}O$	294.1978	294.1976	-0.23
	276	$C_{21}H_{24}$	276.1873	276.1872	-0.09
	261	$C_{20}H_{21}$	261.1638	261.1637	-0.04
	219	$C_{17}H_{15}$	219.1168	219.1167	-0.13
	209	$C_{16}H_{17}$	209.1325	209.1323	-0.22
	181	$C_{14}H_{13}$	181.1012	181.1010	-0.22
	155	$C_{12}H_{11}$	155.0855	155.0854	-0.1
	143	$C_7H_{15}OSi$	143.0887	143.0886	-0.11
	128	$C_{10}H_8$	128.0621	128.0620	-0.01
	117	$C_5H_{13}OSi$	117.073	117.073	0
	115	C_9H_7	115.0542	115.0542	0
	91	C_7H_7	91.0542	91.0542	0
	75	C_2H_7OSi	75.0261	75.0261	0
	73	C_3H_9Si	73.0468	73.0468	0

Table A6. Accurate ion masses from the GC-EI HR MS data of compound **7(C17-TMS)**. The ion at *m/z* 195.1204 indicates it is a C17-TMS isomer.

RT: 21.78					
7(C17-TMS)	Nominal mass [Da]	Composition	Theo. Mass [Da]	Accurate ion mass measured [Da]	Error [ppm]
$[M]^{+\bullet}$	456	$C_{27}H_{44}O_2Si_2$	456.2874	456.2871	-0.69
$[M\text{-}CH_3^{\bullet}]^+$	441	$C_{26}H_{41}O_2Si_2$	441.2640	441.2636	-0.79
$[M\text{-}TMSOH]^{+\bullet}$	366	$C_{24}H_{34}OSi$	366.2373	366.2371	-0.73
$[M\text{-}TMSOH\text{-}CH_3^{\bullet}]^+$	351	$C_{23}H_{31}OSi$	351.2139	351.2136	-0.27
	276	$C_{21}H_{24}$	276.1873	276.1872	-0.06
	261	$C_{20}H_{21}$	261.1638	261.1637	-0.06
	235	$C_{18}H_{19}$	235.1481	235.1481	0
	233	$C_{18}H_{17}$	233.1325	233.1324	-0.06
	219	$C_{17}H_{15}$	219.1168	219.1167	-0.15
	209	$C_{12}H_{21}OSi$	209.1356	209.1358	0.19
	207	$C_{16}H_{15}$	207.1168	207.1164	-0.38
	195	$C_{11}H_{19}OSi$	195.1200	195.1204	0.41
	179	$C_{14}H_{11}$	179.0855	179.0852	-0.31
	157	$C_8H_{17}OSi$	157.1043	157.1042	-0.11
	157	$C_{12}H_{13}$	157.1012	157.1011	-0.04
	156	$C_{12}H_{12}$	156.0934	156.0932	-0.14
	156	$C_{12}H_{12}$	156.0934	156.0889	-4.45
	155	$C_{12}H_{11}$	155.0855	155.0854	-0.1
	143	$C_7H_{15}OSi$	143.0887	143.0886	-0.1
	143	$C_{11}H_{11}$	143.0855	143.0857	0.15
	131	$C_{10}H_{11}$	131.0855	131.0855	0
	91	C_7H_7	91.0542	91.0542	0
	73	C_3H_9Si	73.0468	73.0468	0

Table A7. Accurate ion masses from the EI HR MS data of compound **7'(C17-TMS)**. The ion at *m/z* 195.1205 indicates it is a C17-TMS isomer.

RT: 21.87					
7'(C17-TMS)	Nominal mass [Da]	Composition	Theo. Mass [Da]	Accurate ion mass measured [Da]	Error [ppm]
$[M]^{+\bullet}$	456	$C_{27}H_{44}O_2Si_2$	456.2874	456.2871	-0.66
$[M\text{-}CH_3^{\bullet}]^+$	441	$C_{26}H_{41}O_2Si_2$	441.2640	441.2636	-0.8
$[M\text{-}TMSOH]^{+\bullet}$	366	$C_{24}H_{34}OSi$	366.2373	366.2371	-0.58
$[M\text{-}TMSOH\text{-}CH_3^{\bullet}]^+$	351	$C_{23}H_{31}OSi$	351.2139	351.2135	-0.34
	294	$C_{21}H_{26}O$	294.1978	294.1977	-0.39
	276	$C_{21}H_{24}$	276.1873	276.1872	-0.01
	261	$C_{20}H_{21}$	261.1638	261.1637	-0.12
	249	$C_{19}H_{21}$	249.1638	249.1639	0.12
	235	$C_{18}H_{19}$	235.1481	235.1480	-0.09
	233	$C_{18}H_{17}$	233.1325	233.1324	-0.03
	219	$C_{17}H_{15}$	219.1168	219.1166	0
	209	$C_{12}H_{21}OSi$	209.1356	209.1358	0.15
	207	$C_{16}H_{15}$	207.1168	207.1162	-0.62
	205	$C_{16}H_{13}$	205.1012	205.1010	-0.23
	195	$C_{11}H_{19}OSi$	195.1200	195.1205	0.5
	193	$C_{15}H_{13}$	193.1012	193.1010	-0.16
	192	$C_{15}H_{12}$	192.0934	192.0932	-0.19
	181	$C_{10}H_{17}OSi$	181.1043	181.1042	-0.08
	181	$C_{14}H_{13}$	181.1012	181.1010	-0.15
	179	$C_{14}H_{11}$	179.0855	179.0853	-0.24
	165	$C_{13}H_9$	165.0699	165.0697	-0.18
	157	$C_8H_{17}OSi$	157.1043	157.1042	-0.12
	156	$C_{12}H_{12}$	156.0934	156.0932	-0.15
	155	$C_{12}H_{11}$	155.0855	155.0854	-0.1
	143	$C_7H_{15}OSi$	143.0887	143.0886	-0.08
	131	$C_{10}H_{11}$	131.0855	131.0855	0
	119	C_9H_{11}	119.0855	119.0855	-0.01
	115	C_9H_7	115.0542	115.0542	0
	105	C_8H_9	105.0699	105.0699	0
	91	C_7H_7	91.0542	91.0542	0
	75	C_2H_7OSi	75.0261	75.0261	0
	73	C_3H_9Si	73.0468	73.0468	0

9.3.4 Chromatograms and MS spectra of *in vitro* phase I metabolites

Table A8. Ions found in the GC-EI HR MS spectrum of the S42-mono-OH metabolite **M1a**.

M1a	Nominal mass [Da]	Composition	Theo. Mass [Da]	Accurate ion mass measured [Da]	Error [ppm]
$[M]^{+\bullet}$	456	$C_{27}H_{44}O_2Si_2$	456.2874	456.2875	0.11
$[M\text{-}Me^{\bullet}]^{+}$	441	$C_{26}H_{41}O_2Si_2$	441.2640	441.2640	0
$[M\text{-}TMSOH]^{+\bullet}$	366	$C_{24}H_{34}OSi$	366.2373	366.2376	0.23
$[M\text{-}TMSOH\text{-}Me^{\bullet}]^{+}$	351	$C_{23}H_{31}OSi$	351.2139	351.2140	0.15
	310	$C_{20}H_{26}OSi$	310.1747	310.1750	0.21
	297	$C_{19}H_{25}OSi$	297.1669	297.1671	0.22
	284	$C_{18}H_{24}OSi$	284.1591	284.1592	0.14
	245	$C_{15}H_{21}OSi$	245.1356	245.1359	0.23
	243	$C_{15}H_{19}OSi$	243.1200	243.1202	0.22
	232	$C_{14}H_{20}OSi$	232.1278	232.1280	0.22
	219	$C_{13}H_{19}OSi$	219.1200	219.1201	0.15
	195	$C_{11}H_{19}OSi$	195.1200	195.1199	-0.03
	194	$C_{11}H_{18}OSi$	194.1127	194.1122	-2.55
	193	$C_{11}H_{17}OSi$	193.1043	193.1045	0.14
	157	$C_8H_{17}OSi$	157.1043	157.1045	0.15
	156	$C_8H_{16}OSi$	156.0965	156.0966	0.09
	143	$C_7H_{15}OSi$	143.0887	143.0888	0.10
	117	$C_5H_{13}OSi$	117.0730	117.0731	0.10
	91	$C_3H_{11}OSi$	91.0574	91.0575	0.14
	73	C_3H_9Si	73.0468	73.0469	0.06

Table A9. Ions found in the GC-EI HR MS spectrum of the S42-mono-OH metabolite **M1b**.

M1b	Nominal mass [Da]	Composition	Theo. Mass [Da]	Accurate ion mass measured [Da]	Error [ppm]
$[M\text{-}Me^{\bullet}]^{+}$	441	$C_{26}H_{41}O_2Si_2$	441.2640	441.2644	0.46
$[M\text{-}TMSOH]^{+\bullet}$	366	$C_{24}H_{34}OSi$	366.2373	366.2376	0.26
$[M\text{-}TMSOH\text{-}Me^{\bullet}]^{+}$	351	$C_{23}H_{31}OSi$	351.2139	351.2142	0.35
	337	$C_{22}H_{29}OSi$	337.1982	337.1987	0.52
	295	$C_{19}H_{23}OSi$	295.1513	295.1515	0.22
	245	$C_{15}H_{21}OSi$	245.1356	245.1359	0.27
	243	$C_{15}H_{19}OSi$	243.1200	243.1202	0.23
	232	$C_{14}H_{20}OSi$	232.1278	232.1279	0.63
	219	$C_{13}H_{19}OSi$	219.1200	219.1201	0.13
	209	$C_{12}H_{21}OSi$	209.1356	209.1358	0.19
	207	$C_{12}H_{19}OSi$	207.1200	207.1200	0
	195	$C_{11}H_{19}OSi$	195.1200	195.1201	0.14
	157	$C_8H_{17}OSi$	157.1043	157.1044	0.05
	156	$C_8H_{16}OSi$	156.0965	156.0966	0.15
	117	$C_5H_{13}OSi$	117.0730	117.0731	0.11
	91	$C_3H_{11}OSi$	91.0574	91.0576	0.2
	73	C_3H_9Si	73.0468	73.0468	0

Table A10. Ions found in the GC-EI HR MS spectrum of the S42-mono-OH metabolite **M1c**.

M1c	Nominal mass [Da]	Composition	Theo. Mass [Da]	Accurate ion mass measured [Da]	Error [ppm]
$[M\text{-}Me^{\bullet}]^{+}$	441	$C_{26}H_{41}O_2Si_2$	441.2640	441.2644	0.40
$[M\text{-}TMSOH]^{+\bullet}$	366	$C_{24}H_{34}OSi$	366.2373	366.2375	0.15
$[M\text{-}TMSOH\text{-}Me^{\bullet}]^{+}$	351	$C_{23}H_{31}OSi$	351.2139	351.2141	0.20
	295	$C_{19}H_{23}OSi$	295.1513	295.1513	0
	245	$C_{15}H_{21}OSi$	245.1356	245.1357	0.13
	243	$C_{15}H_{19}OSi$	243.1200	243.1202	0.18
	232	$C_{14}H_{20}OSi$	232.1278	232.1279	0.11
	219	$C_{13}H_{19}OSi$	219.1200	219.1200	0
	209	$C_{12}H_{21}OSi$	209.1356	209.1357	0.12
	195	$C_{11}H_{19}OSi$	195.1200	195.1200	0
	157	$C_8H_{17}OSi$	157.1043	157.1044	0.05
	117	$C_5H_{13}OSi$	117.0730	117.0731	0.07
	73	C_3H_9Si	73.0468	73.0469	0.07

Table A11. Ions found in the GC-EI HR MS spectrum of the S42-bis-OH metabolite **M2a.**

M2a	Nominal mass [Da]	Composition	Theo. Mass [Da]	Accurate ion mass measured [Da]	Error [ppm]
$[M]^{+\bullet}$	544	$C_{30}H_{52}O_3Si_3$	544.3219	544.3225	0.62
$[M\text{-}C_5H_{13}OSi^{\bullet}]^{+}$	427	$C_{25}H_{39}O_2Si_2$	427.2483	427.2482	-0.07
	399	$C_{23}H_{35}O_2Si_2$	399.2170	399.2173	0.33
	364	$C_{24}H_{32}OSi$	364.2217	364.2217	0
$[M\text{-}C_5H_{13}OSi^{\bullet}\text{-}TMSOH]^{+}$	337	$C_{22}H_{29}OSi$	337.1982	337.1983	0.11
	311	$C_{20}H_{27}OSi$	311.1826	311.1832	0.61
	274	$C_{21}H_{22}$	274.1716	274.1718	0.16
	244	$C_{11}H_{24}O_2Si_2$	244.1309	244.1312	0.26
	243	$C_{11}H_{23}O_2Si_2$	243.1231	243.1236	0.46
	231	$C_{10}H_{23}O_2Si_2$	231.1231	231.1233	0.18
	231	$C_{18}H_{15}$	231.1168	231.1177	0.89
	230	$C_{10}H_{22}O_2Si_2$	230.1153	230.1155	0.26
	218	$C_9H_{22}O_2Si_2$	218.1153	218.1153	0
	218	$C_{17}H_{14}$	218.1090	218.1092	0.16
	209	$C_{16}H_{17}$	209.1325	209.1320	-0.46
	207	$C_{16}H_{15}$	207.1168	207.1167	-0.15
	143	$C_6H_{11}O_2Si$	143.0523	143.0523	0
	143	$C_7H_{15}OSi$	143.0887	143.0887	0
	117	$C_5H_{13}OSi$	117.0730	117.0731	0.07
	91	$C_3H_{11}OSi$	91.0574	91.0575	0.09

Table A12. Ions found in the GC-EI-HR MS spectrum of the S42-bis-OH metabolite **M2b**.

M2b	Nominal mass [Da]	Composition	Theo. Mass [Da]	Accurate ion mass measured [Da]	Error [ppm]
$[M]^{+\bullet}$	544	$C_{30}H_{52}O_3Si_3$	544.3219	544.3233	2.57
$[M\text{-}Me^{\bullet}]^{+}$	529	$C_{29}H_{49}O_3Si_3$	529.2984	529.2995	2.08
$[M\text{-}TMSOH]^{+\bullet}$	454	$C_{27}H_{42}O_2Si_2$	454.2718	454.2720	0.20
$[M\text{-}TMSOH\text{-}Me^{\bullet}]^{+}$	439	$C_{26}H_{39}O_2Si_2$	439.2483	439.2486	0.28
	426	$C_{25}H_{38}O_2Si_2$	426.2405	426.2409	0.41
	383	$C_{22}H_{31}O_2Si_2$	383.1857	383.1860	0.28
	334	$C_{18}H_{30}O_2Si_2$	334.1779	334.1779	0
	333	$C_{18}H_{29}O_2Si_2$	333.1701	333.1704	0.34
	331	$C_{18}H_{27}O_2Si_2$	331.1544	331.1546	0.19
	307	$C_{16}H_{27}O_2Si_2$	307.1544	307.1547	0.31
	281	$C_{14}H_{25}O_2Si_2$	281.1388	281.1389	0.14
	231	$C_{10}H_{23}O_2Si_2$	231.1231	231.1231	0
	195	$C_{11}H_{19}OSi$	195.1200	195.1201	0.13
	157	$C_8H_{17}OSi$	157.1043	157.1044	0.07
	143	$C_7H_{15}OSi$	143.0887	143.0887	0
	117	$C_5H_{13}OSi$	117.0730	117.0731	0.11
	73	C_3H_9Si	73.0468	73.0468	0

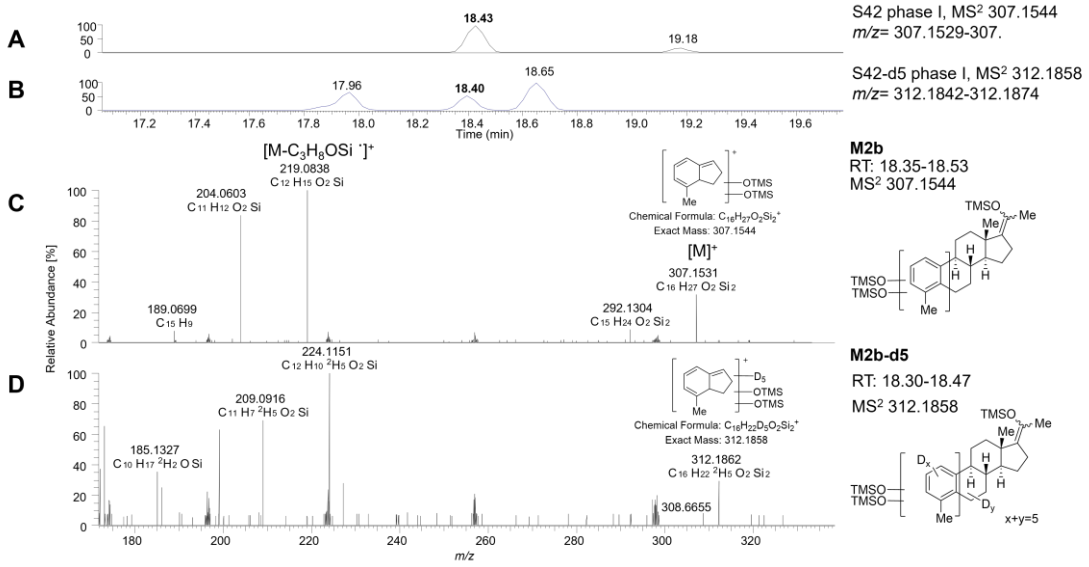

Figure A64. Extracted SICs of the characteristic fragment ions of the TMS derivatized S42-bis-OH metabolites M2b and M2b-d5 at *m /z* 307 and *m/z* 312. MS^2-product ion experiments of the ions at *m/z* 307 (131+88*2 Da) (d0) and *m/z* 312 (131+88*2+5 Da) (d5) of **M2b** and of **M2b-d5**, respectively. In the measurement of this figure, a new column was used. A large retention time shifting was not observed.

Table A13. Ions found in the GC-EI HR MS spectrum of the S42-bis-OH metabolite **M2c**.

M2c	Nominal mass [Da]	Composition	Theo. Mass [Da]	Accurate ion mass measured [Da]	Error [ppm]
$[M]^{+\bullet}$	544	$C_{30}H_{52}O_3Si_3$	544.3219	544.3228	1.91
$[M\text{-}Me^{\bullet}]^{+\bullet}$	529	$C_{29}H_{49}O_3Si_3$	529.2984	529.2995	2.05
$[M\text{-}TMSOH]^{+\bullet}$	454	$C_{27}H_{42}O_2Si_2$	454.2718	454.2720	0.49
$[M\ TMSOH\ \text{-}Me^{\bullet}]^{+\bullet}$	439	$C_{26}H_{39}O_2Si_2$	439.2483	439.2485	0.35
	414	$C_{24}H_{38}O_2Si_2$	414.2405	414.2409	0.96
	402	$C_{23}H_{38}O_2Si_2$	402.2405	402.2407	0.65
	388	$C_{22}H_{36}O_2Si_2$	388.2248	388.2251	0.73
	385	$C_{22}H_{33}O_2Si_2$	385.2014	385.2016	0.75
	359	$C_{20}H_{31}O_2Si_2$	359.1857	359.1858	0.38
	333	$C_{18}H_{29}O_2Si_2$	333.1701	333.1703	0.79
	331	$C_{18}H_{27}O_2Si_2$	331.1544	331.1545	0.21
	320	$C_{17}H_{28}O_2Si_2$	320.1622	320.1622	0
	307	$C_{16}H_{27}O_2Si_2$	307.1544	307.1547	0.81
	281	$C_{14}H_{25}O_2Si_2$	281.1388	281.1389	0.38
	219	$C_{13}H_{19}OSi$	219.1200	219.1200	0
	219	$C_{12}H_{15}O_2Si$	219.0836	219.0837	0.63
	209	$C_{12}H_{21}OSi$	209.1356	209.1357	0.40
	207	$C_{12}H_{19}OSi$	207.1200	207.1200	0
	195	$C_{11}H_{19}OSi$	195.1200	195.1200	0
	157	$C_8H_{17}OSi$	157.1043	157.1044	0.67
	156	$C_8H_{16}OSi$	156.0965	156.0965	0
	143	$C_7H_{15}OSi$	143.0887	143.0887	0
	117	$C_5H_{13}OSi$	117.0730	117.0731	0.49
	91	$C_3H_{11}OSi$	91.0574	91.0575	1.06
	75	C_2H_7OSi	75.0261	75.0261	0
	73	C_3H_9Si	73.0468	73.0468	0

Table A14. Ions found in the GC-EI HR MS spectrum of the S42-tris-OH metabolite **M3a**.

M3a	Nominal mass [Da]	Composition	Theo. Mass [Da]	Accurate ion mass measured [Da]	Error [ppm]
$[M]^{+\bullet}$	632	$C_{33}H_{60}O_4Si_4$	632.3563	632.3589	4.11
$[M\text{-}TMSOH]^{+\bullet}$	542	$C_{30}H_{50}O_3Si_3$	542.3062	542.3069	1.23
	515	$C_{28}H_{47}O_3Si_3$	515.2828	515.2832	0.89
	487	$C_{26}H_{43}O_3Si_3$	487.2515	487.2516	0.41
$[M\text{-}2TMSOH]^{+\bullet}$	452	$C_{27}H_{40}O_2Si_2$	452.2561	452.2563	0.45
$[M\text{-}2TMSOH\text{-}Me^{\bullet}]^{+}$	437	$C_{26}H_{37}O_2Si_2$	437.2327	437.2327	0
$[M\text{-}TMSOH\text{-}C_5H_{13}OSi^{\bullet}]^{+}$	425	$C_{25}H_{37}O_2Si_2$	425.2327	425.2331	1.06
	402	$C_{23}H_{38}O_2Si_2$	402.2405	402.2407	0.57
	400	$C_{23}H_{36}O_2Si_2$	400.2248	400.2249	0.21
	385	$C_{22}H_{33}O_2Si_2$	385.2014	385.2015	0.4
	334	$C_{18}H_{30}O_2Si_2$	334.1779	334.1781	0.75
	333	$C_{18}H_{29}O_2Si_2$	333.1701	333.1698	-0.72
	332	$C_{18}H_{28}O_2Si_2$	332.1622	332.1622	0
	331	$C_{18}H_{27}O_2Si_2$	331.1544	331.1544	0
	320	$C_{17}H_{28}O_2Si_2$	320.1622	320.1622	0
	307	$C_{16}H_{27}O_2Si_2$	307.1544	307.1545	0.38
	281	$C_{14}H_{25}O_2Si_2$	281.1388	281.1388	0
	244	$C_{11}H_{24}O_2Si_2$	244.1309	244.1310	0.33
	243	$C_{11}H_{23}O_2Si_2$	243.1231	243.1233	0.6
	231	$C_{10}H_{23}O_2Si_2$	231.1231	231.1232	0.41
	230	$C_{10}H_{22}O_2Si_2$	230.1153	230.1154	0.34
	218	$C_9H_{22}O_2Si_2$	218.1153	218.1153	0
	169	$C_9H_{17}OSi$	169.1043	169.1043	0
	157	$C_8H_{17}OSi$	157.1043	157.1043	0
	155	$C_7H_{11}O_2Si$	155.0523	155.0523	0
	143	$C_7H_{15}OSi$	143.0887	143.0886	-0.44
	117	$C_5H_{13}OSi$	117.073	117.0731	0.53
	91	$C_3H_{11}OSi$	91.0574	91.0574	0
	73	C_3H_9Si	73.0468	73.0468	0

Table A15. Ions found in the GC-EI HR MS spectrum of the S42-tris-OH metabolite **M3b**.

M3b	Nominal mass [Da]	Composition	Theo. Mass [Da]	Accurate ion mass measured [Da]	Error [ppm]
$[M]^{+\bullet}$	632	$C_{33}H_{60}O_4Si_4$	632.3563	632.3586	2.32
$[M\text{-}Me^{\bullet}]^{+}$	617	$C_{32}H_{57}O_4Si_4$	617.3328	617.3348	1.94
$[M\text{-}TMSOH]^{+\bullet}$	542	$C_{30}H_{50}O_3Si_3$	542.3062	542.3073	1.06
$[M\text{-}TMSOH\text{-}Me^{\bullet}]^{+}$	527	$C_{29}H_{47}O_3Si_3$	527.2828	527.2837	0.92
	502	$C_{27}H_{46}O_3Si_3$	502.2749	502.2755	0.56
	452	$C_{27}H_{40}O_2Si_2$	452.2561	452.2564	0.22
	437	$C_{26}H_{37}O_2Si_2$	437.2327	437.2328	0.09
	388	$C_{22}H_{36}O_2Si_2$	388.2248	388.2251	0.30
	334	$C_{18}H_{30}O_2Si_2$	334.1779	334.1782	0.29
	333	$C_{18}H_{29}O_2Si_2$	333.1701	333.1703	0.29
	332	$C_{18}H_{28}O_2Si_2$	332.1622	332.1623	0.10
	331	$C_{18}H_{27}O_2Si_2$	331.1544	331.1545	0.13
	307	$C_{16}H_{27}O_2Si_2$	307.1544	307.1546	0.18
	281	$C_{14}H_{25}O_2Si_2$	281.1388	281.1388	0
	231	$C_{10}H_{23}O_2Si_2$	231.1231	231.1232	0.14
	157	$C_8H_{17}OSi$	157.1043	157.1043	0
	155	$C_8H_{15}OSi$	155.0887	155.0886	-0.08
	143	$C_7H_{15}OSi$	143.0887	143.0887	0
	131	$C_6H_{15}OSi$	131.0887	131.0887	0
	117	$C_5H_{13}OSi$	117.073	117.0731	0.09
	91	$C_3H_{11}OSi$	91.0574	91.0575	0.10
	73	C_3H_9Si	73.0468	73.0468	0

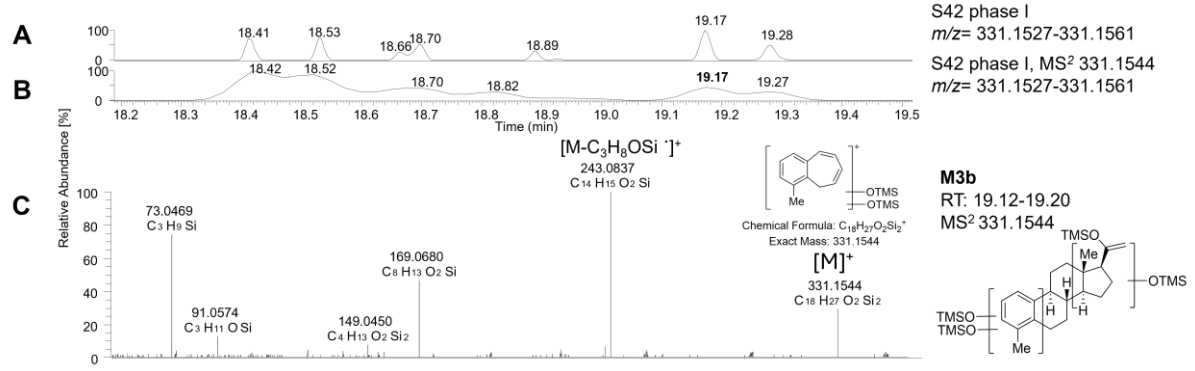

Figure A65. Extracted single ion currents SIC of the characteristic fragment ions of the TMS derivatized S42-tris-OH metabolites M3b at *m/z* 331 (panel A). MS^2-product ion experiments of ions at *m/z* 331 (155+88x2 Da) (d0) of **M3b** (panel B). These measurements were conducted on a new GC column without any influence on the retention time of M3b.

Table A16. Ions found in the GC-EI HR MS spectrum of the S42-tris-OH metabolite **M3c**.

M3c	Nominal mass [Da]	Composition	Theo. Mass [Da]	Accurate ion mass measured [Da]	Error [ppm]
$[M]^{+\bullet}$	632	$C_{33}H_{60}O_4Si_4$	632.3563	632.3588	3.91
$[M\text{-}TMSOH]^{+\bullet}$	542	$C_{30}H_{50}O_3Si_3$	542.3062	542.3071	1.53
$[M\text{-}TMSOH\text{-}Me^{\bullet}]^{+}$	529	$C_{29}H_{49}O_3Si_3$	529.2984	529.2992	1.55
	516	$C_{28}H_{48}O_3Si_3$	516.2906	516.2913	1.46
	500	$C_{27}H_{44}O_3Si_3$	500.2593	500.2597	0.91
	473	$C_{25}H_{41}O_3Si_3$	473.2358	473.2359	0.11
	452	$C_{27}H_{40}O_2Si_2$	452.2561	452.2565	0.73
	439	$C_{26}H_{39}O_2Si_2$	439.2483	439.2483	0
	414	$C_{24}H_{38}O_2Si_2$	414.2405	414.2408	0.71
	402	$C_{23}H_{38}O_2Si_2$	402.2405	402.2408	0.68
	387	$C_{22}H_{35}O_2Si_2$	387.2170	387.2172	0.6
	385	$C_{22}H_{33}O_2Si_2$	385.2014	385.2017	0.77
	371	$C_{21}H_{31}O_2Si_2$	371.1857	371.1859	0.52
	344	$C_{19}H_{28}O_2Si_2$	344.1622	344.1624	0.55
	334	$C_{18}H_{30}O_2Si_2$	334.1779	334.1780	0.41
	333	$C_{18}H_{29}O_2Si_2$	333.1701	333.1700	-0.09
	332	$C_{18}H_{28}O_2Si_2$	332.1622	332.1624	0.36
	331	$C_{18}H_{27}O_2Si_2$	331.1544	331.1543	-0.34
	320	$C_{17}H_{28}O_2Si_2$	320.1622	320.1623	0.13
	307	$C_{16}H_{27}O_2Si_2$	307.1544	307.1546	0.46
	281	$C_{14}H_{25}O_2Si_2$	281.1388	281.1388	0
	243	$C_{11}H_{23}O_2Si_2$	243.1231	243.1233	0.65
	231	$C_{10}H_{23}O_2Si_2$	231.1231	231.1232	0.46
	230	$C_{10}H_{22}O_2Si_2$	230.1153	230.1154	0.58
	183	$C_{10}H_{19}OSi$	183.1200	183.1200	0
	155	$C_8H_{15}OSi$	155.0887	155.0886	-0.16
	155	$C_7H_{11}O_2Si$	155.0523	155.0522	-0.51
	149	$C_4H_{13}O_2Si_2$	149.0449	149.0449	0
	143	$C_7H_{15}OSi$	143.0887	143.0887	0
	143	$C_6H_{11}O_2Si$	143.0523	143.0523	0
	117	$C_5H_{13}OSi$	117.073	117.073	0
	91	$C_3H_{11}OSi$	91.0574	91.0574	0
	73	C_3H_9Si	73.0468	73.0467	-0.81

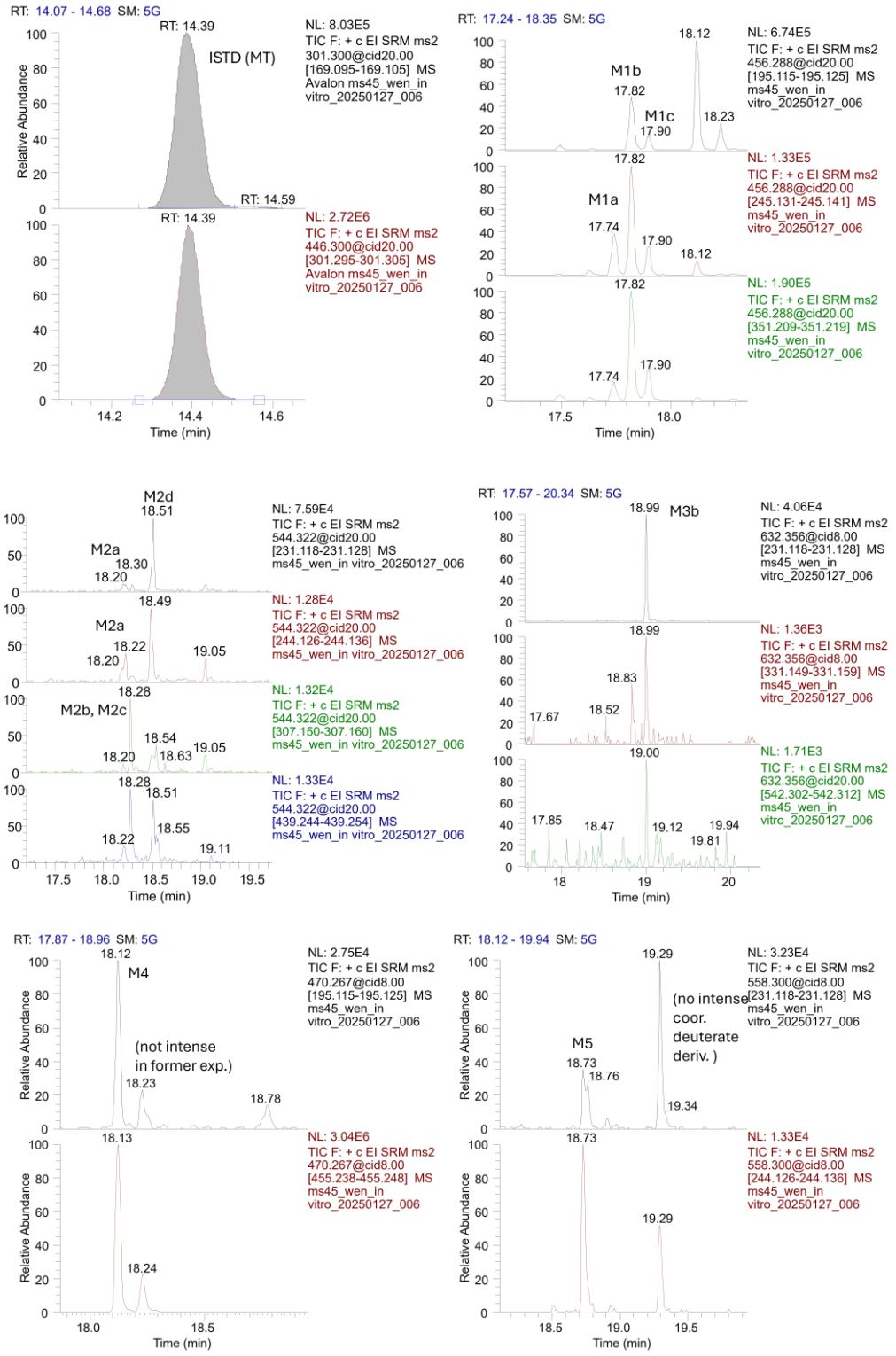

Figure A66. Chromatograms of MRM experiments of different *in vitro* phase I metabolites.

9.3.5 MS spectra of silylated metabolites from rat urine samples

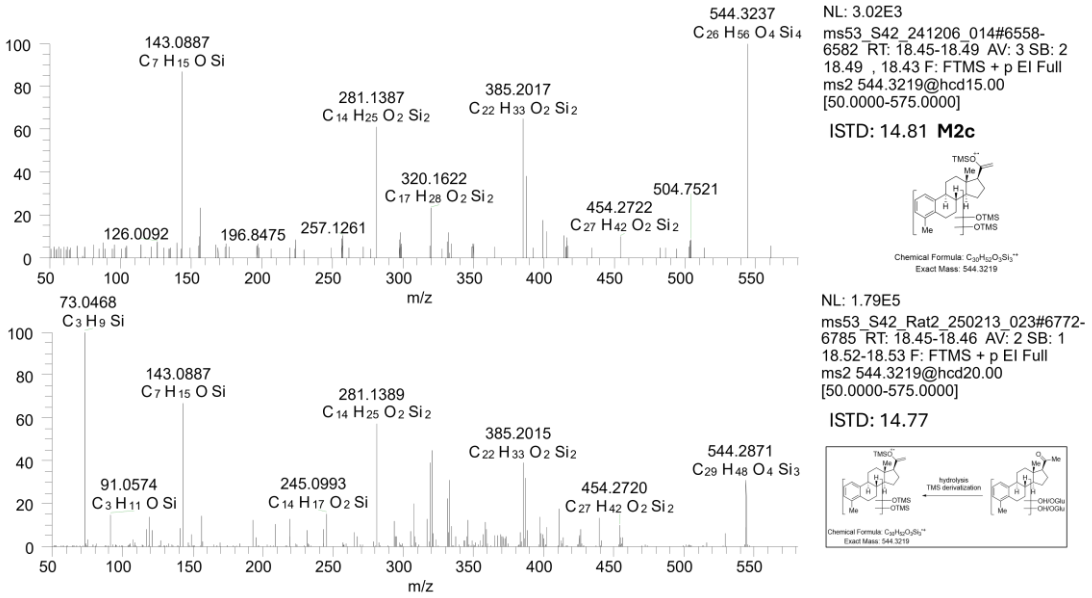

Figure A67. TMS-S42-bis-OH (MS^2 at *m/z* 544) from *In vitro* phase I experiment and Rat 2 urine on day 2 showed similar retention time (18.46 min) and MS spectra.

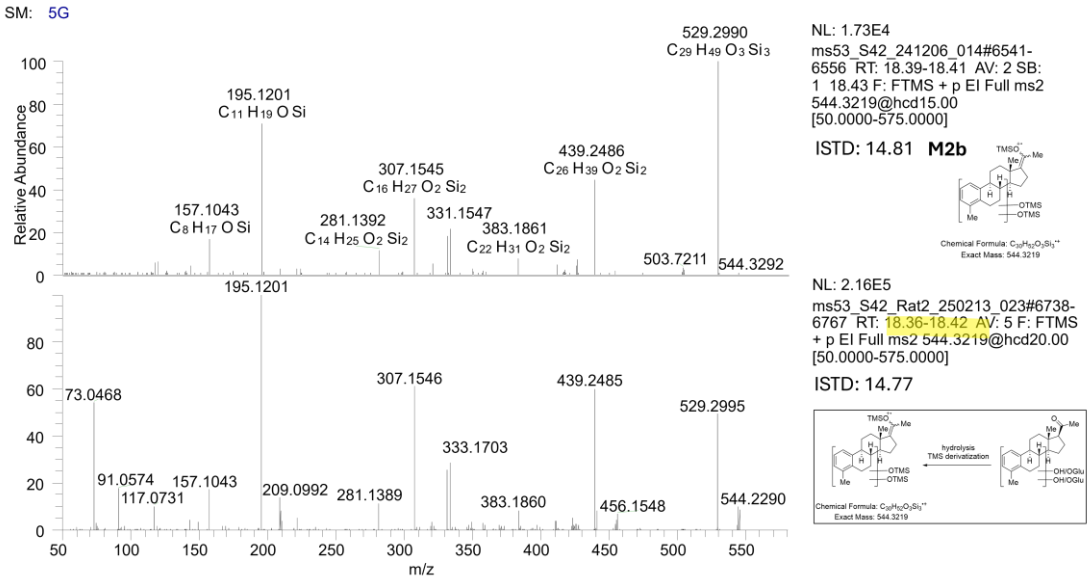

Figure A68. TMS-S42-bis-OH (MS^2 at *m/z* 544) from *In vitro* phase I experiment and Rat 2 urine on day 2 showed similar retention time (18.4 min) and MS spectra.

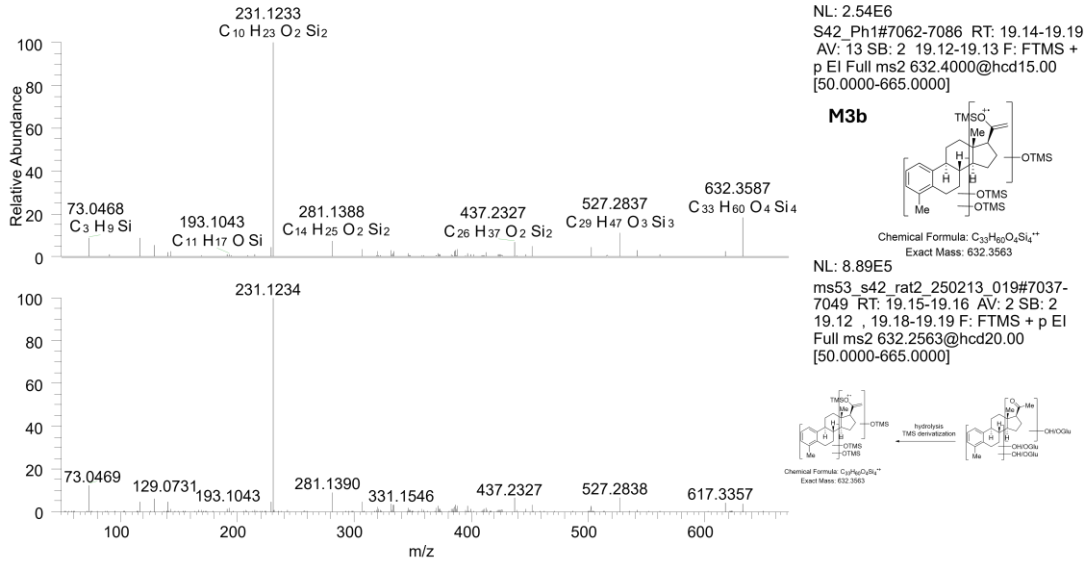

Figure A69. TMS-S42-triss-OH (MS^2 at *m/z* 632) from *In vitro* phase I experiment and Rat 2 urine on day 2 showed similar retention time (19.13 min) and MS spectra.

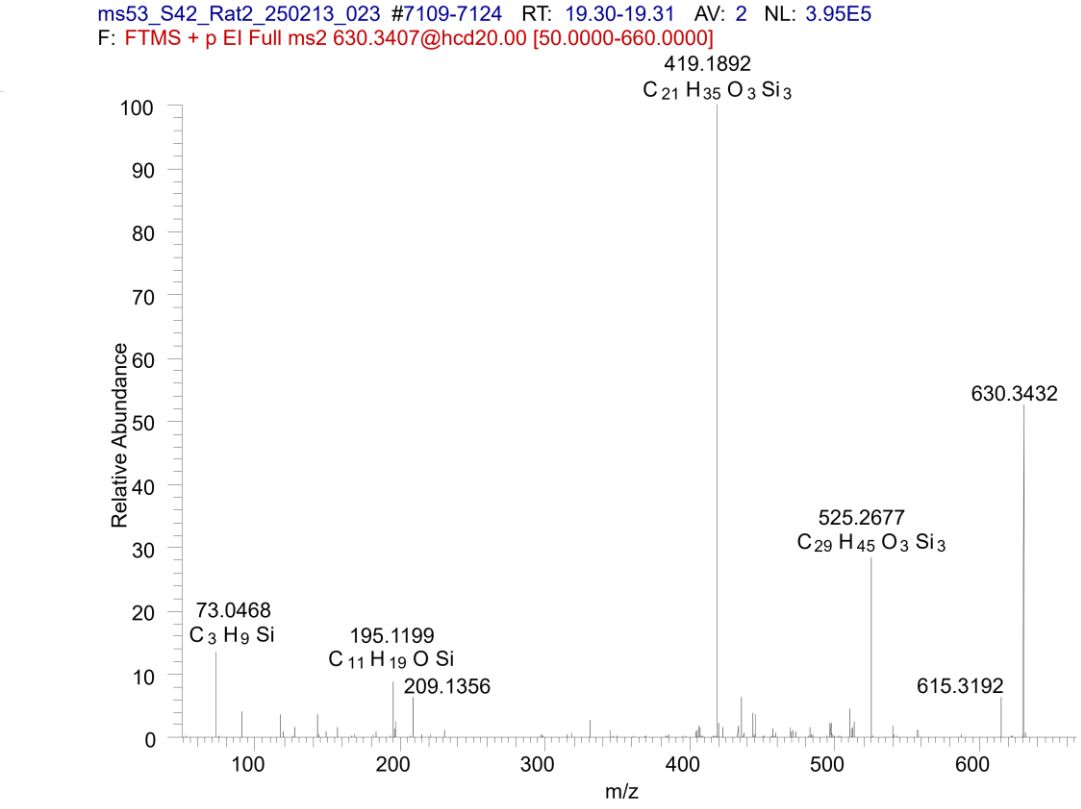

Figure A70. The metabolite S42-tris-OH-2H (molecular mass at *m/z* 630) at RT19.3 min showed a significant ion peak at *m/z* 419, which recommended three TMSO functional groups located at the A and B rings.

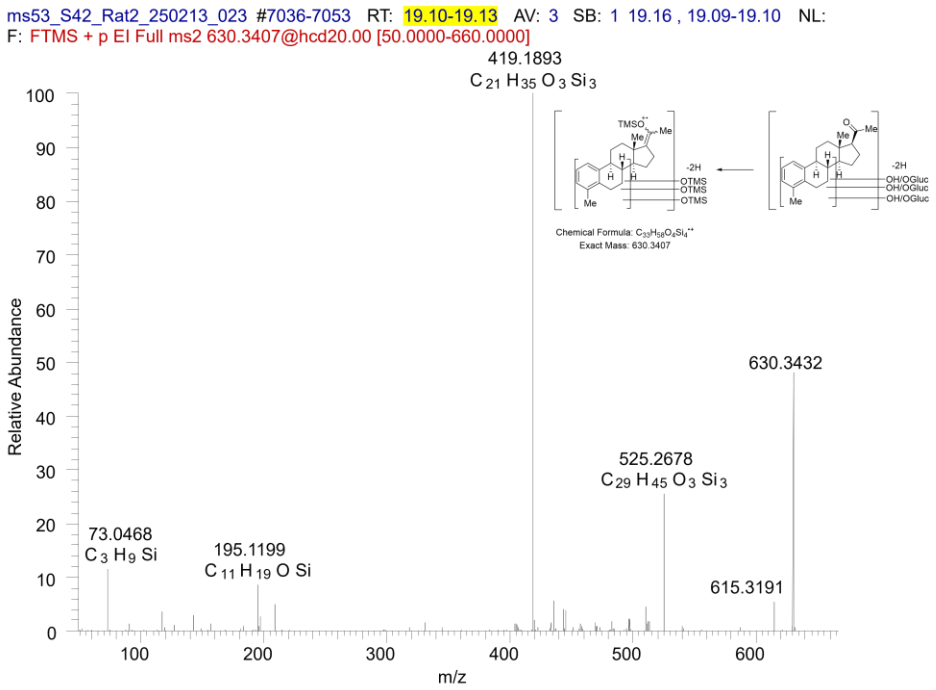

Figure A71. The metabolite S42-tris-OH-2H (molecular mass at *m/z* 630) at RT19.1 min showed a significant ion peak at *m/z* 419, which recommended three TMSO functional groups located at the A and B rings.

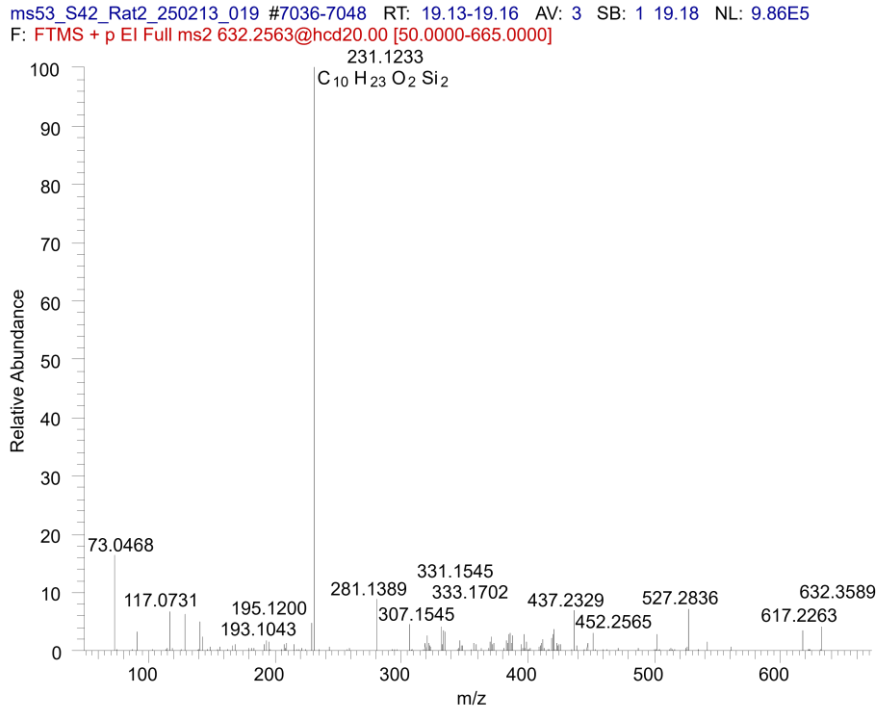

Figure A72. MS^2 spectrum of the S42-tris-OH (*m/z* 632) showed a significant ion peak at *m/z* 231, which indicated a least one hydroxy group. Two TMSO functional groups can be at the A ring by observing the ion peak at *m/z* 281.

9.4 Crystallography data

9.4.1 S42 (**1**) crystal structure

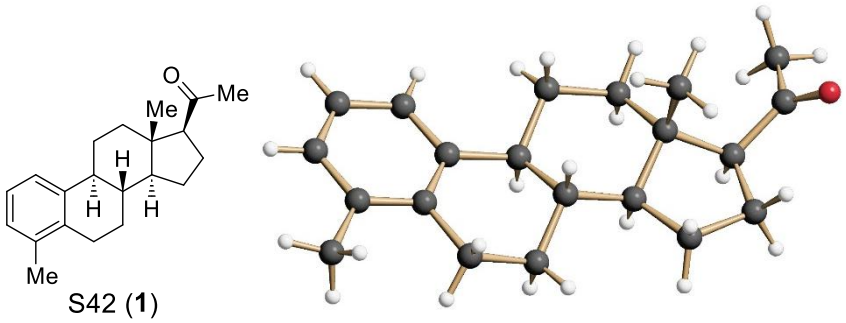

Figure A73. Crystal structure of S42 (**1**).

Empirical formula	$C_{21}H_{26}O_2$	
Moiety formula	$C_{21}H_{26}O_2$	
Formula weight	310.42	
Temperature	100(2) K	
Wavelength	1.54178 Å	
Crystal system	Orthorhombic	
Space group	$P2_12_12_1$	
Unit cell dimensions	a = 7.55400(10) Å	a = 90°.
	b = 12.6579(3) Å	b = 90°.
	c = 16.9785(4) Å	g = 90°.
Volume	1623.45(6) $Å^3$	
Z	4	
Density (calculated)	1.270 Mg/m^3	
Absorption coefficient	0.619 mm^{-1}	
F(000)	672	
Crystal size	0.100 x 0.070 x 0.050 mm^3	
Theta range for data collection	4.357 to 72.207°.	
Index ranges	-9≤h≤9, -15≤k≤15, -20≤l≤20	
Reflections collected	38864	
Independent reflections	3196 [R(int) = 0.0459]	
Completeness to theta = 67.679°	99.9 %	
Absorption correction	Semi-empirical from equivalents	
Max. and min. transmission	0.7536 and 0.6010	
Refinement method	Full-matrix least-squares on F^2	
Data / restraints / parameters	3196 / 0 / 211	
Goodness-of-fit on F^2	1.062	
Final R indices [I>2sigma(I)]	R1 = 0.0277, wR2 = 0.0732	
R indices (all data)	R1 = 0.0281, wR2 = 0.0735	
Absolute structure parameter	0.04(5)	
Extinction coefficient	n/a	
Largest diff. peak and hole	0.226 and -0.164 $e.Å^{-3}$	

9.4.2 S42-d7 (**1-d7**) crystal structure

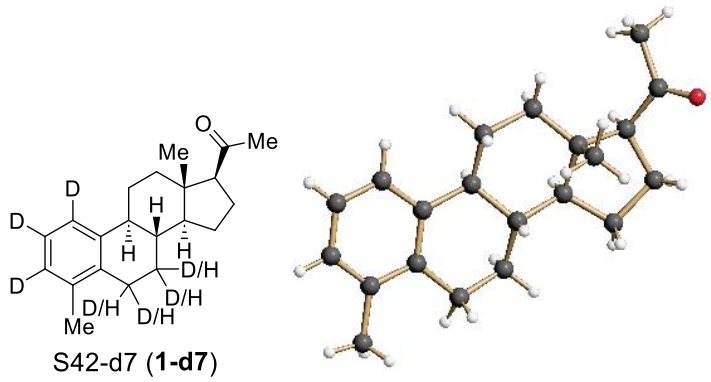

S42-d7 (**1-d7**)

Figure A74. Crystal structure of S42-d7 (**1-d7**).

Empirical formula	$C_{21}H_{28}O$	
Moiety formula	$C_{21}H_{28}O$	
Formula weight	296.43	
Temperature	100(2) K	
Wavelength	1.54178 Å	
Crystal system	Tetragonal	
Space group	$P4_1$	
Unit cell dimensions	a = 7.59240(10) Å	a= 90°.
	b = 7.59240(10) Å	b= 90°.
	c = 28.7445(6) Å	g = 90°.
Volume	1656.96(6) $Å^3$	
Z	4	
Density (calculated)	1.188 Mg/m^3	
Absorption coefficient	0.534 mm^{-1}	
F(000)	648	
Crystal size	0.300 x 0.200 x 0.150 mm^3	
Theta range for data collection	5.828 to 72.431°.	
Index ranges	-9≤h≤9, -9≤k≤9, -35≤l≤34	
Reflections collected	23163	
Independent reflections	3271 [R(int) = 0.0310]	
Completeness to theta = 67.679°	100.0 %	
Absorption correction	Semi-empirical from equivalents	
Max. and min. transmission	0.753 and 0.6178	
Refinement method	Full-matrix least-squares on F^2	
Data / restraints / parameters	3271 / 1 / 202	
Goodness-of-fit on F^2	1.047	
Final R indices [I>2sigma(I)]	R1 = 0.0279, wR2 = 0.0737	
R indices (all data)	R1 = 0.0279, wR2 = 0.0737	
Absolute structure parameter	0.10(5)	
Extinction coefficient	n/a	
Largest diff. peak and hole	0.121 and -0.179 $e.Å^{-3}$	

9.4.3 S42-C20-OH (**2**) crystal structure

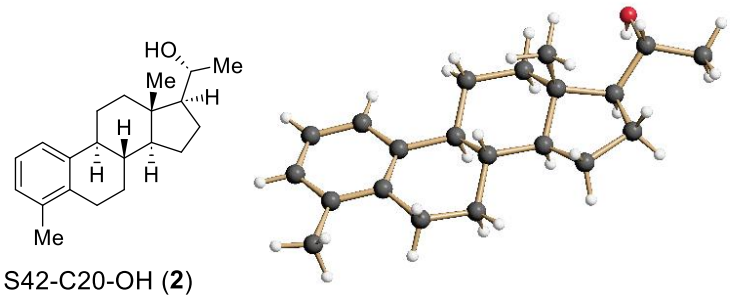

S42-C20-OH (**2**)

Figure A75. Crystal structure of S42-C20-OH (**2**).

Empirical formula	$C_{21}H_{30}O$	
Moiety formula	$C_{21}H_{30}O$	
Formula weight	298.45	
Temperature	100(2) K	
Wavelength	1.54178 Å	
Crystal system	Orthorhombic	
Space group	$P2_12_12_1$	
Unit cell dimensions	a = 9.7544(2) Å	a= 90°.
	b = 15.3033(3) Å	b= 90°.
	c = 47.6318(9) Å	g = 90°.
Volume	7110.2(2) $Å^3$	
Z	16	
Density (calculated)	1.115 Mg/m^3	
Absorption coefficient	0.498 mm^{-1}	
F(000)	2624	
Crystal size	0.150 x 0.100 x 0.050 mm^3	
Theta range for data collection	3.033 to 72.232°.	
Index ranges	-11<=h<=11, -18<=k<=18, -53<=l<=58	
Reflections collected	61287	
Independent reflections	13952 [R(int) = 0.0419]	
Completeness to theta = 67.679°	99.9 %	
Absorption correction	Semi-empirical from equivalents	
Max. and min. transmission	0.7536 and 0.5739	
Refinement method	Full-matrix least-squares on F^2	
Data / restraints / parameters	13952 / 0 / 821	
Goodness-of-fit on F^2	1.064	
Final R indices [I>2sigma(I)]	R1 = 0.0348, wR2 = 0.0893	
R indices (all data)	R1 = 0.0359, wR2 = 0.0901	
Absolute structure parameter	0.09(5)	
Extinction coefficient	n/a	
Largest diff. peak and hole	0.222 and -0.167 $e.Å^{-3}$	

9.4.4 S42-C6*α*-OH (**3**) crystal structure

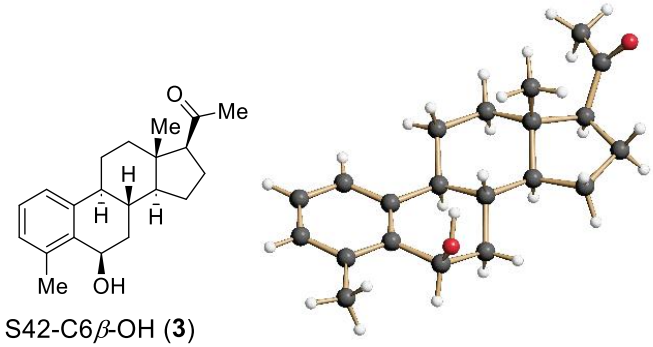

S42-C6*β*-OH (**3**)

Figure A76. Crystal structure of S42-C6*β*-OH (**3**).

Empirical formula	$C_{21}H_{28}O_2$	
Moiety formula	$C_{21}H_{28}O_2$	
Formula weight	312.43	
Temperature	100(2) K	
Wavelength	1.54178 Å	
Crystal system	Monoclinic	
Space group	$P2_1$	
Unit cell dimensions	a = 7.5929(2) Å	a= 90°.
	b = 12.7155(4) Å	b= 103.2080(10)°.
	c = 9.2979(3) Å	g = 90°.
Volume	873.94(5) $Å^3$	
Z	2	
Density (calculated)	1.187 Mg/m^3	
Absorption coefficient	0.575 mm^{-1}	
F(000)	340	
Crystal size	0.250 x 0.150 x 0.050 mm^3	
Theta range for data collection	4.885 to 72.012°.	
Index ranges	-9<=h<=9, -14<=k<=15, -11<=l<=11	
Reflections collected	21537	
Independent reflections	3328 [R(int) = 0.0432]	
Completeness to theta = 67.679°	97.5 %	
Absorption correction	Semi-empirical from equivalents	
Max. and min. transmission	0.7535 and 0.6259	
Refinement method	Full-matrix least-squares on F^2	
Data / restraints / parameters	3328 / 1 / 214	
Goodness-of-fit on F^2	1.066	
Final R indices [I>2sigma(I)]	R1 = 0.0310, wR2 = 0.0849	
R indices (all data)	R1 = 0.0319, wR2 = 0.0851	
Absolute structure parameter	0.08(6)	
Extinction coefficient	n/a	
Largest diff. peak and hole	0.214 and -0.217 $e.Å^{-3}$	

9.4.5 S42-C7*β*-OH (**4**) crystal structure

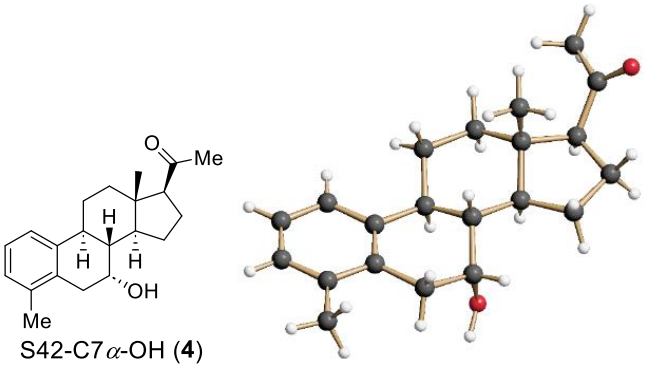

Figure A77. Crystal structure of S42-C7*α*-OH (**4**)

Empirical formula	$C_{21}H_{28}O_2$	
Moiety formula	$C_{21}H_{28}O_2$	
Formula weight	312.43	
Temperature	100(2) K	
Wavelength	1.54178 Å	
Crystal system	Monoclinic	
Space group	$P2_1$	
Unit cell dimensions	a = 10.0460(4) Å	a= 90°.
	b = 5.9063(3) Å	b= 96.257(2)°.
	c = 14.4697(6) Å	g = 90°.
Volume	853.44(7) $Å^3$	
Z	2	
Density (calculated)	1.216 Mg/m^3	
Absorption coefficient	0.589 mm^{-1}	
F(000)	340	
Crystal size	0.150 x 0.070 x 0.070 mm^3	
Theta range for data collection	3.072 to 72.118°.	
Index ranges	-12<=h<=12, -7<=k<=7, -17<=l<=17	
Reflections collected	17795	
Independent reflections	3334 [R(int) = 0.0450]	
Completeness to theta = 67.679°	99.9 %	
Absorption correction	Semi-empirical from equivalents	
Max. and min. transmission	0.7536 and 0.6738	
Refinement method	Full-matrix least-squares on F^2	
Data / restraints / parameters	3334 / 1 / 214	
Goodness-of-fit on F^2	1.051	
Final R indices [I>2sigma(I)]	R1 = 0.0279, wR2 = 0.0714	
R indices (all data)	R1 = 0.0304, wR2 = 0.0718	
Absolute structure parameter	0.01(6)	
Extinction coefficient	n/a	
Largest diff. peak and hole	0.188 and -0.132 $e.Å^{-3}$	

10. Eidesstattliche Erklärung

Hiermit versichere ich an Eides statt, dass ich die vorliegende Dissertation selbstständig und ohne die Benutzung anderer als der angegebenen Hilfsmittel und Literatur angefertigt habe. Alle Stellen, die wörtlich oder sinngemäß aus veröffentlichten und nicht veröffentlichten Werken dem Wortlaut oder dem Sinn nach entnommen wurden, sind als solche kenntlich gemacht. Ich versichere an Eides statt, dass diese Dissertation noch keiner anderen Fakultät oder Universität zur Prüfung vorgelegen hat; dass sie - abgesehen von unten angegebenen Teilpublikationen und eingebundenen Artikeln und Manuskripten - noch nicht veröffentlicht worden ist sowie, dass ich eine Veröffentlichung der Dissertation vor Abschluss der Promotion nicht ohne Genehmigung des Promotionsausschusses vornehmen werde. Die Bestimmungen dieser Ordnung sind mir bekannt. Darüber hinaus erkläre ich hiermit, dass ich die Ordnung zur Sicherung guter wissenschaftlicher Praxis und zum Umgang mit wissenschaftlichem Fehlverhalten der Universität zu Köln gelesen und sie bei der Durchführung der Dissertation zugrundeliegenden Arbeiten und der schriftlich verfassten Dissertation beachtet habe und verpflichte mich hiermit, die dort genannten Vorgaben bei allen wissenschaftlichen Tätigkeiten zu beachten und umzusetzen. Ich versichere, dass die eingereichte elektronische Fassung der eingereichten Druckfassung vollständig entspricht.

Teilpublikationen:

- A comprehensive gas chromatography electron ionization high resolution mass spectrometry study of a new steroidal selective androgen receptor modulator (SARM) compound S42.
  Wen H-C, Wilczek T, Neudörfl J-M, Wagener F, Piper T, Thevis M, Schäfer M. *Journal of Mass Spectrometry* **2024,** *59*(8), e5077.

- Investigations Into Structures of In Vitro–Derived Phase I Metabolites of a Novel 20-Keto-Steroid S42 by GC-EI HR MS Analysis and Chemical Synthesis.
  Wen H-C, Wagener F, Piper T, Neudörfl J-M, Thevis M, Schäfer M. *Drug Testing and Analysis,* **2025**.

26.05.2025, Hui-Chung Wen